Synthesis and characterisation of high silica zeolites with MOR and MFI framework type from South African coal fly ash.

By

Mero-Lee Ursula Cornelius

MSc (Chemistry) – University of the Western Cape

BSc (Honours) Chemistry – University of the Western Cape

BSc degree (Chemical Biology) – Stellenbosch University

A thesis submitted in fulfilment of the requirements of the degree of Doctor of Philosophy in Chemistry in the Chemistry Department, University of the Western Cape.

Supervisors: Prof. Leslie F. Petrik

Dr Asel Sartbaeva

August 2019

Abstract

High-silica zeolites are porous, aluminosilicate materials known for high thermal stability; making these materials favourable for application in various industrial processes involving elevated temperatures. The synthesis of zeolites from alternative feedstock such as coal fly ash has been investigated previously. Coal fly ash is a waste by-product of the coal combustion process, which is main source utilised for energy generation in South Africa. Coal fly ash is an ideal alternative feedstock for zeolites due to the large annual production as well as the rich mineral content (high in silicon and aluminium). Coal fly ash also contains a range of other elements which is known to result in environmental problems such as excessive land-use as well as air, soil, surface water and ground water pollution; including inorganic cations that may influence the zeolite crystallisation process. However, coal fly ash has successfully been utilised for the synthesis of a range of low-silica zeolites. High-silica zeolite synthesis from alternative feedstock has usually focused on the synthesis of zeolite ZSM-5. Furthermore, these synthesis routes commonly utilised additional silicon sources and/or a purification step by reflux treatment with a chelating agent to enhance the feedstock Si/Al ratio prior to crystallisation. This adds complexity to the conversion of coal fly ash to zeolite process, in terms of cost, energy and time.

This research study therefore aimed to synthesise pure, high-silica zeolites from waste South African coal fly ash by utilising a simplified, green synthesis procedure. This was realised by applying a relatively low-temperature alkaline treatment (150 °C for 24 hours) for the extraction of a silicon precursor from coal fly ash, which served as the silicon feedstock for the synthesis of high-silica zeolite ZSM-5. The preparation of highly crystalline and pure zeolite materials was achieved without the need for additional silicon sources or the purification of the silicon extract. Similarly, zeolite mordenite (with large-pore MOR-type framework) and silicate-1 (with medium-pore MFI-type framework) were also synthesised using the coal fly ash-derived silicon precursor. Synthesised zeolites were characterised by a combination of analytical techniques such as XRD, SEM-EDS, FTIR, TGA-DTA/MS and/or nitrogen physisorption (BET). This study also aimed to investigate the influence of different extra-framework cations on the flexibility (and hence, synthetic feasibility) of a model zeolite framework (i.e. zeolite A with an LTA framework) through geometric modelling by using GASP software. This theoretical investigation was carried out to understand the steric effect of some of the major inorganic cations present in coal fly ash on the zeolite crystallisation process.

A simplified, greener synthesis route for the preparation of high-silica zeolites from coal fly ash was developed in this study; that involved a relatively low-temperature alkaline treatment for the extraction of a silicon precursor for high-silica zeolite synthesis (no additional silicon sources or purification steps were required). Furthermore, the solid residue generated in the conversion of coal fly ash to high-silica zeolites was easily recovered and transformed into low-silica zeolite sodalite (with high yield), which makes this process a near-zero waste process. This simplified synthesis process for high-silica zeolite production from coal fly ash waste was used to prepare highly crystalline zeolite mordenite. Zeolite mordenite was synthesised from a coal fly ash-derived silicon precursor using three different hydrothermal synthesis approaches; (i) Organic structure-directing agent-free synthesis (1 SiO_2•0.019 Al_2O_3•0.57 Na_2O•30.1 H_2O), (ii) seed-assisted synthesis (1 SiO_2•0.019 Al_2O_3•0.57 Na_2O•30.1 H_2O with 0.1 wt% mordenite seeds) and (iii) Organic structure-directing agent-assisted synthesis (1 SiO_2•0.019 Al_2O_3•0.46 Na_2O•0.26 TEAOH•30.1 H_2O with no added seed crystals nor NaOH), carried out under static hydrothermal conditions (170 °C for up to 72 hours). The synthesis approaches developed in this study resulted in the crystallisation of pure zeolite mordenite and allowed for control over the chemical composition of zeolite mordenite in terms of Si/Al ratio (between 6 and 15) as well as the morphological properties of zeolite mordenite in terms of both particle shape (prismatic, twinned prismatic, elongated needle-like crystals, hierarchical and spherical agglomerated mordenite crystals formed) and particle size (between 2.5 and 13.6 µm). Furthermore, the preparation of zeolite mordenite with novel hierarchical morphology from a coal fly ash-derived silicon precursor (without the utilisation of a complex organic structure-directing agent such as organosilane compounds) was also achieved in this study. This study therefore presents novel synthesis routes for the preparation of zeolite mordenite (with a range of different material properties) from a coal fly ash-derived silicon precursor.

Similarly, zeolite ZSM-5 and zeosil silicate-1 with different material properties (such as composition, morphology, hydrophilicity and porosity) were synthesised from a coal fly ash-derived silicon precursor under hydrothermal conditions of 160-170 °C for up to 72 hours. These material properties ranged from aluminium-rich, prismatic zeolite ZSM-5 crystals that were highly hygroscopic and microporous (1 SiO_2•0.015 Al_2O_3•0.53 Na_2O•0.10 TPABr•28.3 H_2O) to silicon-rich, spherical zeolite ZSM-5 crystals with both microporosity and mesoporosity (1 SiO_2•0.004 Al_2O_3•0.54 Na_2O•0.10 TPABr•35.4 H_2O) as well as

hydrophobic, all-silica silicate-1 crystals (1 SiO_2•0.004 Al_2O_3•0.49 Na_2O•0.09 TPABr•11.6 H_2O). This study therefore presents a novel synthesis route for the preparation of silicalite-1 from a coal fly ash-derived silicon precursor as well as a simplified, greener synthesis route for the preparation of zeolite ZSM-5 with a range of different material properties. This study therefore presents a novel green synthesis route for the preparation of pure, high-silica zeolites from waste coal fly ash, which was suitable for the design of tailor-made, pure zeolite mordenite and ZSM-5 as well as zeosil silicalite-1 with various properties such as morphology (in terms of crystal shape and size), composition (Si/Al ratio, solid acidity), hydrophilicity/hydrophobicity and porosity. The utilisation of geometric simulation by GASP software to investigate the steric influence of different inorganic cations on a model zeolite framework (zeolite A) was achieved for the first time. The geometric simulation study illustrated that various inorganic cations present in coal fly ash may not be detrimental to the formation of zeolites depending on the cation size as well as the zeolite framework topology. It was found that relatively larger inorganic cations may alter crystallisation processes involved in zeolite synthesis, due to short-range disorder that is caused by the steric strain imposed on the growing zeolite framework.

The synthesis of high-silica zeolites mordenite, ZSM-5 and silicalite-1 from a waste material such as coal fly ash was achieved in this study; the overall conversion process was simplified by the removal of the additional purification step and no additional silicon source was required. This study reports the first synthesis of silicalite-1 from coal fly ash and the first synthesis of zeolite mordenite from coal fly ash (as the sole silicon source). Furthermore, the solid residue generated in the conversion of coal fly ash to high-silica zeolites was easily recovered and transformed into low-silica zeolite sodalite, which makes this process for the synthesis of industrially applicable, high-silica zeolites from coal fly ash a near-zero waste process. Therefore, this study presents a novel green synthesis route for the preparation of pure, high-silica zeolites (such as zeolite mordenite and ZSM-5 as well as silicalite-1) from waste coal fly ash coupled to the production of sodalite (as a by-product). The conversion of a waste material such as coal fly ash to value-added, high-silica zeolites (mordenite, ZSM-5 and silicalite-1) as well as sodalite may be of interest to industries that make use of these materials for catalytic and adsorption processes as well as separation science.

Keywords: Zeolites, waste utilisation, coal fly ash, low temperature alkaline activation, high-silica zeolites, geometric simulation

Declaration

I declare that "Synthesis and characterisation of high silica zeolites with MOR and MFI framework type from South African coal fly ash." is my own work, that it has not been submitted for any degree or examination in any other university, and that all the resources I have used or quoted have been indicated and acknowledged by complete references.

Mero-Lee Ursula Cornelius August 2019

Signature: …….

Acknowledgements

I wish to thank my supervisors, Prof. Leslie Petrik and Dr. Asel Sartbaeva, for their support and guidance during my research project. I am truly grateful for the opportunity to have been part of the Environmental Nano Sciences (ENS) research group (at the University of the Western Cape, South Africa) as well as the Sartbaeva research group (during my research visit at the University of Bath in Bath, United Kingdom). I would like to acknowledge the Environmental Nano Sciences (ENS) research group and Sartbaeva research group for their support during the study and a special thank you to Emmanuel Ameh, Michael Nzadi, Zenzele Ndlovu, Dr. Roland Missengue, Dr. Yun-Chu Chen, Dr. Antony Nearchou, Zoe Jones, Lisa Price and Dr. Stephen Wells for their assistance and support during this research project. To the ENS technical and administration staff (Mrs. Vanessa Kellerman, Ilse Wells and Rallston Richards); your support and assistance during the research has been invaluable. I would also like to thank the National Research Foundation (NRF), Commonwealth Scholarship Commission, Prof. Leslie Petrik and Dr. Asel Sartbaeva for their contributions to the research project funding.

I would like to thank the staff at the Electron Microscope Unit at the University of the Western Cape) and Dr. Remi Bucher from iThemba labs for their kind assistance with SEM, TEM and XRD facilities, respectively. Thank you to the CAF staff (especially Mrs. Mareli Grobbelaar-Moolman) at Stellenbosch University for assistance with elemental analysis during this project. Thank you to Mr. Timothy Lesch for assistance with FTIR analysis during this research project. To the staff of the CCAF facilities at the University of Bath, United Kingdom (Dr. Gabriele Kociok-Kohn, Dr. Philip Fletcher, Dr. Diana Lednitzky and especially Dr. Remi Caistaing), thank you for all your help and kind assistance with various analytical techniques such as XRD, SEM, BET and TGA analysis during my research visit to the University of Bath.

I thank the Almighty God for his grace and for giving me the strength to carry out and complete this body of work. I wish to give my heartfelt thank you and appreciation to my family, friends (old and new) and husband for their continued love, support and encouragement during this time.

Table of Contents

List of Figures

List of Tables

Academic outputs during the research project

Patent in progress

Cornelius, M. -L. U., Ndlovu, N, Z, N., Sedres, G., Ameh, A. E., Sartbaeva, A., & Petrik, L. F. Process involving low temperature fly ash activation for synthesis of high-silica zeolitic materials. Technology Transfer Office, University of the Western Cape, Bellville, Cape Town, South Africa.

Accepted scientific articles

Cornelius, M. -L. U., Price, L., Wells, S. A., Petrik, L. F., & Sartbaeva, A. (2019). The steric influence of extra-framework cations on framework flexibility: an LTA case study. *Zeitschrift für Kristallographie - Crystalline Materials*, 234 (7-8), 461-468. https://doi.org/10.1515/zkri-2019-0016

Oral presentation

Cornelius, M. -L. U., Sartbaeva, A., & Petrik, L. F. (2018). Synthesis of (high-silica) zeolites from South African coal fly ash. Life beyond the PhD conference, 13-17 August 2018, Windsor, United Kingdom.

Poster presentations

Cornelius, M. -L. U., Wells, S. A., Sartbaeva, A., & Petrik, L. F. (2018). Geometric simulations: the influence of extra-framework cations on the flexibility window of zeolite LTA. Groupe Français des Zéolithes (GFZ) 34th Congress, 26-29 March 2018, Cabourg, Normandy, France.

Cornelius, M. -L. U., Sartbaeva, A., & Petrik, L. F. (2018). Synthesis of high-silica zeolites from South African coal fly ash. Annual Bolland Symposium, 14 June 2018, University of Bath, Bath, United Kingdom.

Cornelius, M. -L. U., Sartbaeva, A., & Petrik, L. F. (2018). Synthesis of high-silica zeolites from coal fly ash silicon precursor. British Zeolite Association (BZA) 41st Annual Meeting, 16-19 July 2018, Ambleside, Lake District, United Kingdom.

1 Chapter 1 - Introduction

A brief background of the research project will be presented in this chapter. The gap in the research topic was identified in the literature, which motivated the project. The aims and objectives of the project were to bridge the identified research gap in the topic. This chapter will also present the scope and delimitations of the research project and an outline of the thesis will be presented.

1.1 Background

High-silica zeolites are microporous aluminosilicate materials with Si/Al (SAR) ratios > 5. High-silica zeolites are known for superior thermal stability, solid acidity and shape selectivity and as such, these materials are valuable in industries that utilise high-temperature catalytic and adsorption processes (Payra and Dutta, 2003). Zeolite mordenite is a high-silica zeolite with a large-pore opening of ~0.75 nm that is utilised in adsorption processes involving the separation of compounds in the gas or liquid phase. Zeolite mordenite has also been utilised extensively in the catalysis for hydrocarbon transformations such as alkylation, hydrocracking and hydroisomerisation. One of the best known and most widely used high-silica zeolites is zeolite ZSM-5, which is a medium-pore (~0.55 nm) zeolite applied as a solid acid catalyst in a range of chemical processes involving hydrocarbon transformations such as alcohol dehydration, isomerisation and alkylation and acylation reactions. Another interesting material is the siliceous analogue of the MFI-type zeolite ZSM-5, silicalite-1, which is hydrophobic in nature due to the lack of aluminium in the framework. This hydrophobic material is a viable material for preparation of waterproof membranes and thin films for application in separation science. Hydrophobic silicalite-1 has been utilised for the removal of organic compounds from contaminated water streams (Cheng and Shantz, 2005; Dai et al., 2017; Hincapie et al., 2004; Idris et al., 2019; Lobo, 2003; Maesen, 2007; van den Broeke et al., 1999; Yang et al., 2011).

The synthesis of high-silica zeolites commonly involves an aluminosilicate precursor gel subjected to relatively high temperature (>100 °C) and autogenous pressures. Furthermore, the crystallisation of high-silica zeolites often occurs in the presence of an organic-structure directing agent (OSDA), which is a compound that aids in the organisation of silica and alumina tetrahedra to form the building units of a specific framework. For example, tetrapropylammonium bromide (TPABr) is commonly applied as an OSDA in the synthesis

of MFI-type zeolites such as ZSM-5. The typical precursors for hydrothermal synthesis of zeolites are fumed silica, colloidal silica or sodium silicate solution as sources of silicon as well as sodium aluminate and aluminium hydroxide as aluminium sources (Payra and Dutta, 2003; Yu, 2007). However, a range of naturally occurring materials (such as kaolin clay or diatomite) and waste by-products of industrial processes (such as coal fly ash) have been utilised as alternative sources of silicon and aluminium for the synthesis of zeolites (Aono et al., 2018; Chang and Shih, 2000; Franus, 2012; Hollman et al., 1999; Mignoni et al., 2008; Musyoka et al., 2013). In this study, coal fly ash (CFA) will be utilised as a source of silicon for the formation of high-silica zeolites. CFA is a waste by-product of the coal combustion process that is produced in large quantities annually and is typically destined for disposal to landfills. CFA contains a large amount of silicon and aluminium oxides, in the mineral form of quartz and mullite. The uncontrolled disposal of CFA is accompanied by a range of environmental issues such as surface and ground water pollution, air and soil pollution as well as excessive land-use (Blissett and Rowson, 2012; Shoumkova and Stoyanova, 2012). The utilisation of CFA in other processes such as cement and concrete production has therefore been studied extensively to date (Blissett and Rowson, 2012; Heidrich et al., 2013). An industrially desirable use of CFA is in the conversion of this waste by-product to zeolites; this process is advantageous as a high-value material applicable in many industries (such as petroleum, fine chemicals, etc.) is produced and at the same time a harmful waste product is reduced (Ameh et al., 2016; Missengue et al., 2018; Ndlovu et al., 2017).

The transformation of CFA to zeolites has been investigated for a few years, with emphasis on the synthesis of low-silica zeolites such as zeolite A, X, P and sodalite. Some challenges that face this conversion technology are variability of the ash, low purity of zeolite products, low zeolite yields (particularly in the case of more pure zeolites) and the lack of control of zeolite product properties. More recently, the synthesis of zeolite ZSM-5 from CFA has also been reported. The synthesis of this high-silica zeolite from CFA typically involved the addition of an extra silicon source to enhance the SAR value of the synthesis mixture or a silicon extract from alkaline-activated CFA was treated with concentrated oxalic acid under reflux conditions to remove excess sodium and enhance the SAR value of the material prior to hydrothermal treatment (Ameh et al., 2016; Chareonpanich et al., 2004; Gitari et al., 2016; Kalyankar et al., 2011; Kapure et al., 2017; Krisnandi et al., 2017; Missengue, 2016; Missengue et al., 2017; Missengue et al., 2018; Ndlovu, 2016; Ndlovu et al., 2017;

Vichapund et al., 2014; Vichapund et al., 2017). Zeolite ZSM-5 was synthesised from South African CFA using a high temperature, solid fusion method to extract silicon (and aluminium) from coal fly ash. An additional purification step was utilised to remove excess sodium cations from the silicon extract; involving the treatment of the silicon extract with a concentrated oxalic acid solution under reflux (Missengue, 2016). A novel low-temperature extraction method for the preparation of a silicon extract from CFA was reported in the literature. However, the utilisation of this silicon extract in zeolite ZSM-5 synthesis also involved the oxalic acid treatment step prior to hydrothermal treatment (Ndlovu, 2016). The addition of extra steps and/or chemical reagents to the conversion process (i.e. CFA to high-silica zeolites) is known to be both energy- and cost-intensive. The simplification of this conversion process will create a relatively greener synthesis route compared to literature reported to date (Missengue, 2016; Missengue et al., 2017; Missengue et al., 2018; Ndlovu, 2016).

In this study, the low-temperature alkaline reflux process was utilised for the preparation of a silicon extract as reported in the literature (Ndlovu, 2016). This silicon extract will serve as the silicon precursor material for high-silica zeolite synthesis. However, in this study the silicon precursor will be utilised as is, without the requirement of the oxalic acid treatment step or the addition of extra silicon sources as reported in literature (Chareonpanich et al., 2004; Kalyankar et al., 2011; Kapure et al., 2017; Krisnandi et al., 2017; Missengue, 2016; Missengue et al., 2017; Missengue et al., 2018; Ndlovu, 2016; Vichapund et al., 2014; Vichapund et al., 2017). Furthermore, this silicon precursor will be utilised in the synthesis of silicalite-1 and zeolite mordenite. silicalite-1 has not been synthesised from CFA to date, while zeolite mordenite has been synthesised from naturally occurring materials such as diatomite and mixtures of coal fly ash with either diatomite or rich husk ash (Ahmed et al., 2018; Aono et al., 2018; Johan and Matsue, 2014; Johan et al., 2015; Mignoni et al., 2008). However, zeolite mordenite synthesis from solely CFA as a silicon source has not been reported to date.

The silicon precursor utilised for zeolite synthesis in this study is thought to contain a range of elements due to the rich mineral content of CFA. Inorganic cations in the synthesis mixture of zeolites are known to play an important role in crystallisation and affect the processes of zeolite crystallisation; some cations such as sodium are known as structure-directing while other cations such as divalent calcium have a strong structure-breaking effect (Cejka et al,

2007; Petrik et al., 1995; Valdes et al., 2006; Yu, 2007). Geometric modelling of polyhedral materials (such as zeolites) has been carried out using Geometric Simulation of Polyhedra (GASP) software, which is a simple and fast method of determining the theoretical flexibility range of a polyhedral material (i.e. the flexibility window). The flexibility window of a zeolite material gives information on the likelihood of formation as well as the compressibility of a given zeolite framework (Fletcher et al., 2015; Dawson et al., 2012; Kapko et al., 2010; Sartbaeva et al., 2006; Wells and Sartbaeva, 2012; Wells et al., 2011; Wells et al., 2017). GASP software has mainly been applied to simulate the flexibility window of zeolite frameworks. Some studies have been reported on the effect of extra-framework content (such as water, methanol or NaBr salt) on zeolite framework flexibility (Wells et al., 2015; Wells et al., 2017). To date, the steric influence of extra-framework cations on zeolite framework flexibility has not been reported. In this study, GASP geometric modelling software will be used to gain more insight into the effect of the different cations in the synthesis mixture (as a result of the source of the silicon precursor CFA containing a range of different elements) on the crystallisation of zeolites.

1.2 Problem Statement

Annually, tonnes of CFA are produced as a waste by-product of the coal combustion process. Currently, a small amount of this waste material is re-used and recycled in the construction industry process for cement, concrete and brick production. CFA is also utilised in the mining industry to backfill voids created by mining processes. CFA is a waste material that is rich in minerals and contains a high quantity of silicon and aluminium (which has made it a suitable feedstock for zeolite synthesis). However, CFA also contains a range of hazardous elements and the uncontrolled, large scale disposal of CFA to landfills has a major impact on the surrounding environment. To date, high-silica zeolites have been synthesised from CFA using either high temperature solid fusion or low temperature alkaline reflux conditions for the extraction of a silicon precursor. The current process for the conversion of CFA to high-silica zeolites is also coupled with a purification step (by treatment with concentrated oxalic acid solution under reflux conditions) that was utilised to remove excess sodium and enhance the SAR value of the feedstock (silicon precursor). In some cases, the SAR value of the feedstock has been enhanced by addition of standard chemical reagents to the synthesis mixture for zeolite ZSM-5 synthesis. This study aims to simplify the process for the conversion of CFA into high-silica zeolite ZSM-5 and to evaluate the simplified process as a

potential synthesis route for other high-silica zeolitic materials such as zeolite mordenite and silicalite-1. Furthermore, the study also aims to gain insight into the steric influence of inorganic cations on the formation of zeolites (by GASP simulations) and how the rich mineral content of CFA may impact zeolite crystallisation.

1.3 Aim and Objectives of the Study

The main aim of the study is to synthesise high-silica zeolites mordenite and ZSM-5 as well as zeosil silicalite-1 from a silicon precursor material derived from waste coal fly ash (by using a simplified conversion process).

The objectives of this study include:

1. Low-temperature alkaline activation of coal fly ash and preparation of the silicon precursor material.
2. Synthesis and optimisation (of synthesis parameters) of zeolite mordenite from a CFA-derived silicon precursor.
3. Synthesis and optimisation (of synthesis parameters) of zeolite ZSM-5 from a CFA-derived silicon precursor.
4. Synthesis of the purely siliceous analogue of ZSM-5, silicalite-1 from a CFA-derived silicon precursor.
5. Modelling the effect of extra-framework cations (such as Na^+, Ca^{2+}, K^+ and Cs^+) on a model zeolite framework (LTA) by geometric simulation using GASP software.

This study therefore hypothesises that the CFA-derived silicon precursor may be utilised as a source of silicon for the synthesis of other high-silica zeolites such as mordenite and ZSM-5 with a range of SAR values as well as the synthesis of purely siliceous, MFI-material silicalite-1. This study further hypothesises that the synthesis procedure may be simplified by avoiding the purification of the CFA-derived silicon precursor with a chelating agent (such as oxalic acid), prior to use in hydrothermal synthesis.

1.4 Research Questions

This study aims to answer the following research questions:

- Can the synthesis procedure for high-silica zeolites (such as mordenite, ZSM-5 and silicalite-1) be simplified to avoid the utilisation of additional silicon sources?
- Can the synthesis procedure for high-silica zeolites (such as mordenite, ZSM-5 and silicalite-1) be simplified to avoid the purification of the silicon precursor with a concentrated oxalic acid solution under reflux conditions prior to use in hydrothermal synthesis?
- Can a large-pore, high-silica zeolite such as zeolite mordenite be synthesised from a CFA-derived silicon precursor?
    - Is zeolite mordenite crystallisation possible from a CFA-derived silicon precursor in the absence of an organic structure-directing agent (OSDA)?
    - What range of synthesis parameters result in the crystallisation of zeolite mordenite?
    - What is the effect of seeding on the crystallisation of zeolite mordenite?
    - What is the effect of an OSDA agent on the crystallisation of zeolite mordenite?
- Can medium-pore, high-silica zeolite ZSM-5 be synthesised from a CFA-derived silicon precursor without the oxalic acid treatment step?
    - What range of synthesis parameters result in the crystallisation of zeolite ZSM-5?
    - Can zeolite ZSM-5 with a range of different properties be synthesised from a CFA-derived silicon precursor?
    - What is the effect of different cations (in the synthesis mixture) on the crystallisation of zeolite ZSM-5?
- Can a purely siliceous zeolite such as silicalite-1 be synthesised from a CFA-derived silicon precursor?
- What is the effect of different extra-framework cations on a model zeolite (zeolite A with LTA framework) simulated using the GASP software?

1.5 Research Approach

In this study, a literature review on the synthesis of high-silica zeolites from coal fly ash (and standard chemical reagents) as well as GASP simulations of zeolites were carried out and the research approach was designed accordingly. An overview of the research approach is depicted in Figure 1.1.

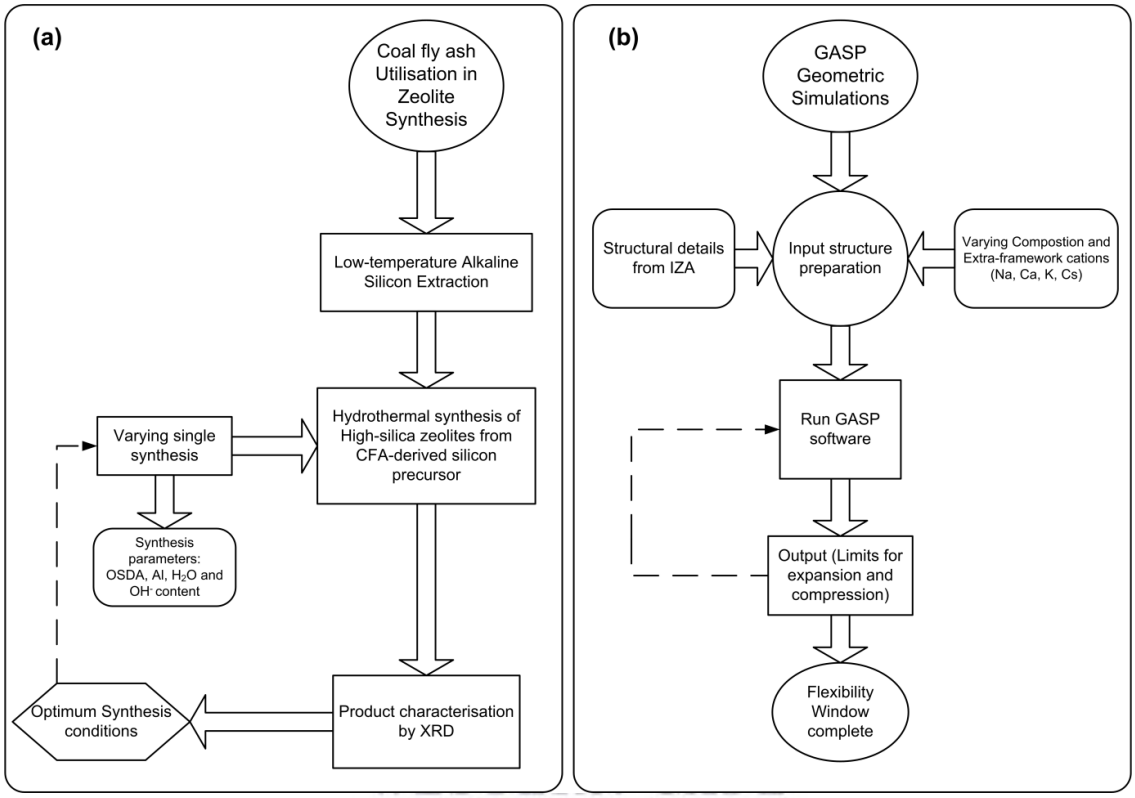

Figure 1.1: Schematic diagram of the research approach for (a) high-silica zeolite synthesis from coal fly ash and (b) GASP modelling of a model zeolite.

A South African coal fly ash-derived silicon precursor material (extracted using a low-temperature alkaline reflux process) was used as the starting material for high-silica zeolite synthesis. The starting material (coal fly ash) and extraction products were characterised by various analytical techniques to determine chemical and physical properties thereof such as chemical and mineralogical composition as well as morphology. As depicted in Figure 1.1, the optimisation of the synthesis of high-silica zeolites from a CFA-derived silicon precursor was carried out in a step-wise manner; the best result in terms of zeolite product crystallinity, determined by X-ray diffraction (XRD), was used as the starting point for subsequent experiments. Selected zeolite products were characterised further to determine material properties such as morphology, SAR value, thermal stability and specific surface area.

GASP simulations were typically carried out using an initial starting structure retrieved from the Database for Zeolite Structures (Baerlocher and McCusker, 2017), the GASP output results (the initial limits for expansion and compression of the zeolite structure) were used as the starting point for subsequent GASP simulations and this process was repeated until the limits of the flexibility window for a particular zeolite was defined.

1.6 Scope and delimitations of the study

A broad range of topics is covered in zeolite science such as synthesis and characterisation methods, applications as well as zeolite modelling. For this study, the literature review discusses zeolite science in general with regard to characteristic zeolite properties, classification as well as synthesis and characterisation methods and applications of zeolites. The literature review mainly focuses on the current methods utilised for the preparation of high-silica zeolites from coal fly ash. The background of the GASP modelling software is also discussed in the literature review. The silicon extraction method from CFA and the target high-silica zeolites were based on the gap analysis of the literature review. In the interest of time, product crystallinity (calculated from XRD) was utilised as the main response factor for the optimisation of high-silica zeolites from a CFA-derived silicon precursor. Selected zeolites were characterised by other analytical techniques to determine the material properties of fly ash based high-silica zeolites compared to the properties of high-silica zeolites (prepared from standard chemical reagents) reported in the literature.

1.7 Thesis Outline

The contents of this thesis will be structured in the following manner:

- Chapter One: Introduction
- Chapter Two: Literature review
- Chapter Three: Research methodology
- Chapter Four: Extraction of silicon from CFA and process overview (zeolite yields)
- Chapter Five: Synthesis of large-pore MOR framework type zeolites
- Chapter Six: Synthesis of medium-pore MFI framework type zeolites
- Chapter Seven: Geometric modelling of the steric influence of extra-framework cation type on a model zeolite framework (LTA) using GASP software
- Chapter Eight: Conclusions and recommendations

2 Chapter 2 - Literature Review

2.1 Introduction

This chapter will present a literature review of the research relevant to this study. Zeolite science covers a wide range of topics from hydrothermal synthesis, material characterisation, various zeolite applications as well as computational modelling of zeolites. In this study, high silica zeolites with MOR- and MFI-type framework were synthesised from CFA (which served as the sole source of silicon feedstock). The literature review will therefore focus on a brief introduction into the history of zeolite science, the characteristic features and properties of zeolites and the hydrothermal synthesis of zeolites including a brief discussion on the crystallisation mechanism and factors that influence zeolite crystallisation (with emphasis on MOR- and MFI-type framework materials). Next, the utilisation of an alternative feedstock (CFA) in the synthesis of zeolites will be presented with emphasis on the current research in the area of high-silica zeolite synthesis from CFA. The analytical techniques utilised in this study for the characterisation of zeolite materials as well as starting materials will also be described. Subsequently, an introduction into the geometric modelling of zeolite frameworks using GASP software will be presented.

2.2 A brief history of zeolite science

Zeolites are microporous, aluminosilicate materials with unique properties that make them suitable for application in important industrial fields such as catalysis and gas adsorption (Bowman, 2003; Payra and Dutta; 2003; Weitkamp, 2000). These unique properties include; thermal stability, high porosity and high surface areas, ion-exchangeability and solid acidity (Mintova et al., 1995). Currently zeolites are commonly synthesised, under hydrothermal conditions, from alkaline aqueous solutions containing precursor (silicon and aluminium) species, a mineralising agent (typically OH^- or F^-) and in some cases, an additional structure directing agent such as organic template molecules (Weitkamp, 2000). However, zeolites were first discovered in 1756 by Axel F. Cronstedt as natural mineral deposits in sedimentary rocks that formed as a result of volcanic activities. To date, more than 60 naturally occurring zeolites have been discovered. Some examples of natural zeolites include analcime (ANA), chabazite (CHA), clinoptilolite (HEU), erionite (ERI), faujasite (FAU), ferrierite (FER), gismondine (GIS), gmelinite (GME) and mordenite (MOR). The natural formation of zeolites under geothermal conditions served as motivation for researchers to prepare synthetic zeolites

in a laboratory and by the 20th century zeolites were first synthesised in a laboratory; with pioneering research undertaken by Richard M. Barrer between 1930 and 1940 (Maesen, 2007; Weitkamp, 2000; Xu et al., 2007). In 1959, the research of Robert M. Milton and Donald W. Breck (Union Carbide) resulted in the preparation of zeolites A and X and these materials still have a major role commercially and in research (Payra and Dutta, 2003; Yu, 2007). At this time, aluminium-rich zeolites were synthesised by mimicking the conditions under which natural zeolites form in nature. Between 1960 and 1970, Mobil researchers synthesised the first silicon-rich zeolites by using organic quaternary alkylammonium cations and amines in the synthesis mixtures for hydrothermal zeolite synthesis. This method resulted in the formation of one of the most widely used silicon-rich zeolites namely ZSM-5 as well as many other silicon-rich zeolites and siliceous analogues of aluminosilicate zeolites. These silicon-rich zeolites possessed a new range of properties such as thermal stability and hydrophobicity and as such, these materials are still widely researched to date (Baerlocher and McCusker, 2017; Corma, 2003; Li et al., 2015; Pan et al., 2019; Payra and Dutta, 2003; Xu et al., 2007). Currently, thousands of synthetic zeolite materials have been discovered that are associated with the ~245 zeolite framework types, as approved by the Structure Commission of the International Zeolite Association (Baerlocher and McCusker, 2017; Yu, 2007).

2.2.1 The structure and properties of the zeolite framework

In general, zeolites are composed of TO_4 tetrahedra as primary building units (PBU); typically silica (SiO_4) and alumina (AlO_4) tetrahedra. These SiO_4 and AlO_4 tetrahedra are connected by a common oxygen atom to form relatively larger structural building units (SBUs) such as single 4-membered ring (S4R), single 5-membered ring (S5R), single 6-membered ring (S6R), single 8-membered ring (S8R), double 4-membered ring (D4R), double 6-membered ring (D6R), *mor* (5^4) and pentasil units (5^8), as depicted in Figure 2.1 (adapted from McCusker and Baerlocher, 2007).

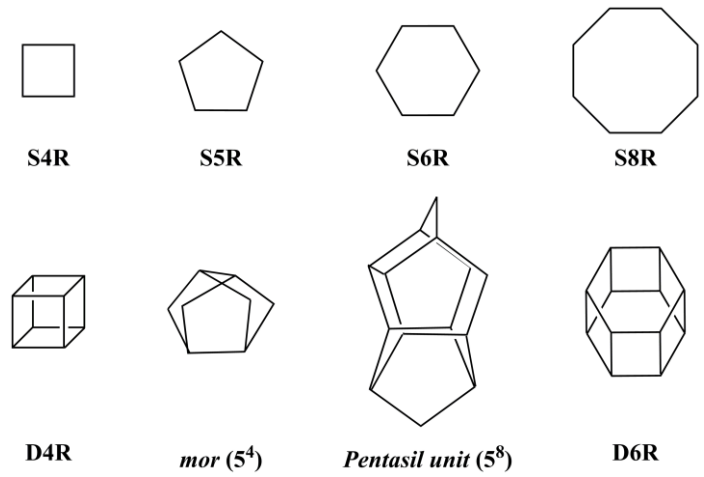

Figure 2.1: Typical structural building units of zeolite framework structures (adapted from McCusker and Baerlocher, 2007).

These SBUs (depicted in Figure 2.1) connect in a particular manner through condensation reactions resulting in the formation of a crystalline zeolite framework, with a specific framework type (Davis and Lobo, 1992; McCusker and Baerlocher, 2007). As mentioned before, the Structure Commission of the International Zeolite Association classified more than 200 zeolite framework types (each assigned a three letter code). Some common framework types are ANA, FAU, GIS, LTA, MFI, MOR and SOD. Each framework possesses a common framework topology, crystal symmetry and pore network (Davis and Lobo, 1992; McCusker and Baerlocher, 2007; Payra and Dutta, 2003). Specific examples of zeolite framework types (of interest to this study) such as LTA, MFI and MOR will be described in more detail.

2.2.1.1 LTA framework

The LTA framework consists of sodalite units (arranged in a primitive cubic manner) joined to each other through oxygen bridges between S4R faces (to yield D4R units). This arrangement of SBUs creates an α-cage in the centre of the unit cell and a three-dimensional pore system with 8-ring pore openings (~0.45 nm in diameter). Zeolite A is the most common material with LTA framework topology. The pore dimensions of the LTA framework makes zeolite A a small-pore zeolite, as depicted in Figure 2.2 (Ameh et al., 2016; Breck et al., 1956; McCusker and Baerlocher, 2007; Payra and Dutta, 2003).

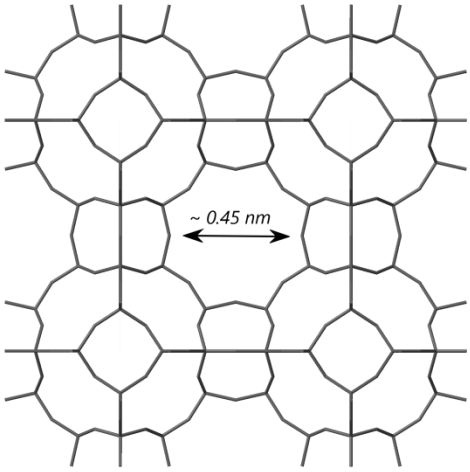

Figure 2.2: LTA framework with small-sized pore openings (adapted from McCusker and Baerlocher, 2017).

2.2.1.2 MFI framework

The MFI framework contains S5Rs that join together to form pentasil units (5^8 units), as depicted in Figure 2.1. Pentasil units are connected through oxygen bridges to form pentasil chains, which link together to form a three dimensional network of interconnected pores. MFI-type zeolites contain two types of 10-ring pore channels; (i) 0.51 x 0.55 nm (along the [1 0 0] direction) and (ii) 0.53 x 0.56 nm (along the [0 1 0] direction). The most common MFI type zeolite material is called zeolite ZSM-5 (Zeolite Sicony Mobil-5). The dimensions of these pore channels in this MFI-type zeolite material makes zeolite ZSM-5 a medium-pore zeolite, as depicted in Figure 2.3 (McCusker and Baerlocher, 2007; Payra and Dutta, 2003).

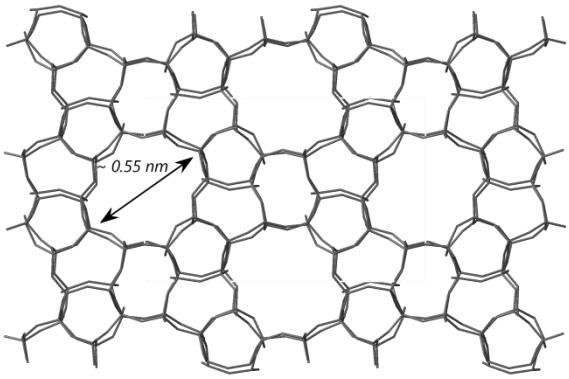

Figure 2.3: MFI framework type material ZSM-5 with medium-sized pore openings (adapted from McCusker and Baerlocher, 2017).

2.2.1.3 MOR framework

The MOR framework is made up of S5Rs that join together to form *mor* SBUs (5^4 units), as depicted in Figure 2.1. The *mor* SBUs join together by sharing edges to form a chain of 5^4 units. These chains are aligned parallel to each other as mirror images to form a two-dimensional pore network made up of 12-ring pore openings along the [0 0 1] direction parallel to the c-axis (0.67 x 0.70 nm) and 8-ring pore openings along the [0 1 0] direction parallel to the b-axis (0.26 x 0.57 nm). However, the MOR framework is commonly described as a one-dimensional framework due to difficulties accessing the relatively smaller 8-ring pore openings of the MOR framework. Zeolite mordenite is the common material type for the MOR framework. The pore dimensions of this framework type (MOR) makes zeolite mordenite a large-pore zeolite, as depicted in Figure 2.4 (Aly et al., 2012; Idris et al., 2019; Jin et al., 2012; McCusker and Baerlocher, 2007; Payra and Dutta, 2003).

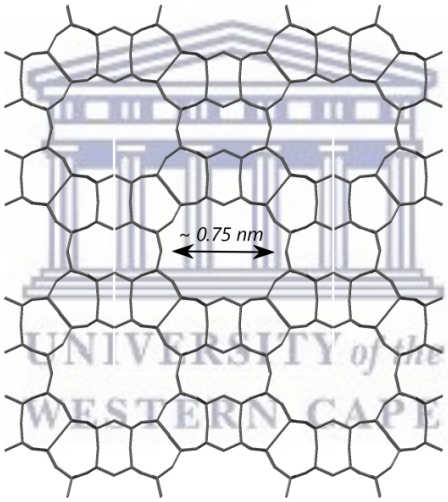

Figure 2.4: MOR framework with large-sized pore openings (adapted from McCusker and Baerlocher, 2017).

2.2.2 Classification of zeolites

Other than zeolite framework type, zeolites may also be grouped according to the chemical composition of the material in terms of Si/Al ratio (SAR) as well as the pore size of the framework. The type of classification is limited to aluminosilicate zeolitic materials, which are the focus of this study. However, it should be noted that frameworks with a range of different chemical compositions have been synthesised such as metallosilicates, aluminophosphates (AlPOs) and silicoaluminophosphates (SAPOs). A range of metallosilicates have been prepared by substituting aluminium with other metals such as boron, gallium, germanium, iron, titanium and zirconium in the zeolite framework (Liu et al.,

2019; Moliner et al., 2013; Payra and Dutta, 2003). These materials are not within the scope of this study and will therefore not be discussed in detail in this review.

2.2.2.1 Chemical composition

The chemical composition (in particular the SAR value) of aluminosilicate zeolites has a significant influence on the properties of the material, which in turn strongly influences the application of the material. For instance, zeolite frameworks with relatively higher SAR values exhibit a greater degree of solid acidity, thermal stability and hydrophobicity. Zeolites may therefore be classified by the degree of aluminium substitution in the framework (i.e. SAR value); low-silica zeolites have SARs ≤ 2, intermediate-silica zeolites have SARs between 2 and 5, high-silica zeolites have SARs >5 (Holderich and van Bekkum, 1991; Payra and Dutta, 2003; Xu et al., 2007). Examples of zeolites with different SARs are listed in Table 2.1.

Table 2.1: Classification of zeolites by SAR value of the framework.

Zeolite classification	SAR value	Zeolite examples (Framework type)
Low-silica	≤ 2	A (LTA), P (GIS), X (FAU), Sodalite (SOD)
Intermediate-silica	2-5	Y (FAU), Ferrierite (FER), Mordenite (MOR), Sodalite (SOD)
High-silica	> 5	Beta (BEA), Ferrierite (FER), Mordenite (MOR), ZSM-5 (MFI)
All-silica (siliceous materials)	∞	Silicalite-1 (MFI), Silicalite-2 (MEL)

As listed in Table 2.1, zeolite A is a low-silica zeolite and typically exhibits a SAR value of 1, while zeolite mordenite may be considered either intermediate- or high-silica zeolite depending on the SAR value of the material (which is commonly >5). Zeolite ZSM-5 is considered a high-silica zeolite with a typical SAR value ≥ 10 and silicalite-1 is the

completely siliceous analogue of zeolite ZSM-5 (Holderich and van Bekkum, 1991; Payra and Dutta, 2003; Weitkamp, 2000). High-silica zeolites are of particular interest in industries that make use of high temperature processes. This is due to the superior thermal stability of these materials, compared to low-silica zeolites, coupled to the appreciable solid acidity of these materials (Lobo, 2003; Maesen, 2007; Payra and Dutta, 2003).

2.2.2.2 Pore size

The well-defined pore architecture of zeolites is another important characteristic that determines the type of applications in which zeolites are used. Zeolite pore structures are characterised by shape, size and the overall dimensionality of the pore channels. The pore openings, depicted in Figure 2.5, serve as windows into the pore network of a zeolite framework and are commonly named (8-ring, 10-ring and 12-ring) according the number of T-atoms that make up the pore opening (Holderich and van Bekkum, 1991; Huang et al., 2014; Weitkamp, 2000).

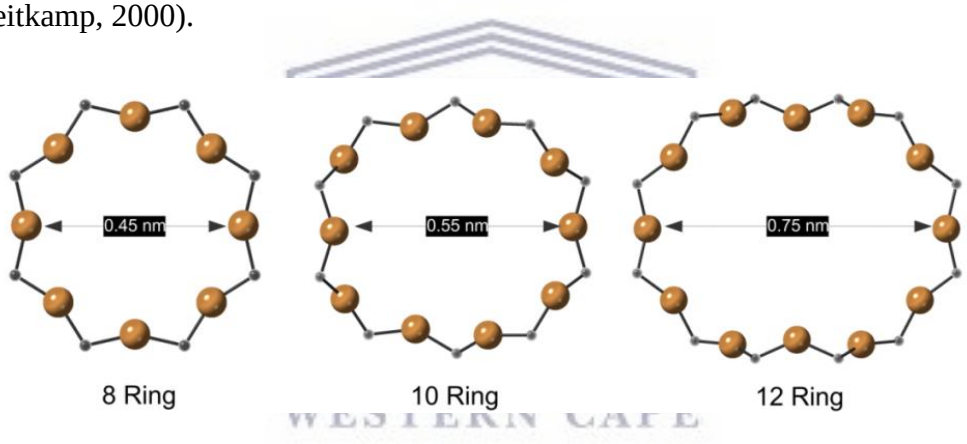

Figure 2.5: Typical pore aperture sizes in 8 ring, 10 ring and 12 ring pore openings.

Zeolites are often classified as small-, medium- and large-pore zeolites depending on the pore aperture size; some examples are listed in Table 2.2 (Holderich and van Bekkum, 1991; Payra and Dutta, 2003).

Table 2.2: Classification of zeolites by pore aperture size.

Zeolite classification	Pore opening (ring size)	Pore size (nm)	Zeolite examples (Framework type)	Pore dimensionality
Small pore	8	~0.45	A (LTA) P (GIS) Sodalite (SOD)	3 3 -
Medium pore	10	~0.55	Ferrierite (FER) ZSM-5 (MFI) Silicalite-1 (MFI)	3 3 3
Large pore	12	~0.75	X and Y (FAU), Beta (BEA), Mordenite (MOR)	3 3 2 (1)

The size of pore apertures for small-pore zeolites such as zeolite A is typically ~0.45 nm, ~0.55 nm for medium-pore zeolites such as zeolite ZSM-5 and 0.75 nm for large-pore zeolites such as zeolite mordenite, as illustrated in Figure 2.5 (Holderich and van Bekkum, 1991; Payra and Dutta, 2003). Zeolites are inherently shape-selective due to the molecular dimensions of these pore openings. This makes zeolitic materials ideal candidates to serve as molecular sieves or catalysts and/or support materials for the conversion and separation of various molecules (Huang et al., 2014; Weitkamp, 2000).

The classification of zeolites using properties such as SAR value and pore size is therefore common since these properties directly influence other characteristics of zeolite such as solid acidity, thermal stability, hydrophobicity as well as porosity. These properties all play a vital role in the application of zeolites; the characteristic properties will therefore be discussed briefly in the next section.

2.2.3 Characteristic properties and uses of zeolites

The characteristic properties of zeolites such as porosity and shape selectivity are attributed to the unique framework topology of these materials, while other unique properties such as solid acidity, thermal stability, hydrophilicity/hydrophobicity and ion-exchangeability arise due to the composition of these materials (Louis and Kiwi-Minsker, 2004; Tao et al., 2006; Valdes et al., 2006; Weitkamp, 2000). A summary of the different zeolite properties is illustrated in Figure 2.6.

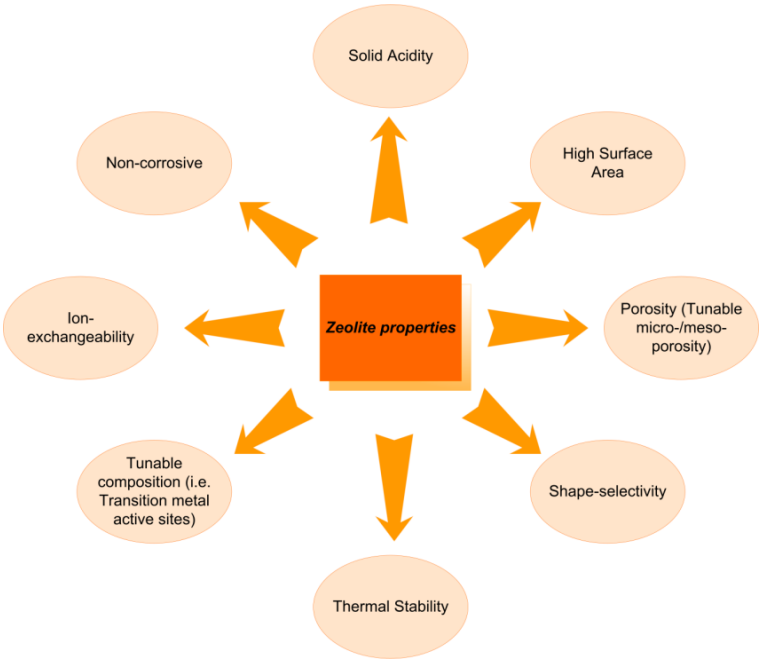

Figure 2.6: The characteristic properties of zeolite materials.

2.2.3.1 Ion-exchangeability

Most zeolites exist as aluminosilicates that possess an overall net negative charge due to the presence of aluminium atoms in the framework. It is therefore common that aluminosilicate zeolites contain extra-framework cations for charge-compensation of the framework. Sodium cations are the most common extra-framework cations in zeolites (Valdes et al., 2006; Weitkamp, 2000). This characteristic feature of zeolites allows for the exchange of cations in aqueous solution; giving zeolites its property of ion-exchangeability. A common application of zeolites is in the laundry detergent industry as a water softening agent, where sodium cations from the zeolite framework replace relatively hard calcium and magnesium cations in water (Valdes et al., 2006; Payra and Dutta, 2003; Weitkamp, 2000; Xu et al., 2007). For purely siliceous zeolites, the zeolite framework is charge neutral due to the lack of trivalent atoms in the framework such as aluminium (Valdes et al., 2006; Weitkamp, 2000).

2.2.3.2 Hydrophobicity/hydrophilicity

Aluminosilicate zeolites with relatively low SAR values are also known for being hygroscopic in nature. However, purely siliceous analogues of zeolites such as silicalite-1 are hydrophobic in nature. The degree of hydrophilicity of a specific zeolite is therefore directly related to SAR value of zeolite. It is therefore possible to design purely hydrophobic siliceous materials or hygroscopic aluminosilicate materials, by controlling the SAR value of the synthesised material. Due to this property zeolites have great potential in separation science,

particularly in the separation of complex mixtures that may not be possible otherwise (Aly et al., 2012; Cheng and Shantz, 2005; van den Broeke et al., 1999; Yang et al., 2011). In particular, hydrophobic zeolitic materials such as silicalite-1 have interesting applications in membrane and thin-film technologies (van den Broeke et al., 1999; Yang et al., 2011).

2.2.3.3 Solid Acidity

The solid acidity of zeolites is attributed to the presence of aluminium atoms in the zeolite framework; which yields Si-O-Al$^-$ sites that may serve as either acidic or basic sites under the appropriate conditions. In the typical as-synthesised form (the sodium form), zeolites serve as Lewis bases due to the net negative charge on framework oxygen atoms (Xie et al., 1994). The sodium form (Na-zeolite) of zeolites may be ion-exchanged using an ammonium salt (typically ammonium nitrate) under reflux conditions and then calcined to produce the acidic form (H-zeolite) of zeolites (Hunger, 2010, Weitkamp, 2000). Both Brönsted and Lewis acid sites may be present in zeolites, as depicted in Figure 2.7 (Hagen, 2015; Louis et al., 2004; Ordonez and Diaz, 2009; Weitkamp, 2000).

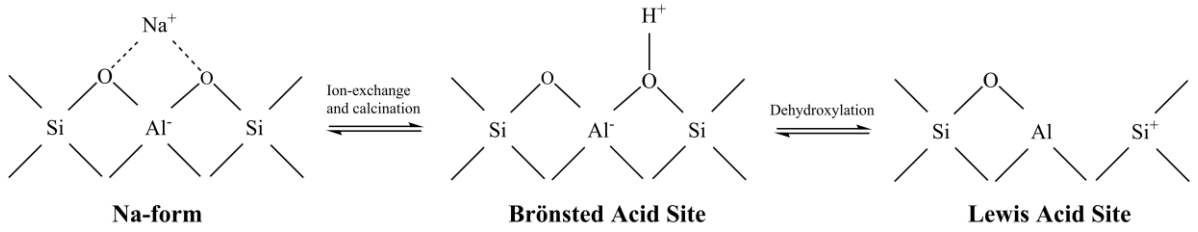

Figure 2.7: Basic and acidic sites (Brönsted and Lewis) in the zeolite framework (adapted from Hagen, 2015).

As depicted in Figure 2.7, the bridging hydroxyl group bonded to a framework aluminium atom serves as Brönsted acid sites in the zeolitic framework. Dehydroxylation of these Brönsted acid sites results in the formation of Lewis acid sites (Hagen, 2015; van Hooff and Roelofsen, 1991; Weitkamp, 2000; Weitkamp and Hunger, 2007; Xie et la., 1994). The degree of solid acidity for a particular zeolite is therefore directly related to the SAR value of the material (Hölderich and van Bekkum, 1991; Louis et al., 2004). In many industries (fine chemical and petroleum), zeolites have been utilised in catalytic applications that typically make use of conventional homogenous Brönsted acids (Hölderich and van Bekkum, 1991; Weitkamp, 2000). Acidic solid zeolites are commonly applied as catalysts in FCC cracking as well as other hydrocarbon transformations in the petroleum industry (Hölderich and van Bekkum, 1991; Holm et al., 2011; Hunger, 2010).

2.2.3.4 Porosity

The zeolite framework contains a pore network with well-defined channels and pores that are of molecular dimensions. Zeolites are highly microporous and exhibit relatively high surface areas. Furthermore, each zeolite framework type possesses specific pore architecture (Huang et al., 2010). The microporous nature of zeolitic materials is one of the major characteristics that make these materials attractive for various molecular applications. According to the International Union of Pure and Applied Chemistry (IUPAC) standard, the pore size of a particular material may be classified in three ways; (i) microporous (≤ 2 nm), (ii) mesoporous (2-50 nm) and (iii) macroporous (> 50 nm). The tunable porosity of zeolites is responsible for the shape-selective nature of these materials; which allow microporous zeolites to discriminate between reactant and/or product molecules based on their size. Zeolites are therefore commonly used as molecular sieves and in shape selective catalytic applications (Thommes et al., 2015; Weitkamp, 2000). However, zeolites have been known to suffer from diffusional constraints during application. As such, the preparation of zeolitic materials with hierarchical pore architecture (materials consisting of more than one pore size type) is currently a major area of research in zeolite science (Liu et al., 2019; Moliner et al., 2013; Musyoka et al., 2014).

2.2.3.5 Thermal Stability

Zeolites are relatively stable and maintain their crystal structure under high temperature conditions. The degree of thermal stability of a particular zeolite is related to the SAR value of the material; the higher the SAR value, the more thermally stable the zeolitic material. The thermal profile of an as-synthesised zeolite material also provides information on the volatile content present in the material such as water, OSDA molecules or other impurities trapped inside the pore network of the zeolite (Holderich and van Bekkum, 1991; McCusker and Baerlocher, 2007; Pál-Borbély, 2007). This property allows zeolites to be applied in catalytic processes that require a relatively high temperature to facilitate the conversion of reactants to products. As such, zeolites are applied in a range of high temperature catalytic processes (Holderich and van Bekkum, 1991; Missengue et al., 2018).

With a combination of these properties (namely thermal stability, high porosity, shape-selectivity and variable solid acidity) high-silica zeolites such as mordenite and ZSM-5 are important catalytic (and adsorption) materials in industries that involve high-temperature processes (Payra and Dutta, 2003). For example, zeolite mordenite plays an important role in

improving the octane rating of petrol (also known as gasoline) by catalysing the isomerisation of alkanes, while zeolite ZSM-5 has a range of important catalytic applications in processes such as the Methanol-to-olefin and Conversion of olefins to gasoline and distillate that are involved in the conversion of feedstock (olefins and alternatives such as alcohols) to valuable commercial products (namely as gasoline and diesel) for the petroleum industry (Dai et al., 2017; Hincapie et al., 2004; Idris et al., 2019; Lobo, 2003; Maesen, 2007). These unique properties of zeolites (as well as the various applications of the material in different industries) are responsible for the interest in these materials and present day research in the field of zeolite science.

2.3 Zeolite synthesis methods

Modern day zeolite science employs hydrothermal synthesis (at elevated temperature and autogenous pressure) as the common route for the preparation of zeolites (Singh and Dutta, 2003; Weitkamp, 2000). Hydrothermal zeolite synthesis is typically achieved by the transformation of a supersaturated alkaline solution containing silicon and aluminium precursors, a mineralising agent, water and cations (inorganic or organic in nature) under hydrothermal conditions. This technique for zeolite preparation allows for fast conversion of precursors to metastable zeolite phases. Other advantages of this technique include minor air pollution as well as low energy cost, which makes hydrothermal synthesis highly attractive for zeolite preparation (Davis and Lobo, 1992; Feijen et al., 1994; Hamilton et al., 1993; Yu, 2007).

A typical zeolite synthesis experiment involves the mixing step, hydrothermal step and a post-synthesis treatment of the solid hydrothermal product. During the mixing step, silicon and aluminium precursor species are combined by stirring (or agitation) under aqueous conditions in the presence of a mineralising agent (sodium hydroxide, NaOH, is typically employed). The synthesis mixture is then subjected to elevated temperatures (typically > 100 °C) and autogenous pressure during hydrothermal treatment, which results in the formation of a crystalline zeolite framework. This solid zeolite product may then be treated after hydrothermal treatment step to alter the material properties (Davis and Lobo, 1992; Feijen et al., 1994; Grand et al., 2016; Hamilton et al., 1993; Singh and Dutta, 2003). The conversion of silicon and aluminium precursor species into a crystalline zeolite framework involves many intricate processes that are sensitive to the composition of the synthesis mixture as well as a range of other factors. An overview of the mechanism of zeolite

crystallisation as well as the influence of various factors on zeolite crystallisation will be discussed briefly in the following sections.

2.3.1 Crystallisation mechanism of zeolites

An understanding of the crystallisation of zeolites is vital for the preparation of tailor-made zeolites with a desired set of properties. The crystallisation of an aluminosilicate zeolite material involves a complex combination of sol-gel chemical reactions and processes such as hydrolysis (depolymerisation), dissolution, condensation (polymerisation) as well as precipitation (Cundy and Cox, 2005; Huo, 2011). A brief overview of the sol-gel processes involved in zeolite crystallisation will be discussed in this section.

During crystallisation of aluminosilicate zeolites, the mineralising agent (typically OH^-) catalyses the hydrolysis (depolymerisation) of silicon and aluminium precursor species to form T-OH groups (T represents either silicon or aluminium in this case). Equations 2.1-2.4 present the hydrolysis reaction of the most condensed $Si(OT)_4$ silicate species (containing four Si-O-T oxo-bridges) sequentially to the least condensed $Si(OH)_4$ silicate species (containing four Si-OH bonds) (Feijen et al., 1994; Lalena et al., 2008; Livage, 1994).

$$Si(OT)_4 + OH^- \rightarrow Si(OH)(OT)_3 + TO^- \text{ (Eq. 2.1)}$$

$$Si(OH)(OT)_3 + OH^- \rightarrow Si(OH)_2(OT)_2 + TO^- \text{ (Eq. 2.2)}$$

$$Si(OH)_2(OT)_2 + OH^- \rightarrow Si(OH)_3(OT) + TO^- \text{ (Eq. 2.3)}$$

$$Si(OH)_3(OT) + OH^- \rightarrow Si(OH)_4 + TO^- \text{ (Eq. 2.4)}$$

Depolymerised silicate and aluminosilicate species are relatively smaller, more soluble and reactive and thus serve as precursor species during the crystallisation of a crystalline zeolite framework through condensation (polymerisation) reactions. Condensation may be separated into two types of mechanisms namely; the olation process and oxolation process. In general, condensation involves the elimination of a water molecule from precursor species (consisting of at least a singular T-OH group) to yield a poly-nuclear species. During the olation process, nucleophilic substitution occurs whereby a negatively charged hydroxide ion (OH-) species is substituted onto a positively charged metal centre which is hydrated (T-OH); this results in the elimination of water. Condensation products achieved through the olation process consist of two T atoms joined together with a hydroxyl bridge (T-OH-T), as illustrated in Equation 2.5 (Lalena et al., 2008; Livage, 1994).

$$Si-(OH)_2 + T-O-T \rightarrow Si(OH)T + TOH + H_2O$$ (Eq. 2.5)

During the oxolation process, condensation occurs through nucleophilic addition instead of nucleophilic substitution that occurs during olation. Equation 2.6 illustrates the condensation of two T-OH metal centres resulting in the formation of a product containing a T-O-T oxo-bridge through the elimination of water (Lalena et al., 2008; Livage, 1994).

$$Si-OH + TOH \rightarrow Si-O-T + H_2O$$ (Eq. 2.6)

The process of olation occurs in a limited range of pH values (typically under acidic conditions). On the other hand, the process of oxolation occurs over a wide range of pH values (Lalena et al., 2008; Livage, 1994). The processes of hydrolysis and condensation (through olation or oxolation) occur during the different stages of zeolite crystallisation. In general, zeolite crystallisation consists of three main stages namely; induction, nucleation and crystal growth as depicted in Figure 2.8 (Cundy and Cox, 2005; Feijen et al., 1994; Grand et al., 2016; Singh and Dutta, 2003).

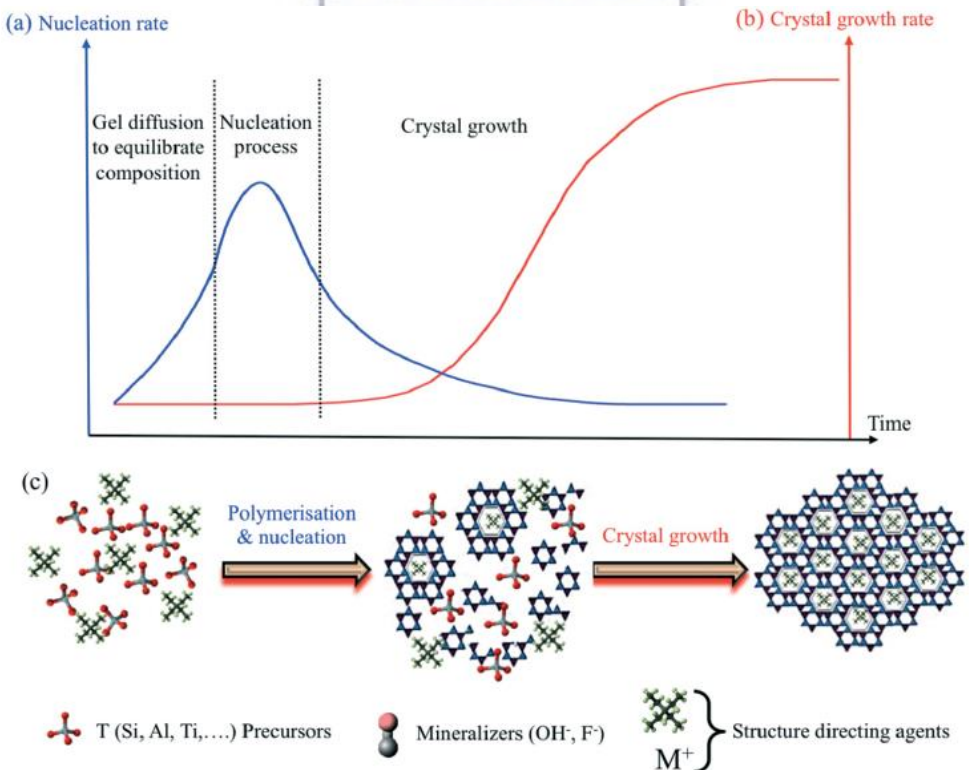

Figure 2.8: An illustration of the nucleation and crystal growth rate of zeolites during crystallisation as well as a schematic representation of zeolite formation (Grand et al., 2016).

Zeolite crystal growth follows the typical sigmoidal shape during zeolite crystallisation as depicted in Figure 2.8. The different stages involved in zeolite crystallisation will be described in the following sections.

2.3.1.1 Induction

During the initial stages of crystallisation, the silicon and aluminium sources undergo hydrolysis (depolymerisation), as illustrated in Equations 2.1-2.4. This process yields more soluble silicate and aluminate species that serve as PBUs for zeolites, as depicted in Figure 2.8. These PBUs undergo dissolution and subsequent condensation (polymerisation) resulting in the formation of an aluminosilicate species in solution, which serves as the precursor gel from which zeolites crystallise. In the induction period, the quantity of aluminosilicate gel increases as the time period increases until the synthesis mixture reaches supersaturation (Cundy and Cox, 2005; Feijen et al., 1994). Supersaturation occurs in solution, at a given temperature, when the solute concentration is relatively higher than concentration of the solute at equilibrium. During zeolite crystallisation, supersaturation of the synthesis mixture is well-known for being the driving force for the formation of zeolites (Cubillas and Anderson, 2010; Myerson, 2002). When the crystallisation process reaches this stage, aluminosilicate precursor species form aggregates in the supersaturated solution through precipitation and the formation of germ nuclei is initiated. Germ nuclei are susceptible to both depolymerisation and polymerisation reactions (as illustrated in Equations 2.1-2.6), depending on the size of these particles and crystallisation conditions. During this phase, germ nuclei grow in time until they reach a critical nuclei size, which enables spontaneous growth that yields stable nuclei (Myerson, 2002).

2.3.1.2 Nucleation

After the induction period (during which stable nuclei are generated in the synthesis solution), the process of nucleation occurs (as depicted in Figure 2.8). Nucleation is typically separated into two types namely; primary nucleation and secondary nucleation. The process of primary nucleation may be further divided into homogeneous and heterogeneous nucleation. Spontaneous nuclei formation occurs during homogeneous nucleation, whereas the formation of nuclei during heterogeneous nucleation occurs due to the presence of impurities in the synthesis mixture. The formation of nuclei due to heterogeneous nucleation may be inhibited by purification of the chemical reagents prior to utilisation in the synthesis mixture. The process of secondary nucleation involves the formation of nuclei as a direct

result of seed crystals (typically of the target zeolite) added to the synthesis mixture (Cubillas and Anderson, 2010; Grand et al., 2016; Huo, 2011). Nucleation is thought to take place at the surface of silica particles, where the boundary between the sol and gel occurs. Due to silica dissolution in this boundary region, this region is thought to contain the largest concentration of nutrient species that is required for nucleation (Cundy and Cox, 2005; Feijen et al., 1994). The process of nucleation is superseded by the process of crystal growth.

2.3.1.3 Crystal growth

The process of crystal growth involves the condensation (polymerisation) of nutrient species onto the surface of growing nuclei, resulting in the formation of the SBUs and further condensation until fully formed zeolite crystals are produced. As depicted in Figure 2.8, the crystal growth rate increases with time and the overall crystal growth process is sigmoidal in nature. The crystallisation of zeolites is considered self-accelerating as a result of the spontaneous nature of the initial stages of the crystallisation process. The inflection point of the crystallisation curve (as depicted in Figure 2.8) separates the period of autocatalytic nucleation and crystal growth from the period of relatively slower crystal growth (Cubillas and Anderson, 2010; Feijen et al., 1994). Both the crystal growth and nucleation processes consume aluminosilicate nutrient species in solution, which results in competition between these two processes. Therefore the rate of nucleation is thought to increase with time, go through a maximum and subsequently decrease with time due to competition with the crystal growth process for precursor species (as depicted in Figure 2.8). The process of crystal growth takes place at the boundary region between the planes of growing crystal and the aluminosilicate solution, by condensation of dissolved aluminosilicate species onto the surface of the growing crystals (Cundy and Cox, 2005; Feijen et al., 1994).

2.3.2 Factors influencing zeolite crystallisation

As discussed above, the chemistry of zeolite formation is complicated and the exact mechanism of zeolite crystallisation is still not fully understood (Grand et al., 2016). However, the factors involved in the preparation of the synthesis mixture (such as chemical composition of the synthesis mixture, silicon and aluminium sources, SAR value, water content, alkalinity, inorganic and organic cations) and the hydrothermal treatment step (temperature and agitation) is known to influence the formation of zeolites as well as the properties of the resultant material (Feijen et al., 1994; Oleksiak and Rimer, 2014; Yu, 2007). One of the main factors influencing the formation of a particular zeolite is the molar regime

of the synthesis mixture, which is typically described by the following notation SiO_2•x Al_2O_3•y Na_2O•z H_2O•n OSDA. The molar regime of the synthesis mixture may be altered by changing the other synthesis parameters such as Si/Al ratio, alkalinity, water content and OSDA amount. The influence of these parameters on the formation of zeolites mordenite and ZSM-5 will be investigated in this study. Therefore, the influence of these synthesis parameters as well as hydrothermal conditions on the formation of zeolites will be discussed in the following sections.

2.3.2.1 Silicon and aluminium sources

The properties of the silicon and aluminium precursor sources play a major role in the process of crystallisation. Sources of silicon typically utilised in zeolite synthesis include fumed silica, tetraethylorthosilicate (TEOS), sodium silicate solution and colloidal silica (Isa et al., 2018; Iwakai et al., 2011; Kamil et al., 2015; Krznaric et al., 2003; Mao et al., 2014; Mitra et al., 2002). The type of zeolite framework that crystallises is significantly influenced by the degree of solubility and reactivity of the silicon source. These factors determine the rate of dissolution and distribution of precursor silicate species in the synthesis solution during the crystallisation process; thereby controlling the rate of nucleation and crystal growth during zeolite synthesis (Burkett and Davis, 1995; Hamilton et al., 1993; Yu, 2007). Furthermore, the particle size and surface area of silicon sources also influence the processes involved in zeolite crystallisation. Silicon sources with high surface area and relatively small particle size exhibits high rates of dissolution under alkaline aqueous conditions compared to silicon sources with relatively lower surface area and larger particle size. The enhanced rate of dissolution (for silicon sources with high surface area and relatively small particle size) promotes fast supersaturation, resulting in enhanced nucleation and the formation of relatively small zeolite crystals. Conversely, silicon sources with relatively low surface area and larger particle size results in slower silica dissolution, reduced nuclei formation and consequently, the formation of relatively larger zeolite crystals, owing to a slower rate of nucleation compared to crystal growth (Meise and Schwochow, 1973; Yu, 2007).

The typical aluminium sources utilised in zeolite synthesis are sodium aluminate, aluminium hydroxide, aluminium nitrate hydrate, aluminium sulphate hydrate and aluminium isopropoxide, which also affects the processes of zeolite crystallisation (Shigemoto et al., 1993; Shigemoto et al., 1995; Yu, 2007). Aluminium sources also control the type of zeolite framework that crystallises as well as the morphology of zeolite crystals. The properties of

the aluminium sources (such as solubility and reactivity) particularly affect the formation of low-silica zeolites such as zeolite A and X, which requires an adequate amount of aluminium in the feedstock to form the precursor species necessary for the assembly of aluminium-rich SBUs that make up these low-silica zeolites (Hamilton et al., 1993; Shigemoto et al., 1993; Liu et al., 2013).

Depending on the silicon source type used during zeolite mordenite synthesis, the crystallisation products and boundary conditions differed. The formation of competing phases of zeolite mordenite such as zeolite Na-P1 and analcime were observed when amorphous silica powder was used as feedstock for hydrothermal synthesis, while the use of colloidal silica resulted in the formation of zeolite mordenite over a wide SAR range (Aono et al., 2016; Zhang et al., 2009). Aono et al., (2018) synthesised zeolite mordenite by utilising a mixture of risk husk ash (which exhibits a high SAR value) and CFA (which exhibits a relatively lower SAR value) as feedstock. The presence of a considerable amount of impurities (such as quartz and mullite) was present in the solid zeolite mordenite product formed. This is due to the type of silicon and aluminium source (rice husk ash and CFA) utilised in the synthesis solution, which is composed of quartz and mullite mineral phases (Aono et al., 2018).

Zeolite ZSM-5 has been synthesised from a range of different silicon and aluminium sources; some of which include fumed silica, sodium silicate solution, colloidal silica, TEOS, sodium aluminate, aluminium sulphate hydrate and aluminium nitrate hydrate (Iwakai et al., 2011; Mitra et al., 2002; Petrik et al., 1995; Petrik, 2009). Zeolite ZSM-5 has also been prepared using alternative feedstock as sources of silicon and aluminium such as kaolin clay, rice husk ash and coal fly ash (Chareonpanich, 2004; Kalyankar, 2011; Kapure, 2017; Krisnandi, 2017; Missengue, 2016; Missengue, 2017; Missengue, 2018; Ndlovu, 2016; Ndlovu, 2017; Vichaphund, 2014; Vichaphund, 2016). Typically, the synthesis methods for zeolite ZSM-5 from alternative feedstock materials included the addition of standard silicon sources to enrich the SAR value of the synthesis mixture. In some cases, a combination of alternative feedstock sources is used for the synthesis of zeolite ZSM-5 (such as high-silica rice husk ash and relatively low-silica CFA) in order to establish the ideal SAR value in the synthesis mixture (Chareonpanich, 2004; Krisnandi, 2017). The conversion of CFA to zeolite ZSM-5 was achieved by using a silicon-rich precursor material extracted from CFA. Prior to use in hydrothermal synthesis of zeolite ZSM-5, the silicon precursor material was treated with a

chelating agent to enrich the SAR value of the material and to remove excess sodium from the material, reported to be a deterrent to zeolite ZSM-5 crystallisation (Ndlovu, 2016; Missengue, 2016).

Silicalite-1 has not been synthesised from CFA to date but is commonly synthesised from standard laboratory reagents such as fumed silica, colloidal silica and TEOS as sources of silicon (Kamil et al., 2015; Petrik et al., 1995; Valtchev et al., 2004; Yang et al., 2011; Zhang et al., 2019). Furthermore, the conversion of pre-formed mesoporous silica materials SBA-15 and SBA-16 into silicalite-1 under hydrothermal conditions was also investigated by Kamil et al., (2015). Kamil et al., (2015) reported that the morphology of silicalite-1 was dependent on the silicon source utilised; fumed silica and TEOS resulted in the formation of nano-sized silicalite-1 crystals, while SBA-16 resulted in the formation of interconnected silicalite-1 crystals and SBA-15 resulted in the formation of relatively large, coffin-shaped silicalite-1 crystals. Zhang et al., (2019) also investigated the influence of different silicon sources such as TEOS and fumed silica (with different particle sizes, 7 and 12 nm) on silicalite-1 crystallisation. It was reported that the particle size of silica utilised in the synthesis mixture corresponded to the particle size of silicalite-1 crystals formed (Zhang et al., 2019).

The solubility and reactivity (as well as other properties such as surface area and particle size) of silicon and aluminium sources influence the formation of zeolites and the morphology of zeolite crystals (Yu, 2007). The source of feedstock is therefore an important factor to consider for the synthesis of tailor-made zeolites with a desired set of properties (required for catalytic and adsorption applications). It should be noted that in this study a solid silicon precursor extracted from CFA using a low temperature alkaline reflux method will be utilised in the synthesis of high-silica zeolites. The properties of this material (such as solubility, particle size and composition) may therefore greatly influence the formation of high-silica zeolites under alkaline, hydrothermal conditions in this study.

2.3.2.2 Si/Al ratio

The type of zeolite framework that crystallises is significantly influenced by the SAR value of the synthesis mixture (Chang and Shih, 2000; Oleksiak and Rimer, 2014; Shigemoto et al., 1993). In general, low-silica and intermediate-silica zeolites (SAR < 5) such as zeolite A, X, P1, analcime and sodalite crystallise from synthesis mixtures with relatively low SAR values and high alkalinity. On the other hand, high-silica zeolites (SAR > 5) such as zeolite mordenite, ZSM-5 and silicalite-1 commonly crystallise from synthesis mixtures with

relatively high SAR values under weakly alkaline conditions or in neutral fluoride synthesis conditions (Feijen et al., 1994; Yu, 2007). The composition of the zeolite product is also influenced by the SAR value of the synthesis mixture, although there is no quantitative correlation between these properties (Oleksiak and Rimer, 2014; Yu, 2007). The typical framework SAR value for low-silica zeolite A and sodalite is 1, intermediate-silica zeolite P1 exhibits a range of SAR values between 2 and 8, while zeolite mordenite may exhibit intermediate- to high-silica compositions (≥ 5) and high-silica zeolite ZSM-5 may have a range of SAR values (> 5). Silicalite-1 is the siliceous analogue of zeolite ZSM-5, with SAR value of ∞ (Eulenberger et al., 1967; Payra and Dutta, 2003; Yu, 2007).

The crystallisation of high-silica zeolite mordenite is dependent on the SAR value of the synthesis mixture. Zeolite mordenite crystallisation was reported in a relatively wide SAR range (up to ~80) by using standard chemical reagents. Relatively high SAR values in the synthesis mixture may result in the formation of zeolite Na-P1, ZSM-5, Beta or analcime depending on the synthesis conditions applied (Aono et al., 2016; Lu et al., 2004; Zhang et al., 2009). In the absence of an OSDA agent, zeolite ZSM-5 is formed from synthesis mixtures with a relatively high SAR value (> 60); however, zeolite mordenite and quartz may also form under these conditions depending on the sodium content in the synthesis mixture. The crystallisation of zeolite ZSM-5 is possible over a range of SAR values when an OSDA agent such as TPA^+ is added to the synthesis mixture (Cheng et al., 2008; Singh and Dutta, 2003). On the other hand, silicalite-1 is prepared from all-silica synthesis mixtures (i.e. with no added aluminium source) (Kamil et al., 2015; Zhang et al., 2019). In this study, a solid silicon precursor extracted from CFA will be utilised to synthesise high-silica zeolites mordenite, ZSM-5 and silicalite-1. In OSDA-free synthesis environments, careful consideration of the SAR value of the synthesis mixture is required for the crystallisation of zeolite mordenite or ZSM-5, since these zeolites crystallise under similar hydrothermal conditions. The optimisation of this factor during zeolite synthesis is therefore required for the formation of these high-silica zeolites with specific SAR values.

2.3.2.3 Alkalinity

Zeolite synthesis typically takes place under alkaline aqueous conditions, with a synthesis mixture described by the molar regime SiO_2•x Al_2O_3•y Na_2O•z H_2O. The alkalinity of the synthesis system is commonly defined as either H_2O/Na_2O or OH^-/SiO_2 ratio (Oleksiak and Rimer, 2014; Yu, 2007). In general, higher degrees of alkalinity in the synthesis system result

in enhanced dissolution of silicon and aluminium feedstock which in turn improves crystallisation kinetics (Cubillas and Anderson, 2010; Oleksiak and Rimer, 2014; Shigemoto et al., 1993). The improved dissolution of nutrient feedstock may also influence the morphology of zeolite crystals formed, by favouring nucleation over crystal growth processes and resulting in the formation of relatively smaller zeolite crystals (Koroglu et al., 2002; Meise and Schwochow, 1973; Mostowicz and Berak, 1985; Sashkina et al., 2017).

The formation of high-silica zeolite mordenite is highly sensitive to the alkalinity of the synthesis system. Low levels of alkalinity in the synthesis system may result in reduced rates of zeolite mordenite crystallisation (Choudhury et al., 1998; Lv et al., 2011; Machado et al., 1999; Oleksiak and Rimer, 2014). During the preparation of zeolite mordenite, the formation of amorphous material or Wairakite has been reported under low alkalinity conditions (Choudhury et al., 1998; Machado et al., 1999). At relatively high alkalinity in the synthesis system, the formation of a denser mineral phase (α-quartz) was reported instead of zeolite mordenite (Lv et al., 2011). On the other hand, zeolite ZSM-5 crystallinity is also influenced by the alkalinity of the synthesis environment. For zeolite ZSM-5, it has been reported that the nucleation rate was more sensitive to changes in alkalinity than crystal growth rate. Furthermore, it was reported that the optimum alkalinity corresponded to the SAR value of the synthesis system (Cheng et al., 2008; Singh and Dutta, 2003). The influence of alkalinity on the formation of silicalite-1 was investigated by Kamil et al., (2015). It was reported that at a relatively low alkalinity, an amorphous material formed and as the alkalinity in the synthesis mixture increased, the crystallinity of silicalite-1 was enhanced (Kamil et al., 2015). A CFA-derived solid silicon precursor will be used in this study for the preparation of high-silica zeolites mordenite and ZSM-5. The alkalinity of the synthesis system will therefore play an important role in the dissolution of the feedstock and subsequent conversion to a crystalline material. This factor will therefore be optimised for the preparation these zeolitic materials from the CFA-derived silicon feedstock.

2.3.2.4 Water content

During the crystallisation of zeolites, water serves as the solvent for the reactions and processes involved. For the crystallisation of a specific zeolite framework, water content in the synthesis mixture needs to be controlled in a defined range since changes in water content influence the concentration of nutrients and consequently, alters the crystallisation process. In general, high water content in the synthesis mixture (i.e. a diluted synthesis mixture) results

in reduced dissolution of the feedstock which in turn slows down the achievement of supersaturation and nucleation. Under these dilute conditions crystal growth processes may therefore be favoured over nucleation, yielding relatively larger zeolite crystals. The opposite effect is typically observed in synthesis systems with low water content (i.e. a synthesis mixture with concentrated nutrients) resulting in the formation of relatively smaller zeolite crystals (Oleksiak and Rimer, 2014; Yu, 2007). Therefore, water content plays a significant role in controlling the morphology of zeolites. Furthermore, water molecules also influence the function of organic structure-directing agents (OSDAs); changes in water content may alter the structure direction of a particular OSDA agent to favour the formation of one zeolite over another by allowing the formation of different SBUs during the initial stages of crystallisation (Yu, 2007).

The water content in the synthesis mixture was reported to influence zeolite mordenite crystallisation (prepared from synthesis mixtures made up of standard laboratory reagents); with water content reported up to z = 78 in some cases (Choudhury et al., 1998; Zhang et al., 2009). Zeolite mordenite formation under dilute conditions resulted in reduced overall crystallisation; longer crystallisation periods were required for the formation of highly crystalline zeolite mordenite (Zhang et al., 2009). Similarly, the synthesis of zeolite ZSM-5 was achieved over a wide range of water content (z = 25-60) in the synthesis mixture; the optimum synthesis conditions were achieved at z = 25 (Cheng et al., 2008). The influence of water content on the formation of zeolite ZSM-5 was investigated under high and low water synthesis environments, using standard chemical reagents (Petrik, 2009). It was reported that water content influenced the crystallisation processes of zeolite ZSM-5 formation; dilute synthesis environments resulted in prolonged crystallisation time (Cheng et al., 2008; Petrik, 2009). In this study, the influence of water content on zeolite mordenite and ZSM-5 formation from a CFA-derived solid silicon precursor will be investigated.

2.3.2.5 Inorganic cations

Inorganic cations are commonly added to the synthesis mixture in the form of a base (MOH, M denotes alkali or alkaline earth metals). Therefore, the addition of inorganic cations into the synthesis mixture simultaneously controls the alkalinity of the synthesis system (Yu, 2007). Inorganic cations play a vital role in zeolite crystallisation, by serving as minor structure-directing agents under aqueous conditions involved in the organisation of silica and alumina precursor species into the PBUs and SBUs of particular zeolite frameworks. The

charge density of cations (based on cationic radius and charge) is reported to influence the interaction of aluminosilicate precursor species with inorganic cations (Feijen et al., 1994; Oleksiak and Rimer, 2014; Liu et al., 2013; Yu, 2007). Inorganic cations are considered structure-forming or structure-breaking depending on their ability to promote the crystallisation of a particular zeolite framework. Sodium cations are the most common inorganic cation utilised in the synthesis of zeolites and is present in most naturally occurring zeolites. Sodium is therefore known as a structure-forming cation in the synthesis of most zeolites. Other inorganic cations such as lithium, calcium, potassium, rubidium and cesium have been reported in the synthesis of zeolites. However, potassium, rubidium and cesium cations are typically considered as structure-breaking cations due to the relatively large cationic radii of these cations (Meng et al., 2017; Petrik et al., 1995; Petrik, 2009; Singh and Dutta, 2003; Wang et al., 2017; Yu, 2007). Inorganic cations may therefore enhance or inhibit the crystallisation of a particular zeolite. Therefore, the type of inorganic cation utilised in the synthesis mixture is an important factor to consider during zeolite synthesis.

The presence of inorganic cations (such as sodium and potassium) in the synthesis mixture influenced the formation of zeolite ZSM-5 and mordenite synthesised using standard chemical reagents (Liu et al., 2014; Mohamed et al., 2005; Petrik, 2009). Structure-forming inorganic cations (such as sodium and lithium with relatively small cationic radii) resulted in the formation of silicon-rich ZSM-5 crystals 5-15 µm in size, while structure-breaking inorganic cations (such as potassium, rubidium and cesium with relatively larger cationic radii) resulted in the formation of relatively larger crystals with an average particle size of 15-25 µm (with twinned morphology in some cases) (Meng et al., 2017; Singh and Dutta, 2003; Wang et al., 2007). Similarly, relatively large potassium cations had a similar effect on the morphology of zeolite ZSM-5 resulting in the formation of relatively larger zeolite ZSM-5 crystals in the presence of nitrate and sulphate anions, due to slower crystallisation processes compared to sodium-containing synthesis mixtures (Petrik, 2009). In the case of zeolite mordenite, highly crystalline material was obtained in the presence of relatively small sodium cations or binary inorganic cation synthesis environments made up of both sodium and potassium cations (Mohamed et al., 2005). Yang et al., (2011) studied the influence of sodium content on the synthesis of silicalite-1. Changes in the sodium content did not significantly influence silicalite-1 crystallinity; however, the particle size of silicalite-1 crystals increased with increasing sodium content in the synthesis mixture (Yang et al., 2011).

The crystallisation of a particular zeolite framework is therefore significantly affected by the inorganic cations present in the synthesis mixture. In this study, a CFA-derived silicon precursor will be used as feedstock for high-silica zeolite synthesis. It is noteworthy that this feedstock may contain a range of inorganic cations in varying amounts, which may influence the crystallisation process for the conversion of the CFA-derived silicon precursor to high-silica zeolites.

2.3.2.6 Organic structure-directing agents

The first reported synthesis of high-silica zeolites was achieved by Barrer and Denny by using tetramethylammonium (TMA) cations as an organic structure-directing agent (OSDA) in the synthesis mixture during hydrothermal treatment. OSDA agents are still utilised for the preparation of high-silica zeolite frameworks as well as novel all-silica analogues of existing zeolite frameworks (Burton and Zones, 2007; Davis and Lobo, 1992). Quaternary alkylammonium cations such as TMA, tetraethylammonium (TEA) and tetrapropylammonium (TPA) are common OSDAs utilised in the synthesis of zeolites with high SAR values (Feijen et al., 1994). OSDA agents are generally thought to function by organising silica and alumina tetrahedra into particular geometries during the early stages of crystallisation (induction and/or nucleation stages). This action of OSDA agents in the synthesis mixture results in the early formation of PBUs and SBUs specific to a particular zeolite framework. As the hydrophobic, high-silica zeolite framework is formed, OSDA molecules will occupy the channels and cages of the framework to avoid contact with the aqueous solution. The incorporation of OSDA molecules in the framework of a zeolite is thought to improve thermodynamic stability of the growing structure, compared to the empty zeolite framework. It is noteworthy that the composition of the synthesis mixture and OSDA type both influence the formation of a particular zeolite structure. Furthermore, the function of the OSDA agent is also affected by the chemistry of the synthesis mixture (Burton and Zones, 2007; Davis and Lobo, 1992; Burkett and Davis, 1995; Grand et al., 2016; Yu, 2007).

An important distinction has been made for the role of organic guest molecules utilised in zeolite synthesis; these organic molecules serve as (i) templating, (ii) OSDA or (iii) space-filling agents. A true templating agent is highly specific and directs the formation of one type of zeolite framework. One such example is known in literature for zeolite ZSM-18 which is synthesised in the presence of a particular tri-quaternary amine ($C_{18}H_{36}N^{+}$). OSDA agents are guest molecules with a particular geometry that corresponds to the void space of the zeolite

framework, while space-filling agents exhibit no structural correlation with the void space in the zeolite framework and merely occupy the space within the zeolite framework (Burton and Zones, 2007; Burkett and Davis, 1995; Davis and Lobo, 1992). Zeolite mordenite has been synthesised in the presence of a range of different OSDA agents namely; tetraethylammonium hydroxide (TEAOH), hexamethyleneimine (HMI), benzene-1,2-diol and benzyltrimethylammonium hydroxide (Jin et al., 2012; Jongkind et al., 1997; Lu et al., 2004; Lv et al., 2011; Mao et al., 2014; Shaikh et al., 1993). Zeolite ZSM-5 is typically synthesised in the presence of TPA^+ cations. However, other OSDA agents have also been utilised in zeolite ZSM-5 synthesis such as tetrapropylammonium bromide (TPABr), tetrabutylammonium bromide (TBABr), 1,2-ethanediamine, 1-propylamine, 1,6-hexanediamine, 1,2-cyclohexanediamine and a range of alcohols; which resulted in changes in ZSM-5 crystal morphology (Missengue et al., 2018; Petrik et al., 1995; Singh and Dutta, 2003). Silicalite-1 is commonly synthesised in the presence of tetrapropylammonium hydroxide (TPAOH), TPABr and TBABr as OSDA agents (Kamil et al., 2015; Petrik et al., 1995; Valtchev et al., 2004; Yang et al., 2011; Zhang et al., 2019). In this study, the common OSDA agents for zeolite mordenite and ZSM-5 such as TEAOH and TPABr will be utilised during hydrothermal synthesis, respectively. Silicalite-1 will also be synthesised in the presence of TPABr, as OSDA agent.

2.3.2.7 Seeding

In zeolite synthesis, seeding describes the use of a small quantity of the desired zeolite added to the synthesis mixture prior to hydrothermal treatment (Feijen et al., 1994; Yu, 2007). The addition of seed crystals to the synthesis mixture is commonly used to favour the crystallisation of a zeolite phase that is thermodynamically unfavourable otherwise. Seed crystals function by (i) supressing the crystallisation of undesired zeolite phases that crystallise as impurities, (ii) enhancing the nucleation of the desired zeolite phase or (iii) improving crystallisation kinetics to promote the crystallisation of the desired zeolite phase. Seeding may provide a cost-effective manner of achieving a particular zeolite phase, without the addition of an OSDA agent (Cundy and Cox, 2003; Grand et al., 2016; Yu, 2007). Seed-assisted zeolite synthesis is commonly applied in the synthesis of zeolite mordenite to promote mordenite crystallisation without the formation of competing phases such as zeolite Na-P1 and analcime (Cysneiros et al., 2016; Lu et al., 2004; Lv et al., 2011; Todorova and Kalvachev, 2015; Ueda et al., 1980; Zhang et al., 2011). The addition of seed crystals to the synthesis mixture for zeolite mordenite synthesis resulted in the control of the morphology of

synthesised zeolite mordenite crystals. In the presence of relatively high seed quantities, a reduction in the particle size of mordenite crystals was observed (Todorova and Kalvachev, 2015; Ueda et al., 1980). Similarly, seed-assisted crystallisation of zeolite ZSM-5 has been reported for the preparation of nano-sized crystals (Gao et al., 2016; Li et al., 2016; Ren et al., 2010; Singh and Dutta, 2003). In some cases, nano-sized ZSM-5 crystals with hierarchical morphology were formed in the presence of an organosilane OSDA by using seed-assisted zeolite crystallisation (Chen et al., 2018; Gao et al., 2016; Li et al., 2016). These studies illustrated how seed-assisted zeolite crystallisation may be utilised to control crystal morphology in terms of particle shape and size as well as favour the crystallisation of a specific zeolite (in the absence of impure mineral phases. In this study, seed-assisted zeolite mordenite crystallisation from a CFA-derived silicon precursor will be investigated (in the absence of an OSDA agent) to determine the influence of this parameter on the mordenite formation.

2.3.2.8 Ageing

The process of ageing refers to the mixing of a homogeneous solution of precursor species for a given time period, before hydrothermal treatment takes place. This process may occur under static or stirred conditions at elevated temperatures or room temperature (Feijen et al., 1994; Oleksiak and Rimer, 2014). Typically, the ageing process is carried out to allow the initial stages of crystallisation such as induction and nucleation to commence prior to the hydrothermal treatment step. During the ageing process, germ nuclei may be formed that remain dormant until an elevated temperature is reached (during the hydrothermal treatment step). Overall, the process of ageing reduces the total crystallisation time period required for zeolite formation by reducing the induction period and enhancing the rate of nucleation during crystallisation. Consequently, the morphology of zeolite crystals is also altered by ageing; relatively smaller zeolite crystals may be formed by using the ageing process prior to hydrothermal treatment (Feijen et al., 1994; Yu, 2007).

Enhanced zeolite mordenite crystallisation occurred at prolonged ageing time periods and the morphology of zeolite mordenite crystals was also influenced by the ageing step. Relatively short ageing times resulted in larger crystals, while longer ageing time produced relatively smaller mordenite crystals (Idris et al., 2019). Similarly, an increase in ageing time (up to 24 hours) resulted in improved zeolite ZSM-5 crystallinity. This was reported to be due to enhanced crystallisation processes such as nucleation and induction. As a result, relatively

smaller zeolite ZSM-5 crystals were formed (Cheng et al., 2008). The conversion of a similar CFA-derived silicon precursor to high-silica zeolite ZSM-5 with high crystallinity was achieved by using an ageing step of 30 minutes at room temperature (Missengue, 2016). In this study, the ageing step (prior to hydrothermal synthesis) was therefore set at 30 minutes throughout the study.

All of these factors highlight that a specific set of synthesis conditions are required for the crystallisation of a specific zeolite framework. Considering zeolite mordenite and ZSM-5 which are made up of similar SBUs, slight variation in these parameters could result in the crystallisation of contaminant zeolite phases or a different zeolite phase altogether. Therefore, careful consideration of these factors is required prior to the hydrothermal synthesis of a particular zeolite. In this study, an alternative silicon precursor (derived from CFA) will be utilised as feedstock for the synthesis of high-silica zeolite mordenite and ZSM-5. The most important factors involved in the crystallisation of these high-silica zeolites (such as SAR value, alkalinity, water content and template content) will be optimised in this study. In the case of zeolite mordenite, the effect of seeding on mordenite formation will also be studied.

2.3.2.9 Crystallisation conditions

During hydrothermal treatment, parameters such as crystallisation temperature (and time period) as well as ageing conditions influence the formation of zeolites (Yu, 2007). The influence of these parameters on zeolite crystallisation will be discussed briefly in this section, with particular interest in high-silica zeolite mordenite and ZSM-5.

2.3.2.9.i Crystallisation temperature and time

Hydrothermal synthesis of a particular zeolite framework is significantly influenced by the choice of hydrothermal (crystallisation) temperature, as this factor will have a major impact on the crystallisation kinetics of the zeolite formation process. For this reason a vast amount of research in the field of zeolite science has placed emphasis on studying how crystallisation temperature influences zeolite formation; results reported in literature showed that a specific zeolite crystallises in a particular range of crystallisation temperatures. The processes of zeolite crystallisation such as induction, nucleation as well as crystal growth are influenced by the crystallisation temperature (Aono et al., 2016; Choudhury et al., 1998; Feijen et al., 1994; Hincapie, et al., 2004; Idris et al., 2019; Kim and Ahn, 1991; Li et al., 2009; Singh et al., 2018; Singh and Dutta, 2003; Yu, 2007; Zhang et al., 2009). Increased hydrothermal temperature is known to enhance the nucleation rate and in particular, the rate of crystal

growth. This typically results in the formation of relatively large zeolite crystals (Feijen et al., 1994; Musyoka et al., 2014; Singh and Dutta, 2003; Yu, 2007). The crystallinity of a zeolite product is affected by the period of hydrothermal treatment applied; enhanced zeolite crystallinity is typically observed with time. Furthermore, zeolites are metastable materials that undergo successive transformations according to Ostwald's law (Feijen et al., 1994; Oleksiak and Rimer, 2014; Yu, 2007). Both hydrothermal synthesis temperature and time period are significant factors to take into account during zeolite synthesis.

Zeolite mordenite crystallisation has been reported over a wide range of crystallisation temperatures (160-200 °C), by using standard chemical reagents to prepare the synthesis mixture without the utilisation of an OSDA agent in most cases (Aono et al., 2016; Choudhury et al., 1998; Hincapie, et al., 2004; Idris et al., 2019; "IZA Synthesis Commission," 2016; Kim and Ahn, 1991; Li et al., 2009; Singh et al., 2018; Zhang et al., 2009). Zeolite ZSM-5 crystallisation is typically carried out at a hydrothermal temperature of 160 °C ("IZA Synthesis Commission," 2016; Missengue et al., 2017; Missengue et al., 2018; Singh and Dutta, 2003). However, a wide range of crystallisation temperatures (130-190 °C) may be applied to achieve zeolite ZSM-5 formation as reported in literature (Cheng et al., 2008; Singh and Dutta, 2003). Similarly, the synthesis of silicalite-1 was also possible over a range of crystallisation temperature from 90 to 230 °C (Kamil et al., 2015; Petrik et al., 1995; Valtchev et al., 2004; Yang et al., 2011; Zhang et al., 2019). In this study, zeolite mordenite, ZSM-5 and silicalite-1 will be synthesised using mild crystallisation temperatures of 160 or 170 °C, based on results for highly crystalline materials reported in the literature.

2.3.2.9.ii Stirring during hydrothermal treatment

The hydrothermal treatment step for zeolite synthesis may be carried out under static or stirred conditions; typically this process is carried out under static conditions. Nevertheless, stirring during hydrothermal synthesis has been reported to improve overall crystallisation kinetics (i.e. shorter crystallisation time period for zeolite formation) as well as influence the morphology of the zeolite crystals formed. Furthermore, stirring has also played a role in the selective formation of a particular zeolite framework type over another (Di Renzo et al., 1991; Hanif et al., 2000; Musyoka et al., 2013; Singh and Dutta, 2003; Yu, 2007).

The physical parameters involved in hydrothermal treatment such as crystallisation temperature (and time period) as well as stirring have a significant impact on the crystallisation kinetics of zeolite formation. These factors also play a role in determining the

zeolite framework type that crystallises for a certain set of chemical conditions; therefore the physical parameters applied during hydrothermal synthesis need to be considered carefully to allow the formation of the desired zeolite framework. The hydrothermal synthesis conditions (i.e. physical parameters) for the formation of zeolite mordenite and ZSM-5 are very similar. In this study, emphasis will therefore be placed on investigating the chemical parameters (such as SAR value, alkalinity, water content, seeding and OSDA content) that influence zeolite crystallisation as discussed in Section 2.4.1.

2.3.3 Post-synthesis treatment of zeolite products

The typical treatment of zeolite products after the hydrothermal step involves cooling the reaction vessel to room temperature, recovering the synthesised zeolite product through filtration. Deionised water is then used to wash the synthesised zeolite product until the pH of the filtrate reaches values < 9. Subsequently, the synthesised zeolite product is then oven dried at relatively low temperatures between 80 and 110 °C (typically overnight). If zeolite synthesis was carried out in the presence of an OSDA agent, a relatively high-temperature calcination step (carried out in air or inert gas) is then carried out to remove the organic molecules from the zeolite framework (Deutschmann et al., 2009; Hagen, 2006; Payra and Dutta, 2003; Yu, 2007). In the case of zeolite mordenite, ZSM-5 and silicalite-1, a calcination step at a temperature of 550 °C (using a slow ramp rate), initially carried out under nitrogen flow then switching to air flow, is typically applied for the removal of OSDA molecules from the zeolite framework (Deutschmann et al., 2009; Hagen, 2006; Singh and Dutta, 2003). Further modification of zeolite products is possible through techniques such as ion-exchange and metal-doping or steaming and desilication/dealumination, which are typically used to alter the chemical or physical properties of the material (Deutschmann et al., 2009; Payra and Dutta, 2003).

2.3.4 Alternative methods of zeolite synthesis

The hydrothermal treatment procedure is widely used in zeolite science. However, many other zeolite synthesis approaches have been developed over the years to produce zeolite materials with different properties. These approaches include microwave-assisted hydrothermal treatment, dry-gel zeolite synthesis, solvo-thermal zeolite synthesis as well as the synthesis of zeolites in various reaction media such as fluoride synthesis or synthesis carried out using organic solvent as the reaction medium. These zeolite synthesis technologies were developed due to the need for zeolites with tailor-made properties suited to

specific applications (Feijen et al., 1994; Singh and Dutta, 2003; Yu, 2007). These techniques are out of the scope of this study and were therefore only mentioned briefly.

2.4 Zeolite synthesis from coal fly ash

In this study, CFA will be used as a source of silicon and aluminium for zeolite synthesis. CFA is a waste by-product of the process of coal combustion. In countries such as South Africa, in which coal is the primary energy source used for the generation of electricity, CFA is produced in millions of tonnes annually (Eskom, 2015). The nature of CFA (siliceous or calcareous) produced during coal combustion is related to the type of coal utilised in the process (Heidrich et al., 2013). Siliceous CFA (also named Class F ash) contains > 70 % of SiO_2, Al_2O_3 and Fe_2O_3/Fe_3O_4 oxides (present as quartz, mullite and hematite/magnetite, respectively) and < 10 % lime. On the other hand, calcareous CFA (also named Class C ash) is composed of ~ 50% of SiO_2, Al_2O_3 and Fe_2O_3/Fe_3O_4 oxides and > 10 % lime (Chang and Shih, 2000; Kruger, 1997; Musyoka et al., 2014; Shigemoto et al., 1995).

CFA is typically destined for disposal to landfills or transported to a different facility for utilisation. The uncontrolled disposal of large quantities of CFA is associated with a range of environmental issues such as surface and ground water pollution, air and soil pollution as well as excessive land-use (Blissett and Rowson, 2012; Shoumkova and Stoyanova, 2012). These environmental issues led to the utilisation of CFA in the cement and concrete production industries as a cheap resource of minerals as well as in the production of geopolymers (Blissett and Rowson, 2012; Heidrich et al., 2013). The rich mineral content of CFA (i.e. high silicon and aluminium content) and the abundance of this waste by-product make CFA a favourable feedstock for the synthesis of zeolites. This CFA conversion technology involves the formation of industrially important materials such as zeolites from a waste by-product, which results in reduced disposal of a harmful waste material (Ameh et al., 2016; Missengue et al., 2018; Musyoka et al., 2014, Ndlovu et al., 2017).

The transformation of CFA to zeolites involves the hydrolysis of dense mineral phases quartz and mullite (typically catalysed by a base) to produce relatively smaller and more reactive silicate and aluminosilicate species. This step is followed by the dissolution of soluble silicate and aluminosilicate species and the subsequent condensation of these reactive silicate and aluminosilicate species to form the crystalline zeolite framework, as discussed in Section 2.4.1 (Murayama et al., 2002; Querol et al., 2002). To date, CFA has typically been utilised

as feedstock in the synthesis of low-silica zeolites such as zeolite A, P, X and hydroxysodalite. This is due to the relatively low SAR value of the CFA material (Chang and Shih, 2000; Holler and Wirsching, 1985; Musyoka et al., 2014; Querol et al., 2002; Shigemoto et al., 1995). The synthesis of high-silica zeolite materials from CFA is currently an area of interest. Zeolite ZSM-5 synthesised from CFA has been reported in the literature (Chareonpanich et al., 2004; Kalyankar et al., 2011; Krisnandi et al., 2017; Missengue, 2016; Missengue et al., 2017; Missengue et al., 2018; Ndlovu, 2016; Vichaphund et al., 2014; Vichaphund et al., 2016). Zeolite mordenite synthesis from combinations of waste and natural materials (such as CFA, rice husk ash, diatomite and kaolin clay) has been reported in the literature (Ahmed et al., 2018; Aono et al., 2018; Johan & Matsue, 2014; Johan et al., 2015; Mignoni et al., 2008). However, other high-silica zeolites such as silicalite-1 and zeolite mordenite have not been synthesis from CFA as the sole silica feedstock.

2.4.1 Conversion technologies for CFA conversion to zeolites

A range of CFA conversion technologies have been developed to date for the transformation of CFA to zeolites. Low-silica zeolites have typically been synthesised using direct alkali-activation of CFA in the liquid phase under reflux conditions (Molina and Poole, 2004; Shoumkova and Stoyanova, 2013; Querol et al., 2002). These zeolites have typically been utilised using the activated material resulting in the formation of zeolites in the presence of unconverted dense mineral phases such as quartz and mullite (Murayama et al., 2002; Querol et al., 2002). A dry CFA alkali-activation method has also been reported for zeolite synthesis from CFA, which typically involves a high-temperature in the presence of a base, followed by dissolution of silicate and aluminosilicate species and the utilisation of the clear solution for the production of pure zeolites (Ameh et al., 2016; Chang and Shih, 1998; Hollman et al., 1999; Molina and Poole, 2004; Musyoka et al., 2014; Shigemoto et al., 1993; Shigemoto et al., 1995; Yaping et al., 2008). Some examples of zeolite synthesis using the liquid phase alkali activation of CFA and solid phase alkali activation CFA will be presented in subsequent sections.

2.4.1.1 Aqueous alkaline treatment of CFA

The liquid phase alkali activation of CFA is typically carried out by mixing CFA with a specific volume of NaOH (with different concentrations up to 5.0 M NaOH) and subjecting the mixture to relatively low-temperature, reflux conditions (80-200 °C) for a given time period (up to 48 hours) (Hollman et al., 1999; Murayama et al., 2002; Shoumkova and

Stoyanova, 2013; Querol et al., 2002). The conversion of CFA to zeolite Na-P1 (40-45 wt% purity) was carried out by mixing CFA with 2 M NaOH at a solid-to-liquid ratio of 1:2.5 at a temperature of 90 °C for 96 hours (Hollman et al., 1999). Shoumkova and Stoyanova (2013) investigated the influence of NaOH and KOH on the formation of zeolites from CFA using the liquid phase alkali activation method under different reflux conditions in terms of temperature (80-110 °C) for 7 hours; with NaOH reported as the superior catalyst for alkali activation of CFA. These conditions resulted in the formation of hydroxysodalite (104 °C for 7 hours) and a mixture of zeolite Na-P1 and A (80 °C for 7 hours). It is noteworthy that the presence of converted quartz and mullite were also obtained for these zeolite samples (Shoumkova and Stoyanova, 2013). Similarly, the synthesis of zeolite Na-P1 from CFA by liquid phase alkaline treatment was reported in the presence of three different bases (NaOH, KOH and Na_2CO_3) under reflux conditions of 120 °C for 3 hours; with the highest zeolite Na-P1 crystallisation rate achieved for NaOH (Murayama et al., 2002). These studies reported the formation of low-silica zeolites (with purity ranging between 40 and 70 wt%) in the presence of unconverted dense mineral phases such as quartz and mullite, depending on the concentration and volume of alkali mixed with CFA and reflux conditions (Hollman et al., 1999; Molina and Poole, 2004; Murayama et al., 2002; Shoumkova and Stoyanova, 2013; Querol et al., 2002).

2.4.1.2 Solid alkaline fusion treatment of CFA

The solid alkaline fusion treatment of CFA is commonly carried out by mixing CFA with a specific mass of NaOH (at CFA/NaOH ratios ranging between) and subjecting the mixture to relatively high-temperature conditions (550 °C) for a given time period (up to 1.5 hours). The solid fusion step is typically followed by a dissolution step and the clear solution (containing silicon and aluminium precursor species) is subjected to hydrothermal treatment to yield the crystalline zeolite framework. This type of CFA activation resulted in enhanced dissolution of dense mineral phases such as quartz and mullite and the formation of highly crystalline zeolite A and X (Ameh et al., 2016; Hollman et al., 1999; Molina and Poole, 2004; Musyoka et al., 2014; Shigemoto and Hayashi, 1993; Shigemoto et al., 1995; Yaping et al., 2008).

The formation of relatively crystalline zeolite X (~62 %) was synthesised by using fusion activation of CFA (at 550 °C for 1 hour), using a CFA/NaOH ratio of 1:1.2 and hydrothermal conditions of 100 °C for 6 hours (Shigemoto and Hayashi, 1993). Under similar conditions, relatively crystalline zeolite A (~60 %) was achieved by the addition of sodium aluminate (at

a $NaAlO_2$/CFA ratio of 0.41 (Shigemoto and Hayashi, 1993). This study served as the basis for further research to improve the crystallinity of zeolite A and X formed from CFA, using similar fusion conditions (Ameh et al., 2016; Hollman et al., 1999; Molina and Poole, 2004; Musyoka et al., 2014). The synthesis of pure zeolite A, P and X from CFA was achieved using the fusion activation method, with a relatively high yield of ~300-600 g zeolite/kg CFA. However, a relatively high fusion temperature of 830-850 °C was utilised (Yaping et al., 2008). Therefore this technology, which makes use of dissolved silicate and aluminate species derived from CFA, provided a method for the production of pure zeolites.

2.4.2 The preparation of high-silica zeolites from CFA

The synthesis of high-silica zeolites from CFA has been carried out using both the liquid phase (low-temperature) and solid phase (high-temperature) CFA activation methods. However, in some cases the SAR value of the synthesis mixture was enhanced by the addition of another silicon source, typically fumed silica, sodium silicate solution or rice husk ash (Aono et al., 2018; Chareonpanich et al., 2004; Johan & Matsue, 2014; Johan et al., 2015; Kalyankar et al., 2011; Krisnandi et al., 2017; Missengue, 2016; Missengue et al., 2017; Missengue et al., 2018; Ndlovu, 2016; Vichaphund et al., 2014; Vichaphund et al., 2016). Zeolite mordenite has also been synthesised from alternative feedstock such as fly ash, rice husk ash and diatomite. Johan and Matsue (2014) synthesised zeolite mordenite directly from diatomite using alkaline ageing (70 °C for 6 hours under dilute alkaline conditions), followed by hydrothermal treatment (170 °C for 72 hours). The formation of zeolite mordenite was reported to crystallise together with quartz under these conditions (Johan and Matsue, 2014). Similarly, Johan et al., (2015) reported that zeolite mordenite was synthesised from diatomite under mild alkaline conditions and hydrothermal conditions of 170 °C for 24 hours. It should be noted that zeolite mordenite crystallised in the presence of analcime under these conditions (Johan et al., 2015). In another study, zeolite mordenite was synthesised using a combination of alternative feedstock (CFA and additional rice husk ash) to prepare a synthesis mixture with the appropriate SAR value (Aono et al., 2018). Aono et al., (2018) synthesised zeolite mordenite by separate liquid alkaline activation of fly ash and rice husk ash and using a mixture of the two solutions as the synthesis mixture for hydrothermal treatment (170 °C for 24 hours). Therefore, the zeolite product (mordenite) also contained unreacted dense mineral phases such as quartz and mullite from the fly ash and/or rice husk ash (Aono et al., 2018). To date, other studies have utilised an additional silica source to

enhance the SAR value of CFA. Therefore, it should be noted that CFA has not been utilised as the sole silicon source for the preparation of pure zeolite mordenite to date.

In terms of zeolite ZSM-5 synthesis from CFA, Chareonpanich et al., (2004) synthesised zeolite ZSM-5 using a mixture of lignite fly ash and sodium silicate solution derived from rice husk ash as feedstock, under hydrothermal conditions of 210 °C for 4 hours at an elevated pressure of 4 bar. Rice husk ash was treated under acidic conditions; the treated rice husk ash was pyrolysed at 600 °C for 1 hour and the resultant powder was dissolved in NaOH to form the sodium silicate solution, which was used to enhance the SAR value. The lignite fly ash was added to the rice husk ash-derived sodium silicate solution together with the OSDA agent (TPABr) to form the synthesis mixture (Chareonpanich et al., 2004). The synthesis of zeolite ZSM-5 from fly ash and rice husk ash was achieved by the activation of the feedstock at a relatively high temperature of 800 and 700 °C, respectively, low-temperature alkaline activation at 100 °C as well as a range of other treatment steps prior to use in hydrothermal treatment at 150 °C for 144 hours (Krisnandi et al., 2017).

Kalyankar et al., (2011) synthesised zeolite ZSM-5 by purifying fly ash prior to hydrothermal treatment, using a few different steps; (i) boiling in deionised water for 2 hours, (ii) drying overnight at 100 °C, (iii) calcination at a temperature of 500 °C for 5 hours and (iv) magnetic separation of the iron-containing minerals in fly ash. The purified powder fly ash was then dissolved in NaOH, mixed with additional silica sol (to enhance the SAR value) and TPABr (Kalyankar et al., 2011). The liquid phase alkaline activation of fly ash (at 90 °C for 3 hours) was used for the dissolution of reactive silicate and aluminosilicate species. Sodium silicate solution was added to the mixture to enhance the SAR value of the synthesis solution, followed by the addition of TPABr to form the synthesis solution which was subjected to hydrothermal treatment at 160 °C for 72 hours (Vichaphund et al., 2014; Vichaphund et al., 2016). These synthesis methods for zeolite ZSM-5 from CFA resulted in a zeolite product that contained unreacted mineral phases such as quartz and mullite from CFA (Chareonpanich et al., 2004; Kalyankar et al., 2011; Krisnandi et al., 2017; Vichaphund et al., 2014; Vichaphund et al., 2016).

Zeolite ZSM-5 was synthesised from South African CFA in three ways; (i) direct synthesis using CFA mixed with fumed silica, (ii) direct synthesis using acid-treated CFA mixed with fumed silica and (iii) a silicon precursor extracted from CFA using a high-temperature fusion step was used as the feedstock for zeolite ZSM-5 synthesis. In all cases, three different

OSDA agents (such as TPABr, 1,6-hexanediamine or 1-propylamine) were investigated for zeolite ZSM-5 formation (Missengue, 2016; Missengue et al., 2017; Missengue et al., 2018). In the first method, CFA was mixed with fumed silica at a 1:1 ratio in deionised water, NaOH and an OSDA agent was then added sequentially while stirring. The synthesis mixture was then aged (20 °C for 12 hours) and subjected to hydrothermal conditions of 120 °C for 24 hours. These conditions resulted in the formation of zeolite ZSM-5 with poor crystallinity in the presence of unreacted quartz and mullite, in some cases analcime was also formed (Missengue, 2016).

In the second method, CFA was mixed with concentrated sulphuric acid at a solid-to-liquid ratio of 1:2, the mixture was then placed in a digestion vessel and subjected to a temperature of 250 °C for 4 hours. The acidic mixture was then added to deionised water at a ratio of 1:3, subjected to reflux conditions (85 °C for 30 minutes, while stirring) and the hot liquid was filtered to collect the acid-treated CFA. It should be noted that the magnetic fraction attached to the magnetic stirrer bar was collected, to reduce the amount of iron-containing minerals in the acid-treated CFA. The acid-treated CFA was washed with boiling deionised water (~300 mL) and dried in an oven overnight at 80 °C. The acid-treated CFA served as the feedstock for zeolite ZSM-5 synthesis and was mixed with fumed silica at a 1:1 ratio, NaOH and an OSDA agent while stirring. The synthesis mixture was aged (stirring for 2 hours at room temperature) and subjected to hydrothermal conditions of 160 °C for 72 hours. Similar to the first method, this method resulted in the formation of zeolite ZSM-5 with poor crystalline in the presence of unreacted quartz and mullite. Consequently, these ZSM-5 zeolites exhibited a relatively low SAR value (4-5) and specific surface area values lower than a commercial zeolite ZSM-5 sample (Missengue, 2016; Missengue et al., 2017).

In the third method, CFA was mixed with NaOH at a ratio of 1:1.2 and fused at a temperature of 550 °C for 1.5 hours. The fused CFA/NaOH was mixed with deionised water (500 mL) for 2 hours at room temperature and filtered. The filtrate was collected, to which concentrated sulphuric acid was added drop-wise to start the precipitation of silica, which serves as the silicon feedstock for zeolite ZSM-5 synthesis without the addition of other silicon sources. Prior to utilisation in hydrothermal synthesis, the silicon precursor was treated with concentrated oxalic acid solution (at a solid-to-liquid ratio of 1:10) under reflux conditions (80 °C for 6 hours) to remove excess sodium and enhance the SAR value of the feedstock. The synthesis mixture was then prepared using the treated silicon precursor, NaOH and an

OSDA agent and aged (stirring for 30 minutes at room temperature) prior to hydrothermal treatment (160 °C for 72 hours). Zeolite ZSM-5 crystallised in the presence of all investigated OSDA agents using the oxalic acid treated silicon precursor that was extracted from CFA via the fusion method. These conditions resulted in the formation of highly crystalline zeolite ZSM-5 without the presence of impurities, with SAR values between 36 and 55 and specific surface area comparable to a commercial ZSM-5 sample. However, zeolite ZSM-5 prepared in the presence of 1,6-hexanediamine exhibited the best catalytic performance in the Methanol-to-Olefin process, while zeolite ZSM-5 synthesis in the presence of TPABr exhibited the highest specific area. It is noteworthy that zeolite ZSM-5 did not form when the silicon extract was used without the oxalic acid treatment step (Missengue, 2016; Missengue et al., 2018).

The synthesis of zeolite ZSM-5 was also synthesised from South African CFA by using a relatively low-temperature alkaline activation method. In this method, magnetic separation of the iron-containing mineral phases in CFA was carried out by mixing CFA with deionised water at a solid-to-liquid ratio of 1:5 and stirring for 24 hours at room temperature. The magnetic fraction of CFA was removed by collecting the material that adhered to the magnetic stirrer bar used for mixing, while the non-magnetic fraction of CFA was collected by filtration and dried overnight at 70 °C (Ndlovu, 2016). The non-magnetic fraction of CFA was then mixed with 8.0 M NaOH at a solid-to-liquid ratio of 1:5 and subjected to low-temperature alkaline activation under reflux conditions (150 °C for 24 hours). Once complete, the mixture was cooled and filtered to collect the filtrate. The precipitation of a silicon extract from the filtrate was achieved by the drop-wise addition of concentrated sulphuric acid until the pH reached 10 (Ndlovu, 2016). The silicon precursor extracted from the non-magnetic fraction of CFA was then treated with oxalic acid, as reported by Missengue (2016), prior to utilisation in the hydrothermal synthesis of zeolite ZSM-5. The oxalic acid treated-silicon precursor was then mixed with deionised water, NaOH and TEAOH (as an OSDA agent) and the synthesis mixture was aged (30 minutes at room temperature) and subjected to a temperature of 160 °C for 72 hours (Ndlovu, 2016).

Therefore the synthesis of pure, highly crystalline, high-silica zeolite ZSM-5 from South African CFA has been previously reported by two different alkaline activation methods (Missengue, 2016; Missengue et al., 2017; Missengue et al., 2018; Ndlovu, 2016). In one case, the hydrolysis of the dense mineral phases of CFA (such as quartz and mullite) was

carried out under high-temperature, solid, alkaline activation conditions of 550 °C for 1.5 hours (Missengue, 2016; Missengue et al., 2018). In the other case, a low-temperature, liquid phase, alkaline activation step was used for the hydrolysis process at 150 °C for 24 hours (Ndlovu, 2016). However, it should be noted that the magnetic separation of iron-containing minerals was carried out prior to the hydrolysis step (Ndlovu, 2016). In both cases, a liquid extraction step was carried out to achieve the dissolution of silicate and aluminosilicate species in deionised water, followed by the precipitation of a high-silica precursor material by a mineral acid. The next step involved the enhancement of the SAR value of the silicon precursor material by treatment with a chelating agent (reflux conditions of 80 °C for 6 hours with concentrated oxalic acid); this purification step also aided in the removal of excess sodium from the silicon precursor material. The purified silicon precursor material was then used as feedstock in the hydrothermal synthesis of zeolite ZSM-5 (Missengue, 2016; Missengue et al., 2017; Missengue et al., 2018; Ndlovu, 2016). The synthesis of zeolite ZSM-5 using the high-temperature CFA activation method resulted in a residual solid waste material after silicon extraction (Missengue, 2016; Missengue et al., 2017; Missengue et al., 2018), while the synthesis of zeolite ZSM-5 using the low-temperature CFA activation method resulted in a residual solid waste material after silicon extraction that was converted to a geopolymer by curing the wet solid waste (for 120 hours at room temperature) followed by "baking" (at 70 °C for 120 hours) (Ndlovu, 2016).

2.4.3 Other CFA mineral extraction methods

A range of investigations into the extraction of individual elements (such as iron, aluminium and silicon) from CFA for different applications has been reported in the literature to date (Gilbert, 2013; Ndlovu, 2016; Sedres, 2016). As mentioned previously, this study aims to synthesise high silica zeolites from CFA through the preparation of a highly siliceous precursor material for utilisation in hydrothermal zeolite synthesis. Therefore this section will emphasise techniques such as magnetic separation of iron-containing minerals in CFA and alkaline treatment of CFA for the extraction of silicon.

2.4.3.1 Iron extraction from CFA

The magnetic separation of iron-containing mineral phases from CFA has been carried out extensively in literature (Gilbert, 2013; Ndlovu, 2016; Sedres, 2016). These studies used a similar approach for magnetic separation; (i) mixing as-received CFA with deionised water at a fixed solid-to-liquid ratio, (ii) separation of magnetic fraction of CFA, non-magnetic

fraction of CFA and the filtrate through filtration and (iii) drying solid products in an oven overnight. The magnetic separation conditions and iron recovery (%) reported for each study is summarised in Table 2.3 (Gilbert, 2013; Ndlovu, 2016; Sedres, 2016).

Table 2.3: Magnetic separation conditions (for extraction of iron minerals from CFA) reported in literature.

Solid:Liquid ratio	Temp. (°C)	Time (h)	Stirring (rpm)	Fe recovery (%)	Citation
1:2	r.t.	6	250	82	Gilbert, 2013
1:2	r.t.	24	-	N.D.*	Ndlovu, 2016
-	r.t.	1	750	26	Sedres, 2016

*N.D. – not determined

As listed in Table 2.3, the most efficient iron removal was achieved by mixing CFA with deionised water at a solid-to-liquid ratio of 1:2 by stirring (250 rpm) at room temperature for 6 hours (Gilbert, 2013).

2.4.3.2 Silicon extraction from CFA

The extraction of silicon from CFA has also been reported in literature (Ndlovu, 2016; Sedres, 2016). In one study, CFA was utilised directly as the starting material for the alkaline extraction of silicon and the silicon was recovered by filtration (Sedres, 2016). In the other case, the non-magnetic fraction of CFA was utilised as the starting material for the alkaline extraction of silicon, the silicon was recovered by filtration and precipitated with a mineral acid such as concentrated sulphuric acid, as described previously (Ndlovu, 2016). The silicon extraction conditions and silicon recovery (%) reported for each study is summarised in Table 2.4 (Ndlovu, 2016; Sedres, 2016).

Table 2.4: Silicon extraction conditions from CFA reported in literature.

Solid:Liquid ratio	[NaOH]	Temp. (°C)	Time (h)	Stirring (rpm)	Si recovery (%)	Citation
1:5	8.0	150	24	-	92	Ndlovu, 2016
1:30	8.0	100	2	-	53	Sedres, 2016

As listed in Table 2.4, the most efficient silicon removal was achieved by mixing the non-magnetic fraction of CFA with 8.0 M NaOH at a solid-to-liquid ratio of 1:5 under reflux

conditions (150 °C for 24 hours) (Ndlovu, 2016). In this study, the magnetic separation method reported by Gilbert (2013) and the low-temperature alkaline silicon extraction method reported by Ndlovu (2016) will be investigated for the preparation of a silicon feedstock, due to the high iron and silicon recovery percentages, respectively. The silicon feedstock material derived from CFA will be utilised in the synthesis of zeolite mordenite as well as the preparation of zeolite ZSM-5 with different properties (such as SAR values and crystal morphology), up to the preparation of the purely siliceous MFI material known as silicalite-1.

2.5 Zeolite characterisation techniques

As discussed previously, the unique characteristics of zeolites are associated with the structure of zeolites (Morris and Wheatley, 2007; van Hooff and Roelofsen, 1991). A wide range of analytical techniques have therefore been utilised to gain insight into the properties of zeolites. An understanding of the structure-function relationship of zeolites is vital in the design of tailor-made zeolites for a particular application. Zeolite characterisation typically involves the analysis of the mineral content, morphology as well as elemental composition. In this section, the principles of the characterisation techniques applied in this study will be described briefly.

2.5.1 Elemental Analysis

Elemental analysis is typically carried out to determine the composition of a particular zeolite or material. Analytical techniques such as X-Ray Fluorescence (XRF) spectroscopy and Inductively-Coupled Plasma-Mass spectroscopy (ICP-MS) are typically applied to determine the elemental composition of material in terms of major and trace elemental analysis, respectively (van Hooff and Roelofsen, 1991).

2.5.1.1 X-Ray Fluorescence Spectroscopy

XRF is a quantitative technique, commonly used to determine the chemical content in a particular material. This technique is non-destructive technique that makes use of high-energy X-rays to determine the chemical composition of a material. Electrons are released from different atoms present in the analyte, when high-energy X-rays irradiate the analyte material. This causes “holes” in the low-lying orbitals that is filled by an electron in a relatively higher energy orbital; the process is accompanied by a release of energy. In the case of XRF, the energy release causes radiation to be emitted from the analyte material that serves as a

fingerprint for a particular atom (van Hooff and Roelofsen, 1991). In this study, the chemical composition of starting materials (such as CFA) and extraction products will be analysed using XRF spectroscopy.

2.5.1.2 Inductively-coupled Plasma-Mass Spectroscopy

The chemical composition of an analyte may be determined by mass spectroscopy (MS). In MS, chemical composition is analysed based on an atomic or molecular mass of different species present in the analyte by converting atoms in the analyte into ionic form in gaseous medium. MS is a highly sensitive analytical technique that only requires a small amount of analyte for accurate determination of the chemical composition. However, MS is a destructive analytical technique (Rouessac and Rouessac, 2013). In ICP-MS, a plasma torch is used to achieve the ionisation of atoms present in the analyte. Charged ionic species pass through either an electric or magnetic field under vacuum, depending on the type of ICP-MS instrument. Charged ionic species accelerate through the field with a particular force that corresponds to the mass-to-charge (m/e) ratio, which gives information of the chemical nature of a particular charged ionic species. ICP-MS is typically used to determine the elemental composition of materials such as inorganic oxides. In this study, ICP-MS will be used to determine the chemical composition of starting materials (such as CFA) and extraction products (Rouessac and Rouessac, 2013).

2.5.2 Morphological Analysis

The morphology (in terms of particle shape and size) of zeolites greatly influences the functionality of the material (van Hooff and Roelofsen, 1991). The characterisation of the morphological properties of zeolites and other materials is typically determined by Scanning emission microscopy (SEM).

2.5.2.1 Scanning Emission Microscopy

SEM is used to determine the morphology of zeolite crystals (typically on the micron-scale) as well as particle size distribution of crystals. During SEM analysis of a particular sample, an electron beam is focused on the sample and causes secondary electrons (or back-scatter primary electrons) to be emitted from the sample. An objective lens focuses the scattered electrons resulting in an image of the sample material (Haber et al., 1995; Terasaki et al., 2007; van Hooff and Roelofsen, 1991). High-resolution (HR)-SEM may be used to achieve greater resolution of the morphology of zeolite crystals (up to the nano-scale). The surface of

the zeolite crystal may also be analysed by using HR-SEM, to gain insight into the growth of zeolite crystals (Terasaki et al., 2007).

2.5.3 Structural Analysis

The mineralogical and structural properties of materials such as zeolites play an important role in the characteristics of the material and thereby influence the applications of the material. The characterisation of the mineralogical and structural properties (such as mineral phase) of zeolites is therefore one of the main methods utilised to evaluate the material properties. The most common analytical technique used to evaluate the structural features of zeolites is X-ray diffraction (XRD).

However, other analytical techniques such as Fourier transform infrared (FTIR), Raman and Nuclear Magnetic Resonance (NMR) spectroscopy are also used to gain insight into the structural properties of materials (Morris and Wheatley, 2007; van Hooff and Roelofsen, 1991). In this study, analytical techniques such as XRD and FTIR will be used to evaluate structural changes and functional groups in the starting material (CFA) as different elements are extracted and XRD will be used as the main analytical technique to evaluate the mineral phase content of the synthesised zeolitic materials.

2.5.3.1 X-Ray Diffraction

The mineralogical content of zeolites and other crystalline material is commonly characterised by XRD. This technique is a simple, non-destructive identification method and depending on the type of instrument (and radiation) utilised XRD may provide more advanced details of a crystalline material that allows for structural modelling. These structural details also include the location of extra-framework cationic species (Haber et al., 2009; Morris and Wheatley, 2007; van Hooff and Roelofsen, 1991). The XRD diffraction pattern for a particular crystalline material (such as zeolites) is created when X-ray radiation (with a particular wavelength, λ) comes into contact with a regular arrangement of atoms in the crystal lattice that correspond to the same order of magnitude as λ (Morris and Wheatley, 2007; van Hooff and Roelofsen, 1991). These XRD diffraction patterns may therefore be thought of as a collection of lattice points (that correspond to atoms) which lie in different planes; these planes are typically annotated by Miller indices (h k l). Each set of lattice planes (h k l) values corresponds to a particular interplanar distance (d) that yields maximum diffraction at a specific angle (θ); this relationship is described by Bragg's law as depicted in Equation 2.7 (Morris and Wheatley, 2007).

$$n\lambda = 2d\ sin\theta \text{ (Eq. 2.7)}$$

In material science, powder XRD is typically utilised to identify the mineral phases present in a material as well as any impurities. The topology of a zeolite framework plays a role in the diffraction pattern of the material. XRD diffraction patterns are therefore fingerprints used for identification of a specific zeolite framework (Morris and Wheatley, 2007; van Hooff and Roelofsen, 1991). As such, XRD data may be used to calculate the degree of crystallinity for a specific zeolite phase in the synthesised product. Relative percentage crystallinity may be calculated by comparison of the intensities of the main diffraction peaks for a particular zeolite phase with that of a sample of the same zeolite phase that is known to be highly crystalline, as depicted in Equation 2.8 (van Hooff and Roelofsen, 1991).

$$\%\ Crystallinity = \frac{Intensity\ of\ (hkl)peak_{Sample}}{Intensity\ of\ (hkl)peak_{Standard}} \times 100\% \text{ (Eq. 2.8)}$$

XRD may also be used to determine the particle size of nano-scaled crystals using the Sherrer equation. However, the application of the Sherrer equation is dependent on the shape of the crystals (Morris and Wheatley, 2007; van Hooff and Roelofsen, 1991). This analytical technique is therefore a powerful and widely applied method for assessing the quality of synthesised zeolitic materials (van Hooff and Roelofsen, 1991). Therefore, XRD will be utilised in this study to determine the crystallinity of synthesised zeolites as well as to monitor changes in the mineral content of the starting material (CFA) and extraction products.

2.5.3.2 Fourier Transform Infrared Spectroscopy

FTIR spectroscopy also provides information on the structural properties of zeolites. In FTIR, the adsorption (or reflection) of electromagnetic radiation in the wavenumber range of 400 to 4000 cm^{-1} by the sample material is analysed. The chemical bonds present in the sample material absorbs the IR radiation and if the chemical bond is present between different atoms, a dipole is created that vibrates at a specific wavelength (or frequency). Absorption (or reflection) occurs when monochromatic light (with the same wavelength as the dipole) irradiates the non-symmetrical bond and is recorded by a spectrometer (Lercher and Jentys, 2007; Rouessac and Rouessac, 2013). For solid powdered materials such as zeolites, the FTIR spectrum is typically monitored in the reflection mode by using a diamond sample cell known as Attenuated Total Reflection (ATR)-FTIR (Rouessac and Rouessac, 2013).

In general, FTIR vibrational spectra of zeolites is typically recorded in the 400-1300 cm^{-1} wavenumber range and gives information of the bending and stretching vibrational modes of T-O bonds present in zeolite framework, where T represents either silicon or aluminium atoms for aluminosilicate zeolitic materials (Lercher and Jentys, 2007). The T-O vibrational modes of zeolites may be divided into two types; (i) structure insensitive bands and (ii) structure sensitive bands. Structure insensitive bands include; the bending T-O vibrational mode (420-500 cm^{-1}), symmetric stretching vibrational mode (650-720 cm^{-1}) and asymmetric stretching vibrational mode (950-1250 cm^{-1}). On the other hand, structure sensitive bands are typically associated with the SBUs of the zeolite framework which include; the symmetric stretching vibrational mode (750-820 cm^{-1}) and the double ring vibrational modes (500-650 cm^{-1}) (Hagen, 2015; Lercher and Jentys, 2007; van Hooff and Roelofsen, 1991). The structure sensitive bands are characteristic for a specific zeolite framework; an example is the ring unit in the MFI framework as observed for zeolite ZSM-5 (at ~550 cm^{-1}). The optical density (OD) ratio of zeolite ZSM-5 may be calculated from FTIR data according to Equation 2.9, which serves as an indication of the degree of crystallinity of the synthesised material. The OD ratio of highly crystalline zeolite ZSM-5 is reported as 0.7-0.8. Amorphous silica content has been reported to possess an OD ratio < 0.7 (Coudurier et al., 1982; Hagen, 2015; Lercher and Jentys, 2007; Shukla and Pandya, 1989; van Hooff and Roelofsen, 1991).

$$\text{Optical density} = \frac{\text{Intensity of } 550cm^{-1}}{\text{Intensity of } 450cm^{-1}} \quad \text{(Eq. 2.9)}$$

FTIR is also used to characterise the solid acidity of zeolite samples, by adsorption of organic molecules such as pyridine to the acidic sites in the zeolite framework. The acidic sites in the zeolite framework (bridging OH groups) are typically observed in the wavenumber range 3550-3650 cm^{-1}; generally more acidic OH groups exhibit a relatively lower wavenumber. Furthermore, terminal OH groups exist on the external zeolite surface, while silanol (OH) groups present in the zeolite framework due to structural defects may also be observed by FTIR spectroscopy (at a wavenumber of ~3740 cm^{-1}). Therefore, ATR-FTIR spectroscopy is a fast, simple method utilised for the characterisation of zeolites (Lercher and Jentys, 2007; Rouessac and Rouessac, 2013). In this study, FTIR will be utilised to monitor changes in the structural properties in the starting material (CFA) and the extraction products. FTIR will also be utilised to characterise selected synthesised zeolite samples and to calculate the OD values of synthesised zeolite ZSM-5 samples according to Equation 2.9.

2.5.4 Textural Analysis by Nitrogen Physisorption

The textural properties of zeolites play an important role in the application of zeolites that involve the transport of molecules through the microporous zeolite framework. The characterisation of zeolite porosity is commonly carried out by nitrogen physisorption, which will be described briefly (Haber et al., 2009; Thommes, 2007; Thommes et al., 2015). The textural properties of materials (such as zeolites) such as specific surface area, pore size (and volume) as well as the pore size distribution may be characterised by nitrogen physisorption. This analytical technique is applied to materials with pore size in the range 0.35-100 nm (Haber et al., 2009; Thommes et al., 2015). In nitrogen physisorption, the adsorption of nitrogen gas molecules onto the sample material and the subsequent desorption of adsorbed nitrogen gas molecules is monitored under continuous gas stream flow (Deutschmann et al., 2009; Haber et al., 2009; Thommes et al., 2015). Physisorption refers to the process involving the interaction of an adsorptive (nitrogen gas molecules in this case) with an adsorbent solid surface (the zeolite surface in this case). When the nitrogen gas molecule is adsorbed to the adsorbent surface of the zeolite, it is referred to as an adsorbate. The physisorption of nitrogen gas molecules onto the zeolite surface involves non-specific intermolecular repulsive and London dispersion forces. In porous materials such as zeolites, the process of physisorption is affected by fluid-wall interactions, fluid-fluid interactions and fluid stability in the confined pore network. This yields an adsorption isotherm with a specific shape, since the textural properties of microporous material varies from that of mesoporous materials as well as macroporous materials (Sing, 1982; Thommes, 2007; Thommes et al., 2015). The IUPAC recently defined six different adsorption isotherm types with additional classification added for type I and IV, as depicted in Figure 2.9.

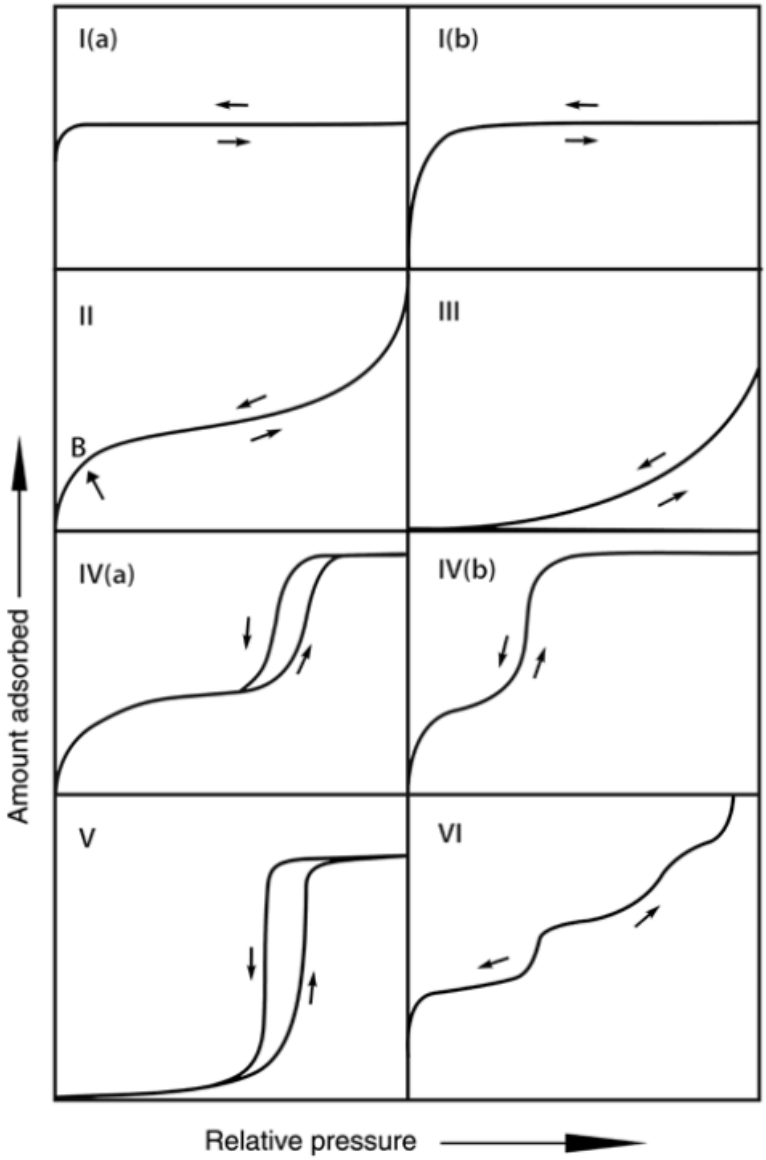

Figure 2.9: Classification of adsorption isotherms, by IUPAC (Thommes et al., 2015).

As depicted in Figure 2.9, the common nitrogen adsorption isotherm types observed for zeolites are type I (a), type I (b), type IV (a) or type IV (b); the isotherm shape depends on the porosity of the zeolite sample (Sing, 1982; Thommes et al., 2015). Type I adsorption isotherms are common for microporous materials such as zeolites exhibiting a high nitrogen uptake at relatively low partial pressure; type I (a) isotherms corresponding to materials with micropores (pore diameter < 1 nm) with a narrow pore size distribution and type I (b) isotherms corresponding to materials with a wide pore size distribution (pore diameter < 2.5 nm) containing relatively large micropores and small mesopores (Thommes, 2007; Thommes et al., 2015). The type IV adsorption isotherm is characteristic of mesoporous

materials; type IV (a) isotherms possess a hysteresis loop (at partial pressures > 0.4) due to capillary condensation in mesopores with diameter > 4 nm and type IV (b) isotherms are indicative of completely reversible nitrogen adsorption and correspond to mesopores with relatively smaller pore diameters, which are cylindrical and conical in shape with tapered ends (Sing, 1982; Thommes, 2007; Thommes et al., 2015). The IUPAC also recently re-defined the different types of hysteresis loops, as depicted in Figure 2.10.

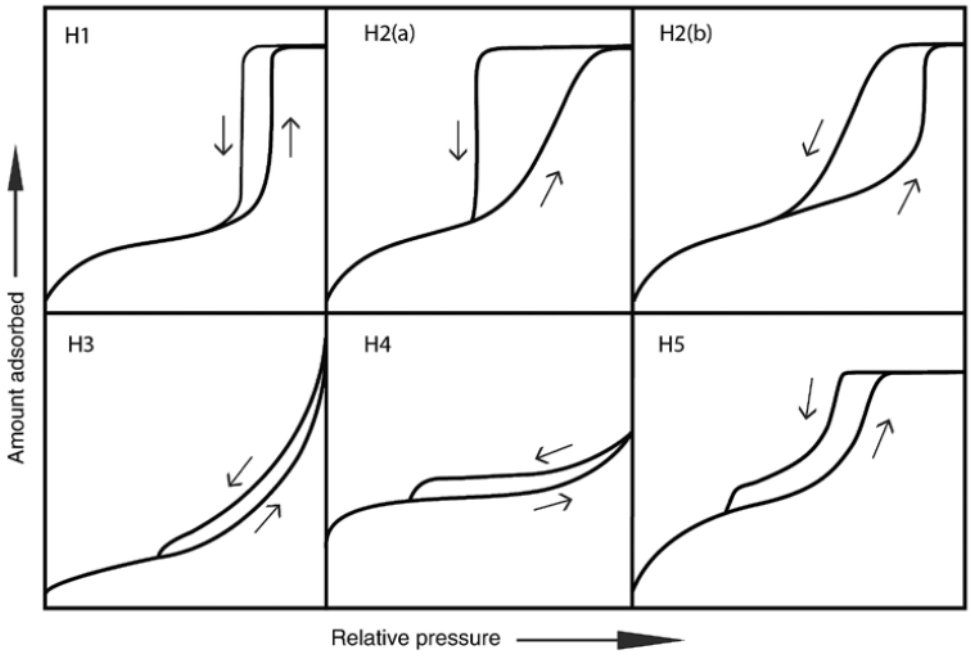

Figure 2.10: Classification of the type of hysteresis loops observed during nitrogen physisorption, by IUPAC (Thommes et al., 2015).

The shape of the hysteresis loop provides information on the pore architecture of the material. For example, the H1 type of hysteresis loop is typically observed for mesoporous materials with a narrow range of pore sizes. Type H2 hysteresis is exhibited by mesoporous materials that commonly experience pore blockages due to the narrow openings to the pore network, as depicted in Figure 2.10 for type H2 (a) hysteresis loop which clearly exhibits the delayed desorption of nitrogen from the material. Similarly, type H2 (b) hysteresis loops arise due to the same reason. However, pore openings in type H2 (b) mesoporous materials is relatively wider than that in type H2 (a) mesoporous materials; resulting in a more gradual desorption branch for H2 (b) type mesoporous materials. Type H3 hysteresis loops are typically observed for mesoporous materials with plate-like crystals that form in an agglomerated manner or mesoporous materials that also contain larger macropores. Type H4 hysteresis

loops are commonly observed for zeolites; with the microporous characteristic of high nitrogen uptake at relatively low partial pressures and slight hysteresis loop at relatively higher partial pressures associated with agglomerated zeolite crystals or mesoporous zeolite crystals. Type H5 hysteresis loops, recently added to the IUPAC classification, are exhibited by mesoporous materials that contain both easily accessible pores as well as relatively smaller pore openings (Sing, 1982; Thommes et al., 2015). This characterisation technique for zeolites therefore provides a range of interesting information on the properties of the synthesised material such as specific surface area, pore size and volume, pore size distribution and also the pore architecture of the material. These textural properties play a significant role in zeolite applications such as adsorption and catalysis. In this study, the textural properties of selected synthesised materials will be investigated by nitrogen physisorption.

2.5.5 Thermal Analysis

The thermal analysis of materials such as zeolites provides information on the thermal stability, water content as well as any other decomposition processes; in some cases thermally induced phase transitions may also be studied. Thermal analysis may also be utilised to detect the presence of impurities in the synthesised material. A range of different thermal experiments have been developed such as Thermogravimetric Analysis (TGA) with Derivative Thermogravimetric (DTG) Analysis as well as Differential Thermal Analysis (DTA). These instruments may be coupled to a Mass Spectrometer (MS) for identification of released compounds (Bourgeat-Lami et al., 1992; Gabelica et al., 1984; Pál-Borbély, 2007). These thermal analysis techniques will be described briefly.

2.5.5.1 Thermogravimetric Analysis (TGA) and Derivative Thermogravimetric (DTG) Analysis

Thermogravimetric analysis (TGA) involves monitoring changes in analyte weight (W) as a function of either (i) time (under isothermal experimental conditions) or (ii) temperature. The TGA experiment may be carried out over a relatively wide range of temperatures (with a programmable heating profile), using an inert (or reactive) gas flow. During the TGA experiment, it is common to determine the derivative of the TGA profile, which is an indication of the rate of weight loss for the analyte (dW/dt); known as Derivative Thermogravimetric (DTG) Analysis (Gabelica et al., 1984; Pál-Borbély, 2007).

2.5.5.2 Differential Thermal Analysis (DTA)

Differential Thermal Analysis (DTA) involves monitoring temperature differences (ΔT) between an inert reference material and the analyte during the TGA experiment; plotted as a function of time or temperature. Under equilibrium conditions the temperature of the reference material, instrument oven and the analyte will be equal. Temperature differences (ΔT) that occur during heating are thought to be due to thermal processes in the analyte material. If the sample temperature is relatively higher than the reference material then the thermal process is exothermic and if the sample temperature is relatively lower than the reference material then the thermal process is endothermic (Gabelica et al., 1984; Pál-Borbély, 2007).

These techniques are commonly applied in combination to study thermal properties of zeolites. Typically, crystalline aluminosilicate zeolites exhibit a relatively low temperature mass loss at ~100 °C due to desorption of water molecules from the zeolite framework. Organic guest molecules in the zeolite framework (such as OSDA agents or trapped reaction products) are typically released from the zeolite framework at a relatively higher temperature (>350 °C) (Bourgeat-Lami et al., 1992; Gabelica et al., 1984; Pál-Borbély, 2007). In this study, thermal analysis (TGA-DTG-DTA) coupled to MS will be used to characterise the water content and OSDA content of synthesised zeolitic materials.

2.6 Computational modelling in zeolite science

The field of zeolite science also incorporates computational chemistry (i.e. theoretical simulations) to gain insight into the material properties, zeolite formation mechanisms as well as adsorption/catalytic activity of zeolites (Dawson et al., 2012; Xu et al., 2007). Computational chemistry also plays a significant role in the rational design of novel or tailor-made zeolites, which is currently a research area that is of great interest in the field of zeolite science (Kapko et al., 2010; Wells and Sartbaeva, 2015; Xu et al., 2007).

In general, typical computational modelling experiments for zeolites involve the following steps (Dawson et al., 2012; Wells and Sartbaeva, 2015; Xu et al., 2007):

- Definition of a zeolite model including structural properties such as crystal symmetry, atoms, bonds, energy terms, force fields, etc.
- Generation of a range of potential zeolite structures by the random arrangement of atoms through application of the Monte Carlo method, reverse Monte Carlo method, etc.
- Evaluation of the generated structures using total energy minimisation to select representative zeolite model structures.
- Visual inspection of selected zeolite model structures and Distance Least Squares (DLS) optimisation to refine the selected group of zeolite model structures.

The cost of this type of modelling process relies on the scale of the model, the type of structure generation method applied as well as the number of steps involved in the structure evaluation and refinement process (Wells and Sartbaeva, 2015; Xu et al., 2007). A relatively fast, simple method for evaluating the feasibility of synthesising a particular zeolite framework was reported in literature (Sartbaeva et al., 2006). This simulation method involved the geometric modelling of zeolites using Geometric Analysis of Structural Polyhedra (GASP) software (Sartbaeva et al., 2006; Wells and Sartbaeva, 2015). This geometric modelling method is relatively low cost compared to other computational methods utilised for zeolite simulations. Furthermore, the model preparation process is relatively simple (Wells and Sartbaeva, 2015). An introduction to GASP software and modelling will therefore presented briefly in the following section.

2.6.1 Geometric modelling of zeolites using GASP software

The GASP software makes use of template-based, geometric simulations on polyhedral materials such as zeolitic frameworks. This is achieved by modelling the tetrahedra of the zeolite framework as rigid units connected through flexible corner atoms. Geometric simulations by GASP software uses short-range, steric strain on the zeolite polyhedra as the main selection criterion; it is noteworthy that dispersion and long-range electrostatic interactions are neglected. A simulated zeolite structure is considered feasible (i.e. relaxed) if framework tetrahedra are ideal with; (i) Si-O bond distances of 1.610 ± 0.001 Å, (ii) O-Si-O bond angles of 109.471 ± 0.001 ° and (iii) no steric strain (overlap) between oxygen atoms (with hard-sphere radius defined as 1.35 Å) in neighbouring tetrahedra (Dawson et al., 2012; Kapko et al., 2010; Sartbaeva et al., 2006; Wells and Sartbaeva, 2012; Wells and Sartbaeva, 2015). Initial investigations using GASP software simulated a range of known zeolite frameworks as purely siliceous frameworks. These siliceous zeolite frameworks were found to be flexible structures with a range of possible framework densities; resulting in the definition of the term "flexibility window" for polyhedral framework materials such as zeolites (Sartbaeva et al., 2006).

The flexibility window is defined as a range of cell parameters (i.e. framework densities) for which zeolite tetrahedra exhibit ideal tetrahedral geometry. The flexibility window is limited by the extension of the Si-O bond (upon expansion) and steric clashes between oxygen atoms (upon compression) (Sartbaeva et al., 2006; Wells and Sartbaeva, 2012; Wells and Sartbaeva, 2015). An extensive collection of known zeolite frameworks (194) were then simulated as purely siliceous using GASP software. It was reported that most of the known zeolite frameworks (182) were flexible structures (as purely siliceous zeolite frameworks). Furthermore, it was possible to model the majority of the other 12 zeolite frameworks as flexibility structures when simulated as mixed chemical compositions (for example, aluminosilicates) (Kapko et al., 2010). Exploring the hypothetical database of zeolite frameworks, 5824 potential new zeolite frameworks were simulated as flexible structures, using GASP software (Dawson et al., 2012). Some common characteristics of known zeolites determined through geometric simulations using GASP software included that; (i) most realisable known zeolite frameworks exhibit framework flexibility as ideal zeolite structures, (ii) most realisable known zeolite frameworks occur as low framework density structures within their flexibility window and (iii) most realisable known zeolite frameworks exhibit multiple compression pathways within their flexibility window. These studies therefore

illustrated the importance of the flexibility window in establishing the feasibility of potential zeolite frameworks (Dawson et al., 2012; Kapko et al., 2010; Sartbaeva et al., 2006; Wells and Sartbaeva, 2012; Wells and Sartbaeva, 2015).

Later GASP simulations included the presence of aluminium atoms in zeolite frameworks such as SOD and GOO (with ordered aluminium distribution throughout the framework). These studies revealed that the presence of aluminium atoms in the zeolite framework allowed for more flexibility, due to relatively longer Al-O bonds. Consequently, aluminosilicate zeolite frameworks were relatively more open structures (Wells et al., 2017). The flexibility window characteristic of zeolite frameworks is therefore inherently important in assessing the potential formation of novel and tailor-made zeolite frameworks in the future.

2.6.2 The investigation of the steric effect of extra-framework content on zeolite flexibility

Recently zeolite frameworks have been simulated using GASP software, with extra-framework content such as solvent molecules and charge-balancing sodium cations, to assess the steric influence of extra-framework content on the flexibility of zeolite frameworks (Wells et al., 2015; Wells et al., 2017). Host-guest interactions between the FAU zeolite framework and extra-framework content such as solvent molecules (water or methanol molecules) were simulated using GASP software to gain insight into the compression behaviour of the FAU framework in the presence of ethanol-methanol-water pressure-transmitting medium (as studied experimentally). In this case, the FAU framework was simulated as a purely siliceous structure and it was reported that the flexibility of the FAU framework was not limited by the presence of a water molecule (together with a methanol molecule) in the beta cage of the framework (Wells et al., 2015). The presence of extra-framework sodium cations and sodium bromide (NaBr) salt in the SOD framework was simulated using GASP software. The presence of extra-framework sodium cations in the SOD framework did not reduce the flexibility window of the material. However, the presence of NaBr salt in the SOD framework limited framework flexibility (Wells et al., 2017). These studies reported that the framework flexibility of zeolites containing extra-framework content was limited based on the steric interactions between extra-framework content and the oxygen atoms of framework tetrahedra (Wells et al., 2015; Wells et al., 2017).

Framework flexibility around extra-framework content is thought to play a role in the zeolite crystallisation process, particularly during the early stages of crystallisation such as the nucleation process. The inherent property of flexibility that zeolites possess allows these

structures to easily accommodate a range of different extra-framework content, without imposing the high-energy cost associated with tetrahedral distortions (Dawson et al., 2012). To date, the steric influence of different inorganic cation content in the zeolite framework (determined using the GASP software) has not been reported. It is not fully understood how inorganic cations influence the crystallisation processes involved in zeolite formation. The utilisation of GASP software may provide insight into the steric influence of different inorganic cations on the flexibility of a particular framework.

In this study, zeolites are synthesised from an alternative silicon source (derived from CFA) which may contain a range of different inorganic cations such as sodium, calcium and potassium due to the nature of the starting material (CFA). Zeolite crystallisation is known to be promoted by sodium cations and inhibited by the presence of certain inorganic cations (particularly calcium and potassium) in the synthesis mixture. The presence of different extra-framework inorganic cations in a model aluminosilicate zeolite framework (LTA) will therefore be simulated using GASP software, to gain insight into the zeolite formation mechanism in the presence of different extra-framework inorganic cations. Zeolite A (an LTA framework type material) has cubic symmetry and a framework SAR value of 1 with an ordered aluminium distribution throughout the framework which makes this material an ideal zeolite to study. The GASP geometric modelling method was chosen based on the relatively simplicity and low cost of the modelling process. The steric constraints placed on this model zeolite framework by the presence of different charge-balancing cations may provide more information on the structure-directing role of inorganic cations during the process of zeolite crystallisation; in particular zeolite crystallisation from fly ash which occurs in the presence of a range of different inorganic cations.

2.7 Chapter Summary

This review aimed to present the research relevant to the topic of the current study. The utilisation of CFA for zeolite synthesis has been an area of interest for years, due to the rich mineral content of this waste material. To date, emphasis has been on the synthesis of low-silica zeolites (A, P, X, Y, sodalite) from CFA. The conversion technology for CFA to zeolites has been plagued by some issues such as variability of the fly ash and low product purity. This lead to the synthesis of zeolites from clear, alkaline solutions extracted from CFA, which has produced highly pure zeolite materials at a relatively lower yield (Chang and Shih, 2000; Franus, 2012; Hollman et al., 1999; Musyoka et al., 2013). Recent studies in this area have focused on using this technology to prepare high-silica zeolites (particularly zeolite ZSM-5) from CFA (Chareonpanich, 2004; Kalyankar, 2011; Krisnandi, 2017; Missengue, 2016; Missengue, 2017; Missengue, 2018; Ndlovu, 2016; Ndlovu, 2017; Vichaphund, 2014; Vichaphund, 2016). According to the literature reported to date, the conversion of CFA into high-silica zeolites (such as zeolite ZSM-5 and mordenite) commonly required the addition of an extra silicon source to enhance the SAR value of the synthesis mixture (Chareonpanich, 2004; Kalyankar, 2011; Krisnandi, 2017; Vichaphund, 2014; Vichaphund, 2016). Alternatively, some researchers extracted a solid silicon feedstock from CFA by using either solid, alkaline fusion conditions (at a relatively high temperature) or liquid, alkaline reflux conditions (at a relatively low temperature). The CFA-derived silicon feedstock was then treated with a chelating agent (such as oxalic acid) under reflux conditions to enhance the SAR value of the CFA-derived silicon feedstock and to remove excess sodium from the CFA-derived silicon feedstock prior to the hydrothermal synthesis of high-silica zeolite ZSM-5 (Ndlovu, 2016; Missengue, 2016; Missengue, 2017; Missengue, 2018). The literature on this topic has been reviewed and the following gaps in the field have been identified:

- The low-temperature alkaline reflux method for the extraction of silicon from CFA provides a highly siliceous material, which will serve as a suitable silicon feedstock for the preparation of a range of high-silica materials with different material properties. However, this process required the purification of the CFA-derived silicon feedstock (using a chelating agent) prior to hydrothermal synthesis. The chelating agent is non-specific and may result in the removal of silicon along with other inorganic cations such as sodium and aluminium, resulting in reduced product yields (Ndlovu, 2016; Missengue, 2016). This study will therefore aim to simplify the

process for the conversion of CFA to high-silica zeolite by removing the additional purification step.

- Zeolite mordenite has been synthesised from mixtures of CFA and rice hush ash, according to literature reported to date (Aono et al., 2018; Johan and Matsue, 2014). However, the preparation of zeolite mordenite has not been achieved by using CFA as the sole silicon source. This study will therefore aim to synthesise zeolite mordenite from a CFA-derived feedstock.
- Current research on the synthesis of zeolite ZSM-5 from a CFA-derived silicon feedstock has been limited to aluminium-rich zeolite ZSM-5. This study will aim to prepare zeolite ZSM-5 with a range of different properties such as chemical compositions (SAR values).
    - The synthesis of silicalite-1 (the siliceous analogue of zeolite ZSM-5) from CFA has not been reported to date. This study will also aim to synthesise silicalite-1 from a CFA-derived feedstock.
- The CFA-derived silicon feedstock utilised in this study for the synthesis of zeolites may be consist of a range of other inorganic elements due the rich mineral nature of CFA. Inorganic extra-framework cations are known to play a role in the crystallisation processes involved in zeolite formation. Inorganic cations are considered either "structure-forming" or "structure-breaking" agents depending on the nature of the cation and the topology of the target zeolite (Cejka et al, 2007; Petrik et al., 1995). Geometric modelling of zeolites using GASP software has been proven to be a fast and simple way to establish the theoretical feasibility of the formation of a particular zeolite framework, by determining whether a given zeolite framework is flexible or not (Dawson et a., 2012; Kapko et al., 2010; Sartbaeva et al., 2006; Wells and Sartbaeva, 2012). To date, the steric influence of extra-framework inorganic cations on the zeolite flexibility (and formation) has not been investigated using GASP software. This study will therefore investigate the influence of different extra-framework inorganic cations on the flexibility of a model zeolite (such as zeolite A with LTA framework) to gain insight into how the inorganic cations present in CFA may enhance or hinder zeolite crystallisation during hydrothermal synthesis.

Current research in the conversion of CFA to high-silica zeolites has focused mainly on zeolite ZSM-5. This study will therefore aim to utilise a CFA-derived silicon feedstock to prepare other high-silica zeolites such as mordenite as well as silicalite-1. Furthermore, a simple method for geometric modelling (using GASP software) will be utilised to gain insight into the steric influence of inorganic cations (present in CFA) on zeolite formation.

3 Chapter 3 - Research Methodology

3.1 Introduction

This chapter will present the research design and methodology used during the investigation of the conversion of South African coal fly ash to high-silica zeolites. This process involves the extraction of iron- and silicon-containing minerals from CFA followed by the utilisation of CFA-derived silicon extract in the hydrothermal synthesis of zeolites mordenite and ZSM-5 as well as zeosil silicalite-1. The procedure for the geometric modelling of a model zeolite framework (LTA) with different extra-framework cations by GASP software will also be presented.

3.2 Materials and chemical reagents

South African coal fly ash from the Arnot coal-fired power station in Mpumalanga was used as the starting material in this study. For this study, a batch of coal fly ash was mixed to form a homogeneous sample that was stored in a sealed container, in a dry area at room temperature. The same batch of coal fly ash was used throughout the investigation to ensure composition variability was kept to a minimum. The materials and chemical reagents utilised in this study are listed in Table 3.1, along with details such as batch number and origin.

Table 3.1: List of chemical reagents used, including the supplier name and batch details.

Reagent Name	Supplier	% Purity	Batch/Lot no.
Coal fly ash	Arnot Power Plant, Mpumalanga, South Africa	-	N/A
Sodium hydroxide pearls	Kimix	97	22012
Potassium hydroxide	Sigma Aldrich	≥85	221473
Calcium hydroxide	Merck	96	K48319847
Cesium hydroxide solution (50 wt% in H_2O)	Acros Organics	99.9	A0339996
Sulphuric acid	Sigma Aldrich	95-98	SHBH9170
Anhydrous aluminium hydroxide	Sigma Aldrich	≥95	MKBP3033V
Anhydrous sodium aluminate	Sigma Aldrich	99	SZBD2200V
Tetrapropylammonium bromide	Sigma Aldrich	98	MKCC0001
Tetraethylammonium hydroxide solution (35 wt% in H_2O)	Sigma Aldrich	35 wt% in H_2O	302929
MOR seed crystals (SAR = 13)	Alfa Aesar (Fisher Scientific)	-	45876.22

3.3 The extraction of silicon from South African coal fly ash for use as starting material in zeolite synthesis

An overview of the process for the synthesis of high-silica zeolites from South African coal fly ash, via silicon extraction, is presented in Figure 3.1.

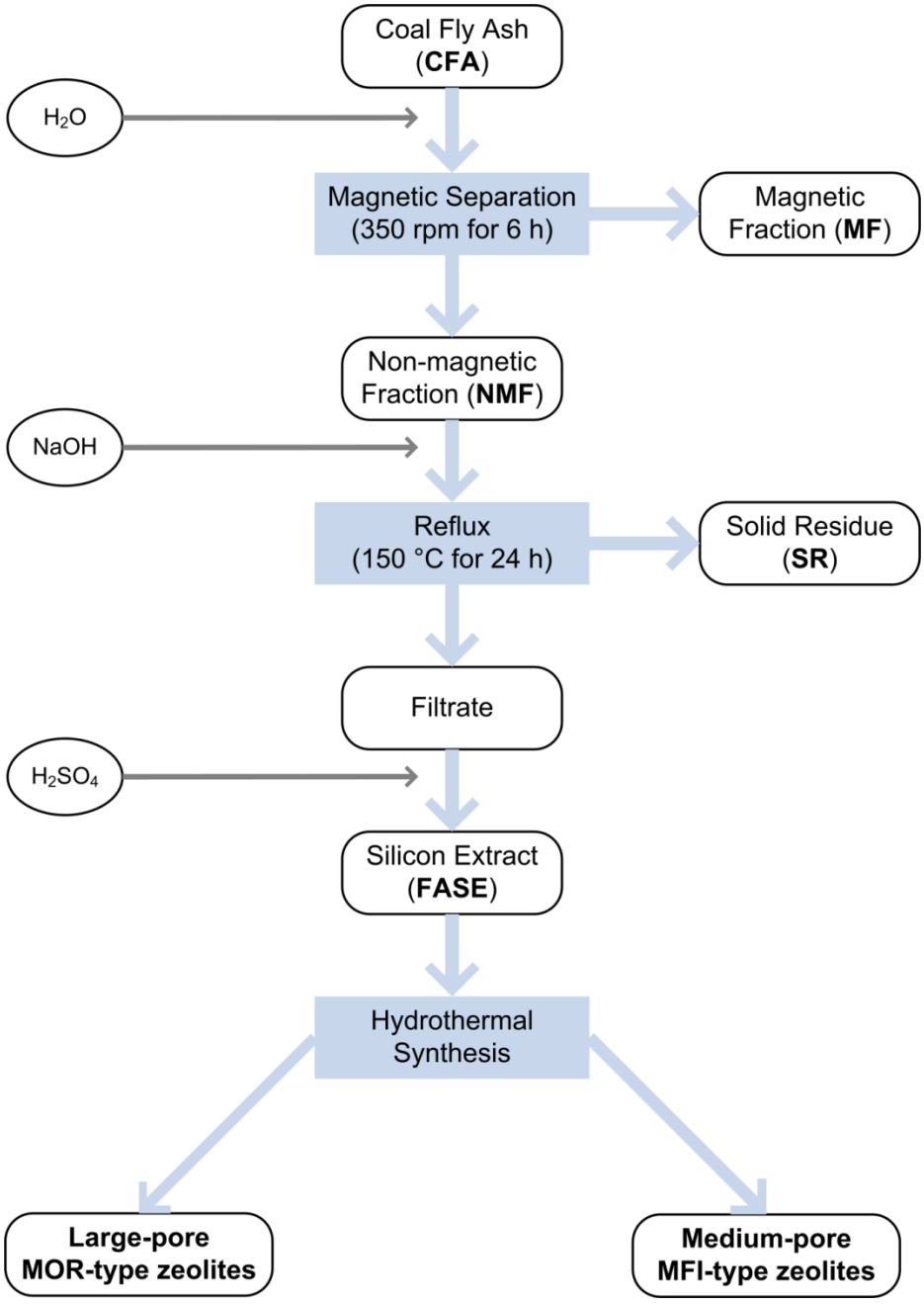

Figure 3.1: A general overview of the transformation process of coal fly ash to high-silica zeolites.

South African coal fly ash from the Arnot power plant in the Mpumalanga province was used as the starting material for this study. Magnetic separation was used to extract the iron (Fe) containing magnetic fraction (MF) while a low-temperature reflux process was used to extract the silicon extract from the non-magnetic fraction (NMF), as depicted in Figure 3.1. Magnetic separation was carried out prior to silicon extraction to avoid the presence of iron in the silicon extract, which may influence crystallisation of zeolites from the CFA-derived silicon precursor (Li et al., 2013; Zhang et al., 2003). These extraction processes are described in more detail in the following sections.

3.3.1 Extraction of Fe (magnetic fraction) from South African coal fly ash

South African coal fly ash (120.0 g) was mixed with deionised water (240 mL) at a solid-to-liquid ratio of 1:2 and stirred at 250 rpm for 6 hours at room temperature, after which a magnet was placed in the beaker containing the mixture and removed after ~ 15 seconds. The magnetic fraction (MF) was removed from the magnet by washing with deionised water. This process was repeated until no visible MF was present on the magnet. The MF was then filtered and washed with deionised water and allowed to dry in an oven at 90 °C overnight. The remaining mixture (containing the non-magnetic fraction of CFA) was filtered; the non-magnetic fraction (NMF) of CFA was collected and dried in an oven at 90 °C overnight. The NMF material was used for the subsequent silicon extraction step.

3.3.2 Extraction of Si from the non-magnetic fraction of South African coal fly ash using a low-temperature, alkaline reflux conditions

A mixture of dried NMF (50.0 g) and 8.0 M NaOH solution (250 mL) was placed in a round-bottomed flask and subjected to reflux conditions at 150 °C for 24 hours, while stirring at 350 rpm. When complete, the mixture was allowed to cool and filtered to yield the solid residue (SR) and filtrate. The SR material was placed in an oven at 70 °C overnight to dry prior to characterisation. The filtrate was collected and placed in a conical flask and conc. H_2SO_4 was added to the filtrate drop-wise until the solution reached a pH of ~10 (at which point the Si precipitate formed). The mixture was filtered to collect the fly ash silicon extract (FASE), which was dried in an oven at 70 °C overnight, for characterisation and utilisation in the synthesis of high-silica zeolites.

3.4 Hydrothermal synthesis of mordenite from CFA-derived silicon precursor (FASE)

The synthesis and step-wise optimisation of zeolite mordenite from South African CFA was investigated in this study. The verified synthesis procedure for zeolite mordenite was used as the starting point for the investigation ("IZA Synthesis Commission", 2016). The synthesis of zeolite mordenite was investigated in a template-free synthesis environment, using the seed-assisted synthesis method as well as using an OSDA agent (tetraethylammonium hydroxide - TEAOH) in the synthesis mixture; the different synthesis protocols for each method will be presented in this section.

3.4.1 Organic structure directing agent-free synthesis of zeolite mordenite from a CFA-derived silicon precursor (FASE)

Zeolite mordenite synthesis was carried out (in the absence of an OSDA agent) under hydrothermal conditions using a synthesis mixture, with the general molar regime $SiO_2 \cdot x\ Al_2O_3 \cdot y\ Na_2O \cdot z\ H_2O$, prepared as follows. The required amount of sodium hydroxide (NaOH) pellets was dissolved in deionised water and (if necessary) the required amount of sodium aluminate was dissolved in the NaOH solution while stirring. Subsequently, the required amount of FASE material was added to the mixture and stirred at 350 rpm at room temperature for 30 minutes to form a homogeneous mixture. The synthesis mixture was then subjected to static hydrothermal treatment in a Teflon-lined pressure vessel at a temperature of 170 °C for a set time period. After hydrothermal treatment was complete, the pressure vessels were allowed to cool down to room temperature. The product was then collected by filtration and washed with deionised water until the filtrate reached a pH of ~7-8. The solid product was then dried in oven at 90 °C overnight and characterisation of as-synthesised solid products was then carried out.

3.4.1.1 Preliminary experiments for OSDA-free synthesis of zeolite mordenite from FASE

Preliminary experiments for the conversion of a CFA-derived silicon precursor (FASE) to zeolite mordenite were carried out under hydrothermal conditions of 170 °C for 24 hours in the absence of an OSDA agent, as reported in literature for the synthesis of zeolite mordenite from standard chemical reagents (Choudhury et al., 1998; Hincapie et al., 2004, Idris et al., 2019; "IZA Synthesis Commission", 2016). The synthesis conditions used for the preliminary zeolite mordenite synthesis experiments are listed in Table 3.2.

Table 3.2: Preliminary experiments for OSDA-free synthesis of zeolite mordenite from a CFA-derived silicon precursor, FASE.

Zeolite code	Molar regime	Variable Parameter	Hydrothermal Treatment	
			Temp. (°C)	Time (hours)
Mor01	1 SiO_2•0.004 Al_2O_3•0.68 Na_2O•30.1 H_2O	-	170	24
Mor02	1 SiO_2•0.019 Al_2O_3•0.70 Na_2O•30.1 H_2O	Amount of Al by $NaAlO_2$ addition	170	24
Mor03	1 SiO_2•0.039 Al_2O_3•0.72 Na_2O•30.1 H_2O			
Mor04	1 SiO_2•0.077 Al_2O_3•0.75 Na_2O•30.1 H_2O			
Mor05	1 SiO_2•0.019 Al_2O_3•0.70 Na_2O•30.1 H_2O	Crystallisation temperature	150	24
Mor06	1 SiO_2•0.039 Al_2O_3•0.72 Na_2O•30.1 H_2O			
Mor07	1 SiO_2•0.077 Al_2O_3•0.75 Na_2O•30.1 H_2O			
Mor08	1 SiO_2•0.019 Al_2O_3•0.52 Na_2O•30.1 H_2O	NaOH content	170	24
Mor09	1 SiO_2•0.019 Al_2O_3•0.54 Na_2O•30.1 H_2O			
Mor10	1 SiO_2•0.019 Al_2O_3•0.56 Na_2O•30.1 H_2O			
Mor11	1 SiO_2•0.019 Al_2O_3•0.57 Na_2O•30.1 H_2O			
Mor12	1 SiO_2•0.019 Al_2O_3•0.58 Na_2O•30.1 H_2O			
Mor13	1 SiO_2•0.019 Al_2O_3•0.60 Na_2O•30.1 H_2O			
Mor14	1 SiO_2•0.019 Al_2O_3•0.61 Na_2O•30.1 H_2O			
Mor15	1 SiO_2•0.019 Al_2O_3•0.64 Na_2O•30.1 H_2O			
Mor02	1 SiO_2•0.019 Al_2O_3•0.70 Na_2O•30.1 H_2O			
Mor11	1 SiO_2•0.019 Al_2O_3•0.57 Na_2O•30.1 H_2O	Crystallisation with time	170	24
Mor16				48
Mor17				72
Mor18				96
Mor19	1 SiO_2•0.019 Al_2O_3•0.57 Na_2O•30.1 H_2O	Crystallisation temperature with time	180	24
Mor20				48
Mor21				72
Mor22			190	24
Mor23				48
Mor24				72

3.4.1.2 Further optimisation of OSDA-free synthesis of zeolite mordenite from FASE

After the preliminary OSDA-free zeolite mordenite synthesis experiments from FASE, further hydrothermal experiments were carried out at 170 °C for 72 hours. The optimisation of synthesis parameters such as aluminium content (by sodium aluminate addition) and water

content (at constant [OH^-]) were carried out as listed in Table 3.3. The optimisation of zeolite mordenite synthesis from a CFA-derived silicon precursor was carried out in a step-wise manner; the best result (in terms of crystallinity) was used as the starting point for subsequent experiments.

Table 3.3: Optimisation of synthesis parameters for OSDA-free synthesis of zeolite mordenite from a CFA-derived silicon precursor, FASE.

Zeolite code	Molar regime	Variable Parameter	Hydrothermal Treatment	
			Temp. (°C)	Time (hours)
Mor25	1 SiO_2•0.010 Al_2O_3•0.56 Na_2O•30.1 H_2O	Amount of Al by $NaAlO_2$ addition	170	72
Mor26	1 SiO_2•0.013 Al_2O_3•0.56 Na_2O•30.1 H_2O			
Mor27	1 SiO_2•0.015 Al_2O_3•0.57 Na_2O•30.1 H_2O			
Mor17	1 SiO_2•0.019 Al_2O_3•0.57 Na_2O•30.1 H_2O			
Mor28	1 SiO_2•0.023 Al_2O_3•0.57 Na_2O•30.1 H_2O			
Mor29	1 SiO_2•0.026 Al_2O_3•0.58 Na_2O•30.1 H_2O			
Mor30	1 SiO_2•0.029 Al_2O_3•0.58 Na_2O•30.1 H_2O			
Mor31	1 SiO_2•0.039 Al_2O_3•0.59 Na_2O•30.1 H_2O			
Mor32	1 SiO_2•0.077 Al_2O_3•0.63 Na_2O•30.1 H_2O			
Mor33	1 SiO_2•0.019 Al_2O_3•0.52 Na_2O•15.1 H_2O	Water content (at constant OH^-/H_2O)	170	72
Mor17	1 SiO_2•0.019 Al_2O_3•0.57 Na_2O•30.1 H_2O			
Mor34	1 SiO_2•0.019 Al_2O_3•0.62 Na_2O•45.2 H_2O			
Mor35	1 SiO_2•0.019 Al_2O_3•0.68 Na_2O•60.2 H_2O			
Mor36	1 SiO_2•0.019 Al_2O_3•0.69 Na_2O•90.4 H_2O			

3.4.2 Seed-assisted synthesis of zeolite mordenite from a CFA-derived silicon precursor (FASE)

The effect of seeding on the synthesis of zeolite mordenite was carried out by adding commercial Na-mordenite crystals to the synthesis mixture prior to hydrothermal treatment, as listed in Table 3.4. The initial synthesis mixture for zeolite mordenite synthesis was prepared as described in Section 3.4.1. Varying amounts of Na-mordenite seeds (0.0025, 0.025 and 0.25 g) were added to the initial synthesis mixture (with a fixed molar regime as listed in Table 3.4) after the ageing period; calculated as 0.1, 1.0 and 10.0 wt% seeds relative to the amount of silicon precursor (FASE) added to the synthesis mixture, respectively. Subsequently, the Na-mordenite seed-containing synthesis mixture was subjected to

hydrothermal treatment at 170 °C for up to 96 hours (at 24 hour intervals). The post-synthesis treatment of as-synthesised zeolites was as described in Section 3.4.1. Solid products were then characterised in the as-synthesised form.

Table 3.4: The effect of seeding amount on the formation of zeolite mordenite from a CFA-derived silicon precursor, FASE.

Zeolite code	Molar regime	Mordenite seeds (g)	Variable Parameter	Hydrothermal Treatment	
				Temp. (°C)	Time (hours)
Mor37	1 SiO_2•0.019 Al_2O_3•0.57 Na_2O•30.1 H_2O	0.0025	Effect of seeding amount monitored over time	170	24
Mor38					48
Mor39					72
Mor40					96
Mor41	1 SiO_2•0.019 Al_2O_3•0.57 Na_2O•30.1 H_2O	0.025		170	24
Mor42					48
Mor43					72
Mor44					96
Mor45	1 SiO_2•0.019 Al_2O_3•0.57 Na_2O•30.1 H_2O	0.25		170	24
Mor46					48
Mor47					72
Mor48					96

3.4.3 Synthesis of zeolite mordenite from a CFA-derived silicon precursor (FASE) in the presence of an OSDA agent

The synthesis of zeolite mordenite in the presence of an OSDA agent (TEAOH) was carried out under hydrothermal conditions of 170 °C for 72 hours from a synthesis mixture (as listed in Table 3.5) prepared as follows. The required amount of sodium hydroxide (NaOH) pellets was dissolved in deionised water, then the required amount of TEAOH was mixed with the NaOH solution while stirring. The required amount of sodium aluminate was then dissolved in the NaOH-TEAOH solution while stirring. Subsequently, the required amount of FASE was added to the mixture, which was then stirred at 350 rpm at room temperature for 30 minutes to form a homogeneous mixture. After ageing was completed, the required amount of Na-mordenite seeds was added to the synthesis mixture (unless stated otherwise). The synthesis mixture was then subjected to static hydrothermal treatment (as described in Table 3.5) and post-synthesis treatment as described in Section 3.4.1. Solid products were then characterised in the as-synthesised form. If required, OSDA (TEAOH) removal was carried

out by calcination in air using a temperature programmed furnace with a heating profile: (1) 1 °C/min up to 150 °C, hold time 1 hour , (2) 1 °C/min up to 250 °C, hold time 1 hour, (3) 1 °C/min up to 350 °C, hold time 1 hour, (4) 1 °C/min up to 450 °C, hold time 1 hour, (5) 1 °C/min up to 550 °C, hold time 3 hours, after which the sample was cooled down to room temperature at a rate of 1 °C/min (holding for 1 hour at 400 °C, 300 °C and 200 °C).

Table 3.5: The effect of OSDA (TEAOH) amount on the synthesis of zeolite mordenite from a CFA-derived silicon precursor, FASE.

Zeolite code	Molar regime	Mordenite seeds (g)	Variable Parameter	Hydrothermal Treatment	
				Temp. (°C)	Time (hours)
Mor43	1 SiO_2•0.019 Al_2O_3•0.57 Na_2O•30.1 H_2O	0.025	Effect of TEOAH amount	170	72
Mor49	1 SiO_2•0.019 Al_2O_3•0.57 Na_2O•0.26 TEAOH•30.1 H_2O				
Mor50	1 SiO_2•0.019 Al_2O_3•0.57 Na_2O•0.53 TEAOH•30.1 H_2O				
Mor51	1 SiO_2•0.019 Al_2O_3•0.57 Na_2O•1.05 TEAOH•30.1 H_2O				
Mor52	1 SiO_2•0.019 Al_2O_3•0.46 Na_2O•0.26 TEAOH•30.1 H_2O	0.025	Effect of TEOAH amount (no additional NaOH)	170	72
Mor53	1 SiO_2•0.019 Al_2O_3•0.46 Na_2O•0.53 TEAOH•30.1 H_2O				
Mor54	1 SiO_2•0.019 Al_2O_3•0.46 Na_2O•1.05 TEAOH•30.1 H_2O				
Mor55	1 SiO_2•0.019 Al_2O_3•0.46 Na_2O•0.26 TEAOH•30.1 H_2O	0	Effect of TEOAH amount (no additional NaOH or seeds)	170	72
Mor56	1 SiO_2•0.019 Al_2O_3•0.46 Na_2O•0.53 TEAOH•30.1 H_2O				
Mor57	1 SiO_2•0.019 Al_2O_3•0.46 Na_2O•1.05 TEAOH•30.1 H_2O				

The influence of aluminium content (by addition of varying amounts of sodium aluminate) on the synthesis of zeolite mordenite in the presence of an OSDA agent (TEAOH) was also investigated in this study. Synthesis mixtures were prepared according to Table 3.6 and subjected to static hydrothermal treatment at 170 °C for 72 hours. Post-synthesis treatment of synthesised products was carried out as described in Section 3.4.3.

Table 3.6: The effect of aluminium content (by sodium aluminate addition) on the synthesis of zeolite mordenite from a CFA-derived silicon precursor, FASE, in the presence of TEAOH.

Zeolite code	Molar regime	Variable Parameter	Hydrothermal Treatment	
			Temp. (°C)	Time (hours)
Mor58	1 SiO_2•0.004 Al_2O_3•0.45 Na_2O•0.53 TEAOH•30.1 H_2O	Al content in the presence of TEOAH (no additional NaOH or seeds)	170	72
Mor56	1 SiO_2•0.019 Al_2O_3•0.46 Na_2O•0.53 TEAOH•30.1 H_2O			
Mor59	1 SiO_2•0.038 Al_2O_3•0.48 Na_2O•0.53 TEAOH•30.1 H_2O			
Mor60	1 SiO_2•0.077 Al_2O_3•0.52 Na_2O•0.53 TEAOH•30.1 H_2O			

3.5 Hydrothermal synthesis of zeolite ZSM-5 and silicalite-1 from a CFA-derived silicon precursor (FASE)

The synthesis of zeolite ZSM-5 from a CFA-derived silicon precursor (FASE) was carried out under static hydrothermal treatment of a synthesis mixture, with the general molar regime SiO_2·x Al_2O_3·y Na_2O·n TPABr z H_2O, prepared as follows. The required amount of sodium hydroxide (NaOH) pellets was dissolved in deionised water and (if necessary) the required amount of aluminium precursor (aluminium hydroxide or sodium aluminate) was dissolved in the NaOH solution while stirring. The required amount of FASE was then added to the mixture, which was stirred at 350 rpm for ~ 5 minutes. The required amount of OSDA, in this case tetrapropylammonium bromide (TPABr), was added to the mixture and the mixture was stirred at room temperature for 30 minutes at 350 rpm to form a homogeneous mixture. The synthesis mixture was then subjected to static hydrothermal treatment in a Teflon-lined pressure vessel at a temperature of 160 °C for 72 hours (unless stated otherwise). After hydrothermal treatment was complete, the pressure vessels were allowed to cool down to room temperature. The product was then filtered and washed with deionised water until the filtrate reached a pH of ~7-8. The solid product was then dried in an oven at 90 °C overnight and characterisation of as-synthesised solid products was then carried out. If required, the OSDA (TPABr) was removed by calcination in air using a temperature programmed furnace as described in Section 3.4.3.

3.5.1 Optimisation of synthesis parameters for zeolite ZSM-5 formation from FASE

The effect of OSDA amount, aluminium content (by aluminium hydroxide or sodium aluminate addition), water content (at constant [OH^-]) and alkalinity on the crystallisation of zeolite ZSM-5 was investigated to determine the optimum conditions for the formation of highly crystalline zeolite ZSM-5 from a CFA-derived silicon precursor (FASE), as described in Table 3.7. The optimisation of zeolite ZSM-5 synthesis from a CFA-derived silicon precursor was also investigated in a step-wise manner; the best result (in terms of crystallinity) was used as the starting point for subsequent experiments.

Table 3.7: Optimisation of synthesis parameters for synthesis of zeolite ZSM-5 from a CFA-derived silicon precursor, FASE, in the presence of an OSDA (TPABr).

Zeolite code	Molar regime	Variable Parameter	Hydrothermal Treatment	
			Temp. (°C)	Time (hours)
Zeo01	1 SiO_2•0.004 Al_2O_3•0.54 Na_2O•0.42 TPABr•35.4 H_2O	Amount of OSDA (TPABr)	160	72
Zeo02	1 SiO_2•0.004 Al_2O_3•0.54 Na_2O•0.10 TPABr•35.4 H_2O			
Zeo03	1 SiO_2•0.004 Al_2O_3•0.54 Na_2O•0.03 TPABr•35.4 H_2O			
Zeo02	1 SiO_2•0.004 Al_2O_3•0.54 Na_2O•0.10 TPABr•35.4 H_2O	Amount of Al by $Al(OH)_3$ addition	160	72
Zeo04	1 SiO_2•0.015 Al_2O_3•0.54 Na_2O•0.10 TPABr•35.4 H_2O			
Zeo05	1 SiO_2•0.058 Al_2O_3•0.54 Na_2O•0.10 TPABr•35.4 H_2O			
Zeo06	1 SiO_2•0.111 Al_2O_3•0.54 Na_2O•0.10 TPABr•35.4 H_2O			
Zeo02	1 SiO_2•0.004 Al_2O_3•0.54 Na_2O•0.10 TPABr•35.4 H_2O	Amount of Al by $NaAlO_2$ addition	160	72
Zeo07	1 SiO_2•0.015 Al_2O_3•0.55 Na_2O•0.10 TPABr•35.4 H_2O			
Zeo08	1 SiO_2•0.025 Al_2O_3•0.56 Na_2O•0.10 TPABr•35.4 H_2O			
Zeo09	1 SiO_2•0.036 Al_2O_3•0.57 Na_2O•0.10 TPABr•35.4 H_2O			
Zeo10	1 SiO_2•0.046 Al_2O_3•0.58 Na_2O•0.10 TPABr•35.4 H_2O			
Zeo11	1 SiO_2•0.058 Al_2O_3•0.59 Na_2O•0.10 TPABr•35.4 H_2O			
Zeo12	1 SiO_2•0.111 Al_2O_3•0.65 Na_2O•0.10 TPABr•35.4 H_2O			
Zeo13	1 SiO_2•0.015 Al_2O_3•0.50 Na_2O•0.10 TPABr•17.7 H_2O	Water content (and NaOH simultaneously)	160	72
Zeo14	1 SiO_2•0.015 Al_2O_3•0.53 Na_2O•0.10 TPABr•28.3 H_2O			
Zeo07	1 SiO_2•0.015 Al_2O_3•0.55 Na_2O•0.10 TPABr•35.4 H_2O			
Zeo15	1 SiO_2•0.015 Al_2O_3•0.60 Na_2O•0.10 TPABr•53.1 H_2O			
Zeo16	1 SiO_2•0.015 Al_2O_3•0.49 Na_2O•0.10 TPABr•28.3 H_2O	NaOH content	160	72
Zeo14	1 SiO_2•0.015 Al_2O_3•0.53 Na_2O•0.10 TPABr•28.3 H_2O			
Zeo17	1 SiO_2•0.015 Al_2O_3•0.61 Na_2O•0.10 TPABr•28.3 H_2O			
Zeo18	1 SiO_2•0.015 Al_2O_3•0.84 Na_2O•0.10 TPABr•28.3 H_2O			

3.5.2 The crystallisation of zeolite ZSM-5 with time

The crystallisation of zeolite ZSM-5 from a CFA-derived silicon precursor (FASE) was monitored with time at a hydrothermal temperature of 160 °C from a synthesis mixture with fixed molar regime at 24 hour intervals between 48 and 144 hours (2-6 days), as described in Table 3.8.

Table 3.8: Monitoring the formation of zeolite ZSM-5 from a CFA-derived silicon precursor, FASE, in the presence of an OSDA (TPABr) under static hydrothermal treatment at 160 °C over time.

Zeolite code	Molar regime	Variable Parameter	Hydrothermal Treatment	
			Temp. (°C)	Time (hours)
Zeo19	1 SiO_2•0.015 Al_2O_3•0.53 Na_2O•0.10 TPABr•28.3 H_2O	Crystallisation with time	160	16
Zeo20				24
Zeo21				48
Zeo14				72
Zeo22				96
Zeo23				120
Zeo24				144

3.5.3 The effect of extra-framework cation type on the crystallisation of zeolite ZSM-5

The effect of different cations (M = calcium, potassium and cesium) on the formation of zeolite ZSM-5 from a CFA-derived silicon precursor (FASE) was carried out by substituting the NaOH mineralising agent in the synthesis mixture with the corresponding M-OH bases, by keeping the overall [OH^-] of the synthesis mixture constant. It is noteworthy that the silicon precursor (FASE) contains a high quantity of sodium, as listed in Table 3.9, making these M-synthesis mixtures a dual cation synthesis environment. The crystallisation of zeolite ZSM-5 was carried out at a hydrothermal temperature of 160 °C for a set time period of 72 hours from synthesis mixtures prepared as described in Table 3.9. The typical post-synthesis treatment was carried out, as described in Section 3.5.

Table 3.9: The effect of extra-framework cation on the formation of zeolite ZSM-5 from a CFA-derived silicon precursor, FASE, in the presence of an OSDA (TPABr).

Zeolite code	Molar regime	Variable Parameter	Hydrothermal Treatment	
			Temp. (°C)	Time (hours)
Zeo14	1 SiO_2•0.015 Al_2O_3•0.53 Na_2O•0.10 TPABr•28.3 H_2O	Counter-cation type (Na, Ca, K, Cs) by addition of M-OH base	160	72
Zeo25	1 SiO_2•0.015 Al_2O_3•0.45 Na_2O•0.08 CaO•0.10 TPABr•28.3 H_2O			
Zeo26	1 SiO_2•0.015 Al_2O_3•0.45 Na_2O•0.08 K_2O•0.10 TPABr•28.3 H_2O			
Zeo27	1 SiO_2•0.015 Al_2O_3•0.45 Na_2O•0.08 Cs_2O•0.10 TPABr•28.3 H_2O			

3.5.4 Synthesis of silicalite-1 from CFA-derived FASE

The synthesis of zeosil silicalite-1 from a CFA-derived silicon precursor (FASE) was carried out under static hydrothermal conditions of 170 °C for 48 hours, from a synthesis mixture (prepared as described in Section 3.5) with a molar regime, as described in Table 3.10. Post-synthesis treatment of the synthesised product was carried out as described in Section 3.4.3.

Table 3.10: Synthesis conditions for preparation of silicalite-1 from a CFA-derived silicon precursor, FASE, in the presence of an OSDA (TPABr).

Zeolite code	Molar regime	Hydrothermal Treatment	
		Temp. (°C)	Time (hours)
Sil01	1 SiO_2•0.004 Al_2O_3•0.49 Na_2O•0.09 TPABr•11.6 H_2O	170	48

3.6 Characterisation techniques

In this study, a range of characterisation techniques were used to determine the properties of the starting material and as-synthesised zeolite products. Material properties such as crystallinity, morphology, thermal stability and porosity are vital in the design of zeolites for specific applications. The experimental details of the analytical techniques used to monitor these properties will be described in more detail in the following sections.

3.6.1 Elemental analysis

The elemental composition of as-received South African CFA and extraction products (NMF, MF, SR and FASE) was determined by the quantitative analytical technique X-ray fluorescence (XRF) spectroscopy and/or Laser ablation- inductively-coupled plasma-mass spectrometry (LA-ICP-MS) and semi-quantitative analytical technique Energy dispersive spectroscopy (EDS). Semi-quantitative EDS was also utilised to analyse the composition of as-synthesised zeolites.

The major elemental composition of South African CFA and the extraction products were analysed by XRF spectroscopy, while the trace elemental composition of these materials were analysed by LA-ICP-MS spectroscopy. The XRF sample preparation was carried by crushing the sample material with a jaw crusher to form a fine (particle size ~70 µm) powder. The fine powdered sample material was milled with the use of a tungsten-carbide Zibb mill. The milled, powdered sample material was mixed with high purity mixture of trace and rare-earth elements (which consists of 32.83% $LiBO_2$, 66.67 % $Li_2B_4O_7$ and 0.50 % LiI) at a 1:10 mass ratio and a fused disc was prepared for XRF analysis. The elemental analysis of the sample material was carried out on a PANalytical Axios Wavelength Dispersive spectrometer with the use of SuperQ PANalytical software. The spectrometer was fitted with a Rhodium tube and scintillation detector, a gas-flow proportional counter that makes use of an Argon-Methane gas mixture in a 90:10 mixture was also coupled to the spectrometer. The analysis conditions were set to 50 kV and 50 mA and external standards (Basalt JB-1 and BE-N) were used to determine the standard deviation of the analysis by this equipment. The SuperQ PANalytical software was used to correct for matrix effects in the sample material by applying theoretical alpha factors and measuring the line-overlap factors compared to the raw intensities.

The LA-ICP-MS sample preparation was carried out by preparing fused discs as described above. Subsequently, these discs were coarsely crushed and a chip of the sample was mounted onto a disk which was mapped and polished prior to analysis. The trace elemental analysis of the sample material was then determined by LA-ICP-MS on an Agilent 7500ce ICP-MS instrument equipped with a Resonetics 193 nm Excimer laser. During the ablation phase, a helium gas flow at a flow-rate of 350 mL/min mixed with nitrogen flow (4 mL/min) and argon flow (900 mL/min) was utilised. A Traceable NIST 612 standard for calibration of

the instrument and the % SiO_2 (determined by XRF measurement) was used as an internal standard for quantification of trace elements.

An estimation of the elemental composition of as-synthesised zeolite products were carried out by semi-quantitative elemental analysis by EDS. The sample preparation for EDS was carried out by placing a small amount of powdered material onto a conductive carbon layer mounted on a metal stub. In most cases, samples were analysed uncoated. If coating was required for imaging, samples were coated with a layer of gold-palladium/gold using a Quorum Q150T ES/Edwards S150B sputter coater. The EDS spectrometer (which was coupled to a scanning emission microscope) was used to determine the average Si/Al (SAR) and Na/Al ratios of synthesised zeolite materials by spot analysis of at least 10 sites for a given sample.

3.6.2 Mineralogical analysis by X-ray diffraction

The mineralogical content of South African CFA, extraction products (NMF, MF, SR and FASE) and as-synthesised zeolites products was determined by powder X-ray diffraction (XRD) using flat-plate geometry. Powdered samples were loaded into a clear, plastic disk and flattened until smooth and level with the top edge of the disk. XRD analysis was then carried out by using a powder PANalytical PW3830 X-Ray generator and XRD measurements were carried out at 40 kV and 25 mA using Cu $K\alpha_1$ radiation (λ = 0.154 nm). In some cases, a powder Bruker D8-Advance X-ray diffractometer with the same X-ray radiation source was used. The identification of mineral phases in sample materials was carried out by using Philips X'Pert Graphics and Identification software and JCPDS International Centre for Diffraction Data (1997) database. The collection of simulated zeolite XRD diffraction patterns was also used to identify zeolite phases present in synthesised products (Treacy and Higgins, 2007).

3.6.3 Morphological analysis by Scanning emission microscopy

The morphology (particle shape and size) of South African CFA, extraction products (NMF, MF, SR and FASE) and as-synthesised zeolite products was analysed by Scanning emission microscopy (SEM). Powdered samples were prepared for SEM imaging as described in Section 3.6.1 for EDS. SEM imaging was carried out using a Zeiss Auriga field emission gun (FEG)-scanning emission microscope at 5.0 kV. In some cases, SEM imaging was carried out on a JEOL JSM-6480LV SEM. The images obtained by SEM were processed by using ImageJ Software.

3.6.4 Structural analysis by Fourier transform infrared spectroscopy

Structural properties of South African CFA and extraction products (NMF, MF, SR and FASE) were analysed by Fourier transform infrared (FTIR) spectroscopy. Selected as-synthesis zeolite products were also analysed by FTIR. The sample material was ground into a fine powder, which was placed onto the sample slot of the Perkin Elmer (ATR)-FTIR Spectrum Two instrument. FTIR measurements were carried out in the wavelength range of 400 to 4000 cm^{-1}, collected using Spectrum software.

3.6.5 Textural analysis by Nitrogen physisorption

Nitrogen (N_2) physisorption was used to analyse the textural properties (such as BET surface area, micropore and total pore volume as well as pore size distribution) of selected synthesised zeolite products (in the Na-form). A known mass (~0.2 g) of sample material was degassed prior to N_2 physisorption. Ex-situ degassing was carried out at 100 °C for ~2 hours under vacuum, followed by in-situ degassing at 300 °C (ramp rate = 10 °C/min) for ~5 hours under vacuum. N_2 physisorption measurements were then carried out using a Micromeritics 3Flex instrument at -196 °C. The specific surface area of sample materials was determined using the Brunauer-Emmett-Teller (BET) method in the relative pressure range of 0.0001 to 0.05. The total pore volume was determined using single-point adsorption at a relative pressure of 0.99. The t-plot method was used to determine the micropore volume of sample materials, while the pore size distribution of sample materials was determined by applying the Barrett-Joyner-Halenda (BJH) method to the adsorption branch of the isotherm.

3.6.6 Thermogravimetric Analysis and Differential Thermal Analysis coupled to Mass Spectrometry

The thermal evolution of water and decomposition of organic compounds in the framework of zeolites were characterised by Thermogravimetric Analysis (TGA) coupled to Differential Thermal Analysis (DTA) and Differential Scanning Calorimetry (DSC) as well as a Mass Spectrometer (MS). Measurements were carried out on a Setaram Setsys Evolution 16 TGA-DTA-DSC analyser equipped with a Pfeiffer GSD 320 mass spectrometer. The sample material (~0.020 g) was loaded into an alumina crucible and the experiment was carried out under air flow of 20 mL/min at a heating rate of 10 °C/min up to 650 °C. Mass spectrometry was carried out using the online MS under helium flow.

3.7 Geometric modelling of the LTA framework with different extra-framework cations using GASP software

GASP software was used to simulate the flexibility window of a model zeolite framework (LTA), which is the framework type of zeolite A with cubic symmetry. As a starting point for the GASP simulations, the purely siliceous LTA framework was modelled. Subsequently, the dehydrated aluminosilicate LTA framework (with a SAR value of 1) was simulated using GASP software. Different extra-framework cations (M) were then introduced into the dehydrated framework, such as sodium (Na^+), calcium (Ca^{2+}), potassium (K^+) and cesium (Cs^+) and these M-LTA frameworks were also simulated by GASP. It is noteworthy that GASP simulations model extra-framework cations as steric objects and electrostatic effects associated with this positively-charged extra-framework content are neglected for the purpose of the simulation. Therefore, the aluminosilicate M-LTA frameworks may be compared to the empty aluminosilicate framework directly. The preparation of input structures for the GASP simulation will be discussed in subsequent sections.

3.7.1 Preparation of input structures for GASP geometric simulations

In all cases, input structures were prepared in CIF file format with unit cell parameters defined in P1 symmetry, as required by GASP software. A 2.2.2 supercell of the dehydrated LTA framework was generated (using GASP) based on a CIF file retrieved from the Database of Zeolite Structures (Baerlocher and McCusker, 2017; Pluth and Smith, 1980); which enables the visualisation of the alpha-cage of the LTA framework. Using this LTA supercell, an input file was generated for GASP containing other structural information such as steric radii for framework atoms (0.26 Å for silicon, 0.40 Å for aluminium, 1.35 Å for oxygen) and relevant T-O bond lengths.

3.7.1.1 Siliceous LTA framework and aluminosilicate LTA framework

The siliceous LTA framework and aluminosilicate LTA framework (SAR = 1) input structures were prepared as discussed in Section 3.7.1, with properties listed in Table 3.11, for utilisation in GASP.

Table 3.11: Starting cell parameters and T-O bond lengths used in GASP simulations of cubic LTA frameworks (Siliceous and aluminosilicate).

Framework	Starting cell parameter, *a* (Å)	T-O bond length (Å)
Siliceous LTA	23.838	1.61
Aluminosilicate LTA (SAR = 1)	24.555	1.68

3.7.1.2 Different extra-framework cations in the aluminosilicate LTA framework

The aluminosilicate M-LTA framework (SAR = 1) containing extra-framework cations (M = Na^+, Ca^{2+}, K^+ or Cs^+) input structures were prepared as discussed in Section 3.7.1, with properties listed in Table 3.12, for utilisation in GASP. Extra-framework cations were assigned hard-sphere Pauling ionic radii of 0.95 Å (Na^+), 0.99 Å (Ca^{2+}), 1.33 Å (K^+) and (1.69 Å) (Cs^+) as reported in literature (Pauling, 1927). Cation site occupation for each M-LTA framework is defined per unit cell, as listed in Table 3.12, according to literature (Breck et al., 1956; Pluth and Smith, 1980; Psycharis et al., 2004; Reed and Breck, 1956).

Table 3.12: Starting cell parameters, T-O bond lengths and cation sites occupation of cubic Na-LTA, Ca-LTA, K-LTA and Cs-LTA input structures used in GASP simulations.

Framework	Starting cell parameter (Å)	T-O bond length (Å)	M^{n+} Radius (Å)	Site I	Site II	Site III	Total M^{n+}/unit cell
Na-LTA	24.555	1.68	0.95	8	4	-	12
Ca-LTA	24.555	1.68	0.99	6	-	-	6
K-LTA	24.555	1.68	1.33	8	4	-	12
Cs-LTA	24.555	1.68	1.69	8	4	-	12

3.7.2 GASP geometric simulations

GASP simulations were carried out as described in the literature (Sartbaeva et al., 2006; Wells et al., 2002; Wells and Sartbaeva, 2012; Wells and Sartbaeva, 2015). GASP software utilises template based geometric simulation to establish the flexibility window of zeolites by simulating the framework as tetrahedra connected together through flexible corner atoms. For the GASP simulations, zeolite compression is limited by framework oxygen contact and zeolite expansion is limited by the length of T-O-T bonds with the T-O bond length variation constraint set to 0.01 Å (Sartbaeva et al., 2006; Wells and Sartbaeva, 2015).

3.8 Chapter Summary

This chapter served to present the experimental details of the synthesis of high-silica zeolites (mordenite and ZSM-5) as well as zeosil silicalite-1 from a CFA-derived silicon precursor (FASE). South African CFA from a coal-fired power station in the Mpumalanga province was used as the starting material in this study. A silicon precursor material (FASE) was prepared from CFA by magnetic separation followed by a low-temperature, alkaline reflux step. The silicon precursor (FASE) was utilised in the synthesis of high-silica zeolites, without the need for additional silicon sources or any pre-treatment with oxalic acid to remove excess sodium or enhance the SAR value of the material. The characterisation techniques (namely XRF, ICP-MS, XRD, SEM-EDS, FTIR and Nitrogen physisorption) utilised to analyse the properties of starting materials and synthesised products (such as chemical composition, crystallinity, morphology, thermal stability and porosity) were also described in this chapter. Furthermore, details of geometric modelling simulations (by GASP software) to study the effect of different extra-framework cations on the flexibility of a model zeolite framework (LTA) were also presented in this chapter.

4 Chapter 4 - Extraction of silicon from CFA and process overview (zeolite yields)

4.1 Introduction

In this chapter, the preparation of a silicon precursor material from CFA for utilisation in zeolite synthesis will be discussed. To date, two different approaches (solid fusion and liquid alkaline reflux conditions) have been utilised for the synthesis of high-silica zeolite ZSM-5 from CFA. However, the addition of supplementary silicon sources or treatment of silicon precursors has been reported in many cases to alter the SAR value of the synthesis mixture prior to hydrothermal treatment (Missengue et al., 2017; Missengue et al., 2018; Ndlovu, 2016; Vichaphund et al., 2014; Vichaphund et al., 2017). A novel low-temperature approach to zeolite ZSM-5 synthesis from CFA was reported that involved magnetic separation of iron-containing phases from CFA followed by low-temperature alkaline reflux (Ndlovu, 2016). The high-silica precursor material was then precipitated using a mineral acid. Subsequently, a purification step involving the removal of excess sodium from the silica precursor, by treatment with concentrated oxalic acid under reflux conditions, was carried out prior to use of the treated high-silica precursor in hydrothermal zeolite synthesis (Ndlovu, 2016; Ndlovu, 2017). In this study, the extraction of a high-silica precursor from South African Arnot CFA for zeolite synthesis is carried out using low-temperature reflux conditions, as reported by Ndlovu, (2016). This study aims to achieve the synthesis of high-silica zeolites without the oxalic acid purification step prior to hydrothermal treatment, since this step results in the loss of silicate species and adds extra complexity and chemical use to the synthesis method.

In this chapter, the preparation of the starting material (a silicon extract, FASE from South African Arnot CFA) for utilisation in high-silica zeolite synthesis will be presented. The characterisation of extraction products by analytical techniques such as XRF, ICP-MS, XRD, FTIR and SEM will be presented in this chapter to evaluate the elemental composition, mineralogical content, structural and morphological properties, respectively, of the resultant silicon precursor compared to as-received CFA. Furthermore, an overview of the extraction process will be presented along with sample yields for the synthesis of high-silica zeolites (ZSM-5 and mordenite) and silicalite-1 using this simplified procedure.

4.2 Characterisation of CFA

As-received South African Arnot CFA was characterised by XRF, ICP-MS, XRD, FTIR and SEM to determine the major and minor elemental composition as well as the mineralogical, structural and morphological properties, respectively (as described in Section 3.6).

4.2.1 Elemental analysis

The major elemental composition (calculated on a dry weight basis) of as-received Arnot CFA was characterised by XRF spectroscopy; XRF results are presented on a dry mass basis as listed in Table 4.1 with relative standard deviation values reported.

Table 4.1: Major elemental composition (dry weight) of as-received Arnot CFA characterised by XRF spectroscopy (n = 3).

Major elements	wt%	Relative standard deviation
SiO_2	56.50	0.14
Al_2O_3	27.58	0.16
Fe_2O_3	6.02	0.13
CaO	5.62	0.02
TiO_2	1.60	0.01
MgO	1.57	0.01
K_2O	0.57	0.01
P_2O_5	0.37	0.01
Na_2O	0.10	0.00
MnO	0.05	0.00
Cr_2O_3	0.02	-
Sum	100.00	-
SAR	1.02	-
L.O.I	7.43	0.42

The main oxide components present in as-received Arnot CFA ash were of silicon, aluminium, iron and calcium, as listed in Table 4.1. CFA also contained a significant amount of carbon and/or moisture; as indicated by the L.O.I value of 7.43 wt% which signifies the mass lost upon ignition at 1000 °C (Blissett and Rowson, 2012). As listed in Table 4.1, the total content of silicon, aluminium and iron oxides was > 70 wt%. Arnot CFA may therefore be classified as class F type fly ash. Arnot CFA also contained other elements in major and minor quantities such as titanium, magnesium, potassium, phosphorous, sodium, manganese and chromium.

The trace elemental analysis of as-received Arnot CFA was characterised by ICP-MS; results are listed in Table 4.2.

Table 4.2: Trace elemental composition of as-received Arnot CFA characterised by ICP-MS.

Trace elements	ppm	Relative standard deviation
Ba	872.70	4.43
Sr	806.80	5.42
Zr	399.80	10.06
Ce	175.30	7.37
V	119.70	0.11
Ni	87.30	2.61
La	86.45	5.87
Nd	66.60	7.32
Y	62.56	12.05
Zn	50.80	9.34
Pb	42.30	36.76
Cu	41.70	3.01
Th	34.08	5.63
Nb	29.64	12.36
Rb	28.01	1.90
Sc	27.50	3.44
Co	24.97	2.70
Pr	18.08	8.17
Sm	13.18	3.93
Gd	11.38	1.79
Dy	11.04	4.17
Hf	10.85	0.81
U	9.31	7.38
Er	6.26	4.73
Yb	5.98	7.45
Cs	5.38	6.38
Mo	4.28	3.59
Ta	2.36	12.32
Ho	2.21	6.39
Eu	2.20	6.73
Tb	1.72	8.24
Tm	0.85	7.31
Lu	0.84	7.11

As-received Arnot CFA contains a range of trace elements, as listed in Table 4.2. Compared to XRF analysis, the relative standard deviation of trace elements determined by ICP-MS was relatively higher due to the small quantities in which these elements are present in CFA, which results in lower precision in analytical quantification of these elements.

Some of the trace elements present in CFA are useful nutrients for plants (Cu and Zn), while other trace elements such as Ni, Pb, Sr and Zr may be harmful to animal and plant life (Shaheen et al., 2014). Of the 17 rare-earth elements (REEs) that make up the earth's crust such as Sc, Y and the lanthanide series (La to Lu), CFA contains 16 REEs as listed in Table 4.2 (highlighted in grey). The most abundant REE in the earth's crust is Ce (63 ppm) and the least abundant REE is Tm (0.30 ppm) element (McLoed and Shaulis, 2018; Rudnick and Gao, 2003). Compared to the earth's crust, CFA contains a relatively higher level of REEs (as listed in Table 4.2) and may therefore serve as a source of REEs for extraction and industrial utilisation. Similarly, the presence of trace levels of 16 REEs was observed in South African Matla CFA (Eze et al., 2013). CFA also contains elements Th and U in trace amounts; which may decay to radioactive isotopes such as radium, radon and thoron (Lauer et al., 2015).

The controlled disposal of CFA is imperative to prevent environmental issues associated with the release of harmful and toxic elements into the air, soil and surface- and ground-water. However, the uncontrolled and excessive disposal of CFA may result in (i) pollution of water bodies that affects aquatic life, (ii) changes in soil pH, soil water retention, compaction of soil and nutrient content of soil (which may affect plant and terrestrial life) as well as (iii) air pollution caused by particulate matter (Heidrich et al., 2013; Shaheen et al., 2014; Shoumkova and Stoyanova, 2012). The conversion of CFA into zeolitic materials may therefore serve as a remediation method to alleviate the environmental impact associated with large scale CFA disposal.

4.2.2 Mineralogical analysis

The mineral content of as-received Arnot CFA was characterised by XRD, as depicted in Figure 4.1.

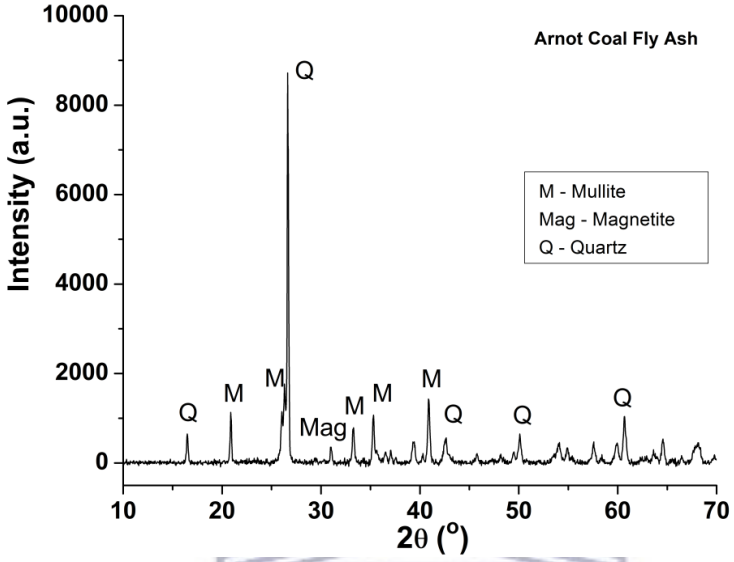

Figure 4.1: XRD diffraction pattern of as-received Arnot CFA.

As-received Arnot CFA contained mainly quartz and mullite mineral phases; diffraction peaks corresponding to magnetite were also observed in Figure 4.1. The mineral phase quartz is made up of silicon oxide, while mullite is an aluminosilicate mineral and magnetite is a mineral made up of iron (FeII and FeIII) oxides. Quartz and mullite are dense mineral phases that typically require harsh conditions (such as high alkalinity and/or high temperature) for the depolymerisation and dissolution of silicon and aluminium species (Nasrazadani and Raman, 1993; Ojha et al., 2004; Wdowin et al., 2014). The mineralogical content of as-received CFA determined by XRD corresponded well with the elemental composition of the material (as observed by XRF in Table 4.1).

4.2.3 Structural analysis

The structural analysis of as-received Arnot CFA was carried out by FTIR spectroscopy, as depicted in Figure 4.2. The major mineral phases that constitute CFA, namely quartz and mullite, are composed of silica and alumina tetrahedra with varying degrees of polymerisation. Therefore the FTIR vibrational bands observed in Figure 4.2 are mainly due to T-O vibrational modes of these minerals (T represents either aluminium or silicon atoms). Strong vibrational bands were observed at 445, 553, 778, 903, 995, 1090 and 1405 cm^{-1} for Arnot CFA (Criado et al., 2007; Fernandez-Jimenez and Palomo, 2005; Livage, 1994).

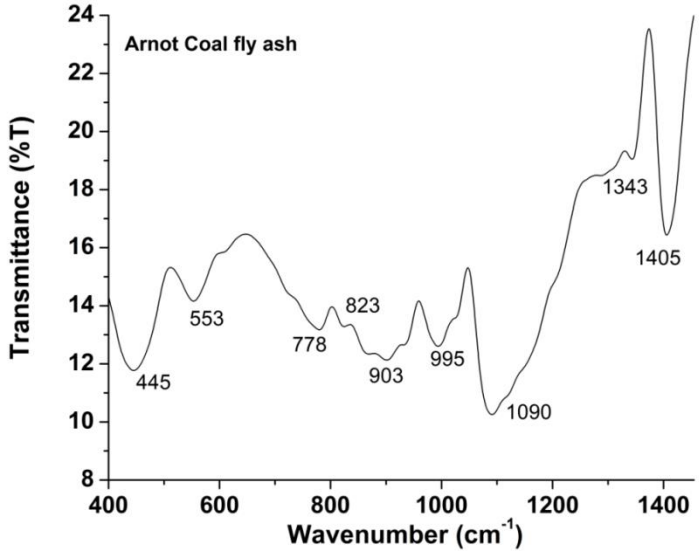

Figure 4.2: FTIR spectrum of as-received Arnot CFA.

FTIR vibrational band assignments for as-received Arnot CFA are listed in Table 4.3.

Table 4.3: FTIR vibrational band assignments of as-received Arnot CFA.

Wavenumber (cm^{-1})	Assignment
445	Si-O-T bending
553	Si-O-Al stretching (mullite)
778	Si-O-T symmetric stretching
823	
903	
995	Si-O-T asymmetric stretching
1090	
1343	Bicarbonates
1405	Carbonates

Vibrational bands associated with T-O vibrational modes were assigned as internal bending mode (445 cm^{-1}), symmetric stretching modes (553-823 cm^{-1}) and asymmetric modes (903-1090 cm^{-1}). The vibrational band at 823 cm^{-1} may also be due to the Si-OH stretching vibration. Vibrational bands observed at 445, 778, 823, 903, 995 and 1090 cm^{-1} are associated with vibrational T-O modes in quartz, while the band at 553 cm^{-1} is associated with vibrational T-O modes in mullite (Criado et al., 2007; Fernandez-Jimenez and Palomo, 2005). The broad T-O asymmetric stretching band at 1090 cm^{-1}, with a tail towards higher wavenumbers, indicates the dense nature of silicate (and aluminosilicate) species present in CFA (Böke et al., 2015; Livage, 1994). The strong vibrational band observed at 1405 cm^{-1}

was attributed to the presence of carbonate species in Arnot CFA (in particular, carbon-oxygen bonds), while the weak band at 1343 cm^{-1} may be associated with bicarbonate species (Miller and Wilkins, 1952).

4.2.4 Morphological analysis

The morphology of as-received CFA was characterised by SEM, as depicted in Figure 4.3.

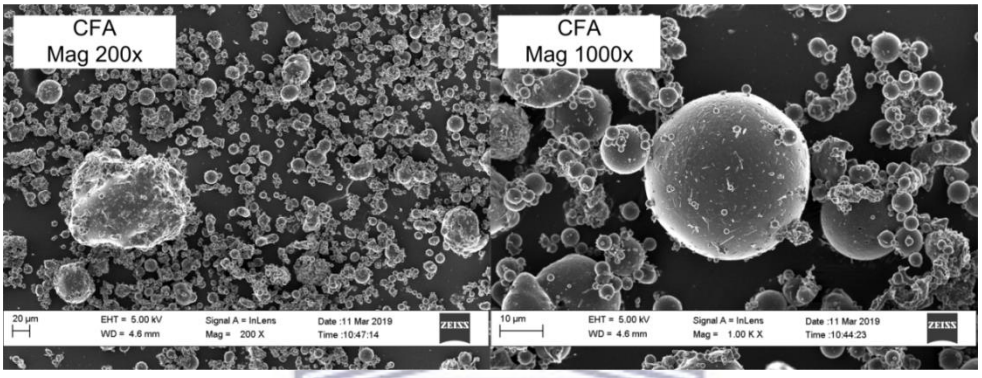

Figure 4.3: SEM micrograph of as-received Arnot CFA.

As-received Arnot CFA consisted of relatively large, irregularly shaped particles (60-175 µm) as well as spherical particles of varying particle size (0.5-40 µm), as depicted in Figure 4.3. The morphology of CFA depends on the thermal processes that take place during the combustion of coal; factors such as combustion temperature and post-combustion cooling rate all play a role in the resultant nature and morphology of CFA. The smooth outer appearance of these spherical particles in CFA is attributed to glass-like aluminosilicate coatings formed during the combustion process (Blissett and Rowson, 2012; Franus, 2012).

4.3 The preparation of the silicon extract from CFA

In this section, the preparation of the silicon extract (FASE) from CFA (as described in Section 3.3) will be discussed. The extraction process involved magnetic separation of iron-containing species from CFA resulting in the magnetic fraction (MF) and non-magnetic fraction (NMF). The FASE material was then prepared by low-temperature reflux of the NMF material with a NaOH solution, which yielded a solid residue (SR) and filtrate. The filtrate was subsequently used to precipitate the FASE material by H_2SO_4 addition. The characterisation of extraction products by XRF, ICP-MS, XRD, FTIR and SEM will be discussed in this section, to monitor changes in the elemental, mineralogical, structural and morphological properties of the material.

4.3.1 Magnetic separation of iron-containing components from CFA

The magnetic separation of iron-containing minerals from CFA was carried out by using a simple method, as described in Section 3.3.1. High levels of iron in the synthesis solution have been reported to cause the inhibition of zeolite ZSM-5 crystallisation (Li et al., 2013; Zhang et al., 2003). The magnetic fraction (MF) and non-magnetic fraction (NMF) collected after the process was characterised by XRF, ICP-MS, XRD, FTIR and SEM to evaluate the separation process.

4.3.1.1 Elemental analysis

The major elemental composition (calculated on a dry weight basis) of the NMF and MF material was characterised by XRF spectroscopy; results are listed in Table 4.4. The enrichment factor (EF) for each element was calculated (according to Equation 4.1) relative to the concentration of the element in the starting material (CFA); these results are also listed in Table 4.4.

$$Enrichment\ factor\ (EF) = {Quantity_x}/{Quantity_{x_{CFA}}} \quad \text{Eq (4.1)}$$

Table 4.4: Major elemental composition (dry weight) and enrichment factors (EF) for each element of the non-magnetic and magnetic fraction of CFA characterised by XRF spectroscopy (n = 3).

	Non-magnetic fraction			Magnetic fraction		
Major elements	wt%	Relative standard deviation	EF	wt%	Relative standard deviation	EF
SiO_2	57.88	0.31	1.02	31.06	2.32	0.55
Al_2O_3	29.86	0.36	1.08	14.88	1.02	0.54
Fe_2O_3	2.70	0.09	0.45	45.57	3.69	7.57
CaO	5.24	0.12	0.93	4.84	0.12	0.86
TiO_2	1.66	0.01	1.04	0.94	0.06	0.59
MgO	1.52	0.02	0.97	1.89	0.02	1.20
K_2O	0.61	0.00	1.06	0.28	0.02	0.48
P_2O_5	0.37	0.00	1.01	0.29	0.01	0.80
Na_2O	0.09	0.01	0.95	0.03	0.01	0.35
MnO	0.04	0.00	0.83	0.19	0.01	3.64
Cr_2O_3	0.02	0.00	0.89	0.02	0.00	1.04
Sum	100.00	-	-	100.00	-	-
SAR	0.97	-	-	1.04	-	-
L.O.I	8.03	0.20	-	0.40	0.28	-

The main constituents of the NMF material were SiO_2 and Al_2O_3 (> 70 wt%), as listed in Table 4.4. The elements Si, Al, Ti, K and P exhibited an EF > 1, which illustrated that these elements were enriched in the NMF compared to the starting material (CFA). On the other hand, other elements (such as Fe, Ca, Mg, Na, Mn and Cr) with an EF < 1 were reduced in concentration in the NMF compared to CFA. The MF material consisted of mainly iron oxides (45.57 wt%) as well as SiO_2 (31.06 wt%) and Al_2O_3 (14.88 wt%) that may have adhered to the magnetic particles during the separation process. Most of the elements (such as Si, Al, Ca, Ti, K, P and Na) were reduced in the MF material compared to CFA, while other elements (such as Fe, Mg, Mn and Cr) were enriched in the MF material compared to CFA. The elements Fe (EF = 7.57) and Mn (EF = 3.64) were highly enriched in the MF material compared to CFA. These results illustrated that the majority of the iron oxide minerals were therefore easily separated into the MF material from as-received CFA during this simple magnetic separation process, resulting in the NMF material that is largely free of iron oxide minerals.

The trace elemental composition of the NMF and MF materials was analysed by ICP-MS, as listed in Table 4.5. The enrichment factor (EF) for each trace element was calculated (according to Equation 4.1) relative to the concentration of the element in the starting material (CFA); results are listed in Table 4.5. Most of the trace elements in the NMF material (such as Ba, Sr, Zr, La, Nd, Y, Zn, Pb, Cu, Th, Nb, Rb, Sc, Pr, Sm, Gd, Dy, Hf, U, Er, Yb, Cs, Mo, Ta, Ho, Eu, Tb, Tm and Lu) exhibited an EF > 1, which illustrates that these elements were enriched in the NMF material compared to CFA. Other trace elements (such as Ce, V, Ni and Co) exhibited an EF < 1, which illustrates that these elements were reduced in concentration in the NMF material compared to CFA. Therefore, the majority of REEs (with the exception of Ce) were enriched in the NMF material by using the simple magnetic separation process to remove the iron-containing mineral phases (i.e. the MF material) from CFA. Furthermore, compared to the earth's crust, the REE content of NMF material is highly enriched (Rudnick and Gao, 2003). In the MF material, most of the trace elements (such as Ba, Sr, Zr, Ce, La, Nd, Y, Pb, Th, Nb, Rb, Sc, Pr, Sm, Gd, Dy, Hf, Er, Yb, Cs, Ta, Ho, Eu, Tb, Tm and Lu) exhibited an EF < 1, which illustrates that these elements were reduced in concentration in the MF material compared to CFA. On the other hand, trace elements such as V, Ni, Zn, Cu, Co, U, Mo exhibited an EF > 1, which illustrates that these elements were enriched in the MF material compared to CFA. It is noteworthy that the MF material

contained highly enriched levels of the transition metals Co (EF = 2.98), Ni (EF = 2.10), Mo (EF = 1.91), Zn (EF = 1.57) and Cu (EF = 1.41). The magnetic separation process may therefore serve as a simple procedure for concentrating REEs into the NMF material, while concentrating a specific set of transition metals (such as Fe, Mn, Co, Ni, Mo, Zn and Cu) into the MF material.

Table 4.5: Trace elemental composition and enrichment factors (EF) for each element of the non-magnetic and magnetic fraction of CFA characterised by ICP-MS (n = 3).

	Non-magnetic fraction			Magnetic fraction		
Trace elements	ppm	Relative standard deviation	EF	ppm	Relative standard deviation	EF
Ba	913.00	7.87	1.05	743.90	18.90	0.85
Sr	838.50	8.20	1.04	605.37	21.15	0.75
Zr	422.97	8.09	1.06	267.40	22.70	0.67
Ce	188.13	1.23	0.94	116.57	6.23	0.66
V	119.07	1.64	0.99	126.10	3.31	1.05
Ni	62.30	1.98	0.71	183.47	10.72	2.10
La	92.90	1.04	1.07	56.85	2.08	0.66
Nd	70.67	1.02	1.06	44.70	2.22	0.67
Y	67.91	0.49	1.09	45.98	1.22	0.73
Zn	59.20	0.88	1.17	79.70	4.75	1.57
Pb	50.00	1.41	1.18	26.49	2.27	0.63
Cu	47.97	4.06	1,15	58.83	16.01	1.41
Th	37.49	0.53	1.10	20.99	0.81	0.62
Nb	31.89	0.65	1.08	18.81	1.11	0.63
Rb	30.34	0.43	1.08	14.11	0.94	0.50
Sc	30.77	0.16	1.12	22.16	0.93	0.81
Co	21.96	0.52	0.88	74.37	4.37	2.98
Pr	19.48	0.10	1.08	12.10	0.63	0.67
Sm	13.78	0.47	1.05	8.78	0.62	0.67
Gd	12.48	0.52	1.10	8.29	0.51	0.73
Dy	12.19	0.12	1.10	7.96	0.39	0.72
Hf	11.45	0.19	1.06	7.43	0.53	0.68
U	9.70	0.19	1.04	9.59	0.17	1.03
Er	6.88	0.15	1.10	4.62	0.24	0.74
Yb	6.26	0.11	1.05	4.37	0.35	0.73
Cs	5.84	0.06	1.09	2.40	0.25	0.45
Mo	4.28	0.28	1.00	8.19	0.39	1.91
Ta	2.54	0.02	1.08	1.37	0.11	0.58
Ho	2.42	0.04	1.10	1.57	0.12	0.71
Eu	2.55	0.04	1.16	1.67	0.11	0.76
Tb	1.88	0.02	1.09	1.23	0.04	0.72
Tm	0.95	0.01	1.12	0.63	0.02	0.74
Lu	0.93	0.04	1.10	0.61	0.02	0.73

4.3.1.2 Mineralogical analysis

The mineralogical content of as-received CFA, MF and NMF was characterised by XRD, as depicted in Figure 4.4.

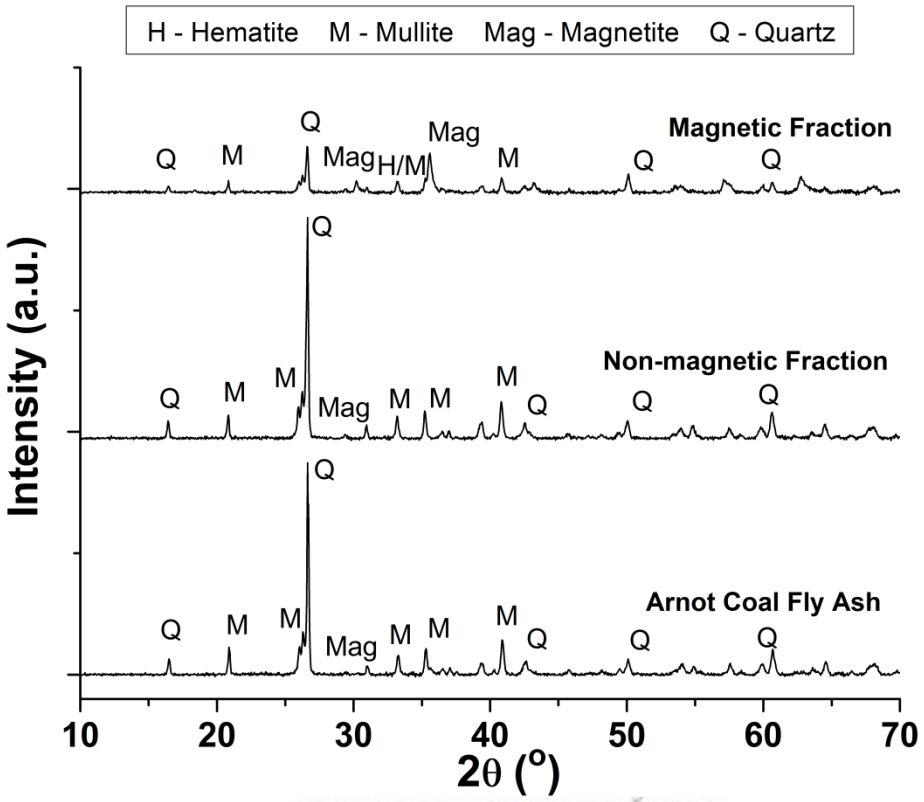

Figure 4.4: XRD diffraction patterns for Arnot CFA, magnetic fraction and non-magnetic fraction generated by magnetic separation.

The NMF material consisted of mainly quartz and mullite, as depicted in Figure 4.4, which compares well with the mineral content of as-received CFA. However, the presence of the diffraction peak associated with magnetite was still present in the NMF material. The MF material consisted of iron oxide minerals, magnetite (FeII and FeIII) and hematite (FeIII) (Ojha et al., 2004; Wdowin et al., 2014), as well as quartz and mullite minerals (which may have adhered to the magnetic particles during the separation process).

4.3.1.3 Structural analysis

The structural analysis of CFA, NMF and MF materials was characterised by FTIR spectroscopy, as depicted in Figure 4.5.

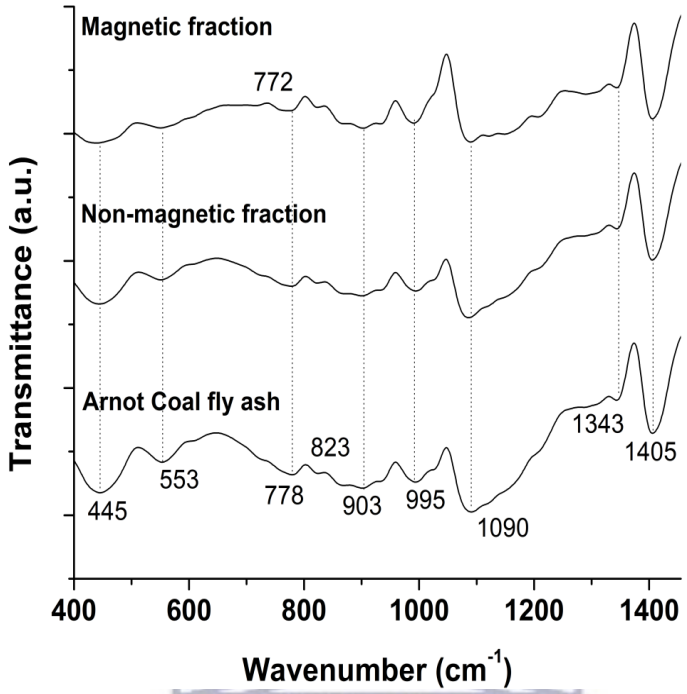

Figure 4.5: FTIR spectra of as-received Arnot CFA, magnetic fraction and non-magnetic fraction generated by magnetic separation.

FTIR vibrational bands, observed in Figure 4.5, for CFA, NMF and MF materials were similar due the presence of various silicate species (of the same degree of polymerisation) in these materials. FTIR vibrational band assignments for CFA, NMF and MF materials are summarised in Table 4.6.

Table 4.6: FTIR vibrational band assignments of as-received Arnot CFA, magnetic fraction and non-magnetic fraction generated by magnetic separation.

Wavenumber (cm^{-1})			
Arnot CFA	Non-magnetic fraction	Magnetic fraction	Assignment
445	445	445	Si-O-Si bending Fe-O stretching (FeIII)
553	553	554	Si-O-Al stretching (mullite) Fe-O stretching (FeIII)
778	778	772	Si-O-T symmetric stretching
823	821	821	
903	903	903	Si-O-T asymmetric stretching
995	995	991	
1090	1084	1090	
1343	1346	1345	Bicarbonates
1405	1405	1405	Carbonates

The presence of iron oxide was not clearly detected by IR. FTIR vibrational bands for Fe-O stretching modes in iron (III) oxide species in hematite and magnetite typically appear at 445 and 553 cm^{-1}, which corresponds to the Si-O-T bending and Si-O-Al stretching vibrational modes associated with quartz and mullite (Nasrazadani and Raman, 1993; Ojha et al., 2004).

4.3.1.4 Morphological analysis

The morphology of the MF and NMF materials generated by the magnetic separation process was characterised by SEM and compared to that of as-received Arnot CFA, as depicted in Figure 4.6.

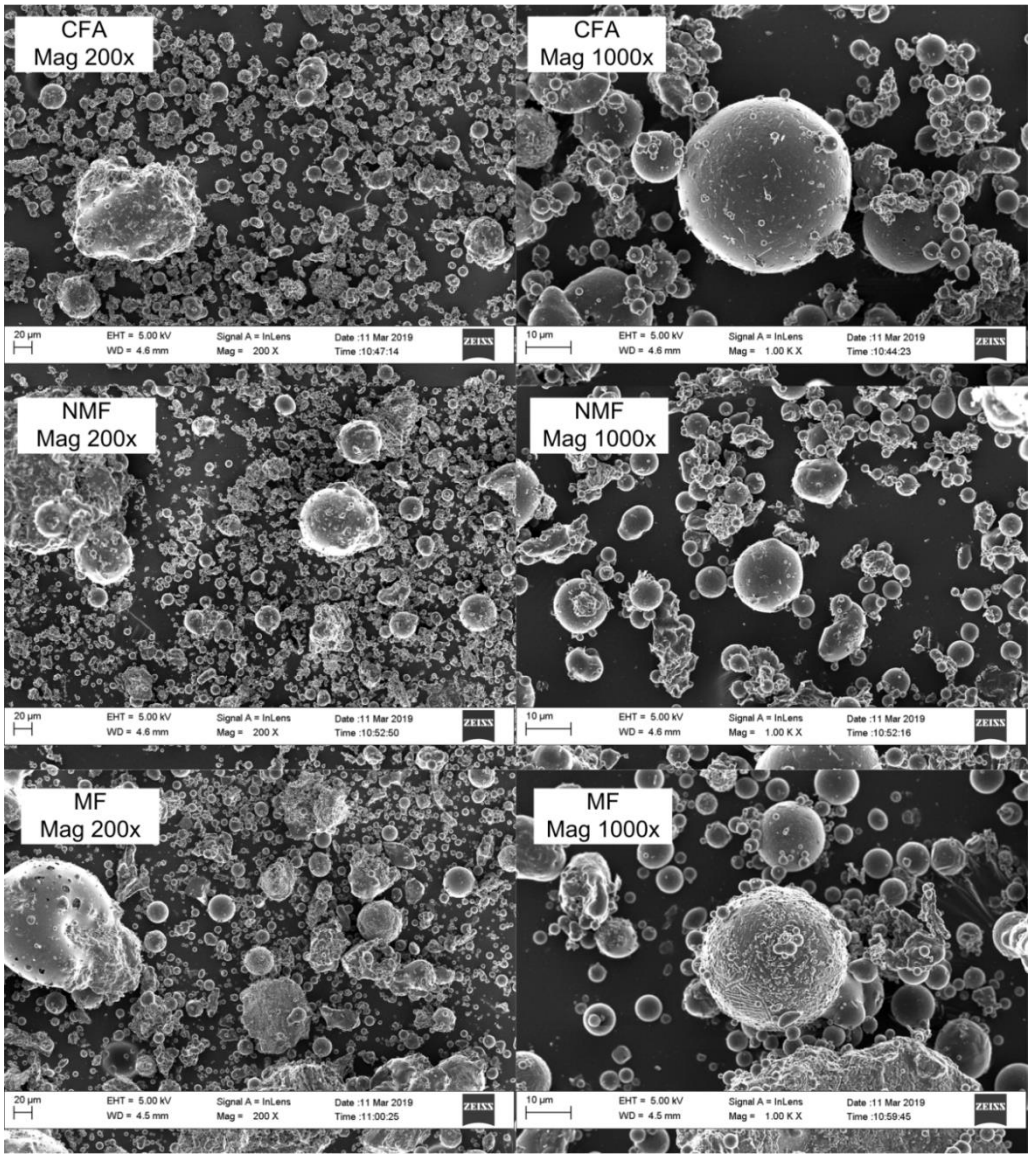

Figure 4.6: SEM micrograph of as-received Arnot CFA, Magnetic fraction and Non-magnetic fraction generated by magnetic separation.

As expected, the morphology of the NMF material was comparable to the morphology of as-received Arnot CFA; both spherical and irregularly shaped particles were observed in Figure 4.6. The morphology of the MF material also resembled that of CFA, this is due to the presence of a significant amount of quartz in the MF material (as determined by XRD in Figure 4.4). The presence of aggregated, rod-like structures (thought to be iron oxide particles) on the surface of CFA particles in the MF material was observed in Figure 4.6. Furthermore, the presence of large, hollow-sphere CFA particles containing relatively smaller CFA particles (some of which may be magnetic particles) was also observed in the MF material. These factors may account for the significant amount of silicon oxide (quartz) observed in the magnetic fraction of CFA (as determined by XRF and XRD in Table 4.4 and Figure 4.4, respectively).

Semi-quantitative EDS analysis was carried out to determine the average elemental composition of as-received Arnot CFA, MF and NMF materials; 10 spots were analysed in different sites of the samples and results are listed in Table 4.7. The elemental composition of CFA and NMF were relatively similar, as depicted in Table 4.7, with the exception of iron and titanium that was reduced in the NMF material. The main constituents of the MF material were iron, silicon and aluminium. These results correspond well with the major elemental composition determined by XRF spectroscopy (as listed in Table 4.4).

Table 4.7: Average elemental composition of as-received Arnot CFA, Magnetic fraction and Non-magnetic fraction generated by magnetic separation characterised by EDS (10 spots).

	Average elemental composition (wt%)		
Element	CFA	Non-magnetic fraction	Magnetic fraction
Si	47.04	54.35	29.63
Al	34.51	33.11	18.71
Fe	6.17	3.24	40.97
Ca	5.95	4.77	7.43
Ti	4.14	2.89	0.93
K	1.28	1.08	0.22
Mg	0.70	0.55	1.94
S	0.20	-	0.07
Na	-	-	0.10

During the magnetic separation process, the majority of iron-containing mineral phases were removed from the bulk of the CFA to yield the NMF material. However, the presence of

some silicon-containing minerals was observed in the MF material. The adherence of magnetic particles to silicon-containing minerals may have been a contributing factor to this effect, as discussed previously. The magnetic separation process resulted in a high mass yield of the NMF material (~91.6 %) and a relatively lower mass yield of the MF material (~8.4 %), which corresponds to an Fe recovery of 63.6 %. The efficiency of the iron removal process in this study was therefore improved compared to a study in literature, which reported an Fe recovery of 26 % from South African CFA using a similar magnetic separation process (Sedres, 2016). However, a highly efficient magnetic separation was reported by Gilbert, (2013) using similar methodology, with an Fe recovery of 82 %. Repeated magnetic separation and/or further washing of the MF material may reduce the amount of silicon in the MF material and improve the Fe recovery. The MF material may be utilised for the recovery of iron for the preparation of nano-iron, for example, as reported in literature (Gilbert, 2013). However, this was not within the scope of this study. The NMF material was used in subsequent experiments for the extraction of silicon.

4.3.2 Extraction of the silicon precursor (FASE) from CFA

The extraction of silicon (for zeolite synthesis) from the NMF material of CFA was carried out by low-temperature reflux under alkaline conditions, followed by filtration to collect the dissolved silicate species and subsequent precipitation to form the solid silicon-containing precursor (FASE), as described in Section 3.3.2. The products of the silicon extraction such as FASE and the solid residue (SR) were characterised by XRF, ICP-MS, XRD, FTIR and SEM.

4.3.2.1 Elemental analysis

The major elemental composition (calculated on a dry weight basis) of the FASE and SR material collected after silicon extraction was characterised by XRF spectroscopy and EF values for each element was calculated according to Equation 4.1 relative to CFA; results are listed in Table 4.8.

Table 4.8: Major elemental composition (dry weight) and enrichment factors (EF) for each element of the fly ash silicon extract and solid residue characterised by XRF spectroscopy (n = 3).

	Fly ash silicon extract			Solid Residue		
Major elements	wt%	Relative standard deviation	EF	wt%	Relative standard deviation	EF
SiO_2	70.70	2.50	1.25	40.02	0.97	0.71
Al_2O_3	0.49	0.14	0.02	26.83	1.21	0.97
Fe_2O_3	0.02	0.01	0.00	2.19	0.04	0.36
CaO	0.05	0.02	0.01	4.92	0.03	0.88
TiO_2	0.07	0.02	0.05	1.50	0.06	0.94
MgO	b.d.l	b.d.l	0.00	1.39	0.03	0.88
K_2O	0.45	0.11	0.78	0.39	0.07	0.68
P_2O_5	0.03	0.01	0.09	0.13	0.00	0.35
Na_2O	28.18	1.56	295.25	22.56	1.27	236.37
MnO	b.d.l	b.d.l	0.00	0.04	0.00	0.77
Cr_2O_3	b.d.l	b.d.l	0.00	0.02	0.00	0.89
Sum	100.00	-		100.00	-	-
SAR	71.66	-		0.75	-	-
L.O.I	7.23	2.18		18.59	1.12	-

*b.d.l – below detection limits of instrument

Both the FASE and SR materials were highly hygroscopic in nature as indicated by the significant L.O.I values of 7.23 and 18.59 wt%, respectively, as listed in Table 4.8. The FASE material was composed of mainly silicon and sodium oxides (70.70 and 28.18 wt%, respectively) with a low aluminium oxide content (0.49 wt%). The FASE material also contained 0.45 wt% of potassium oxide, while other oxides were below the detection limits of the instrument or present in very small quantities. The main element enriched in the FASE material (by the alkaline activation and precipitation of silicon process) was Si with an EF value of 1.25, as listed in Table 4.8. It is noteworthy that Na exhibited an EF value of ~295, due to the addition of NaOH during the alkaline reflux process. The other elements (such as Al, Fe, Ca, Ti, Mg, K, P, Mn and Cr) were reduced in the FASE material compared to CFA (most of which exhibited EF values << 1). It is noteworthy that the FASE material is nearly free of iron (0.02 wt%) and aluminium (0.49 wt%), as listed in Table 4.8, with a SAR value of ~72 that makes it a suitable feedstock for high-silica zeolite synthesis.

The SR material was composed of mainly silicon, aluminium and sodium oxides (40.02, 26.83 and 22.56 wt%, respectively) and also contained a considerable amount of calcium

oxide (4.92 wt%). The SR material was also highly enriched with Na (EF value of ~236) due to the addition of NaOH during the alkaline reflux process. The SAR value of the SR material was 0.75, which makes the SR material a suitable material for the synthesis of aluminium-rich zeolites such as zeolite A, X and sodalite. As listed in Table 4.8, most of the major elements from the NMF material (such as Al, Ca, Ti, Mg, K, Mn and Cr) were retained in the SR material, while most of these elements were excluded from the FASE material or present in very small quantities.

The alkaline reflux process therefore yielded a highly siliceous material (FASE) that was mainly composed of the element of interest (namely silicon) and was nearly free of aluminium and iron. The FASE material also exhibited a relatively high SAR value of ~72, which is more than 70 times the SAR value of CFA (as listed in Table 4.1). This is important to enable easy tailoring of the molar composition of synthesis mixtures that may utilise a CFA-derived silicon feedstock; particularly in the case of high-silica zeolites. The dissolution and precipitation of the FASE material from the NMF using the relatively low-temperature, alkaline reflux method was therefore thought to be successful.

The trace elemental composition of the FASE and SR material collected after silicon extraction was analysed by ICP-MS, as listed in Table 4.9. The EF value for each trace element was calculated (according to Equation 4.1) relative to the concentration of the element in the starting material (CFA); results are listed in Table 4.9. In general, the trace elemental composition of the SR material was relatively high compared to the trace elemental composition of the FASE material, as listed in Table 4.9. In the FASE material, particular trace elements such as Dy, Er, Eu, Gd, Nd, Sm, Tb, Tm and Yb were below the detection limits of the instrument. However, it is noteworthy that most of the trace elements exhibited an EF value < 1 for both the FASE material and the SR material compared to CFA, with a few exceptions. In the SR material, trace elements such as Zr and REEs (Ce and Hf) were enriched compared to CFA (with an EF >1), as listed in Table 4.9. It is noteworthy that these trace elements (Zr, Ce and Hf) were also enriched in the SR material compared to the NMF material. These results illustrate that most of the trace elements present in the NMF material were retained in the SR material in comparison to the FASE material. However, these trace elements may also have been present in the filtrate generated during precipitation of the silicon feedstock (FASE). The SR material contains relatively enriched levels of REEs

compared to the earth's crust (Rudnick and Gao, 2003). However, the highest enrichment of REEs was observed for the NMF material, as listed in Table 4.5.

Table 4.9: Trace elemental composition and enrichment factors (EF) for each element of the fly ash silicon extract and solid residue was characterised by ICP-MS (n = 3).

	Fly ash silicon extract			Solid residue		
Trace elements	ppm	Relative standard deviation	EF	ppm	Relative standard deviation	EF
Ba	47.60	11.40	0.05	751.40	30.46	0.86
Sr	3.76	0.94	0.00	688.27	35.05	0.85
Zr	84.40	8.20	0.21	492.67	20.16	1.23
Ce	0.57	0.02	0.00	259.13	18.13	1.48
V	28.55	6.95	0.16	28.01	1.56	0.16
Ni	6.05	0.16	0.05	48.57	2.67	0.41
La	0.10	0.00	0.00	75.37	4.53	0.86
Nd	0.00	0.00	0.00	57.73	3.37	0.67
Y	0.09	0.04	0.00	56.06	3.84	0.84
Zn	57.65	33.35	0.92	30.33	3.52	0.48
Pb	38.20	0.20	0.75	20.73	6.82	0.41
Cu	10.48	1.53	0.25	41.16	4.96	0.97
Th	0.03	0.00	0.00	30.35	2.20	0.73
Nb	2.12	1.05	0.06	25.14	1.37	0.74
Rb	13.91	3.15	0.47	9.26	0.85	0.31
Sc	3.48	0.38	0.12	23.93	1.03	0.85
Co	0.59	0.11	0.02	16.72	1.00	0.61
Pr	0.01	0.00	0.00	15.89	0.97	0.64
Sm	b.d.l	b.d.l	0.00	11.09	0.69	0.61
Gd	b.d.l	b.d.l	0.00	10.09	0.58	0.77
Dy	b.d.l	b.d.l	0.00	10.05	0.46	0.88
Hf	2.16	0.18	0.20	12.98	0.62	1.18
U	1.68	0.90	0.15	7.29	0.94	0.67
Er	b.d.l	b.d.l	0.00	5.70	0.31	0.61
Yb	b.d.l	b.d.l	0.00	5.38	0.41	0.86
Cs	2.01	0.59	0.34	1.33	0.36	0.22
Mo	1.09	0.35	0.20	0.96	0.13	0.18
Ta	0.35	0.14	0.08	1.97	0.12	0.46
Ho	0.01	0.00	0.00	1.88	0.18	0.80
Eu	b.d.l	b.d.l	0.00	2.07	0.17	0.94
Tb	b.d.l	b.d.l	0.00	1.55	0.09	0.70
Tm	b.d.l	b.d.l	0.00	0.83	0.05	0.49
Lu	0.02	0.00	0.02	0.80	0.07	0.93

The low-temperature, alkaline reflux method for the preparation of a silicon precursor material (for utilisation in zeolite synthesis) therefore serves as a dissolution step (for quartz and mullite mineral phases in the NMF material) as well as a purification step (by which many impurities from CFA are excluded from the silicon precipitate formed during the silicon extraction process).

4.3.2.2 Mineralogical analysis

The mineral content of the products of the silicon extraction process (FASE and SR) were characterised by XRD, as depicted in Figure 4.7, and compared to the NMF material.

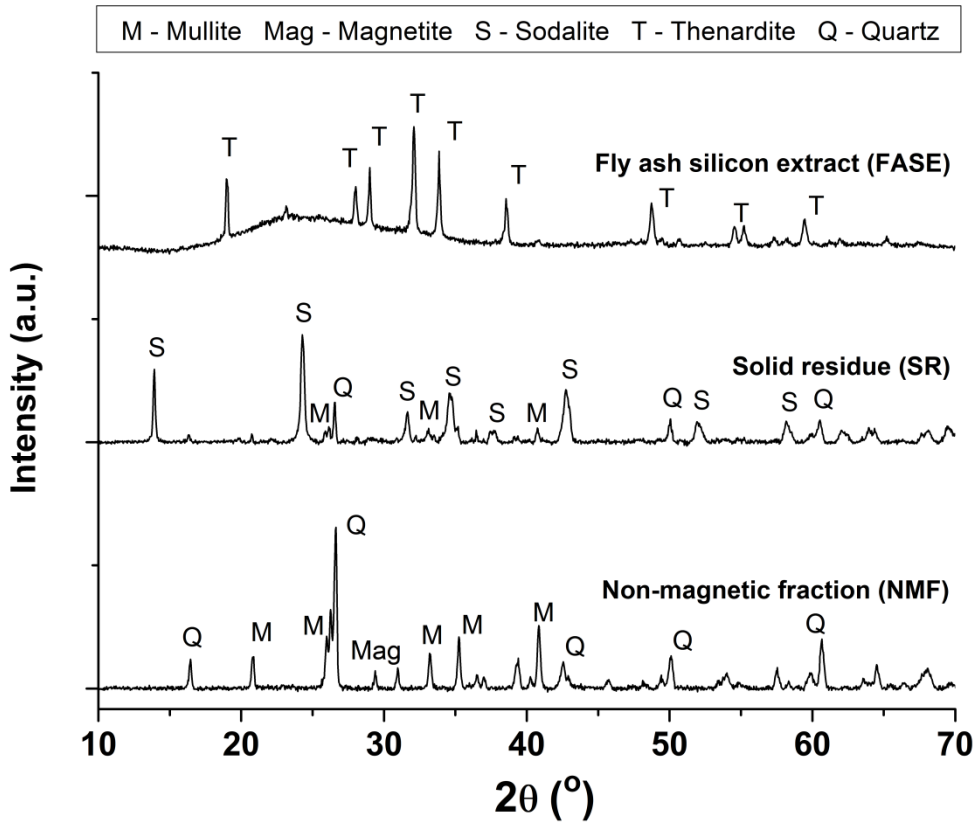

Figure 4.7: XRD diffraction patterns of fly ash silicon extract and solid residue generated during the silicon extraction process from the NMF material.

As depicted in Figure 4.7, the FASE material consisted of amorphous silica (observed between 2θ values of 15 and 35°) as well as the crystalline mineral phase Thernadite composed of $Na_2(SO_4)$ (Brichni et a., 2016; Lafuente et al., 2015). The presence of Thernadite is as a result of the precipitation of the FASE material from a high sodium, aqueous solution by using H_2SO_4. The diffraction pattern of the SR material (that remained

after the silicon extraction process) mainly contained diffraction peaks at 2θ values of ~13.9, 24.3, 31.5, 34.6, 37.7 and 42.8° corresponding to synthetic sodalite as well as minor diffraction peaks associated with quartz and mullite (Criado et al., 2007; Fernandez-Jimenez and Palomo, 2005; Treacy and Higgins, 2007). This indicates that quartz and mullite present in the NMF material of CFA was highly susceptible to dissolution under the alkaline, reflux conditions used in this study (150 °C for 24 hours); and could also be directly converted to a low-silica zeolite such as sodalite. The more soluble silicate (and aluminosilicate) species dissolved into aqueous solution and was precipitated to yield the FASE material containing mainly amorphous silica, while other silicon species remaining in the solid residue underwent further dissolution and condensation reactions during the alkaline, reflux process (as described in Section 3.3.2) to yield the crystalline sodalite product.

4.3.2.3 Structural analysis

The structural analysis of NMF, FASE and SR materials were characterised by FTIR spectroscopy, as depicted in Figure 4.8; which shows (a) full FTIR spectra as well as (b) a closer look at the wavenumber range corresponding to asymmetrical T-O stretching bands.

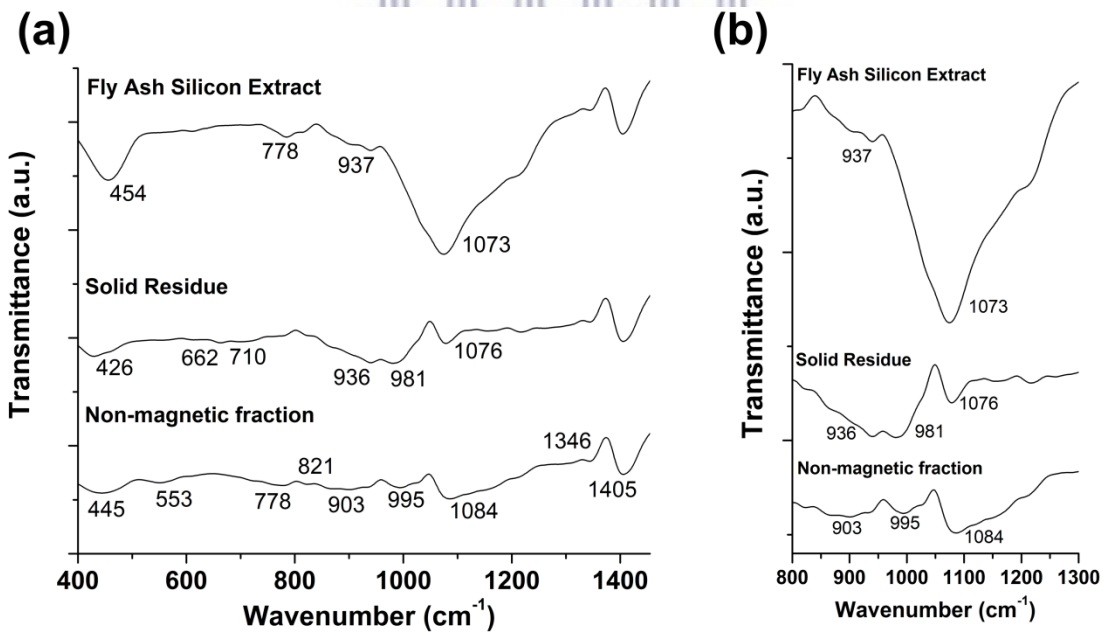

Figure 4.8: FTIR spectra of Non-magnetic fraction, Fly ash silicon extract and Solid residue generated during the silicon extraction process (a) 1400-400 cm^{-1} and (b) 1300-800 cm^{-1}.

The FASE and SR materials exhibited FTIR vibrational spectra that were different from that of the NMF material, as depicted in Figure 4.8; the presence of carbonate species (1405 cm^{-1})

was the main similarity observed in these materials. This illustrates a significant change in the structural order of silicate and aluminosilicate species in these materials; these differences are clearly illustrated in Figure 4.8 (b) which shows the presence of different asymmetrical T-O stretching bands. FTIR vibrational band assignments are listed in Table 4.10.

Table 4.10: FTIR vibrational band assignments of Non-magnetic fraction, Fly ash silicon extract and Solid residue materials.

Wavenumber (cm^{-1})			
Non-magnetic fraction	Fly ash silicon extract	Solid residue	Assignment
445	454	426	Si-O-T bending
553	-	-	Si-O-Al stretching (mullite)
-	-	662	
778	778	710	Si-O-T symmetric stretching
821	-	-	
903	937	936	Si-OH asymmetric stretching
995	-	981	Si-O-T asymmetric stretching
1084	1073	1076	
1346	1346	1346	Bicarbonates
1405	1405	1405	Carbonates

The FASE material contained four main vibrational bands at 454, 778, 937 and 1073 cm^{-1}. These vibrational bands are all attributed to T-O vibrational modes in amorphous silica present in the FASE material. The vibrational band at 454 cm^{-1} is attributed to bending vibrations in T-O bonds, while the vibrational band at 778 cm^{-1} may be due to Si-OH stretching or symmetric T-O stretching. The broad, asymmetric T-O stretching vibrational ranging between wavenumbers of 1250 and 850 cm^{-1} indicates the presence of silicate species of varying degrees of polymerisation in the FASE material, as depicted in Figure 4.8 (b). This broad vibrational band was centred at 1073 cm^{-1}, which indicates that mainly $SiO(OH)_3^-$ silicate species are present in the FASE material (Silva et al., 2012; Yang et al., 2008). The medium vibrational band at 937 cm^{-1} is associated with asymmetric stretching of T-OH bonds in relatively less condensed silicate species such as monomeric $Si(OH)_4$ silicate species (Silva et al., 2012).

As observed in Figure 4.8, the SR material contained five main vibrational bands at 426, 662, 710, 936, 981 and 1076 cm^{-1}. The T-O bending (426 cm^{-1}), T-O symmetric stretching (662 cm^{-1}) and T-O asymmetric stretching (936-1076 cm^{-1}) vibrational bands were observed

for the SR material. These bands appeared at a relatively lower wavenumber in the SR material due to the presence of aluminium in this material (Fernandez-Jimenez and Palomo, 2005). The FTIR vibrational spectrum of the SR material was similar to that of sodalite reported in literature (Criado et al., 2007). Vibrational bands observed in the SR material are therefore mainly attributed to T-O vibrational modes in sodalite and to a lesser extent quartz, since the 1076 cm^{-1} vibrational band was weakened as observed in Figure 4.8 (b).

4.3.2.4 Morphological analysis

The morphology of the FASE and SR materials generated by the silicon extraction process was characterised by SEM and compared to that of the NMF material, as depicted in Figure 4.9.

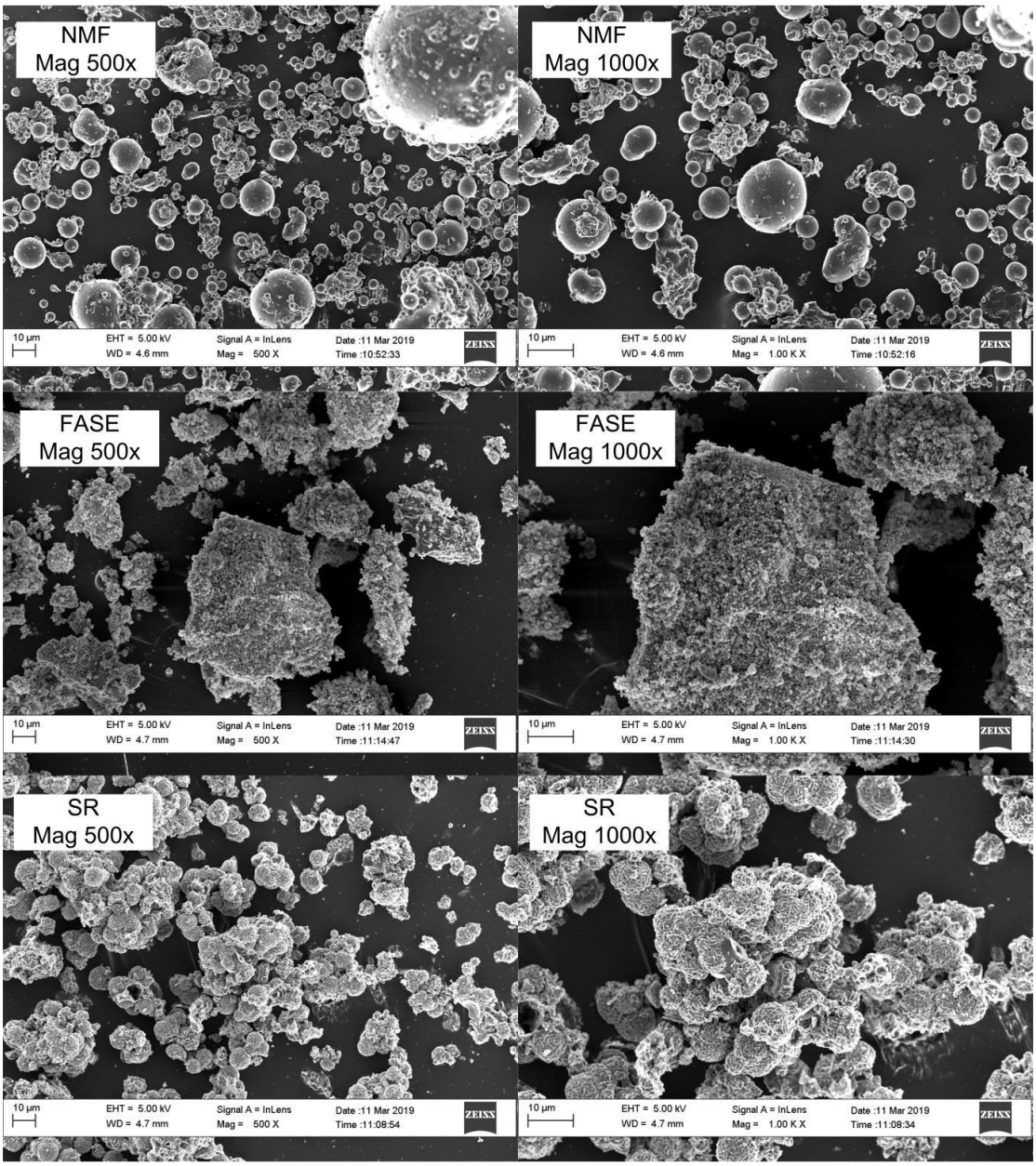

Figure 4.9: SEM micrograph of Non-magnetic fraction, Fly ash silicon extract and Solid residue.

The morphology of the FASE material was irregular in shape and varying particle sizes were observed, as depicted in Figure 4.9. The relatively larger FASE particles (7-100 µm) were composed of agglomerated smaller particles (0.1-0.3 µm). The SR material exhibited the typical morphology of sodalite. A closer look at the morphology of the SR material (sodalite) is depicted in Figure 4.10.

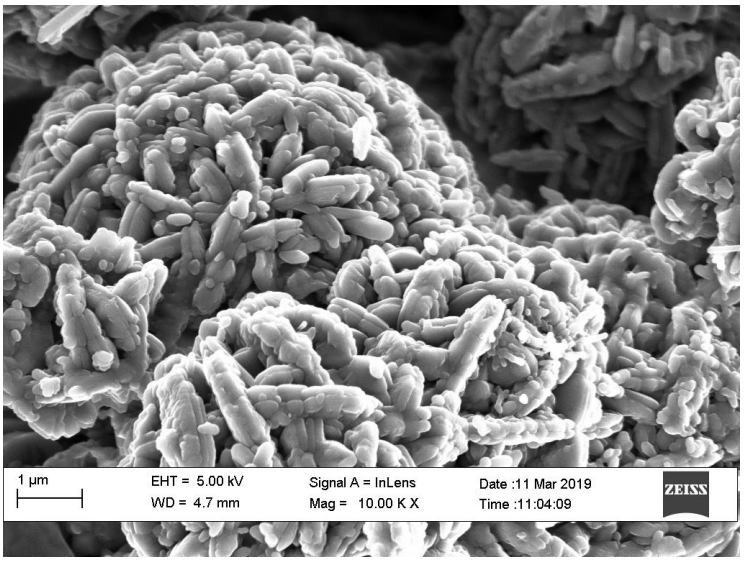

Figure 4.10: SEM micrograph of the Solid residue material at 10000x magnification.

As depicted in Figure 4.10, the SR material consisted of intergrown platelets that agglomerate in a spherical manner (Li et al., 2015; Luo et al., 2016; Reyes et al., 2013). These sodalite particles exhibited an average particle size of ~6.7 µm, confirming the direct formation of a zeolite mineral phase. Semi-quantitative EDS analysis of the NMF, FASE and SR materials were carried out; results are listed in Table 4.11.

Table 4.11: Average elemental composition of the Non-magnetic fraction, Fly ash silicon extract and Solid residue characterised by EDS (10 spots).

	Average elemental composition (wt%)		
Element	Non-magnetic fraction	Fly ash silicon extract	Solid residue
Si	54.35	69.92	30.55
Al	33.11	0.22	25.81
Ca	3.24	-	7.44
Fe	4.77	0.06	3.97
Ti	2.89	-	2.67
K	1.08	0.24	0.05
Mg	0.55	-	1.50
S	-	9.45	-
Na	-	20.12	27.72
Zr	-	-	0.29
SAR	1.6	317.8	1.2

The FASE material was mainly composed of silicon and sodium, as listed in Table 4.11. The presence of a minor quantity of sulphur in the FASE material was detected by EDS; this may indicate the presence of sulphates in this material due to the precipitation of the silicon feedstock (FASE) using sulphuric acid. The SR material contained mainly silicon, aluminium and sodium, which is typical of zeolitic materials. The presence of other elements in the SR material such as Ca, Fe, Ti, Mg, Zr and K were also detected by EDS. The SR material possessed a SAR value of 1.2, which compares well with the SAR value of sodalite (1.0) reported in literature (Herreros et al., 1994; Treacy and Higgins, 2007). Compared to elemental analysis carried out by XRF (as listed in Table 4.8), the average elemental composition determined by semi-quantitative EDS corresponded reasonably well for major elements; differences observed between the two analytical techniques are thought to be due to the relatively lower sensitivity of the EDS technique compared to XRF spectroscopy. These results illustrate that the low-temperature, alkaline reflux method (150 °C for 24 hours) not only directly yielded a zeolite product (namely sodalite) but was also suitable for the preparation of the silicon extract that is highly siliceous and free of most of the other components of CFA. It is noteworthy that this method does not require the use of the additional oxalic acid purification step for the preparation of a highly siliceous CFA silicon extract (Missengue et al., 2017; Missengue, 2018; Ndlovu, 2016). Furthermore, the utilisation of the high-temperature, alkaline activation fusion step or the addition of an aluminium source was not required for the crystallisation of zeolite sodalite.

Compared to standard silica sources used in zeolite synthesis (such as sodium silicate solution, fumed silica and Ludox AS-40 colloidal silica), the FASE material contained relatively high Na content and was composed of relatively large silica particles. Sodium silicate solution is prepared by the dissolution of a silica source in an alkaline solution and typically contains high silica content (45.5 wt%) and varying sodium content (10-51 wt%) depending on the method of preparation. Fumed silica consists of amorphous silica particles with high purity (99.8 wt%) and an average particle size of 0.012-0.3 µm. Colloidal silica (such as Ludox AS-40) is made up of a ~40 wt% silica suspension in deionised water and contains less than 0.10 wt% Na and 0.02 wt% sulphates; the colloidal silica particles exhibit an average particle size of 20-24 nm (Isa et al., 2018; Iwakai et al., 2011; Kamil et al., 2015; Krznaric et al., 2003; Mitra et al., 2002).

The particle size of the FASE material compares well with that of fumed silica. However, FASE particles were present as large agglomerates of relatively small particles which may affect the rate of silica dissolution. Consequently, the rate of crystallisation of zeolites from this CFA-derived silicon precursor may be affected. Furthermore, the high Na content in the FASE material may also influence zeolite crystallisation process. Nevertheless, the FASE material contains high silica content and is derived from a waste material (CFA) which makes it a favourable starting material for potential utilisation in the synthesis of high-silica zeolites such as ZSM-5 and mordenite as well as silicalite-1.

4.4 Process overview and zeolite yields from the conversion of fly ash derived silicon extract to high-silica zeolites

In this section, the preparation of the FASE material (that will serve as a silica source for zeolite synthesis presented in subsequent chapters) from CFA will be compared to other silicon extraction methods utilised for the synthesis of high-purity zeolites from CFA. An overview of the conversion of CFA to pure, high-silica zeolites (further discussed in Chapter 5 and 6) and low-purity sodalite is illustrated in Figure 4.11.

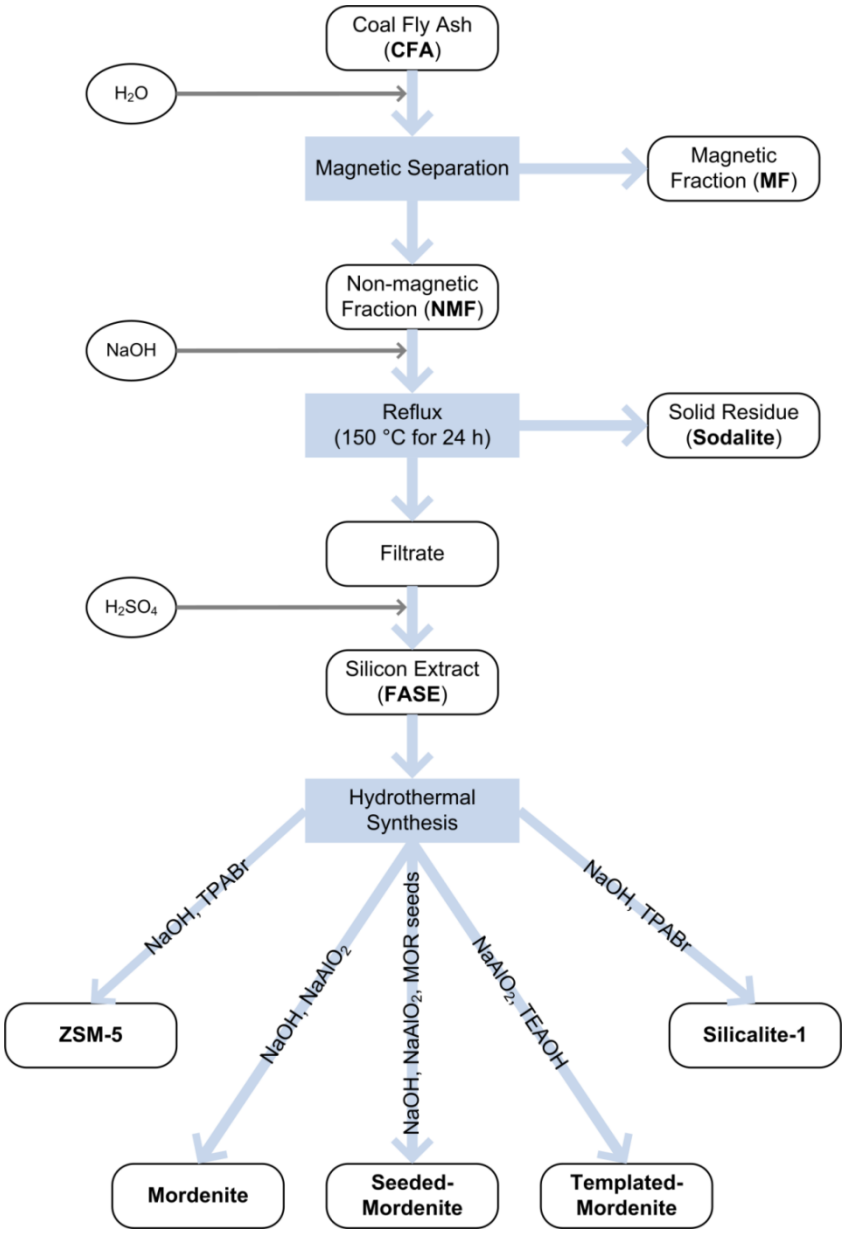

Figure 4.11: An overview of the conversion of CFA to high-silica zeolite via low-temperature silicon extraction.

Under the conditions utilised in this study, a highly siliceous extract was prepared from CFA by a relatively low-temperature alkaline reflux for potential utilisation in the synthesis of high-silica zeolitic materials such as zeolite mordenite (Chapter 5) as well as ZSM-5 and silicalite-1 (Chapter 6), as depicted in Figure 4.11. The solid residue collected by filtration after the low-temperature alkaline reflux treatment was observed to be low-purity sodalite. Sodalite is a small-pore zeolitic material that has application in cation exchange as well as gas adsorption (Henmi, 1987; Li et al., 2015; Luo et al., 2016; Shoumkova and Stoyanova, 2013). Sodalite synthesised in this manner contained a range of elements as listed in Table 4.8 and 4.9, which may influence the application of this material. This material is therefore thought to be more suited to gas adsorption applications where contamination of the gas feed stream is not likely to occur. The direct formation of sodalite as the "solid residue" makes this process for silicon extraction from CFA (for high-silica zeolite synthesis) an almost zero-waste method. Further optimisation of the direct conversion of CFA to sodalite may be useful for the preparation of pure phase sodalite; however, this aspect fell outside the scope of this study.

The FASE material was further utilised as a silicon precursor in the synthesis of high-silica zeolites (to be presented in detail in Chapter 5 and 6). A sample material of each synthesised zeolite (see Chapter 5 and 6) was chosen to calculate the zeolite yield (in grams per kg of CFA) and percentage zeolite yield (based on SiO_2 added to the synthesis mixture as the FASE material) according to Equation 4.2 and Equation 4.3, respectively; results are listed in Table 4.12.

$$Zeolite\ yield\ (based\ on\ CFA\ input) = {Mass\ (g)_{Zeolite}}/{1\ kg_{CFA}} \quad \text{Eq (4.2)}$$

$$Zeolite\ yield\ (based\ on\ SiO_2\ input) = {Zeolite_{Output}}/{SiO_{2_{Input}}} \times 100\ \% \quad \text{Eq (4.3)}$$

Table 4.12: Zeolite yields for high-silica zeolites (per kg of CFA and based on SiO_2 input) synthesised from FASE.

Zeolite (sample code)	Zeolite yield (g/kg CFA)	% Zeolite yield (based on SiO_2 input)
Zeolite ZSM-5 (Zeo03)	162	64
Zeolite mordenite (Mor17)	94	37
Zeolite mordenite-seeded (Mor38)	102	40
Zeolite mordenite-templated (Mor55)	157	62
Silicalite-1 (Sil01)	95	37
Sodalite (SR)	972	~100

The percentage zeolite yield (based on SiO_2 input) ranged between 37 and 100 %, as listed in Table 4.12. The conversion of SiO_2 to sodalite is reported as ~100 %, since a minor quantity of unconverted quartz was still present in the material. On the other hand, the conversion of SiO_2 (from the FASE material) into high-silica zeolites was relatively low (37-64 %). In some cases (for example Mor17, Mor38 and silicalite-1 synthesis) a substantial amount of SiO_2 wastage occurred. In the case of mordenite synthesis, this may be attributed to the low aluminium content of the FASE material. In the case of Mor38 synthesis, the addition of seed crystals did not have a significant impact on the zeolite yield. It is noteworthy that the presence of an OSDA agent in the synthesis mixture improved the conversion process (of FASE to zeolites) and enhanced the percentage zeolite yield for zeolite mordenite Mor55 (62 %) as well as zeolite ZSM-5 Zeo03 (64 %). OSDA agents have an important role in zeolite synthesis; these compounds are responsible for the organisation of silicon and aluminium oxide tetrahedra into specific building units for zeolite formation (Burton and Zones, 2007; Yu, 2007). In this study, increased feedstock (SiO_2 from FASE) utilisation occurred as a result of the presence of an OSDA agent in the synthesis mixture.

In terms of CFA utilisation and conversion, the yield of high-silica zeolites is low (94-162 g/kg CFA) compared to the yield of sodalite (972 g/kg CFA), as observed in Table 4.12. Compared to literature, the yield of high-silica zeolites with high purity from the CFA-derived FASE material is relatively low compared to the yield of low-silica zeolites synthesised from CFA. Higher zeolite yields (300-560 g/kg CFA) have been reported for the synthesis of zeolites A, P and X from CFA by using solid alkali fusion at high temperatures (830-850 °C) for the preparation of a clear solution containing silica and alumina, which was subsequently utilised in zeolite synthesis (Yaping et al., 2008). This high-temperature method

for the conversion of CFA to zeolites is more suited to the preparation of low-silica zeolites, since the clear solution contains high aluminium content and would require further processing for utilisation as a starting material in high-silica zeolite synthesis. The yield of high-purity zeolite P synthesised from CFA in a two-step process using low-temperature silicon extraction was reported as 85 g/kg CFA (Hollman et al., 1999). This low-temperature process is more comparable to the silicon extraction process utilised in this study and the yield of high-purity, high silica zeolites from the FASE material extracted from CFA is comparable and slightly improved compared to the yield of zeolite P reported by Hollman et al., (1999). These studies illustrate the compromise that exists between utilisation of high-temperature alkaline CFA treatment methods (which results in high conversion of CFA to high-aluminium zeolites) and a low-temperature alkaline CFA treatment method (whereby a silicon-rich precursor is generated suitable for high-silica zeolite synthesis).

The silicon extraction process utilised in this study resulted in a highly siliceous material that was used in the synthesis of highly pure, high-silica zeolites from a waste feedstock; with an appreciable zeolite yield (up to 162 g/kg CFA). The purity of these high-silica zeolites allows for the application of these materials in various industries such as the petroleum or fine chemical industry. However, further optimisation of the extraction and conversion process of the FASE material into high-silica zeolites is possible to achieve higher yields and consequently, avoid wastage of feedstock SiO_2. The silicon extraction process also resulted in the formation of a high yield of sodalite (972 g/kg CFA) as a by-product. Therefore this study presents a novel, simplified method for the preparation of high-silica zeolites from a CFA-derived silicon extract (without the requirement of an additional oxalic acid purification step or additional silicon sources) that is closer to a zero-waste synthesis route than methods reported in the literature to date (Missengue et al., 2017; Missengue et al., 2018; Ndlovu, 2016; Vichaphund et al., 2014; Vichaphund et al., 2017).

4.5 Chapter Summary

The utilisation of a relatively low-temperature method for the extraction of a highly siliceous material (FASE) from CFA was achieved in this study. During the preparation of the FASE material, the changes in different extraction products were also monitored to determine the fate of the different elements in CFA. As-received South African CFA (from the Arnot power station) was found to possess a high level of REEs compared to the earth's crust. The magnetic separation process resulted in highly enriched REE levels in the non-magnetic fraction (NMF) of CFA, while most of the transition metal elements (such as Fe, Mn, Co, Ni, Mo, Zn and Cu) were enriched in the magnetic fraction (MF) of CFA. The magnetic separation process may therefore serve as a simple method for the enrichment and separation of REEs and transition metals of CFA.

The highly siliceous material (FASE) generated by the low-temperature silicon extraction method was composed of mainly silicon and sodium with very low aluminium content and did not require further treatment (for example oxalic acid treatment for the removal of excess sodium and enhancement of the SAR value or addition of silicon sources to adjust the SAR value) as reported in the literature (Missengue, 2016; Ndlovu, 2016). It is noteworthy that most of the elements from CFA were not present in the FASE material. This highly siliceous material (FASE) extracted from CFA may therefore serve as an ideal silicon precursor in the synthesis of high-silica zeolites such as ZSM-5 and mordenite as well as silicalite-1. Furthermore, the low-temperature silicon extraction method utilised in this study resulted in the formation of sodalite (with an appreciable yield) as a by-product. Sodalite formation was therefore possible in a relatively high-sodium environment, as well as in the presence of a range of elements originating from the NMF of CFA.

This study therefore presents a novel method, which is closer to a zero-waste synthesis route, for the conversion of CFA to high-silica zeolites (mordenite, ZSM-5 and silicalite-1) than reported in the literature to date. The utilisation of the FASE material as a silicon precursor in the synthesis of high-silica zeolites such as mordenite and ZSM-5 as well as silicalite-1 will be discussed in greater detail in subsequent chapters.

5 Chapter 5 - Synthesis of large-pore MOR framework type zeolites

5.1 Introduction

Zeolite mordenite has been synthesised from standard chemical reagents as well as other silicon-containing materials such as kaolin clay and diatomite. A combination of CFA with rice husk ash or diatomite has also been utilised as the starting material for zeolite mordenite synthesis (Aono et al., 2018; Johan and Matsue, 2014; Johan et al., 2015). However, the utilisation of a waste material such as CFA as the sole starting material for the synthesis of pure zeolite mordenite has not been investigated extensively, according to literature reported to date. In this study, the synthesis and optimisation of zeolite mordenite from a silicon extract (FASE) prepared from South African CFA (as discussed in Chapter 4) was investigated. The verified synthesis procedure for zeolite mordenite was used as the starting point for the investigation, using the FASE material as the sole source of silicon in zeolite synthesis, as described in Section 3.4.1.

This chapter will present the synthesis and optimisation of zeolite mordenite from a CFA-derived silicon extract (FASE), in the absence of an OSDA agent or seeds. Synthesis parameters such as alkalinity, aluminium and water content were varied sequentially to determine the influence of these parameters on zeolite mordenite formation; the optimum result, after varying each chosen parameter, was used as the baseline for subsequent investigations (as described in Section 3.4.1.1 and 3.4.1.2). The effect of seeding amount on the formation of zeolite mordenite by addition of commercial mordenite powder to the synthesis mixture prior to hydrothermal treatment was then investigated (as described in Section 3.4.2). The effect of OSDA (TEAOH) agent addition (of varying amounts) to the synthesis mixture on the formation of zeolite mordenite was also studied (as described in Section 3.4.3). The optimisation process for zeolite mordenite synthesis was monitored using the crystallinity of mordenite as the main response factor (determined by XRD diffraction). Selected zeolite samples (MOR framework type) were characterised further by SEM, FTIR and TGA-DTA to determine properties of synthesised materials such as morphology, structural composition and thermal properties (thermal stability, water and template content), respectively.

5.2 OSDA-free hydrothermal synthesis of zeolite mordenite from fly ash silicon extract

The synthesis of zeolite mordenite from standard chemical reagents, in the absence of an OSDA agent has been reported extensively in literature (Aono et al., 2016; Choudhury et al., 1998; Hincapie, et al., 2004; Idris et al., 2019; "IZA Synthesis Commission," 2016; Kim and Ahn, 1991; Li et al., 2009; Singh et al., 2018; Zhang et al., 2009). The verified synthesis protocol for zeolite mordenite involves hydrothermal treatment (170 °C for 24 hours) of a synthesis gel with molar regime, 1 SiO_2•0.03 Al_2O_3•0.20 Na_2O•26 H_2O, prepared using silica gel as the silicon source, sodium aluminate as the aluminium source and sodium hydroxide as the mineralising agent (Kim and Ahn, 1991). A similar synthesis protocol to the verified synthesis for zeolite mordenite was reported in literature for the preparation of zeolite mordenite with SAR value of 15. However, in this case hydrothermal treatment was carried out at 180 °C for 24 hours using fumed silica as a silica source (Li et al., 2009). Zhang et al, (2009) reported the synthesis of highly crystalline zeolite mordenite from a synthesis gel with molar regime 1 SiO_2•0.052 Al_2O_3•0.23 Na_2O•7.95 H_2O, prepared using colloidal silica and sodium aluminate as feedstock; hydrothermal treatment was carried out at 170 °C for 96 hours. In this study, the verified synthesis protocol for zeolite mordenite was therefore utilised as the starting point for the preparation of zeolite mordenite using the FASE material as the main feedstock.

5.2.1 Preliminary synthesis of zeolite mordenite using verified synthesis method

The synthesis conditions for zeolite mordenite, taken from the verified method (Kim and Ahn, 1991), was followed using a silicon precursor (FASE) extracted from CFA as the starting material. Synthesis mixtures with the following general molar regime (1 SiO_2•x Al_2O_3•y Na_2O•30.1 H_2O) was subjected to static hydrothermal treatment at 170 °C for 24 hours. The first synthesis experiment was carried out in the absence of any additional aluminium or silicon source and the synthesis mixture had a molar regime of 1 SiO_2•0.004 Al_2O_3•0.68 Na_2O•30.1 H_2O; the difference in the initial molar regime utilised in this study compared to the verified synthesis method for zeolite mordenite preparation from standard chemical reagents ("IZA Synthesis Commission", 2016) was due to the presence of low aluminium and high sodium content in the FASE material derived from CFA (as presented in Table 4.8, Section 4.3.2). The amount of aluminium content in the synthesis mixture was then varied by the addition of sodium aluminate (x = 0.02-0.08, y = 0.68-0.75) to the synthesis mixture (prepared as described in Table 3.2, Section 3.4.1.1); to determine the influence of

the SAR value of the synthesis mixture on the crystallisation of zeolite mordenite. Figure 5.1 depicts XRD diffractograms of as-synthesised zeolite products crystallised from synthesis mixtures with different sodium aluminate content, under hydrothermal conditions of 170 °C for 24 hours; analcime peaks are indexed in green and Na-P1 (GIS) peaks are indexed in purple.

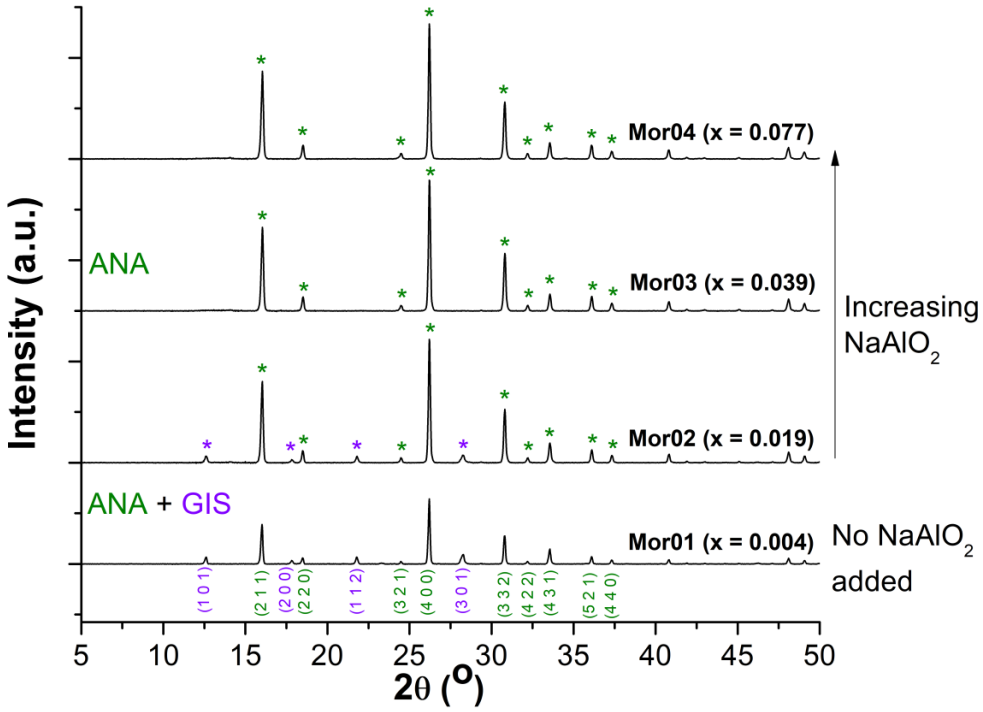

Figure 5.1: XRD diffractograms of as-synthesised zeolite products synthesised under hydrothermal conditions of 170 °C for 24 hours, using different amounts of sodium aluminate in the synthesis mixture (1 SiO_2•x Al_2O_3•y Na_2O•30.1 H_2O; x = 0.004-0.08 and y = 0.68-0.75). Key: ANA - Analcime, GIS - zeolite Na-P1

The main mineral phase that crystallised under the verified synthesis method conditions using FASE as the silicon source in synthesis mixture compositions (1 SiO_2•x Al_2O_3•y Na_2O•30.1 H_2O; x = 0.004-0.08 and y = 0.68-0.75) was analcime, as depicted in Figure 5.1 (peaks annotated in green). Relatively lower aluminium content in the synthesis mixture (x = 0.004-0.02, y = 0.68-0.70) resulted in the formation of analcime as the major phase as well as minor diffraction peaks corresponding to the Gismondine framework (zeolite Na-P1) at 2θ values of ~12.5, 17.6, 21.7 and 28.1° with peaks annotated in purple (Treacy and Higgins, 2007). Increasing the aluminium content in the synthesis mixture under these conditions resulted in enhanced analcime crystallinity; no other mineral phases were present under these conditions. Mineral phases analcime and zeolite Na-P1 are known to be competing crystallising phases during mordenite synthesis (Aono et al., 2016; "IZA Synthesis Commission," 2016).

Analcime and zeolite Na-P1 are denser zeolite structures than zeolite mordenite. According to Ostwald's law of successive transformations, metastable mineral phases such as zeolite mordenite crystallise and with time (or enhanced crystallisation processes) are transformed into more dense mineral phases such as analcime (Davis and Lobo, 1992; Feijen et al., 1994; Maldonado et al., 2012; Oleksiak and Rimer, 2014; Yu, 2007). The crystallisation temperature was therefore lowered to 150 °C (24 hours) to investigate the influence of temperature on crystallisation products (as described in Table 3.2, Section 3.4.1.1); XRD diffractograms of as-synthesised products are depicted in Figure 5.2.

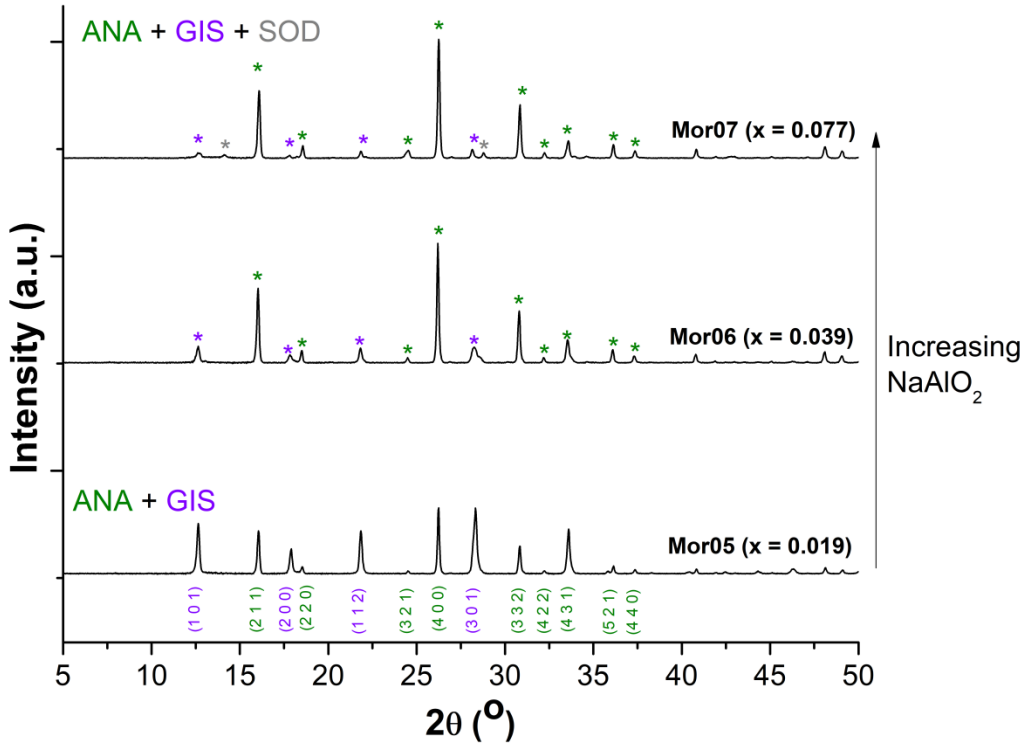

Figure 5.2: XRD diffractograms of as-synthesised zeolite products synthesised under hydrothermal conditions of 150 °C for 24 hours, using different amounts of sodium aluminate in the synthesis mixture (1 SiO_2•x Al_2O_3•y Na_2O•30.1 H_2O; x = 0.004-0.08 and y = 0.68-0.75). Key: ANA - Analcime, GIS - zeolite Na-P1, SOD - Sodalite

A reduction in the crystallisation temperature did not result in the formation of zeolite mordenite, as depicted in Figure 5.2. The crystallisation of analcime in the presence of Na-P1 was observed under these conditions. At relatively low aluminium content (x = 0.02, y = 0.70), the co-crystallisation of analcime with Na-P1 was observed. On the other hand, at a relatively high aluminium content (x = 0.08, y = 0.75), the presence of two minor peaks associated with sodalite were observed at 2θ values of ~14.1 and ~28.8 °. The reduced crystallisation temperature had an effect on the crystallisation products; however, zeolite

mordenite formation did not occur under these crystallisation conditions as observed in Figure 5.1 and 5.2. This indicated that the synthesis mixture compositions investigated were close to the boundary conditions for analcime and zeolite Na-P1, not the boundary conditions required for the crystallisation of zeolite mordenite.

According to literature, the crystallisation of zeolite mordenite was observed in the hydrothermal temperature range of 160-200 °C. Furthermore, the synthesis mixture utilised in this study contained a high Na_2O content compared to synthesis mixtures for mordenite synthesis reported in literature (Aono et al., 2016; Choudhury et al., 1998; Hincapie, et al., 2004; Idris et al., 2019; "IZA Synthesis Commission," 2016; Kim and Ahn, 1991; Li et al., 2009; Singh et al., 2018; Zhang et al., 2009). It is noteworthy that the FASE material utilised as the feedstock for zeolite synthesis contains a high sodium content (as discussed in Section 4.3.2). Further investigations into the influence of alkalinity (and other synthesis parameters) on zeolite mordenite crystallisation were then carried out to better understand the boundary regions between zeolite mordenite, analcime and Na-P1.

5.2.2 The effect of alkalinity on zeolite mordenite crystallisation

The crystallisation of zeolite mordenite is reported to be sensitive to the alkalinity of the synthesis mixture (Lv et al., 2011; Oleksiak and Rimer, 2014). The alkalinity of the synthesis mixture, with general molar regime 1 SiO_2•0.02 Al_2O_3•y Na_2O•30.1 H_2O, was varied by using different amounts of NaOH (y = 0.52-0.70) in the preparation of the synthesis mixture, as described in Table 3.2, Section 3.4.1.1. Figure 5.3 depicts XRD diffractograms of as-synthesised zeolite products synthesised at 170 °C (for 24 hours) from synthesis mixtures with varying alkalinity (all other synthesis parameters kept constant).

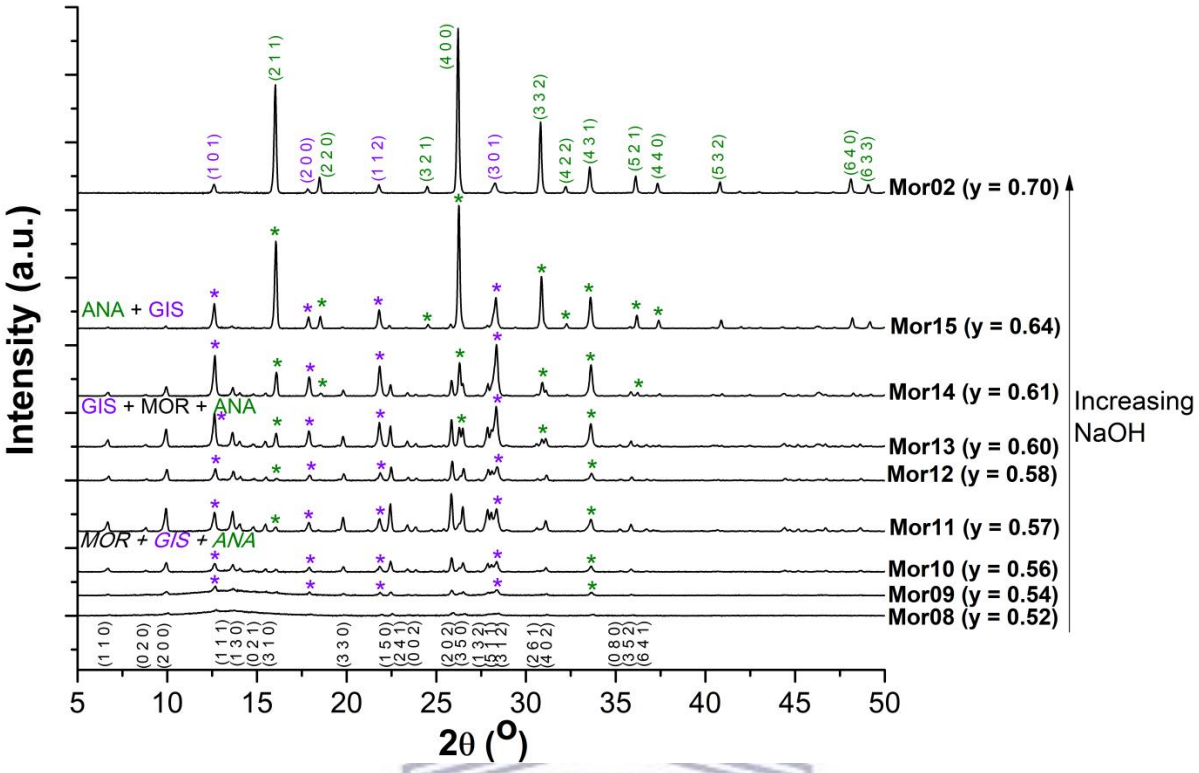

Figure 5.3: XRD diffractograms of as-synthesised zeolite products synthesised under hydrothermal conditions of 170 °C for 24 hours from synthesis mixtures (1 SiO_2•0.02 Al_2O_3•y Na_2O•30.1 H_2O) with varying alkalinity (y = 0.52-0.70). Key: MOR - zeolite mordenite, ANA - Analcime, GIS - zeolite Na-P1

Under the synthesis conditions investigated, the alkalinity of the synthesis mixture had a significant influence on crystallisation products, as observed in Figure 5.3. At very low alkalinity (y = 0.52-0.54), the crystallisation products were mainly composed of an amorphous material but contained a few mordenite peaks (samples Mor08 and Mor09). This is expected at extremely low alkalinity where the hydroxide concentration in the synthesis mixture may be inadequate to facilitate the dissolution of precursor materials, which may consequently impede other crystallisation processes. As the alkalinity increased (y = 0.56-0.58), more crystalline zeolite mordenite was formed with minor Na-P1 and analcime diffraction peaks present as observed in Figure 5.3 (samples Mor10-Mor12). The highest crystallinity for zeolite mordenite was observed for sample Mor11 (y = 0.57). At intermediate alkalinity (y = 0.60-0.61), the major mineral phase was zeolite Na-P1 which crystallised in the presence of zeolite mordenite and analcime as observed in Figure 5.3 (samples Mor13 and Mor14). As observed in Figure 5.3, relatively higher alkalinity (y ≥ 0.64) resulted in the formation of analcime as the major mineral phase. As observed in Figure 5.3, analcime crystallised in the presence of both Na-P1 and mordenite at y = 0.64 (sample Mor15), while the presence of Na-P1 as the only minor phase was observed at y = 0.70 (sample Mor02).

Under these synthesis conditions, relatively low alkalinity was suitable for the crystallisation of zeolite mordenite, while intermediate alkalinity was suitable for Na-P1 crystallisation and high alkalinity for analcime.

These results compare well with literature; low alkalinity was reported to result in the formation of either amorphous material or wairakite (Choudhury et al., 1998; Machado et al., 1999) while high alkalinity was reported to yield a denser mineral phase α-quartz (Lv et al., 2011). However, due to the presence of minor peaks associated with the competing, denser mineral phases (such as analcime and Na-P) in the most crystalline zeolite mordenite sample (Mor11), the crystallisation of mordenite from a fixed synthesis mixture (corresponding to sample Mor11) was monitored over time.

5.2.2.1 Monitoring the crystallisation of zeolite mordenite with time

The crystallisation of zeolite mordenite from a synthesis mixture with a fixed molar regime (1 SiO_2•0.02 Al_2O_3•0.57 Na_2O•30.1 H_2O) under hydrothermal conditions of 170 °C was monitored with time at intervals of 24 hours between 1 and 4 days, as described in Table 3.2, Section 3.4.1.1. Figure 5.4 represents the XRD diffractograms of as-synthesised zeolites prepared under these conditions.

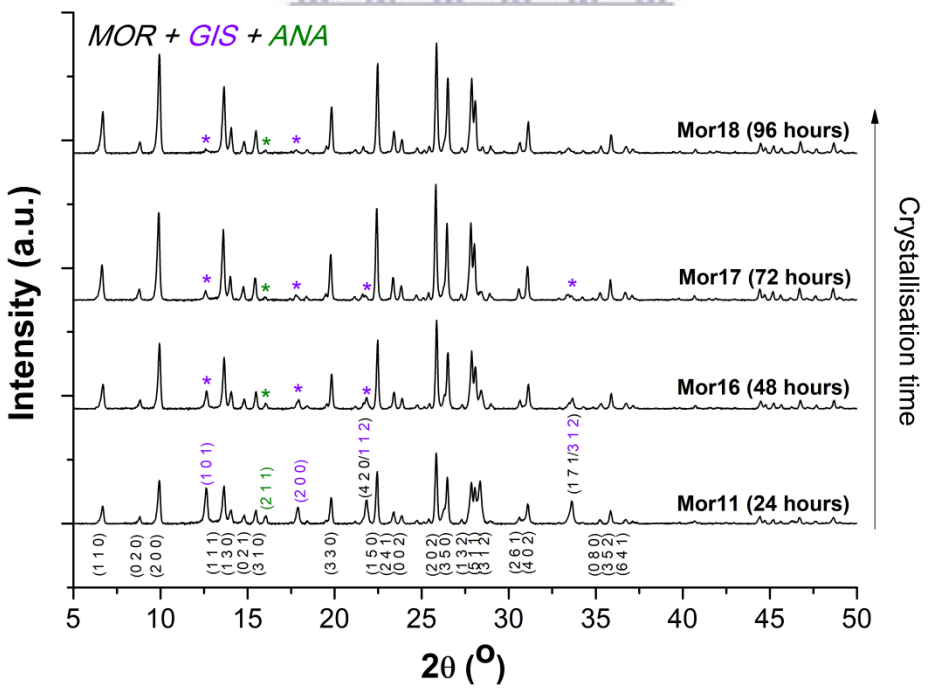

Figure 5.4: XRD diffractograms of as-synthesised zeolite mordenite products synthesised under hydrothermal temperature of 170 °C from a fixed synthesis mixture (1 SiO_2•0.02 Al_2O_3•0.57 Na_2O•30.1 H_2O), monitored over time between 24 and 96 hours. Key: MOR - zeolite mordenite, ANA - Analcime, GIS - zeolite Na-P1

As expected the crystallinity of zeolite mordenite improved with crystallisation time, as observed in Figure 5.4. On the other hand, the crystallinity of minor competing phases Na-P1 and analcime decreased with crystallisation time. The main diffraction peaks for zeolite mordenite (2θ = 9.77, 22.20, 25.63, 27.67 and 27.87°) were used to calculate the relative crystallinity of zeolite mordenite samples (relative to a highly crystalline sample Mor17); the crystallisation curve is depicted in Figure 5.5.

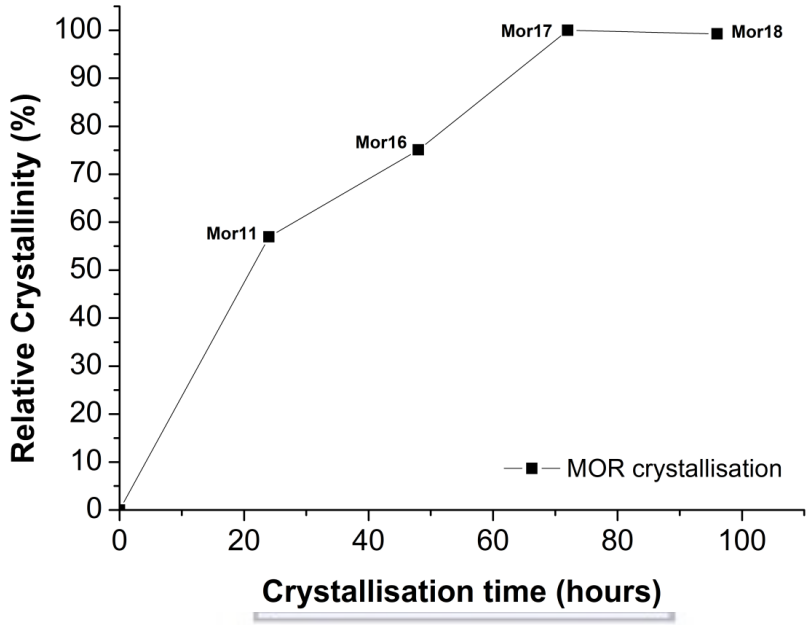

Figure 5.5: Crystallisation curve for zeolite mordenite synthesised from a fixed synthesis mixture (1 SiO_2•0.02 Al_2O_3•0.57 Na_2O•30.1 H_2O) at hydrothermal temperature of 170 °C.

As observed in Figure 5.5, the relative crystallinity of zeolite mordenite increased with time from ~57 % crystallinity after 24 hours of hydrothermal treatment, to ~75 % crystallinity after 48 hours and ~100 % after 72-96 hours. The formation of highly crystalline zeolite mordenite was therefore considered complete after 72 hours of hydrothermal treatment. Similar results were reported in literature, the synthesis of highly crystalline zeolite mordenite from a synthesis mixture prepared with colloidal silica and sodium aluminate under hydrothermal conditions of 170 °C for 96 hours (Zhang et al., 2009). However, zeolite mordenite crystallisation from standard reagents was reported after 24 hours of hydrothermal treatment at relatively high temperatures of 180 °C (Li et al., 2009) and up to 200 °C (Aono et al., 2016). Therefore the effect of crystallisation temperatures (> 170 °C) on zeolite mordenite formation was investigated with time between 24 and 72 hours.

5.2.3 The effect of crystallisation temperature on zeolite mordenite formation with time

Crystallisation temperature is known to play an important role on the formation of zeolite mordenite. Zeolite mordenite is reported to crystallise in the hydrothermal temperature range of 160-200 °C (Aono et al., 2016; Choudhury et al., 1998; Hincapie, et al., 2004; Idris et al., 2019; "IZA Synthesis Commission," 2016; Kim and Ahn, 1991; Li et al., 2009; Singh et al., 2018; Zhang et al., 2009). The formation of zeolite mordenite from a synthesis mixture, with fixed molar regime 1 SiO_2•0.02 Al_2O_3•0.57 Na_2O•30.1 H_2O, subjected to hydrothermal conditions of 180 °C (and 190 °C) was monitored between 24 and 72 hours, as described in Table 3.2, Section 3.4.1.1. Figure 5.6 depicts XRD diffractograms of as-synthesised zeolite products crystallised at 180 °C at 24 hour intervals up to 72 hours. The crystallisation of zeolite mordenite was observed after 24 hours of hydrothermal treatment at 180 °C, with minor Na-P1 and analcime peaks observed in Figure 5.6. As the crystallisation period was prolonged (to 48 hours), the crystallinity of zeolite mordenite was slightly enhanced as expected. However, analcime crystallisation was also enhanced as the crystallisation period increased (up to 72 hours) and peaks corresponding to Na-P1 were no longer observed.

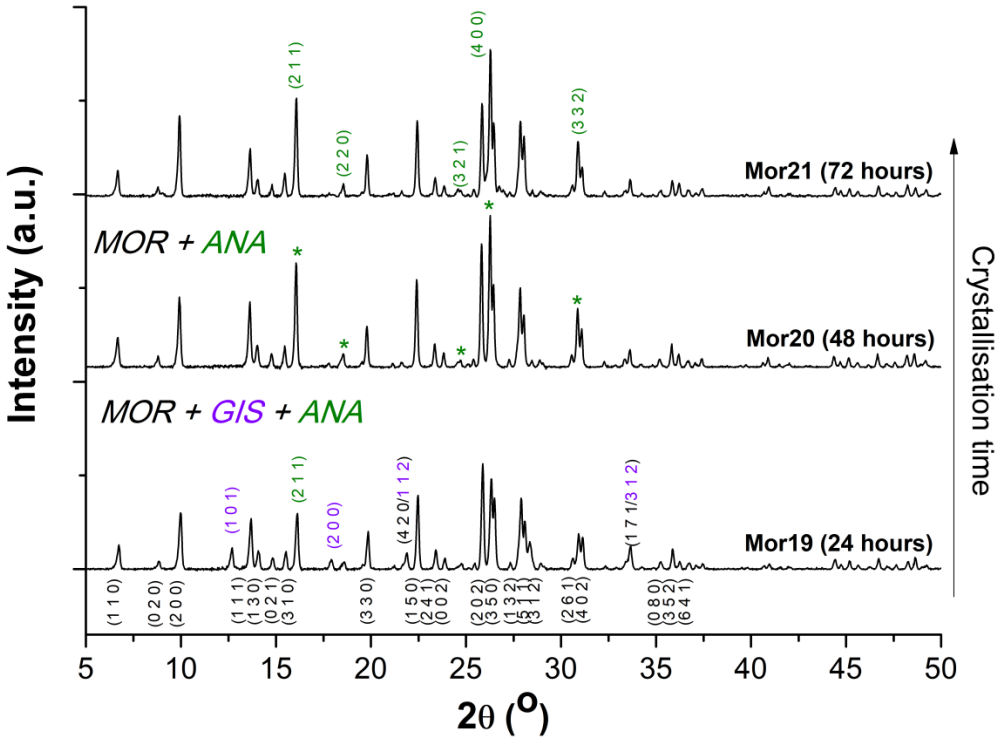

Figure 5.6: XRD diffractograms of as-synthesised zeolite mordenite products synthesised under hydrothermal temperature of 180 °C from a fixed synthesis mixture (1 SiO_2•0.02 Al_2O_3•0.57 Na_2O•30.1 H_2O), monitored over time between 24 and 72 hours. Key: MOR - zeolite mordenite, ANA - Analcime, GIS - zeolite Na-P1

Figure 5.7 depicts XRD diffractograms of as-synthesised zeolite products crystallised at 190 °C at 24 hour intervals up to 72 hours.

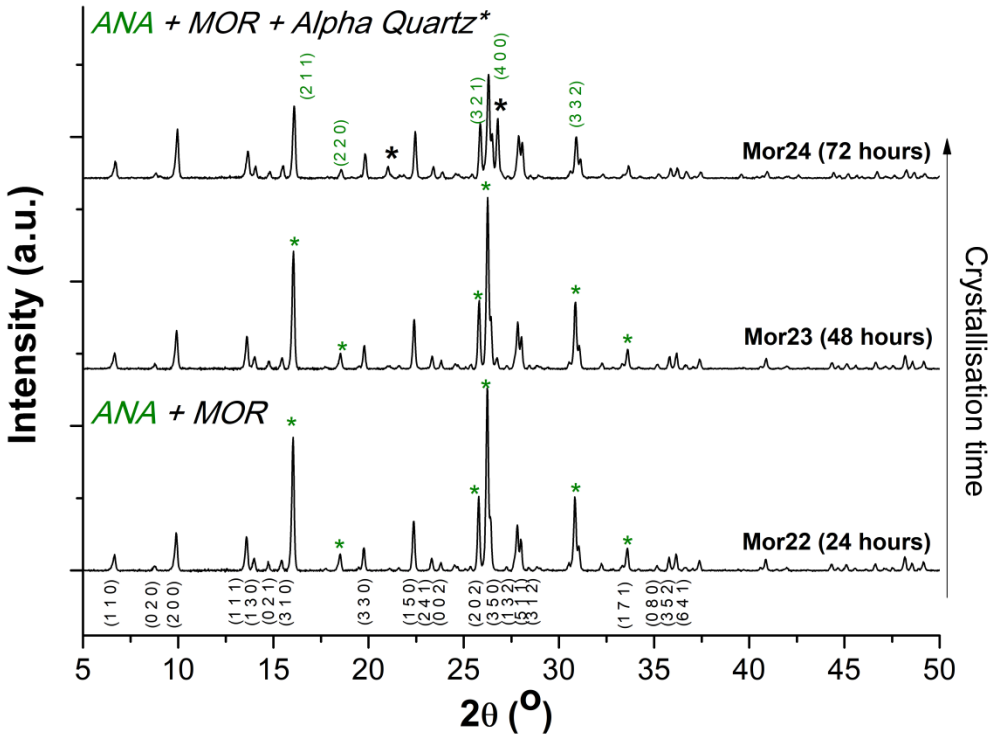

Figure 5.7: XRD diffractograms of as-synthesised zeolite mordenite products synthesised under hydrothermal temperature of 190 °C from a fixed synthesis mixture (1 SiO_2•0.02 Al_2O_3•0.57 Na_2O•30.1 H_2O), monitored over time between 24 and 72 hours. Key: MOR - zeolite mordenite, ANA - Analcime

The co-crystallisation of analcime and mordenite was observed under hydrothermal conditions of 190 °C between 24 and 72 hours, as depicted in Figure 5.7. At prolonged crystallisation period of 72 hours, diffraction peaks (2θ = 21.0 and 26.7°) associated with alpha quartz were also observed (marked by an * in Figure 5.7). The enhancement of crystallisation processes at prolonged periods at a hydrothermal temperature of 180 and 190 °C therefore resulted in the formation of more dense mineral phases such as analcime and alpha quartz. The relative crystallinity of as-synthesised zeolite products crystallised under hydrothermal temperature of 180 and 190 °C between 24 and 72 hours was calculated relative to a highly crystalline zeolite mordenite sample (Mor17); crystallisation curves for zeolite synthesis at hydrothermal temperatures of 170-190 °C are depicted in Figure 5.8.

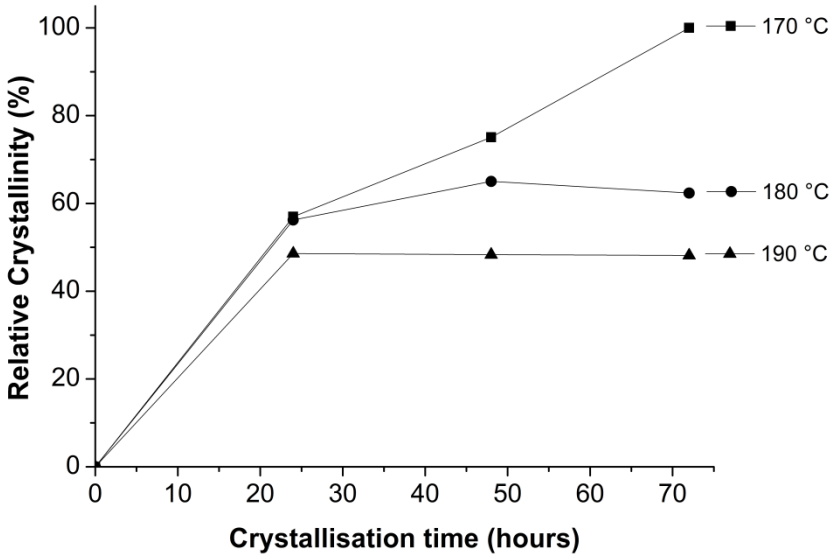

Figure 5.8: Crystallisation curves for zeolite mordenite synthesised from a fixed synthesis mixture (1 SiO_2•0.02 Al_2O_3•0.57 Na_2O•30.1 H_2O) at hydrothermal temperatures between 170 and 190 °C.

As depicted in Figure 5.8, the crystallinity of zeolite mordenite was highly dependent on the crystallisation temperature. Between 24 and 48 hours of crystallisation, the crystallisation of zeolite mordenite (as well as zeolite crystallinity) was relatively similar at hydrothermal temperatures of 170 and 180 °C. After 72 hours of crystallisation, zeolite mordenite crystallisation was enhanced at 170 °C, while zeolite mordenite formation reached a plateau at 180 °C and the formation of analcime was enhanced. At a relatively higher crystallisation of 190 °C, zeolite mordenite formation was supressed and a plateau in the crystallinity was observed between 24 and 72 hours of hydrothermal treatment and analcime formation was favoured. The most crystalline zeolite mordenite prepared from the FASE material was therefore achieved after 72 hours of crystallisation at 170 °C.

The crystallisation of zeolite mordenite from standard chemical reagents was possible in a wide range of hydrothermal temperatures (160-200 °C) as discussed previously (Aono et al., 2016; Choudhury et al., 1998; Hincapie, et al., 2004; Idris et al., 2019; "IZA Synthesis Commission," 2016; Kim and Ahn, 1991; Li et al., 2009; Singh et al., 2018; Zhang et al., 2009). The crystallisation of highly crystalline zeolite mordenite from FASE was more favourable at a hydrothermal temperature of 170 °C; this may be due to differences in the properties of the FASE material compared to standard chemical reagents (as discussed in Section 4.3.2). The OSDA-free synthesis of highly crystalline zeolite mordenite, using FASE as a silicon source, was achieved from a synthesis mixture (with molar regime 1 SiO_2•0.02

Al_2O_3•0.57 Na_2O•30.1 H_2O) under hydrothermal conditions of 170 °C for 72 hours. Subsequent optimisation experiments for the synthesis of zeolite mordenite were therefore carried out at hydrothermal conditions of 170 °C for 72 hours. The effect of aluminium content (by sodium aluminate addition) was investigated once again using the optimum synthesis conditions (sample Mor17) as the starting point for the investigated.

5.2.4 The effect of aluminium content (by sodium aluminate addition) on zeolite mordenite crystallisation

The effect of aluminium content (by sodium aluminate addition to the synthesis mixture) on the formation of zeolite mordenite was investigated, as described in Table 3.2, Section 3.4.1.1. Figure 5.9 depicts XRD diffractograms of as-synthesised zeolites crystallised at 170 °C for 72 hours from a synthesis mixture (1 SiO_2•x Al_2O_3•y Na_2O•30.1 H_2O) with varying amounts of aluminium content (x = 0.01-0.08, y = 0.56-0.63) achieved by sodium aluminate addition.

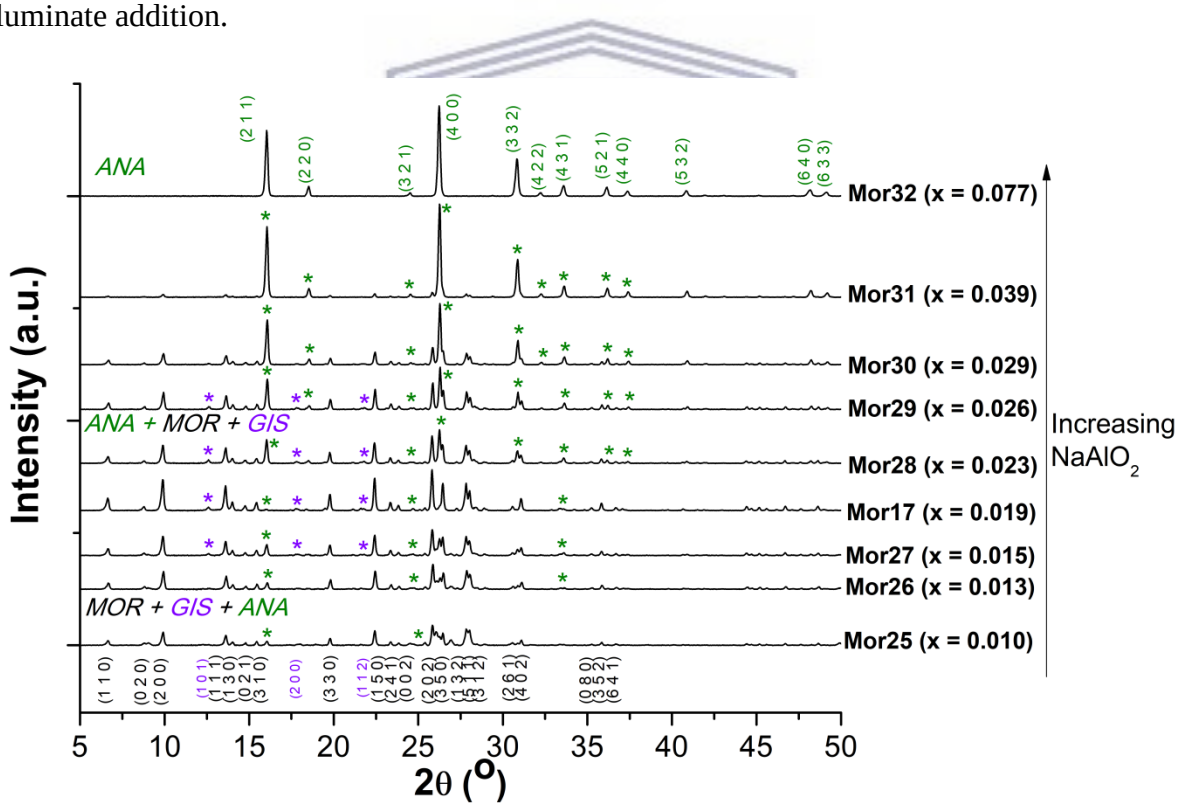

Figure 5.9: XRD diffractograms of as-synthesised zeolite mordenite products synthesised under hydrothermal conditions of 170 °C for 72 hours with different aluminium content (achieved by sodium aluminate addition) in the synthesis mixture with molar regime 1 SiO_2•x Al_2O_3•y Na_2O•30.1 H_2O (x = 0.01-0.08, y = 0.56-0.63). Key: MOR - zeolite mordenite, ANA - Analcime, GIS - zeolite Na-P1

The crystallisation of zeolite mordenite was significantly influenced by the amount of additional aluminium content (achieved by sodium aluminate addition) present in the synthesis mixture, as described in Figure 5.9, under these synthesis conditions. At relatively low additional aluminium content (x = 0.01-0.02, y = 0.56-0.57), zeolite mordenite crystallised as the major phase with minor Na-P1 and analcime peaks present (as observed for samples Mor25-Mor27 and Mor17 in Figure 5.9). At relatively intermediate additional aluminium content (x = 0.023-0.04, y = 0.57-0.59), analcime crystallised as the major phase together with zeolite mordenite and/or Na-P1 (as observed for samples Mor28-Mor31 in Figure 5.9). Whereas at relatively higher additional aluminium content (x = 0.08, y = 0.63) for sample Mor32, analcime crystallised as the major mineral phase under the synthesis conditions investigated. The highest relative crystallinity of zeolite mordenite was achieved at x = 0.02, as observed for sample Mor17 in Figure 5.9; this synthesis mixture composition (1 SiO_2·0.02 Al_2O_3·0.57 Na_2O·30.1 H_2O) was therefore used in subsequent optimisation experiments.

The crystallisation of zeolite mordenite from standard chemical reagents was possible in a relatively wide range of SAR values (of the synthesis mixture) from x = 0.08-0.12, with x > 0.12 resulting in the favourable crystallisation of analcime and/or Na-P1 at relatively high hydrothermal temperatures (≥ 170 °C) and amorphous material or analcime and/or Na-P1 at relatively lower hydrothermal temperatures (≤ 170 °C) (Aono et al., 2016). Another study which utilised colloidal silica (Ludox AM30) and sodium aluminate as feedstock, reported the crystallisation of highly crystalline zeolite mordenite in the SAR range (as investigated in this study) with x = 0.013-0.079 under hydrothermal conditions of 170 °C for 72-96 hours (Zhang et al., 2009). The synthesis of zeolite mordenite from the FASE material was more sensitive to the SAR value of the synthesis mixture and highly crystalline zeolite mordenite crystallised in the lower range of SAR values; this range is very narrow compared to literature. In this study, the crystallisation of analcime was favourable; this may be due to the high sodium content in the FASE material. The next synthesis parameter that was investigated was water content in the synthesis mixture (at constant [OH^-]) and the optimum synthesis conditions for zeolite mordenite crystallisation (sample Mor17) was utilised as the starting point for subsequent optimisation experiments.

5.2.5 The effect of water content on zeolite mordenite crystallisation

The effect of water content (at constant [OH^-]) in the synthesis mixture on the crystallinity of zeolite mordenite was investigated by varying the amount of 1.6 wt% NaOH solution used in the synthesis mixture (1 SiO_2•0.02 Al_2O_3•y Na_2O•z H_2O), as described in Table 3.3, Section 3.4.1.2. This was done in order to keep the overall OH^-/H_2O ratio of the synthesis mixture constant. Figure 5.10 depicts XRD diffractograms of as-synthesised zeolites crystallised at 170 °C for 72 hours from a synthesis mixture with different water content.

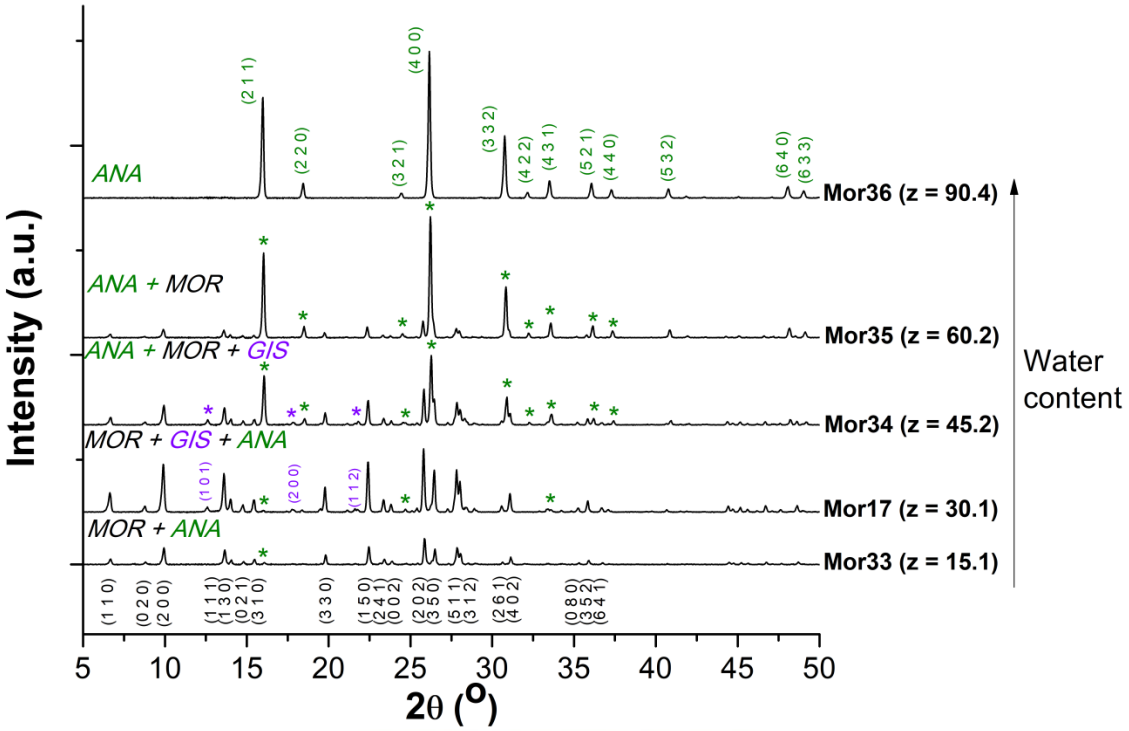

Figure 5.10: XRD diffractograms of as-synthesised zeolite mordenite products synthesised under hydrothermal conditions of 170 °C for 72 hours with different water content (at constant alkalinity) in the synthesis mixture with molar regime 1 SiO_2•0.02 Al_2O_3•y Na_2O•z H_2O (z = 15.1-60.2). Key: MOR - zeolite mordenite, ANA - Analcime, GIS - zeolite Na-P1

The water content in the synthesis mixture had a significant influence on the zeolite products that crystallised, as observed in Figure 5.10. Relatively low water content synthesis systems (z = 15.1-30.1) resulted in the crystallisation of zeolite mordenite as the major mineral phase, with analcime and Na-P1 present as minor phases (as observed for samples Mor33 and Mor17 in Figure 5.10). However, at very low water content (z = 15.1, as in sample Mor33) the crystallinity of zeolite mordenite was reduced. An intermediate water content (as observed for samples Mor34 and Mor35 in Figure 5.10) in the synthesis system (z = 45.2-60.2) resulted in the co-crystallisation of analcime and zeolite mordenite, with Na-P1 present as a minor phase (at z = 60.2). Relatively higher water content synthesis systems (z = 90.4)

resulted in the formation of pure analcime (as observed for sample Mor36 in Figure 5.10). It is noteworthy that as the water content was increased, the sodium content in the synthesis mixture also increased (as listed in Table 3.3, Section 3.4.1.2). However, due to the small increments by which sodium content changed in the investigated range, the sodium content was considered insignificant compared to changes in the water content.

In general, increasing the water content in the synthesis system dilutes the silicon and aluminium concentration in the synthesis mixture, which may impede the achievement of supersaturation as well as the other zeolite crystallisation processes such as nucleation and crystal growth (Oleksiak and Rimer, 2014; Yu, 2007). The crystallisation of zeolite mordenite from standard laboratory reagents was reported from synthesis mixtures containing water in the range of z = 7.7 to 60.8. As expected, a longer crystallisation period was required under high water content (dilution of nutrients) synthesis conditions (Zhang et al., 2009). Considerably higher water content (z = ~78) has also been reported for the crystallisation of zeolite mordenite (Choudhury et al., 1998). However, in this study the opposite effect was observed; initially the crystallisation of zeolite mordenite was observed and subsequently, the transformation into analcime was enhanced with increasing water content. This may be due to the fact that overall OH^-/H_2O ratio of the synthesis mixture was kept constant, which may have resulted in enhanced dissolution of nutrients as the water content was increased. Under the condition utilised in this study, zeolite mordenite crystallisation from the FASE material was favoured in synthesis systems with relatively low water content (i.e. high nutrient concentration). Whereas, analcime crystallisation was favoured in synthesis systems with relatively high water content (i.e. low nutrient concentration). The OSDA-free zeolite mordenite formation from the FASE material was therefore favoured in a well-defined range of molar compositions.

5.2.6 Further characterisation of highly crystalline zeolite mordenite

The most crystalline zeolite mordenite sample (Mor17) was characterised further by SEM-EDS, FTIR and TGA/DTA-MS. The morphology of zeolite mordenite sample Mor17 (with the highest crystallinity) was analysed by SEM microscopy and EDS was used to determine the average SAR ratio of the synthesised zeolite mordenite crystals. Figure 5.11 depicts SEM micrographs of as-synthesised zeolite sample Mor17, which was composed of mainly highly crystalline zeolite mordenite and minor Na-P1 and analcime peaks (as observed in Figure 5.4).

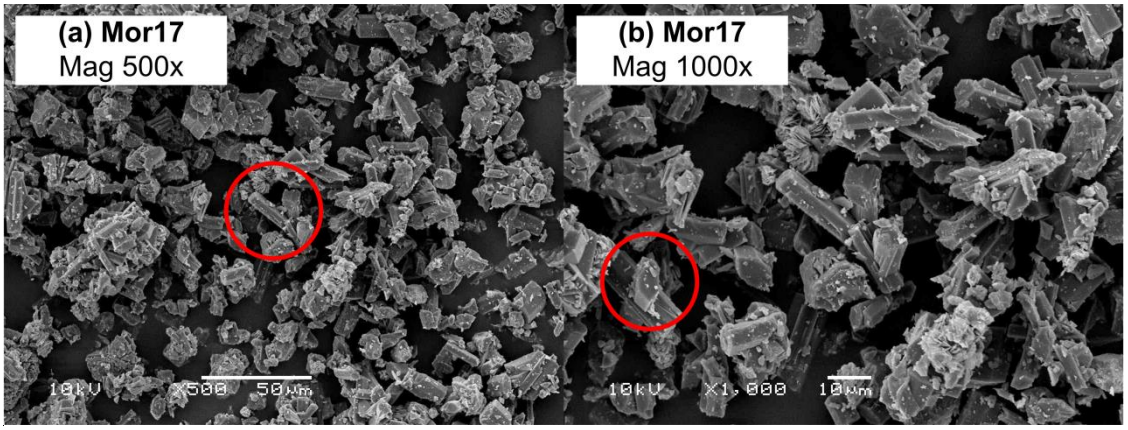

Figure 5.11: SEM micrograph of as-synthesised sample Mor17 crystallised at 170 °C for 72 hours from a synthesis mixture with molar regime 1 SiO_2•0.019 Al_2O_3•0.57 Na_2O•30.1 H_2O (a) 500x and (b) 1000x magnification.

As-synthesised zeolite mordenite (sample Mor17) crystals exhibited the typical prismatic shape reported for zeolite mordenite. The average particle size of zeolite mordenite was calculated to be 13.6 µm using ImageJ software. There was no uniformity in terms of the aspect ratios for the synthesised mordenite crystals; mordenite crystals were either long and thin or short and wide prismatic crystals as encircled in Figure 5.11 (a) and (b), respectively. EDS (n = 10) was used to determine the SAR ratio of the synthesised product Mor17, which was calculated to be 10.3 (comparable to the value of 8.6 reported for zeolite mordenite synthesised using the verified synthesis method). The structural properties of highly crystalline zeolite mordenite sample Mor17 was analysed by FTIR spectroscopy; the FTIR vibrational spectrum is depicted in Figure 5.12.

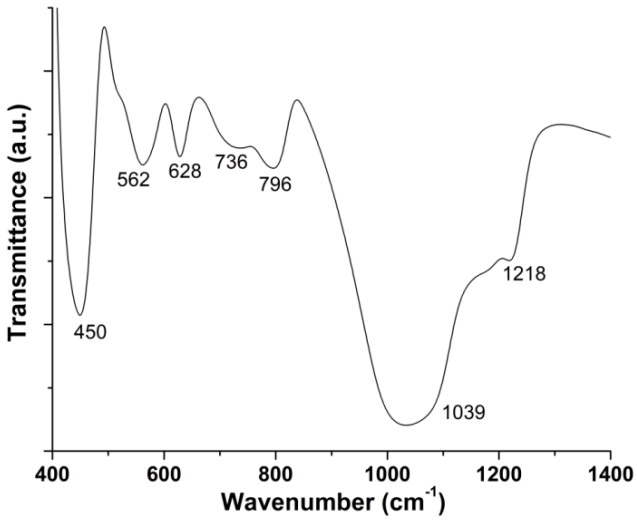

Figure 5.12: FTIR vibrational spectrum of as-synthesised sample Mor17 crystallised at 170 °C for 72 hours from a synthesis mixture with molar regime 1 SiO_2•0.019 Al_2O_3•0.57 Na_2O•30.1 H_2O.

Five main FTIR vibrational bands were observed for highly crystalline mordenite sample Mor17 at wavenumbers of 450, 562, 628, 736, 796 and 1039 cm^{-1}, as observed in Figure 5.12, with a weak shoulder band at 1218 cm^{-1}. These bands are associated with different T-O vibrational modes in the crystalline aluminosilicate Mor17 sample. Sample Mor17 contained the characteristic vibrational bands for zeolite mordenite (Aly et al., 2012; Johan and Matsue, 2014; Nassar et al., 2017). FTIR vibrational band assignments for highly crystalline zeolite mordenite sample Mor17 are summarised in Table 5.1.

Table 5.1: FTIR vibrational band assignments for as-synthesised sample Mor17 crystallised at 170 °C for 72 hours from a synthesis mixture with molar regime 1 SiO_2•0.019 Al_2O_3•0.57 Na_2O•30.1 H_2O.

Wavenumber (cm^{-1})	Assignment
450	Si-O-T bending
562	Ring structure vibrations
628	Ring structure vibrations
736	Si-O-T symmetric stretching (internal) of S4R units
796	Si-O-T symmetric stretching (external)
1039	Si-O-T asymmetric stretching (internal)
1218	Si-O-T asymmetric stretching (external)

The FTIR vibrational bands are assigned according to literature (Aly et al., 2012; Criado et al., 2007; Fernandez-Jimenez and Palomo, 2005; Johan and Matsue, 2014; Mozgawa et al., 2005; Nassar et al., 2017), as listed in Table 5.1. For sample Mor17, the T-O bending vibration was observed at 450 cm^{-1}, vibrations in double ring structures at 562 and 628 cm^{-1}, symmetric T-O stretching vibrations were observed at 736 cm^{-1} (internal linkages) associated with S4R units and 796 cm^{-1} (external linkages), while asymmetric T-O stretching vibrations were observed at 1039 cm^{-1} (internal linkages) and 1218 cm^{-1} (external linkages). The relatively lower wavenumber of symmetric and asymmetric T-O stretching vibrations was due to the high aluminium content in these sample (Johan and Matsue, 2014; Mozgawa et al., 2005; Nassar et al., 2017). The Thermogravimetric (TG) analysis curve (solid line) and its Derivative Thermogravimetric (DTG) analysis curves (dotted line) for as-synthesised sample as well as the Differential Thermal Analysis (DTA) analysis curve for Mor17 are depicted in Figure 5.13; the experiment was carried out in air. The MS spectrum for sample Mor17 containing fragments of interest was monitored during the TGA experiments, as described in Section 3.6.6; results are depicted in Figure 5.14.

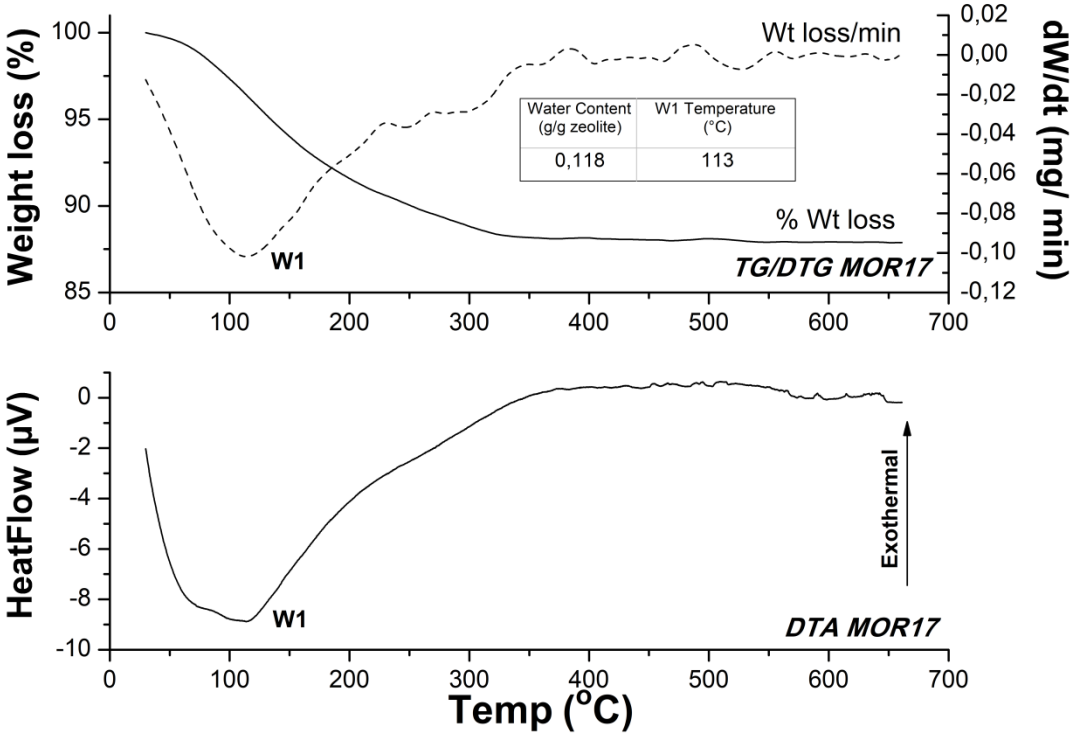

Figure 5.13: TGA/DTG/DTA analysis (carried out in air) of as-synthesised sample Mor17 crystallised at 170 °C for 72 hours from a synthesis mixture with molar regime 1 SiO_2•0.019 Al_2O_3•0.57 Na_2O•30.1 H_2O.

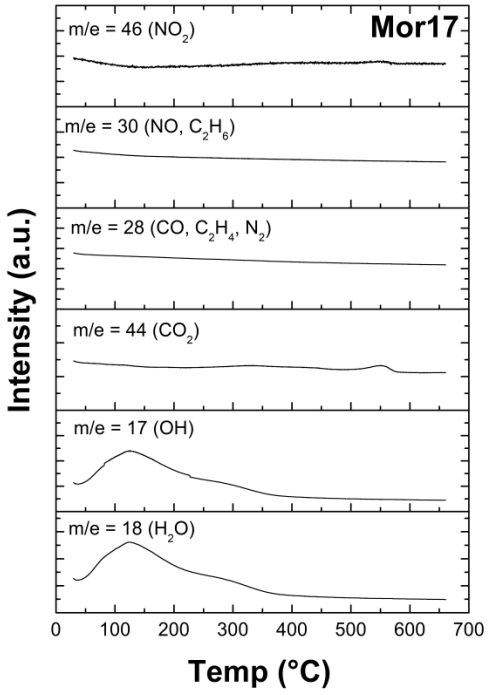

Figure 5.14: MS spectrum of as-synthesised sample Mor17 crystallised at 170 °C for 72 hours from a synthesis mixture with molar regime 1 SiO_2•0.019 Al_2O_3•0.57 Na_2O•30.1 H_2O.

As depicted in Figure 5.13, a water loss peak was observed at a temperature of 113 °C. However, water loss from the zeolite framework occurred over a wide temperature range (up to 350 °C), as depicted in Figure 5.13 and Figure 5.14. The release of carbon dioxide from the zeolite mordenite framework at a temperature of ~550 °C was detected by MS, as depicted in Figure 5.14. Nevertheless, zeolite mordenite (Mor17) was thermally stable up to 650 °C. The thermal analysis of as-synthesised zeolite Mor17 revealed that the highly crystalline mordenite sample was highly hygroscopic containing 0.118 g of H_2O/g zeolite (11.8 %), which is likely due to presence of a relatively large amount of aluminium in the zeolite framework as well as the high void volume of the microporous zeolite framework.

The thermal profile of zeolite mordenite synthesised from the CFA-derived FASE material is similar to zeolite mordenite synthesised from standard chemical reagents (sodium silicate solution and aluminium sulphate) with high silicon content (SAR = 16.7) as reported in the literature (Choudhury et al., 1998). A similar thermal analysis profile was also reported for crystalline mordenite synthesised from standard chemical reagent (Ludox AS30 colloidal silica and aluminium nitrate) with a SAR value of 15.6 (Aly et al., 2012). The total water loss for this material occurred at ~109 C, with a total water content reported as 6 % (Aly et al., 2012). This is almost half the amount of water present in the crystalline mordenite sample (Mor17) synthesised in this study, which was 11.8 %. Zeolite Mor17 exhibited a lower SAR value (10.3) compared to the samples reported in literature. The amount of water adsorbed to a zeolite framework is directly related to the amount of aluminium present in the framework (Pál-Borbély, 2007). The difference in water content between these samples may therefore be attributed the difference in aluminium content in these samples. However, it should be noted that similar water content for zeolite mordenite was reported by Choudhury et al., (1998) and Cysneiros et al., (2016). These results illustrate that highly crystalline mordenite may be synthesised from a CFA-derived silicon precursor (FASE), with properties comparable to that of zeolites synthesis from standard chemical reagents, without the need for addition of OSDA agents.

5.3 Seed-assisted hydrothermal synthesis of zeolite mordenite from fly ash silicon extract

During zeolite synthesis, the addition of seed crystals (of the target zeolite phase) to the synthesis mixture is typically used to promote the crystallisation of a thermodynamically unfavourable zeolite phase. This is achieved either by preventing the crystallisation of unwanted zeolite phases (i.e. impurities) or influencing nucleation of the target zeolite phase or enhancing crystallisation kinetics in favour of the target zeolite. Seed-assisted zeolite synthesis may be utilised as a method to prevent the need for OSDA agents (Cundy and Cox, 2003; Grand et al., 2016; Yu, 2007). The utilisation of a small amount of mordenite seed crystals (relative to the feedstock) has been utilised to promote the formation of zeolite mordenite (Cysneiros et al., 2016; Lu et al., 2004; Lv et al., 2011; Todorova and Kalvachev, 2015; Ueda et al., 1980; Zhang et al., 2011). In this study, commercial mordenite powder (SAR = 13) was used as seed crystals added to the synthesis mixtures prior to hydrothermal treatment (as described in Table 3.4, Section 3.4.2) to promote the crystallisation of zeolite mordenite without any competing mineral phases such as zeolite Na-P1 and analcime. The effect of seeding amount on the crystallisation of zeolite mordenite at 170 °C was monitored over time.

5.3.1 The effect of seeding amount on zeolite mordenite crystallisation

The crystallisation of zeolite mordenite from the optimised synthesis mixture (1 SiO_2•0.02 Al_2O_3•0.57 Na_2O•30.1 H_2O) in the presence of mordenite seed crystals of varying amounts (0.0025, 0.025 and 0.25 g) and no added OSDA agent was monitored over time, as described in Table 3.4, Section 3.4.2. XRD diffractograms of as-synthesised products are depicted in Figures 5.15-5.17. The crystallisation curves for zeolite mordenite synthesis in the presence of varying amounts of seed crystals (0.0025, 0.025 and 0.25 g) compared to the zeolite mordenite synthesis system without added seed crystals are depicted in Figure 5.18.

5.3.1.1 Mineralogy and crystallinity

XRD diffractograms of as-synthesised zeolite products prepared using a general molar regime (1 SiO_2•0.02 Al_2O_3•0.57 Na_2O•30.1 H_2O) in the presence of a fixed amount of seed crystals (0.0025 g), at a hydrothermal temperature of 170 °C monitored over time, are depicted in Figure 5.15.

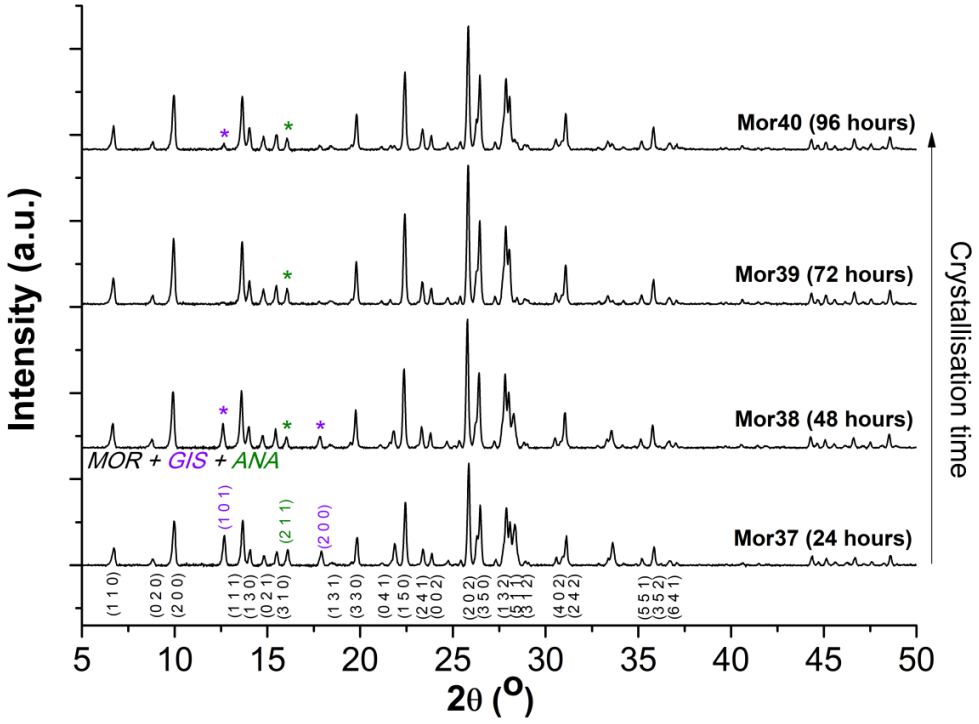

Figure 5.15: XRD diffractograms of as-synthesised Na-mordenite zeolites Mor37-40 synthesised at 170 °C, monitored with time, from a synthesis mixture with molar regime 1 SiO_2•0.019 Al_2O_3•0.57 Na_2O•30.1 H_2O in the presence of a fixed amount of seed crystals (0.0025 g). Key: MOR - zeolite mordenite, ANA - Analcime, GIS - zeolite Na-P1

The crystallisation of zeolite mordenite occurred in the presence of a small amount of zeolite mordenite seed crystals (0.0025 g) between 24 to 96 hours of crystallisation at 170 °C, as observed in Figure 5.15. As the crystallisation time increased, the crystallinity of zeolite mordenite increased (up to 72 hours). In the early stages of mordenite crystallisation (24-48 hours), the presence of the competing phases such as Na-P1 and analcime were observed (sample Mor37 and Mor38 as depicted in Figure 5.15). However, highly crystalline zeolite mordenite was formed after 48 hours of crystallisation as observed in Figure 5.15 (sample Mor38). After 72 hours of crystallisation (sample Mor39), highly crystalline zeolite mordenite was formed and other mineral phases such as Na-P1 and analcime were supressed. XRD diffractograms of as-synthesised zeolite products prepared using a general molar regime (1 SiO_2•0.02 Al_2O_3•0.57 Na_2O•30.1 H_2O) in the presence of a fixed amount of seed crystals (0.025 g), at a hydrothermal temperature of 170 °C monitored over time, are depicted in Figure 5.16.

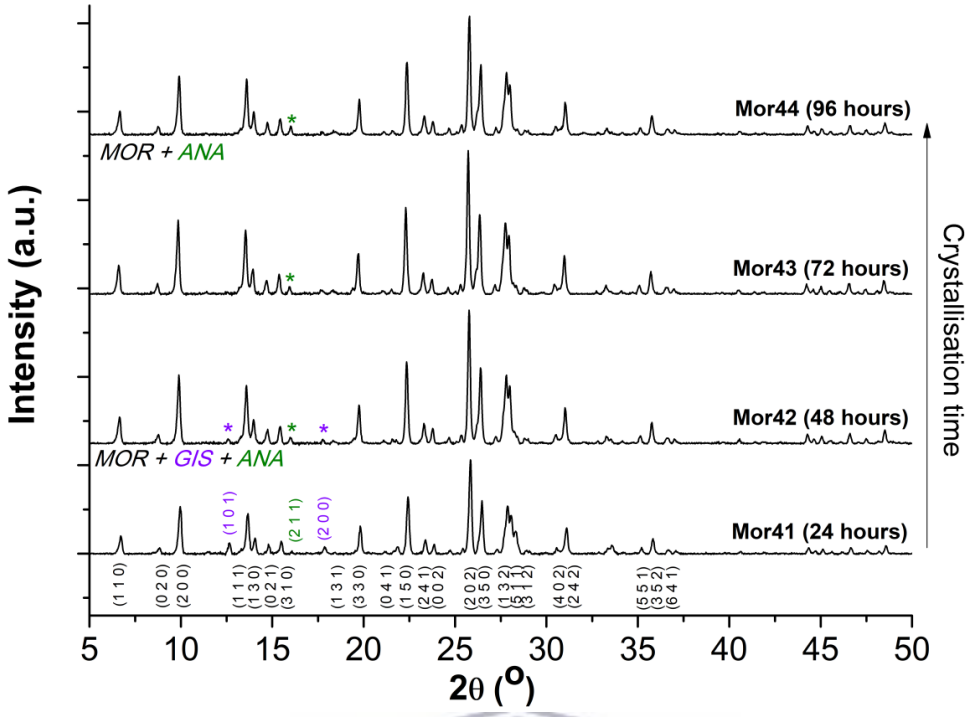

Figure 5.16: XRD diffractograms of as-synthesised Na-mordenite zeolites Mor41-44 synthesised at 170 °C, monitored with time, from a synthesis mixture with molar regime 1 SiO_2•0.019 Al_2O_3•0.57 Na_2O•30.1 H_2O in the presence of a fixed amount of seed crystals (0.025 g). Key: MOR - zeolite mordenite, ANA - Analcime, GIS - zeolite Na-P1

The crystallisation of zeolite mordenite occurred in the presence of a relatively small amount mordenite seed crystals (0.025 g) between 24 to 96 hours of crystallisation at 170 °C, as observed in Figure 5.16. In this case, the crystallinity of zeolite mordenite was enhanced (up to 72 hours) as the crystallisation time increased. The competing phases Na-P1 and analcime were observed as minor peaks in the crystallisation product formed in 24 hours (sample Mor41). After 48 hours of crystallisation (sample Mor42), highly crystalline zeolite mordenite was formed with minimal competing phases present as observed in Figure 5.16. XRD diffractograms of as-synthesised zeolite products prepared using a general molar regime (1 SiO_2•0.02 Al_2O_3•0.57 Na_2O•30.1 H_2O) in the presence of a fixed amount of seed crystals (0.25 g), at a hydrothermal temperature of 170 °C monitored over time, are depicted in Figure 5.17.

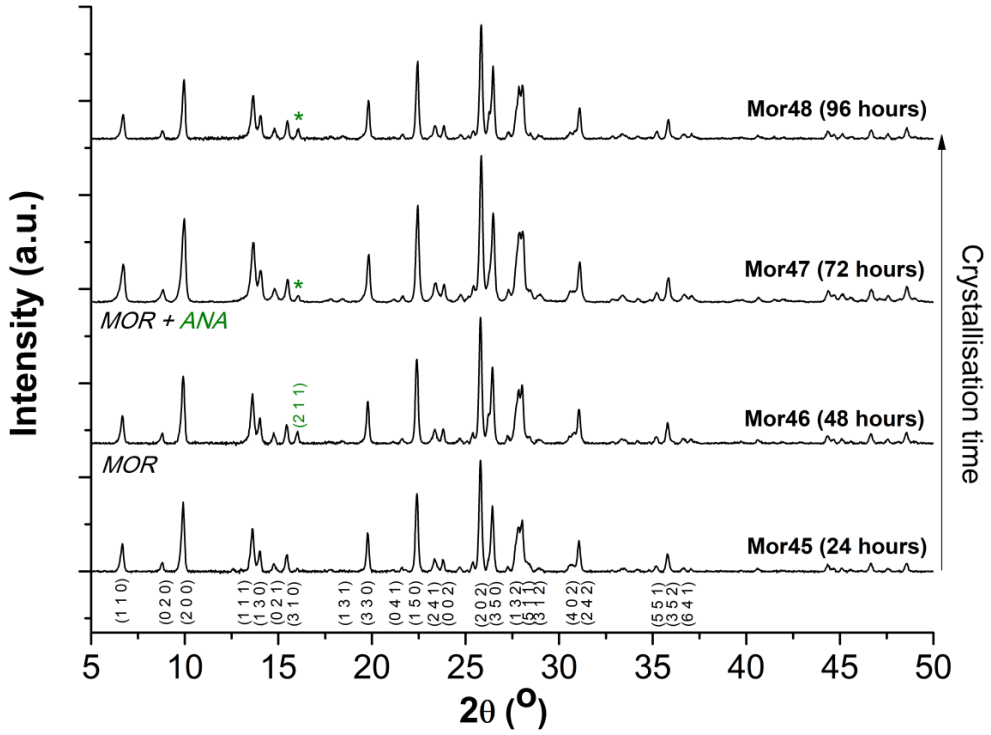

Figure 5.17: XRD diffractograms of as-synthesised Na-mordenite zeolites Mor45-48 synthesised at 170 °C, monitored with time, from a synthesis mixture with molar regime 1 SiO_2•0.019 Al_2O_3•0.57 Na_2O•30.1 H_2O in the presence of a fixed amount of seed crystals (0.25 g). Key: MOR - zeolite mordenite, ANA - Analcime

The crystallisation of zeolite mordenite occurred in the presence of a relatively larger amount mordenite seed crystals (0.25 g) between 24 to 96 hours of crystallisation at 170 °C, as observed in Figure 5.17. When a relatively larger amount of seeding crystals were added to the synthesis mixture, the formation of pure, crystalline zeolite mordenite was observed in the absence of competing phases after 24 hours of crystallisation (Mor45). As depicted in Figure 5.17, highly crystalline zeolite mordenite was also observed after 48-96 hours of crystallisation (Mor46-Mor48); however the appearance of a diffraction peak associated with analcime at 2θ value of ~16° was present in these samples. This illustrates the role of seeding in zeolite synthesis; whereby the crystallisation of competing phases may be supressed in the presence of seed crystals through enhancement of the crystallisation kinetics of the target zeolite phase (Grand et al., 2016). This is a particularly significant achievement for methods that make use of alternative feedstock for zeolite synthesis; as is the case in this study which utilises the CFA-derived silicon precursor as the main feedstock for zeolite synthesis, in the absence of an OSDA agent.

The crystallisation curves of seeded mordenite samples and mordenite synthesised in the absence of seed crystals are depicted in Figure 5.18; percentage relative crystallinity of each seeded mordenite sample was calculated relative to highly crystalline commercial mordenite.

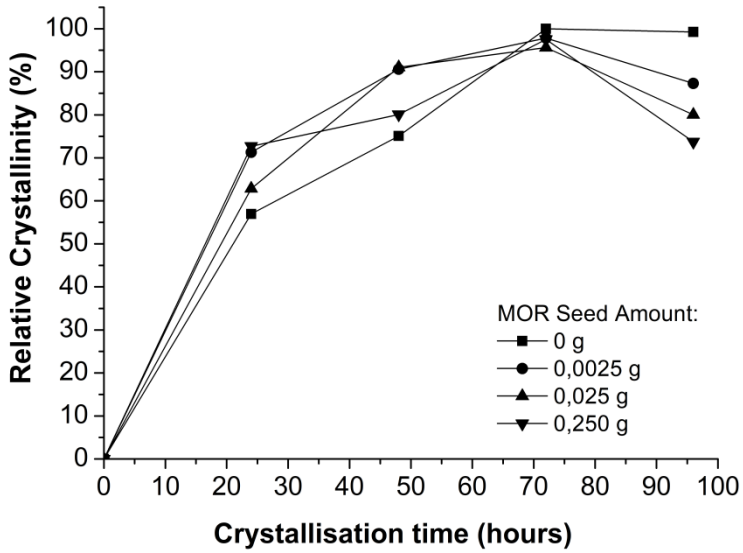

Figure 5.18: Crystallisation curves for as-synthesised Na-mordenite zeolites prepared from synthesis mixtures with a molar regime of 1 SiO_2•0.019 Al_2O_3•0.57 Na_2O•30.1 H_2O in the absence of added seed crystals (0 g) or in the presence of varying seed crystal amounts (0.025-0.25 g).

As depicted in Figure 5.18, the presence of zeolite mordenite seed crystals in the synthesis mixture enhanced the crystallisation rate of zeolite mordenite from the CFA-derived FASE material compared to the unseeded synthesis system (samples Mor11 and Mor16-18). A relatively low seed content (0.0025 and 0.025 g of mordenite seed crystals) resulted in the crystallisation of highly crystalline zeolite mordenite (~90 % relative crystallinity) after 48 hours of hydrothermal treatment at 170 °C, as depicted in Figure 5.18. In all cases (seeded mordenite synthesis and mordenite synthesis in the absence of seed crystals), highly crystalline zeolite mordenite with a relative crystallinity of ~100 % was formed after 72 hours of hydrothermal treatment at 170 °C. The utilisation of a small quantity of seed crystals in the synthesis of zeolite mordenite may therefore reduce the total time period required for the conversion of the FASE material into the crystalline zeolite mordenite framework, by reducing the induction period and enhancing mordenite crystallisation. Therefore, mordenite seed crystals may be incorporated into the synthesis procedure for zeolite mordenite from CFA to supress the crystallisation of the competing phases of zeolite mordenite (such as zeolite Na-P1 and analcime) and reduce the crystallisation time.

Similar results were reported in literature for the formation of zeolite mordenite from synthesis solutions with high silicon content in the presence of natural mordenite seed crystals (~3.0 to 18.5 wt%) (Ueda et al., 1980). Interestingly, Ueda et al., (1980) also reported that zeolite mordenite was able to crystallise from synthesis solutions containing analcime seed crystals. This may explain the presence of minor analcime peaks in mordenite samples prepared from the FASE material in both the unseeded (Section 5.2) and seeded synthesis systems. Todorova and Kalvachev, (2015) also reported the rapid crystallisation of zeolite mordenite in the presence of varying amounts of synthetic mordenite seed crystals (1.0 to 5.0 wt%). In this study, mordenite seed crystals are thought to behave as nucleation sites in the synthesis solution and favour the crystallisation of highly crystalline and pure zeolite mordenite after 24 hours of crystallisation (in the presence of a relatively small amount of seed crystals) using a CFA-derived silicon feedstock.

5.3.1.2 Morphology and composition

The effect of seeding amount on the morphology of zeolite mordenite was analysed by SEM and EDS was used to determine the average SAR ratio. SEM micrographs of as-synthesised Na-zeolites crystallised at 170 °C for 72 hours in the presence of varying amounts of zeolite mordenite seed crystals (0.0025-0.25 g) are depicted in Figure 5.19, compared to the morphology of zeolite mordenite seed crystals that were added to the synthesis mixtures.

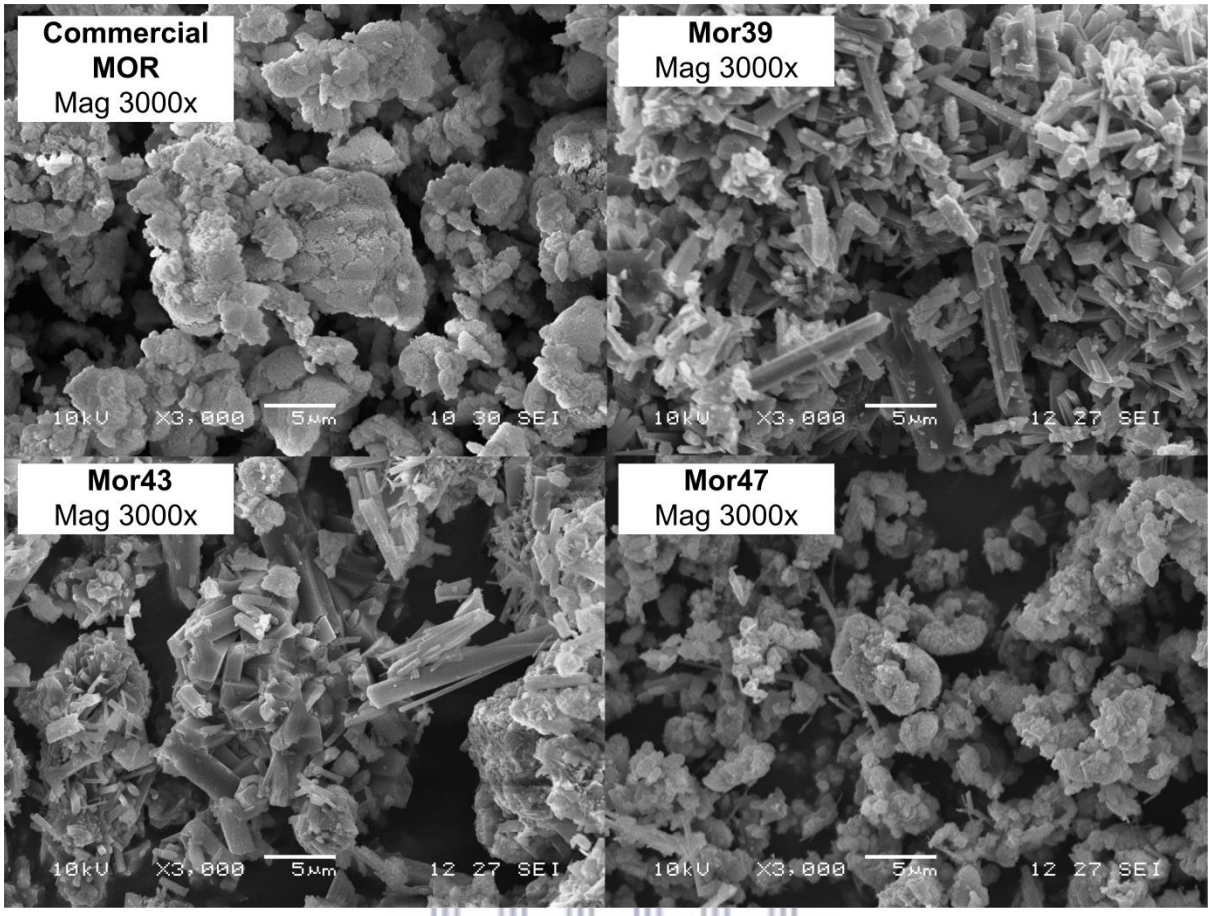

Figure 5.19: SEM micrograph (3000x magnification) of as-synthesised Na-zeolites Mor39, Mor43 and Mor47 synthesised at 170 °C for 72 hours in the presence of varying amounts of mordenite seed crystals (0.0025, 0.025 and 0.25 g, respectively) in the synthesis mixture with molar regime 1 SiO_2•0.019 Al_2O_3•0.57 Na_2O•30.1 H_2O, compared to commercial zeolite mordenite.

The morphology of zeolite mordenite formed in the presence of seed crystals was dependent on the amount of seed crystals added to the synthesis mixture, as depicted in Figure 5.19. Relatively higher seed content of 0.25 g (Mor47) resulted in the formation of small, sphere-like, agglomerated mordenite crystals similar to the morphology of the seed crystals. At relatively low seed content of 0.0025 g (Mor39) and 0.025 g (Mor43), the crystallisation of elongated needle-like mordenite crystals was observed (as depicted in Figure 5.19). It is noteworthy that these mordenite samples exhibit a similar needle-like morphology as the unseeded synthesis system (as depicted in Figure 5.11 for sample Mor17). However, mordenite crystals formed in seeded synthesis systems were relatively smaller than the mordenite crystals formed in the unseeded synthesis system. The average particle size and SAR values for as-synthesised Na-zeolites determined from EDS are summarised in Table 5.2.

Table 5.2: Properties of as-synthesised Na-zeolites Mor39, Mor43 and Mor47 such as average particle size (determined using ImageJ) and relative composition (determined by EDS analysis n=10), synthesised at 170 °C for 72 hours in the presence of varying amounts of mordenite seed crystals (0.0025, 0.025 and 0.25 g, respectively) in the synthesis mixture with molar regime 1 SiO_2•0.019 Al_2O_3•0.57 Na_2O•30.1 H_2O, compared to commercial zeolite mordenite.

Sample	Commercial mordenite seed amount added to the synthesis mixture (g)	Average particle size (µm)	SAR value	Na/Al ratio
Commercial mordenite	-	2.1	7.8	-
Mor39	0.0025	4.6	6.5	0.6
Mor43	0.025	4.4	6.3	0.01
Mor47	0.25	2.5	6.9	0.6

As listed in Table 5.2, the particle size of zeolite mordenite crystals was influenced by the amount of seed crystals added to the synthesis mixture, while the SAR value of seeded mordenite crystals was unaffected. Typically, zeolite mordenite synthesised from standard chemical reagent exhibits an SAR value in the range of ~5-17 (Aly et al., 2012; Choudhury et al., 1998; Holderich and van Bekkum, 1991). This indicates that seed crystals influenced the processes of nucleation and crystal growth during the transformation of the synthesis mixture into crystalline zeolite mordenite. Zeolite mordenite seed crystals exhibited an average particle size of 2.1 µm, as listed in Table 5.2. At low seed content of 0.0025 g (Mor39) and 0.025 g (Mor43) in the synthesis mixture, the particle size of mordenite crystals was relatively large at 4.6 and 4.4 µm, respectively. The relatively small amount of mordenite seed crystals added to the synthesis mixture serves as a surface on which rapid crystal growth may occur in the synthesis solution while the nucleation process is inhibited; this may have resulted in the formation of relatively large crystals (Ueda et al., 1980). At a relatively higher seed content of 0.25 g (Mor47), the particle size of mordenite crystals was relatively smaller (2.5 µm). In this case, the presence of a large amount of mordenite seed crystals in the synthesis mixture serves as nuclei and crystal growth of multiple "nuclei" occurs depleting the nutrients in the feedstock and consequently, these processes result in the formation of small zeolite mordenite crystals.

These results are similar to the changes in mordenite morphology observed in the presence of different amounts of mordenite seed crystals (Todorova and Kalvachev, 2015; Ueda et al., 1980). Todorova and Kalvachev, (2015) reported that an increase in the seed amount from 1

wt% to 5 wt% resulted in a reduction in zeolite mordenite particle size from 15 to 1-2 µm compared to the unseeded mordenite seeds (50 µm). Similar results were reported by Ueda et al., (1980). In this case, the synthesis of zeolite mordenite from the CFA-derived FASE material behaved similar to synthesis systems which made use of standard chemical reagents. Furthermore, the addition of mordenite seed crystals in the synthesis of zeolite mordenite (from the CFA-derived FASE material) may therefore be used to control the morphology of mordenite crystals in terms of both particle size and shape.

5.3.1.3 Thermal Stability

The thermal analysis of as-synthesised seeded mordenite samples Mor39, Mor43 and Mor47 (prepared using varying amounts of seed crystals under hydrothermal conditions of 170 °C for 72 hours) was analysed by TGA/DTG/DTA analysis in air, results are depicted in Figure 5.20. MS spectra for samples Mor39, Mor43 and Mor47 (with fragments of interest) are depicted in Figure 5.21. The thermal degradation profiles of zeolite mordenite samples synthesised in the presence of seed crystals (Mor39, Mor43 and Mor47) exhibited the same weight loss profile, as depicted in Figure 5.20, despite the differences in zeolite mordenite morphology as depicted in Figure 5.19.

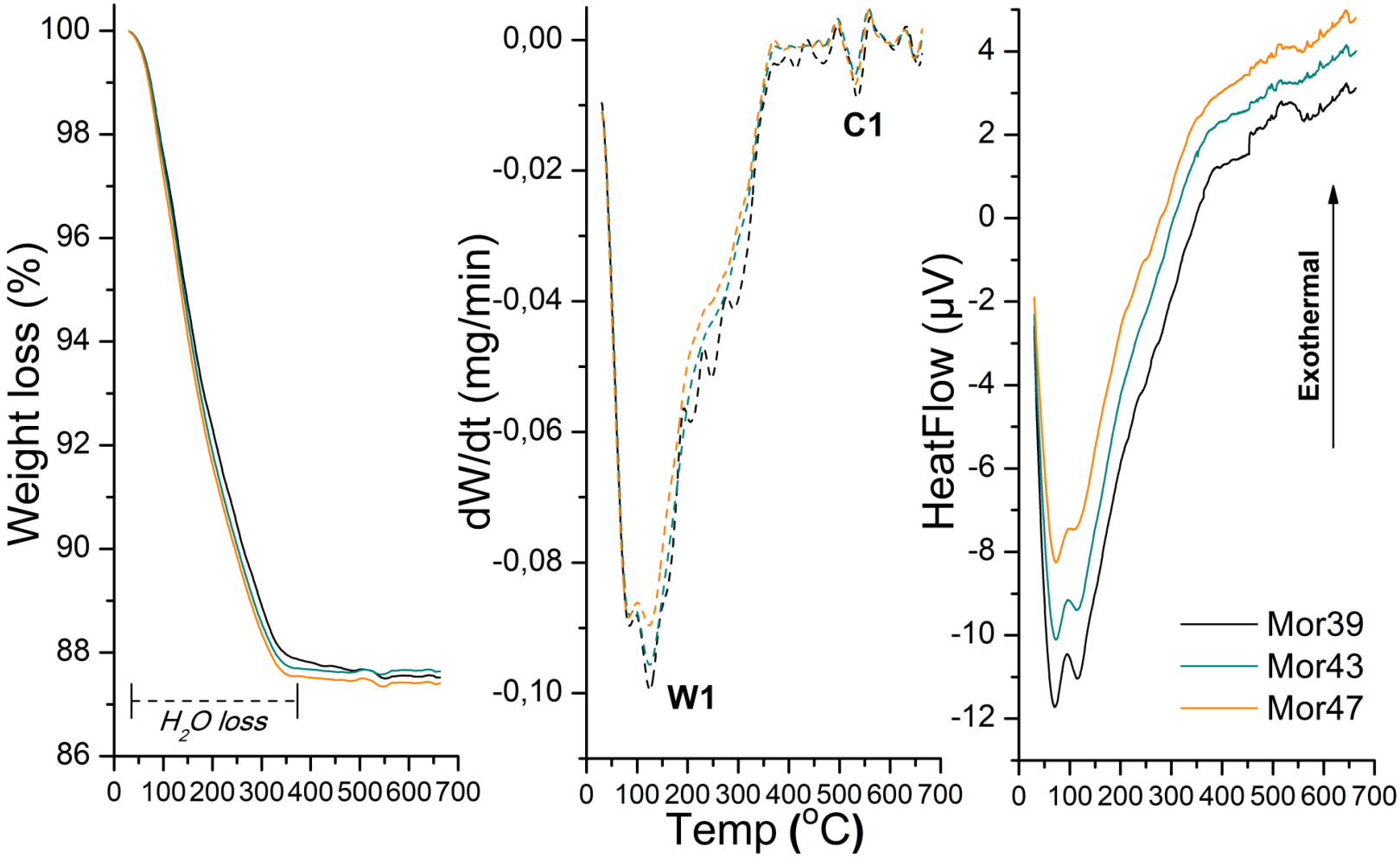

Figure 5.20: TGA/DTG/DTA analysis of as-synthesised zeolite mordenite samples Mor39, Mor43 and Mor47 synthesised at 170 °C for 72 hours, in the presence of varying amounts of mordenite seed crystals (0.0025-0.25 g) in the synthesis mixture with molar regime 1 SiO_2•0.019 Al_2O_3•0.57 Na_2O•30.1 H_2O.

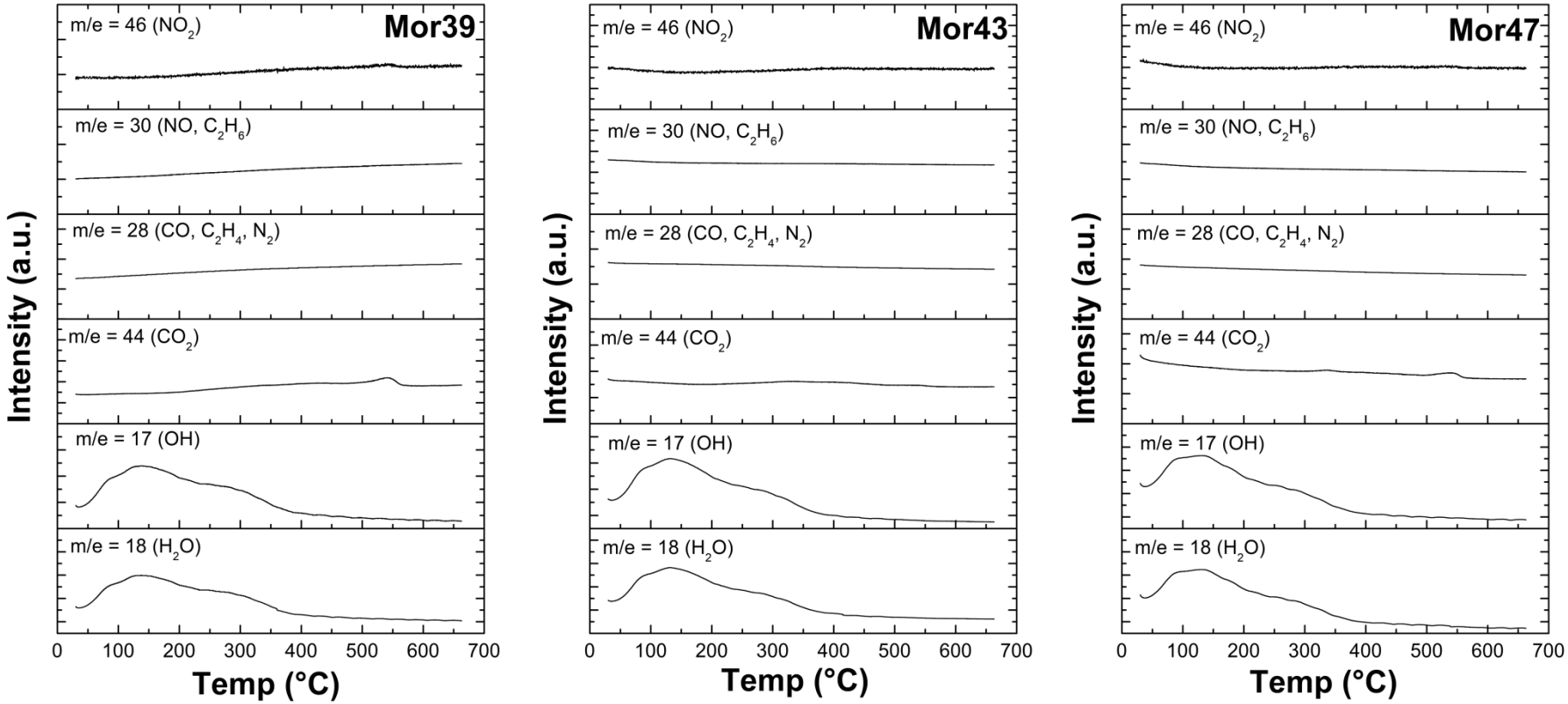

Figure 5.21: MS spectra of as-synthesised zeolite mordenite samples Mor39, Mor43 and Mor47 synthesised at 170 °C for 72 hours, in the presence of varying amounts of mordenite seed crystals (0.0025-0.25 g) in the synthesis mixture with molar regime 1 SiO_2•0.019 Al_2O_3•0.57 Na_2O•30.1 H_2O.

A summary of the thermal properties of as-synthesised zeolite mordenite samples prepared in the presence of varying amounts of seed crystals is listed in Table 5.3.

Table 5.3: Summary of information gathered from TGA analysis for as-synthesised zeolite mordenite samples Mor39, Mor43 and Mor47 synthesised at 170 °C for 72 hours, in the presence of varying amounts of mordenite seed crystals (0.0025-0.25 g) in the synthesis mixture with molar regime 1 SiO_2•0.019 Al_2O_3•0.57 Na_2O•30.1 H_2O; with water and extra-framework content reported as per gram of zeolite.

Sample	Temp. W1 peak (°C)	Water content (g/g zeolite)	Temp. C1 peak (°C)	Carbonate content (g/g zeolite)
Mor39	125	0.121	535	0.0017
Mor43	125	0.123	532	0.0004
Mor47	125	0.124	532	0.0012

As listed in Table 5.3, these samples exhibited two mass loss sections; (i) the main endothermic mass loss due to physisorbed water released from the pores of the MOR framework (annotated as W1 in Figure 5.20) and (ii) the exothermic mass loss associated with carbonate species (annotated as C1 in Figure 5.20) (Gabelica et al., 1984; Pál-Borbély, 2007). These results are confirmed by the MS spectra as depicted in Figure 5.21. Due to the similar aluminium content in these mordenite samples (synthesised in the presence of seed crystals), the water content of these materials was also similar at ~0.12 g/g of zeolites (~12 %) as listed in Table 5.3. Zeolite mordenite synthesised in the presence of seed crystals is therefore highly hygroscopic. These samples compare well to the unseeded zeolite mordenite sample Mor17 (as depicted in Figure 5.13) as well as mordenite samples synthesised from standard chemical reagents as reported in literature (Aly et al., 2012; Choudhury et al., 1998; Cysneiros et al., 2016).

The utilisation of synthetic zeolite mordenite as seed crystals in the synthesis of zeolite mordenite from the CFA-derived FASE material (without additional OSDA agent) resulted in enhanced crystallisation of zeolite mordenite and suppressed the formation of competing zeolite Na-P1 and analcime. Highly pure and crystalline zeolite mordenite was formed in the presence of a relatively small amount of seed crystals (0.0025 g) after 24 hours of crystallisation at 170 °C. Furthermore, this study illustrated that the addition of seed crystals to the synthesis mixture for mordenite synthesis from a CFA-derived silicon feedstock may also be used to control the particle size and shape; this is vital for the production of zeolite mordenite (with varying properties) for utilisation in different applications. However, it

should be noted that sample Mor17 (synthesised in the absence of seed crystals and OSDA agent at 170 °C for 72 hours) was highly crystalline (~100%). Therefore, the seeded-synthesis system mainly offers the advantage of enhanced mordenite crystallisation (~24-48 hours of crystallisation for relatively crystalline mordenite formation) and product purity (suppression of competing phases) in comparison to the unseeded-synthesis system.

5.4 OSDA-assisted hydrothermal synthesis of zeolite mordenite from fly ash silicon extract

In the past, the utilisation of OSDA agents in zeolite synthesis resulted in the formation of new high-silica zeolite frameworks and novel high-silica compositions for existing zeolites (Burton and Zones, 2007). The role of OSDA agents in zeolite synthesis is typically the organisation of precursor silicate species into the structural building units of a particular framework topology (Burton and Zones, 2007; Burkett and Davis, 1995; Davis and Lobo, 1992; Grand et al., 2016). The synthesis of zeolite mordenite with high SAR ratios (up to 37 in some cases) have been reported in the presence of various OSDA agents such as TEAOH, HMI, benzene-1,2-diol, benzyltrimethylammonium hydroxide (Jin et al., 2012; Jongkind et al., 1997; Lu et al., 2004; Lv et al., 2011; Mao et al., 2014; Shaikh et al., 1993). The dual-templating method was also utilised for the synthesis of zeolite mordenite in presence of OSDA agents (TEAOH and hexamethyleneimine, HMI), which was reported to cooperatively aid in mordenite nucleation and crystallisation in high silicon synthesis environments (Jin et al., 2012; Lv et al., 2011).

In this study, TEAOH was utilised as an OSDA agent in the synthesis of zeolite mordenite from the FASE material as described in Section 3.4.3. The effect of OSDA amount on the crystallisation of zeolite mordenite was investigated in the presence of a relatively small amount of seed crystals (0.025g), using a fixed molar regime 1 SiO_2•0.02 Al_2O_3•0.57 Na_2O•30.1 H_2O (corresponding to the optimum conditions determined in Section 5.2). The synthesis procedure for OSDA-assisted zeolite mordenite was subsequently altered by removal of the mineralising agent (NaOH) and then seed crystals from the synthesis mixture, to determine the influence of TEAOH amount (in the absence of these compounds) on zeolite mordenite crystallinity, morphology and thermal properties analysed by XRD, SEM and TGA/DTG/DTA coupled to MS, respectively. Furthermore, the influence of aluminium content (by sodium aluminate addition) of the synthesis mixture on zeolite mordenite crystallinity (determined by XRD) was investigated in the presence of TEAOH using the optimum result from the investigations on the OSDA-assisted zeolite mordenite.

5.4.1 The effect of OSDA amount on zeolite mordenite crystallisation

Zeolite mordenite crystallisation from synthesis mixtures with the general molar regime 1 SiO_2•0.02 Al_2O_3•0.57 Na_2O•30.1 H_2O•n TEAOH, with varying amounts of TEAOH, was investigated as described in Table 3.5, Section 3.4.3. These synthesis mixtures contained a fixed amount of seed crystals (0.025 g) to aid in the formation of zeolite mordenite.

5.4.1.1 Mineralogy and crystallinity

XRD diffractograms of as-synthesised zeolite products prepared using a general molar regime 1 SiO_2•0.02 Al_2O_3•0.57 Na_2O•30.1 H_2O•n TEAOH and varying amounts of OSDA agent (TEAOH) n = 0-1.05, in the presence of a fixed amount of seed crystals (0.025 g) under hydrothermal conditions (170 °C for 72 hours) are depicted in Figure 5.22. The percentage relative crystallinity for each sample was calculated relative to highly crystalline commercial mordenite and results are listed in Table 5.4.

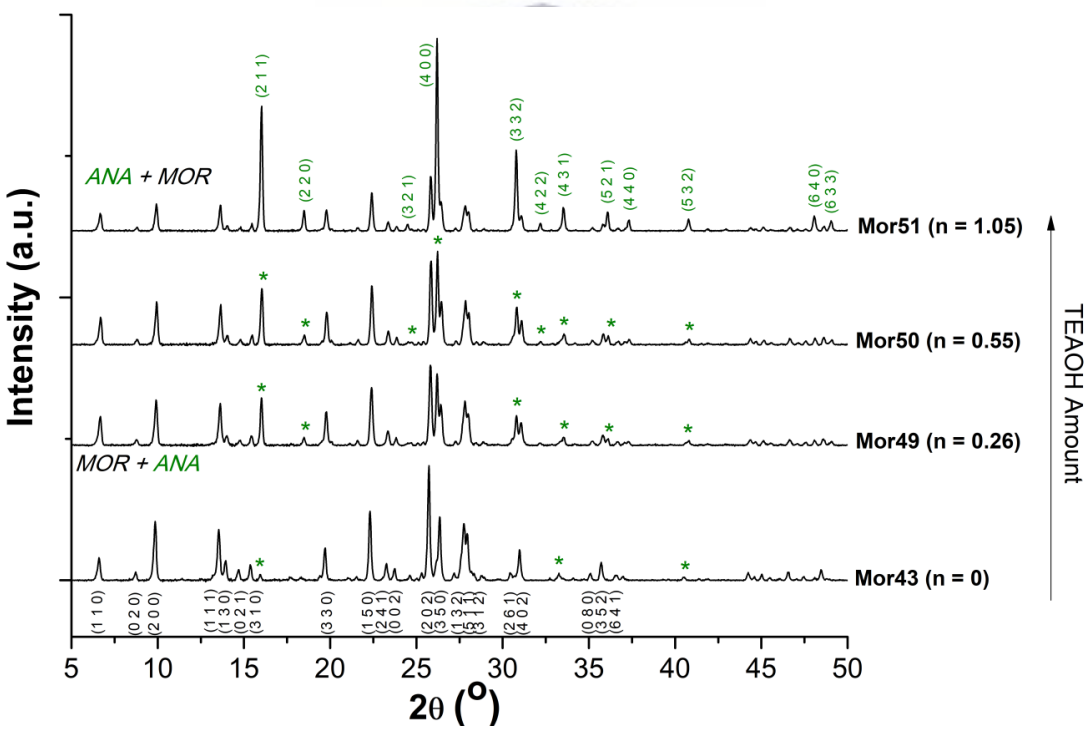

Figure 5.22: XRD diffractograms of as-synthesised Na-zeolites Mor43, Mor49-51 synthesised under hydrothermal conditions (170 °C for 72 hours) using varying amounts of ODSA agent (TEAOH) and a fixed amount of seed crystals (0.025 g) in the synthesis mixture with molar regime 1 SiO_2•0.019 Al_2O_3•0.57 Na_2O•n TEAOH•30.1 H_2O (n = 0-1.05). Key: MOR - zeolite mordenite, ANA - Analcime

As depicted in Figure 5.22, compared to sample Mor43 (synthesised in the absence of OSDA agent) the addition of an OSDA agent to the synthesis mixture resulted in the co-crystallisation of zeolite mordenite with analcime at relatively low TEAOH content for

samples Mor49 and Mor50 (n = 0.26-0.53) and the crystallisation of analcime was favoured over zeolite mordenite formation at relatively higher TEAOH content (n = 1.05) as observed for sample Mor51.

Table 5.4: Relative crystallinity of as-synthesised Na-zeolites Mor43, Mor49-51 synthesised in the presence of varying TEAOH amount (with 0.025g of mordenite seed crystals) in the synthesis mixture with molar regime 1 SiO_2•0.019 Al_2O_3•0.57 Na_2O•n TEAOH•30.1 H_2O (n = 0-1.05), determined using XRD data.

Sample	TEAOH molar content in synthesis mixture (moles)	% Relative Crystallinity
Mor43	0	95.6
Mor49	0.26	71.9
Mor50	0.55	72.1
Mor51	1.05	44.1

As listed in Table 5.4, the crystallinity of zeolite mordenite decreased from ~96% (sample Mor43 synthesised in the absence of OSDA agent) to ~44% at relatively high TEAOH content (n = 1.05). This is due to the enhanced crystallisation of analcime under these conditions. This may be attributed to the relatively higher hydroxide concentration in the synthesis mixture caused by the addition of the OSDA agent under these conditions, compared to sample Mor17.

5.4.1.2 Morphological and composition

The effect of OSDA amount on the morphology of zeolite mordenite was analysed by SEM coupled to EDS (to determine average SAR values of these materials). SEM micrographs of as-synthesised Na-zeolites crystallised at 170 °C for 72 hours with either no or varying amounts of OSDA agent (TEAOH) in the presence of a fixed amount of seed crystals (0.025 g) are depicted in Figure 5.23.

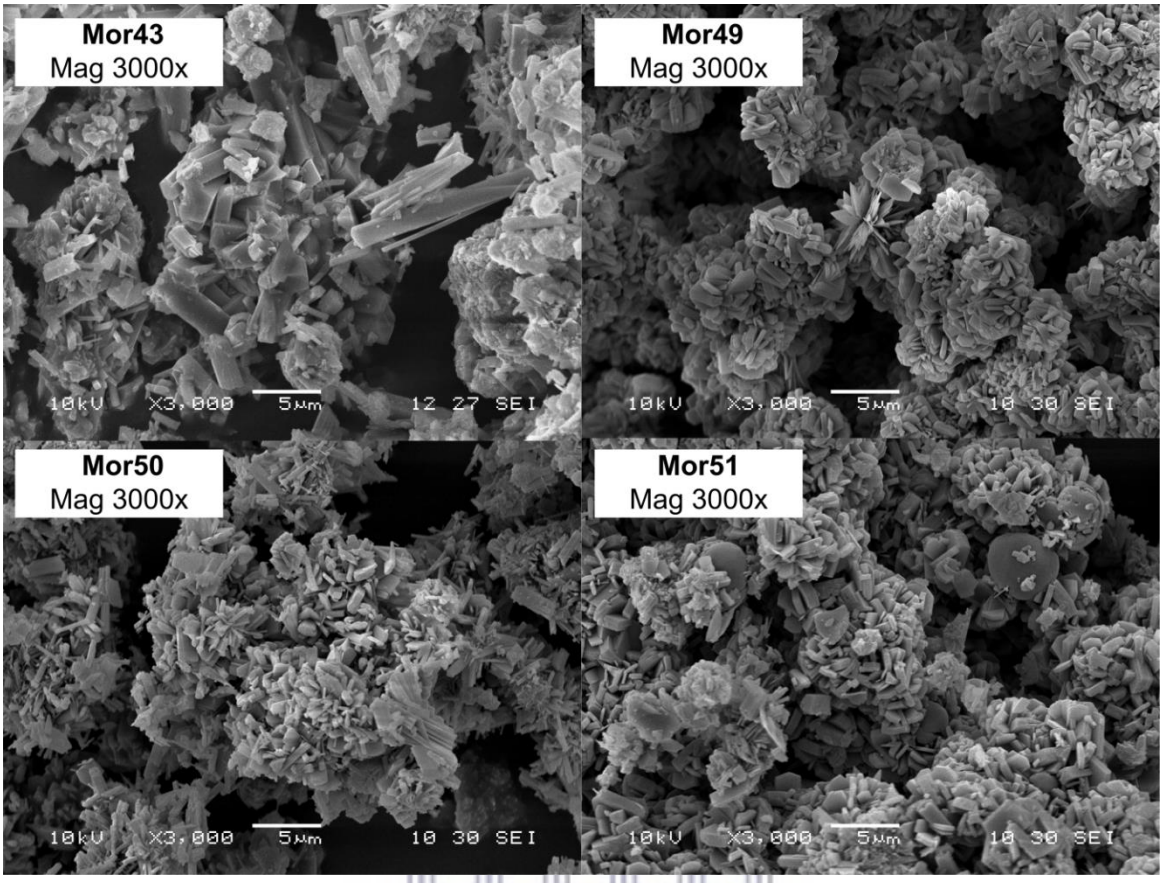

Figure 5.23: SEM micrograph (3000x magnification) of as-synthesised Na-zeolites Mor43, Mor49-51 synthesised under hydrothermal conditions (170 °C for 72 hours) using varying amounts of ODSA agent (TEAOH) and a fixed amount of seed crystals (0.025 g) in the synthesis mixture with molar regime 1 SiO_2•0.019 Al_2O_3•0.57 Na_2O•n TEAOH•30.1 H_2O (n = 0-1.05).

Compared to Mor43 (synthesised in the absence of OSDA agent) it was observed that in the presence of TEAOH as an OSDA agent in the synthesis mixture, needle-like zeolite mordenite crystals formed in an agglomerated manner (as observed in Figure 5.23 for samples Mor49-Mor51). As the TEAOH content was increased the presence of relatively larger, spherical analcime crystals was observed in the synthesised product (as depicted in Figure 5.23 for sample Mor51). The average particle size and SAR values for as-synthesised Na-zeolites determined from EDS are summarised in Table 5.5.

Table 5.5: Properties of as-synthesised Na-zeolites Mor43, Mor49-51 such as average particle size (determined using ImageJ) and relative composition (determined by EDS analysis n=10), synthesised under hydrothermal conditions (170 °C for 72 hours) using varying amounts of ODSA agent (TEAOH) and a fixed amount of seed crystals (0.025 g) in the synthesis mixture with molar regime 1 SiO_2•0.019 Al_2O_3•0.57 Na_2O•n TEAOH•30.1 H_2O (n = 0-1.05).

Sample	TEAOH molar content in synthesis mixture (moles)	Average particle size (µm)	SAR value	Na/Al ratio
Mor43	0	4.4	6.3	0.01
Mor49	0.26	2.1	8.2	0.4
Mor50	0.55	2.4	8.1	0.5
Mor51	1.05	7.8	7.2	0.5

As listed in Table 5.5, low TEAOH content (n = 0.26-0.53 for samples Mor49 and Mor50, respectively) resulted in a reduced particle size (2.1-2.4 µm) for agglomerated zeolite mordenite crystals and increase in the SAR value for these crystals. At high TEAOH content, the formation of large analcime crystals (7.8 µm) were observed together with agglomerated needle-like mordenite crystals. The presence of TEAOH in the synthesis mixture resulted in an increase in the SAR of the synthesised product, as listed in Table 5.5. However, the increase in SAR values of the synthesised product was not as pronounced as expected. This may be due to the presence of analcime, with common SAR value of ~1 (a much lower SAR value than zeolite mordenite), as a minor phase in synthesised products Mor49 and Mor50 and as the major phase in synthesis product Mor51.

The presence of TEAOH in the synthesis mixture therefore favoured mordenite nucleation over crystal growth. In this case it is noteworthy that the effect of the OSDA agent (TEAOH) on crystallisation processes outweighs the effect of the small amount of mordenite seeding crystals added to the synthesis mixture. As discussed in Section 5.3, the opposite effect was observed during mordenite crystallisation in the presence of a small amount of seed crystals from the OSDA-free synthesis environment (Todorova and Kalvachev, 2015; Ueda et al., 1980). Under the synthesis conditions utilised in this study, the presence of an OSDA agent in the synthesis mixture during the conversion of the CFA-derived FASE material to zeolite mordenite allowed for control over the crystal size of mordenite crystals. However, enhanced crystallisation processes resulted in the formation of a competing phase such as spherical analcime crystals.

5.4.1.3 Thermal Stability

The thermal analysis of as-synthesised zeolite mordenite samples Mor49-Mor51 and Mor43, prepared using varying amounts of TEAOH (in the presence of a small amount of seed crystals) under hydrothermal conditions of 170 °C for 72 hours, was analysed by TGA/DTG/DTA analysis in air coupled to MS spectrometry for identification of released compounds; results are depicted in Figure 5.24 and Figure 5.25, respectively.

As observed in Figure 5.24, zeolite mordenite samples synthesised either with no TEAOH or with varying amounts of TEAOH (in the presence of a small amount of mordenite seed crystals) contained four mass loss sections related to the endothermic release of physisorbed water (W1 and W2) from the MOR/ANA framework as well as the exothermic degradation and release of OSDA (T1 and T2) from the pores of the MOR framework; compared to the sample Mor43 synthesised in the absence of OSDA agent which only contained a mass loss related to the release of physisorbed water (W1). Samples Mor49 and Mor50 exhibited similar TGA/DTG and DTA thermal profiles as well as MS spectra with main mass loss sections at W1 and T1, as depicted in Figure 5.24 and 5.25, respectively. These samples are made up of mainly zeolite mordenite with analcime present as a minor phase (as observed in Figure 5.22). Whereas sample Mor51 (consisted of mainly analcime as observed in Figure 5.22) exhibited the main mass loss due to the release of physisorbed water, annotated as W2 in Figure 5.24.

As depicted in Figure 5.25, the low temperature mass loss between r.t. and ~350 °C was due to water evolution from the pores of the MOR framework (H_2O and OH fragments observed at m/e = 18 and 17, respectively) and the high temperature mass loss at ~420 °C (and in some cases at ~530 °C) was due to the release of TEAOH/TEA^+ degradation products (most likely H_2O, OH, CO_2, CO/C_2H_4, NO, NO_2 observed at m/e = 18, 17, 44, 28, 30 and 46, respectively) from the pores of the MOR framework. As observed in Figure 5.25, at 600 °C the degradation and oxidation of TEA^+ to yield H_2O and CO_2 was complete.

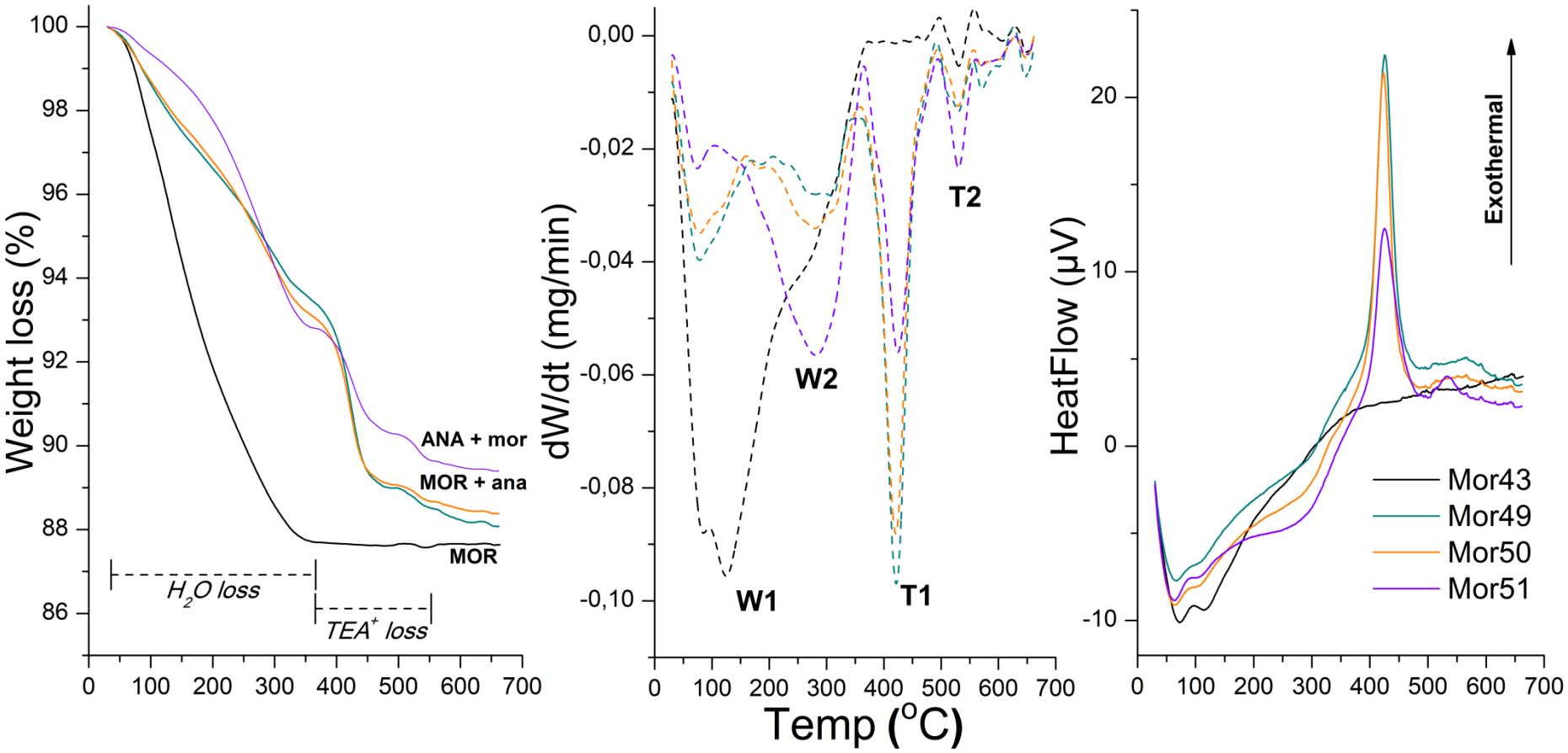

Figure 5.24: TGA/DTG/DTA analysis of as-synthesised Na-zeolites Mor43, Mor49-51 synthesised under hydrothermal conditions (170 °C for 72 hours) using varying amounts of ODSA agent (TEAOH) and a fixed amount of seed crystals (0.025 g) in the synthesis mixture with molar regime 1 SiO_2•0.019 Al_2O_3•0.57 Na_2O•n TEAOH•30.1 H_2O (n = 0-1.05).

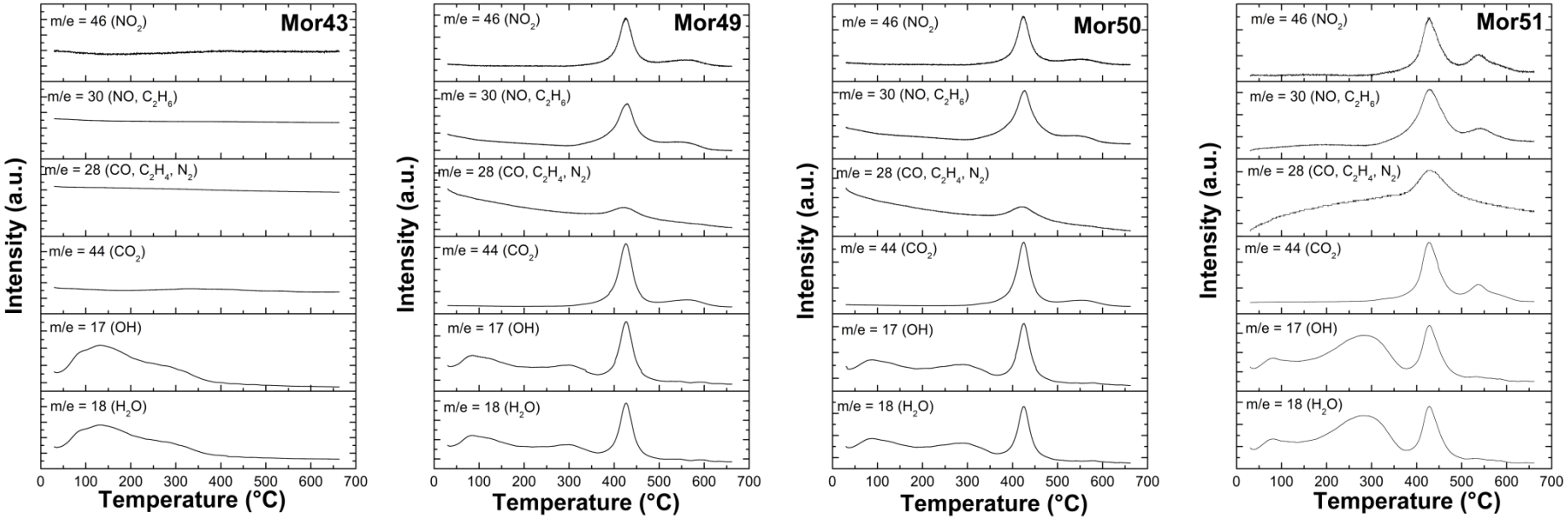

Figure 5.25: MS spectra of as-synthesised Na-zeolites Mor43, Mor49-51 synthesised under hydrothermal conditions (170 °C for 72 hours) using varying amounts of ODSA agent (TEAOH) and a fixed amount of seed crystals (0.025 g) in the synthesis mixture with molar regime 1 SiO_2•0.019 Al_2O_3•0.57 Na_2O•n TEAOH•30.1 H_2O (n = 0-1.05).

A summary of the thermal properties of as-synthesised zeolite mordenite samples prepared either without or with varying TEAOH amounts, in the presence of 0.025 g of mordenite seed crystals, is listed in Table 5.6.

Table 5.6: Summary of information gathered from TGA analysis for as-synthesised zeolite samples Mor43, Mor49-Mor51 synthesised under hydrothermal conditions (170 °C for 72 hours) using varying amounts of ODSA agent (TEAOH) and a fixed amount of seed crystals (0.025 g) in the synthesis mixture with molar regime 1 SiO_2•0.019 Al_2O_3•0.57 Na_2O•n TEAOH•30.1 H_2O (n = 0-1.05), with water and template content reported as per gram of zeolite.

Sample	Temp. W1 peak (°C)	Temp. W2 peak (°C)	Water content (g/g zeolite)	Temp. T1 peak (°C)	Temp. T2 peak (°C)	TEAOH content (g/g zeolite)
Mor43	125	532	0.123	-	-	-
Mor49	77	280	0.064	421	529	0.052
Mor50	77	278	0.068	421	529	0.046
Mor51	74	281	0.071	424	530	0.033

As listed in Table 5.6, the total water content of synthesised samples varied depending on the SAR value of the material. Sample Mor43 (with SAR value of 6.3) contained relatively higher water content (~0.12 g/g zeolite) than relatively more siliceous mordenite samples Mor49-Mor51 prepared in the presence of an OSDA agent (~0.06 g/g zeolite). This is as expected since aluminium-rich zeolites are considered relatively more hydrophilic than siliceous zeolites (Bourgeat-Lami et al., 1992). The main release of physisorbed water (W1) from samples Mor49 and Mor50 occurred at a relatively low temperature (~77 °C) compared to sample Mor51, which exhibited the main loss of physisorbed water at a relatively higher temperature of 281 °C (W2). This is thought to be due to the difference in the morphology of mordenite crystals (relatively small needle-like crystals) compared to analcime crystals (relatively larger, spherical crystals) as observed in Figure 5.23; which results in different diffusional pathways for molecules during thermal treatment in air.

Regarding the degradation of the OSDA agent (TEAOH), the low temperature mass loss at ~420 °C (annotated T1 in Figure 5.24) is associated with TEAOH molecules/TEA^+ cations counter-balancing anionic framework charges at zeolitic acid sites (Si-O-Al^- sites) in the pores of the MOR framework, while the high temperature mass loss at ~530 °C (annotated T2 in Figure 5.24) is associated with TEAOH/TEA^+ cations in less accessible sites in the pores and channels of the MOR framework experiencing diffusional constraints during the thermal

treatment of the samples in air (Bourgeat-Lami et al., 1992; Lohse et al., 1996; Pál-Borbély, 2007). In this case, diffusional constraints are thought to be due to the agglomerated nature of zeolite mordenite crystals as observed in Figure 5.23. It is noteworthy that TEA^+ incorporation into the synthesised product was dependent on the crystallinity of zeolite mordenite (i.e. a decrease in the TEA^+ content in the synthesised product was observed as the relative crystallinity of zeolite mordenite decreased as listed in Table 5.6). This illustrates that the OSDA agent (TEAOH) plays a role in mordenite crystallisation; however, these organic cations were not incorporated into the analcime framework during the crystallisation process.

The synthesis of high-silica zeolite mordenite (up to SAR of ~30, crystal size ~8 µm) from high-silica synthesis mixtures prepared from standard chemical reagents in the presence of mordenite seed crystals (4 wt%) and TEAOH as the OSDA agent, under hydrothermal conditions of 170 °C for 72 hours was reported in literature (Lu et al., 2004). Mordenite crystals reported by Lu et al., (2004) were relatively large compared to the mordenite crystals synthesised from a CFA-derived silicon feedstock in this study under similar conditions (2.1-4.4 µm). Overall, results reported by Lu et al., (2004) are comparable to the findings of this investigation on the effect of TEAOH amount of the crystallisation of zeolite mordenite in the presence of a small amount of seed crystals (0.025 g). In this study, the addition of TEAOH into the synthesis mixture during zeolite mordenite synthesis from the CFA-derived FASE material (in the presence of mordenite seed crystals) resulted in the preferential formation of analcime under the synthesis conditions investigated. The enhanced crystallisation may also have been caused by the increased alkalinity of the synthesis system due to the addition of TEAOH to the synthesis mixture. Therefore, the addition of TEAOH to the synthesis mixture during the synthesis of zeolite mordenite was carried out without added NaOH as mineralising agent, in the presence of a fixed amount of mordenite seed crystals.

5.4.2 The effect of OSDA agent on zeolite mordenite crystallisation, in the absence of NaOH

The crystallisation of zeolite mordenite from synthesis mixtures with the general molar regime 1 SiO_2•0.02 Al_2O_3•0.46 Na_2O•30.1 H_2O•n TEAOH with varying amounts of TEAOH (n = 0.26-1.05), in the presence of a fixed amount of seed crystals (0.025 g), was investigated (as described in Table 3.5, Section 3.4.3). This set of experiments was carried out in the absence of additional NaOH as a mineralising agent, to improve the crystallisation kinetics

towards the formation of crystalline zeolite mordenite without the formation of competing phases such as analcime or zeolite Na-P1.

5.4.2.1 Mineralogy and crystallinity

XRD diffractograms of as-synthesised zeolite products crystallised at 170 °C for 72 hours from synthesis mixtures with no added NaOH and a fixed molar regime (1 SiO_2•0.02 Al_2O_3•0.46 Na_2O•30.1 H_2O•n TEAOH) with varying amounts of TEAOH (n= 0.26-1.05) in the presence of a fixed amount of seed crystals (0.025 g) are depicted in Figure 5.26. The percentage relative crystallinity for each sample was calculated relative to highly crystalline commercial mordenite and results are listed in Table 5.7.

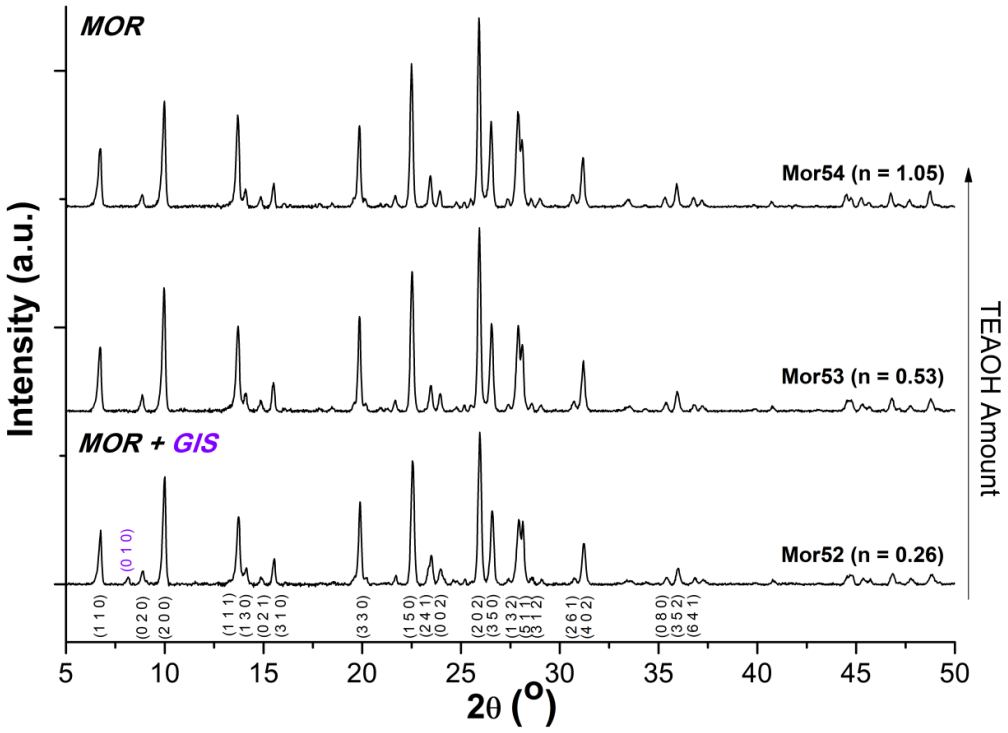

Figure 5.26: XRD diffractograms of as-synthesised Na-zeolites Mor52-54 synthesised using varying amounts of ODSA agent (TEAOH), a fixed amount of seed crystals (0.025 g), without NaOH added in the synthesis mixture with molar regime 1 SiO_2•0.019 Al_2O_3•0.46 Na_2O•n TEAOH•30.1 H_2O (n = 0.26-1.05). Key: MOR - zeolite mordenite, GIS - zeolite Na-P1

In the presence of varying amounts of TEAOH (n = 0.26-1.05) and a small amount of mordenite seed crystals (0.025 g) without the addition of NaOH as mineralising agent, the crystallisation of pure zeolite mordenite was observed as depicted in Figure 5.26; with the exception of a minor peak at 2θ value of ~8.1° associated with Gismondine observed for sample Mor52 which crystallised at low TEAOH content (n = 0.26).

Table 5.7: Relative crystallinity of as-synthesised Na-zeolites Mor52-54 synthesised in the presence of varying TEAOH amount (with 0.025g of mordenite seed crystals, no added NaOH) in the synthesis mixture with molar regime 1 SiO_2•0.019 Al_2O_3•0.46 Na_2O•n TEAOH•30.1 H_2O (n = 0.26-1.05), determined using XRD data.

Sample	TEAOH molar content in synthesis mixture (moles)	% Relative Crystallinity
Mor52	0.26	75.2
Mor53	0.55	90.1
Mor54	1.05	89.3

As depicted in Table 5.7, the crystallinity of zeolite mordenite increased as the TEAOH content in the synthesis mixture increased (in the absence of NaOH as mineralising agent). This effect was observed up to n = 0.56, after which the crystallinity reached a plateau. These results further indicate that mordenite crystallisation is highly sensitive to the alkalinity of the synthesis system. Under the conditions investigated for the conversion of the CFA-derived FASE material to zeolite mordenite, the crystallisation of zeolite mordenite was favoured over the crystallisation of competing phases such as analcime or zeolite Na-P1 in the presence of an OSDA agent such as TEAOH and a small amount of mordenite seed crystals (0.025 g) without the addition of NaOH as a mineralising agent. Highly crystalline zeolite mordenite was achieved over the entire range of TEAOH content investigated (n = 0.26-1.05) and highly pure zeolite mordenite was observed at a relatively low TEAOH content in the synthesis mixture (n = 0.53).

5.4.2.2 Morphological and composition

SEM micrographs of as-synthesised Na-zeolites crystallised at 170 °C for 72 hours with varying amounts of OSDA agent (TEAOH) in the presence of a fixed amount of mordenite seed crystals (0.025 g), without the addition of NaOH, are depicted in Figure 5.27.

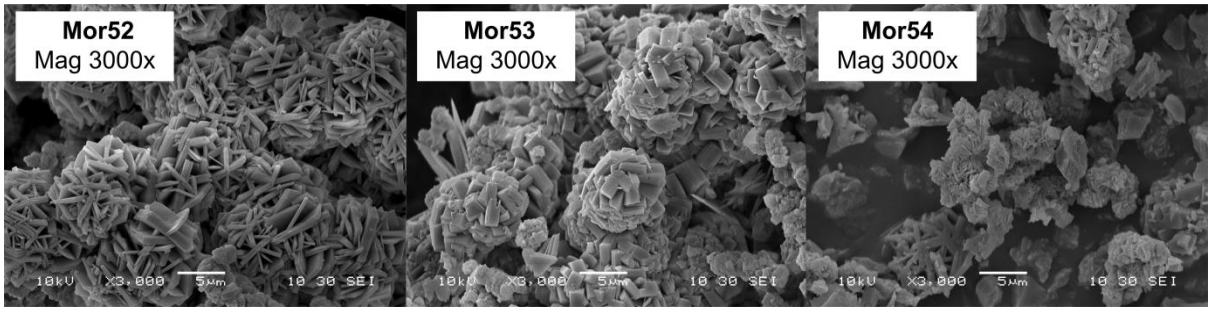

Figure 5.27: SEM micrographs (3000x magnification) of as-synthesised Na-zeolites Mor52-54 synthesised under hydrothermal conditions (170 °C for 72 hours) using varying amounts of ODSA agent (TEAOH) and a fixed amount of seed crystals (0.025 g), without NaOH added in the synthesis mixture with molar regime 1 SiO_2•0.019 Al_2O_3•0.46 Na_2O•n TEAOH•30.1 H_2O (n = 0.26-1.05).

As depicted in Figure 5.27, at relatively low TEAOH content (n = 0.26) for sample Mor52 zeolite mordenite crystals formed as relatively thin platelets, in a highly agglomerated manner. Highly crystalline sample Mor53 exhibited similar crystal morphology, however these crystals were relatively thicker compared to sample Mor52. The morphology of sample Mor54 contained a mixture of prismatic mordenite crystals as well as agglomerated platelets as observed in Figure 5.27. The morphology of sample Mor52 resembles that of hierarchical zeolite X synthesised from a clear solution extracted from CFA (Musyoka et al., 2014). Interestingly, Musyoka et al., (2014) also reported that hierarchical zeolite X formed in the presence of Na-P1 as a minor phase. The average particle size and SAR values for as-synthesised Na-zeolites determined from EDS are summarised in Table 5.8.

Table 5.8: Properties of as-synthesised Na-zeolites Mor52-54 such as average particle size (determined using ImageJ) and relative composition (determined by EDS analysis n=10), synthesised under hydrothermal conditions (170 °C for 72 hours) using varying amounts of ODSA agent (TEAOH) and a fixed amount of seed crystals (0.025 g), without added NaOH in the synthesis mixture with molar regime 1 SiO_2•0.019 Al_2O_3•0.46 Na_2O•n TEAOH•30.1 H_2O (n = 0.26-1.05).

Sample	TEAOH molar content in synthesis mixture (moles)	Average particle size (μm)	SAR value	Na/Al ratio
Mor52	0.26	7.2	14.6	0.4
Mor53	0.55	6.7	12.1	0.4
Mor54	1.05	5.8	10.0	0.03

As listed in Table 5.8, the average particle size of agglomerated zeolite mordenite crystals decreased as the TEAOH content in the synthesis mixture increased. The Na/Al ratio of these materials was relatively low between 0.03 and 0.4 (<<1). This value is typically 1 in aluminosilicate zeolites prepared in the absence of an OSDA agent. This illustrates that TEA^+ cations may be present in the MOR framework as charge-balancing cations. Highly crystalline zeolite mordenite sample Mor53 exhibited a relatively high SAR value of 12.1; this is as expected for the crystallisation of zeolites in the presence of an OSDA agent. The SAR value of zeolite mordenite samples Mor52-Mor54 ranged between 10 and 14.6, as listed in Table 5.8, and decreased with an increase in TEAOH content in the synthesis mixture.

In this study, the precursor material (FASE) is highly siliceous and a small amount of sodium aluminate was added to the synthesis mixture to aid in the formation of zeolite mordenite (as described in Section 3.4.3); this resulted in a synthesis mixture that was highly siliceous. It is therefore proposed that at relatively low TEAOH content (n = 0.26-0.53) in the synthesis mixture, the formation of a few aluminium-rich nuclei occurs followed by the condensation of siliceous species onto the growing crystal surface during crystal growth resulting in relatively large zeolite mordenite crystals with a high SAR value. At relatively high TEAOH content (n = 1.05), it is proposed that during the initial stages of crystallisation a relatively larger quantity of aluminium-rich nuclei form around the OSDA agent, followed by the condensation of silicate species onto the growing crystal surface during crystal growth that results in the formation of relatively smaller zeolite mordenite crystals with relatively lower SAR values. In this way relatively larger, siliceous zeolite mordenite crystals formed at low

TEAOH content in the synthesis mixture, while relatively smaller, aluminium-rich zeolite mordenite crystals were formed at relatively higher TEAOH content in the synthesis mixture.

5.4.2.3 Thermal Stability

The thermal analysis of as-synthesised zeolite mordenite samples Mor52-Mor54, prepared using varying amounts of TEAOH in the presence of a small amount of mordenite seed crystals (with no added NaOH) under hydrothermal conditions of 170 °C for 72 hours, was analysed by TGA/DTG/DTA analysis in air coupled to MS; results are depicted in Figure 5.28 and Figure 5.29, respectively. As observed in Figure 5.28, zeolite mordenite samples synthesised with varying amounts of TEAOH (in the presence of a small amount of mordenite seed crystals, with no added NaOH) exhibited four mass loss sections related to the endothermic release of physisorbed water (W1 and W2) as well as the exothermic degradation and release of OSDA (T1 and T2) from the MOR framework. The relatively high temperature mass loss sections W2 and T2 (observed during the thermal treatment in air) are due to diffusional constraints of compounds situated in less accessible sites in the pores and channels of the MOR framework, as discussed previously.

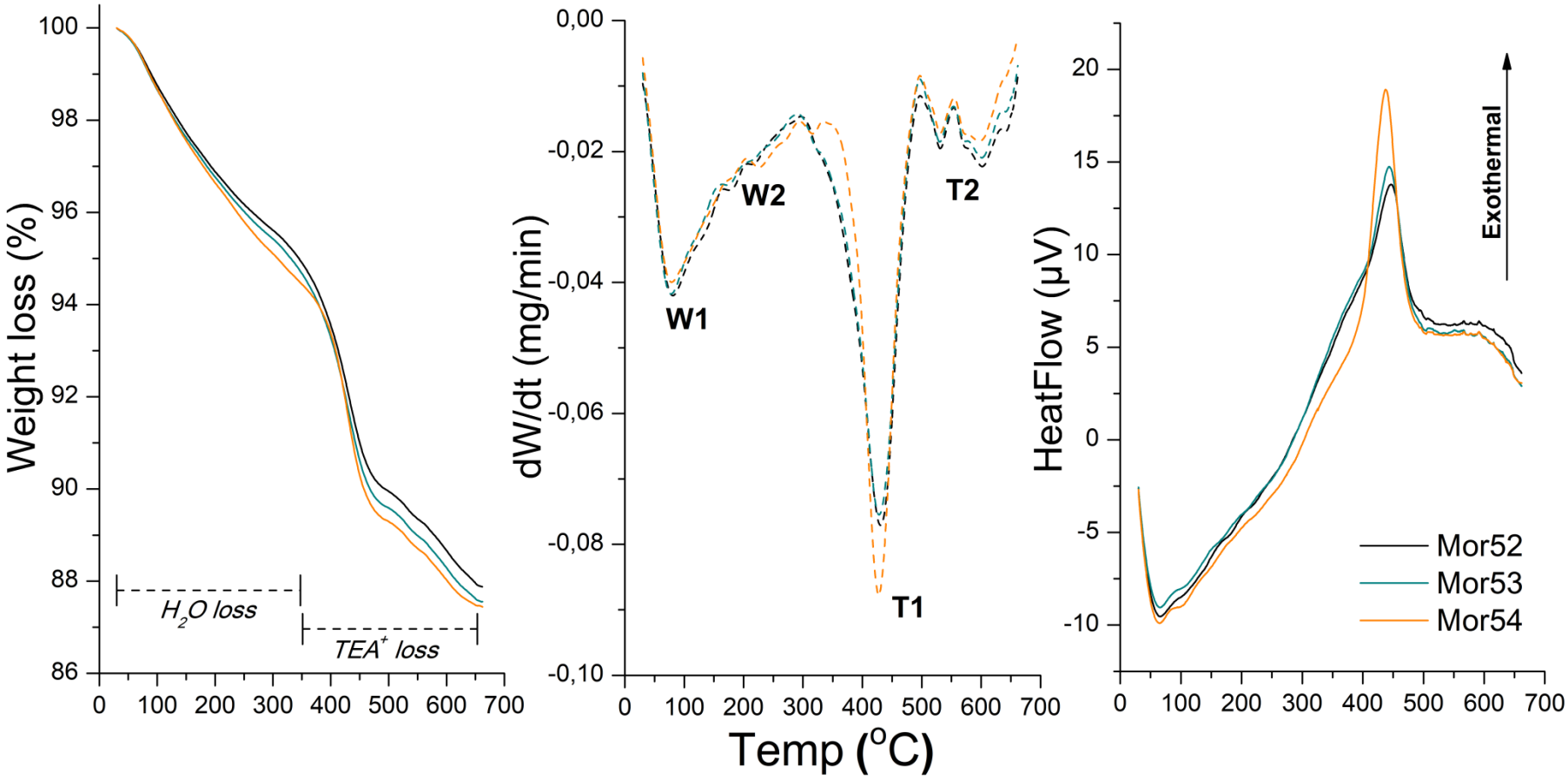

Figure 5.28: TGA/DTG/DTA analysis of as-synthesised Na-zeolites Mor52-54 synthesised under hydrothermal conditions (170 °C for 72 hours) using varying amounts of ODSA agent (TEAOH) in the absence of NaOH, with a fixed amount of seed crystals (0.025 g) in the synthesis mixture with molar regime 1 SiO_2•0.019 Al_2O_3•0.46 Na_2O•n TEAOH•30.1 H_2O (n = 0.26-1.05).

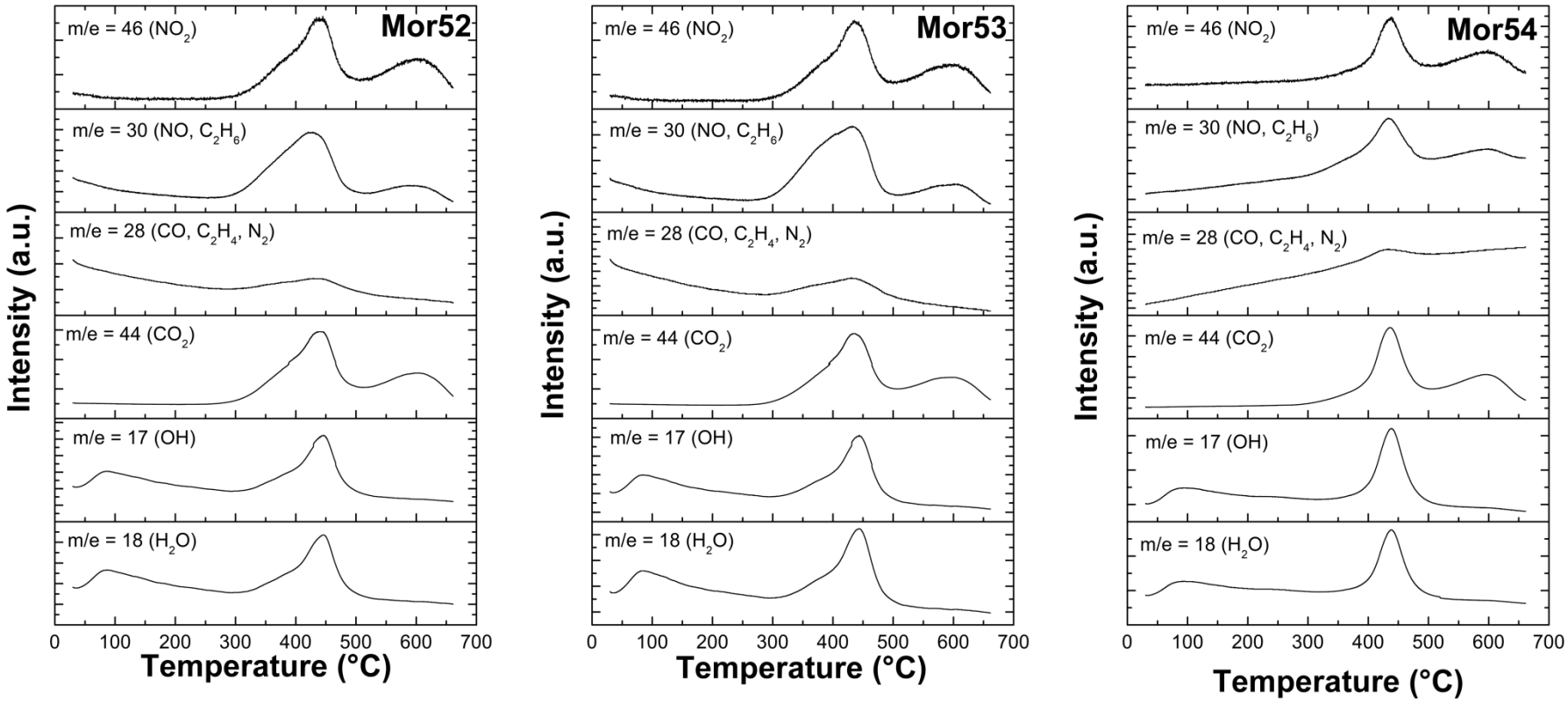

Figure 5.29: MS spectra of as-synthesised Na-zeolites synthesised under hydrothermal conditions (170 °C for 72 hours) using varying amounts of ODSA agent (TEAOH) in the absence of NaOH, with a fixed amount of seed crystals (0.025 g) in the synthesis mixture with molar regime 1 SiO_2•0.019 Al_2O_3•0.46 Na_2O•n TEAOH•30.1 H_2O (n = 0.26-1.05).

Samples Mor52 and Mor53 exhibited similar TGA/DTG and DTA thermal profiles as well as MS spectra with a gradual release of TEAOH/TEA^+ from the MOR framework, as observed in Figure 5.28 and 5.29. Sample Mor54 exhibited similar thermal degradation profiles; however, the release of TEAOH/TEA^+ occurred in a more narrow temperature range (with onset at a relatively higher temperature as depicted in Figure 5.28). This may be due to the relatively higher SAR value of this zeolite compared to sample Mor 52 and Mor53. As listed in Table 5.8, the Na/Al ratio of zeolite mordenite sample Mor54 was very low 0.03 (<< 1), which indicated that the OSDA agent (TEAOH) also served as a charge-balancing cation (TEA^+) to the negative framework charges at zeolite acidic sites ($Si\text{-}O\text{-}Al^-$). The interaction of TEA^+ cations with the framework of mordenite sample Mor54 may therefore be relatively stronger compared to sample Mor52 and Mor53 that exhibited Na/Al ratios of 0.4, which is proposed to cause the difference in the thermal degradation profile shape. The results observed by MS correlated with these findings, as depicted in Figure 5.29.

These results also correlate well with the differences in the morphology of zeolite mordenite samples Mor52-Mor54 in terms of particle shape as well as particle size, as listed in Table 5.8. As-synthesised zeolite mordenite samples Mor52 and Mor53 are highly intergrown, large platelet-like crystals which may contain inter-crystalline mesopores that allowed for relatively low temperature release of some TEA^+ components from the pores of the MOR framework. However these large mordenite crystals (samples Mor52 and Mor53) resulted in slower diffusion through the pores of the MOR framework and consequently, TEA^+ was released over a broad temperature range with a relatively low temperature for the onset of TEA^+ release as observed in Figure 5.29. On the other hand, as-synthesised mordenite sample Mor54 was made up of smaller mordenite crystals (prismatic and platelet-like) that allowed for easy diffusion of TEA^+ components through the pores of the MOR framework and resulted in a well-defined temperature region associated with the loss of TEA^+ components from the pores of the MOR framework, as observed in Figure 5.28 and 5.29. The thermal properties of as-synthesised zeolite mordenite samples prepared in the presence of varying TEAOH amounts (without added NaOH) and 0.025 g of mordenite seed crystals are listed in Table 5.9.

Table 5.9: Summary of information gathered from TGA analysis for as-synthesised zeolite samples Mor52-Mor54 zeolites synthesised under hydrothermal conditions (170 °C for 72 hours) using varying amounts of ODSA agent (TEAOH) in the absence of NaOH, with a fixed amount of seed crystals (0.025 g) in the synthesis mixture with molar regime 1 SiO_2•0.019 Al_2O_3•0.46 Na_2O•n TEAOH•30.1 H_2O (n = 0.26-1.05), with water and template content reported as per gram of zeolite.

Sample	Temp. W1 peak (°C)	Temp. W2 peak (°C)	Water content (g/g zeolite)	Temp. T1 peak (°C)	Temp. T2 peak (°C)	TEAOH content (g/g zeolite)
Mor52	81	178	0.047	430	531/602	0.062
Mor53	78	174	0.049	428	531/602	0.064
Mor54	79	227	0.052	428	531/598	0.063

As expected the water content in zeolite mordenite samples Mor52-54 increased as the SAR value of samples decreased, as listed in Table 5.9. The overall TEAOH content in the synthesised material was not dependent on the SAR value of the material or the initial TEAOH content in the synthesis mixture. In this case, it may be concluded that TEAOH molecules were occluded in the pores and channels of the MOR framework and TEA^+ cations also served as counter-balancing cations for negative charges in the MOR framework (such as acidic sites).

Under these synthesis conditions, highly crystalline (~90 %), pure zeolite mordenite was crystallised at 170 °C for 72 hours from a synthesis mixture (with molar regime 1 SiO_2•0.02 Al_2O_3•0.45 Na_2O•30.1 H_2O•0.53 TEAOH), in the presence of a small amount of mordenite seed crystals (0.025 g) and without added NaOH. The utilisation of TEAOH content higher than (n = 0.53) in the synthesis mixture for the crystallisation of highly crystalline, pure zeolite mordenite is therefore considered a waste of OSDA agent. These results were more comparable to literature on the synthesis of zeolite mordenite (crystal size of ~8 µm) from a synthesis mixture made up of standard chemical reagents, in the presence of TEAOH and mordenite seed crystals (4 wt%) under hydrothermal conditions of 170 °C for 72 hours (Lu et al., 2004). It is noteworthy that only 1 wt% of mordenite seed crystals were utilised to achieve the highly crystalline zeolite mordenite samples in the presence of TEAOH in this study compared to the 4 wt% of mordenite seed crystals reported in the literature (Lu et al., 2004). Subsequently, the effect of TEAOH amount on the crystallisation of zeolite mordenite from the FASE material in the absence of mordenite seed crystals (with no added NaOH) was investigated using a molar regime of 1 SiO_2•0.02 Al_2O_3•0.46 Na_2O•30.1 H_2O•0.53 TEAOH.

5.4.3 The effect of OSDA agent on zeolite mordenite crystallisation, in the absence of NaOH and seeds

The formation of zeolite mordenite from synthesis mixtures with the general molar regime 1 SiO_2•0.02 Al_2O_3•0.46 Na_2O•30.1 H_2O•n TEAOH with varying amounts of TEAOH (n = 0.26-1.05) was carried out as described in Table 3.5, Section 3.4.3, in the absence of additional NaOH as a mineralising agent and without seed crystals under hydrothermal conditions of 170 °C for 72 hours.

5.4.3.1 Mineralogy and crystallinity

XRD diffractograms of as-synthesised zeolite products crystallised at 170 °C for 72 hours prepared using a general molar regime 1 SiO_2•0.02 Al_2O_3•0.46 Na_2O•30.1 H_2O•n TEAOH with varying amounts of TEAOH (n = 0.26-1.05), with neither NaOH nor seed crystals added to the synthesis mixtures are depicted in Figure 5.30. The percentage relative crystallinity for each sample was calculated relative to highly crystalline commercial mordenite and results are listed in Table 5.10.

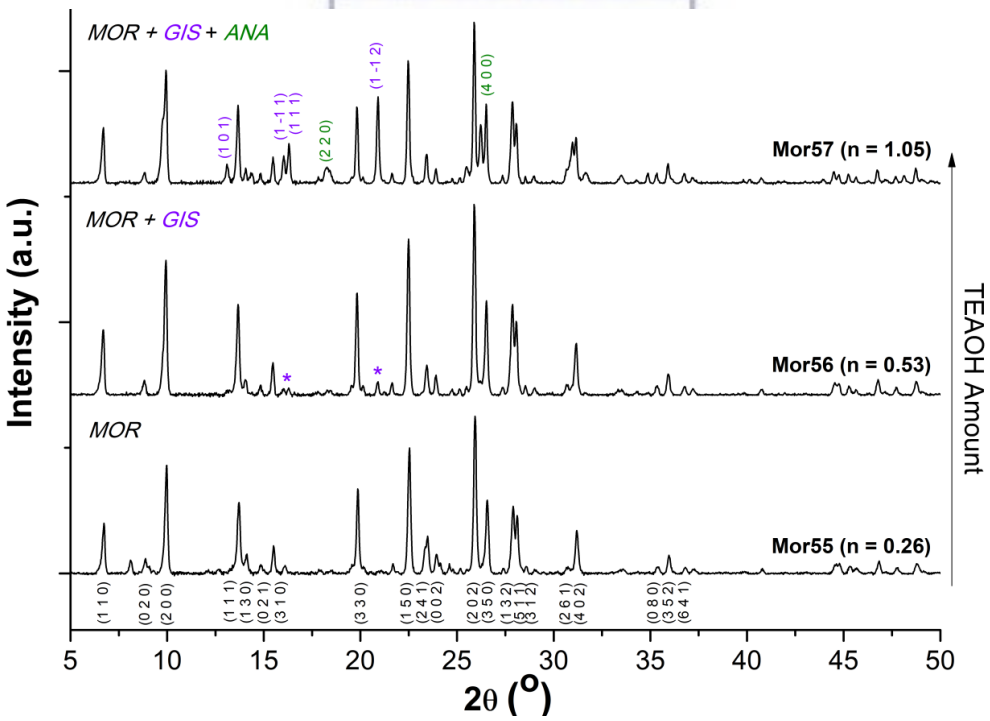

Figure 5.30: XRD diffractograms of as-synthesised Na-zeolites Mor55-57 synthesised using varying amounts of ODSA agent (TEAOH), without NaOH or seed crystals added in the synthesis mixture with molar regime in the synthesis mixture with molar regime 1 SiO_2•0.019 Al_2O_3•0.46 Na_2O•n TEAOH•30.1 H_2O (n = 0.26-1.05). Key: MOR - zeolite mordenite, ANA - Analcime, GIS - zeolite Na-P1

In the presence of varying amounts of TEAOH (n = 0.26-1.05), without the addition of seed crystals or NaOH, the crystallisation of pure zeolite mordenite was observed at a relatively low TEAOH content in the synthesis mixture (n = 0.26 for sample Mor55) as observed in Figure 5.30. As the TEAOH content in the synthesis was increased, the appearance of peaks corresponding to the competing phases analcime and Na-P1 were observed.

Table 5.10: Relative crystallinity of as-synthesised Na-zeolites Mor55-57 synthesised in the presence of varying TEAOH amount (without seed crystals or NaOH) in the synthesis mixture with molar regime in the synthesis mixture with molar regime 1 SiO_2•0.019 Al_2O_3•0.46 Na_2O•n TEAOH•30.1 H_2O (n = 0.26-1.05), determined using XRD data.

Sample	TEAOH molar content in synthesis mixture (moles)	% Relative Crystallinity
Mor55	0.26	78.8
Mor56	0.55	99.4
Mor57	1.05	81.5

As listed in Table 5.10, as the TEAOH content in the synthesis mixture was increased, the crystallinity of zeolite mordenite was enhanced in the presence of TEAOH up to n = 0.53 (sample Mor56). Further addition of TEAOH (n = 1.05 for sample Mor57) resulted in the formation of competing phases analcime and Na-P1 (as observed in Figure 5.30) and consequently, the crystallinity of zeolite mordenite reduced.

Compared to the seeded, OSDA synthesis system (presented in Section 5.4.2), zeolite mordenite crystallisation was enhanced in the presence of a relatively small quantity of OSDA agent, TEAOH (n = 0.26) in the absence of competing phases analcime or Na-P1. However, it should be noted that the crystallinity of this sample (Mor55) was slightly lower than the pure zeolite mordenite sample crystallised in the presence of both TEAOH and seed crystals. Nevertheless, the conversion of the CFA-derived FASE material to highly crystalline and pure zeolite mordenite may be achieved by addition of TEAOH (in the absence of both NaOH and seed crystals) to the synthesis mixture according to the molar regime 1 SiO_2•0.02 Al_2O_3•0.46 Na_2O•30.1 H_2O•0.26 TEAOH under the conditions used in this study, which reduces the cost of reagents while obtaining relatively crystalline (and high purity) zeolite mordenite using a CFA-derived silicon feedstock.

5.4.3.2 Morphological and composition

SEM micrographs of as-synthesised Na-zeolites crystallised at 170 °C for 72 hours with varying amounts of TEAOH (n = 0.26-1.05), without the addition of NaOH or seed crystals to the synthesis mixture, are depicted in Figure 5.31.

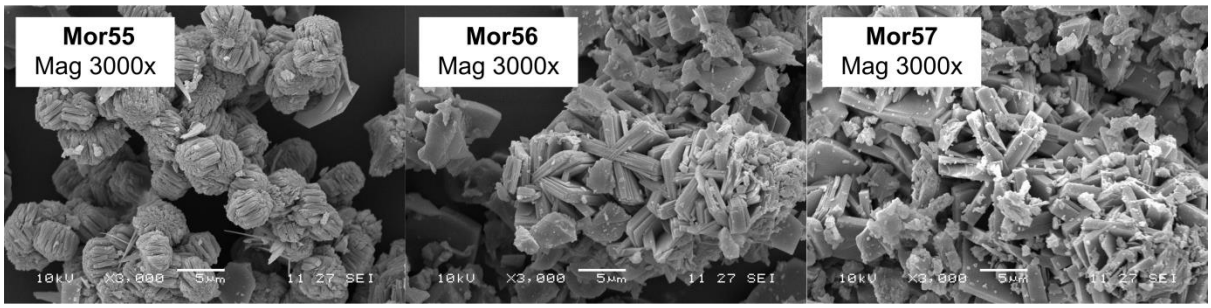

Figure 5.31: SEM micrographs (3000x magnification) of as-synthesised Na-zeolites Mor55-57 synthesised under hydrothermal conditions (170 °C for 72 hours) using varying amounts of ODSA agent (TEAOH), without NaOH or seed crystals added in the synthesis mixture with molar regime in the synthesis mixture with molar regime 1 SiO_2•0.019 Al_2O_3•0.46 Na_2O•n TEAOH•30.1 H_2O (n = 0.26-1.05).

As depicted in Figure 5.31, zeolite mordenite sample Mor55 crystals were thin prismatic crystals that formed as spherical agglomerates. Sample Mor56 and Mor57 exhibited similar morphology in terms of particle shape; these prismatic mordenite crystals were broader in size and agglomerated in a twinned manner. Zeolite mordenite crystals, with similar morphology to sample Mor55, prepared from synthesis mixtures (made up of pure chemical reagents) with relatively low SAR values and high water content (i.e. diluted nutrients) was reported in the literature (Zhang et al., 2009). Similar twinned mordenite crystals were reported in the literature as petal-like crystals by Mao et al., (2014). The average particle size and SAR values for as-synthesised Na-zeolites determined from EDS are summarised in Table 5.11.

Table 5.11: Properties of as-synthesised Na-zeolites Mor55-57 such as average particle size (determined using ImageJ) and relative composition (determined by EDS analysis n=10), synthesised under hydrothermal conditions (170 °C for 72 hours) using varying amounts of ODSA agent (TEAOH), without NaOH or seed crystals added in the synthesis mixture with molar regime in the synthesis mixture with molar regime 1 SiO_2•0.019 Al_2O_3•0.46 Na_2O•n TEAOH•30.1 H_2O (n = 0.26-1.05).

Sample	TEAOH molar content in synthesis mixture (moles)	Average particle size (µm)	SAR value	Na/Al ratio
Mor55	0.26	5.3	10.6	0.4
Mor56	0.55	7.3	11.9	0.02
Mor57	1.05	9.8	11.1	0.4

As listed in Table 5.11, the average particle size of zeolite mordenite crystals increased as the TEAOH content in the synthesis mixture increased (from 5.3 to 9.8 µm). In this case (in the absence of seed crystals and NaOH in the synthesis mixture) crystal growth was favoured at relatively high TEAOH content (n = 1.05 for sample Mor57), which resulted in the formation of relatively large zeolite mordenite crystals. The SAR value of zeolite mordenite samples Mor55-Mor57 was relatively similar ~10.6-11.9, while Na/Al ratios of the synthesised materials varied slightly with the SAR value. It is noteworthy that the Na/Al ratios for zeolite mordenite samples Mor55-Mor57 was relatively low 0.02-0.4 (<<1). As discussed previously, this indicates that the OSDA in synthesised samples is mainly present in the charge-balancing cation form (TEA^+).

5.4.3.3 Thermal Stability

The thermal analysis of as-synthesised zeolite mordenite samples Mor55-Mor57, prepared using varying amounts of TEAOH (in the absence of NaOH and seed crystals) under hydrothermal conditions of 170 °C for 72 hours, was analysed by TGA/DTG/DTA analysis coupled to MS; results are depicted in Figure 5.32 and Figure 5.33, respectively. As observed in Figure 5.32, zeolite mordenite samples Mor55-57 synthesised with varying amounts of TEAOH (in the absence of mordenite seed crystals and NaOH) exhibited four mass loss sections related to the endothermic release of physisorbed water (W1 and W2) as well as the exothermic degradation and release of the OSDA agent (T1 and T2) from the pores of the MOR framework. Slight differences in the thermal profiles of samples are thought to be due to differences in the morphology of these samples (as depicted in Figure 5.31). As the TEAOH content in the synthesis mixture was increased, the average particle size of the mordenite crystals increased which in turn resulted in increased diffusional constraints during the thermal treatment of these samples in air.

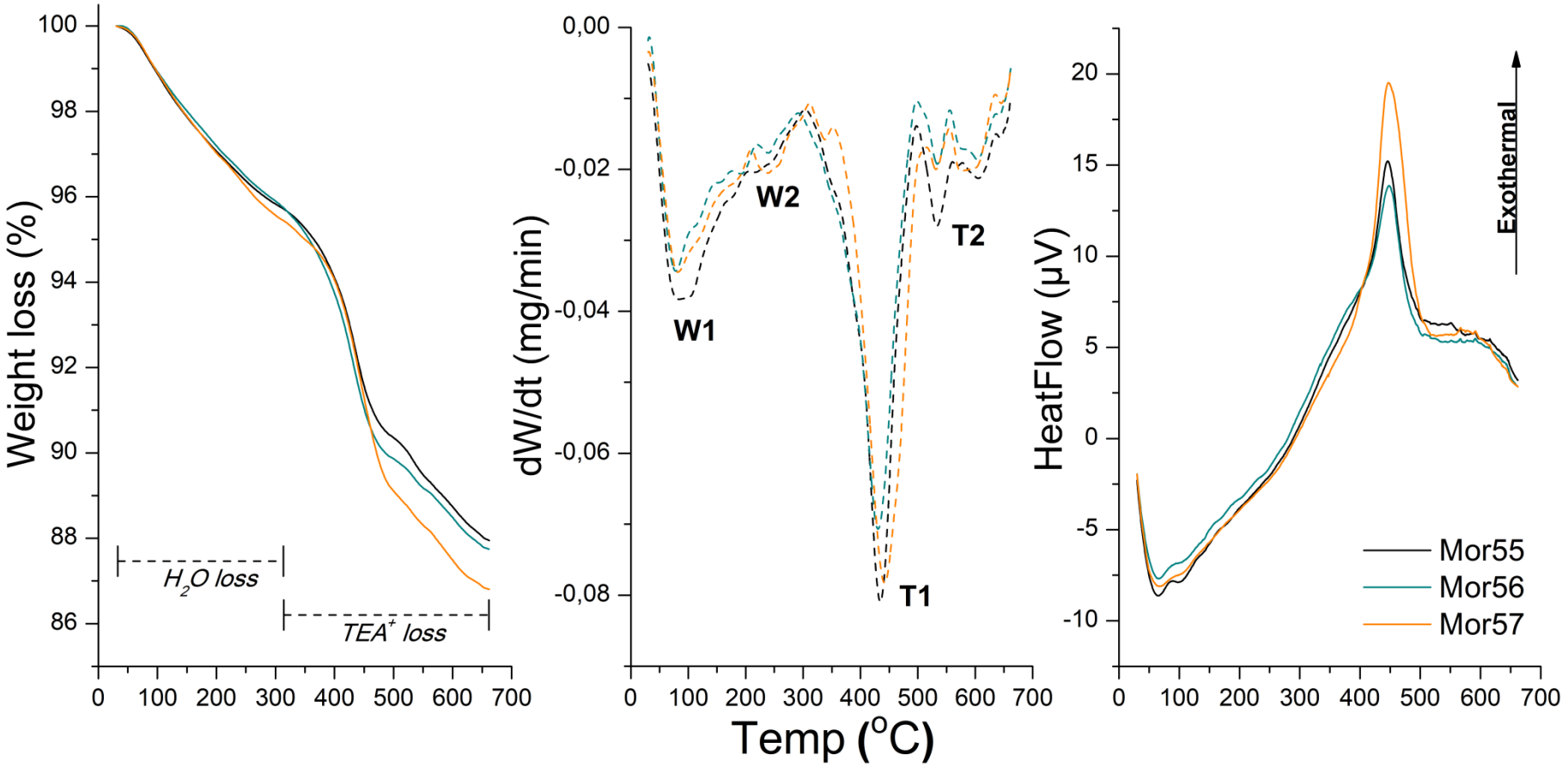

Figure 5.32: TGA/DTG/DTA analysis of as-synthesised Na-zeolites Mor55-57 synthesised under hydrothermal conditions (170 °C for 72 hours) using varying amounts of ODSA agent (TEAOH) in the absence of NaOH and seeds in the synthesis mixture with molar regime in the synthesis mixture with molar regime 1 SiO_2•0.019 Al_2O_3•0.46 Na_2O•n TEAOH•30.1 H_2O (n = 0.26-1.05).

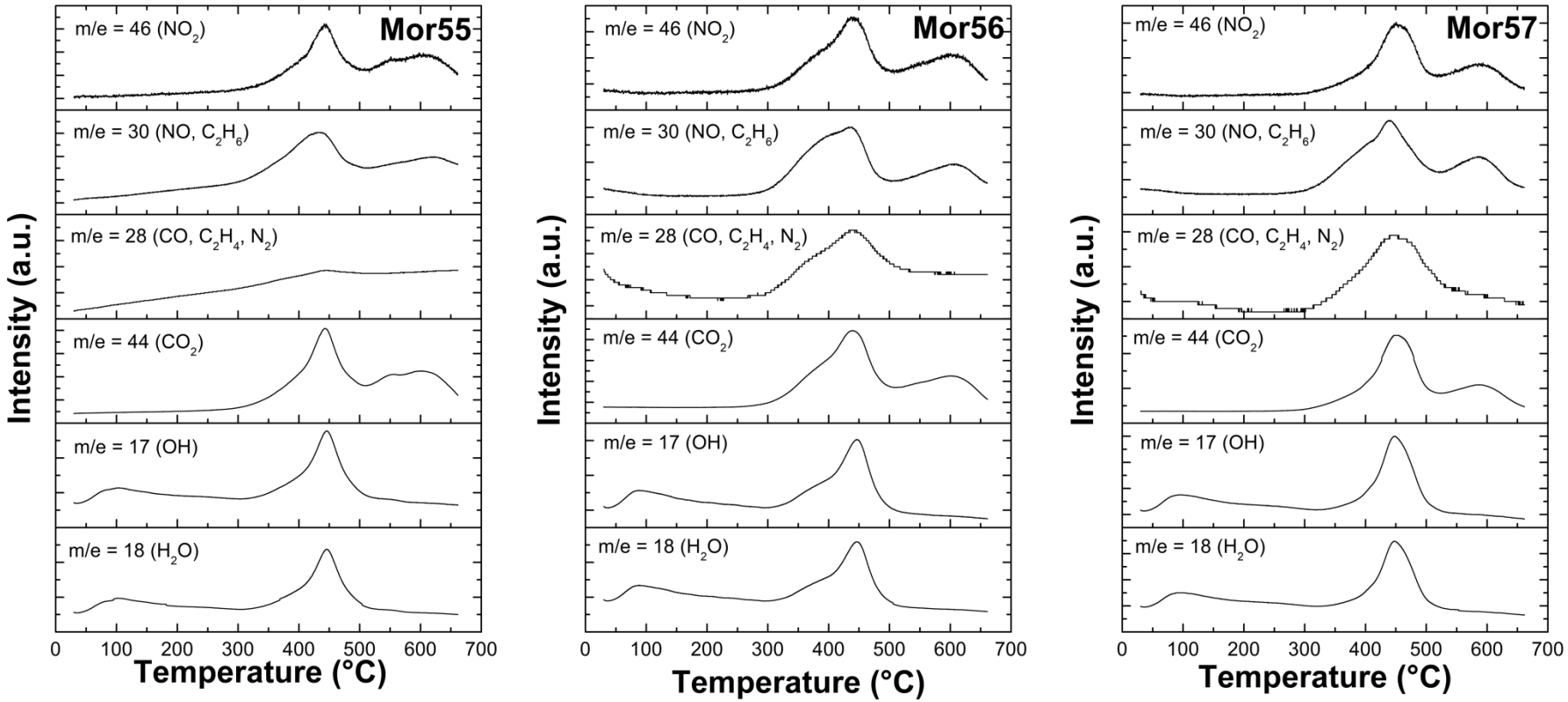

Figure 5.33: MS spectra of as-synthesised Na-zeolites Mor55-57 synthesised under hydrothermal conditions (170 °C for 72 hours) using varying amounts of ODSA agent (TEAOH) in the absence of NaOH and seeds in the synthesis mixture with molar regime in the synthesis mixture with molar regime 1 SiO_2•0.019 Al_2O_3•0.46 Na_2O•n TEAOH•30.1 H_2O (n = 0.26-1.05).

A summary of the thermal properties of as-synthesised zeolite mordenite samples Mor55-57 prepared in the presence of varying TEAOH amounts (without additional NaOH or mordenite seed crystals) is listed in Table 5.12.

Table 5.12: Summary of information gathered from TGA analysis for as-synthesised zeolite samples Mor55-Mor57 synthesised under hydrothermal conditions (170 °C for 72 hours) using varying amounts of ODSA agent (TEAOH), without NaOH or seed crystals added in the synthesis mixture with molar regime in the synthesis mixture with molar regime 1 SiO_2•0.019 Al_2O_3•0.46 Na_2O•n TEAOH•30.1 H_2O (n = 0.26-1.05), with water and template content reported as per gram of zeolite.

Sample	Temp. W1 peak (°C)	Temp. W2 peak (°C)	Water content (g/g zeolite)	Temp. T1 peak (°C)	Temp. T2 peak (°C)	TEAOH content (g/g zeolite)
Mor55	91	217	0.044	435	533/606	0.065
Mor56	82	239	0.040	442	531/587	0.073
Mor57	78	239	0.045	431	534/603	0.076

As listed in Table 5.12, the water content of synthesised zeolites Mor55-57 was relatively similar and corresponded well with the SAR values of these materials (as listed in Table 5.11). However, the amount of TEA^+ incorporated into the synthesised product increased as the TEAOH content in the synthesis mixture increased. This trend corresponds well with the increased crystallinity of zeolite mordenite as listed in Table 5.11 (with sample Mor57 as the exception). These samples exhibited a relatively higher TEAOH content compared to zeolite mordenite samples Mor52-Mor54 (as listed in Table 5.9). It is therefore proposed that in the absence of seed crystals (Mor55-57), relatively more TEAOH is incorporated into the mordenite framework of the synthesised product. On the other hand, when seed crystals were present in the synthesis mixture together with TEAOH (Mor52-54), a relatively lower TEAOH content was present in the synthesised product. This indicates that seeding reduces the amount of OSDA agent required to yield highly crystalline zeolite mordenite, by serving as nucleation sites and resulting in enhanced crystallisation of zeolite mordenite. This is an important factor to consider when designing cost-effective zeolite production processes.

The synthesis of zeolite mordenite in the presence of varying TEAOH content was reported in literature using synthesis mixtures made up of TEOS, aluminium sulphate hydrate and NaOH and hydrothermal conditions between 170 and 200 °C (for up to 96 hours); relatively large mordenite crystals (20 x 10 µm to 50 x 50 µm) with different morphologies were reported Mao et al., (2014). Mao et al., (2014) reported that spherical mordenite crystals were

formed in the presence of TEAOH (particle size increased as the TEAOH content increased), while column-like crystals formed in the absence of TEAOH. These results are similar to the zeolite mordenite samples synthesised in this study (in the presence of varying amounts of TEAOH and in the absence of seed crystals and NaOH). The morphologies of zeolite mordenite samples Mor55 (spherical agglomerates of small crystals) and Mor56/Mor57 (twinned), observed in Figure 5.31, may be due to the formation of relatively small mordenite crystals in solution during the early stages of zeolite crystallisation that aggregate into relatively larger sized crystals (spherical or twinned crystals in this study) to reduce surface potential of the growing crystals (Mao et al., 2014; Zhang et al., 2009).

Under these synthesis conditions, crystalline (~79 %), pure zeolite mordenite was crystallised at 170 °C for 72 hours from a synthesis mixture with molar regime 1 SiO_2•0.02 Al_2O_3•0.46 Na_2O•30.1 H_2O•0.26 TEAOH, in the absence of mordenite seed crystals and without added NaOH. Therefore this study illustrated that highly pure, crystalline zeolite mordenite may be synthesised using the CFA-derived FASE material in the presence of a small quantity of OSDA agent without the need for NaOH as a mineralising agent or mordenite seed crystals. It should be noted that highly crystalline zeolite mordenite (99.4 %) may by synthesised using relatively higher TEAOH content (n = 0.53), however the presence of minor Na-P1 peaks were also present in this sample. Furthermore, this study also illustrates that zeolite mordenite crystals with different morphologies (in terms of shape and size) may be prepared from a CFA-derived silicon precursor (FASE) by using a small amount of TEAOH in the absence of seed crystals and NaOH. Subsequent investigations were carried out using the synthesis conditions of the most crystalline mordenite sample (Mor56).

5.4.4 The effect of Al content in the presence of a OSDA agent on zeolite mordenite crystallisation (no added NaOH or seeds)

The crystallisation of zeolite mordenite from synthesis mixtures with the general molar regime (1 SiO_2•x Al_2O_3•y Na_2O•30.1 H_2O•0.53 TEAOH) in the presence of TEAOH with no additional sodium aluminate (x = 0.004, y = 0.45) and varying amounts of sodium aluminate (x = 0.02-0.08, y = 0.46-0.52) was carried out as described in Table 3.6, Section 3.4.3 (in the absence of additional NaOH as a mineralising agent and mordenite seed crystals), to determine if the utilisation of TEAOH in the synthesis mixture influenced the crystallisation boundary region for zeolite mordenite (in terms of SAR value of the synthesis mixture).

5.4.4.1 Mineralogy and crystallinity

XRD diffractograms of as-synthesised zeolite products prepared using a general molar regime 1 SiO_2•x Al_2O_3•y Na_2O•30.1 H_2O•0.53 TEAOH with no additional sodium aluminate (x = 0.004, y = 0.45) and varying amounts of sodium aluminate (x = 0.02-0.08, y = 0.46-0.52), in the presence of an OSDA agent (TEAOH) are depicted in Figure 5.34. The percentage relative crystallinity for each sample was calculated relative to highly crystalline commercial mordenite and results are listed in Table 5.13.

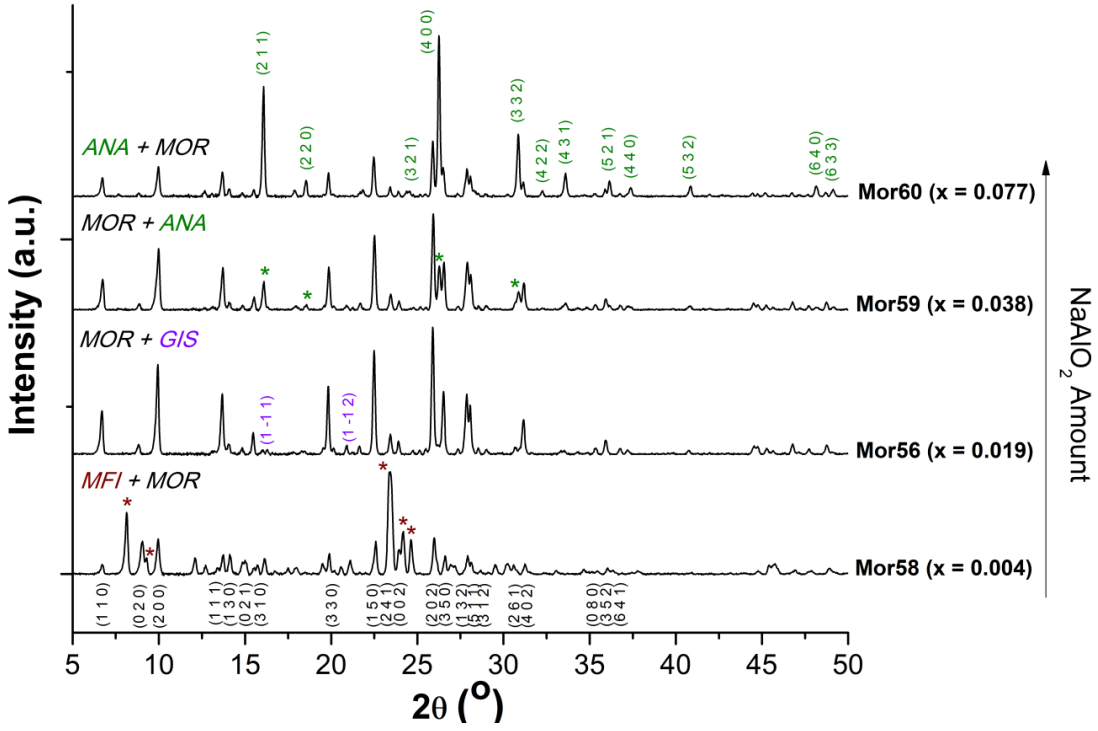

Figure 5.34: XRD diffractograms of as-synthesised Na-zeolites Mor56, Mor58-60 synthesised using varying amounts of sodium aluminate in the presence of an ODSA agent (TEAOH), without NaOH or seed crystals added in the synthesis mixture with molar regime 1 SiO_2•x Al_2O_3•y Na_2O•30.1 H_2O•0.53 TEAOH (x = 0.004-0.08, y = 0.45-0.52). Key: MOR - zeolite mordenite, MFI - zeolite ZSM-5, ANA - Analcime, GIS - zeolite Na-P1

As depicted in Figure 5.34, the crystallisation of zeolite mordenite in the presence of TEAOH as OSDA agent and varying aluminium content in the synthesis mixture resulted in the formation of zeolite ZSM-5 at high SAR values of the synthesis mixture (x = 0.004 and y = 0.45 for sample Mor58) when no sodium aluminate was added to the synthesis mixture, zeolite mordenite at intermediate SAR values of the synthesis mixture (x = 0.02-0.04 and y = 0.46-0.52 for samples Mor56 and Mor59) and analcime at relatively low SAR values (x = 0.08 for sample Mor60).

Table 5.13: Relative crystallinity of as-synthesised Na-zeolites Mor56, Mor58-60 synthesised using varying amounts of sodium aluminate in the presence of an ODSA agent (TEAOH), without NaOH or seed crystals added in the synthesis mixture with molar regime 1 SiO_2•x Al_2O_3•y Na_2O•30.1 H_2O•0.53 TEAOH (x = 0.004-0.08, y = 0.45-0.52), determined using XRD data.

Sample	AlO_2 molar content in synthesis mixture (moles)	NaO_2 molar content in the synthesis mixture (moles)	% Relative Crystallinity
Mor58	0.004	0.45	31.2
Mor56	0.019	0.46	99.4
Mor59	0.038	0.48	72.7
Mor60	0.077	0.52	35.6

As listed in Table 5.13, the crystallinity of zeolite mordenite increased as the aluminium content in the synthesis mixture increased (up to x = 0.02 and y = 0.46). However, the mordenite sample formed at x = 0.04 (y = 0.48) was also relatively crystalline. The most crystalline zeolite mordenite sample (99.4 %) formed at relatively low additional sodium aluminate (x = 0.02 and y = 0.46) in the synthesis mixture as observed for sample Mor56 in Figure 5.34.

The OSDA-assisted zeolite mordenite formation from the FASE material is therefore slightly wider in terms of SAR value of the synthesis mixture. This illustrates that the boundary region for zeolite mordenite crystallisation may be extended (in terms of SAR value of the synthesis mixture) by utilisation of an OSDA agent such as TEAOH in the synthesis mixture during hydrothermal treatment. The boundary conditions for the synthesis of zeolite mordenite from a CFA-derived silicon precursor in the presence of an OSDA agent (such as TEAOH) may be further extended for synthesis parameters such as alkalinity and water content.

The synthesis of zeolite mordenite from standard laboratory reagents in the presence of TEAOH was possible in a defined SiO_2/Al_2O_3 range of 15 to 30 as reported in literature, with SiO_2/Al_2O_3 values above or below this range resulting in the formation of an amorphous material (Mao et al., 2014). On the other hand, the formation of zeolite ZSM-5 or beta was reported during the synthesis of zeolite mordenite from synthesis mixtures with relatively high SiO_2/Al_2O_3 values (≥ 20) in the presence of TEAOH and mordenite seed crystals (Lu et al., 2004). The synthesis of zeolite mordenite in the presence of TEAOH and HMI as OSDA agents (as well as 4 wt% mordenite seed crystals) resulted in the formation of zeolite ZSM-5

as an impurity at a relatively low SiO_2/Al_2O_3 value of 30 and quartz as a major product at relatively high SiO_2/Al_2O_3 values (≥ 35) as reported in literature (Lv et al., 2011). Similarly, the presence of impurities and amorphous material was observed during the synthesis of zeolite mordenite from a synthesis mixture with a relatively high SiO_2/Al_2O_3 ratio of 30 (in the presence of TEAOH and CTAB) (Jin et al., 2012). In this study, synthesis mixtures with relatively high SiO_2/Al_2O_3 ratios of 25 (Mor59) and 50 (Mor56) prepared from a CFA-derived silicon precursor (FASE) resulted in the formation of highly crystalline zeolite mordenite. However, as mentioned previously, further investigations into the boundary regions for OSDA-assisted zeolite mordenite synthesis from a CFA-derived silicon precursor FASE may be carried out in the future to determine the exact boundary regions in the presence of TEAOH.

5.5 Chapter summary

This chapter presented the synthesis of highly crystalline zeolite mordenite from the CFA-derived silicon precursor (FASE) using three different hydrothermal synthesis approaches; (i) OSDA-free synthesis, (ii) seed-assisted synthesis and (iii) OSDA-assisted synthesis. The OSDA-free synthesis of highly crystalline zeolite mordenite from a CFA-derived silicon precursor (FASE) was achieved in this study, without the addition of an extra source of silicon or the utilisation of an extra purification step prior to hydrothermal treatment to remove excess sodium and enhance the SAR value of the feedstock. This study therefore reports the first synthesis of zeolite mordenite from a silicon feedstock derived solely from CFA. However, zeolite mordenite crystallised from the OSDA-free synthesis environment contained a small amount of impurities (competing mineral phases such as analcime and Na-P1). Zeolite mordenite formation from CFA-derived FASE material was favoured in synthesis environments with relatively low water content (high SiO_2/H_2O), high SAR values and low alkalinity (low OH^-/SiO_2). The optimum conditions for the formation of highly crystalline zeolite mordenite from a CFA-derived silicon feedstock was found to be a molar regime of 1 SiO_2•0.019 Al_2O_3•0.57 Na_2O•30.1 H_2O and hydrothermal conditions of 170 °C for 72 hours.

Seeded mordenite synthesis systems (prepared from the CFA-derived silicon precursor FASE) enhanced the crystallisation kinetics for zeolite mordenite formation and supressed the formation of the competing phases of zeolite mordenite such as zeolite Na-P1 and analcime. The utilisation of seeding during zeolite mordenite synthesis from the CFA-derived silicon precursor FASE may be used to reduce the total crystallisation time required for the crystallisation of highly crystalline and pure zeolite mordenite; this was achieved using a relatively small amount of mordenite seed crystals (0.1 wt%) which may have a minor influence on the cost of the process. Furthermore, seeding may also be used to control the morphology of zeolite mordenite prepared from CFA-derived silicon precursor FASE in terms of both particle shape (elongated needle-like, spherical agglomerates) and size (2.5-4.6 μm).

OSDA-assisted mordenite synthesis systems (prepared from the CFA-derived silicon precursor FASE) in the presence of a relatively small amount of TEAOH (n = 0.26) resulted in the formation of highly crystalline zeolite mordenite. The presence of TEAOH in the synthesis mixture resulted in zeolite mordenite crystals with varying morphologies in terms

of particle shape (prismatic, spherical agglomerates, twinned prismatic, hierarchical crystals) and size (5-10 µm) as well as different SAR values (10-15), depending on the synthesis conditions utilised. Furthermore, the utilisation of TEAOH in the synthesis of zeolite mordenite from the CFA-derived silicon precursor FASE also resulted in the extension of the SiO_2/Al_2O_3 boundary conditions for the preparation of zeolite mordenite. It is noteworthy that this study presented the first synthesis of zeolite mordenite with hierarchical morphology.

This study therefore illustrated how these different synthesis strategies may be used in the preparation of zeolite mordenite (from the CFA-derived silicon precursor FASE) control the properties of the resultant material such as morphology and composition; tailoring these material properties are vital for the production of zeolite mordenite that may utilised in a range of different applications.

6 Chapter 6 - Synthesis of medium-pore MFI framework type zeolites

6.1 Introduction

This section will present the synthesis of medium pore zeolites (with the MFI framework type) using a coal fly ash silicon extract (FASE) as the silicon-containing starting material. Various researchers have reported the synthesis of Zeolite ZSM-5 from coal fly ash (Chareonpanich et al., 2004; Kalyankar et al., 2011; Vichaphund et al., 2014; Vichaphund et al., 2016; Kapure et al., 2017; Krisnandi et al., 2017; Ndlovu, 2016; Ndlovu et al., 2017; Missengue, 2016; Missengue et al., 2017; Missengue et al., 2018). Zeolite ZSM-5 was previously synthesised from South African coal fly ash using a method that involved a high temperature, solid fusion step to extract silicon (and aluminium) from coal fly ash. Subsequently, an additional purification step was added to remove excess sodium cations from the FASE material and this process involved the treatment of the FASE material with a concentrated oxalic acid solution under reflux conditions (Missengue et al., 2018). A novel low-temperature extraction method for the synthesis of zeolite ZSM-5 was reported in the literature (Ndlovu, 2016). However, this synthesis still involved the oxalic acid treatment of the FASE material prior to the hydrothermal synthesis of zeolite ZSM-5.

The aim of this study was therefore to further simplify the synthesis protocol for zeolite ZSM-5 from a South African fly ash silicon extract by using relatively low temperature conditions for silicon extraction (Ndlovu, 2016) and without using an additional purification step (namely the oxalic acid treatment of the FASE material). The optimal synthesis conditions for the preparation of zeolite ZSM-5 from a CFA-derived silicon extract (without the oxalic acid treatment step) were investigated in this study. Synthesis parameters (OSDA content, aluminium and water content as well as alkalinity) were varied sequentially to determine the influence of these parameters on zeolite ZSM-5 formation; the optimum result from each investigated parameter was used as the baseline for subsequent investigations (as described in Section 3.5). Furthermore, the study aimed to prepare zeolite ZSM-5 with a range of SAR ratios (i.e. with varying solid acidity) as well as the siliceous analogue of ZSM-5 (silicalite-1). The characterisation of synthesised materials by XRD, FTIR, SEM and TGA will be presented in this chapter along with a comparison of the properties of silicalite-1 with some of the synthesised aluminosilicate ZSM-5 zeolites.

6.2 Hydrothermal synthesis of zeolite ZSM-5

The synthesis of zeolite ZSM-5 was carried out by using the silicon precursor extracted from coal fly ash (FASE prepared as described in Chapter 4) as the starting material for the hydrothermal process. In this section, the synthesis and optimisation of zeolite ZSM-5 from FASE will be discussed. The effect of various synthesis parameters (such as OSDA content, aluminium source and content, water content, alkalinity and counter-cation type) on the crystallisation of zeolite ZSM-5 will be discussed in this section by comparing materials properties such as crystallinity, morphology, SAR value, thermal stability, water content and TPABr content determined by characterisation techniques such as XRD, SEM-EDS, FTIR and TGA.

6.2.1 The effect of OSDA (TPABr) amount on zeolite ZSM-5 crystallisation

The synthesis of zeolite ZSM-5 from a CFA-derived silicon precursor (FASE) was carried out under static hydrothermal conditions of 160 °C for 72 hours, from a synthesis mixture with the following molar regime (1 SiO_2•0.004 Al_2O_3•0.54 Na_2O•n TPABr•35.4 H_2O), where n = 0.03-0.42. As presented in Table 3.7, the amount of the OSDA agent (TPABr) in the synthesis mixture (1 SiO_2•0.004 Al_2O_3•0.54 Na_2O•n TPABr•35.4 H_2O) was reduced for samples Zeo02 (n = 0.10) and Zeo03 (n = 0.03), compared to sample Zeo01, to determine the minimum amount of TPABr required to achieve zeolite ZSM-5 with relatively high crystallinity.

6.2.1.1 Mineralogy and crystallinity

Figure 6.1 illustrates XRD diffractograms of as-synthesised zeolite ZSM-5 samples crystallised from synthesis mixtures with varying amounts of TPABr, as described in Table 3.7.

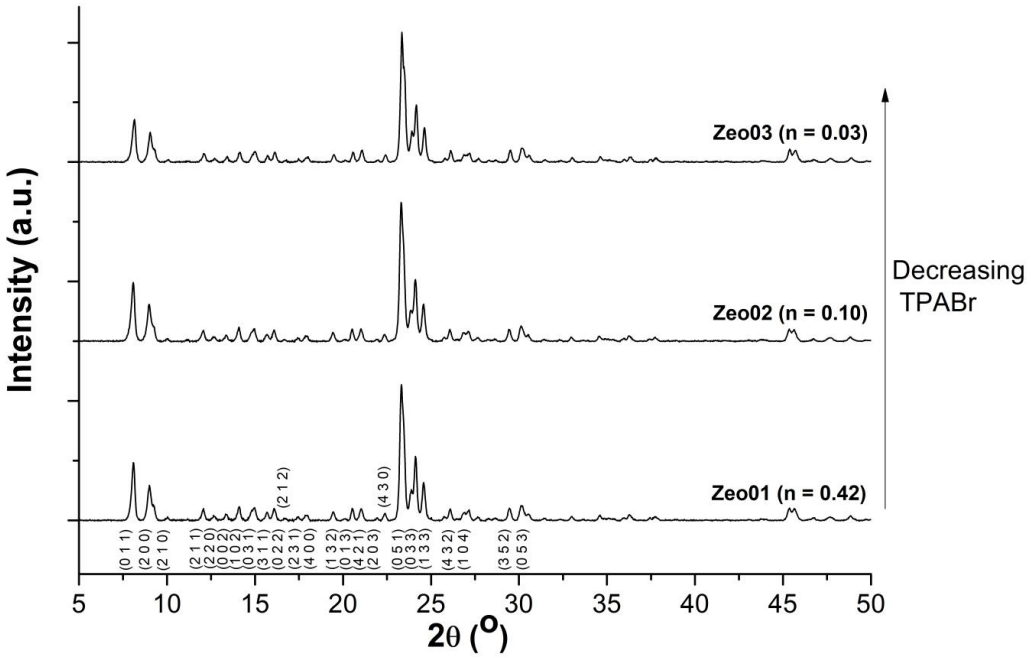

Figure 6.1: XRD diffractograms of as-synthesised zeolite Na-ZSM-5 products Zeo01-03 synthesised under hydrothermal conditions of 160 °C for 72 hours, with different amounts of TPABr in the synthesis mixture with molar regime 1 SiO_2•0.004 Al_2O_3•0.54 Na_2O•n TPABr•35.4 H_2O (n = 0.03-0.42).

As-synthesised zeolite samples Zeo01-03 contained the main diffraction peaks corresponding to the MFI framework (zeolite ZSM-5) at 2θ values of ~7.96, ~8.83, ~23.32, ~24.04 and ~24.45°, as depicted in Figure 6.1. These samples all exhibited high crystallinity, however low angle peaks at 2θ values of ~7.96 and ~8.83° appear to have low intensities due to the presence of TPA^+ cations occluded in the pores of the zeolite framework. The relative crystallinity of each sample was calculated using the most crystalline ZSM-5 sample (Zeo23) as a reference pattern, according to Equation 2.8, and results are summarised in Table 6.1. The optical density (OD) ratio of synthesised zeolites, determined from FTIR according to Equation 2.9, was also used to estimate the relative crystallinity as listed in Table 6.1.

Table 6.1: Relative crystallinity of Na-zeolite samples Zeo01-03 synthesised with different amounts of TPABr in the synthesis mixture with molar regime 1 SiO_2•0.004 Al_2O_3•0.54 Na_2O•n TPABr•35.4 H_2O (n = 0.03-0.42), determined using XRD and FTIR data.

Sample	TPABr amount added to the synthesis mixture (moles)	Relative Crystallinity	
		XRD (% crystallinity)	FTIR (optical density ratio)
Zeo01	0.42	96.2	0.89
Zeo02	0.10	96.9	0.95
Zeo03	0.03	83.4	0.94

According to the results of relative crystallinity calculated from XRD data as listed in Table 6.1, all synthesised samples were highly crystalline zeolite ZSM-5. In terms of phase purity, the crystallisation of zeolite ZSM-5 from a CFA-derived silicon precursor (FASE) in the presence of TPABr was not sensitive to the amount of TPABr utilised in the synthesis mixture. A reduction in TPABr amount of 75% (sample Zeo02) did not affect the crystallinity of zeolite ZSM-5; however, further reduction in TPABr content (for sample Zeo03) resulted in a loss in crystallinity of ~13.5%. The OD ratio of crystalline zeolite ZSM-5 is reported to be 0.7-0.8, while materials containing amorphous silica content are reported to exhibit OD ratios less than 0.7 (Coudurier et al., 1982; Shukla and Pandya, 1989). The estimation of crystallinity using the optimal density ratio determined from FTIR data also revealed that these samples were highly crystalline, as listed in Table 6.1. However, XRD diffraction was more sensitive to changes in crystallinity. The de-templating calcination of as-synthesised zeolite samples was carried out in air at 550 °C for 3 hours using a slow temperature ramp rate (as described in Section 3.4.3) to determine if the crystallinity of samples were retained. XRD diffractograms of de-templated zeolites Zeo01-03 are depicted in Figure 6.2.

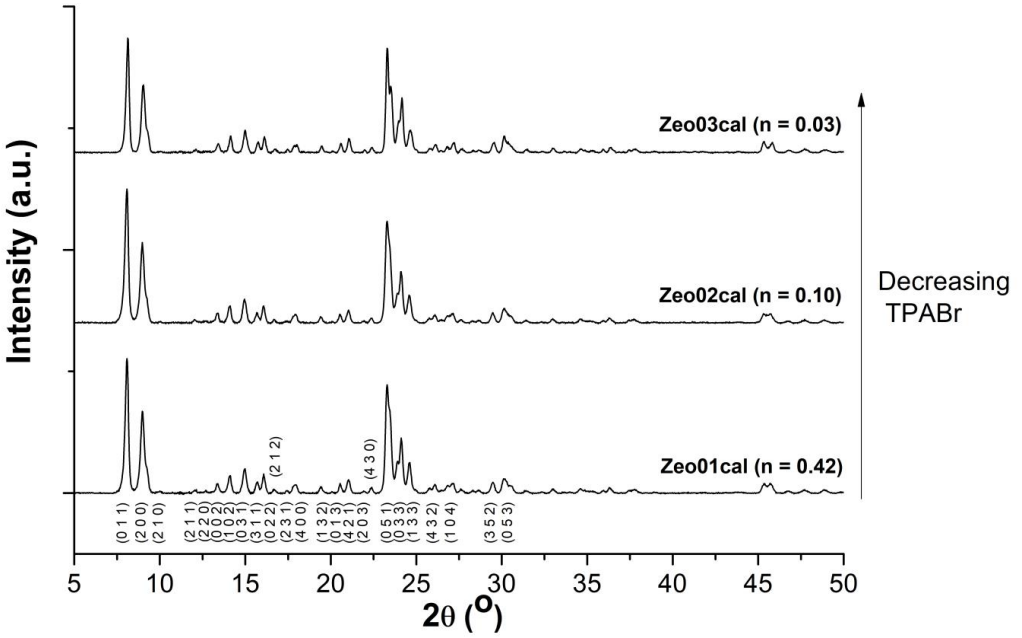

Figure 6.2: XRD diffractograms of de-templated zeolite Na-ZSM-5 products synthesised under hydrothermal conditions of 160 °C for 72 hours, using different amounts of TPABr in the synthesis mixture with molar regime 1 SiO_2•0.004 Al_2O_3•0.54 Na_2O•n TPABr•35.4 H_2O (n = 0.03-0.42) and calcined in air at 550 °C for 3 hours.

De-templated zeolite ZSM-5 samples Zeo01cal-03cal contained the five main diffraction peaks associated with zeolite ZSM-5, as depicted in Figure 6.2. After the removal of TPA^+ cations from the zeolite framework through calcination, the intensity of low angle peaks at ~7.96 and ~8.83° improved which further proved that TPA^+ cations were occluded in the pores of the zeolite framework. However, the relative crystallinity of samples Zeo01-03 were not affected; samples Zeo01cal and Zeo02cal exhibited relatively the same high crystallinity, while sample Zeo03cal had relatively lower crystallinity compared to these two samples.

6.2.1.2 Morphology and composition

SEM was carried out to determine the influence of TPABr content on the morphology of as-synthesised zeolite ZSM-5 samples Zeo01-03; results are depicted in Figure 6.3. The average particle size for each sample was determined using the image processing software ImageJ, while EDS was used to determine the SAR and Na/Al ratios of as-synthesised samples; these results are summarised in Table 6.2.

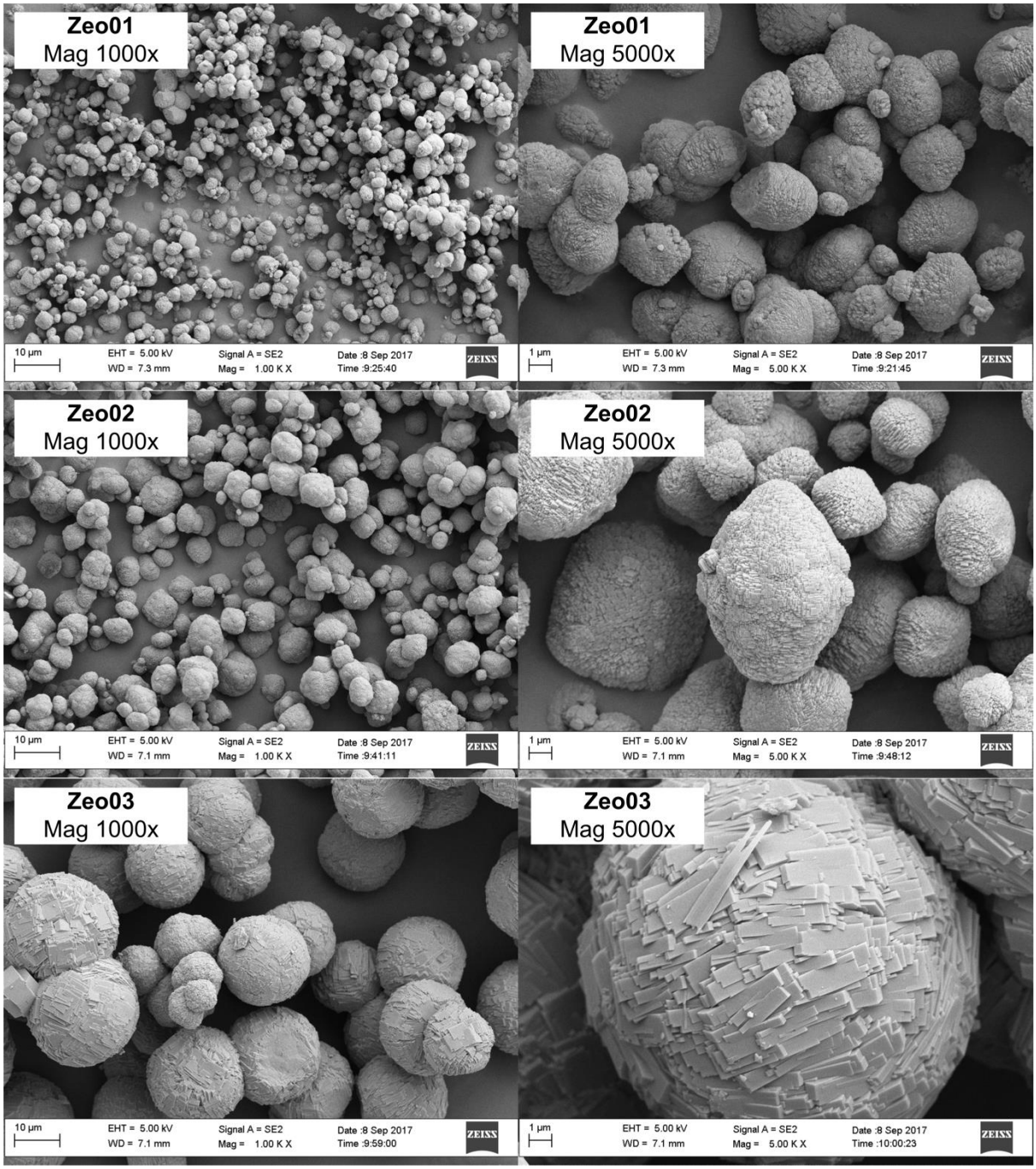

Figure 6.3: SEM micrograph (at 1000x and 5000x magnification) of as-synthesised Na-zeolite ZSM-5 samples Zeo01-03 synthesised under hydrothermal conditions (160 °C for 72 hours) with different amounts of TPABr in the synthesis mixture with molar regime 1 SiO_2•0.004 Al_2O_3•0.54 Na_2O•n TPABr•35.4 H_2O (n = 0.03-0.42).

As-synthesised Na-zeolite ZSM-5 samples Zeo01-03 exhibited a similar morphology in terms of the particle shape, as observed in Figure 6.3. These zeolite samples crystallised in a highly agglomerated manner resulting in the formation of large ellipsoid (samples Zeo01 and Zeo02) and spherical (sample Zeo03) particles. The particle shape of synthesised zeolites suggests that crystal growth occurred in three dimensions compared to the usual 2-dimensionl growth

mechanism for zeolite ZSM-5 that results in the formation of hexagonal-prismatic crystals with "coffin-like" morphology (Kadja et al., 2016). This mechanism of crystal growth may be due to the aluminium-deficiency in the synthesis mixture that caused a change in the electrostatic environment of the TPA^+ cations and consequently, changed the crystallisation mechanism for zeolite ZSM-5 in the presence of the OSDA agent. The morphology of ZSM-5 samples Zeo01 and Zeo02 resemble the morphology of hierarchical zeolite ZSM-5 prepared by (i) low temperature synthesis in the presence of TPABr or (ii) with the aid of mesoporous silica functionalised by organosilane phenylaminopropyl-trimethoxysilane, which serves as the mesoporogen (Kadja et al., 2016; Wang et al., 2017). Sample Zeo03 exhibited a similar morphology to zeolite ZSM-5 crystals prepared using n-butylamine as a templating agent and in the presence of seed crystals as well as NaCl (Wu et al., 2014).

Table 6.2: Properties of as-synthesised Na-zeolite ZSM-5 samples Zeo01-03 such as average particle size (determined using ImageJ) and relative composition (determined by EDS analysis n=10), synthesised under hydrothermal conditions (160 °C for 72 hours) with different amounts of TPABr in the synthesis mixture with molar regime 1 SiO_2•0.004 Al_2O_3•0.54 Na_2O•n TPABr•35.4 H_2O (n = 0.03-0.42).

Sample	TPABr amount added to the synthesis mixture (moles)	Average particle size (µm)	SAR value	Na/Al ratio
Zeo01	0.42	3.0	81.7	1.7
Zeo02	0.10	4.9	92.8	1.3
Zeo03	0.03	16.1	201.7	2.1

The average particle size of as-synthesised zeolite ZSM-5 samples Zeo01-03 varied depending on the amount of TPABr that was used in the preparation of the synthesis mixture, as presented in Table 6.2. As the TPABr amount increased, the particle size of zeolite samples decreased. As-synthesised zeolite ZSM-5 samples Zeo01 and Zeo02 exhibited similar particle shape and size with average particle size of 3.0 and 4.9 µm, respectively. On the other hand, as-synthesised zeolite ZSM-5 sample Zeo03 exhibited a relatively larger average particle size of 16.1 µm. The Na/Al ratio of ZSM-5 crystals was relatively similar for all samples, as listed in Table 6.2. The SAR value of synthesised zeolite ZSM-5 varied as the TPABr amount in the synthesis mixture changed. A decrease in OSDA amount (from sample Zeo01 to Zeo03) resulted in an increase in the SAR value of as-synthesised ZSM-5 samples from 81.7 to 201.7.

In this study, the CFA-derived silicon precursor (FASE) is rich in silicon and very low in aluminium (as listed in Table 4.8, Chapter 4) and no additional aluminium source was added to the synthesis mixture. It was therefore expected that the synthesis products would be highly siliceous. Changes in the crystal size and SAR value may be attributed to OSDA-feedstock interactions as the TPABr amount in the synthesis mixture was reduced. At relatively high TPABr content in the synthesis mixture (Zeo01 and Zeo02), nucleation is favoured over crystal growth processes resulting in the formation relatively small ZSM-5 crystals with relatively low SAR values, as listed in Table 6.2. On the other hand, a relatively low TPABr content in the synthesis mixture (Zeo03) favoured the crystal growth processes resulting in the formation of relatively larger ZSM-5 crystals with a relatively higher SAR value. Under these synthesis conditions, the formation of nuclei around the OSDA agent during the initial stages of zeolite crystallisation may have depleted the aluminium content in the synthesis mixture. Crystal growth, involving the condensation of silicate species onto the growing crystal surface, may have occurred resulting in highly siliceous ZSM-5 crystals in all cases. Similar results were observed for zeolite mordenite synthesis from a CFA-derived silicon precursor in the presence of varying amounts of OSDA agent (TEAOH), as presented in Section 5.4.2.

6.2.1.3 Thermal Stability

The thermal analysis of as-synthesised zeolite ZSM-5 samples Zeo01-03, prepared using varying amounts of TPABr (with no additional aluminium source) under hydrothermal conditions of 160 °C for 72 hours, was analysed by TGA/DTG/DTA analysis in air coupled to MS spectrometry for identification of released compounds; results are depicted in Figure 6.4 and Figure 6.5, respectively. The thermal profiles of as-synthesised zeolite samples Zeo01-03 exhibited two mass loss regions; (1) up to 250 °C and (2) between 250 and 550 °C, as illustrated in Figure 6.4 and Figure 6.5. The initial mass loss was attributed to the release of water physisorbed to the zeolite surface (annotated as W1 in Figure 6.4), while the second mass loss was attributed to the decomposition and release of the OSDA compound (TPA^+) occluded in the pores of the zeolite (annotated as T1 in Figure 6.4) (Frantz et al., 2016; Neves et al., 2019; Pál-Borbély, 2007). It is noteworthy that zeolite Zeo01 and Zeo02 exhibited similar thermal profiles, as depicted in Figure 6.4.

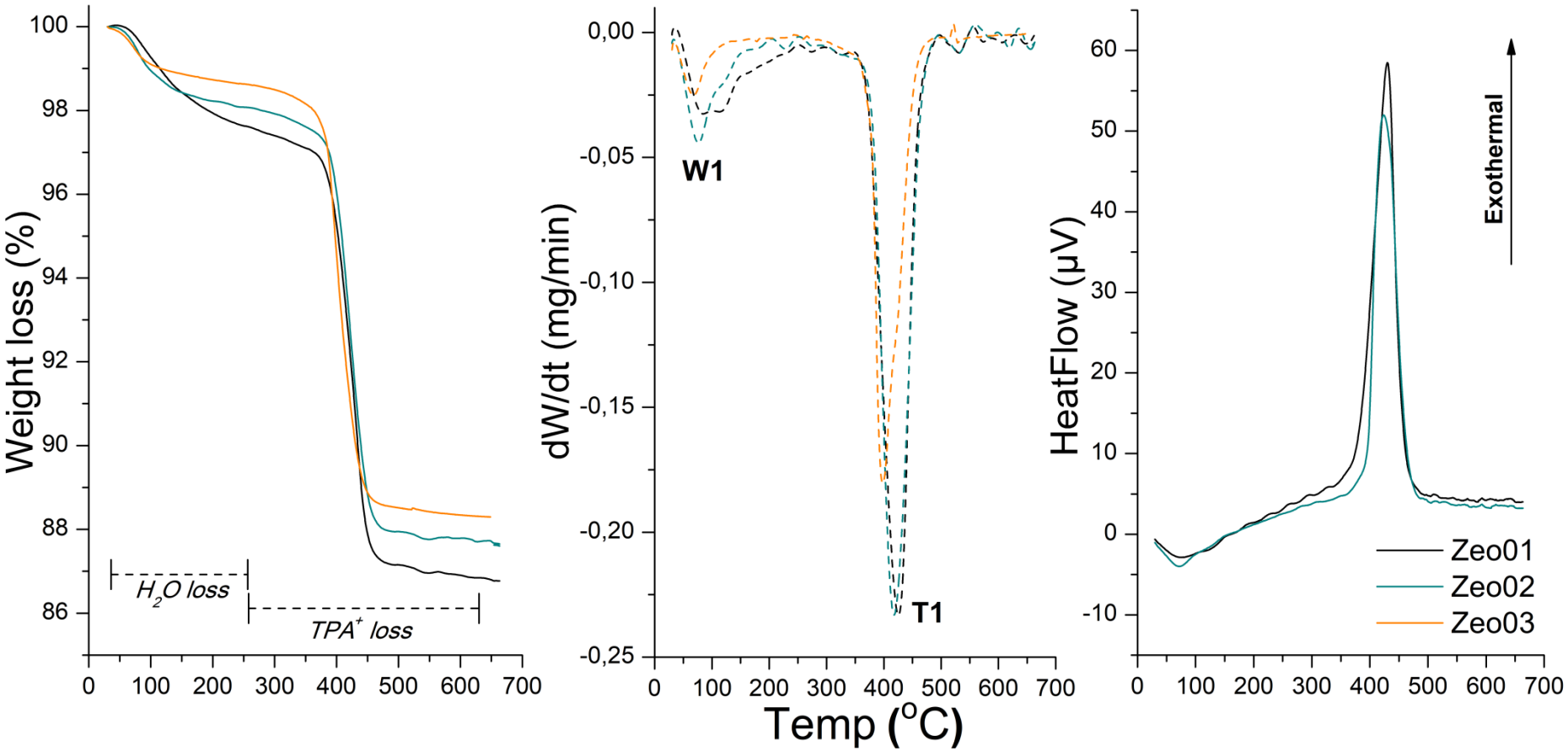

Figure 6.4: TGA/DTG/DTA analysis of as-synthesised Na-zeolites Zeo01-03 synthesised under hydrothermal conditions (160 °C for 72 hours) using varying amounts of ODSA agent (TPABr) in the synthesis mixture (1 SiO_2•0.004 Al_2O_3•0.54 Na_2O•n TPABr•35.4 H_2O) with n = 0.03-0.42, no additional aluminium source was added.

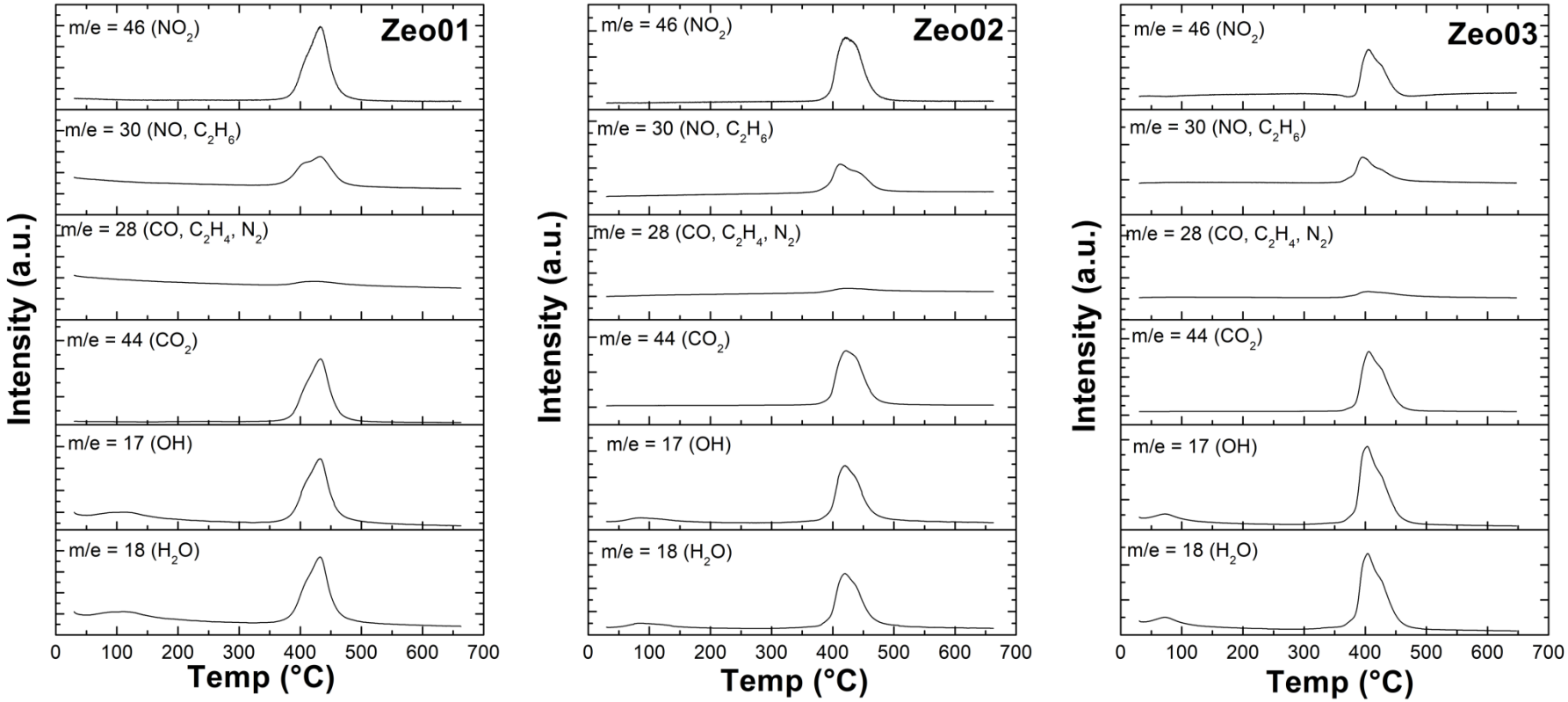

Figure 6.5: MS spectra of as-synthesised Na-zeolites Zeo01-03 synthesised under hydrothermal conditions (160 °C for 72 hours) using varying amounts of ODSA agent (TPABr) in the synthesis mixture (1 SiO_2•0.004 Al_2O_3•0.54 Na_2O•n TPABr•35.4 H_2O) with n = 0.03-0.42, no additional aluminium source was added.

A summary of the water content and TPABr content in the zeolite samples, calculated from the TGA analysis as per gram of the zeolite, is listed in Table 6.3. The water content per gram of zeolite was calculated between room temperature and 250 °C, while TPABr content was calculated between 250 and 550 °C.

Table 6.3: Summary of information gathered from TGA analysis for as-synthesised zeolite samples Zeo01-03, with water and template content reported as per gram of zeolite, synthesised under hydrothermal conditions (160 °C for 72 hours) with different amounts of TPABr in the synthesis mixture with molar regime 1 SiO_2•0.004 Al_2O_3•0.54 Na_2O•n TPABr•35.4 H_2O (n = 0.03-0.42).

Sample	Temp. W1 peak (°C)	Water content (g/g zeolite)	Temp. T1 peak (°C)	TPABr content (g/g zeolite)
Zeo01	98	0.021	415	0.111
Zeo02	82	0.023	418	0.104
Zeo03	68	0.014	398	0.103

As-synthesised zeolite samples Zeo01 and Zeo02 contained relatively similar amounts of water (~0.021 and 0.023 g H_2O/g zeolite respectively), as presented in Table 6.3. On the other hand, as-synthesised zeolite sample Zeo03 had considerably lower water content at 0.014 g H_2O/g zeolite, which illustrated that Zeo03 was relatively more siliceous than zeolites Zeo01 and Zeo02. Although there was no trend in the water content of zeolites as the TPABr amount in the synthesis mixture was varied, the temperature at which water was released from the MFI framework (W1 peak, as depicted in Figure 6.4) increased as the amount of template in the synthesis mixture increased (i.e. as the particle size and SAR of synthesised zeolites decreased). This was not expected since the release temperature of a particular compound is expected to increase with increasing length of the diffusion pathway (i.e. larger particle size, agglomerated particles and/or less porous materials). The observed shift in the W1 temperature is therefore thought to be due to differences in the porosity of synthesised materials. The amount of TPABr incorporated into the zeolite framework was relatively similar (~0.103-0.111 g TPABr/g zeolite), which illustrated that the amount of OSDA incorporation into the zeolite framework was independent of the amount of OSDA in the synthesis mixture and independent of the SAR value of the material. Furthermore, as depicted in Figure 6.4 and 6.5, OSDA degradation and release from the MFI framework occurred at a relatively low temperature of ~398-418 °C, which indicated that the OSDA molecules occluded in the pores of zeolite framework were loosely associated with the framework (Bourgeat-Lami et al., 1992; Pál-Borbély, 2007). Furthermore, the relatively

narrow temperature range observed for the release of OSDA components from these zeolite ZSM-5 samples (as depicted in Figure 6.4 and 6.5) is indicative of the potential ease of diffusion of reactants and/or products through the zeolite framework.

The TPA^+ cation is the most common OSDA agent utilised in the synthesis of zeolite ZSM-5 (Missengue et al., 2018; Petrik et al., 1995; Singh and Dutta, 2003). Highly crystalline zeolite ZSM-5 synthesised from a CFA-derived silicon precursor (FASE) was achieved using a relatively lower TPABr content compared to literature on the synthesis of ZSM-5 from a CFA-derived silicon extract (generated using a high-temperature fusion step) using TPABr as the OSDA agent (Missengue et al., 2018). The morphology of zeolite ZSM-5 crystals synthesised by Missengue et al., (2018) was prismatic ("coffin-shaped") with an average crystal dimensions of 6.5 x 2.6 µm. Spherical ZSM-5 crystals (with varying crystal size) were synthesised from standard chemical reagents (such as colloidal silica) by Petrik et al., (1995). In this study, the synthesis of zeolite ZSM-5 from a CFA-derived silicon precursor (FASE) resulted in the formation of micron-sized, spherical/ellipsoidal ZSM-5 crystals. Differences in the formation of ZSM-5 compared to literature are thought to be due to the silicon feedstock (FASE) utilised in this study.

The crystallinity of zeolite ZSM-5 samples synthesised from a CFA-derived silicon precursor was dependent on the OSDA (TPABr) amount present in the synthesis mixture, as depicted in Figure 6.1. Due to the relatively higher crystallinity of sample Zeo02 compared to sample Zeo03, further experiments were carried out using the synthesis procedure described for sample Zeo02 (as described in Table 3.7, Section 3.5). The synthesis procedure for sample Zeo02 used 25 mass% TPABr of the amount of TPABr used in the synthesis procedure for sample Zeo01. Therefore, a reduction in the TPABr amount by 75 mass% was achieved for the preparation of highly crystalline ZSM-5 from a coal fly ash silicon extract (FASE) without the oxalic acid treatment step, as reported in literature (Missengue, 2016; Ndlovu, 2016), or an additional silicon and/or aluminium source.

6.2.2 The effect of aluminium content on zeolite ZSM-5 crystallisation

The influence of aluminium source on the crystallisation of zeolite ZSM-5 from a CFA-derived silicon precursor was investigated by making use of two different aluminium sources, aluminium hydroxide and sodium aluminate. The effect of aluminium source on the mineralogy, crystallinity, morphology, composition and thermal properties of synthesised materials was characterised and will be presented in subsequent sections.

6.2.2.1 The effect of aluminium hydroxide addition on zeolite ZSM-5 crystallisation

The effect of aluminium content on zeolite ZSM-5 crystallinity was carried out by the addition of varying amounts of aluminium hydroxide (x moles) to the synthesis mixture for sample Zeo02 (1 SiO_2•x Al_2O_3•0.54 Na_2O•0.10 TPABr•35.4 H_2O), where x = 0.004-0.111, as described in Table 3.7 (Section 3.5). The synthesis of zeolite ZSM-5 from a CFA-derived silicon feedstock was carried out under static hydrothermal conditions of 160 °C for 72 hours. The aluminium content in the synthesis mixture was varied to determine the influence of SAR value of the starting synthesis mixture on the crystallinity, morphology and thermal properties of zeolite ZSM-5.

6.2.2.1.i Mineralogy and crystallinity

XRD diffractograms for as-synthesised products crystallised at 160 °C for 72 hours from synthesis mixtures with a molar regime 1 SiO_2•x Al_2O_3•0.54 Na_2O•0.10 TPABr•35.4 H_2O with varying Al content by aluminium hydroxide addition (with x = 0.004-0.111) are depicted in Figure 6.6.

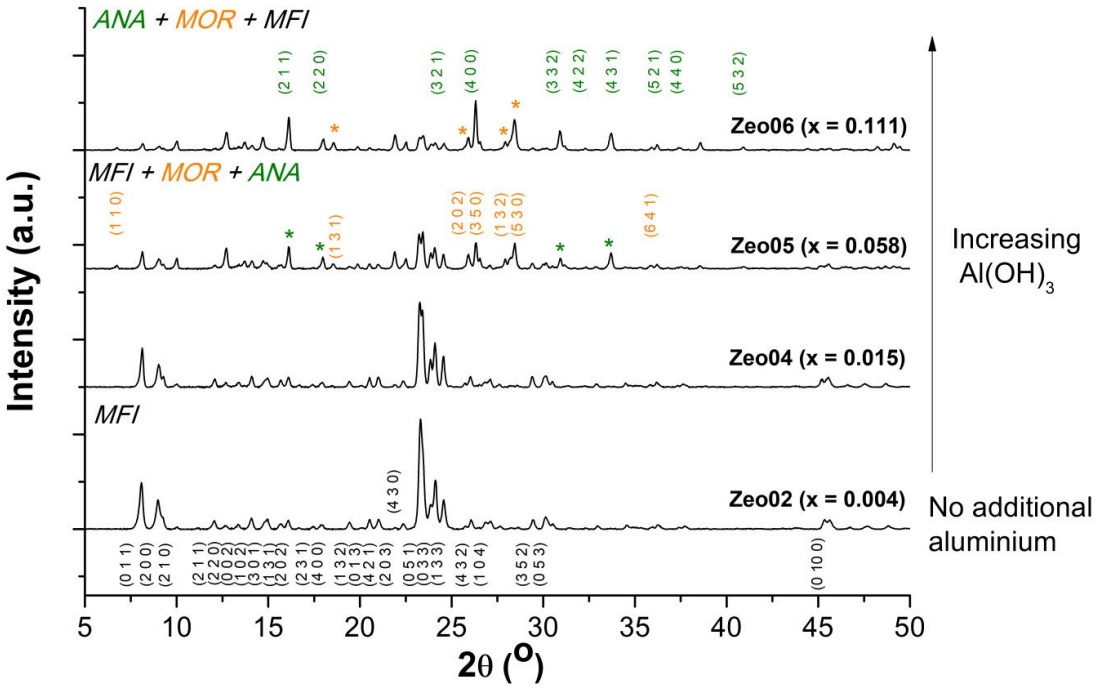

Figure 6.6: XRD diffractograms of as-synthesised zeolite products synthesised under hydrothermal conditions of 160 °C for 72 hours, from a synthesis mixture (1 SiO_2•x Al_2O_3•0.54 Na_2O•0.10 TPABr•35.4 H_2O) with varying amounts of additional aluminium hydroxide (x = 0.004-0.111). Key: MFI - zeolite ZSM-5, MOR - zeolite mordenite, ANA - Analcime

As-synthesised zeolite sample Zeo04 was prepared from a synthesis mixture with the molar regime 1 SiO_2•0.015 Al_2O_3•0.54 Na_2O•0.10 TPABr•35.4 H_2O by the addition of aluminium

hydroxide. The diffraction pattern observed for sample Zeo04 exhibited the main diffraction peaks associated with zeolite ZSM-5, as depicted in Figure 6.6. As-synthesised zeolite sample Zeo05, prepared from a synthesis mixture with the molar regime 1 SiO_2•0.058 Al_2O_3•0.54 Na_2O•0.10 TPABr•35.4 H_2O by the addition of aluminium hydroxide, exhibited the main diffraction peaks associated with zeolite ZSM-5 (indexed in black) as well as the main diffraction peaks for zeolite mordenite at 2θ values of 6.51, 25.63, 26.25, 27.49 and 27.87° (indexed in orange), with minor diffraction peaks corresponding to analcime at 2θ values of 15.81, 25.96 and 30.54° (indexed in green), as depicted in Figure 6.6. As-synthesised zeolite sample Zeo06 was prepared from a synthesis mixture with the molar regime 1 SiO_2•0.111 Al_2O_3•0.54 Na_2O•0.10 TPABr•35.4 H_2O by the addition of aluminium hydroxide. Zeolite sample Zeo06 was composed of analcime as the major phase and also contained diffraction peaks for zeolites ZSM-5 and mordenite as minor phases. The relative crystallinity of each sample was calculated, according to Equation 2.8, using the most crystalline sample (Zeo23) as a reference pattern and the OD ratio of synthesised materials were determined from FTIR data; results are summarised in Table 6.4.

Table 6.4: Relative crystallinity of as-synthesised Na-ZSM-5 zeolites Zeo02, Zeo04-06, synthesised under hydrothermal conditions of 160 °C for 72 hours, from a synthesis mixture (1 SiO_2•x Al_2O_3•0.54 Na_2O•0.10 TPABr•35.4 H_2O) with varying amounts of additional aluminium hydroxide (x = 0.004-0.111), determined using XRD and FTIR data.

Sample	Al_2O_3 added to the synthesis mixture as aluminium hydroxide(moles)	Relative Crystallinity	
		XRD (% crystallinity)	FTIR (optical density ratio)
Zeo02	0.004	96.9	0.95
Zeo04	0.015	82.1	0.95
Zeo05	0.058	33.9	1.06
Zeo06	0.111	13.5	1.22*

*Analcime mineral phase

The crystallisation of zeolite ZSM-5 from synthesis mixtures containing additional aluminium (by using aluminium hydroxide as the Al precursor) was relatively sensitive to the SAR value of the synthesis mixture. Increased aluminium content in the synthesis mixture resulted in a decrease in zeolite ZSM-5 crystallinity, as listed in Table 6.4. As the SAR value of the synthesis mixture was decreased, the co-crystallisation of zeolite ZSM-5 and mordenite occurred and eventually zeolite analcime crystallised as the major phase.

6.2.2.1.ii Morphology and composition

The influence of aluminium content (by aluminium hydroxide addition) on the morphology of as-synthesised Na-zeolite ZSM-5 samples Zeo04-06 compared to Zeo02 was investigated by SEM coupled to EDS; micrographs of synthesised materials are depicted in Figure 6.7. The average particle size, SAR and Na/Al ratios of as-synthesised samples are listed in Table 6.5.

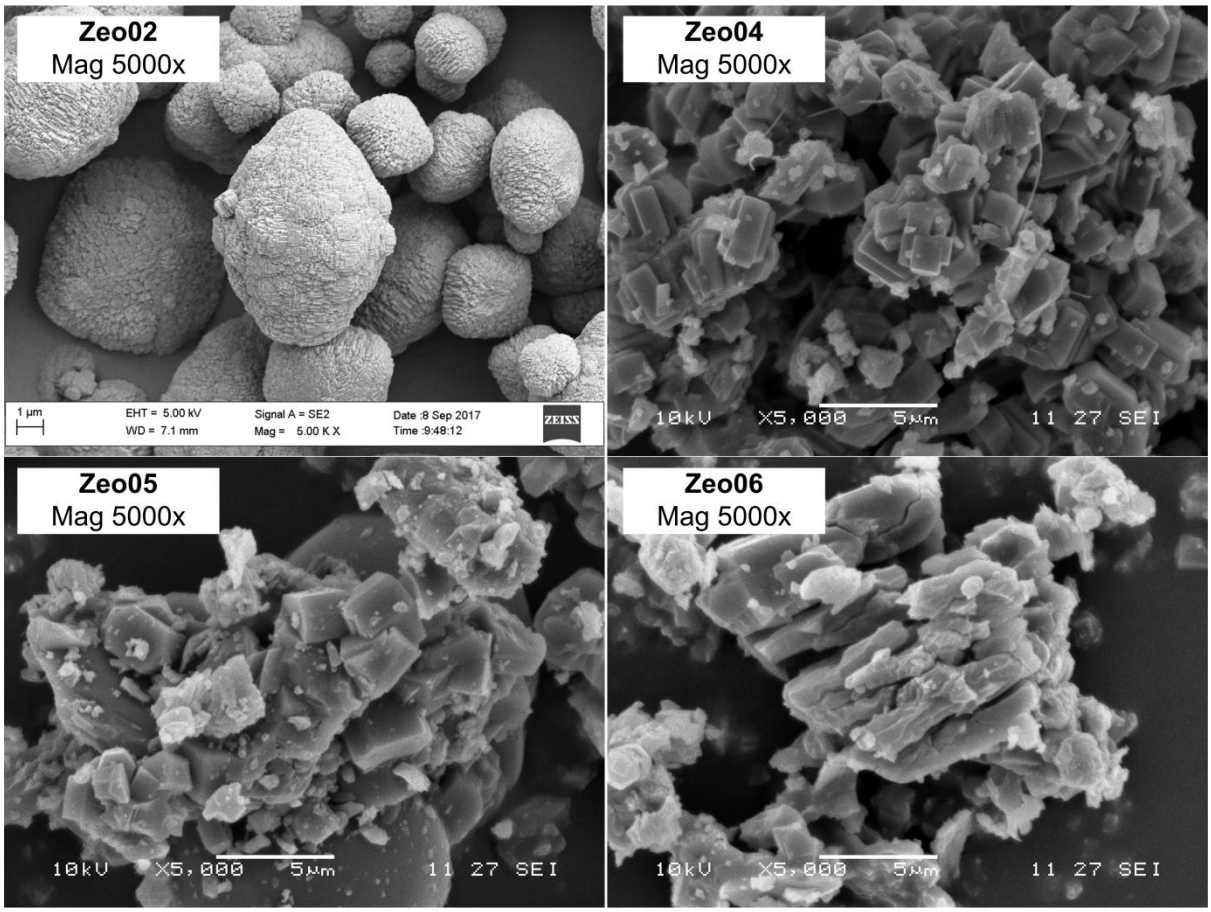

Figure 6.7: SEM micrographs (5000x magnification) of as-synthesised Na-zeolite ZSM-5 samples Zeo02, Zeo04-06 synthesised under hydrothermal conditions of 160 °C for 72 hours, from a synthesis mixture (1 SiO_2•x Al_2O_3•0.54 Na_2O•0.10 TPABr•35.4 H_2O) with varying amounts of additional aluminium hydroxide (x = 0.004-0.111).

The addition of aluminium to the synthesis mixture (in the form of aluminium hydroxide) had a significant effect on the morphology of ZSM-5 crystals, as depicted in Figure 6.7. Addition of a small amount of aluminium hydroxide resulted in ZSM-5 crystals with the typical prismatic ("coffin-shaped") morphology (Zeo04), in contrast to the ellipsoidal ZSM-5 crystals synthesised in the absence of an additional source of aluminium (Zeo02).

Table 6.5: Properties of as-synthesised Na-ZSM-5 zeolites Zeo02, Zeo04-06 such as average particle size (determined using ImageJ) and relative composition (determined by EDS analysis n=10), synthesised under hydrothermal conditions of 160 °C for 72 hours, from a synthesis mixture (1 SiO_2•x Al_2O_3•0.54 Na_2O•0.10 TPABr•35.4 H_2O) with varying amounts of additional aluminium hydroxide (x = 0.004-0.111).

Sample	Al_2O_3 added to the synthesis mixture as aluminium hydroxide(moles)	Average particle size (µm)	SAR value	Na/Al Ratio
Zeo02	0.004	4.9	92.8	1.3
Zeo04	0.015	2.5	21.4	2.9
Zeo05	0.058	2.3	10.3	1.4
Zeo06	0.111	14.6	5.3	1.2

As listed in Table 6.5, sample Zeo04 synthesised with a small amount of aluminium hydroxide exhibited a relatively smaller crystal size with an average particle size of 2.5 µm compared to sample Zeo02 (4.9 µm), which was synthesised without additional aluminium. Furthermore, sample Zeo04 exhibited an SAR value of 21.4 which was much lower than the SAR value for sample Zeo02 (92.8). The presence of a relatively small amount of additional aluminium hydroxide in the synthesis solution was therefore able to change the crystal growth mechanism of zeolite ZSM-5 crystals, from three dimensional growth (no additional aluminium source) to two dimensional growth (a small amount of aluminium hydroxide added), to produce relatively smaller, prismatic crystals. The addition of a small amount of aluminium hydroxide to the synthesis mixture therefore favoured the nucleation rate over the rate of crystal growth, resulting in the formation of smaller ZSM-5 crystals (Cubillas and Anderson, 2010; Yu, 2007). However, the presence of relatively higher amounts of aluminium hydroxide resulted in the formation of zeolite mordenite and analcime crystals together with zeolite ZSM-5 crystals, as depicted in Figure 6.7 (sample Zeo05 and Zeo06). The typical zeolite mordenite crystal morphology is clearly visible in sample Zeo05, while the presence of relatively larger spherical analcime crystals was observed in both sample Zeo05 and Zeo06.

6.2.2.1.iii Thermal Stability

The thermal analysis of as-synthesised samples Zeo02 (no additional aluminium source) and Zeo04-06 (prepared with different amounts of aluminium hydroxide added to the synthesis mixture) was carried out by TGA/DTG/DTA analysis in air coupled to MS, as depicted in Figure 6.8 and 6.9.

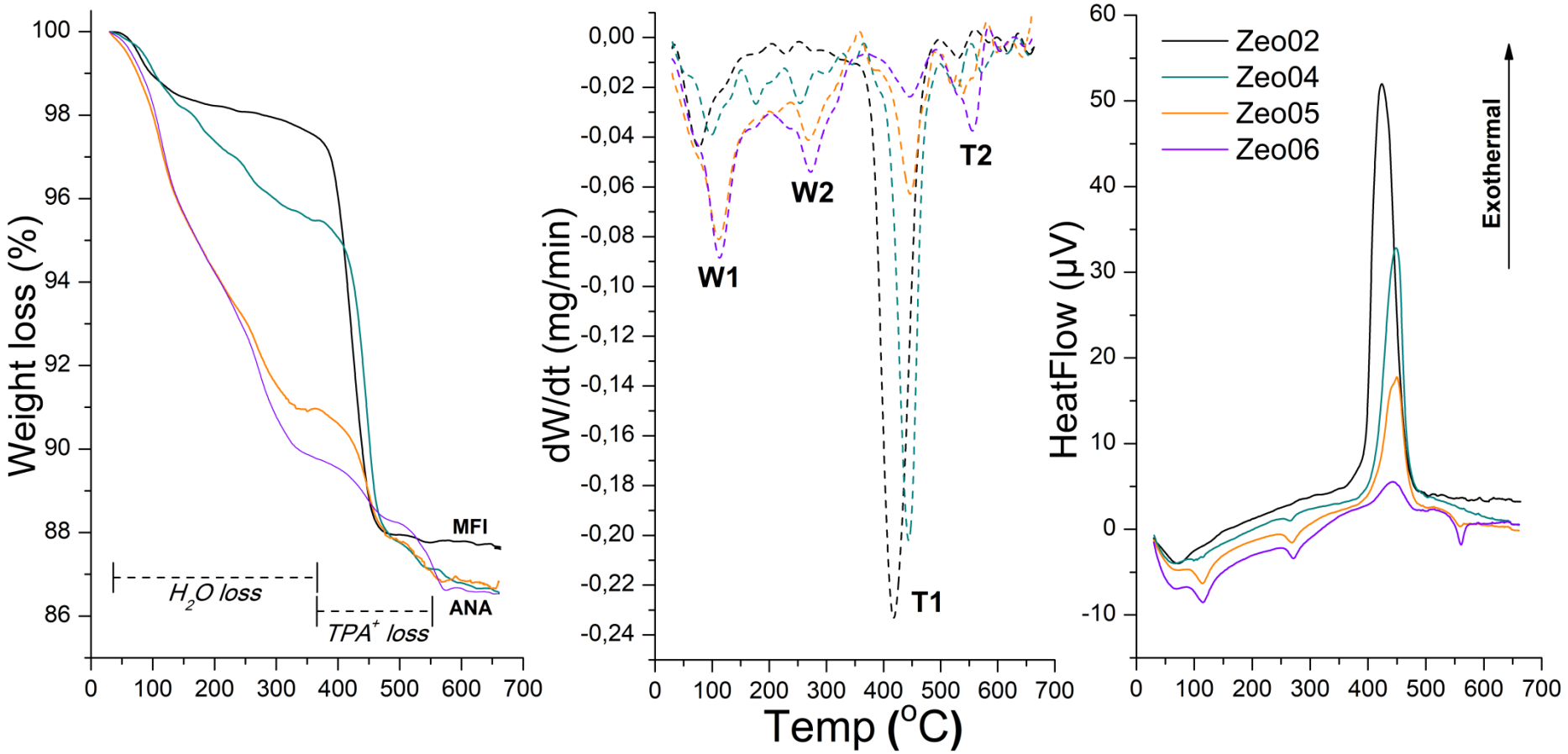

Figure 6.8: TGA/DTG/DTA analysis of as-synthesised Na-zeolites synthesised under hydrothermal conditions (160 °C for 72 hours) using no additional aluminium source (Zeo02) and varying amounts of aluminium hydroxide (Zeo04-06) in the synthesis mixture (1 SiO_2•x Al_2O_3•0.54 Na_2O•0.10 TPABr•35.4 H_2O) with x = 0.004-0.111.

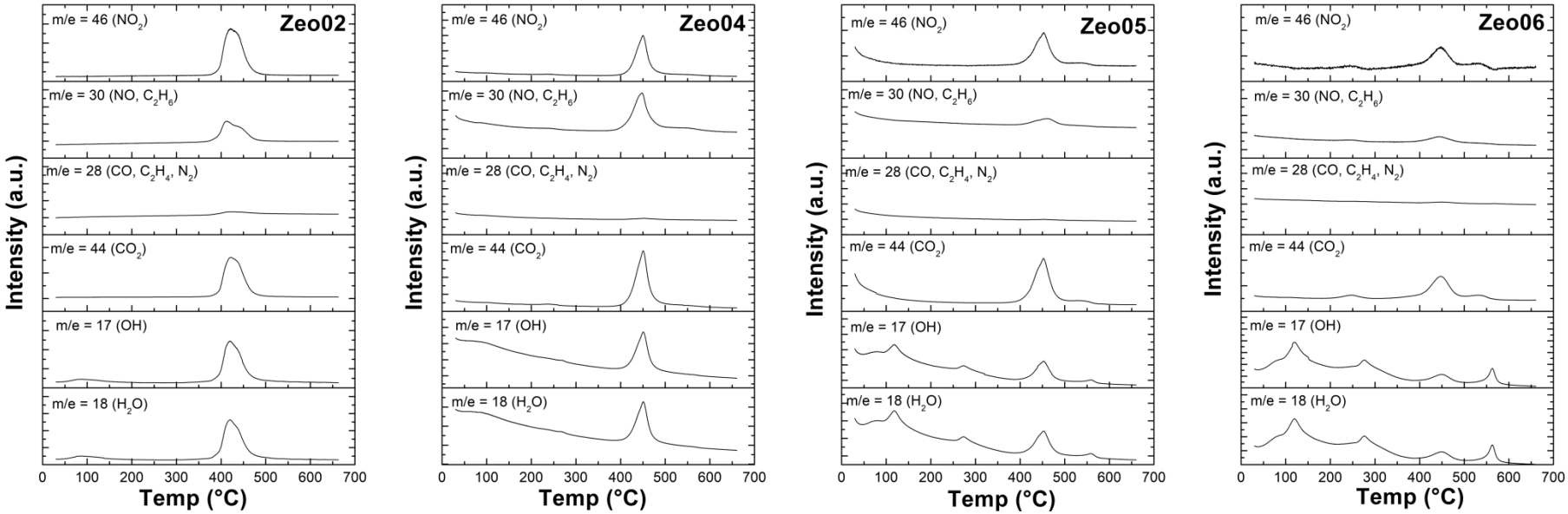

Figure 6.9: MS spectra of as-synthesised Na-zeolites synthesised under hydrothermal conditions (160 °C for 72 hours) using no additional aluminium source (Zeo02) and varying amounts of aluminium hydroxide (Zeo04-06) in the synthesis mixture (1 SiO_2•x Al_2O_3•0.54 Na_2O•0.10 TPABr•35.4 H_2O) with x = 0.004-0.111.

The thermal analysis of as-synthesised samples Zeo04-06 compared to sample Zeo02 revealed two distinct types of mass loss profiles, as depicted in Figure 6.8. These mass loss profiles corresponded to the mineralogical content of the zeolite samples as depicted in Figure 6.6. Zeolite ZSM-5 samples Zeo02 and Zeo04 exhibited a relatively similar mass loss profile, while zeolite samples containing mineral phases zeolite mordenite and analcime (Zeo05 and Zeo06) exhibited a more complex mass loss profile (as depicted in Figure 6.8 and 6.9). The main mass losses were annotated as W1 and W2 for mass loss regions associated with the desorption and release of physisorbed H_2O molecules from the zeolite framework (determined from MS spectra in Figure 6.9) as well as T1 and T2 mass loss regions that correspond to the degradation and release of TPABr molecules from the zeolite ZSM-5 pores and channels (determined from MS spectra in Figure 6.9).

A summary of the thermal properties of as-synthesised zeolites Zeo04-06 compared to Zeo02 are presented in Table 6.6. The initial mass loss due to desorption of physisorbed water occurs at two temperatures; W1 at ~ 100 °C and W2 at ~ 250 °C. Mass loss W1 is due to the desorption of water from the surface of zeolites, while mass loss W2 is thought to be due to the release of water from (i) less accessible sites in the pores and channels of the zeolite ZSM-5 framework due to pore blockages caused by crystal agglomeration (particularly for sample Zeo04) or (ii) larger mordenite/analcime crystals that cause diffusional constraints (particularly in the case of samples Zeo05 and Zeo06).

Table 6.6: Summary of information gathered from TGA analysis for as-synthesised zeolite samples Zeo02, Zeo04-06, reported as per gram of zeolite, synthesised under hydrothermal conditions of 160 °C for 72 hours, from a synthesis mixture (1 SiO_2•x Al_2O_3•0.54 Na_2O•0.10 TPABr•35.4 H_2O) with varying amounts of additional aluminium hydroxide (x = 0.004-0.111).

Sample	Temp. W1 peak (°C)	Temp. W2 peak (°C)	Water content (g/g zeolite)	Temp. T1 peak (°C)	Temp. T2 peak (°C)	TPABr content (g/g zeolite)
Zeo02	82	-	0.023	418	-	0.104
Zeo04	98	254	0.045	444	528	0.084
Zeo05	110	268	0.091	447	540	0.038
Zeo06	113	272	0.101	447	556	0.032

Similarly, two mass losses T1 and T2 were associated with the release of the TPABr molecules from the zeolite frameworks. Mass loss T1 at the relatively low temperature of ~ 400-450 °C is typically associated with the degradation and release of TPABr molecules occluded in the pores and channels of zeolite ZSM-5 (as observed for samples Zeo02 and

Zeo04). On the other hand, the relatively higher temperature mass loss T2 at ~ 550 °C (as observed for sample Zeo04) is thought to be due to the degradation and release of TPABr molecules occluded in less accessible sites in the pores and channels of the zeolite framework, which experience diffusional constraints during the thermal analysis of the zeolite samples in air (Bourgeat-Lami et al., 1992; Lohse et al., 1996; Pál-Borbély, 2007). It is noteworthy that sample Zeo02 did not exhibit the higher temperature mass loss regions, illustrating no diffusional constraints for either water or OSDA agents to be released from the zeolite ZSM-5 framework. Different, high temperature mass losses associated with the degradation and release of the OSDA agent from zeolite ZSM-5 was also reported in the literature (Wang et al., 2017).

6.2.2.2 The effect of sodium aluminate addition on zeolite ZSM-5 crystallisation

The effect of aluminium content on zeolite ZSM-5 crystallinity was carried out by the addition of varying amounts of sodium aluminate (x moles) to the synthesis mixture for sample Zeo02 (1 SiO_2•x Al_2O_3•y Na_2O•0.10 TPABr•35.4 H_2O), where x = 0.004-0.111 and y = 0.54-0.65, as described in Table 3.7 (Section 3.5). Sodium aluminate addition to the synthesis mixture was carried out using equimolar amounts for samples Zeo07, Zeo11 and Zeo12 compared to the addition of aluminium hydroxide in samples Zeo04-06 as described in Table 3.7 and further experiments for samples Zeo08-10 were carried out by varying the aluminium content between samples Zeo07 and Zeo11. The synthesis of zeolite ZSM-5 from a CFA-derived silicon feedstock was carried out under static hydrothermal conditions of 160 °C for 72 hours. The aluminium content in the synthesis mixture (using a different aluminium source such as sodium aluminate) was varied to determine the influence of SAR value of the starting synthesis mixture on the crystallinity, morphology and thermal properties of zeolite ZSM-5.

6.2.2.2.i Mineralogy and crystallinity

XRD diffractograms for as-synthesised products crystallised at 160 °C for 72 hours from synthesis mixtures with a molar regime 1 SiO_2•x Al_2O_3•y Na_2O•0.10 TPABr•35.4 H_2O, with varying Al content by sodium aluminate addition (with x = 0.004-0.111 and y = 0.54-0.65) are depicted in Figure 6.10. The relative crystallinity of each sample was calculated, according to Equation 2.8, using the most crystalline sample (Zeo23) as a reference pattern and the OD ratio was determined from FTIR data; results are summarised in Table 6.7. XRD diffraction patterns of as-synthesised samples Zeo07 and Zeo08 (synthesised from synthesis

mixtures with relatively low Al content; x = 0.015 and 0.025 and y = 0.55 and 0.56, respectively) exhibited the main diffraction peaks associated with zeolite ZSM-5, without any other mineral phases present. However, these ZSM-5 samples were relatively less crystalline compared to as-synthesised sample Zeo02 (as listed in Table 6.7). As the aluminium content in the synthesis mixture was increased (by sodium aluminate addition), the appearance of diffraction peaks associated with analcime was observed. Zeolite ZSM-5 and analcime therefore co-crystallised together at intermediate Al content levels, as observed for samples Zeo09-11 (x = 0.036, 0.046 and 0.058 and y = 0.57, 0.58 and 0.59, respectively) in Figure 6.10. At relatively high Al content (x = 0.111 and y = 0.65) as in sample Zeo12, diffraction peaks associated with analcime were observed.

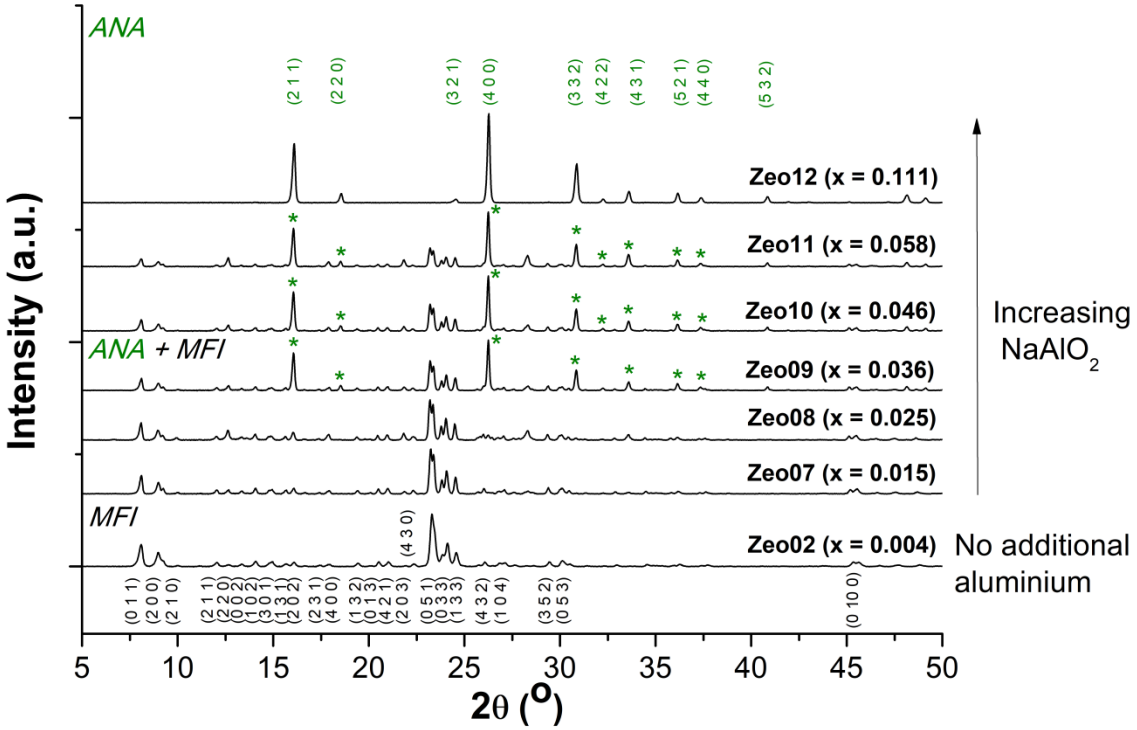

Figure 6.10: XRD diffractograms of as-synthesised zeolite products Zeo02, Zeo07-12 synthesised under hydrothermal conditions of 160 °C for 72 hours, from a synthesis mixture (1 SiO_2•x Al_2O_3•y Na_2O•0.10 TPABr•35.4 H_2O) with varying amounts of additional sodium aluminate (x = 0.004-0.111, y = 0.54-0.65). Key: MFI - zeolite ZSM-5, ANA - Analcime

As listed in Table 6.7, the relative percentage crystallinity of zeolite ZSM-5 decreased as the aluminium content in the synthesis mixture increased (by sodium aluminate addition). This is thought to be due to (i) changes in the crystallisation of ZSM-5 in the presence of sodium aluminate as an additional aluminium source as well as (ii) the favourable crystallisation of the analcime mineral phase at lower SAR values of the synthesis mixture. It is noteworthy

that in this case FTIR spectroscopy was not able to differentiate between crystalline mineral phases.

Table 6.7: Relative crystallinity of as-synthesised zeolites Zeo02, Zeo07-12 synthesised under hydrothermal conditions of 160 °C for 72 hours, from a synthesis mixture (1 SiO_2•x Al_2O_3•y Na_2O•0.10 TPABr•35.4 H_2O) with varying amounts of additional sodium aluminate (x = 0.004-0.111, y = 0.54-0.65), determined using XRD and FTIR data.

Sample	Al_2O_3 added to the synthesis mixture as sodium aluminate (moles)	Na_2O added to the synthesis mixture (moles)	Relative Crystallinity	
			XRD (% crystallinity)	FTIR (optical density ratio)
Zeo02	0.004	0.54	96.9	0.95
Zeo07	0.015	0.55	85.3	1.04
Zeo08	0.025	0.56	80.9	0.96
Zeo09	0.036	0.57	58.9	0.99
Zeo10	0.046	0.58	55.0	1.03
Zeo11	0.058	0.59	35.3	1.07
Zeo12	0.111	0.65	0.0	1.18

The crystallisation of zeolite ZSM-5 from synthesis mixtures containing additional aluminium from a different aluminium precursor such as sodium aluminate was relatively sensitive to changes in SAR value of the synthesis mixture, as was observed for the synthesis of zeolite ZSM-5 in the presence of additional aluminium hydroxide in Figure 6.6. In the case of sodium aluminate addition, no competition between zeolite ZSM-5 and mordenite crystallisation occurred. Furthermore, decreasing the SAR values of the synthesis mixture (as described in Table 3.7, Section 3.5) resulted in the co-crystallisation of zeolite ZSM-5 and analcime only at intermediate aluminium content and at the lowest SAR value (corresponding to x = 0.111 and y = 0.65) for the synthesis mixture, analcime crystallised without any other mineral phases. A comparison of highly crystalline zeolite ZSM-5 samples Zeo04 and Zeo07 (prepared using aluminium hydroxide and sodium aluminate, respectively) is depicted in Figure 6.11.

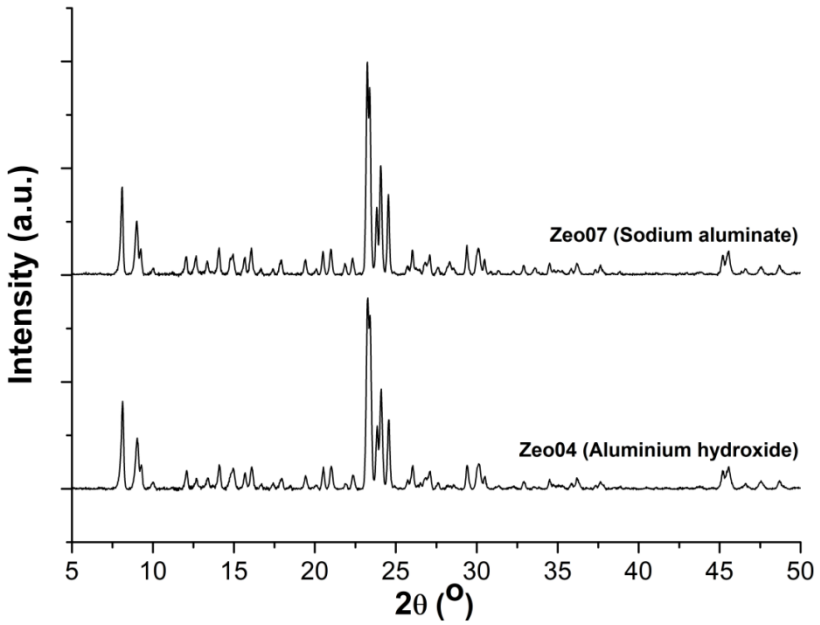

Figure 6.11: XRD diffractograms of as-synthesised zeolite ZSM-5 products prepared from a synthesis mixture with molar regime 1 SiO_2•0.015 Al_2O_3•0.55 Na_2O•0.10 TPABr•35.4 H_2O containing either aluminium hydroxide (Zeo04) or sodium aluminate (Zeo07) as an aluminium source, under hydrothermal conditions of 160 °C for 72 hours.

XRD diffraction patterns of sample Zeo04 and Zeo07 (depicted in Figure 6.11) both exhibited relatively high crystallinity as listed in Table 6.4 and Table 6.7, respectively. However, sample Zeo07 (prepared with sodium aluminate) was slightly more crystalline (85.3%) than sample Zeo04 (prepared with aluminium hydroxide), which exhibited a relative crystallinity of 82.1%. Sample Zeo07 was therefore used as a baseline for further investigations on the influence of synthesis parameters on ZSM-5 crystallisation due to the relatively higher ZSM-5 crystallinity of the sample compared to sample Zeo04, ease of dissolution of the aluminium precursor as well as the lack of ZSM-5/mordenite competition in this synthesis system.

6.2.2.2.ii Morphology and composition

The effect of aluminium content (by sodium aluminate addition) on the morphology of as-synthesised Na-zeolite samples Zeo07-12 was investigated by SEM coupled to EDS, compared to sample Zeo02 (synthesised with no additional aluminium source); micrographs of synthesised materials are depicted in Figure 6.12. Other properties such as the average particle size, SAR and Na/Al ratios of as-synthesised samples are listed in Table 6.8.

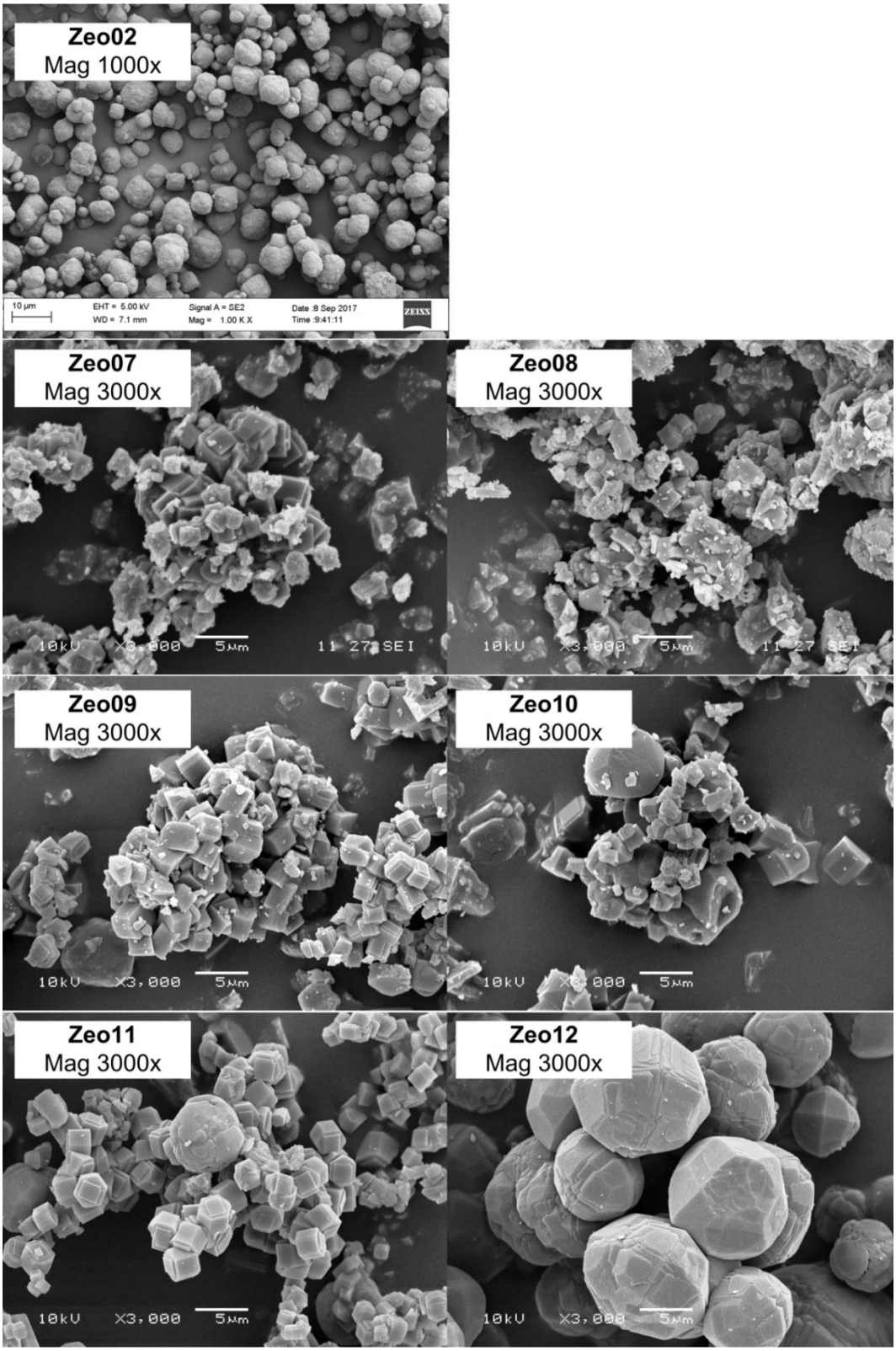

Figure 6.12: SEM micrograph of as-synthesised Na-zeolite ZSM-5 samples Zeo07-12 (3000x magnification) compared to sample Zeo02 (1000x magnification), prepared with different amounts of sodium aluminate in the synthesis mixture with molar regime 1 SiO_2•x Al_2O_3•y Na_2O•0.10 TPABr•35.4 H_2O (x = 0.004-0.111, y = 0.54-0.65) under hydrothermal conditions of 160 C for 72 hours.

The addition of sodium aluminate influenced the morphology of zeolite ZSM-5 crystals, as depicted in Figure 6.12. The addition of relatively small amounts of sodium aluminate (Zeo07 and Zeo08) resulted in the formation of prismatic ZSM-5 crystals with reduced crystal size compared to sample Zeo02. Relatively intermediate amounts of sodium aluminate in the synthesis mixture resulted in the formation of well-defined prismatic ZSM-5 crystals (~3 µm in size) and relatively larger spherical analcime crystals (~10 µm in size), as depicted in Figure 6.12 (Zeo09-11). At high aluminium content in the synthesis mixture (Zeo12), the presence of solely large, spherical analcime crystals were observed with an average particle size of ~10 µm (as listed in Table 6.8).

Table 6.8: Properties of as-synthesised Na-ZSM-5 zeolites Zeo02, Zeo07-12 such as average particle size (determined using ImageJ) and relative composition (determined by EDS analysis n=10), prepared with different amounts of sodium aluminate in the synthesis mixture with molar regime 1 SiO_2•x Al_2O_3•y Na_2O•0.10 TPABr•35.4 H_2O (x = 0.004-0.111, y = 0.54-0.65) under hydrothermal conditions of 160 C for 72 hours.

Sample	Al_2O_3 added to the synthesis mixture as sodium aluminate (moles)	Na_2O added to the synthesis mixture (moles)	Average particle size (µm)	SAR value	Na/Al Ratio
Zeo02	0.004	0.54	4.9	92.8	1.3
Zeo07	0.015	0.55	1.9	30.5	0.5
Zeo08	0.025	0.56	2.7	18.5	0.5
Zeo09	0.036	0.57	3.0	7.5	0.5
Zeo10	0.046	0.58	3.2	6.4	0.5
Zeo11	0.058	0.59	2.6	5.6	0.6
Zeo12	0.111	0.65	9.9*	3.0	0.6

*Analcime crystals

An increase in the amount of sodium aluminate added to the synthesis mixture resulted in decreased SAR values for synthesised zeolites; from 92.8 (no additional sodium aluminate) to 3.0 (for x = 0.111 and y = 0.65) as presented in Table 6.8. The relatively lower SAR values for zeolite ZSM-5 samples Zeo07 (30.5) and Zeo08 (18.5), compared to sample Zeo02 (92.8), illustrates the enhanced incorporation of aluminium into the zeolite framework as the aluminium content in the synthesis mixture was increased. Synthesised zeolites Zeo02, Zeo07 and Zeo08 exhibited SAR values which are typical for zeolite ZSM-5 (≥ 10-15) (Sklenak et al., 2009; Xu, 2007). Synthesised zeolite Zeo12, composed of the mineral phase analcime as depicted in Figure 5.10, exhibited a SAR value of 3. This is typical for zeolite analcime that commonly has a SAR value in the range of 1.8-2.8 (Hartman and Fogler, 2007; Ming and

Gooding, 1988). As expected, synthesised materials composed of both zeolite ZSM-5 and analcime exhibited intermediate SAR values, as listed in Table 6.8.

6.2.2.2.iii Thermal Stability

The TGA profiles of as-synthesised zeolites Zeo02, Zeo07-12 prepared with different amounts of sodium aluminate added to the synthesis mixture are depicted in Figure 6.13, TGA analysis was carried out in air. A summary of the water and TPABr content in as-synthesised zeolite samples is presented in Table 6.9 along with the temperatures at which each component is released from the as-synthesised materials.

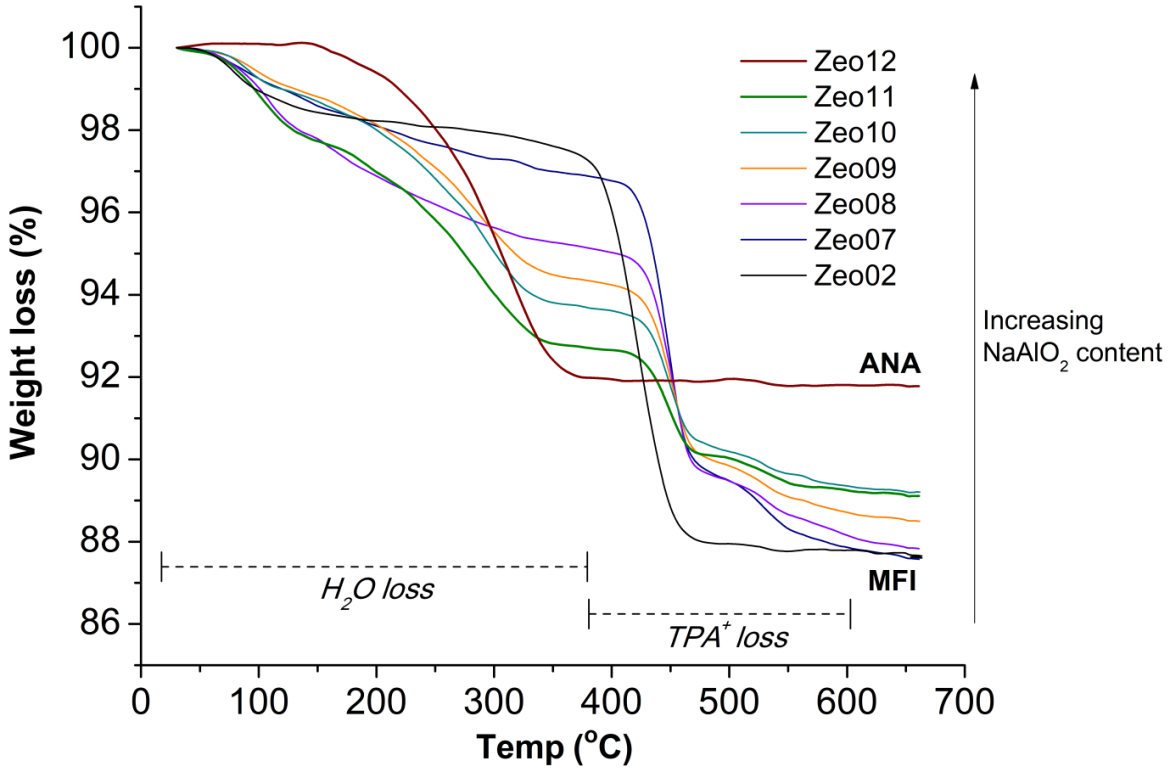

Figure 6.13: Thermal gravimetric (TG) analysis curve for as-synthesised zeolite samples Zeo02, Zeo07-12 prepared with different amounts of sodium aluminate in the synthesis mixture with molar regime 1 SiO_2•x Al_2O_3•y Na2O•0.10 TPABr•35.4 H_2O (x = 0.004-0.111, y = 0.54-0.65) under hydrothermal conditions of 160 C for 72 hours.

Table 6.9: Summary of information gathered from TGA analysis for as-synthesised zeolite samples Zeo02, Zeo07-Zeo12, reported as per gram of zeolite, prepared with different amounts of sodium aluminate in the synthesis mixture with molar regime 1 SiO_2•x Al_2O_3•y Na_2O•0.10 TPABr•35.4 H_2O (x = 0.004-0.111, y = 0.54-0.65) under hydrothermal conditions of 160 C for 72 hours.

Sample	Temp. W1 peak (°C)	Temp. W2 peak (°C)	Water content (g/g zeolite)	Temp. T1 peak (°C)	Temp. T2 peak (°C)	TPABr content (g/g zeolite)
Zeo02	82	-	0.023	418	-	0.104
Zeo07	89	-	0.030	446	529	0.089
Zeo08	108	-	0.047	449	532	0.066
Zeo09	97	280	0.057	449	529	0.053
Zeo10	90	293	0.063	448	529	0.044
Zeo11	101	280	0.073	448	533	0.033
Zeo12	-	314	0.080	-	-	-

As depicted in Figure 6.13 and Table 6.9, the water content in the zeolite framework increased as the aluminium content in the synthesis mixture increased (i.e. SAR value of the synthesised zeolite decreased). This is as expected since highly siliceous zeolites are thought to be hydrophobic, while aluminium-rich zeolites are known to be hydrophilic due to the net negative charge of the framework as a direct consequence of the presence of aluminium atoms in the framework (Frantz et al., 2016; Hölderich and van Bekkum, 1991; Santen and Vogel, 1989). Conversely, the amount of OSDA incorporated into the as-synthesised zeolite framework decreased as the aluminium content in the synthesis mixture increased. This is likely due to changes in the mineralogy of synthesised materials as the aluminium content in the synthesis increased, as depicted in Figure 6.10. The correlation of the water content (i.e. hydrophilicity) and OSDA content in the as-synthesised zeolite material with SAR value of the as-synthesised is presented graphically in Figure 6.14.

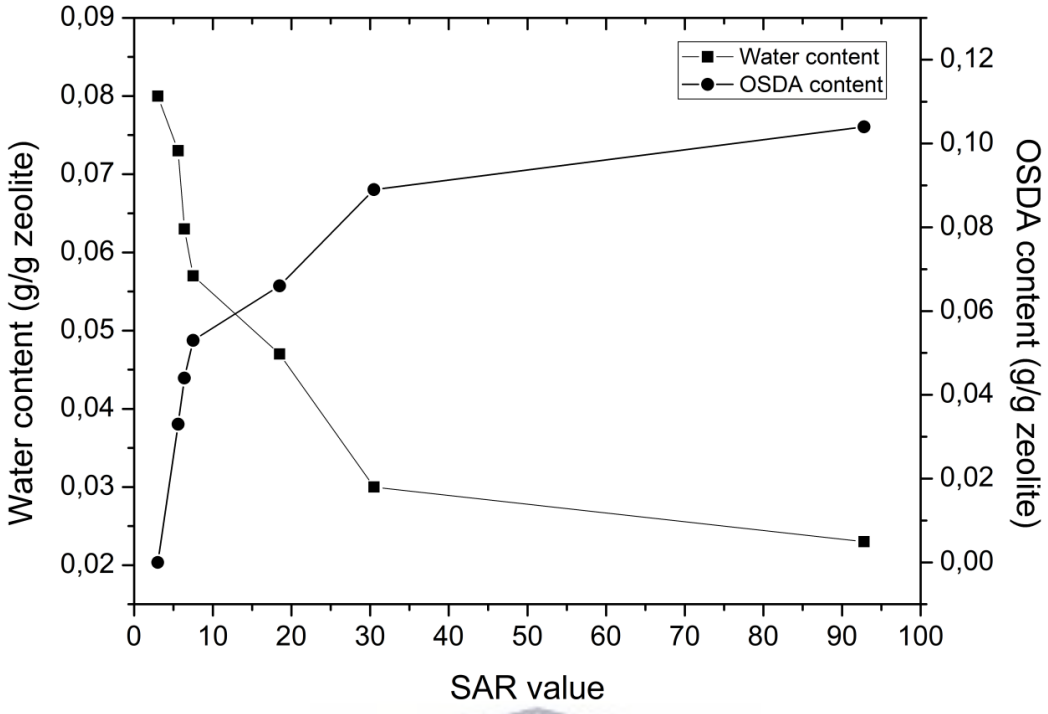

Figure 6.14: The SAR value of as-synthesised zeolite material versus the water content and OSDA content in the as-synthesised materials.

TGA/DTG/DTA spectra of as-synthesised zeolite samples were grouped according to similar mineralogy (as determined using Figure 6.10); spectra of as-synthesised samples corresponding to zeolite ZSM-5 (Zeo02, Zeo07-08) are depicted in Figure 6.15 with the corresponding MS spectra of these materials depicted in Figure 6.16.

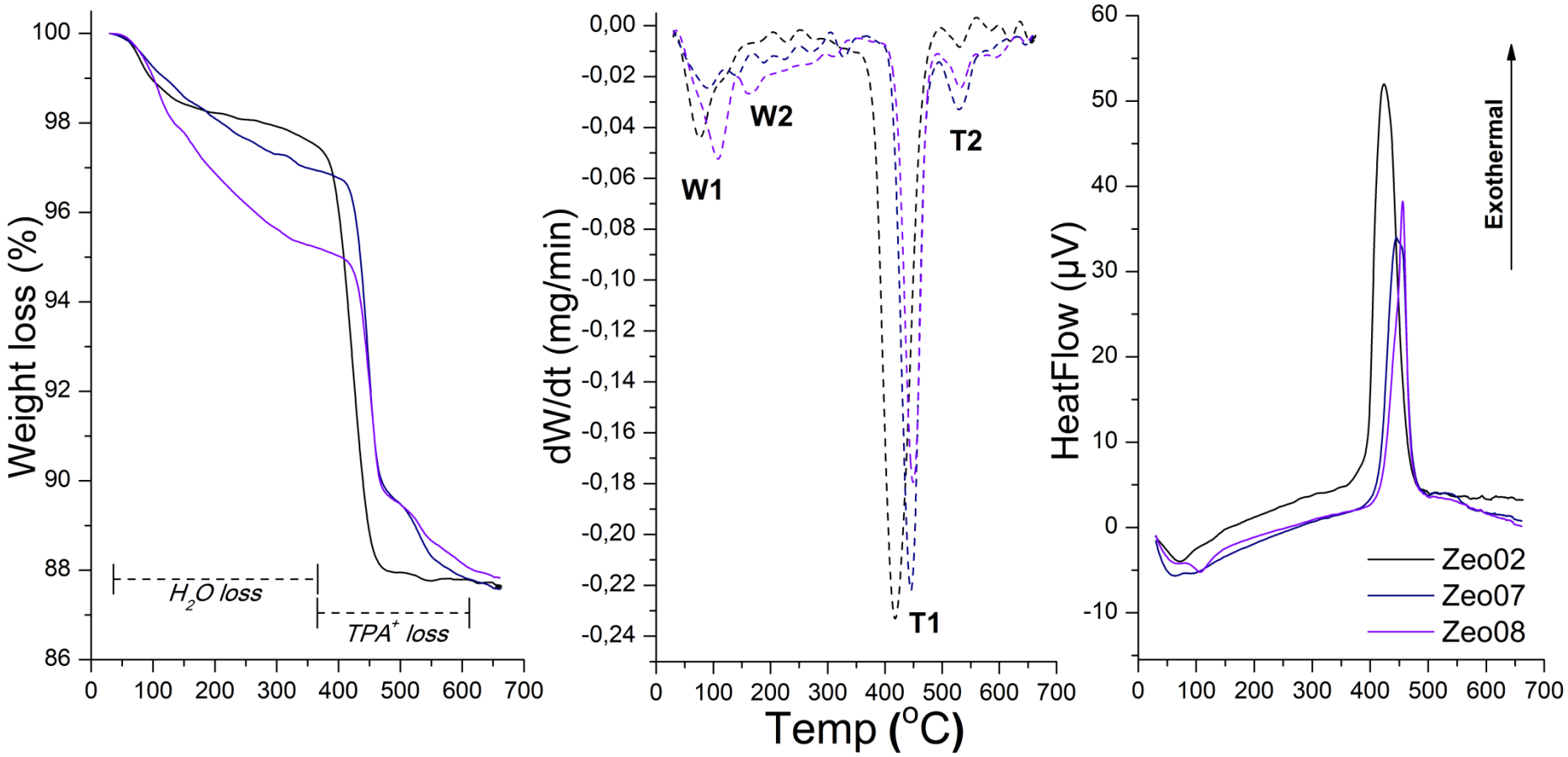

Figure 6.15: TGA/DTG/DTA analysis of as-synthesised Na-zeolites synthesised under hydrothermal conditions (160 °C for 72 hours) using no additional aluminium source (Zeo02) and varying amounts of sodium aluminate (Zeo07-08) in the synthesis mixture with molar regime 1 SiO_2•x Al_2O_3•y Na_2O•0.10 TPABr•35.4 H_2O (x = 0.004-0.025, y = 0.54-0.56).

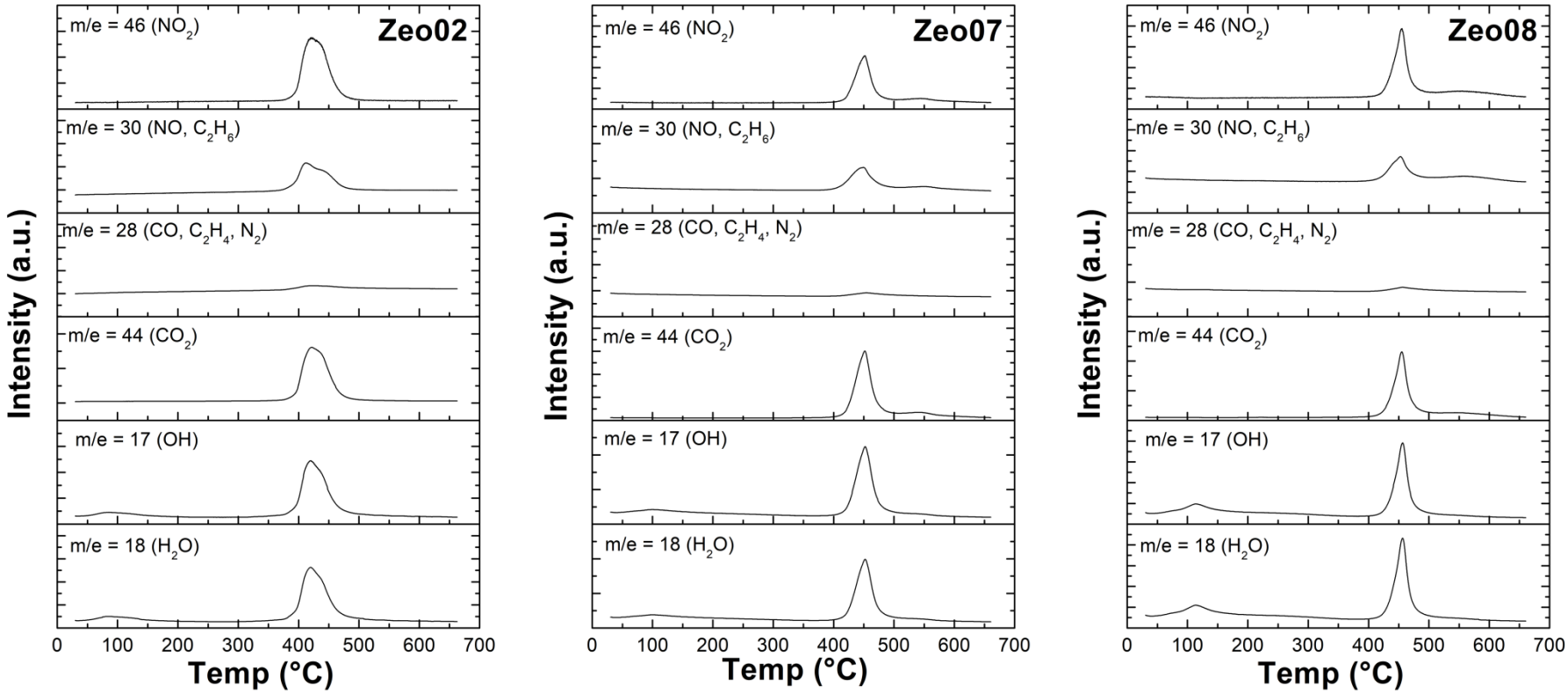

Figure 6.16: MS spectra of as-synthesised Na-zeolites synthesised under hydrothermal conditions (160 °C for 72 hours) using no additional aluminium source (Zeo02) and varying amounts of sodium aluminate (Zeo07-08) in the synthesis mixture with molar regime 1 SiO_2•x Al_2O_3•y Na_2O•0.10 TPABr•35.4 H_2O (x = 0.004-0.025, y = 0.54-0.56).

As-synthesised zeolite samples Zeo02, Zeo07 and Zeo08 exhibited similar thermal profiles, as depicted in Figure 6.15 and 6.16. These samples all exhibited a low temperature (W1) mass loss at ~ 80-110 °C associated with the release of physisorbed water from the pores and channels of synthesised zeolites. As-synthesised sample Zeo02 exhibited one distinct, high temperature mass loss (T1) at ~ 418 °C associated with the degradation and release of TPABr molecules occluded in pores and channels of the zeolite ZSM-5 framework, which illustrated that no diffusional constraints occurred for sample Zeo02. On the other hand, as-synthesised samples Zeo07 and Zeo08 exhibited two distinct temperatures (T1 and T2) related to the degradation and release of TPABr molecules from the zeolite ZSM-5 framework; (i) relatively lower temperature mass loss T1 at ~ 449 °C associated with the degradation and release of TPABr molecules occluded in the pores and channels of the zeolite ZSM-5 framework and (ii) relatively higher temperature T2 at ~ 529 °C attributed to the degradation and release of TPA^+ cations that served as counter-balancing cations (together with sodium cations) for negative framework charges at the acidic sites (Si-O-Al^- sites) in the pores of the MFI framework, since the Na/Al ratio of the as-synthesised zeolites Zeo07 and Zeo08 was less than 1 (as observed in Table 6.8). Furthermore, this relatively high temperature mass loss T2 may also be due to the degradation and release of TPABr molecules from less accessible pores in the zeolite ZSM-5 framework, which may be due to crystal agglomeration of ZSM-5 as observed in Figure 6.12 (Neves et al., 2019; Pál-Borbély, 2007).

TGA/DTG/DTA spectra of as-synthesised samples (Zeo09-11) corresponding to co-crystallised zeolite ZSM-5 and analcime are depicted in Figure 6.17 with the corresponding MS spectra of these materials depicted in Figure 6.18. As-synthesised zeolite samples Zeo09-11 exhibited similar thermal profiles as depicted in Figure 6.17 and Figure 6.18. Both a low temperature (W1) mass loss at ~ 90-100 °C and relatively higher temperature (W2) mass loss at ~ 280-290 °C was observed for these samples, associated with the release of physisorbed water from two different porous environments; (i) in the MFI framework of ZSM-5 crystals (W1) and (ii) in the ANA framework of analcime crystals (W2). The relatively higher temperature at which water is released from the analcime crystals may be due to diffusional constraints caused by the larger crystals (~10 µm). As reported for samples Zeo02, Zeo07 and Zeo08, these samples also exhibited two mass loss regions at T1 and T2 (listed in Table 6.9) associated with the degradation and release of TPA^+/TPABr molecules from different geometric environments in the porous MFI framework of zeolite ZSM-5, as described previously.

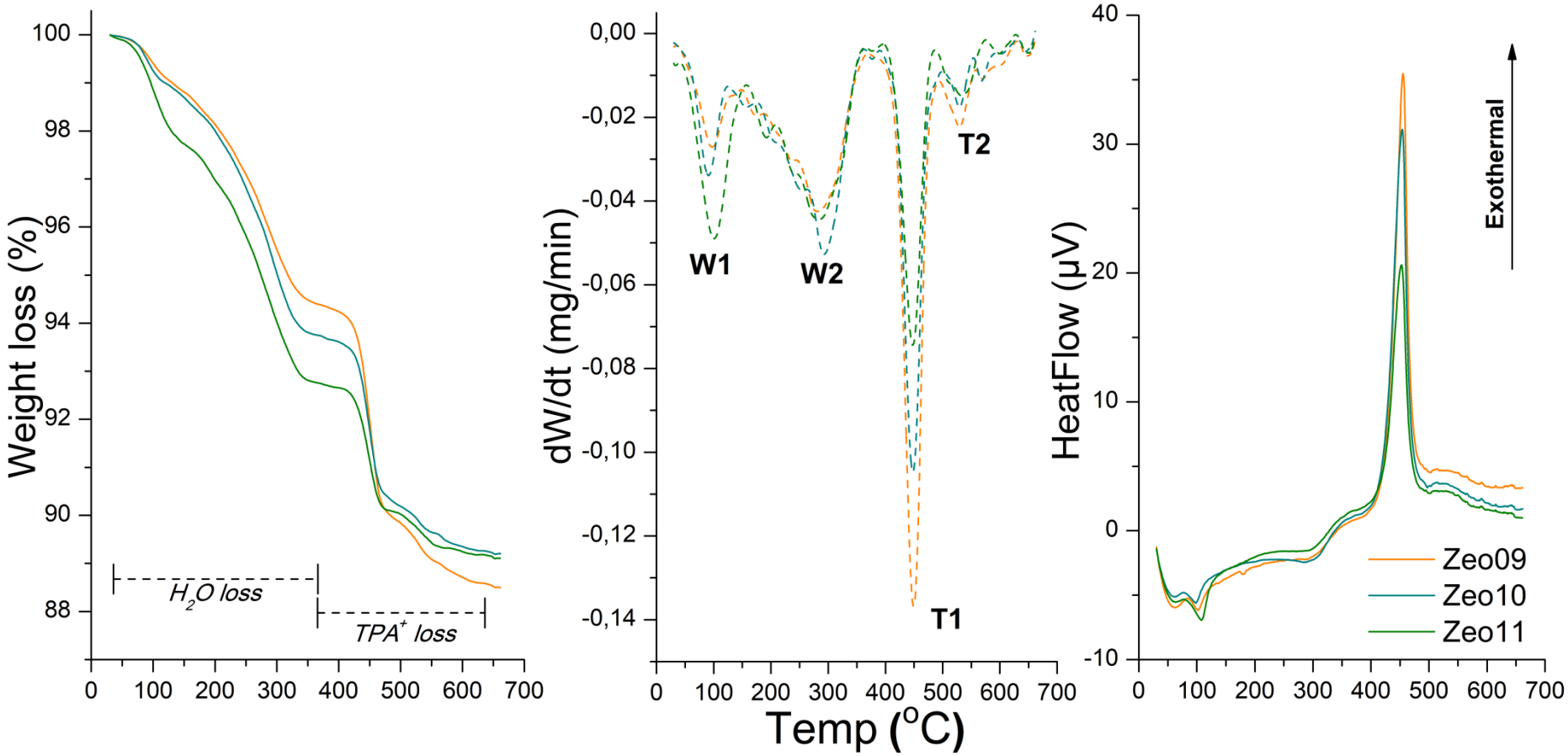

Figure 6.17: TGA/DTG/DTA analysis of as-synthesised Na-zeolites synthesised under hydrothermal conditions (160 °C for 72 hours) using varying amounts of sodium aluminate (Zeo09-11) in the synthesis mixture with molar regime 1 SiO_2•x Al_2O_3•y Na_2O•0.10 TPABr•35.4 H_2O (x = 0.036-0.058, y = 0.57-0.59).

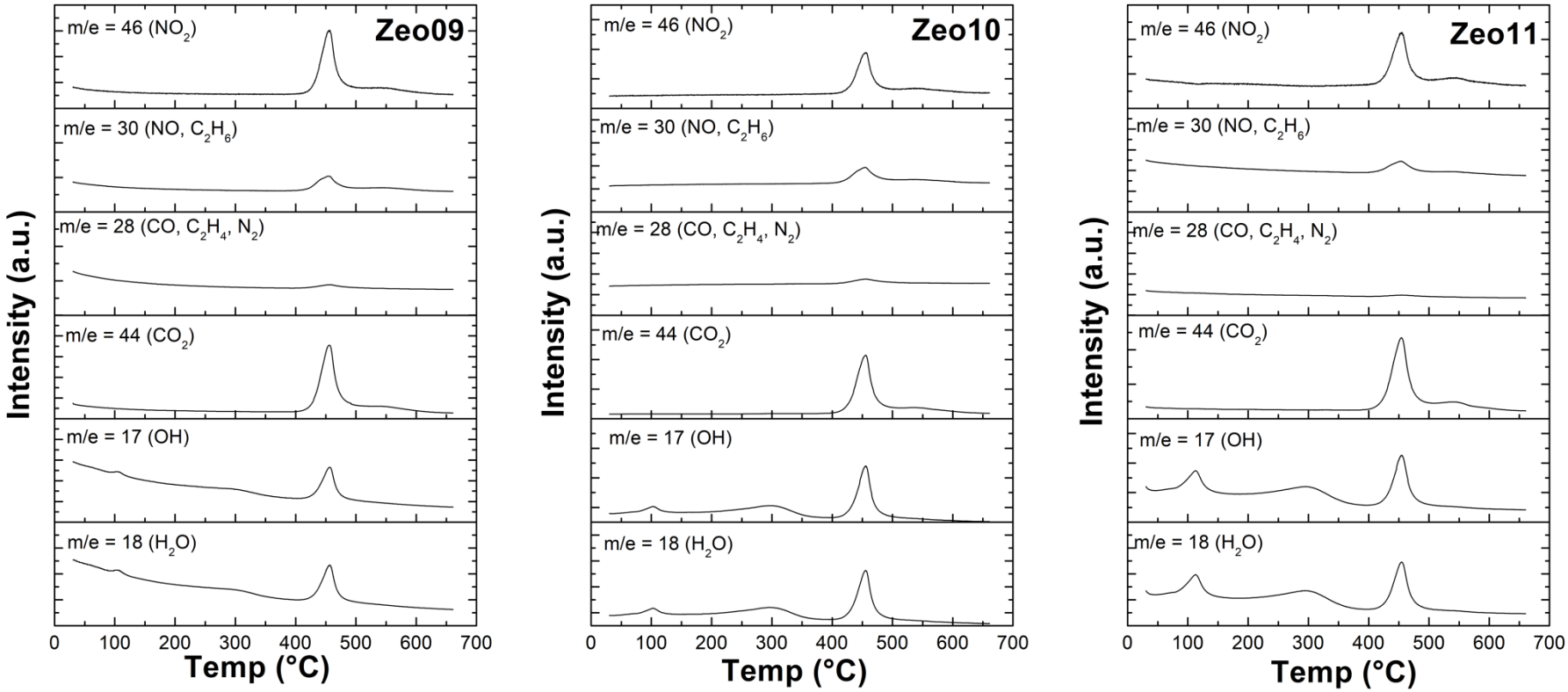

Figure 6.18: MS spectra of as-synthesised Na-zeolites synthesised under hydrothermal conditions (160 °C for 72 hours) using varying amounts of sodium aluminate (Zeo09-11) in the synthesis mixture with molar regime 1 SiO_2•x Al_2O_3•y Na_2O•0.10 TPABr•35.4 H_2O (x = 0.036-0.058, y = 0.57-0.59).

TGA/DTG/DTA spectra of as-synthesised sample (Zeo12) corresponding to analcime are depicted in Figure 6.19 with the corresponding MS spectra depicted in Figure 6.20. The thermal profile of as-synthesised zeolite sample Zeo12 (depicted in Figure 6.19) contained a major mass loss at a temperature of 314 °C (W2) associated with the release of physisorbed water from the pores of analcime framework. This temperature was relatively low compared to the temperature at which organic compounds (occluded in zeolitic pores) are typically released from zeolite frameworks (Pál-Borbély, 2007; Frantz et al., 2016). Furthermore, MS spectra confirmed that this high temperature peak was due to the evolution of water from the synthesised material. This indicates that the OSDA compound (TPABr) was not incorporated into the ANA framework of zeolite analcime. Therefore, the decrease in OSDA content in the as-synthesised zeolite material as the SAR value of the material increased (as depicted in Figure 6.14) is thought to be due to the changes in the mineralogy of the material as well as the SAR value of the synthesised material. As observed in Table 6.8 and 6.9, highly siliceous ZSM-5 samples (such as Zeo02) exhibited a relatively higher OSDA content in the MFI framework compared to aluminium-rich ZSM-5 samples (Zeo07 and Zeo08). This study therefore illustrates the importance of OSDA agents in the stabilisation of silicon-rich frameworks during the zeolite crystallisation process.

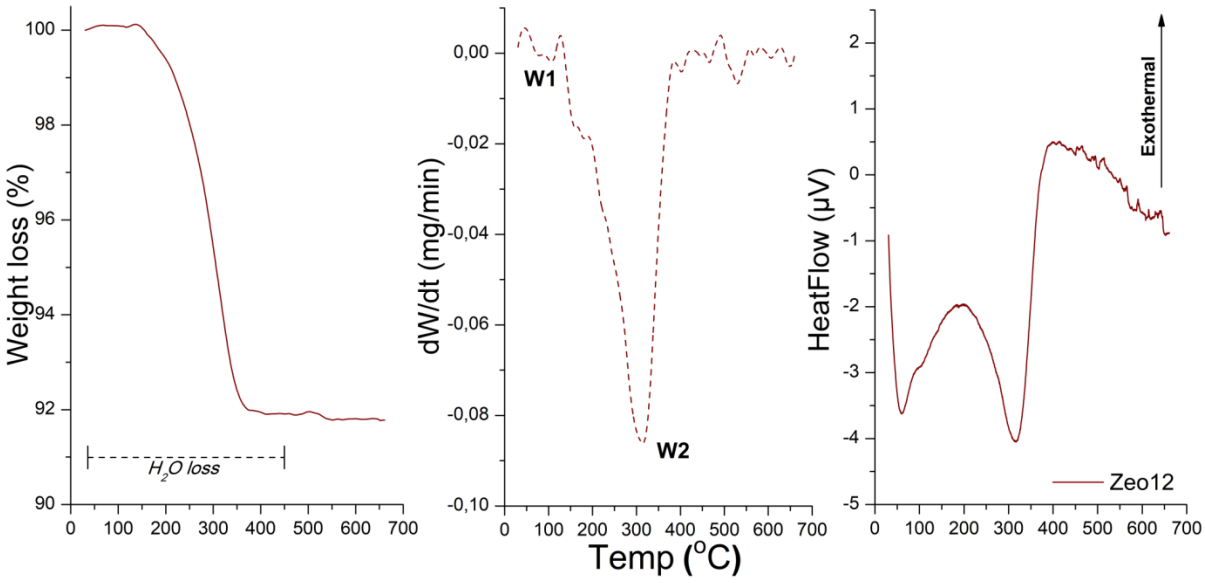

Figure 6.19: TGA/DTG/DTA analysis of as-synthesised Na-zeolite sample Zeo12 (analcime) synthesised under hydrothermal conditions (160 °C for 72 hours) from a synthesis mixture with molar regime 1 SiO_2•0.111 Al_2O_3•0.65 Na_2O•0.10 TPABr•35.4 H_2O.

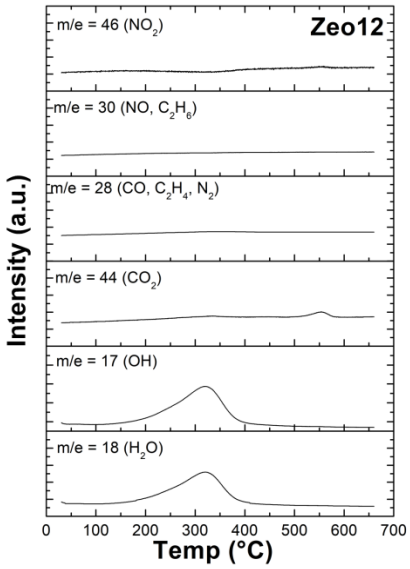

Figure 6.20: MS spectra of as-synthesised Na-zeolite sample Zeo12 (analcime) synthesised under hydrothermal conditions (160 °C for 72 hours) from a synthesis mixture with molar regime 1 SiO_2•0.111 Al_2O_3•0.65 Na_2O•0.10 TPABr•35.4 H_2O.

This investigation on the thermal degradation profiles of as-synthesised zeolites further illustrates the importance of choosing the appropriate molar regime to achieve to the desired properties of the resultant material such as (i) mineral phase, (ii) SAR value (i.e. solid acidity) and (iii) hydrophilicity/hydrophobicity.

The crystallisation of highly crystalline zeolite ZSM-5 from a CFA-derived silicon feedstock was dependent on the SAR value of the synthesis (in the case of aluminium hydroxide or sodium aluminate addition to the synthesis mixture). However, the formation of zeolite ZSM-5 from synthesis systems made up of aluminium hydroxide as a source of aluminium was more sensitive and resulted in co-crystallisation of zeolite ZSM-5 and mordenite. The synthesis systems containing sodium aluminate as an additional source of aluminium was less sensitive to changes in the SAR value of the synthesis mixture and resulted in the formation of zeolite ZSM-5 without competition with zeolite mordenite. Differences between the synthesis system containing aluminium hydroxide and sodium aluminate may be due to the chemical composition of the CFA-derived silicon precursor (as presented in Table 4.8, Section 4.3.2). The crystallisation of zeolite ZSM-5 was observed over a wide range of SAR values (~40-250). Similar findings have been reported in literature (Aono et al., 2016; Cheng et al., 2008; Singh and Dutta, 2003; Zhang et al., 2009). As reported previously, further investigations were carried out using the synthesis procedure for sample Zeo07 (with sodium aluminate as an additional source of aluminium), as described in Table 3.7 in Section 3.5, as

the baseline for further experiments due to ease of dissolution of the aluminium precursor as well as the lack of competition with zeolite mordenite.

6.2.3 The effect of water content (at constant alkalinity) on zeolite ZSM-5 crystallisation

The effect of water content (at constant [OH^-]) in the synthesis mixture on zeolite ZSM-5 crystallinity was carried out by varying the amount of 1.2 wt% NaOH solution used in the synthesis mixture (1 SiO_2•0.015 Al_2O_3•y Na_2O•0.10 TPABr•z H_2O), with water content varied in the range z = 17.7-53.1 and sodium aluminate added as an additional source of aluminium, as described in Table 3.7, Section 3.5. This was done in order to keep the overall OH^-/H_2O ratio of the synthesis mixture constant. Hydrothermal synthesis of the synthesis mixture containing a CFA-derived silicon precursor (FASE) was carried out under static hydrothermal conditions of 160 °C for 72 hours.

6.2.3.1 Mineralogy and crystallinity

XRD diffractograms of as-synthesised products crystallised at 160 °C for 72 hours, with varying water content in the synthesis mixture are depicted in Figure 6.21. The relative crystallinity of each sample was calculated, according to Equation 2.8, using the most crystalline sample (Zeo23) as a reference and the OD ratio was determined from FTIR data; results are summarised in Table 6.10.

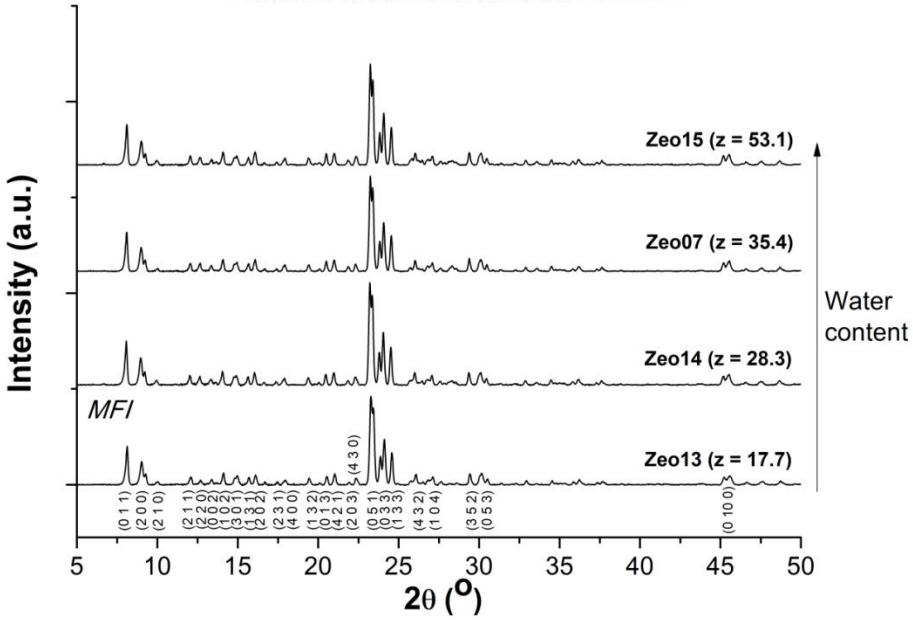

Figure 6.21: XRD diffractograms of as-synthesised zeolite ZSM-5 samples Zeo07 and Zeo13-15 synthesised under hydrothermal conditions of 160 °C for 72 hours, with varying water content in the synthesis mixture with molar regime 1 SiO_2•0.015 Al_2O_3•y Na_2O•0.10 TPABr•z H_2O (z = 17.7-53.1). Key: MFI - zeolite ZSM-5

Table 6.10: Relative crystallinity of as-synthesised Na-ZSM-5 zeolites Zeo07 and Zeo13-15 prepared under hydrothermal conditions of 160 °C for 72 hours, with varying water content in the synthesis mixture with molar regime 1 SiO_2•0.015 Al_2O_3•y Na_2O•0.10 TPABr•z H_2O (z = 17.7-53.1), determined using XRD and FTIR data.

Sample	Water content added to the synthesis mixture (moles)	Relative Crystallinity	
		XRD (% crystallinity)	FTIR (optical density ratio)
Zeo13	17.7	82.9	0.98
Zeo14	28.3	95.8	0.93
Zeo07	35.4	85.3	1.04
Zeo15	53.1	92.7	0.95

Zeolite ZSM-5 was able to crystallise from synthesis mixtures containing a CFA-derived silicon precursor (FASE) over a wide range of water content (z = 17.7 - 53.1), as observed in Figure 6.21. However, water content had an impact on the crystallinity of zeolite ZSM-5, as listed in Table 6.10. At relatively low water content z = 17.7, the formation of zeolite ZSM-5 without any minor phase was observed, as depicted in Figure 6.21. Relatively higher level of water content $z \geq 28.3$, enhanced the crystallinity of zeolite ZSM-5 (with the exception of sample Zeo07). However, samples Zeo14 (z = 28.3) exhibited the highest crystallinity in this range and further zeolite ZSM-5 synthesis investigations were therefore conducted using z = 28.3.

6.2.3.2 Morphology and composition

The influence of water content (at constant alkalinity) on the morphology of as-synthesised zeolite samples Zeo13-15 was characterised by SEM coupled to EDS and compared to sample Zeo07, as depicted in Figure 6.22. The properties of as-synthesised samples Zeo13-15 and Zeo07 such as average particle size, SAR and Na/Al values are listed in Table 6.11.

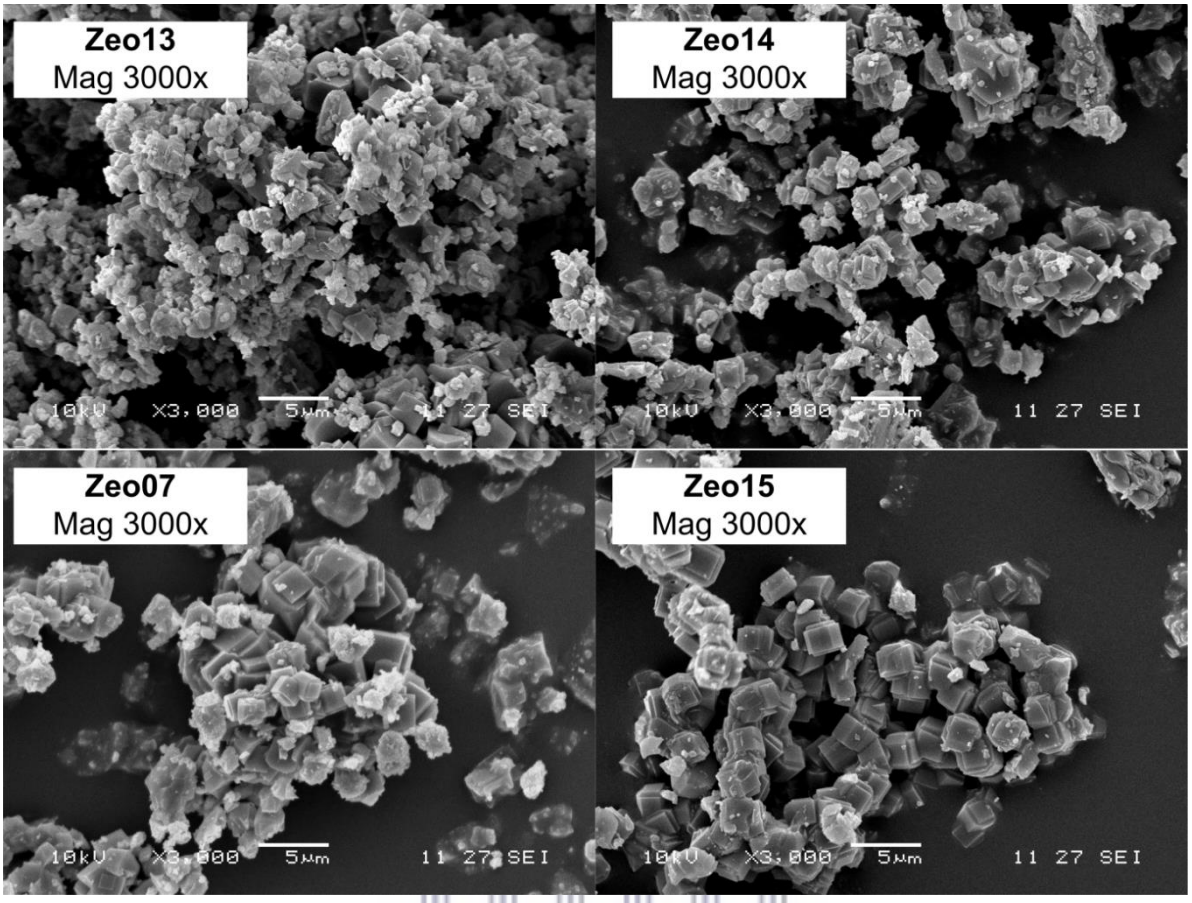

Figure 6.22: SEM micrograph (3000x magnification) of as-synthesised Na-zeolite ZSM-5 samples Zeo07, Zeo13-15 synthesised under hydrothermal conditions of 160 °C for 72 hours, with varying water content (constant alkalinity) in the synthesis mixture with molar regime 1 SiO_2•0.015 Al_2O_3•y Na_2O•0.10 TPABr•z H_2O (z = 17.7-53.1).

Table 6.11: Properties of as-synthesised Na-ZSM-5 zeolite samplesZeo07 and Zeo13-15 such as average particle size (determined using ImageJ) and relative composition (determined by EDS analysis n=10), prepared under hydrothermal conditions of 160 °C for 72 hours, with varying water content (constant alkalinity) in the synthesis mixture with molar regime 1 SiO_2•0.015 Al_2O_3•y Na_2O•0.10 TPABr•z H_2O (z = 17.7-53.1).

Sample	Water content added to the synthesis mixture (moles)	Average particle size (µm)	SAR value	Na/Al Ratio
Zeo13	17.7	0.9	28.6	0.8
Zeo14	28.3	1.8	22.7	0.5
Zeo07	35.4	1.9	30.5	0.5
Zeo15	53.1	2.4	26.7	0.6

Changes in the water content of the synthesis mixture did not influence the particle shape of zeolite ZSM-5 crystals, as depicted in Figure 6.22. However, the average particle size of zeolite ZSM-5 crystals was influenced by the water content in the synthesis mixture while the SAR values of synthesised materials were relatively similar (~ 23-31). As the water content in the synthesis mixture was reduced, the average particle size of ZSM-5 crystals was also reduced as listed in Table 6.11. Low water content (z = 17.7) resulted in relatively smaller, prismatic zeolite ZSM-5 crystals (~ 1 µm in size), while relatively higher water content (z = 53.1) resulted in relatively larger, prismatic ZSM-5 crystals (2.4 µm in size). The crystallisation mechanism is significantly affected by the water content in the synthesis mixture since this parameter influences other factors such as precursor concentration, solution viscosity, etc. that play vital roles in precursor transport during the crystallisation process. At reduced water content, the nucleation rate is most likely favoured over the crystal growth process for ZSM-5 formation which may be due to relatively higher precursor concentrations under these conditions (Cubillas and Anderson, 2010; Petrik, 2009; Sashkina et al., 2017).

6.2.3.3 Thermal Stability

The thermal analysis of as-synthesised zeolite ZSM-5 samples Zeo07, Zeo13-15, prepared using varying water content (at constant alkalinity) under hydrothermal conditions of 160 °C for 72 hours, was analysed by TGA/DTG/DTA analysis in air coupled to MS spectrometry for identification of released compounds; results are depicted in Figure 6.23 and Figure 6.24, respectively. The thermal profiles of as-synthesised zeolite samples Zeo07, Zeo13-15 (synthesised using varying water content in the synthesis mixture) were relatively similar as depicted in Figure 6.23 and Figure 6.24. A mass loss region related to the release of physisorbed water from the pores and channels of the zeolite ZSM-5 framework (W1) as well as two mass loss regions related to the degradation and release of the TPABr molecules from the pores and channels of the zeolite ZSM-5 framework (T1 and T2) were observed in Figure 6.23 and 6.24.

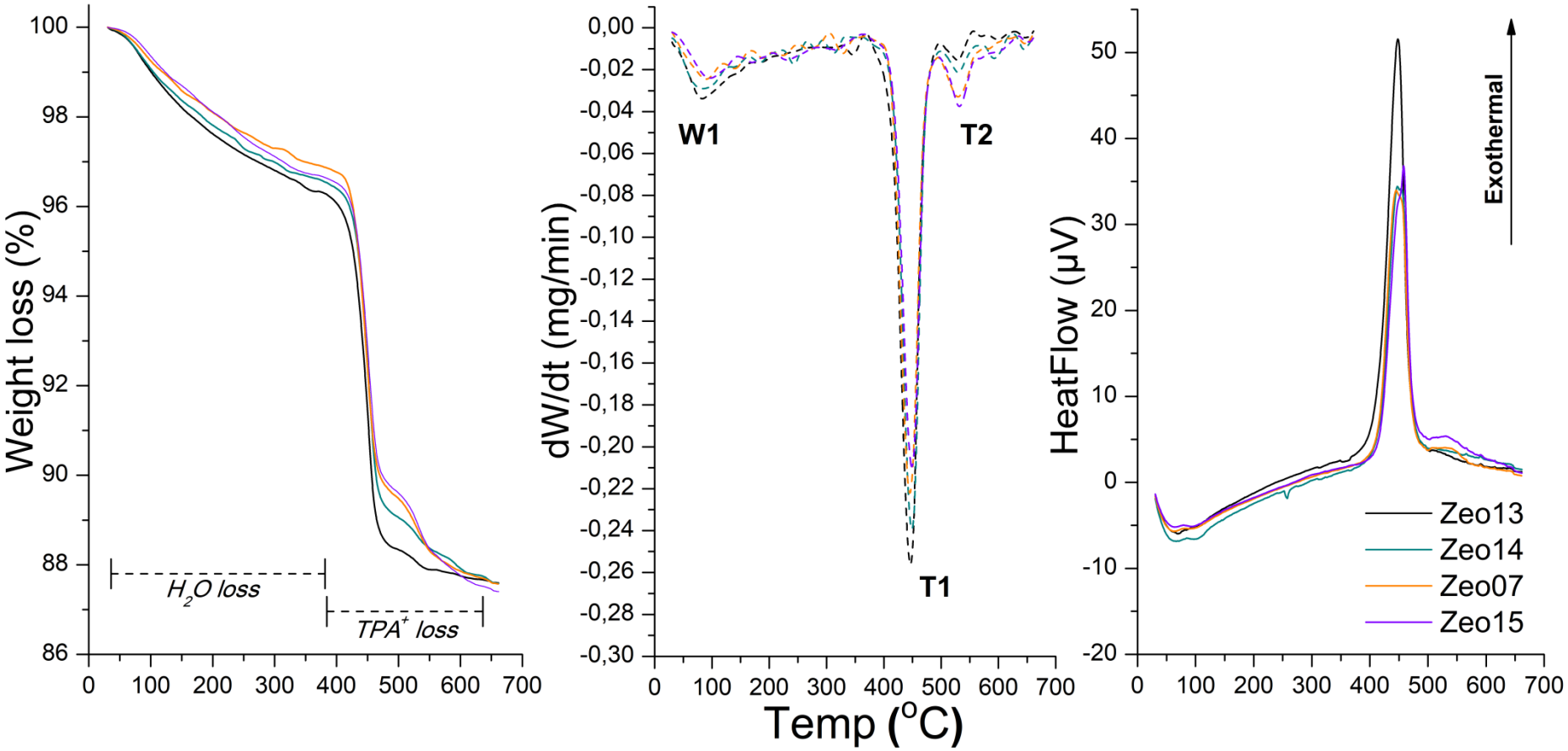

Figure 6.23: TGA/DTG/DTA analysis of as-synthesised Na-zeolite samples Zeo07, Zeo13-15 synthesised under hydrothermal conditions (160 °C for 72 hours) with varying water content (at constant alkalinity) in the synthesis mixture with molar regime 1 SiO_2•0.015 Al_2O_3•y Na_2O•0.10 TPABr•z H_2O (z = 17.7-53.1).

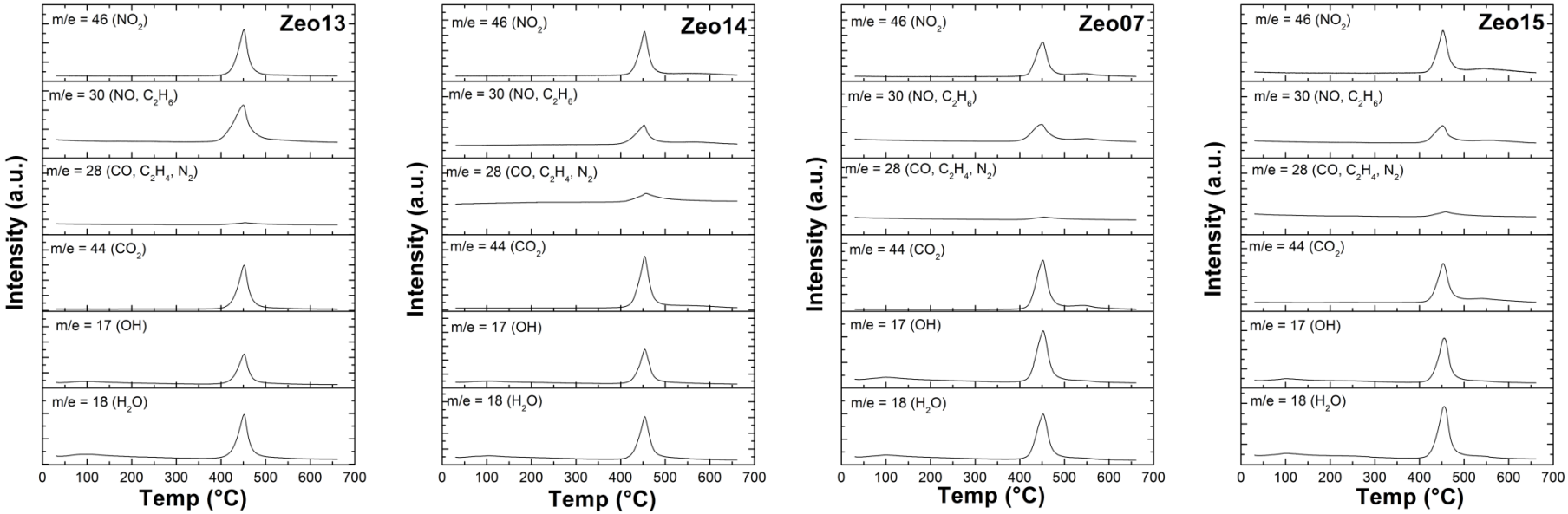

Figure 6.24: MS spectra of as-synthesised Na-zeolite samples Zeo07, Zeo13-15 synthesised under hydrothermal conditions (160 °C for 72 hours) with varying water content (at constant alkalinity) in the synthesis mixture with molar regime 1 SiO_2•0.015 Al_2O_3•y Na_2O•0.10 TPABr•z H_2O (z = 17.7-53.1).

A summary of the properties of the as-synthesised materials such as water and TPABr content is presented in Table 6.12.

Table 6.12: Summary of information gathered from TGA analysis for as-synthesised zeolite samples Zeo07 and Zeo13-15, reported as per gram of zeolite, prepared prepared under hydrothermal conditions of 160 °C for 72 hours, with varying water content (constant alkalinity) in the synthesis mixture with molar regime 1 SiO_2•0.015 Al_2O_3•y Na_2O•0.10 TPABr•z H_2O (z = 17.7-53.1).

Sample	Temp. W1 peak (°C)	Water content (g/g zeolite)	Temp. T1 peak (°C)	Temp. T2 peak (°C)	TPABr content (g/g zeolite)
Zeo13	82	0.037	446	528	0.085
Zeo14	84	0.033	448	529	0.085
Zeo07	89	0.030	446	529	0.089
Zeo15	97	0.033	448	532	0.086

As listed in Table 6.12, zeolite ZSM-5 samples synthesised with different amounts of water in the synthesis mixture possessed similar water content (0.030-0.037 g/ zeolite) in the zeolite framework; these samples also exhibited a relatively similar SAR value ~23-30 (determined by EDS as reported in Table 6.11). This is as expected since zeolite water content is directly related to the aluminium content in the framework, as reported in the literature (Frantz et al., 2016; Hölderich and van Bekkum, 1991; Santen and Vogel, 1989). However, the temperature at which water was released from the zeolite ZSM-5 framework increased as the water content in the material increased (as listed in Table 6.12), corresponding to the increased particle size (as listed in Table 6.11). This may be due to the relatively longer diffusional pathway for released H_2O through the zeolite ZSM-5 framework as the particle size increased. Consequently, the W1 mass loss peak increased in temperature (from 82 to 97 °C) as the water content of the synthesis mixture was increased as depicted in Figure 6.23.

These samples also exhibited similar TPABr content (0.085-0.089 g/g zeolite), as listed in Table 6.12. A relatively low temperature mass loss (T1) at 446-448 °C and a relatively high temperature mass loss (T2) at 528-532 °C were observed for the degradation and release of occluded TPABr molecules from slightly different geometric environments in the zeolite framework, as discussed previously. As listed in Table 6.11, the Na/Al ratios of as-synthesised ZSM-5 samples were less than one. Therefore, the relatively high temperature mass loss T2 may also be due to the TPA^+ cations present as charge-balancing species (together with sodium cations) in the zeolite framework associated with acidic Si-O-Al^- sites. An interesting correlation between water content in the synthesis mixture and mass loss peaks

T1 and T2 were noted, as annotated in Figure 6.23. The decrease in the T1 mass loss region (and increase in the T2 mass loss region) corresponded to the increase in water content in the synthesis mixture, which is also thought to be due to the increased diffusion pathway for TPA^+ fragments as the crystal size of the zeolite ZSM-5 particles increased. In this case, the main factor influencing the thermal profile of zeolite ZSM-5 samples was the crystal size of synthesised ZSM-5 crystals. At a relatively low water content in the synthesis mixture (z = 17.7) for sample Zeo13, zeolite ZSM-5 crystals with no diffusional constraints for the release of water/OSDA agent was observed; this sample is therefore expected to be more active in catalysis. These results signify that a slight change in the dimension of zeolite particles has a significant impact on the transport of reactant/product molecules through the zeolite ZSM-5 framework, which is vital in the application of these materials in areas such as catalysis or adsorption (Zhang et al., 2009).

The synthesis of zeolite ZSM-5 from a CFA-derived silicon precursor (FASE) was therefore achieved over a relatively wide range of water content (z = ~17-53). Similar results were reported in literature for the synthesis of zeolite ZSM-5 from standard chemical reagents achieved with water content in the range of z = 25-60, with the optimum ZSM-5 formation reported at z = 25 (Cheng et al., 2008). Varying the water content in the synthesis mixture for zeolite ZSM-5 also resulted in changes in the crystallisation processes and morphology of zeolite ZSM-5, resulting in longer crystallisation periods under dilute conditions (Cheng et al., 2008; Petrik, 2009). Petrik (2009) reported that spherical ZSM-5 crystals formed under dilute conditions, while twinned ZSM-5 crystals formed under concentrated precursor conditions. In this study, increasing the water content on the synthesis mixture for the synthesis of zeolite ZSM-5 from a CFA-derived silicon precursor (FASE) did not significantly influence the crystallinity of zeolite ZSM-5; however, changes in the morphology (in terms of crystal size) were observed. This study therefore illustrates that it is possible to tune the ZSM-5 crystallisation mechanisms to favour the process of nucleation over crystal growth (at reduced water content in the synthesis mixture) or the process of crystal growth over nucleation (at reduced TPABr content in the synthesis mixture) as reported in Section 6.2.1. This is an important achievement for the synthesis of high-silica zeolites from an alternative feedstock (such as the CFA-derived silicon feedstock utilised in this study). In this study, the highest crystallinity was achieved for sample Zeo14 (with z = 28.3) and the synthesis conditions for sample Zeo14 (as described in Table 3.7, Section 3.5) was therefore used as the baseline for further investigations.

6.2.4 The effect of alkalinity (NaOH content) on zeolite ZSM-5 crystallisation

The effect of alkalinity on zeolite ZSM-5 crystallinity was carried out by hydrothermal synthesis of synthesis mixture containing a CFA-derived silicon precursor (FASE) under static hydrothermal condition of 160 °C for 72 hours by varying the NaOH added to the synthesis mixture, with the following general molar regime 1 SiO_2•0.015 Al_2O_3•y Na_2O•0.10 TPABr•28.3 H_2O (with y = 0.49-0.84), as described in Table 3.7, using a small amount of sodium aluminate as an additional source of aluminium. It is noteworthy that the total Na_2O amount (y) was calculated based on the NaOH added to the synthesis mixture, the amount of Na_2O originating from the CFA-derived silicon precursor (FASE) as determined by XRF (as reported in Table 4.8, Section 4.3.2) as well as the amount of Na_2O originating from the addition of a very small amount of sodium aluminate to the synthesis mixture.

6.2.4.1 Mineralogy and crystallinity

XRD diffractograms of as-synthesised products crystallised at 160 °C for 72 hours from synthesis mixtures with a molar regime 1 SiO_2•0.015 Al_2O_3•y Na_2O•0.10 TPABr•28.3 H_2O, with varying alkalinity are depicted in Figure 6.25. The relative crystallinity of each sample was calculated, according to Equation 2.8, using the most crystalline sample (Zeo23) as a reference pattern and the OD ratio was determined from FTIR data; results are summarised in Table 6.13.

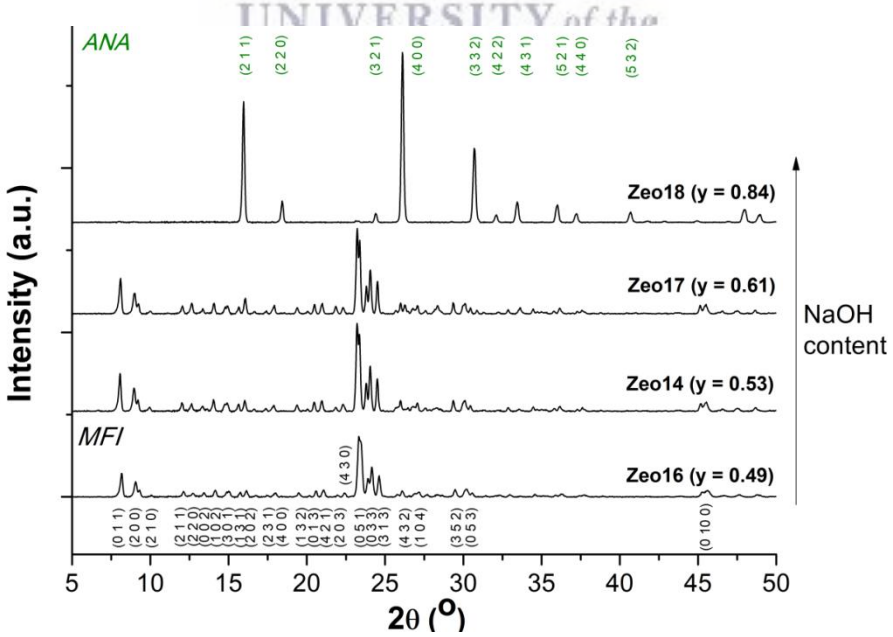

Figure 6.25: XRD diffractograms of as-synthesised zeolite ZSM-5 products Zeo14 and Zeo16-18 synthesised under hydrothermal conditions of 160 °C for 72 hours, with varying alkalinity (NaOH content) of the synthesis mixture with molar regime 1 SiO_2•0.015 Al_2O_3•y Na_2O•0.10 TPABr•28.3 H_2O (y = 0.49-0.84). Key: MFI - zeolite ZSM-5, ANA – Analcime

Table 6.13: Relative crystallinity of as-synthesised Na-ZSM-5 zeolites Zeo14 and Zeo16-18, prepared under hydrothermal conditions of 160 °C for 72 hours, with varying alkalinity (NaOH content) of the synthesis mixture with molar regime 1 SiO_2•0.015 Al_2O_3•y Na_2O•0.10 TPABr•28.3 H_2O (y = 0.49-0.84), determined using XRD and FTIR data.

Sample	NaO_2 content added to the synthesis mixture (moles)	Relative Crystallinity	
		XRD (% crystallinity)	FTIR (optical density ratio)
Zeo16	0.49	63.1	0.99
Zeo14	0.53	95.8	0.93
Zeo17	0.61	87.3	0.98
Zeo18	0.84	6.0	1.18

Low levels of alkalinity (y = 0.49-0.61) for samples Zeo16, Zeo14 and Zeo17 resulted in the formation of zeolite ZSM-5, as observed in Figure 6.25. At relatively high alkalinity (y = 0.84) for sample Zeo18, the formation of only analcime was observed. Relatively high alkalinity is known to favour the formation of dense mineral phases such as analcime due to enhanced crystallisation processes (Lv et al., 2011; Machado et al., 1999; Oleksiak and Rimer, 2014). As listed in Table 6.13, relatively low levels of alkalinity (y = 0.53-0.61) in the synthesis mixture resulted in highly crystalline zeolite ZSM-5; the highest crystallinity observed for sample Zeo14 (y = 0.53). Further investigations on the synthesis of zeolite ZSM-5 were therefore carried out at an alkalinity of y = 0.53.

6.2.4.2 Morphology and composition

The influence of alkalinity on the morphology of as-synthesised zeolite samples Zeo16-18 was characterised by SEM coupled to EDS and compared to sample Zeo14, as depicted in Figure 6.26. Other properties of as-synthesised samples Zeo16-18 and Zeo14 such as average particle size, SAR and Na/Al ratios are listed in Table 6.14.

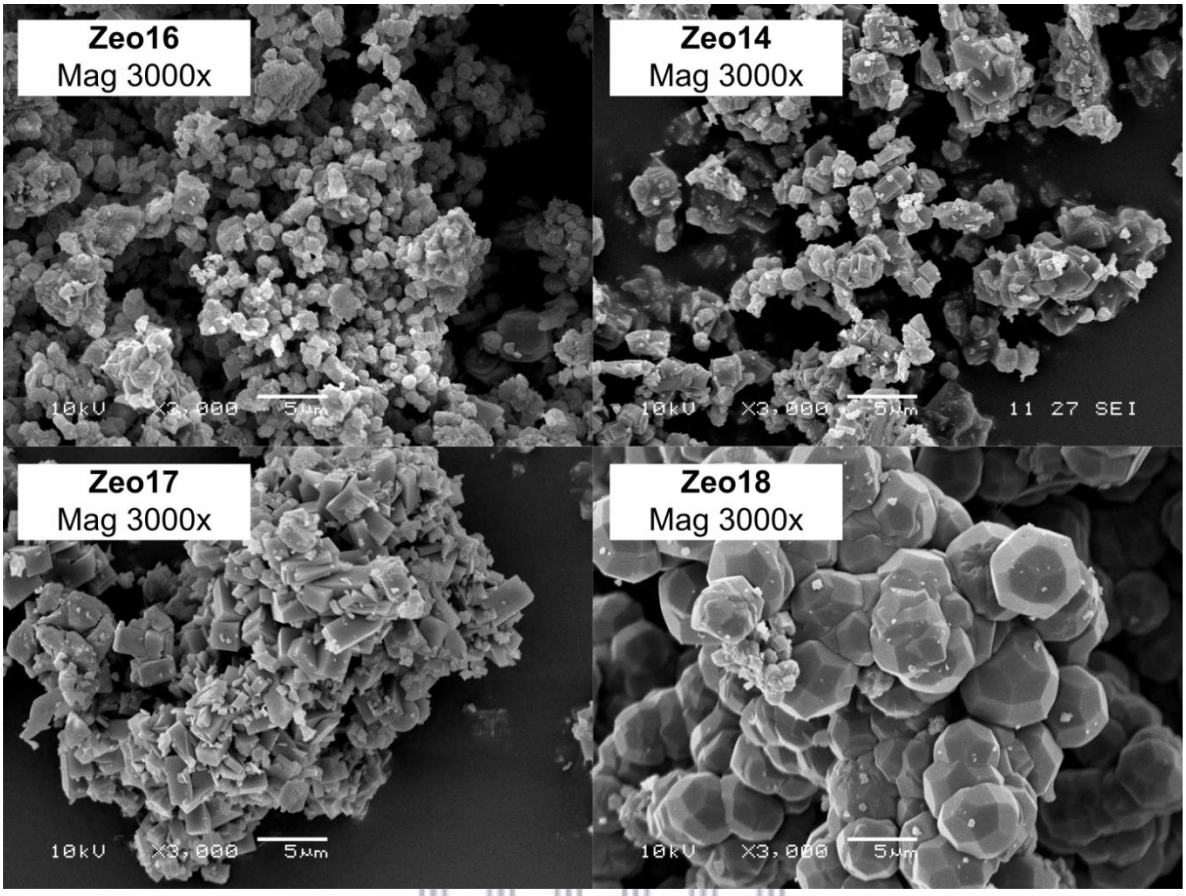

Figure 6.26: SEM micrograph (3000x magnification) of as-synthesised Na-zeolite ZSM-5 samples Zeo14, Zeo16-18 synthesised with varying alkalinity in the synthesis mixture with molar regime 1 SiO_2•0.015 Al_2O_3•y Na_2O•0.10 TPABr•28.3 H_2O (y = 0.49-0.84) under hydrothermal conditions of 160 °C for 72 hours.

Table 6.14: Properties of as-synthesised zeolites Na-ZSM-5 samples such as average particle size (determined using ImageJ) and relative composition (determined by EDS analysis n=10), prepared with varying alkalinity in the synthesis mixture with molar regime 1 SiO_2•0.015 Al_2O_3•y Na_2O•0.10 TPABr•28.3 H_2O (y = 0.49-0.84) under hydrothermal conditions of 160 °C for 72 hours.

Sample	NaO_2 content added to the synthesis mixture (moles)	Average particle size (µm)	SAR value	Na/Al Ratio
Zeo16	0.49	1.2	28.6	0.9
Zeo14	0.53	1.8	22.7	0.5
Zeo17	0.61	3.1	17.4	0.4
Zeo18	0.84	5.0*	2.5	0.6

*Analcime crystals

The degree of alkalinity of the synthesis mixture had a significant effect on the morphology of zeolite crystals, as depicted in Figure 6.26. As listed in Table 6.14, an increase in the alkalinity of the synthesis mixture resulted in an increase in the average particle size and a slight decrease in the SAR value of the synthesised material. At relatively high alkalinity (y = 0.84) for sample Zeo18, mainly spherical analcime crystals were observed, that were relatively large (5.0 µm) and exhibited a low SAR value of 2.5 (as depicted in Figure 6.26 for sample Zeo18). In the case of ZSM-5 zeolites (samples Zeo16, Zeo14 and Zeo17), relatively higher alkalinity in the synthesis mixture resulted in the formation of ZSM-5 crystals with an increased average particle size from 1.2 to 3.1 µm and a slight decrease in the SAR value from 28.6 to 17.4 for samples Zeo16 to Zeo17, respectively.

Higher alkalinity levels in the synthesis mixture are known to enhance the dissolution of nutrients, which may have favoured the crystal growth process in this case (Cubillas and Anderson, 2010; Mostowicz and Berak, 1985). The nucleation process has also been reported to be highly sensitive to the alkalinity of the synthesis system (Mostowicz and Berak, 1985; Sashkina et al., 2017; Yu, 2007). Relatively low levels of alkalinity (y = 0.49 and 0.53) for zeolite ZSM-5 samples Zeo16 and Zeo14 favoured the nucleation process over the crystal growth process, resulting in the formation of many nuclei that undergo relatively slower crystal growth during zeolite crystallisation. Conversely, a relatively high level of alkalinity (y = 0.61) for zeolite ZSM-5 sample Zeo17 favoured the crystal growth process and resulted in the formation of relatively larger ZSM-5 crystals. Further, as-synthesised zeolite ZSM-5 sample Zeo17 exhibited favourable crystal growth in a direction resulting in longer “coffin-

like" ZSM-5 crystals (i.e. greater crystal aspect ratio) compared to zeolite ZSM-5 samples Zeo16 and Zeo14, as depicted in Figure 6.26.

6.2.4.3 Thermal Stability

The thermal analysis of as-synthesised zeolite ZSM-5 samples Zeo14, Zeo16-18, prepared using varying alkalinity in the synthesis mixture under hydrothermal conditions of 160 °C for 72 hours, was analysed by TGA/DTG/DTA analysis in air coupled to MS for identification of released compounds; results are depicted in Figure 6.27 and Figure 6.28, respectively. The thermal profiles of as-synthesised samples Zeo16, Zeo14 and Zeo17 were similar as depicted in Figure 6.27 and Figure 6.28. These results correspond to the mineral content of the samples as depicted in Figure 6.25. It is noteworthy that the thermal profile of sample Zeo18 resembles that of sample Zeo12; both samples are composed of the mineral phase analcime, as depicted in Figure 6.27 and 6.19, respectively.

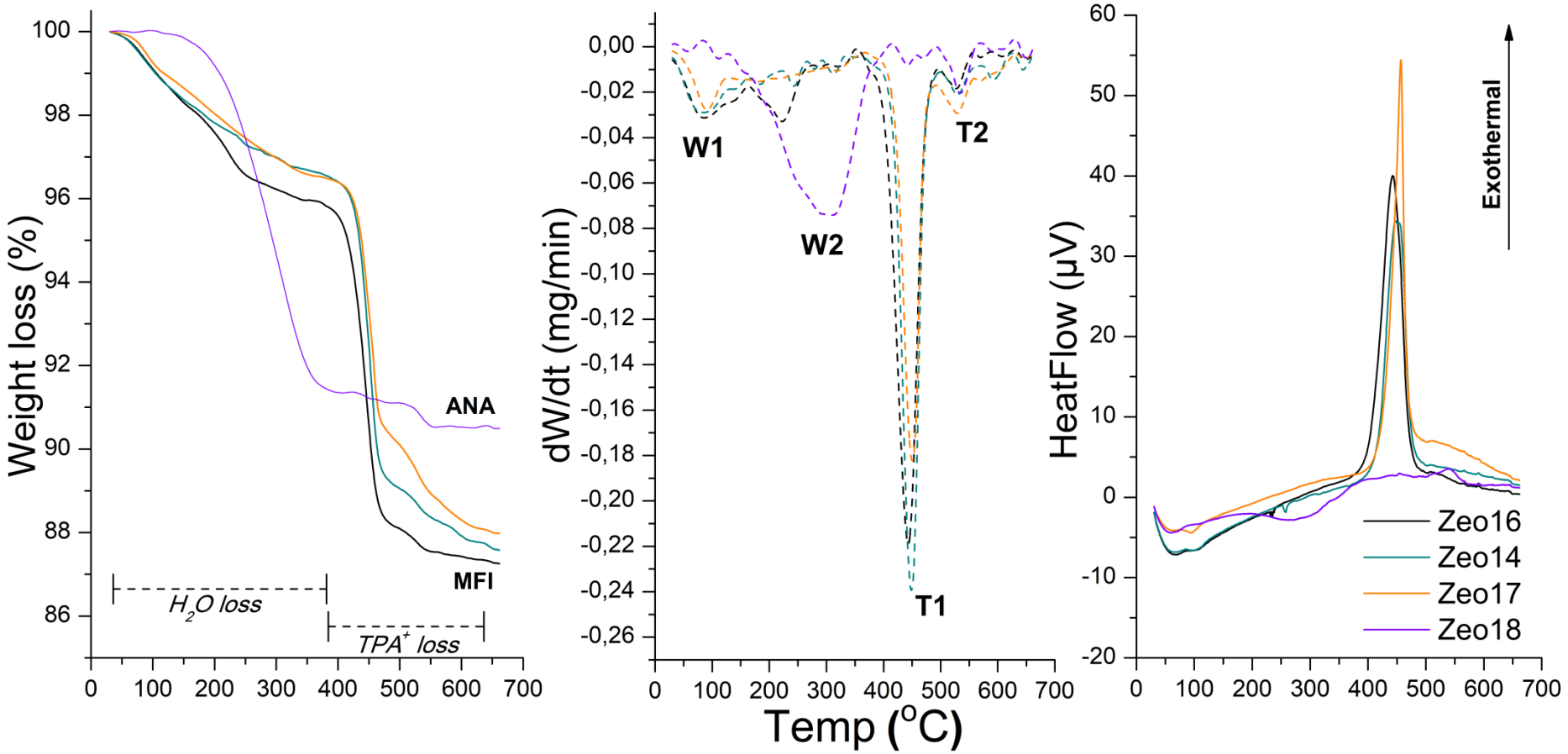

Figure 6.27: TGA/DTG/DTA analysis of as-synthesised Na-zeolite samples Zeo14, Zeo16-18 synthesised under hydrothermal conditions (160 °C for 72 hours) with varying alkalinity in the synthesis mixture with molar regime 1 SiO_2•0.015 Al_2O_3•y Na_2O•0.10 TPABr•28.3 H_2O (y = 0.49-0.84).

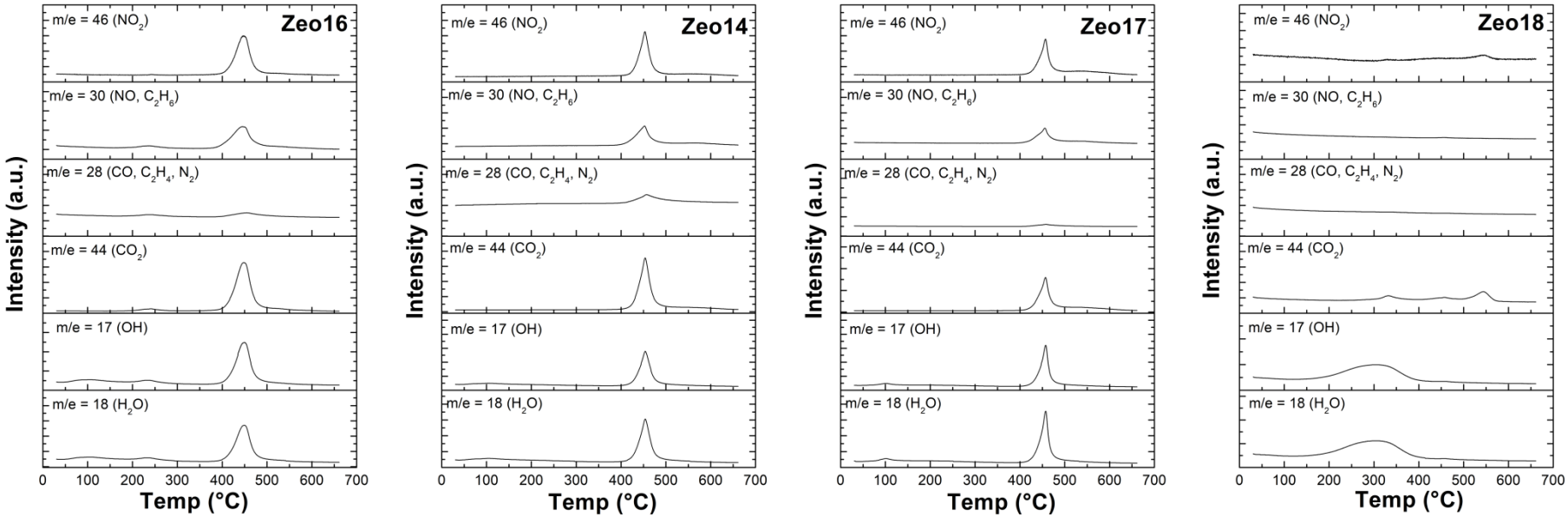

Figure 6.28: MS spectra of as-synthesised Na-zeolite samples Zeo14, Zeo16-18 synthesised under hydrothermal conditions (160 °C for 72 hours) with varying alkalinity in the synthesis mixture with molar regime 1 SiO_2•0.015 Al_2O_3•y Na_2O•0.10 TPABr•28.3 H_2O (y = 0.49-0.84).

A summary of properties of as-synthesised zeolite samples such as water and TPABr content are presented in Table 6.15. The water content in as-synthesised samples Zeo16, Zeo14 and Zeo17 was relatively similar (0.033-0.040 g/g zeolite) as presented in Table 6.15; this is as expected since these samples exhibited similar SAR values as determined from EDS as presented in Table 6.14. These high-silica zeolite ZSM-5 samples were still relatively low in Al content and therefore contained a relatively low amount of water in the pores and channels of the zeolite framework. The main mass loss for zeolite ZSM-5 samples (attributed to the release of physisorbed water from the pores and channels of the zeolite ZSM-5 framework) was at a relatively low temperature (W1) of 84-91 °C. On the other hand, a relatively high temperature mass loss (W2) at 303 °C was observed for sample Zeo18. This sample also exhibited relatively high water content of 0.086 g/g zeolite, as listed in Table 6.15 (similar observations were noted for Zeo12 which was also composed of solely analcime as a mineral phase as listed in Table 6.9).

Table 6.15: Summary of information gathered from TGA analysis for as-synthesised zeolite samples Zeo14 and Zeo16-18, reported as per gram of zeolite, prepared with varying alkalinity in the synthesis mixture with molar regime 1 SiO_2•0.015 Al_2O_3•y Na_2O•0.10 TPABr•28.3 H_2O (y = 0.49-0.84) under hydrothermal conditions of 160 °C for 72 hours.

Sample	Temp. W1 peak (°C)	Temp. W2 peak (°C)	Water content (g/g zeolite)	Temp. T1 peak (°C)	Temp. T2 peak (°C)	TPABr content (g/g zeolite)
Zeo16	85	222	0.040	443	527	0.084
Zeo14	84	-	0.033	448	529	0.085
Zeo17	91	-	0.035	450	529	0.079
Zeo18	-	303	0.086	-	534	0.009

In terms of OSDA content, two mass loss regions T1 (~450 °C) and T2 (~529 °C) were observed for zeolite ZSM-5 samples (as presented in Table 6.15) corresponding to (i) the thermal degradation and release of TPABr molecules occluded in the pores and channels of the zeolite ZSM-5 framework and (ii) the degradation and release of TPA^+ cations serving as charge-balancing species to framework acidic Si-O-Al^- sites or TPABr molecules released from less accessible sites in the zeolite ZSM-5 framework, respectively (Burkett and Davis, 1995; Pál-Borbély, 2007). The latter may be due to the increased particle size of zeolite ZSM-5 crystals as the alkalinity increased (as listed in Table 6.14), which may have resulted in an increased diffusional pathway for TPA^+/TPABr molecules through the pore network of the zeolite framework. Overall, the total OSDA content (0.079-0.085 g/g zeolite) in the as-synthesised zeolite ZSM-5 samples (Zeo16, Zeo14 and Zeo17) varied slightly as the

alkalinity of the synthesis mixture was changed and corresponded to the crystallinity of zeolite ZSM-5 as listed in Table 6.13; the highest crystallinity exhibited the highest OSDA content (per quantity of zeolite formed). The water content in the synthesised materials varied in a similar manner, as listed in Table 6.15. These results illustrated the total OSDA content incorporated in mainly governed by the zeolite framework geometry. However, it should be noted that OSDA content in zeolite ZSM-5 framework may also be altered slightly by varying the amount of OSDA agent added to the synthesis mixture (as discussed in Section 6.2.1).

In this study, a specific degree of alkalinity (y = 0.53-0.61) in the synthesis mixture was required for the crystallisation of highly crystalline zeolite ZSM-5 from a CFA-derived silicon precursor. According to literature, the alkalinity of the synthesis mixture should be tailored according to the SAR value of the synthesis mixture to achieve favourable crystallisation kinetics and the formation of the desired zeolite framework (Cheng et al., 2008; Machado et al., 1999; Oleksiak and Rimer, 2014; Singh and Dutta, 2003). The alkalinity of the synthesis mixture (prepared using standard chemical reagents as feedstock in an OSDA-free synthesis environment) has been reported to influence the morphology of zeolite ZSM-5; with ZSM-5 crystal size reduced at relatively high alkalinity in the synthesis system (Cheng et al., 2008). As mentioned previously, the process of nucleation is reported to be highly sensitive to alkalinity (Mostowicz and Berak, 1985; Sashkina et al., 2017; Yu, 2007) and was reported to be enhanced at relatively high degrees of alkalinity (y = 7-10) by Cheng et al., (2008). The difference observed in this study, compared to literature, are thought to be due to the relatively higher sodium cation content originating from the CFA-derived silicon precursor (as described in Table 4.8, Section 4.3.2) as well as the presence of the OSDA agent in the synthesis mixture, which resulted in favourable nucleation at a relatively low alkalinity and enhanced crystal growth at a relatively higher alkalinity. The optimum alkalinity for the crystallisation of highly crystalline zeolite ZSM-5 from a CFA-derived silicon precursor (FASE) was achieved at y = 0.53 (for sample Zeo14), which was utilised as the baseline for further investigations.

6.2.5 Monitoring zeolite ZSM-5 crystallisation over time

The crystallisation of zeolite ZSM-5 was monitored over a period of up to 144 hours (6 days), using a fixed molar regime of 1 SiO_2•0.015 Al_2O_3•0.53 Na_2O•0.10 TPABr•28.3 H_2O, prepared as described in Table 3.8, using sodium aluminate as a source of aluminium.

6.2.5.1 Mineralogy and crystallinity

Figure 6.29 depicts XRD diffractograms of as-synthesised products crystallised at 160 °C for different time periods up to 144 hours (6 days). A crystallisation curve for the formation of zeolite ZSM-5 (from a CFA-derived silicon precursor) over time is depicted in Figure 6.30; relative percentage crystallinity was calculated, according to Equation 2.8, using sample Zeo23 as the reference pattern.

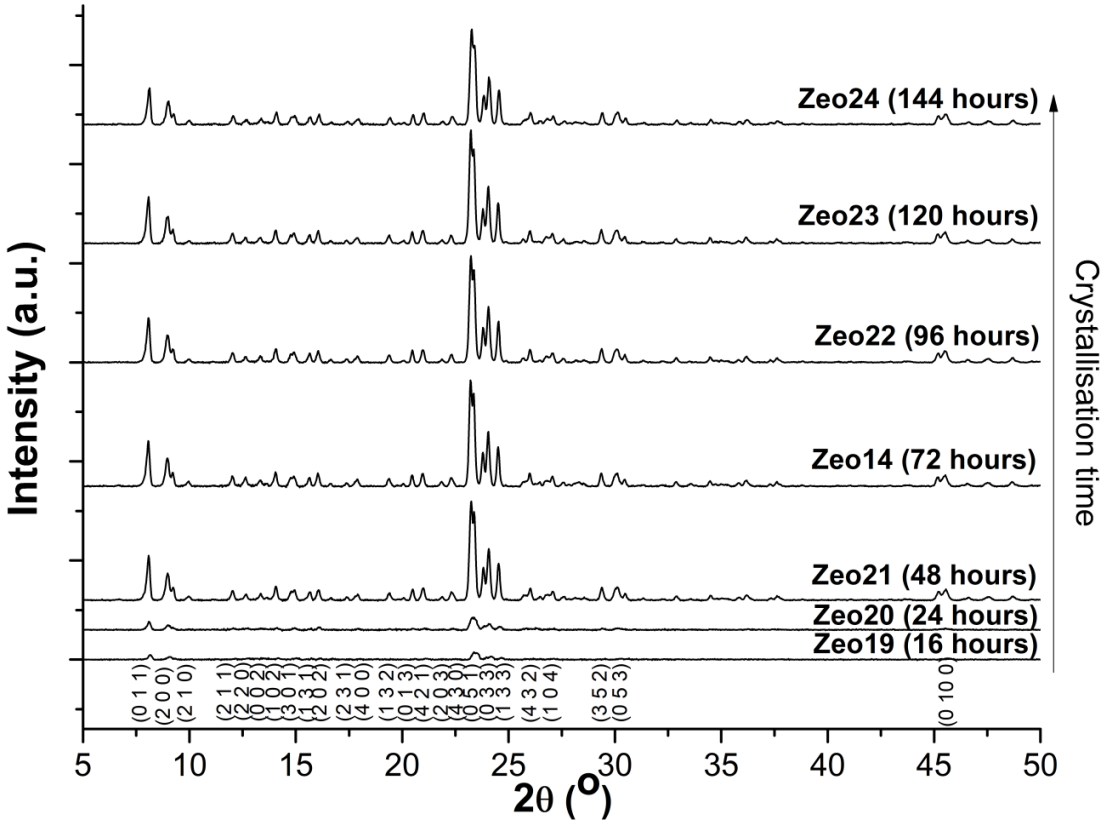

Figure 6.29: XRD diffractograms of as-synthesised zeolite ZSM-5 products synthesised from a CFA-derived silicon precursor (FASE) at 160 °C for up to 144 hours (6 days), using a fixed molar regime 1 SiO_2•0.015 Al_2O_3•0.53 Na_2O•0.10 TPABr•28.3 H_2O.

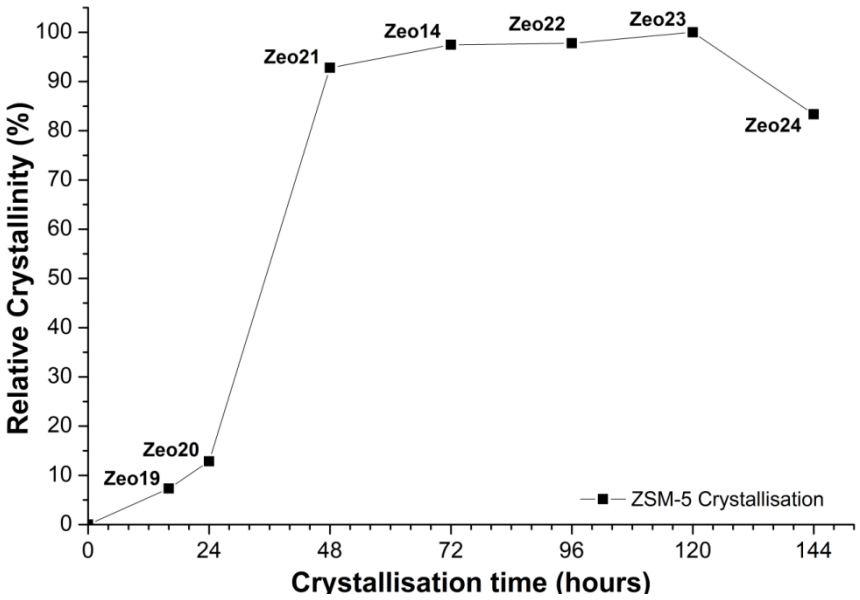

Figure 6.30: Crystallisation curve for zeolite ZSM-5 synthesised from a CFA-derived silicon precursor (FASE) at 160 °C for up to 144 hours (6 days), using a fixed molar regime 1 SiO_2•0.015 Al_2O_3•0.53 Na_2O•0.10 TPABr•28.3 H_2O.

As observed in Figure 6.29 and Figure 6.30, the crystallinity of zeolite ZSM-5 increased as the crystallisation time increased up to 120 hours (5 days), after which the crystallinity of zeolite ZSM-5 decreased slightly. No significant difference in the crystallinity of ZSM-5 samples synthesised between 48 and 120 hours (2 and 5 days) was observed. Zeolite ZSM-5 crystallisation exhibited a typical sigmoidal crystal growth curve, as reported in literature for zeolite formation (Grand et al., 2016). Therefore, the crystallisation of zeolite ZSM-5 from a CFA-derived silicon precursor (FASE) is considered complete after 48 hours (2 days) of static hydrothermal synthesis at 160 °C.

6.2.5.2 Morphology and composition

The changes in morphology of as-synthesised materials formed during the crystallisation process of zeolite ZSM-5 over a period of up to 144 hours (6 days) was monitored by SEM and EDS, as depicted in Figure 6.31. Other properties of as-synthesised zeolite samples Zeo14, Zeo19-24 such as average particle size, SAR and Na/Al ratios are listed in Table 6.16, with the properties of the relatively larger particles observed for sample Zeo19 and Zeo20 marked with an asterisk.

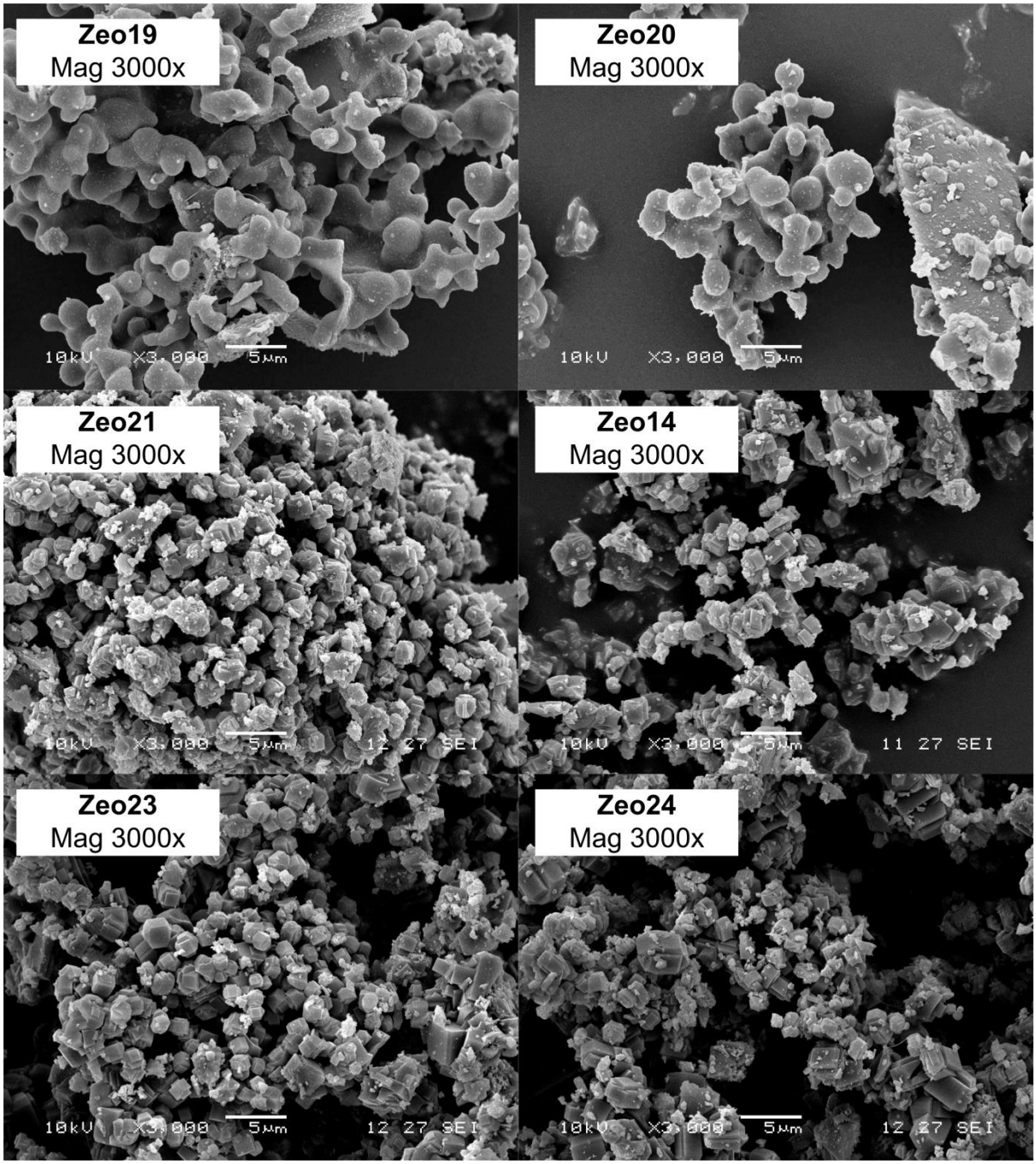

Figure 6.31: SEM micrograph (3000x magnification) of as-synthesised Na-zeolite ZSM-5 samples Zeo14, Zeo19-24 synthesised from a CFA-derived silicon precursor (FASE) at 160 °C for up to 144 hours (6 days), using a fixed molar regime 1 SiO_2•0.015 Al_2O_3•0.53 Na_2O•0.10 TPABr•28.3 H_2O.

As-synthesised materials crystallised for 16-24 hours were amorphous, large materials with an average particle size of 78.9 and 36.4 µm, respectively, as depicted in Figure 6.31 (Zeo19 and Zeo20). These samples also contained small amounts of globular and/or prismatic ZSM-5 crystals (~ 1.1-2.4 µm in size), which formed on the surface of the relatively larger, amorphous particles. The large amorphous material was siliceous (SAR = ~30-33) and

contained relatively high sodium content (Na/Al ratio = ~11-13), as listed in Table 6.16, which corresponds to the composition of the CFA-derived silicon precursor (FASE) used as the silicon feedstock in this study (as presented in Section 4.3.2). The initial ZSM-5 crystals (formed on the surface of the large, amorphous particles) exhibited a relatively low SAR value of ~12-13 and high sodium content (Na/Al ratios of 1.8-3.0), which is not common for zeolite ZSM-5 crystals. After 48 hours of crystallisation (sample Zeo21), the formation of well-defined prismatic ZSM-5 crystals was observed. As the crystallisation period was prolonged, there was no change in the crystal morphology in terms of particle shape. However, a slight increase in the average particle size of zeolite ZSM-5 crystals was observed from 1.1 to 2.2 µm (as expected). Zeolite ZSM-5 crystals exhibited relatively similar SAR values of ~23-31 and a low Na/Al ratio (<1), indicating that the OSDA agent (TPA^+ cations) may serve as charge-balancing cations (together with sodium cations) in the zeolite ZSM-5 framework.

Table 6.16: Properties of as-synthesised zeolites Na-ZSM-5 samples such as average particle size (determined using ImageJ) and relative composition (determined by EDS analysis n=10), prepared using a CFA-derived silicon precursor (FASE) at 160 °C for up to 144 hours (6 days) with a fixed molar regime 1 SiO_2•0.015 Al_2O_3•0.53 Na_2O•0.10 TPABr•28.3 H_2O.

Sample	Crystallisation time (h)	Average particle size (µm)	SAR value	Na/Al Ratio
Zeo19	16	2.4 (78.9)*	11.8 (30.5)*	3.0 (12.6)*
Zeo20	24	1.1 (36.4)*	12.7 (32.5)*	1.8 (11.6)*
Zeo21	48	1.7	30.0	0.7
Zeo14	72	1.8	22.7	0.5
Zeo22	96	1.6	30.1	0.4
Zeo23	120	2.0	31.3	0.6
Zeo24	144	2.2	26.0	0.5

*Large amorphous material

It is noteworthy that initial ZSM-5 crystals (formed on the surface of the large, amorphous silica particles) exhibited a SAR value lower (~12-13) than the highly crystalline ZSM-5 crystals (~23-31). Therefore, the distribution of aluminium throughout the framework of the zeolite ZSM-5 crystals is not expected to be uniform. These observations reveal some interesting details about the crystallisation of zeolite ZSM-5 crystals from the CFA-derived silicon precursor (FASE). In the presence of a small amount of an additional aluminium source such as sodium aluminate, the rate of dissolution of the feedstock (namely the CFA-derived FASE and sodium aluminate) plays an important role in the crystallisation

mechanism and morphology of zeolite ZSM-5 (Mostowicz and Berak, 1985; Sashkina et al., 2017; Yu, 2007). It may therefore be deduced that the aluminium source (sodium aluminate) exhibited a relatively higher rate of dissolution compared to the CFA-derived silicon precursor (FASE) during the crystallisation process under the investigated conditions. This resulted in the formation of aluminium-rich nuclei and initial ZSM-5 crystals on the surface of silica particles. Subsequently, the aluminium feedstock (which was in short supply) depleted over time and crystal growth occurred mainly by the relatively slower dissolution of the silicon feedstock. This crystal growth mechanism of zeolite ZSM-5 crystals from a CFA-derived silicon precursor (FASE) resulted in the uneven distribution of aluminium throughout the framework of the zeolite ZSM-5 crystals.

6.2.5.3 Thermal Stability

The crystallisation of zeolite ZSM-5 from a synthesis mixture with a fixed molar regime (1 SiO_2•0.015 Al_2O_3•0.53 Na_2O•0.10 TPABr•28.3 H_2O) from a CFA-derived silicon precursor (FASE) was followed over time and analysed by TGA/DTG/DTA analysis in air coupled to MS, as depicted in Figure 6.32 and Figure 6.33, respectively. As observed in Figure 6.32 and Figure 6.33, two types of thermal profiles were observed for the as-synthesised products; (i) Zeo19 and Zeo20 and (ii) Zeo21-24, Zeo14 corresponding to 16-24 hours and 48-144 hours of crystallisation, respectively.

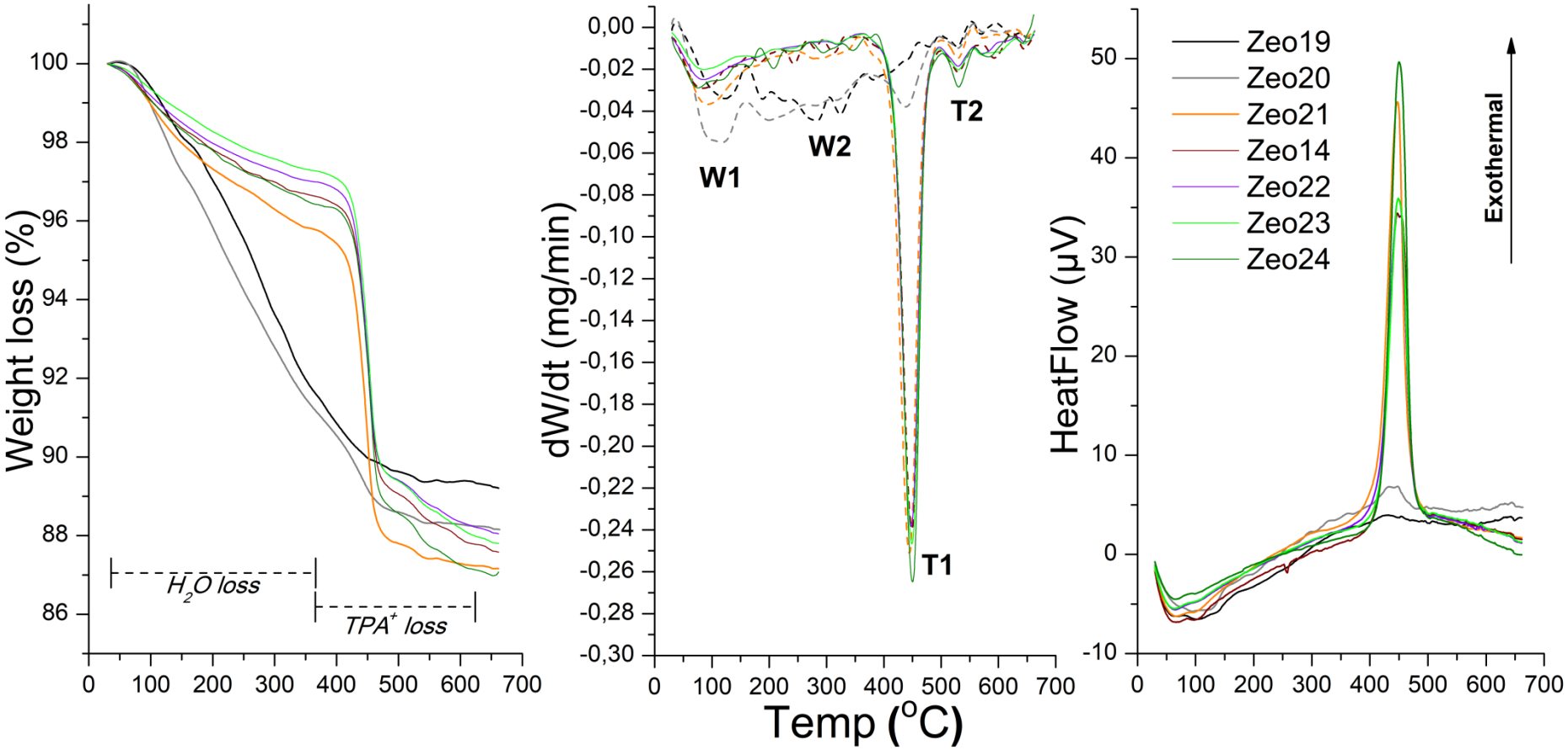

Figure 6.32: TGA/DTG/DTA spectra of as-synthesised Na-zeolite ZSM-5 samples Zeo14, Zeo19-24 synthesised from a CFA-derived silicon precursor (FASE) at 160 °C for up to 144 hours (6 days), using a fixed molar regime 1 SiO_2•0.015 Al_2O_3•0.53 Na_2O•0.10 TPABr•28.3 H_2O.

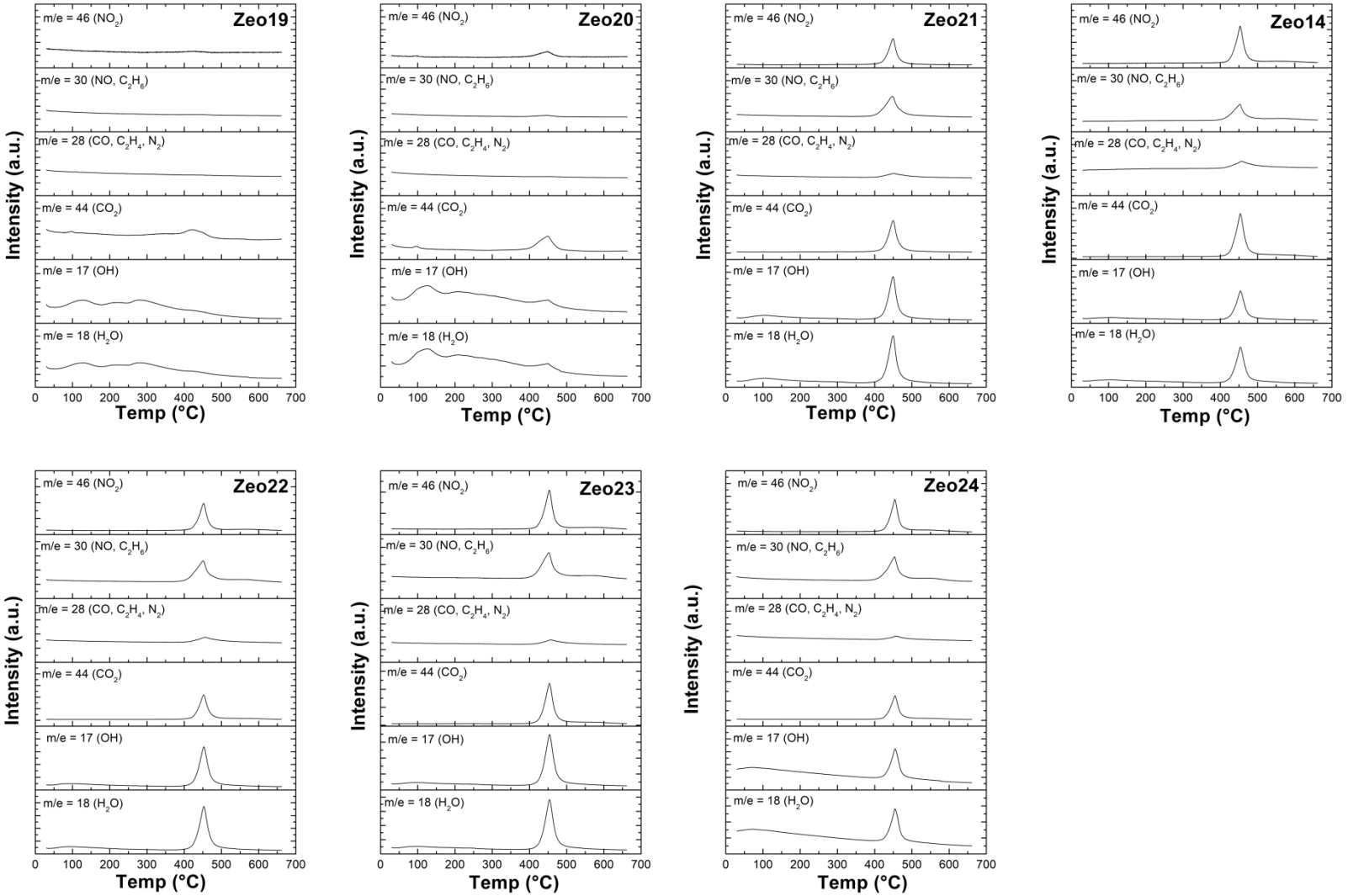

Figure 6.33: MS spectra of as-synthesised Na-zeolite ZSM-5 samples Zeo14, Zeo19-24 synthesised from a CFA-derived silicon precursor (FASE) at 160 °C for up to 144 hours (6 days), using a fixed molar regime 1 SiO_2•0.015 Al_2O_3•0.53 Na_2O•0.10 TPABr•28.3 H_2O.

A summary of properties for as-synthesised materials such as water and TPABr content are presented in Table 6.17.

Table 6.17: Summary of information gathered from TGA analysis for as-synthesised zeolite samples Zeo14 and Zeo19-24, reported as per gram of zeolite, prepared using a CFA-derived silicon precursor (FASE) at 160 °C for up to 144 hours (6 days) with a fixed molar regime 1 SiO_2•0.015 Al_2O_3•0.53 Na_2O•0.10 TPABr•28.3 H_2O.

Sample	Temp. W1 peak (°C)	Temp. W2 peak (°C)	Water content (g/g zeolite)	Temp. T1 peak (°C)	Temp. T2 peak (°C)	TPABr content (g/g zeolite)
Zeo19	124	280	0.106	-	528	-
Zeo20	109	200	0.090	438	530	0.027
Zeo21	92	-	0.043	444	529	0.083
Zeo14	84	-	0.033	448	529	0.085
Zeo22	85	-	0.030	448	529	0.082
Zeo23	85	-	0.028	449	530	0.086
Zeo24	76	-	0.035	450	530	0.088

As-synthesised materials prepared after 16-24 hours of crystallisation (Zeo19-20) contained two mass loss regions associated with the desorption of physisorbed water, the first mass loss was observed at a relatively low temperature of 109-124 °C (W1) and the second at a relatively higher temperature of 200-280 °C (W2), as observed in Figure 6.32 and Figure 6.33. As-synthesised sample Zeo19 also exhibited a high temperature mass loss at 528 °C (T2), which was due to the desorption of adsorbed carbon dioxide (as observed in Figure 6.33). As-synthesised sample Zeo20 contained a small amount of TPABr (0.027 g/g zeolite) that was released at a temperature of 438 °C (T1) and 530 °C (T2) after 24 hours of crystallisation (as observed in Figure 6.33 and listed in Table 6.17). The presence of the W1 and T1 mass loss regions for sample Zeo20 signified the onset of the formation of a crystalline MFI framework after 24 hours of the crystallisation process. As-synthesised zeolite ZSM-5 samples crystallised after 48 hour exhibited similar thermal degradation profiles. The main mass losses were due to the desorption of physisorbed water (W1) at a temperature of ~ 76-92 °C and the degradation and release of the TPABr molecules occluded in the pores and channels of the zeolite ZSM-5 framework at a temperature of ~ 448 °C (T1) (Frantz et al., 2016; Neves et al., 2019). It is noteworthy that the water content and OSDA content remained relatively similar for highly crystalline zeolite ZSM-5 samples (Zeo14, Zeo21-24) at 0.03-0.04 g/g zeolite and ~0.08-0.09 g/g zeolite, respectively, as listed in Table 6.17. These thermal degradation profiles for CFA-derived zeolite ZSM-5 are similar to

reports in literature for zeolite ZSM-5 synthesised from standard chemical reagents (Araya and Lowe, 1985; Pál-Borbély, 2007).

The investigation of the crystallisation of zeolite ZSM-5 from a CFA-derived silicon precursor (FASE) over time therefore revealed interesting details on the formation mechanism. It is proposed that zeolite ZSM-5 crystals are formed over time by the formation of aluminium-rich nuclei and initial crystals (on the surface of silica particles), followed by crystal growth through the condensation of mainly silicate species to form a highly crystalline zeolite ZSM-5. A similar solution-mediated growth mechanism was reported in literature for LTA and FAU materials from colloidal synthesis mixtures; whereby an initial aluminosilicate gel agglomerates into amorphous aluminosilicate particles, then nano-sized zeolite crystals form on these amorphous aluminosilicate particles and further crystal growth processes resulted in the formation of fully crystalline, micron-sized zeolite crystals (Grand et al., 2016). In this study, the synthesis of highly crystalline zeolite ZSM-5 crystals (1.7 µm in size) was achieved from a CFA-derived silicon precursor (FASE) after 48 hours (2 days) of crystallisation at 160 °C.

6.2.6 The influence of extra-framework cation type on the crystallisation of zeolite ZSM-5

The influence of extra-framework cation type on zeolite ZSM-5 crystallisation was carried out by hydrothermal treatment of synthesis mixtures containing a silicon precursor (FASE) extracted from coal fly ash under static hydrothermal condition of 160 °C for 72 hours; using either sodium hydroxide, calcium hydroxide, potassium hydroxide or cesium hydroxide as a mineralising agent. In each case, the overall alkalinity of the synthesis mixture was kept constant compared to the synthesis system prepared using NaOH (sample Zeo14) and synthesis mixtures were prepared as described in Table 3.9 (with general molar regime 1 SiO_2•0.015 Al_2O_3•0.45 Na_2O•0.08 M_xO•0.10 TPABr•28.3 H_2O). It should be noted that these synthesis systems are dual-inorganic cation systems due to the significant amount of Na_2O introduced into the synthesis mixture originating from the CFA-derived silicon precursor (FASE). The amount of Na_2O in the synthesis mixture due to the addition of a very small amount of sodium aluminate was constant throughout and thought to be insignificant in comparison.

6.2.6.1 Mineralogy and crystallinity

XRD diffractograms of as-synthesised products crystallised at 160 °C for 72 hours from synthesis mixtures with a molar regime 1 SiO_2•0.015 Al_2O_3•0.45 Na_2O•0.08 M_xO•0.10

TPABr•28.3 H_2O at constant alkalinity and M= sodium, calcium, potassium and cesium, with sodium aluminate used as an additional aluminium source, are depicted in Figure 6.34. The relative crystallinity was calculated, according to Equation 2.8, using the most crystalline sample (Zeo23) as a reference pattern and OD ratios was determined from FTIR data; results are summarised in Table 6.18.

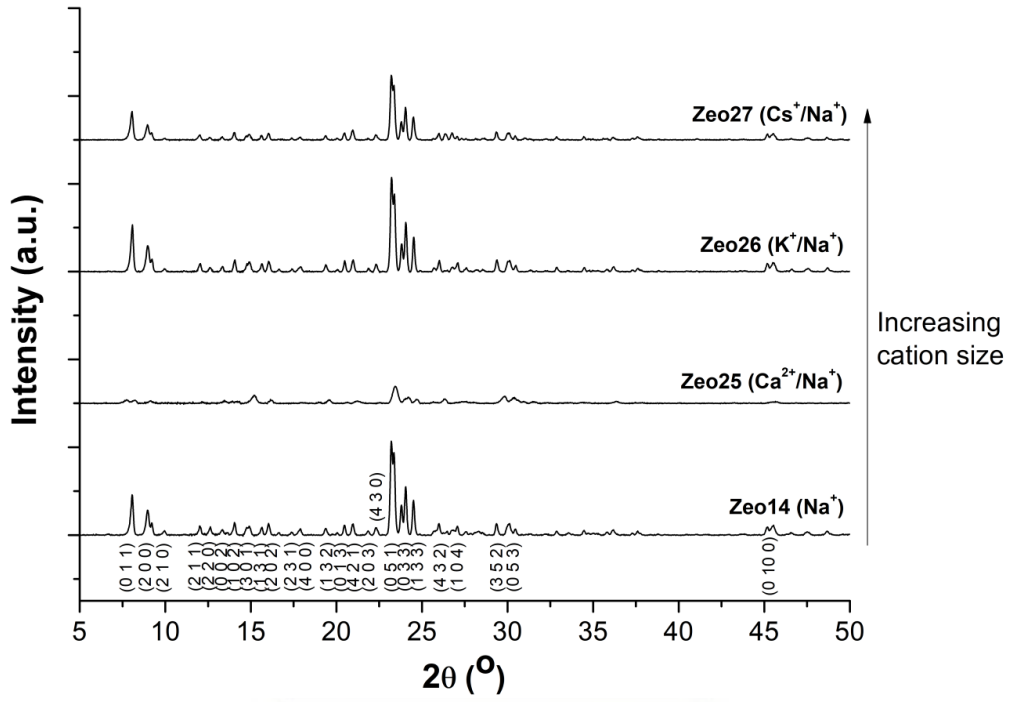

Figure 6.34: XRD diffractograms of as-synthesised zeolite ZSM-5 products synthesised under hydrothermal conditions of 160 °C for 72 hours, with varying extra-framework cations in the synthesis mixture (1 SiO_2•0.015 Al_2O_3•0.45 Na_2O•0.08 M_xO_y•0.10 TPABr•28.3 H_2O) in the form of M-OH (M= Na^+, Ca^{2+}, K^+ or Cs^+).

Table 6.18: Relative crystallinity of as-synthesised zeolites M-ZSM-5 products synthesised under hydrothermal conditions of 160 °C for 72 hours, with varying extra-framework cations in the synthesis mixture (1 SiO_2•0.015 Al_2O_3•0.45 Na_2O•0.08 M_xO_y•0.10 TPABr•28.3 H_2O) in the form of M-OH (M= Na^+, Ca^{2+}, K^+ or Cs^+), determined using XRD and FTIR data.

Sample	NaO_2 added to the synthesis mixture (moles)	M_xO_y added to the synthesis mixture (moles)	Relative Crystallinity	
			XRD (% crystallinity)	FTIR (optical density ratio)
Zeo14-Na	0.53	-	95.8	0.93
Zeo25-Ca/Na	0.45	0.08	11.2	1.52
Zeo26-K/Na	0.45	0.08	98.0	0.86
Zeo27-Cs/Na	0.45	0.08	61.5	0.86

In this study, monovalent cations such as sodium, potassium and cesium with varying cationic radii (0.95, 1.33 and 1.69 Å, respectively) were investigated as well as divalent calcium, which has a similar cationic radius as sodium (0.99 Å) (Pauling, 1927). All synthesis systems resulted in the formation of relatively crystalline zeolite ZSM-5, as observed in Figure 6.34 and listed in Table 6.18, with the exception of sample Zeo25-Ca/Na that was mainly amorphous in nature. The relatively crystalline nature of zeolite samples Zeo14, Zeo26-27 may be due to the high sodium content in the synthesis mixture due to the CFA-derived silicon precursor (FASE), which contains a relatively large amount of sodium (as listed in Table 4.8, Section 4.3.2). Highly crystalline zeolite ZSM-5 was synthesised in the presence of relatively large potassium cations. Therefore monovalent cations of a particular cationic size (such as sodium and potassium, in this case) served as structure-forming species and were able to easily charge-compensate for the negative framework charges in zeolite ZSM-5, without causing strain on the growing framework during the crystallisation process (Meng et al., 2017; Petrik, 2009; Yu, 2007).

It should be noted that the addition of certain inorganic cations such as calcium or cesium inhibited the crystallisation of zeolite ZSM-5 compared to the sodium containing synthesis system (as observed in Figure 6.34); divalent calcium cations were detrimental to the crystallisation of zeolite ZSM-5, while cesium cations only impeded zeolite ZSM-5 crystallisation. Although calcium cations have a similar ionic radius to sodium cations, the inhibition of zeolite ZSM-5 crystallisation in the presence of divalent calcium cations in the synthesis mixture may be due to the structure-breaking behaviour of this divalent cation, which causes instability in the growing zeolite framework during the crystallisation processes (Meng et al., 2017; Petrik et al., 1995; Petrik, 2009; Wang et al., 2017; Yu, 2007). On the other hand, the relatively large ionic radius of cesium, compared to sodium and potassium, is thought to be responsible for the relatively lower crystallisation of zeolite ZSM-5 in the presence of cesium cations. Therefore, a correlation between cation size (for monovalent cations) and the crystallisation of zeolite ZSM-5 from dual-inorganic cation synthesis environments was observed in this study, while divalent calcium was detrimental to zeolite ZSM-5 crystallisation.

6.2.6.2 Morphology and composition

The influence of different counter-cations (Na^+, Ca^{2+}, K^+ and Cs^+) on the morphology of zeolite ZSM-5 (from dual-inorganic cation synthesis environments) was characterised by

SEM coupled to EDS, as depicted in Figure 6.35 (samples Zeo14, Zeo25-27). Other properties of as-synthesised samples Zeo14, Zeo25-27 such as average particle size, SAR and Na/Al ratios are listed in Table 6.19. The nature of the counter-cation type in the synthesis mixture (in addition to sodium cations originating from the CFA-derived silicon precursor FASE) had a significant effect on the morphology of ZSM-5 crystals both in terms of particle size and shape, as depicted in Figure 6.25. As listed in Table 6.19 for monovalent cation synthesis systems (Zeo14-Na, Zeo26-K/Na, Zeo27-Cs/Na), the amount of aluminium incorporated into the MFI framework was not significantly influenced by the change in counter-cation type in the synthesis mixture since the SAR values of these as-synthesised zeolites were relatively similar (~23-29). It is noteworthy that TPA^+ cations also served as charge-balancing species in crystalline zeolite ZSM-5 samples, since the total M/Al ratio was less than one.

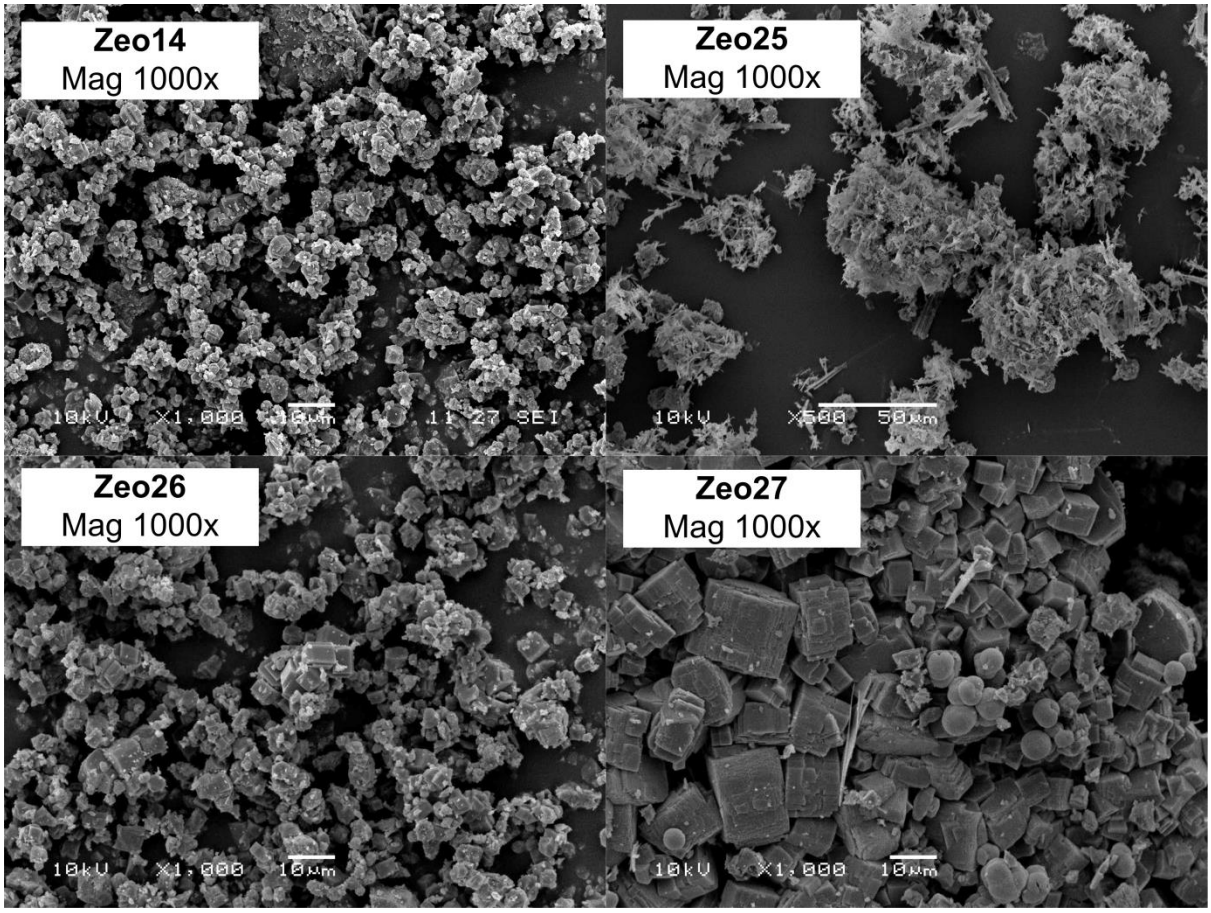

Figure 6.35: SEM micrograph (1000x magnification) of as-synthesised Na-zeolite ZSM-5 samples 146-148, 136 synthesised under hydrothermal conditions of 160 °C for 72 hours, with varying extra-framework cations in the synthesis mixture (1 SiO_2•0.015 Al_2O_3•0.45 Na_2O•0.08 M_xO_y•0.10 TPABr•28.3 H_2O) in the form of M-OH (M= Na^+, Ca^{2+}, K^+ or Cs^+).

Table 6.19: Properties of as-synthesised zeolites M-ZSM-5 samples such as average particle size (determined using ImageJ) and relative composition (determined by EDS analysis n=10), prepared under hydrothermal conditions of 160 °C for 72 hours, with varying extra-framework cations in the synthesis mixture (1 SiO_2•0.015 Al_2O_3•0.45 Na_2O•0.08 M_xO_y•0.10 TPABr•28.3 H_2O) in the form of M-OH (M= Na^+, Ca^{2+}, K^+ or Cs^+).

Sample-M	NaO_2 added to the synthesis mixture (moles)	M_xO_y added to the synthesis mixture (moles)	Average particle size (µm)	SAR value	Na/Al Ratio	M/Al Ratio
Zeo14-Na	0.53	-	1.8	22.7	0.5	-
Zeo25-Ca/Na	0.45	0.08	4.0	57.6	4.1	25.4
Zeo26-K/Na	0.45	0.08	3.5	28.9	0.4	0.2
Zeo27-Cs/Na	0.45	0.08	8.3	26.1	0.1	n.d.

The average particle size of ZSM-5 crystals increased as the ionic radius of the counter-cation increased (Na^+<K^+<Cs^+). Zeolite ZSM-5 crystals synthesised in a Na^+ and Na^+/K^+ environment exhibited a prismatic crystal shape while ZSM-5 crystals synthesised in a Na^+/Cs^+ environment exhibited three types of crystals shapes; (1) spherical crystals, (2) prismatic crystals and (3) enlarged prismatic crystals with platelet like morphology on the surface of the crystal, as depicted in Figure 6.35.

The nature of the charge-balancing cation in the synthesis mixture is known to have a structure-directing effect during the crystallisation of zeolites. However, this effect is reported to be minor in comparison to the structure-directing effect of organic compounds such as TPA^+ cations (Petrik, 2009; Yu, 2007). However, in this study it was observed that simple changes in charge-balancing cation type influenced the crystal morphology of zeolite ZSM-5 synthesised from a CFA-derived silicon precursor (FASE). The morphology of zeolite Cs-ZSM-5 is similar to the morphology of hierarchical ZSM-5 synthesised by the dual-templating method using TPABr and CTAB (Yu et al., 2016). The synthesis of zeolite ZSM-5 in the presence of other inorganic charge-balancing cations in the synthesis mixture (such as Li^+, K^+, Rb^+ and Zn^{2+}) has also been reported to influence the morphology of crystals (Meng et al., 2017; Wang et al., 2007). However, it is not clear exactly how inorganic cations may result in a similar impact on crystal morphology as other complex organic template molecules such as CTAB, etc (that are typically utilised for the synthesis of hierarchical zeolites).

6.2.6.3 Thermal Stability

The thermal analysis of as-synthesised samples Zeo25-27, compared to the thermal properties of highly crystalline zeolite Zeo14, was carried out by TGA/DTG/DTA in air coupled to MS, as depicted in Figure 6.36 and Figure 6.37, respectively. These samples were prepared with different counter-cations such as sodium, calcium, potassium and cesium cations in a dual-inorganic cation synthesis mixture. As-synthesised zeolite ZSM-5 samples (Zeo14, Zeo26-27) synthesised in the presence of mineralising agents containing Na^+, K^+ and Cs^+ as charge-balancing cations (in a dual-inorganic cation synthesis environment) exhibited similar thermal degradation profiles, as depicted in Figure 6.36 and Figure 6.37. Whereas, as-synthesised sample Zeo25 synthesised in the presence of Ca^{2+} cations (in addition to sodium cations) exhibited a significantly different thermal degradation profile.

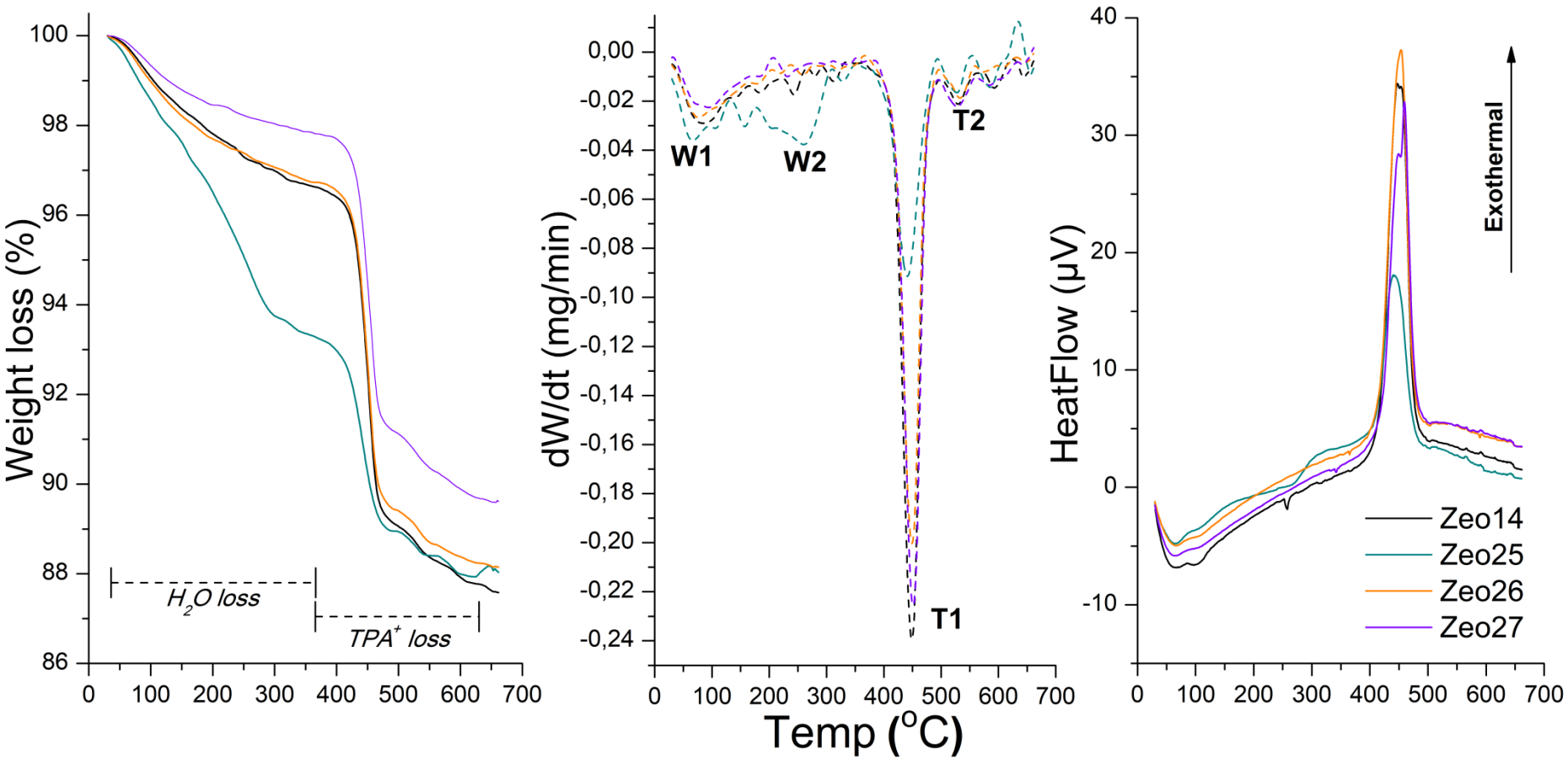

Figure 6.36: Thermal gravimetric (TG) analysis curve (solid line) and its derivative DTG (dotted line) for as-synthesised zeolite samples Zeo14, Zeo25-27 synthesised under hydrothermal conditions of 160 °C for 72 hours, with varying extra-framework cations in the synthesis mixture (1 SiO_2•0.015 Al_2O_3•0.45 Na_2O•0.08 M_xO_y•0.10 TPABr•28.3 H_2O) in the form of M-OH (M= Na^+, Ca^{2+}, K^+ or Cs^+).

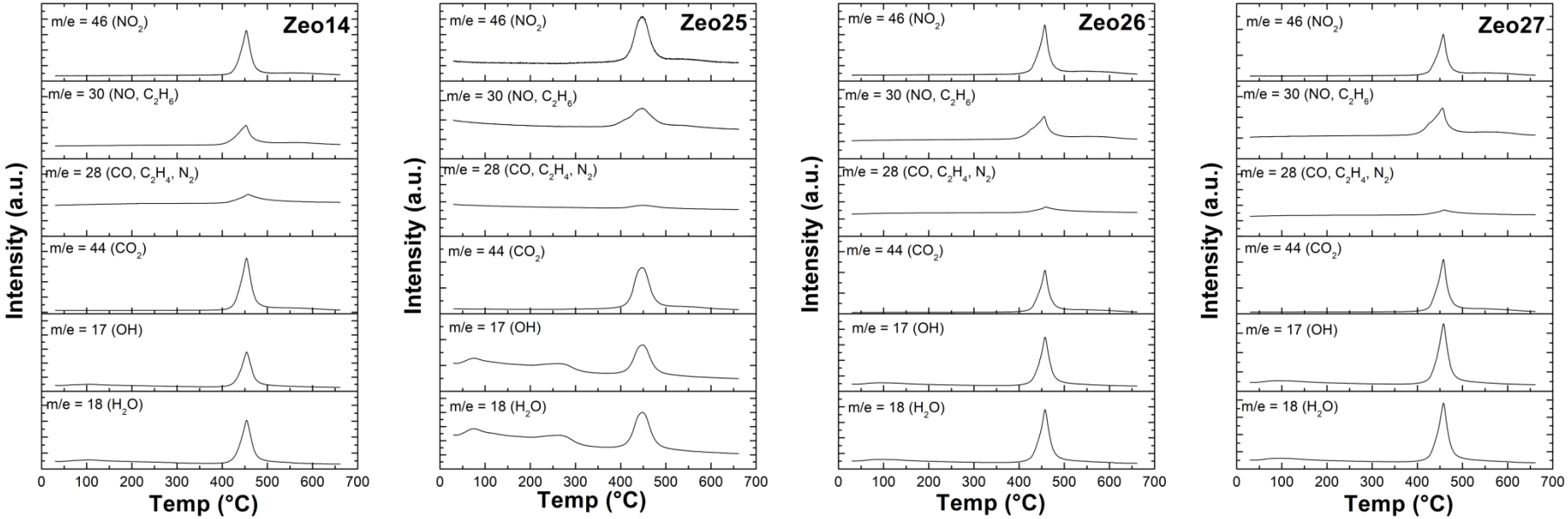

Figure 6.37: MS spectra for as-synthesised zeolite samples Zeo14, Zeo25-27 synthesised under hydrothermal conditions of 160 °C for 72 hours, with varying extra-framework cations in the synthesis mixture (1 SiO_2•0.015 Al_2O_3•0.45 Na_2O•0.08 M_xO_y•0.10 TPABr•28.3 H_2O) in the form of M-OH (M= Na^+, Ca^{2+}, K^+ or Cs^+).

A summary of properties for as-synthesised materials Zeo14, Zeo25-27 such as water and TPABr content are presented in Table 6.20.

Table 6.20: Summary of information gathered from TGA analysis for as-synthesised zeolite samples Zeo14 and Zeo25-27, reported as per gram of zeolite, prepared under hydrothermal conditions of 160 °C for 72 hours, with varying extra-framework cations in the synthesis mixture (1 SiO_2•0.015 Al_2O_3•0.45 Na_2O•0.08 M_xO_y•0.10 TPABr•28.3 H_2O) in the form of M-OH (M= Na^+, Ca^{2+}, K^+ or Cs^+).

Sample	Temp. W1 peak (°C)	Temp. W2 peak (°C)	Water content (g/g zeolite)	Temp. T1 peak (°C)	Temp. T2 peak (°C)	TPABr content (g/g zeolite)
Zeo14-Na	84	-	0.033	448	529	0.085
Zeo25-Ca/Na	67	260	0.066	441	525	0.053
Zeo26-K/Na	77	-	0.032	449	533	0.082
Zeo27-Cs/Na	86	-	0.021	451	528	0.077

As-synthesised zeolite ZSM-5 samples (Zeo14, Zeo25-26) exhibited relatively similar water content (0.02-0.03 g/g zeolite) and TPABr content (0.08-0.09 g/g zeolite), as listed in Table 6.20. As-synthesised sample Zeo25 exhibited relatively higher water content (0.07 g/g zeolite) released over a broad temperature range between room temperature and ~300 °C (as depicted in Figure 6.37) and a relatively lower TPABr content (0.053 g/g zeolite), compared to highly crystalline zeolite samples (Zeo14, Zeo26-27). This is due to the amorphous nature of the Zeo25 material, as reported previously in Section 6.2.6.1. Furthermore, the thermal degradation profile of as-synthesised sample Zeo25 (synthesised in the presence of calcium cations) is comparable to the as-synthesised materials (Zeo19 and Zeo20) synthesised in the presence of sodium cations for a relatively shorter crystallisation period (16-24 hours), as observed in Figure 6.32 and Figure 6.33.

In this study, relatively crystalline zeolite ZSM-5 was synthesised from a CFA-derived silicon precursor in the presence of different inorganic cations such as potassium and cesium. Similar results have been reported in literature for the synthesis of zeolite ZSM-5 in the presence of different inorganic cations such as sodium, lithium, potassium, rubidium and cesium; whereby the morphology of ZSM-5 crystals was influenced by the cation size. However, it should be noted that these M-ZSM-5 zeolites were prepared from synthesis mixtures containing one inorganic cation (Meng et al., 2017; Petrik, 2009; Singh and Dutta, 2003; Wang et al., 2007).

The crystallisation of a particular zeolite framework is known to be affected by the inorganic cations present in the synthesis mixture (Petrik, 2009; Yu, 2007). This study therefore illustrated that the presence of various inorganic charge-balancing cations (in particular monovalent cations) such as potassium and cesium in the synthesis mixture is not detrimental to the synthesis of zeolite ZSM-5 from a CFA-derived silicon precursor but may result in changes in the crystallisation processes involved in the formation of crystalline zeolite ZSM-5.

6.3 Hydrothermal synthesis of silicalite-1

The synthesis of pure zeolite silicalite-1 (MFI framework type) from coal fly ash has not been reported in literature to date. Silicalite-1 is the hydrophobic, siliceous analogue for zeolite ZSM-5. Silicalite-1 has interesting applications in catalysis, adsorption and separation science and the application of this material in membrane and thin-film technologies has gained interest due to the hydrophobic nature of the material (Cheng and Shantz, 2005; van den Broeke et al., 1999; Yang et al., 2011). The synthesis of zeolite silicalite-1 from South African coal fly ash was investigated using a CFA-derived silicon precursor (FASE) as an alternative starting material to conventional silicon sources such as fumed silica or sodium silicate solution. The crystallisation of zeolite silicalite-1 was carried out using a synthesis mixture with a fixed molar regime (1 SiO_2•0.004 Al_2O_3•0.49 Na_2O•0.09 TPABr•11.6 H_2O) under hydrothermal conditions of 170 °C for 48 hours (2 days), as described in Table 3.10, similar to synthesis conditions reported in literature (Kamil et al., 2015; Petrik et al., 1995). The characterisation of synthesised zeolites carried out by XRD, SEM-EDS, FTIR and TGA/DTG/DTA coupled to MS spectrometry will be presented in subsequent sections.

6.3.1 Characterisation of silicalite-1

Figure 6.38 represents the XRD diffractogram of zeolite Sil01 synthesised from a CFA-derived silicon precursor (FASE) under hydrothermal conditions of 170 °C for 48 hours (2 days) using a molar regime of 1 SiO_2•0.004 Al_2O_3•0.49 Na_2O•0.09 TPABr•11.6 H_2O. Highly crystalline MFI-type zeolite was synthesised under these conditions, as observed in Figure 6.38. The main diffraction peaks for the MFI framework (2θ = ~7.96, ~8.83, ~23.32, ~24.04 and ~24.45°) were observed for the as-synthesised sample Sil01.

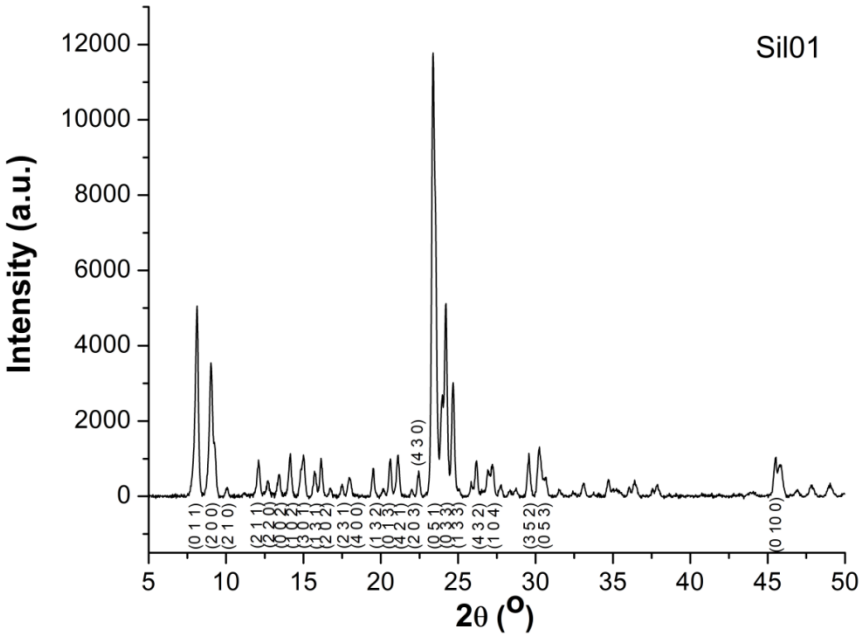

Figure 6.38: XRD diffractogram of as-synthesised zeolite sample Sil01 crystallised at a hydrothermal temperature of 170 °C for 48 hours from a synthesis mixture with molar regime 1 SiO_2•0.004 Al_2O_3•0.49 Na_2O•0.09 TPABr•11.6 H_2O.

The morphology of as-synthesised zeolite sample Sil01 was analysed by SEM and EDS was used to determine the average SAR value of the sample, as depicted in Figure 6.39 and 6.40, respectively. Figure 6.40 also presents the average elemental composition for as-synthesised zeolite sample Sil01.

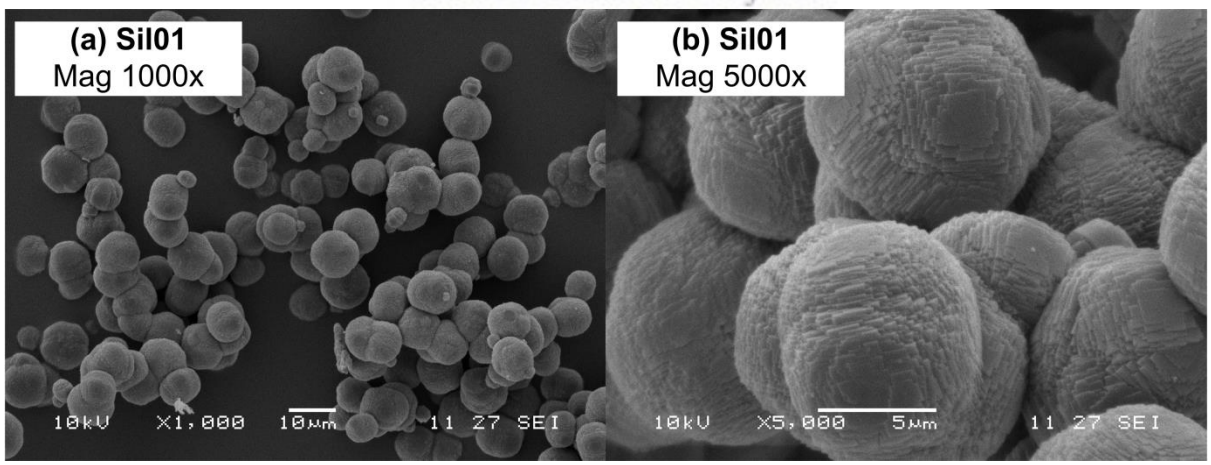

Figure 6.39: SEM micrograph of as-synthesised sample Sil01 crystallised at 170 °C for 48 hours from a synthesis mixture with molar regime 1 SiO_2•0.004 Al_2O_3•0.49 Na_2O•0.09 TPABr•11.6 H_2O (a) at X1000 and (b) at X5000 magnification.

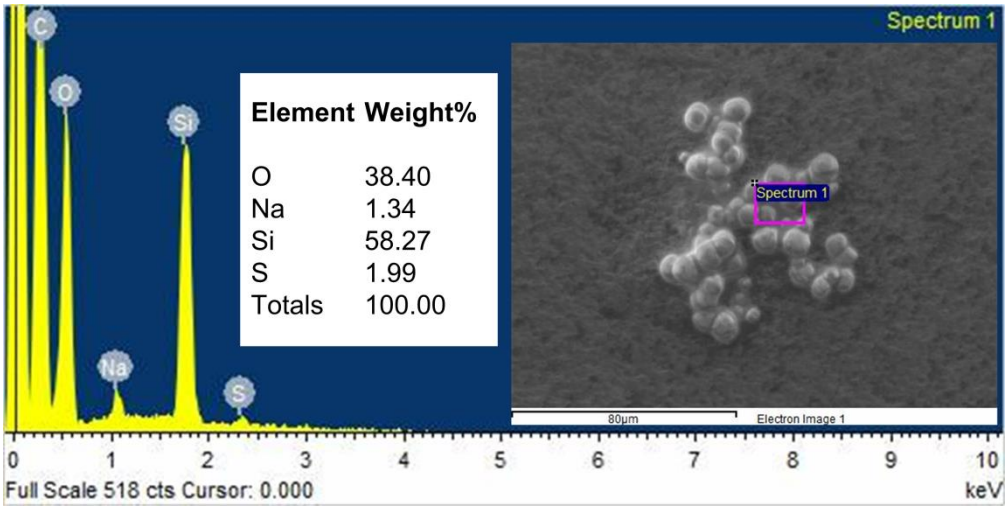

Figure 6.40: An example of an EDS spectrum of as-synthesised sample Sil01 crystallised at 170 °C for 48 hours from a synthesis mixture with molar regime 1 SiO_2•0.004 Al_2O_3•0.49 Na_2O•0.09 TPABr•11.6 H_2O, with an inset of the average elemental composition of as-synthesised Sil01 crystals (determined by EDS analysis n=10).

As depicted in Figure 6.39 and 6.40, as-synthesised zeolite sample Sil01 crystals were spherical in shape, with an average particle size of 8.3 µm calculated using ImageJ software. EDS was used to determine the average elemental composition of synthesised product, which illustrated that no aluminium was present in the material and the synthesised product is therefore the MFI-type material known as silicalite-1. The as-synthesised silicalite-1 also contained sodium (1.3 wt%) and sulphur (2.0 wt%), which is thought to be due to the presence of these elements in the CFA-derived silicon precursor (FASE), as listed in Table 4.8 (Section 4.3.2). Upon closer examination of the crystal surfaces depicted in Figure 6.39 (b), these spherical silicalite-1 crystals were similar in morphology to that of highly siliceous ZSM-5 (reported in Section 6.2.1).

The thermal profile of as-synthesised sample Sil01 was carried out by TGA/DTG/DTA in air coupled to MS, as depicted in Figure 6.41 and 6.42, respectively, with a summary of the thermal properties of the synthesised material presented in Table 6.21.

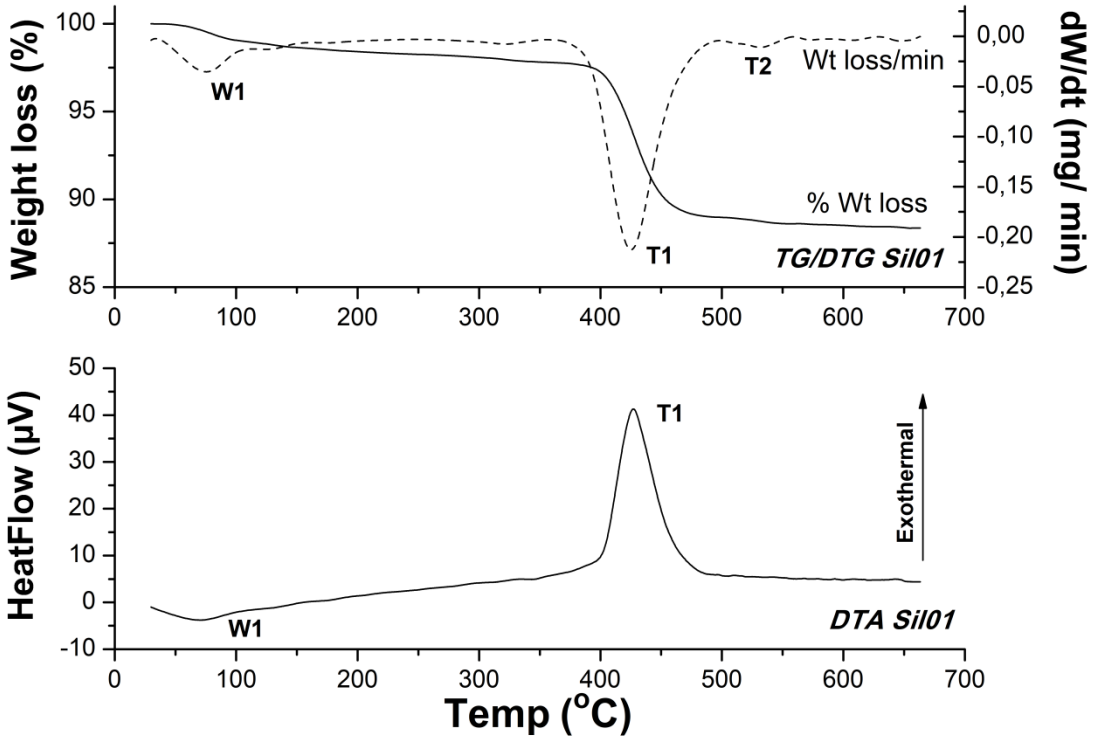

Figure 6.41: TGA/DTG/DTA spectra of as-synthesised zeolite Sil01 crystallised at 170 °C for 48 hours from a synthesis mixture with molar regime 1 SiO_2•0.004 Al_2O_3•0.49 Na_2O•0.09 TPABr•11.6 H_2O.

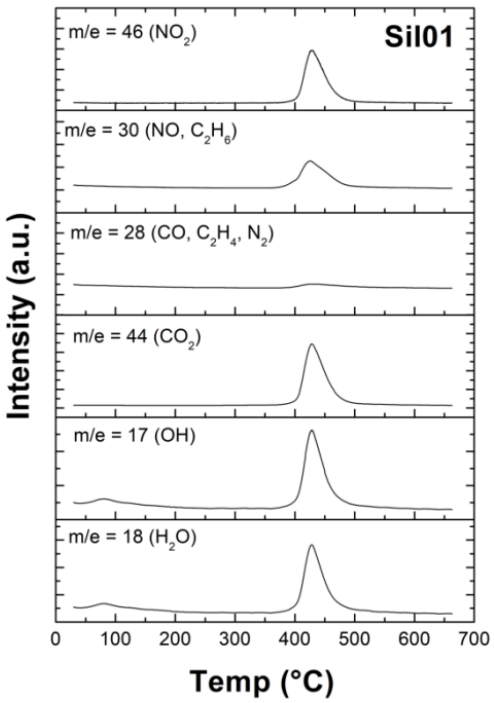

Figure 6.42: MS spectra of as-synthesised zeolite Sil01 crystallised at 170 °C for 48 hours from a synthesis mixture with molar regime 1 SiO_2•0.004 Al_2O_3•0.49 Na_2O•0.09 TPABr•11.6 H_2O, with an inset of thermal properties and H_2O and TPABr content.

Table 6.21: Summary of information gathered from TGA analysis for as-synthesised zeosil sample Sil01, reported as per gram of zeolite, prepared using a synthesis mixture with molar regime 1 SiO_2•0.004 Al_2O_3•0.49 Na_2O•0.09 TPABr•11.6 H_2O under hydrothermal conditions of 170 °C for 48 hours.

Sample	Temp. W1 peak (°C)	Water content (g/g zeolite)	Temp. T1 peak (°C)	Temp. T2 peak (°C)	TPABr content (g/g zeolite)
Sil01	75	0.022	423	532	0.092

The thermal profile of as-synthesised sample Sil01 contained three mass loss regions, as depicted in Figure 6.41 and Figure 6.42. Mass loss W1 is associated with the release of physisorbed water from the pores and channels in the MFI framework of silicalite-1. As listed in Table 6.21, the water content of this material was very low at 0.022 g/g zeolite, which confirms the hydrophobic nature of the material compared to aluminium-rich MFI-type materials such as zeolite ZSM-5 (Pál-Borbély, 2007). Two other mass loss regions associated with the degradation and release of the OSDA agent (TPABr) were observed for this material; (i) the main mass loss T1 which is due to the degradation and release of TPABr molecules occluded in the pores and channels in the MFI framework of silicalite-1 and (ii) a small T2 mass loss region due to the release of TPABr molecules from less accessible sites in the MFI framework of silicalite-1 (which may be attributed to the relatively crystal size of silicalite-1 particles as observed in Figure 6.39). The total OSDA content in the MFI framework (silicalite-1) was 0.092 g/g zeolite, as listed in Table 6.21.

In this study, a purely siliceous MFI-type material (silicalite-1) was synthesised from a CFA-derived silicon precursor (FASE). The synthesis material was comparable to silicalite-1 synthesised from standard chemical reagents (Kamil et al., 2015; Petrik et al., 1995). The preparation of spherical silicalite-1 crystal was achieved using colloidal silica and TBABr as an OSDA agent by Petrik et al., (1995), while Kamil et al., (2015) synthesised silicalite-1 using TEOS as a silicon source and TPAOH as the OSDA agent. According to literature reported to date, this study presents the first method for the preparation of silicalite-1 from CFA.

6.4 Comparison of selected MFI samples (with varying SAR ratios)

This study illustrated that the crystallisation of zeolite ZSM-5 from a CFA-derived silicon precursor (FASE) from synthesis mixtures with a wide range of molar compositions was possible. These synthesised materials exhibited different physical properties. Comparisons between the properties of selected MFI-type zeolites with different SAR values from 18.5 (ZSM-5) up to ∞ (silicalite-1) are listed in Table 6.22, with correlations between SAR value and water/OSDA content depicted in Figure 6.43.

Table 6.22: Properties of selected MFI type materials synthesised from a CFA-derived silicon precursor (FASE).

Zeolite	SAR value	Particle size (µm)	Particle shape	Water content (g/g zeolite)	Template content (g/g zeolite)	BET surface area (m^2/g)	Mesopore Surface Area (m^2/g)	Micropore Volume (cm^3/g)	Total Pore Volume (cm^3/g)
Zeo08	18.5	2.7	p	0.047	0.066	n.d.	n.d.	n.d.	n.d.
Zeo04	21.4	2.5	p	0.045	0.084	359.8	144.1	0.089	0.210
Zeo07	30.5	1.9	p	0.030	0.089	281.5	121.9	0.070	0.178
Zeo03	81.7	16.1	s	0.014	0.103	461.4	195.42	0.109	0.314
Zeo02	92.8	4.9	s	0.023	0.104	459.0	391.2	0.044	0.447
Zeo01	201.7	3.0	s	0.021	0.111	423.3	154.3	0.108	0.265
Sil01	∞	8.3	s	0.022	0.092	414.7	172.4	0.099	0.283

*p - prismatic, s - spherical

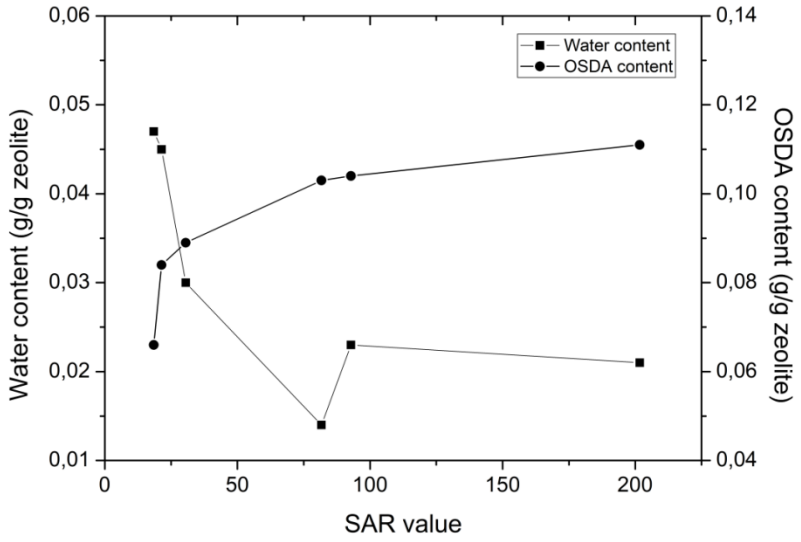

Figure 6.43: The SAR value of selected as-synthesised ZSM-5 materials versus the water content and OSDA content in the as-synthesised materials.

The SAR value of synthesised zeolites played an important role in the properties of zeolites such as water content (hydrophobicity/hydrophilicity) as well as the template content in the MFI framework, as depicted in Table 6.22. As such, a good correlation between SAR value and water/OSDA agent content was observed for zeolite ZSM-5 samples, as Figure 6.43 (with the exception of samples Zeo03 and Sil01). Furthermore, highly siliceous MFI crystals were found to exhibit spherical morphology (with relatively larger crystals) whereas relatively aluminium-rich MFI crystals were prismatic in shape and relatively smaller in size.

The textural properties of synthesised MFI-type zeolites (such as BET and mesopore surface area as well as micropore and total pore volume) were also characterised by N_2 physisorption, as listed in Table 6.22 (see Appendix B for nitrogen adsorption isotherms). The typical BET surface area of zeolite ZSM-5 is reported as ~ >400 m^2/g with a micropore volume of ~0.18-0.21 cm^3/g. The well-defined siliceous MFI materials (with spherical morphology) exhibited BET surface areas comparable to that reported for ZSM-5 in literature (Du and Wu, 2007; Nijkamp et al., 2001; Perez-Page et al., 2016; Solcova et al., 2011) as well as commercial samples tested using the same equipment. Samples Zeo02 and Zeo03 exhibited a slightly larger BET surface area (459 and 461 m^2/g, respectively) than commercial ZSM-5 samples. However, aluminium-rich ZSM-5 samples exhibited slightly lower BET surface areas than expected which may be due to the highly agglomerated nature of the morphology of these samples as observed previously.

It is noteworthy that synthesised MFI materials exhibit similar pore size distributions, with micropore volume of ~0.090 cm^3/g and total pore volume of ~0.170 cm^3/g; illustrating that these materials are all microporous. This is also evident from the type I adsorption isotherm observed for these materials (see Appendix). However, synthesised MFI sample Zeo02 exhibited a type I adsorption isotherm with slightly different N_2 uptake characteristic of type I and IV adsorption isotherms (Thommes et al., 2015). Consequently, this material (Zeo02) exhibited a relatively larger total pore volume (0.447 cm^3/g) and relatively lower micropore volume (0.044 cm^3/g), compared to other microporous MFI materials. The hysteresis loop of the N_2 adsorption isotherm of sample Zeo02 (which indicates capillary condensation in mesopores during the desorption process) was relatively small; this indicated the intercrystalline mesopore nature of these MFI crystals (Thommes et al., 2015). This is likely due to the morphology of the synthesised sample, which is similar to hierarchical zeolite ZSM-5 samples synthesised using more complex templating agents and synthesis techniques

as reported previously, in Section 5.2.1.2. This hierarchical ZSM-5 material may be an interesting candidate for overcoming the diffusional constraints reported for zeolite ZSM-5 during catalytic applications, without suffering from the recovery problems associated with nano-sized zeolite crystals (Moliner et al., 2014; Wang et al., 2017). On the other hand, aluminium rich ZSM-5 samples may be useful in applications that require high acidity while silicalite-1 may be used in the separation of complex mixtures (Cheng and Shantz, 2005; Kadja et al., 2016; Yang et al., 2011).

The ability to fine-tune the properties of MFI-type zeolites (such as crystal size, SAR, solid acidity, porosity, etc.) is an important tool for the rational design of materials (from alternative and/or waste feedstock), which are custom-made for particular applications in the field of catalysis and adsorption. This is the first study that presents the conversion of a CFA to pure, highly crystalline MFI-type materials (such as zeolite ZSM-5 and silicalite-1) with a range of different properties such as SAR value ranging from aluminium-rich ZSM-5 (SAR = 18.5) up to Silicalite-1 (SAR = ∞), according to literature to date.

6.5 Chapter Summary

The synthesis of highly crystalline medium-pore MFI-type zeolites (ZSM-5 and silicalite-1) was achieved from a silicon precursor extracted from coal fly ash; this extraction was carried out under mild conditions. Furthermore, the methodology used in this study eliminated the need for the purification of the coal fly ash-derived silicon extract by oxalic acid treatment prior to hydrothermal synthesis of zeolite ZSM-5 and illustrated that zeolite ZSM-5 crystallisation is possible from FASE in high sodium synthesis environments. This study revealed how simple changes in the synthesis conditions (i.e. molar regime) can alter the properties of the resultant zeolitic material from aluminium-rich, prismatic, microporous ZSM-5 to high-silica, spherical, hierarchical ZSM-5 and relatively hydrophobic, highly-siliceous silicalite-1 crystals. It is important to note that this is the first reported synthesis of highly siliceous silicalite-1 synthesis from a CFA-derived starting material as well as the first reported synthesis of a range of zeolite ZSM-5 material with different properties (SAR values in particular) from CFA. In this study, the type of counter-cation in the synthesis mixture was shown to have a significant influence on the morphology of the resultant ZSM-5 zeolites. The cation size and charge were observed to influence the resultant zeolite morphology. In the next chapter, geometric simulations will be used to explore the influence of cation type on a model zeolite to get more insight into this effect.

7 Chapter 7 - Geometric modelling of the influence of extra-framework cation type on a model zeolite framework (LTA) using GASP software

7.1 Introduction

CFA is a waste material that is rich in silicon and aluminium, the building blocks of zeolites. However, CFA also contains a range of different elements (as presented in Chapter 4). Zeolite synthesis from CFA may be influenced by the various elements present in the feedstock (CFA). Zeolite synthesis from CFA has resulted in the formation of zeolite X with a novel hierarchical morphology (Musyoka et al., 2014). In this study, interesting observations were also made regarding the morphology of zeolite mordenite (Chapter 5) and ZSM-5 (Chapter 6) synthesised from a CFA-derived silicon extract. During zeolite ZSM-5 synthesis in a dual-cation synthesis environment, cation size and charge were observed to influence relative crystallinity and crystal morphology (as observed in Section 6.2.6). In the case of zeolite mordenite synthesis, a reduction in the sodium cation content of the synthesis mixture resulted in a novel morphology for zeolite MOR (as observed in Section 5.4.2). This was thought to be due to the presence of impurities (such as inorganic cations) in the CFA-derived silicon precursor (FASE). Inorganic cations are known to possess a minor structure-directing function (Petrik, 2009; Yu, 2007). However, it is not fully understood how cations in the synthesis mixture may influence crystallisation processes and potentially, result in novel zeolite morphologies.

The steric constraints that charge-balancing, extra-framework cations place on the framework flexibility of zeolites may provide insight into the influence of these cations on zeolite formation. Geometric modelling software (GASP) may be used to evaluate the framework flexibility of zeolites (i.e. the feasibility of formation of a particular zeolite framework) (Sartbaeva et al., 2006; Sartbaeva et al., 2008; Wells et al., 2015; Wells and Sartbaeva, 2012). A range of zeolite frameworks have been simulated using GASP, including zeolite frameworks with extra-framework content such as organic template molecules, solvent molecules and charge-balancing sodium cations, to assess the flexibility of these frameworks (Fletcher et al., 2015; Nearchou et al., 2019; Sartbaeva et al., 2008; Wells et al., 2011; Wells et al., 2015; Wells et al., 2017; Wells and Sartbaeva, 2012). High-pressure powder XRD diffraction coupled with GASP modelling was utilised to investigate the influence of an OSDA agent (18-crown-6 ether) on the compression mechanism of different zeolite

frameworks such as EMT, FAU, KFI and RHO (all synthesised in the presence of 18-crown-6 ether). The presence of organic 18-crown-6-ether molecules in the pores of zeolite frameworks EMT, KFI and RHO served as a structure-directing agent during zeolite formation (since the presence of the OSDA agent enhanced the compressibility of these frameworks with the exception of the EMT framework that was unaffected and unusually large). On the other hand, the 18-crown-6 ether molecules occluded in the pores of FAU did not enhance the compressibility of the framework; 18-crown-6 ether is therefore thought to behave as a space-filling agent in the formation of the FAU framework (Fletcher et al., 2015; Nearchou et al., 2019). It was reported that the presence of sodium cations in the SOD framework did not significantly influence the framework flexibility (Wells et al., 2017).

The GASP simulation of the steric effect of different inorganic cations on a particular zeolite framework has not been reported to date. In this chapter, the influence of different extra-framework cations (such as sodium, calcium, potassium and cesium) on the framework flexibility and compression mechanism of a model zeolite A (LTA framework) simulated by GASP will be presented. Zeolite A (with LTA framework) has cubic symmetry and a framework Si/Al ratio of 1 with an ordered aluminium distribution throughout the framework, making it an ideal framework for simulation studies (Čejka et al., 2007; Liu et al., 2010; Martin-Calvo et al., 2014). The aim of the study was to determine how inorganic cations (which may be present in the CFA-derived silicon extract) may influence the crystallisation of zeolites, by utilisation of geometric modelling software GASP to evaluate the framework flexibility of the zeolitic material in the presence of different inorganic extra-framework cations (as described in Section 3.7).

7.2 Geometric simulation of the flexibility windows of LTA frameworks (Siliceous and aluminosilicate)

The geometric simulation of empty siliceous and aluminosilicate LTA frameworks was carried out by GASP software as the starting point for the investigation, as described in Section 3.7.1.1 (with cell parameters listed in Table 3.11). The simulation results are presented in Figure 7.1 for the siliceous LTA (grey) and aluminosilicate LTA (orange) framework. The starting cell parameters that were used as input values for the GASP simulation are presented as black data points, these ambient cell parameter values were retrieved from the Database for Zeolite Structures (Baerlocher and McCusker, 2017; Pluth

and Smith, 1980). A summary of the limits of the flexibility window for the LTA frameworks is also presented in Table 7.1.

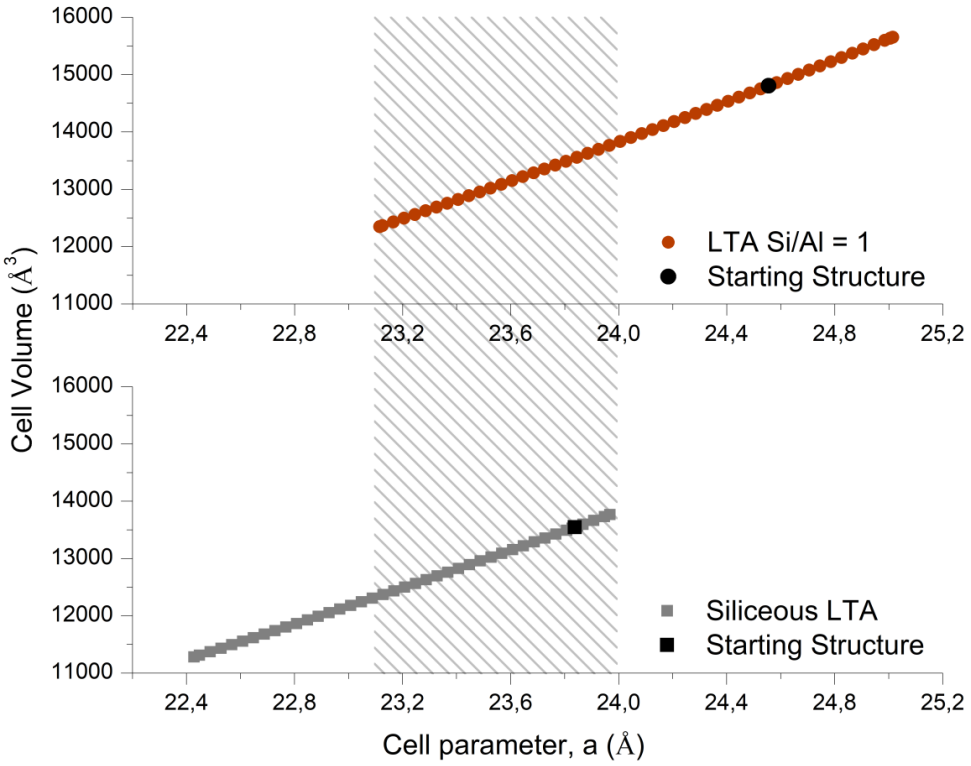

Figure 7.1: GASP simulated flexibility windows of siliceous LTA and aluminosilicate LTA.

Table 7.1: Starting cell parameters and flexibility window limits of the cubic LTA framework (siliceous and Si/Al ratio = 1) simulated using GASP.

Framework	Starting cell parameter, a (Å)	Lower window edge (Å)	Compressed cell volume (Å^3)	Upper window edge (Å)	Expanded cell volume (Å^3)
Siliceous LTA	23.838	22.428	13769	23.968	11282
LTA (Si/Al = 1)	24.555	23.115	12350	25.015	15653

The flexibility window of the siliceous LTA framework ranged between cell parameter values a = 22.428 Å and 23.968 Å; cell volume values corresponding to these limits are listed in Table 7.1. The (a) compressed, (b) starting and (c) expanded LTA structures representing the flexibility window limits are illustrated in Figure 7.2, in which silica tetrahedra are

represented in grey. A typical observation for open framework structures such as zeolites is that the starting structure exists close to the upper limit of the flexibility window; a less dense and consequently low-energy geometry for the framework (Wells et al., 2017). In both the expanded and contracted structures, the geometry of the 8-ring window is altered from an octagonal window under ambient conditions (Figure 7.2 b) to a more square-shaped window (Figure 7.2 a and c).

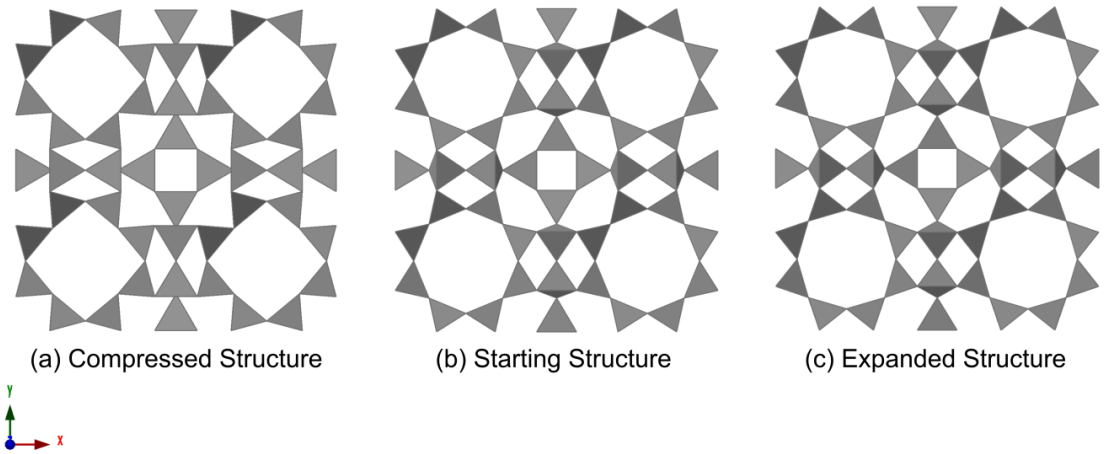

Figure 7.2: Flexibility window limits of the LTA framework, with grey silica tetrahedra.

The flexibility window range for aluminosilicate LTA was ranged between a = 23.115 Å and 25.015 Å, as listed in Table 7.1. The overlapping regions of the flexibility window of siliceous LTA and aluminosilicate LTA were shaded as depicted in Figure 7.1. The compressed region of the aluminosilicate LTA flexibility window corresponds to the expanded region of the siliceous LTA flexibility window due to the relatively longer lengths of T-O bonds due to aluminium incorporation into the LTA framework (Wells et al., 2017). It should be noted that the overall theoretical mechanism of compression for the siliceous and aluminosilicate LTA frameworks was the same. As depicted in Figure 7.3, the distortion of the 8 ring window geometry in the aluminosilicate LTA framework was observed upon compression similar to that observed for the siliceous LTA framework.

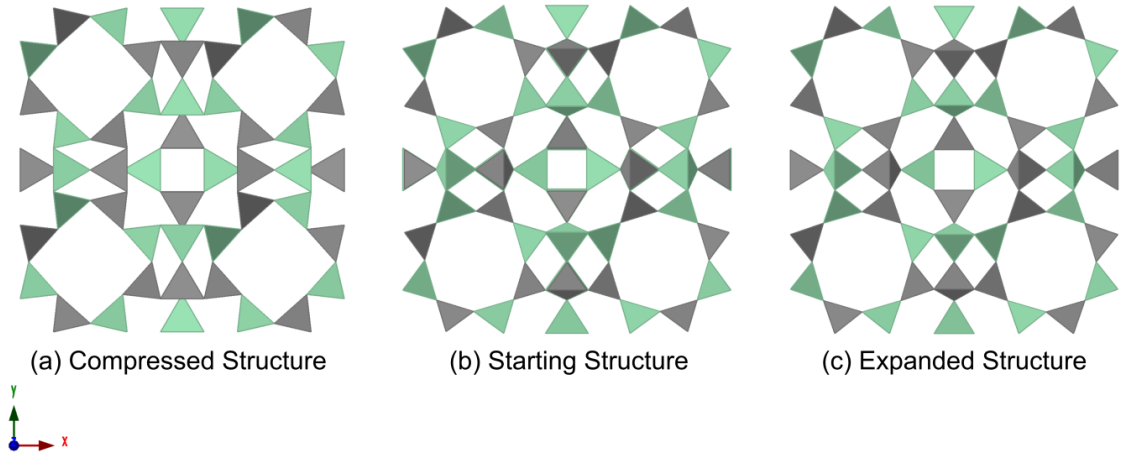

Figure 7.3: Flexibility window limits of aluminosilicate LTA framework (Si/Al ratio = 1), with grey silica tetrahedra and green alumina tetrahedra.

Although the theoretical compression mechanism for the aluminosilicate LTA framework was the same as that of the siliceous LTA framework, the incorporation of aluminium atoms into the LTA framework allows for more flexible and open zeolite framework. Typically, zeolite frameworks with a high framework-aluminium content (i.e. low SAR value) form easily (without the addition of an OSDA agent); some examples include the LTA, FAU and SOD framework (Lobo, 2003; Payra and Dutta, 2003; Weitkamp, 2000; Yu, 2007).

7.3 Geometric simulation of the flexibility windows of M-LTA frameworks (M = Na, Ca, K or Cs extra-framework cations)

The flexibility window of the aluminosilicate LTA framework in the presence of varying extra-framework cations such as Na^+, Ca^{2+}, K^+ and Cs^+ was simulated using GASP software. These cations commonly occupy three different sites in the framework (as depicted in Figure 7.4) depending on cation size and charge (Breck et al., 1956; Reed and Breck, 1956).

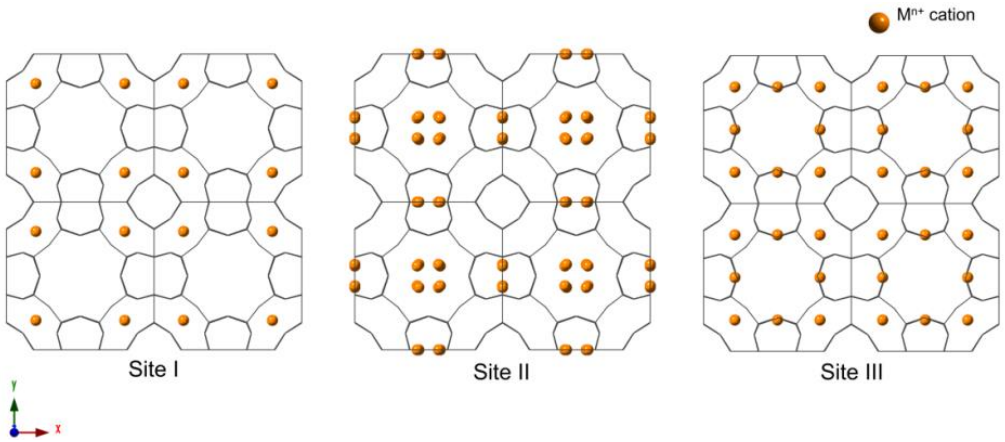

Figure 7.4: Typical cation sites in the LTA framework.

Figure 7.4 represents extra-framework cations positioned in/near the centre of the 6-ring window of sodalite cages (site I), slightly off-centre in the 8-ring window of α cages (site II) and opposite the 4-rings on the interior of α cages (site III). High site occupancies are observed for site I (0.97) and II (0.24). On the other hand, site III typically has insignificant site occupancy of 0.07 (Baerlocher and McCusker, 2017). According to literature (Breck et al., 1956), dehydrated aluminosilicate Na-LTA consists of a total of 12 sodium cations for each unit cell; 8 sodium cations in site I and 4 sodium cations in site II positions. Similar observations have been reported for potassium and it was expected that monovalent cesium may occupy the same sites in order to charge-balance the LTA framework. However, dehydrated aluminosilicate Ca-LTA framework contains 6 cations for every unit cell (all positioned in site I) since calcium is a divalent cation (Breck et al., 1956; Lobo, 2003; Reed and Breck, 1956).

The GASP geometric simulation results of the flexibility window of aluminosilicate LTA frameworks with extra-framework cations (sodium, calcium and potassium) are depicted in Figure 7.5. The flexibility window limits for each M-LTA framework is summarised in Table 7.2. Cation site type and content (per unit cell) was allocated as described previously (and listed in Table 3.12).

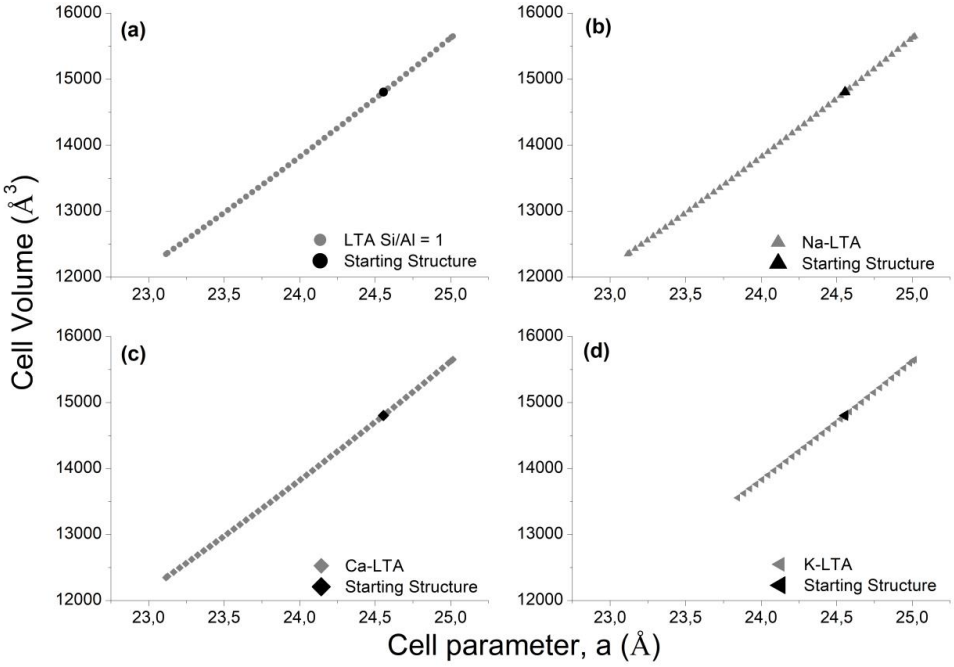

Figure 7.5: GASP simulated flexibility windows of aluminosilicate M-LTA frameworks (b)-(d) compared to aluminosilicate LTA without cation content (a).

Table 7.2: Starting cell parameters and flexibility window limits of the cubic LTA framework (Si/Al = 1) simulated by GASP simulation with different extra-framework cations.

Framework	Starting cell parameter, a (Å)	Lower window edge (Å)	Compressed cell volume (Å^3)	Upper window edge (Å)	Expanded cell volume (Å^3)
LTA (Si/Al = 1)	24.555	23.115	12350	25.015	15653
Na-LTA	24.555	23.115	12350	25.015	15653
Ca-LTA	24.555	23.115	12350	25.015	15653
K-LTA	24.555	23.845	13558	25.015	15653
Cs-LTA	24.555	n.d.	n.d.	n.d.	n.d.

The LTA framework containing sodium and calcium as charge-balancing cations exhibited flexibility windows identical to that of the empty aluminosilicate LTA framework, as depicted in Figure 7.5 (a)-(c). This indicates that the theoretical compressibility of the LTA framework was not influenced by the presence of extra-framework content (sodium or calcium cations). Similar results were observed for the SOD framework containing sodium extra-framework cations (Wells et al., 2017). Sodium and calcium have similar ionic radii and were not expected to significantly strain the LTA framework. The starting structures for

Na-LTA and Ca-LTA are illustrated in Figure 7.6 and 7.7, respectively, compared to the compressed and expanded structures.

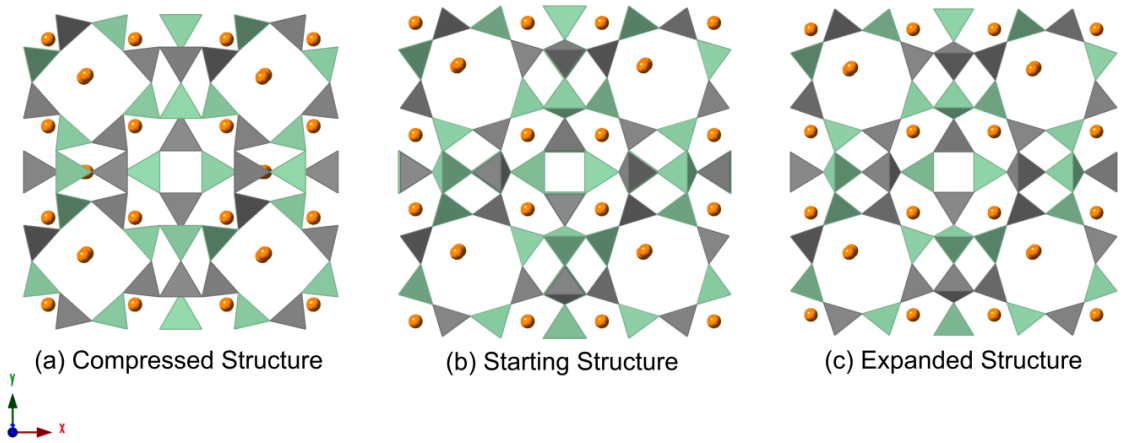

Figure 7.6: Flexibility window limits of aluminosilicate LTA framework (Si/Al ratio = 1) with sodium as extra-framework cation, grey silica tetrahedra and green alumina tetrahedra.

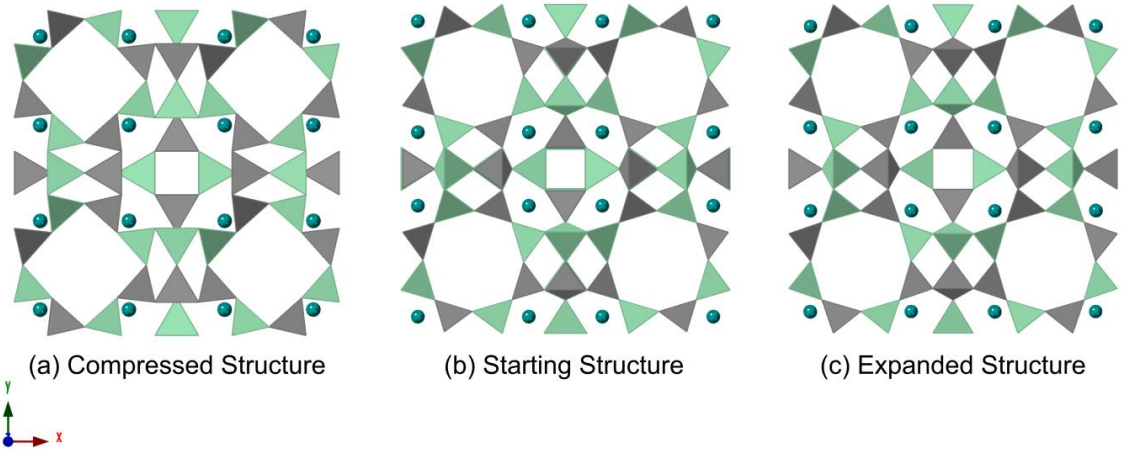

Figure 7.7: Flexibility window limits of aluminosilicate LTA framework (Si/Al ratio = 1) with calcium as extra-framework cation, grey silica tetrahedra and green alumina tetrahedra.

These figures for Na-LTA (Figure 7.6) and Ca-LTA (Figure 7.7) further illustrate that the collective movements of polyhedra during the expansion and contraction process (i.e. the compression mechanism for the framework) is identical to the compression mechanism observed for the empty LTA framework (as depicted in 7.3).

As depicted in Figure 7.5 (d), the theoretical compressibility of the K-LTA framework was reduced compared that of the Na-LTA framework. Steric constraints on the LTA framework arose from filling the LTA cation sites with potassium cations, which have a relatively larger

ionic radius than sodium and calcium cations. This restricted the framework flexibility for the LTA framework and altered the theoretical compression mechanism, as illustrated in Figure 7.8. Upon compression of the K-LTA framework, the theoretical compression mechanism exhibited a cooperative rotation of polyhedra in a symmetry-breaking manner. This is unlike the theoretical compression mechanisms observed for the empty LTA framework or the other M-LTA frameworks. Furthermore, the distortion of the 8-ring window is also different than previous cases in terms of geometry and orientation with respect to the cell axes. In this case, the distortion of the 8-ring window geometry from an octahedral (Figure 7.8 b) to a square/rhomboidal shape (Figure 7.8 a and c) was observed.

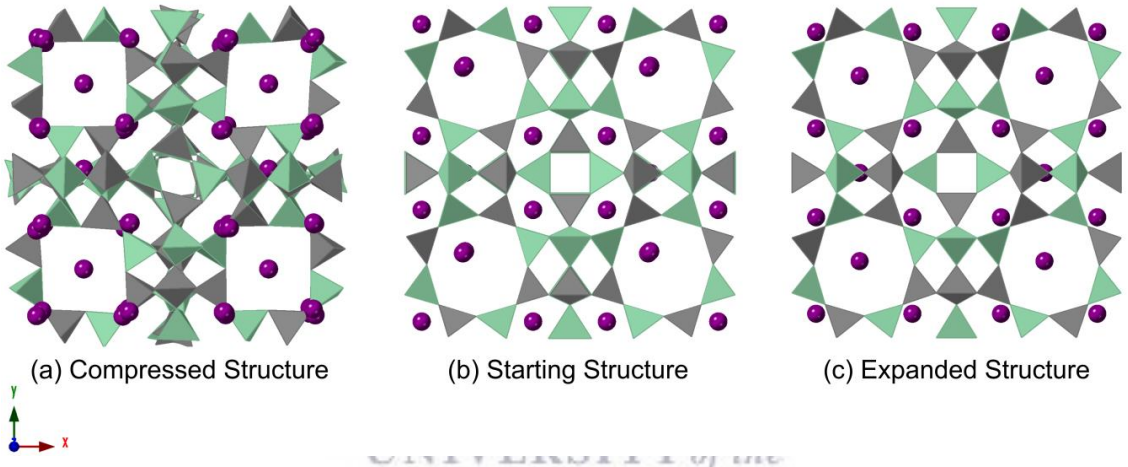

Figure 7.8: Flexibility window limits of aluminosilicate LTA framework (Si/Al ratio = 1) with potassium as extra-framework cation, grey silica tetrahedra and green alumina tetrahedra.

In the case of the Cs-LTA framework, the theoretical compression mechanism was not determined by GASP simulation. The presence of cesium cations in the LTA framework (as described in Table 3.12) caused significant clashes (i.e. steric strain) with the framework oxygen atoms around the site 1 cation positions, which resulted in a LTA framework without a flexibility window. This is due to the relatively large ionic radius of the cesium cations compared to sodium, calcium and potassium. Cesium cations located in site I (6-ring face) were expected to cause more steric strain than those located in site II (8-ring face) positions. This emphasises the importance of cation size, as this factor influences the type of building units formed which in turn directs the crystallisation of specific zeolite frameworks (Yu, 2007).

In this geometric simulation study, it was determined that small sodium cations easily fill cation site I corresponding to the 6-ring opening of the sodalite unit as well as the cation site II corresponding to the 8-ring opening of the alpha cage. The presence of sodium as extra-framework species in the LTA framework did not cause steric strain or influence the compression mechanism of the framework and the overall flexibility of the framework was retained. On the other hand, relatively larger potassium cations resulted in steric hinderance which significantly influenced the compression behaviour of the framework and reduced the overall framework flexibility. The implication of these geometric simulations is that sodium cations allow for greater flexibility of the LTA framework during zeolite A synthesis and will therefore guide its formation more favourably than relatively larger cations such as potassium and cesium. For zeolite A synthesis, potassium cations may therefore be referred to as structure-breaking agents (due to the symmetry-breaking effect caused by steric strain on the LTA framework). Furthermore, relatively larger cesium cations may also be considered structure-breaking agents in the synthesis of zeolite A (since no flexibility window was observed). Based on the results presented in this study for calcium, it is proposed that the poor structure-direction often observed in the presence of calcium cations, as reported in literature (Petrik et al., 1995; Petrik, 2009; Valdés et al., 2006), may be due to the electrostatic effects caused by the divalent cations during the crystallisation process.

This simple geometric modelling study (using GASP software) therefore illustrates the importance of cation properties (such as size and location) as charge-balancing species on the formation of zeolites. The structure-directing effect of a specific cation is also influenced by the topology of the zeolite framework. As reported in literature, zeolite frameworks with sodalite or gmelinite cages are preferentially formed in the presence of sodium cations, while frameworks consisting of cancrinite cages were preferentially formed in the presence of potassium cations (or other relatively large cations) (Yu, 2007). Zeolite frameworks with relatively larger pore networks such as KFI, LTL, MER and RHO are able to accommodate potassium or cesium cations as charge-balancing species. In these cases, potassium and cesium cations are considered structure-directing agent (Auerbach et al., 2003; Čejka et al., 2007; Chatelain et al., 1995; Liu et al., 2010; Nearchou and Sartbaeva, 2015; Yu, 2007). This type of GASP geometric evaluation may therefore be extended to understanding the potential steric effect of various cations on the formation of different zeolite framework topologies.

7.4 Comparison of the experimental results for M-ZSM-5 (MFI) synthesis and GASP geometric simulations of M-LTA frameworks

In this study, zeolite ZSM-5 (MFI framework type) was synthesised in the presence of different extra-framework cations (together with sodium cations originating from the CFA-derived silicon precursor) to determine the influence of inorganic cation type on the morphology and formation of zeolite ZSM-5. In these dual-cation synthesis environments, inorganic cations compete with sodium cations for positions as charge-balancing species. Depending on the size and location of these cations (as well as cationic charge), zeolite formation may either be enhanced, unaffected or impeded.

As observed in Section 6.2.6, monovalent cations (sodium and potassium) favoured the formation of highly crystalline zeolite ZSM-5 while divalent calcium cations significantly retarded the crystallisation of zeolite ZSM-5, even though sodium cations were present in the synthesis mixture. The crystallisation of zeolite ZSM-5 was impeded in the presence of cesium cations (in the presence of sodium cations) compared to the sodium and potassium synthesis systems; this was attributed to the relatively larger cationic radius of the cesium cation compared to sodium as well as potassium. In this study, monovalent sodium and potassium cations are therefore considered "structure-directing' agents for the synthesis of zeolite ZSM-5. Conversely, divalent calcium is thought to be a "structure-breaking" cation for zeolite ZSM-5 synthesis, which is likely due to the electrostatic interactions of these cations in aqueous solution during the crystallisation process (as reported for the zeolite A case study). Although cesium cations altered the crystallisation of zeolite ZSM-5, the formation of zeolite ZSM-5 in the presence of cesium cations was achieved. Therefore, cesium is also thought to be a structure-directing agent for zeolite ZSM-5.

The crystallisation of MFI framework in the presence of different cations did not completely mirror the geometric simulation results for the model M-LTA framework. This may be due to the difference in (i) the total number of cations present in the LTA and MFI framework and/or (ii) the geometry of the LTA and MFI framework. Zeolite A (LTA) commonly contains 12 monovalent cations per unit cell, while zeolite ZSM-5 is expected to contain fewer cations per unit cell due to the relatively higher SAR value of the material (McCusker and Baerlocher, 2007). An illustraion of the small-pore LTA and medium-pore MFI frameworks are depicted in Figure 7.9 showing the largest pore openings for each framework.

The largest pore opening for the LTA framework is the 8-ring window of the alpha-cage, which has a diameter of ~ 0.45 nm. This is relatively smaller than the largest pore opening of the MFI framework (a 10-ring window with a diameter of ~ 0.55 nm), as depicted in Figure 7.9.

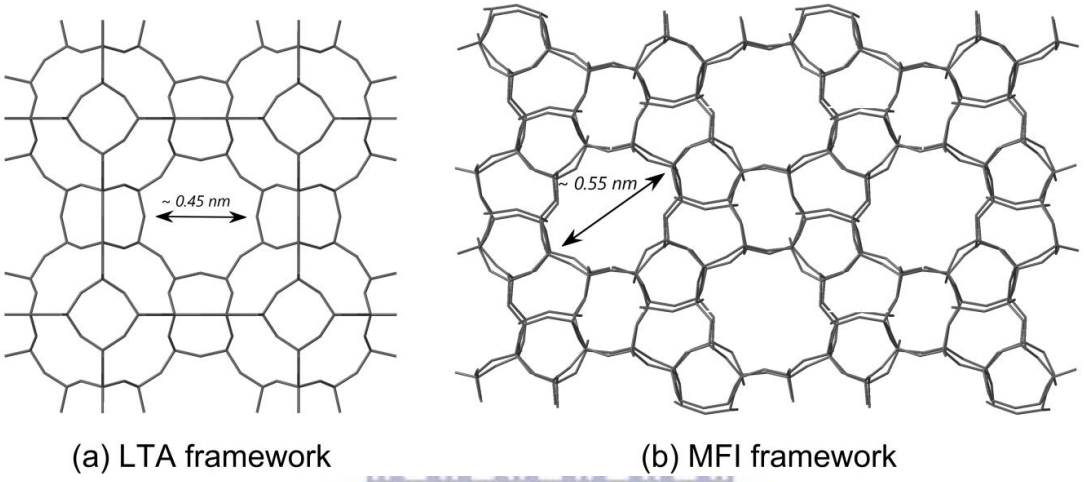

Figure 7.9: The pore openings of the (a) LTA and (b) MFI framework

The typical cation sites for zeolite A (LTA) were outlined previously and illustrated in Figure 7.4. The cation sites for zeolite ZSM-5 (MFI) are reported to be (i) in the 5-ring along the straight channel, (ii) in the 5-ring along the sinusoidal channel and (iii) in the alpha site of the framework (inside the 10-ring pore channel) (Zhidomirov et al., 2012). The 10-ring channels of the MFI framework may therefore easily accommodate cations that are relatively larger than sodium (such as potassium and cesium), without causing the steric strain observed in the LTA framework (as depicted in Figure 7.8). The difference in the geometry of the LTA and MFI framework is therefore thought to be responsible for the favourable synthesis of zeolite ZSM-5 in the presence of relatively larger cations (such as potassium and cesium) in this study. Similar results were reported in the literature for the synthesis of zeolite ZSM-5 in the presence of different cations (sodium and potassium) (Petrik, 2009).

Based on the geometric simulation results in this study, the presence of inorganic cations (in addition to sodium cations) in CFA is not thought to be detrimental to the formation of zeolites from CFA with the exception of calcium cations; this has been proven experimentally for a few zeolites (Chang and Shih, 2000; Missengue et al., 2018; Musyoka et al., 2014; Ndlovu et al., 2017; Shigemoto et al., 1995). However, the crystallisation processes

involved in zeolite synthesis may be influenced by the presence of relatively larger cations in the synthesis mixture due to short-range steric strain caused in the zeolite framework by these extra-framework species, depending on the framework topology of the target zeolite as well as the relative concentration of the inorganic cationic impurities. These changes in the crystallisation kinetics of zeolites may be responsible for the hierarchical morphology of zeolite X synthesised from CFA (Musyoka et al., 2014); as well as the hierarchical morphology of zeolite mordenite synthesised from a CFA-derived silicon precursor in this study (as depicted in Figure 5.26, Section 5.2.6).

7.5 Chapter Summary

The geometric and steric influence of extra-framework cations on the flexibility of the LTA framework was investigated using GASP software. The siliceous and aluminosilicate LTA frameworks were modelled as empty structures and compared to cation-containing LTA structures (Na-LTA, Ca-LTA, K-LTA and Cs-LTA). The theoretical compressibility of the LTA framework was observed to be sensitive to the presence of framework aluminium due to relatively longer Al-O bond lengths that resulted in more flexibility of T-O-Si bridging angles. In turn, this gives rise to a more flexible and open zeolite framework. The theoretical compressibility of the LTA framework was unrestricted by the presence of relatively small extra-framework cations such as sodium and calcium. On the other hand, relatively larger extra-framework cations (such as potassium and cesium) restricted the theoretical compressibility of the LTA framework. In the case of Cs-LTA, no flexibility window was observed. The presence of large extra-framework potassium cations altered the compression mechanism of the LTA (with respect to empty aluminosilicate LTA and Na-LTA). It should be noted that the structure-directing/breaking effect observed in this study for zeolite A (with LTA framework) based on inorganic cation size is limited to relatively small-pore zeolites with similar framework topologies; this effect may therefore be different for medium- and large-pore zeolite frameworks.

It was therefore concluded that cation size and charge as well as location may play a significant role in the structure-direction and formation of flexible, open zeolite frameworks. Furthermore, the presence of impurities (such as inorganic cations) in CFA is not thought to be detrimental to zeolite formation but may impede crystallisation processes due to the short-range steric effects caused by relatively larger cations (such as potassium and cesium), depending on zeolite framework topology.

8 Chapter 8 - Conclusions and recommendations

8.1 Introduction

This chapter serves to present the main findings of the study as well as recommendations for research that may be carried out in this field in the future.

8.2 Main findings of the study

The utilisation of a CFA-derived silicon precursor as feedstock for high-silica zeolite synthesis was achieved in this study, without the need for (i) treatment with a chelating agent (typically utilised to enhance the SAR value of the synthesis mixture and to remove excess sodium cations) or (ii) additional silicon sources (also commonly utilised to enhance the SAR value of the synthesis mixture). The synthesis of pure, highly crystalline, high-silica zeolites (such as zeolite mordenite and ZSM-5) from a waste material was achieved in this study as well as the synthesis of purely siliceous MFI-type framework material silicalite-1. Overall, CFA was converted to (i) pure, high-silica zeolites from the CFA-derived silicon precursor as well as (ii) a high yield of sodalite from the solid residue generated during the alkaline activation step. The preparation of high-silica zeolite mordenite and ZSM-5 (as well as silicalite-1) in this manner therefore provides a near-zero waste process for the conversion of CFA to value-added, high-silica zeolitic materials. Furthermore, geometric modelling by GASP software was used in this study to illustrate the steric influence of different extra-framework cations on the flexibility (and hence, synthetic feasibility) of a model zeolite framework (i.e. the LTA framework). More details on these findings will be presented in the following sections.

8.2.1 Preparation of the CFA-derived silicon feedstock

The extraction of a highly siliceous precursor material (FASE) from CFA was achieved in this study by using two steps; (i) a magnetic separation process to remove the iron-containing mineral phases from CFA yielding the magnetic fraction (MF) and (ii) a relatively low-temperature alkaline treatment of the non-magnetic fraction (NMF) of CFA was carried out by mixing NMF with an 8.0 M NaOH solution at a solid-to-liquid ratio of 1:5 under reflux conditions (150 °C for 24 hours) for the dissolution and precipitation of the silicon precursor material (FASE).

The magnetic separation process was found to be a simple method for the separation and enrichment of the components in CFA such as REEs (into the NMF material) and transition metals (into the MF material), which is a significant finding for the extraction of specific components from CFA for different applications. The extraction of a silicon precursor material (FASE) was achieved using a relatively low-temperature alkaline method. The extracted silicon precursor material (FASE) was silicon-rich and contained a low level of aluminium (with a SAR value of ~72) and almost no iron was present in the FASE material (due to the magnetic separation process). Therefore, the CFA-derived silicon precursor material (FASE) generated in this study served as silicon feedstock for high-silica zeolite synthesis without the need for an extra silicon source (for SAR enrichment) or treatment with a chelating agent (for SAR enrichment and removal of excess sodium). Furthermore, the silicon extraction method resulted in the formation of sodalite (with a high yield) as a by-product of the extraction process. The utilisation of CFA for the synthesis of pure, high-silica zeolites using this methodology therefore presents a method that is closer to a zero-waste synthesis route from an alternative feedstock (such as CFA), compared to methods utilised in literature to date.

8.2.2 Synthesis of large-pore MOR-type framework zeolites

In this study, zeolite mordenite (with large-pore MOR-type framework) was synthesised from a CFA-derived silicon feedstock using three different hydrothermal synthesis approaches; (i) OSDA-free synthesis (1 SiO_2•0.019 Al_2O_3•0.57 Na_2O•30.1 H_2O), (ii) seed-assisted synthesis (1 SiO_2•0.019 Al_2O_3•0.57 Na_2O•30.1 H_2O with 0.1 wt% seeds) and (iii) OSDA-assisted synthesis (1 SiO_2•0.019 Al_2O_3•0.46 Na_2O•0.26 TEAOH•30.1 H_2O with no added seed crystals nor NaOH), carried out under static hydrothermal conditions (170 °C for up to 72 hours). In the OSDA-free synthesis approach, highly crystalline zeolite mordenite was synthesised using a CFA-derived silicon precursor material (FASE) as the sole source of silicon, without the utilisation of an extra purification step prior to hydrothermal treatment to remove excess sodium and enhance the SAR value of the feedstock. This is the first study to present the conversion of CFA to zeolite mordenite in this manner, according to literature reported to date.

The seed-assisted synthesis of zeolite mordenite from a CFA-derived silicon precursor (FASE) allowed for the enhanced crystallisation of zeolite mordenite, while suppressing the formation of competing mineral phases such as zeolite Na-P1 and analcime resulting in a

reduced overall crystallisation time for highly pure and crystalline zeolite mordenite formation. It is noteworthy that this effect was achieved using a relatively small quantity of commercial mordenite seed crystals (0.1 wt%). The utilisation of the seed-assisted synthesis method for zeolite mordenite (from a CFA-derived silicon precursor) also allowed for the control of zeolite mordenite morphology in terms of particle shape (from spherical agglomerated crystals to elongated needle-like crystals) and crystal size (from 2.5 to 4.6 µm), depending on the synthesis conditions utilised.

The OSDA-assisted synthesis of zeolite mordenite from a CFA-derived silicon precursor (FASE) resulted in the formation of pure, highly crystalline zeolite mordenite, by using only a small quantity of TEAOH (n = 0.26) and no added seed crystals, and allowed for the extension of the boundary conditions for zeolite mordenite formation in terms of the SAR value of the synthesis mixture. Furthermore, it was found that the need for a mineralising agent such as NaOH in the crystallisation of pure, crystalline zeolite mordenite was not required due to the utilisation of a small quantity of TEAOH (which served as both mineralising agent and OSDA agent) in the synthesis mixture. The utilisation of TEAOH as an OSDA agent in the synthesis of zeolite mordenite also allowed for control over properties of the zeolite material such as morphology and composition. The morphology of zeolite mordenite crystals changed in terms of particle shape (with prismatic, twinned prismatic, hierarchical and spherical agglomerated crystals observed) and particle size (from 5 to 10 µm), while the SAR value of zeolite mordenite crystals varied between 10 and 15, depending on the synthesis conditions utilised. This study also presented the first synthesis of zeolite mordenite with hierarchical morphology without the utilisation of complex OSDA agents such as CTAB or other organosilane compounds (according to literature presented to date). Therefore, this study illustrated that it is possible to control the properties of zeolite mordenite (such as morphology and composition in terms of SAR value) synthesised from a CFA-derived silicon precursor by using these three different types of synthesis approaches, which is vital for the preparation of zeolites tailor-made for particular applications.

8.2.3 Synthesis of medium-pore MFI-type framework zeolites

In this study, medium-pore MFI-type framework zeolites such as ZSM-5 and silicalite-1 were synthesised from a CFA-derived silicon precursor material (FASE) as the sole source of silicon, without the utilisation of an extra purification step prior to hydrothermal treatment to remove excess sodium and enhance the SAR value of the feedstock; illustrating that zeolite

ZSM-5 crystallisation is possible from a CFA-derived silicon feedstock in high sodium synthesis environments.

MFI-type zeolite materials (ZSM-5 and silicate-1) with a range of different properties such as morphology, composition, hydrophilicity and porosity were synthesised from a CFA-derived silicon precursor (FASE) in this study; from aluminium-rich, prismatic zeolite ZSM-5 crystals that were highly hygroscopic and microporous (1 SiO_2•0.015 Al_2O_3•0.53 Na_2O•0.10 TPABr•28.3 H_2O) to silicon-rich, spherical zeolite ZSM-5 crystals with both microporosity and mesoporosity (1 SiO_2•0.004 Al_2O_3•0.54 Na_2O•0.10 TPABr•35.4 H_2O) as well as hydrophobic, all-silica silicate-1 crystals (1 SiO_2•0.004 Al_2O_3•0.49 Na_2O•0.09 TPABr•11.6 H_2O) prepared under hydrothermal conditions of 160 or 170 °C for up to 72 hours This study presents the first synthesis of silicate-1 from CFA, as well as the first synthesis of zeolite ZSM-5 from a CFA-derived silicon precursor (FASE) with a range of different properties (without the need for SAR enrichment by the addition of an extra silicon source or treatment with a chelating agent), according to literature to date. This study therefore provides simple synthesis routes for the design of tailor made, pure MFI-type zeolite materials (such as ZSM-5 and silicalite-1) from CFA with various properties such as crystal size, composition (SAR, solid acidity), hydrophilicity/hydrophobicity and porosity, which is of vital importance to industries that make use of MFI-type zeolites (ZSM-5 and silicalite-1) for processes involving catalysis and adsorption as well as separation science.

8.2.4 Steric influence of extra-framework inorganic cations on the LTA framework (zeolite A)

This study also utilised geometric simulations by GASP software to understand the influence of different inorganic, extra-framework cations (Na^+, Ca^{2+}, K^+ and Cs^+) on a model zeolite such as zeolite A (with small-pore, LTA framework). The theoretical compressibility (which is an indicator of synthetic feasibility) of zeolite A was unrestricted in the presence of sodium and calcium cations, while potassium cations restricted the theoretical compressibility of zeolite A and altered the compression mechanism. The theoretical compressibility of zeolite A was completely hindered by the presence of cesium cations as extra-framework cations (with no framework flexibility observed). It was therefore proposed that relatively small, monovalent cations served as structure-directing agents in the formation of zeolite A, while relatively larger cations such as cesium cations may behave as a structure-breaking agent in the formation of zeolite A. The steric influence of the different inorganic, extra-framework

cations is dependent on cation size as well as the framework topology of the zeolite (in this case a small-pore zeolite such as zeolite A was studied); this effect may therefore be different in zeolites with medium- and large-pore framework topologies such as zeolite ZSM-5 and mordenite. This geometric simulation study using GASP software served to illustrate that the various components in CFA are not detrimental to the formation of zeolites depending on the cation size and charge as well as the framework topology of the desired zeolite. However, relatively larger inorganic cations in CFA may impede the crystallisation processes involved in zeolite synthesis by causing short-range disorder through steric strain in the growing zeolite framework.

8.3 Recommendations for future studies

- In this study, a two-step process (involving magnetic separation and a low-temperature alkaline silicon extraction method) was utilised for the preparation of a silicon precursor (FASE) from CFA. The CFA-derived silicon precursor (FASE) was in turn utilised as silicon feedstock for high-silica zeolite synthesis. It is proposed that the magnetic separation process may be removed from the protocol, to further simplify the process of silicon extraction from CFA. However, it should be noted that the presence of iron in the feedstock for zeolite synthesis may influence the crystallisation process.
- In this study, a relatively low yield of pure, high-silica zeolites from a CFA-derived silicon feedstock was achieved that may be improved by further optimisation of the silicon extraction process. The silicon extraction process also produced a high yield of sodalite, which may be used in various gas adsorption applications. Furthermore, the silicon extraction process may also be optimised for high yields other low-silica zeolites as the by-product of the silicon precursor extraction process, such as zeolite A and X, which have great value in various applications such as catalysis and adsorption.
- Further characterisation and application of zeolite mordenite samples synthesised from a CFA-derived silicon precursor (FASE) is required to determine the quality and catalytic activity of these CFA-derived zeolites compared to commercially available zeolite mordenite.

- Similarly, further characterisation and catalytic application of zeolite ZSM-5 samples synthesised from a CFA-derived silicon precursor (FASE) is required for comparison with commercially available zeolite ZSM-5.
- The influence of various synthesis parameters on the formation of silicalite-1 from the CFA-derived silicon precursor (FASE) may be investigated further as well as the application of CFA-derived silicalite-1 in various separation applications that require hydrophobic materials.
- In terms of the geometric simulation study (using GASP software) that was utilised to determine the influence of different inorganic, extra-framework cations on the theoretical compressibility (i.e. synthetic feasibility) of zeolite A; the same type of geometric simulation study may be carried out on other zeolite frameworks (using refined zeolite structures with known cation positions and content).

References

Ahmed, K. R., Travkina, O. S., Grigor'eva, N. G., & Kutepov, B. I. (2018). Catalytic activity of mordenite from natural source in the dimerization of α-methylstyrene. *IOP Conference Series: Materials Science and Engineering*, 454, 012029. https://doi.org/10.1088/1757-899X/454/1/012029

Aly, H. M., Moustafa, M. E., & Abdelrahman, E. A. (2012). Synthesis of mordenite zeolite in absence of organic template. *Advanced Powder Technology*, 23 (6), 757-760. https://doi.org/10.1016/j.apt.2011.10.003

Ameh, A. E., Musyoka, N. M., Fatoba, O. O., Syrtsova, D. A., Teplyakov, V. V., & Petrik, L. F. (2016). Synthesis of zeolite NaA membrane from fused fly ash extract. *Journal of Environmental Science and Health, Part A*, 51 (4), 348-356. https://doi.org/10.1080/10934529.2015.1109410

Aono, H., Kaji, N., Itagaki, Y., Johan, E., & Matsue, N. (2016). Synthesis of mordenite and its composite material using chemical reagents for Cs decontamination. *Journal of the Ceramic Society of Japan*, 124 (5), 617-623. https://doi.org/10.2109/jcersj2.15317

Aono, H., Kunimoto, T., Takahashi, R., Itagaki, Y., Johan, E., & Matsue, N. (2018). Cs+ decontamination properties of mordenites and composite materials synthesized from coal fly ash and rice husk ash. *Journal of Asian Ceramic Societies*, 6 (3), 213-221. https://doi.org/10.1080/21870764.2018.1489940

Araya, A., & Lowe, B. M. (1986.). Effect of organic species on the synthesis and properties of ZSM-5. *Zeolites*, 6 (2), 111-118.

Auerbach, S., Carrado, K., & Dutta, P. (2003). Handbook of Zeolite Science and Technology. The United States of America: Marcel Dekker, Inc. https://doi.org/10.1201/9780203911167

Baerlocher, C., & McCusker, L. B. (2017). Database of Zeolite Structures. Retrieved October 1, 2018, from http://www.iza-structure.org/databases/

Blissett, R. S., & Rowson, N. A. (2012). A review of the multi-component utilisation of coal fly ash. *Fuel*, 97, 1-23. https://doi.org/10.1016/j.fuel.2012.03.024

Böke, N., Birch, G. D., Nyale, S. M., & Petrik, L. F. (2015). New synthesis method for the production of coal fly ash-based foamed geopolymers. *Construction and Building Materials*, 75, 189-199. https://doi.org/10.1016/j.conbuildmat.2014.07.041

Bourgeat-Lami, E., Renzo, F. D., Fajula, F., Mutin, P. H & Des Courieres, T. (1992). Mechanism of the thermal decomposition of tetraethylammonium in zeolite beta. *Journal of Physical Chemistry*, 96 (9), 3807-3811.

Bowman, R. S. (2003). Applications of surfactant-modified zeolites to environmental remediation. *Microporous and Mesoporous Materials*, 61 (1), 43-56. https://doi.org/10.1016/S1387-1811(03)00354-8

Breck, D. W., Eversole, W. G., Milton, R. M., Reed, T. B., & Thomas, T. L. (1956). Crystalline Zeolites. I. The properties of a new synthetic zeolite, type A. *Journal of the American Chemical Society*, 78 (23), 5963-5971. https://doi.org/10.1021/ja01604a001

Brichni, A., Hammi, H., Aggoun, S., & Mnif, A. (2016). Optimisation of magnesium oxychloride cement properties by silica glass. *Advances in Cement Research*, 28 (10), 654-663. https://doi.org/10.1680/jadcr.16.00024

Burkett, S. L., & Davis, M. E. (1995). Mechanisms of structure direction in the synthesis of pure-silica zeolites. 1. Synthesis of TPA/Si-ZSM-5. *Chemistry of Materials*, 7 (5), 920-928. https://doi.org/10.1021/cm00053a017

Burton, A. W., & Zones, S. I. (2007). Organic molecules in zeolite synthesis: Their preparation and structure-directing effects. In Introduction to Zeolite Science and Practice. Edited by Čejka, J., van Bekkum, H., Corma, A., & Schüth, F. The Netherlands: Elsevier B. V. https://doi.org/10.1016/S0167-2991(07)80793-2

Čejka, J., van Bekkum, H., Corma, A., & Schüth, F. (2007). Introduction to zeolite science and practice. 3rd Edition. Retrieved October 2, 2018 from http://public.eblib.com/choice/publicfullrecord.aspx?p=311426

Chang, H.-L., & Shih, W.-H. (2000). Synthesis of zeolites A and X from fly ashes and their ion-exchange behavior with cobalt ions. *Industrial & Engineering Chemistry Research*, 39 (11), 4185-4191. https://doi.org/10.1021/ie990860s

Chareonpanich, M., Namto, T., Kongkachuichay, P., & Limtrakul, J. (2004). Synthesis of ZSM-5 zeolite from lignite fly ash and rice husk ash. *Fuel Processing Technology*, 85 (15), 1623-1634. https://doi.org/10.1016/j.fuproc.2003.10.026

Chatelain, T., Patarin, J., Fousson, E., Soulard, M., Guth, J. L., & Schulz, P. (1995). Synthesis and characterization of high-silica zeolite RHO prepared in the presence of 18-crown-6 ether as organic template. *Microporous Materials*, 4 (2), 231-238. https://doi.org/10.1016/0927-6513(95)00009-X

Chen, H., Wang, Y., Sun, C., Wang, X., & Wang, C. (2018). Synthesis of hierarchical ZSM-5 zeolites with CTAB-containing seed silicalite-1 and its catalytic performance in methanol to propylene. *Catalysis Communications*, 112, 10-14. https://doi.org/10.1016/j.catcom.2018.04.017

Cheng, C.-H., & Shantz, D. F. (2005). Silicalite-1 growth from clear solution: Effect of the structure-directing agent on growth kinetics. *The Journal of Physical Chemistry B*, 109 (29), 13912-13920. https://doi.org/10.1021/jp050733b

Cheng, Y., Liao, R. H., Li, J. S., Sun, X. Y., & Wang, L. J. (2008). Synthesis research of nanosized ZSM-5 zeolites in the absence of organic template. *Journal of Materials Processing Technology*, 206 (1-3), 445-452. https://doi.org/10.1016/j.jmatprotec.2007.12.054

Choudhury, M., Borthakur, P. C., & Borac, T. (1998). Synthesis and characterisation of silicious mordenite. *Indian Journal of Chemical Technology*, 5, 1-6.

Corma, A. (2003). State of the art and future challenges of zeolites as catalysts. *Journal of Catalysis*, 216 (1-2), 298-312. https://doi.org/10.1016/S0021-9517(02)00132-X

Coudurier, G., Naccache, C., & Vedrine, J. C. (1982). Uses of i.r. spectroscopy in identifying ZSM zeolite structure. *Journal of the Chemical Society, Chemical Communications*, (24), 1413-1415. https://doi.org/10.1039/c39820001413

Criado, M., Fernández-Jiménez, A., & Palomo, Á. (2007). Alkali activation of fly ash: Effect of the SiO_2/Na_2O ratio: Part I: FTIR study. *Microporous and Mesoporous Materials*, 106 (1-3), 180-191. https://doi.org/10.1016/j.micromeso.2007.02.055

Cubillas, P. & Anderson, M. W. (2010). Synthesis mechanism: Crystal growth and nucleation. In Zeolites and Catalysis: Synthesis, Reactions and Applications. Edited by

Čejka, J., Corma, A. & Zones, S. Germany: Wiley-VCH Verlag GmbH & Co. KGaA. https://doi.org/10.1002/9783527630295.ch1

Cundy, C. S., & Cox, P. A. (2003). The hydrothermal synthesis of zeolites: History and development from the earliest days to the present time. *Chemical Reviews*, 103 (3), 663-702. https://doi.org/10.1021/cr020060i

Cundy, C. S., & Cox, P. A. (2005). The hydrothermal synthesis of zeolites: Precursors, intermediates and reaction mechanism. *Microporous and Mesoporous Materials*, 82 (1-2), 1-78. https://doi.org/10.1016/j.micromeso.2005.02.016

Cysneiros, O. M. S., Silva, B. J. B., Silva, A. O. S., Alencar, S. L., Santos, R. B., Soares, P. F. M., Mendonca, T. R. D., Sousa Junior, L. V., Santos, J. R. (2016). Crystallization of mordenite zeolite with seed addition in reaction mixtures with different SiO_2/Al_2O_3 ratios. *Scientia Plena*, 12 (4), 1-11.

Dai, G., Hao, W., Xiao, H., Ma, J., & Li, R. (2017). Hierarchical mordenite zeolite nano-rods bundles favourable to bulky molecules. *Chemical Physics Letters*, 686, 111-115. https://doi.org/10.1016/j.cplett.2017.08.036

Davis, M. E., & Lobo, R. F. (1992). Zeolite and molecular sieve synthesis. *Chemistry of Materials*, 4 (4), 756-768. https://doi.org/10.1021/cm00022a005

Dawson, C. J., Kapko, V., Thorpe, M. F., Foster, M. D., & Treacy, M. M. J. (2012). Flexibility as an indicator of feasibility of zeolite frameworks. *Journal of Physical Chemistry C*, 116 (30), 16175-16181. https://doi.org/10.1021/jp2107473

Deutschmann, O., Knözinger, H., Kochloefl, K., & Turek, T. (2009). Heterogeneous catalysis and solid catalysts. In Ullmann's Encyclopedia of Industrial Chemistry. Germany: Wiley-VCH Verlag GmbH & Co. KGaA. https://doi.org/10.1002/14356007.a05_313.pub2

Di Renzo, F., Remoué, F., Massiani, P., Fajula, F., Figueras, F., & Thierry Des, C. (1991). Crystallization kinetics of zeolite TON. *Zeolites*, 11 (6), 539-548. https://doi.org/10.1016/S0144-2449(05)80002-8

Du, X., & Wu, E. (2007). Porosity of microporous zeolites A, X and ZSM-5 studied by small angle X-ray scattering and nitrogen adsorption. *Journal of Physics and Chemistry of Solids*, 68 (9), 1692-1699. https://doi.org/10.1016/j.jpcs.2007.04.013

Eskom Integrated results for 2015, Facts sheet with additional information. (2015). Retrieved June 27, 2019, from Eskom website: http://www.eskom.co.za/IR2015/Pages/Default.aspx

Eulenberger, G. R., Shoemaker, D. P., & Keil, J. G. (1967). Crystal structures of hydrated and dehydrated synthetic zeolites with faujasite aluminosilicate frameworks. I. The dehydrated sodium, potassium, and silver forms. *The Journal of Physical Chemistry*, 71 (6), 1812-1819. https://doi.org/10.1021/j100865a040

Eze, C. P., Fatoba, O., Madzivire, G., Ostrovnaya, T. M., Petrik, L. F., Frontasyeva, M. V., & Nechaev, A. N. (2013). Elemental composition of fly ash: A comparative study using nuclear and related analytical techniques. *Chemistry-Didactics-Ecology-Metrology*, 18 (1-2), 19-29. https://doi.org/10.2478/cdem-2013-0014

Feijen, E. J. P., Martens, J. A., & Jacobs, P. A. (1994). Zeolites and their mechanism of synthesis. In Zeolites and Related Microporous Materials: State of the Art 1994 - Proceedings of the 10th International Zeolite Conference, Garmisch-Partenkirchen, Germany, 17-22 July 1994. Edited by Weitkamp, J., Karge, H.G., Pfeifer, H., & Hölderich, W. https://doi.org/10.1016/S0167-2991(08)64074-4

Fernández-Jiménez, A., & Palomo, Á. (2005). Mid-infrared spectroscopic studies of alkali-activated fly ash structure. *Microporous and Mesoporous Materials*, 86 (1-3), 207-214. https://doi.org/10.1016/j.micromeso.2005.05.057

Fletcher, R. E., Wells, S. A., Leung, K. M., Edwards, P. P., & Sartbaeva, A. (2015). Intrinsic flexibility of porous materials; theory, modelling and the flexibility window of the EMT zeolite framework. *Acta Crystallographica Section B Structural Science, Crystal Engineering and Materials*, 71 (6), 641-647. https://doi.org/10.1107/S2052520615018739

Frantz, T. S., Ruiz, W. A., da Rosa, C. A., & Mortola, V. B. (2016). Synthesis of ZSM-5 with high sodium content for CO_2 adsorption. *Microporous and Mesoporous Materials*, 222, 209-217. https://doi.org/10.1016/j.micromeso.2015.10.022

Franus, W. (2012). Characterization of X-type zeolite prepared from coal fly ash. *Polish Journal of Environmental Studies*, 21 (2), 337-343.

Gabelica, Z., J, B. N., Derouane, E. G., & Gilson, J.-P. (1984). The use of combined thermal analysis to study crystallization, pore structure, catalytic activity and deactivation of synthetic zeolites. *Clay Minerals*, 19 (5), 803-824. https://doi.org/10.1180/claymin.1984.019.5.10

Gao, Y., Wu, G., Ma, F., Liu, C., Jiang, F., Wang, Y., & Wang, A. (2016). Modified seeding method for preparing hierarchical nanocrystalline ZSM-5 catalysts for methanol aromatisation. *Microporous and Mesoporous Materials*, 226, 251-259. https://doi.org/10.1016/j.micromeso.2015.11.066

Gilbert, C. (2013). Synthesis and characterisation of iron nanoparticles by extraction from iron rich waste material for the remediation of acid mine drainage (MSc Thesis). University of the Western Cape, Bellville, Cape Town, South Africa.

Gitari, M. W., Musyoka, N. M., & Petrik, L. F. (2016). Hydrothermal conversion of South African coal fly ash into pure phase zeolite Na-P1. Zeolites - Useful Minerals. https://doi.org/10.5772/63399

Grand, J., Awala, H., & Mintova, S. (2016). Mechanism of zeolites crystal growth: New findings and open questions. *CrystEngComm*, 18 (5), 650-664. https://doi.org/10.1039/C5CE02286J

Haber, J., Block, J. H., & Delmon, B. (2009). Manual of methods and procedures for catalyst characterization (Technical Report). *Pure and Applied Chemistry*, 67 (8-9), 1257-1306. https://doi.org/10.1351/pac199567081257

Hagen, J. (2015). Industrial catalysis: A practical approach. 3rd Edition. Germany: WILEY-VCH Verlag GmbH & Co. KGaA.

Hamilton, K. E., Coker, E. N., Sacco, A., Dixon, A. G., & Thompson, R. W. (1993). The effects of the silica source on the crystallization of zeolite NaX. *Zeolites*, 13 (8), 645-653. https://doi.org/10.1016/0144-2449(93)90137-R

Hanif, N., Anderson, M. W., Alfredsson, V., & Terasaki, O. (2000). The effect of stirring on the synthesis of intergrowths of zeolite Y polymorphs. *Physical Chemistry Chemical Physics*, 2 (14), 3349-3357. https://doi.org/10.1039/B002314K

Hartman, R. L., & Fogler, H. S. (2007). Understanding the dissolution of zeolites. *Langmuir*, 23 (10), 5477-5484. https://doi.org/10.1021/la063699g

Heidrich, C., Weir, A., & Feuerborn, H.-J. (2013). Coal combustion products: a global perspective. Retrieved April 4, 2019 from http://www.flyash.info

Henmi, T. (1987). Increase in cation exchange capacity of coal fly ash by alkali treatment. *Clay Science*, 6 (6), 277-282. https://doi.org/10.11362/jcssjclayscience1960.6.277

Herreros, B., He, H., Barr, T. L., & Klinowski, J. (1994). ESCA Studies of framework silicates with the sodalite structure: 1. Comparison of purely siliceous sodalite and aluminosilicate sodalite. *The Journal of Physical Chemistry*, 98 (4), 1302-1305. https://doi.org/10.1021/j100055a042

Hincapie, B. O., Garces, L. J., Zhang, Q., Sacco, A., & Suib, S. L. (2004). Synthesis of mordenite nanocrystals. *Microporous and Mesoporous Materials*, 67 (1), 19-26. https://doi.org/10.1016/j.micromeso.2003.09.026

Hölderich, W.F. & van Bekkum, H. (1991). Zeolites in Organic Syntheses. In Introduction to Zeolite Science and Practice. Edited by van Bekkum, H., Flanigen, E.M., & Jansen, J.C. The Netherlands: Elsevier B.V. https://doi.org/10.1016/S0167-2991(08)63614-9

Höller, H., & Wirsching, U. (1985). Zeolite formation from fly ash. *Fortschritte der Mineralogie*, 63 (1), 21-43.

Hollman, G. G., Steenbruggen, G., & Janssen-Jurkovičová, M. (1999). A two-step process for the synthesis of zeolites from coal fly ash. *Fuel*, 78 (10), 1225-1230. https://doi.org/10.1016/S0016-2361(99)00030-7

Holm, M. S., Taarning, E., Egeblad, K., & Christensen, C. H. (2011). Catalysis with hierarchical zeolites. *Catalysis Today*, 168 (1), 3-16. https://doi.org/10.1016/j.cattod.2011.01.007

Huang, S., Liu, X., Yu, L., Miao, S., Liu, Z., Zhang, S., Xie, S., & Xu, L. (2014). Preparation of hierarchical mordenite zeolites by sequential steaming-acid leaching-alkaline treatment. *Microporous and Mesoporous Materials*, 191, 18-26. https://doi.org/10.1016/j.micromeso.2014.02.039

Huang, Y., Wang, K., Dong, D., Li, D., Hill, M. R., Hill, A. J., & Wang, H. (2010). Synthesis of hierarchical porous zeolite NaY particles with controllable particle sizes. *Microporous and Mesoporous Materials*, 127 (3), 167-175. https://doi.org/10.1016/j.micromeso.2009.07.026

Hunger, M. (2010). Catalytically active sites: Generation and characterization. In Zeolites and Catalysis: Synthesis, Reactions and Applications. Edited by Čejka, J., Corma, A., & Zones, S. Germany: Wiley-VCH Verlag GmbH & Co. KGaA. https://doi.org/10.1002/9783527630295.ch17

Huo, Q. (2011). Synthetic chemistry of the inorganic ordered porous materials. In Modern Inorganic Synthetic Chemistry. Edited by Xu, R., Pang, W., & Huo, Q. The Netherlands: Elsevier B.V. https://doi.org/10.1016/B978-0-444-53599-3.10016-2

Idris, A., Khalil, U., AbdulAziz, I., Makertihartha, I. G. B. N., Subagjo, Laniwati, M., Al-Betar, A. -R., Mukti, R. R., & Muraza, O. (2019). Fabrication zone of OSDA-free and seed-free mordenite crystals. *Powder Technology*, 342, 992-997. https://doi.org/10.1016/j.powtec.2018.09.041

Isa, M. A., Chew, T. L., & Yeong, Y. F. (2018). Zeolite NaY synthesis by using sodium silicate and colloidal silica as silica source. *IOP Conference Series: Materials Science and Engineering*, 458, 012001. https://doi.org/10.1088/1757-899X/458/1/012001

Iwakai, K., Tago, T., Konno, H., Nakasaka, Y., & Masuda, T. (2011). Preparation of nano-crystalline MFI zeolite via hydrothermal synthesis in water/surfactant/organic solvent using fumed silica as the Si source. *Microporous and Mesoporous Materials*, 141 (1-3), 167-174. https://doi.org/10.1016/j.micromeso.2010.11.001

IZA Synthesis Commission. (2016). Retrieved April 4, 2019, from http://www.iza-online.org/synthesis/default.htm

Jin, Y., Li, Y., Zhao, S., Lv, Z., Wang, Q., Liu, X., & Wang, L. (2012). Synthesis of mesoporous MOR materials by varying temperature crystallizations and combining ternary organic templates. *Microporous and Mesoporous Materials*, 147 (1), 259-266. https://doi.org/10.1016/j.micromeso.2011.06.023

Johan, E., & Matsue, N. (2014). Synthesis of mordenite from diatomite and its application for VOCs adsorption. *Transactions of the Materials Research Society of Japan*, 39 (1), 23-26. https://doi.org/10.14723/tmrsj.39.23

Johan, E., Yoshida, K., Munthali, M. W., Matsue, N., Itagaki, Y., & Aono, H. (2015). Adsorption characteristics of Cs^+ onto artificial zeolites synthesized from coal fly ash and

diatomite. *Journal of the Ceramic Society of Japan*, 123 (1444), 1065-1072. https://doi.org/10.2109/jcersj2.123.1065

Jongkind, H., Datema, K. P., Nabuurs, S., Seive, A., & Stork, W. H. J. (1997). Synthesis and characterisation of zeolites using saturated cyclic amines as structure-directing agents. *Microporous Materials*, 10 (4), 149-161. https://doi.org/10.1016/S0927-6513(97)00005-9

Kadja, G. T. M., Mukti, R. R., Liu, Z., Rilyanti, M., Ismunandar, Marsih, I. N., Ogura, M., Wakihara, T., & Okubo, T. (2016). Mesoporogen-free synthesis of hierarchically porous ZSM-5 below 100 °C. *Microporous and Mesoporous Materials*, 226, 344-352. https://doi.org/10.1016/j.micromeso.2016.02.007

Kalyankar, A. N., Choudhari, A. L., & Joshi, A. A. (2011). Low frequency dielectric properties of fly ash based zeolite ZSM-5. *International Journal of Basic and Applied Research*, 1, 59-63.

Kamil, M. S. M., Manikandan, K., Elangovan, S. P., Ogura, M., & Cheralathan, K. K. (2015). Crystallization of amorphous silica to silicalite-1: Effect of nature of silica sources and tetrapropylammonium hydroxide concentration. *Indian Journal of Chemistry. Section A. Inorganic, physical, theoretical & analytical*, 54 (4), 469-477.

Kapko, V., Dawson, C., Treacy, M. M. J., & Thorpe, M. F. (2010). Flexibility of ideal zeolite frameworks. *Physical Chemistry Chemical Physics*, 12 (30), 8531-8541. https://doi.org/10.1039/c003977b

Kapure, G. P. (2017). Synthesis of valuable zeolitic material from coal fly ash as industrial waste, its post modification and characterizations. *International Research Journal of Science* and *Engineering*, 5 (4), 49-58.

Kim, G. J., & Ahn, W. S. (1991). Direct synthesis and characterization of high-SiO_2-content mordenites. *Zeolites*, 11 (7), 745-750. https://doi.org/10.1016/S0144-2449(05)80183-6

Köroğlu, H. J., Sarıoğlan, A., Tatlıer, M., Erdem-Şenatalar, A., & Tunç Savaşçı, Ö. (2002). Effects of low-temperature gel aging on the synthesis of zeolite Y at different alkalinities. *Journal of Crystal Growth*, 241 (4), 481-488. https://doi.org/10.1016/S0022-0248(02)01321-0

Krisnandi, Y. K., Yanti, F. M., & Murti, S. D. S. (2017). Synthesis of ZSM-5 zeolite from coal fly ash and rice husk: Characterization and application for partial oxidation of methane to methanol. *IOP Conference Series: Materials Science and Engineering*, 188, 012031. https://doi.org/10.1088/1757-899X/188/1/012031

Kruger, R. A. (1997). Fly ash beneficiation in South Africa: Creating new opportunities in the market-place. *Fuel*, 76 (8), 777-779. https://doi.org/10.1016/S0016-2361(96)00190-1

Krznaric, I., Antoni, T., Broni, J., Suboti, B., & Thompson, R. W. (2003). Influence of silica sources on the chemical composition of aluminosilicate hydrogels and the results of their hydrothermal treatment. *Croatica Chemica Acta*, 76 (1), 7-17.

Lafuente, B., Downs, R. T., Yang, H., & Stone, N. (2015). Highlights in Mineralogical Crystallography. Retrieved from http://rruff.info/

Lalena, J.N., Cleary, D.A., Carpenter, E.E., & Dean, N.F. (2008). Solid-liquid reactions. In Inorganic Materials Synthesis and Fabrication. The United States of America: John Wiley & Sons, Inc. https://doi.org/10.1002/9780470191576

Lauer, N. E., Hower, J. C., Hsu-Kim, H., Taggart, R. K., & Vengosh, A. (2015). Naturally occurring radioactive materials in coals and coal combustion residuals in the United States. *Environmental Science & Technology*, 49 (18), 11227-11233. https://doi.org/10.1021/acs.est.5b01978

Lercher, J.A. & Jentys, A. (2007). Infrared and raman spectroscopy for characterizing zeolites. In Introduction to Zeolite Science and Practice. Edited by Čejka, J., van Bekkum, H., Corma, A., & Schüth, F. The Netherlands: Elsevier B. V. https://doi.org/10.1016/S0167-2991(07)80801-9

Li, B., Sun, B., Qian, X., Li, W., Wu, Z., Sun, Z., Qiao, M., Duke, M., & Zhao, D. (2013). In-situ crystallization route to nanorod-aggregated functional ZSM-5 microspheres. *Journal of the American Chemical Society*, 135 (4), 1181-1184. https://doi.org/10.1021/ja309194z

Li, J., Corma, A., & Yu, J. (2015). Synthesis of new zeolite structures. *Chemical Society Reviews*, 44 (20), 7112-7127. https://doi.org/10.1039/C5CS00023H

Li, M., Oduro, I. N., Zhou, Y., Huang, Y., & Fang, Y. (2016). Amphiphilic organosilane and seed assisted hierarchical ZSM-5 synthesis: Crystallization process and structure.

Microporous and Mesoporous Materials, 221, 108-116. https://doi.org/10.1016/j.micromeso.2015.09.028

Li, X., Prins, R., & van Bokhoven, J. A. (2009). Synthesis and characterization of mesoporous mordenite. *Journal of Catalysis*, 262 (2), 257-265. https://doi.org/10.1016/j.jcat.2009.01.001

Liu, C., Gu, W., Kong, D., & Guo, H. (2014). The significant effects of the alkali-metal cations on ZSM-5 zeolite synthesis: From mechanism to morphology. *Microporous and Mesoporous Materials*, 183, 30-36. https://doi.org/10.1016/j.micromeso.2013.08.037

Liu, Q., Mace, A., Bacsik, Z., Sun, J., Laaksonen, A., & Hedin, N. (2010). NaKA sorbents with high CO_2-over-N_2 selectivity and high capacity to adsorb CO_2. *Chemical Communications*, 46 (25), 4502-4504. https://doi.org/10.1039/C000900H

Liu, X., Wang, Y., Cui, X., He, Y., & Mao, J. (2013). Influence of synthesis parameters on NaA zeolite crystals. *Powder Technology*, 243, 184-193. https://doi.org/10.1016/j.powtec.2013.03.048

Liu, Z., Zhu, J., Wakihara, T., & Okubo, T. (2019). Ultrafast synthesis of zeolites: Breakthrough, progress and perspective. *Inorganic Chemistry Frontiers*, 6 (1), 14-31. https://doi.org/10.1039/C8QI00939B

Livage, J. (1994). Sol-gel chemistry and molecular sieve synthesis. In Advanced Zeolite Science and Applications. Edited by Jansen, J.C., Stocker, M., Karge, H.G., & Weitkamp, J. The Netherlands: Elsevier B.V. https://doi.org/10.1016/S0167-2991(08)60763-6

Lobo, R. F. (2003). Introduction to the structural chemistry of zeolites. In Handbook of Zeolite Science and Technology. Edited by Auerbach, S. M., Carrado, K. A., & Dutta, P. K. The United States of America: Marcel Dekker, Inc. https://doi.org/10.1201/9780203911167-9

Lohse, U., Altrichter, B., Donath, R., Fricke, R., Jancke, K., Parlitz, B., & Schreier, E. (1996). Synthesis of zeolite beta. Part 1.-Using tetraethylammonium hydroxide/bromide with addition of chelates as templating agents. *J. Chem. Soc., Faraday Trans.*, 92 (1), 159-165. https://doi.org/10.1039/FT9969200159

Louis, B., & Kiwi-Minsker, L. (2004). Synthesis of ZSM-5 zeolite in fluoride media: An innovative approach to tailor both crystal size and acidity. *Microporous and Mesoporous Materials*, 74 (1-3), 171-178. https://doi.org/10.1016/j.micromeso.2004.06.016

Lu, B., Tsuda, T., Oumi, Y., Itabashi, K., & Sano, T. (2004). Direct synthesis of high-silica mordenite using seed crystals. *Microporous and Mesoporous Materials*, 76 (1), 1-7. https://doi.org/10.1016/j.micromeso.2004.07.008

Lu, B., Tsuda, T., Sasaki, H., Oumi, Y., Itabashi, K., Teranishi, T., & Sano, T. (2004). Effect of aluminum source on hydrothermal synthesis of high-silica mordenite in fluoride medium, and it's thermal stability. *Chemistry of Materials*, 16 (2), 286-291. https://doi.org/10.1021/cm030576y

Luo, J., Zhang, H., & Yang, J. (2016). Hydrothermal synthesis of sodalite on alkali-activated coal fly ash for removal of lead ions. *Procedia Environmental Sciences*, 31, 605-614. https://doi.org/10.1016/j.proenv.2016.02.105

Lv, A., Xu, H., Wu, H., Liu, Y., & Wu, P. (2011). Hydrothermal synthesis of high-silica mordenite by dual-templating method. *Microporous and Mesoporous Materials*, 145 (1), 80-86. https://doi.org/10.1016/j.micromeso.2011.04.027

Machado, F. J., López, C. M., Centeno, M. A., & Urbina, C. (1999). Template-free synthesis and catalytic behaviour of aluminium-rich MFI-type zeolites. *Applied Catalysis A: General*, 181 (1), 29-38. https://doi.org/10.1016/S0926-860X(98)00383-4

Maesen, T. (2007). The zeolite scene - An overview. In Studies in Surface Science and Catalysis. Edited by Čejka, J., van Bekkum, H., Corma, A., & Schüth, F. The Netherlands: Elsevier B. V. https://doi.org/10.1016/S0167-2991(07)80789-0

Maldonado, M., Oleksiak, M. D., Chinta, S., & Rimer, J. D. (2013). Controlling crystal polymorphism in organic-free synthesis of Na-zeolites. *Journal of the American Chemical Society*, 135 (7), 2641-2652. https://doi.org/10.1021/ja3105939

Mao, Y., Zhou, Y., Wen, H., Xie, J., Zhang, W., & Wang, J. (2014). Morphology-controlled synthesis of large mordenite crystals. *New Journal of Chemistry*, 38 (7), 3295-3301. https://doi.org/10.1039/C3NJ01601C

Martin-Calvo, A., Parra, J. B., Ania, C. O., & Calero, S. (2014). Insights on the anomalous adsorption of carbon dioxide in LTA zeolites. *The Journal of Physical Chemistry C*, 118 (44), 25460-25467. https://doi.org/10.1021/jp507431c

McCusker, L. B., & Baerlocher, C. (2007). Zeolite structures. In Introduction to Zeolite Science and Practice. Edited by Čejka, J., van Bekkum, H., Corma, A., & Schüth, F. The Netherlands: Elsevier B. V. https://doi.org/10.1016/S0167-2991(07)80790-7

McLeod, C. L., & Shaulis, B. J. (2018). Rare earth elements in planetary crusts: Insights from chemically evolved igneous suites on earth and the moon. *Minerals*, 8 (10), 455-478. https://doi.org/10.3390/min8100455

Meise, W., & Schwochow, F. E. (1973). Kinetic studies on the formation of zeolite A. *Advances in Chemistry*, 121, 169-178. https://doi.org/10.1021/ba-1973-0121.ch014

Meng, L., Mezari, B., Goesten, M. G., Wannapakdee, W., Pestman, R., Gao, L., Wiesfeld, J., & Hensen, E. J. M. (2017). Direct synthesis of hierarchical ZSM-5 zeolite using cetyltrimethylammonium as structure directing agent for methanol-to-hydrocarbons conversion. *Catalysis Science & Technology*, 7 (19), 4520-4533. https://doi.org/10.1039/C7CY01603D

Mignoni, M. L., Petkowicz, D. I., Machado, N. R. C. F., & Pergher, S. B. C. (2008). Synthesis of mordenite using kaolin as Si and Al source. *Applied Clay Science*, 1-2 (41), 99-104. https://doi.org/10.1016/j.clay.2007.09.010

Miller, F. A., & Wilkins, C. H. (1952). Infrared spectra and characteristic frequencies of inorganic ions. *Analytical Chemistry*, 24 (8), 1253-1294. https://doi.org/10.1021/ac60068a007

Ming, D. W., & Gooding, J. L. (1988). Zeolites on Mars: Possible environmental indicators in soils and sediments. *Lunar and Planetary Institute Workshop on Mars Sample Return Science*, 124-125.

Mintova, S., Valtchev, V., & Kanev, I. (1995). Structure-controlled effect of organic templates on zeolite crystallization. *Molecular Engineering*, 4 (4), 369-373. https://doi.org/10.1007/BF01019469

Missengue, R., Losch, P., Musyoka, N., Louis, B., Pale, P., & Petrik, L. (2018). Conversion of South African coal fly ash into high-purity ZSM-5 zeolite without additional source of silica or alumina and its application as a methanol-to-olefins catalyst. *Catalysts*, 8 (4), 124-138. https://doi.org/10.3390/catal8040124

Missengue, R. N. M. (2016). Synthesis of ZSM-5 zeolite from South African fly ash and its application as solid catalyst (PhD Thesis, University of the Western Cape). Retrieved June 28, 2019 from http://etd.uwc.ac.za/xmlui/handle/11394/5431

Missengue, R. N. M., Losch, P., Sedres, G., Musyoka, N. M., Fatoba, O. O., Louis, B., Pale, P., & Petrik, L. F. (2017). Transformation of South African coal fly ash into ZSM-5 zeolite and its application as an MTO catalyst. *Comptes Rendus Chimie*, 20 (1), 78-86. https://doi.org/10.1016/j.crci.2016.04.012

Mitra, A., Wang, Z., Cao, T., Wang, H., Huang, L., & Yan, Y. (2002). Synthesis and corrosion resistance of high-silica zeolite MTW, BEA, and MFI coatings on steel and aluminum. *Journal of the Electrochemical Society*, 149 (10), B472-B478. https://doi.org/10.1149/1.1507784

Mohamed, M. M., Salama, T. M., Othman, I., & Ellah, I. A. (2005). Synthesis of high silica mordenite nanocrystals using o-phenylenediamine template. *Microporous and Mesoporous Materials*, 84 (1), 84-96. https://doi.org/10.1016/j.micromeso.2005.05.017

Molina, A., & Poole, C. (2004). A comparative study using two methods to produce zeolites from fly ash. *Minerals Engineering*, 17 (2), 167-173. https://doi.org/10.1016/j.mineng.2003.10.025

Moliner, M., Martínez, C., & Corma, A. (2014). Synthesis strategies for preparing useful small pore zeolites and zeotypes for gas separations and catalysis. *Chemistry of Materials*, 26 (1), 246-258. https://doi.org/10.1021/cm4015095

Moliner, M., Rey, F., & Corma, A. (2013). Towards the rational design of efficient organic structure-directing agents for zeolite synthesis. *Angewandte Chemie International Edition*, 52 (52), 13880-13889. https://doi.org/10.1002/anie.201304713

Morris, R. E., & Wheatley, P. S. (2007). Diffraction techniques applied to zeolites. In Introduction to Zeolite Science and Practice. Edited by Čejka, J., van Bekkum, H., Corma,

A., & Schüth, F. The Netherlands: Elsevier B. V. https://doi.org/10.1016/S0167-2991(07)80799-3

Mostowicz, R., & Berak, J. M. (1985). Factors influencing the crystal morphology of ZSM-5 type zeolites. In Zeolites Synthesis, Structure, Technology and Application. Edited by B. Držaj, B., & Hočevar, S., & Pejovni, S. https://doi.org/10.1016/S0167-2991(08)65269-6

Mozgawa, W., Król, M., Dyczek, J., & Deja, J. (2014). Investigation of the coal fly ashes using IR spectroscopy. *Spectrochimica Acta Part A: Molecular and Biomolecular Spectroscopy*, 132, 889-894. https://doi.org/10.1016/j.saa.2014.05.052

Murayama, N., Yamamoto, H., & Shibata, J. (2002). Mechanism of zeolite synthesis from coal fly ash by alkali hydrothermal reaction. *International Journal of Mineral Processing*, 64 (1), 1-17. https://doi.org/10.1016/S0301-7516(01)00046-1

Musyoka, N. M., Petrik, L. F., Hums, E., Baser, H., & Schwieger, W. (2014). In situ ultrasonic diagnostic of zeolite X crystallization with novel (hierarchical) morphology from coal fly ash. *Ultrasonics*, 54 (2), 537-543. https://doi.org/10.1016/j.ultras.2013.08.005

Musyoka, Nicholas M., Petrik, L. F., Fatoba, O. O., & Hums, E. (2013). Synthesis of zeolites from coal fly ash using mine waters. *Minerals Engineering*, 53, 9-15. https://doi.org/10.1016/j.mineng.2013.06.019

Myerson, A.S. (2002). Handbook of industrial crystallization. 2nd Edition. United Kingdom: Butterworth-Heinemann.

Nasrazadani, S., & Raman, A. (1993). The application of infrared spectroscopy to the study of rust systems - II. Study of cation deficiency in magnetite produced during its transformation to maghemite and hematite. *Corrosion Science*, 34 (8), 1355-1365.

Nassar, M. Y., Abdelrahman, E. A., Aly, A. A., & Mohamed, T. Y. (2017). A facile synthesis of mordenite zeolite nanostructures for efficient bleaching of crude soybean oil and removal of methylene blue dye from aqueous media. *Journal of Molecular Liquids*, 248, 302-313. https://doi.org/10.1016/j.molliq.2017.10.061

Ndlovu, N. Z. N., Missengue, R. N. M., Petrik, L. F., & Ojumu, T. (2017). Synthesis and characterization of faujasite zeolite and geopolymer from South African coal fly ash. *Journal*

of Environmental Engineering, 143 (9), 04017042. https://doi.org/10.1061/(ASCE)EE.1943-7870.0001212

Ndlovu, N. Z. N. (2016). Synthesis of zeolite (ZSM-5 and Faujasite) and geopolymer from South African coal fly ash (M(Tech)). Cape Peninsula University of Technology, Bellville, Cape Town, South Africa.

Nearchou, A., Cornelius, M.-L. U., Skelton, J. M., Jones, Z. L., Cairns, A. B., Collings, I. E., Raithby, P. R., Wells, S. A., & Sartbaeva, A. (2019). Intrinsic flexibility of the EMT zeolite framework under pressure. *Molecules*, 24 (3), 641. https://doi.org/10.3390/molecules24030641

Nearchou, A., & Sartbaeva, A. (2015). Influence of alkali metal cations on the formation of zeolites under hydrothermal conditions with no organic structure directing agents. *CrystEngComm*, 17 (12), 2496-2503. https://doi.org/10.1039/C4CE02119C

Neves, T. M., Fernandes, J. O., Lião, L. M., Deise da Silva, E., Augusto da Rosa, C., & Mortola, V. B. (2019). Glycerol dehydration over micro- and mesoporous ZSM-5 synthesized from a one-step method. *Microporous and Mesoporous Materials*, 275, 244-252. https://doi.org/10.1016/j.micromeso.2018.09.006

Nijkamp, M. G., Raaymakers, J. E. M. J., van Dillen, A. J., & de Jong, K. P. (2001). Hydrogen storage using physisorption - materials demands. *Applied Physics A*, 72 (5), 619-623. https://doi.org/10.1007/s003390100847

Ojha, K., Pradhan, N. C., & Samanta, A. N. (2004). Zeolite from fly ash: Synthesis and characterization. *Bulletin of Materials Science*, 27 (6), 555-564. https://doi.org/10.1007/BF02707285

Oleksiak, M. D., & Rimer, J. D. (2014). Synthesis of zeolites in the absence of organic structure-directing agents: Factors governing crystal selection and polymorphism. *Reviews in Chemical Engineering*, 30 (1), 1-49. https://doi.org/10.1515/revce-2013-0020

Ordonez, S., & Diaz, E. (2009). Basic zeolites: Structure, preparation and environmental applications. In Handbook of zeolites: Structure, properties and applications. Edited by Wong, T. T. The United States of America: Nova Science Publishers, Inc.

Pál-Borbély, G. (2007). Thermal Analysis of Zeolites. In Characterization II. Edited by Karge, H. G., & Weitkamp, J. Germany: Springer. https://doi.org/10.1007/3829_002

Pan, T., Wu, Z., & Yip, A. C. K. (2019). Advances in the green synthesis of microporous and hierarchical zeolites: A short review. *Catalysts*, 9 (3), 274-291. https://doi.org/10.3390/catal9030274

Payra, P. & Dutta, P.K. (2003). Zeolites: A primer. In Handbook of Zeolite Science and Technology. Edited by Auerbach, S. M., Carrado, K. A., & Dutta, P. K. The United States of America: Marcel Dekker, Inc.

Pérez-Page, M., Makel, J., Guan, K., Zhang, S., Tringe, J., Castro, R. H. R., & Stroeve, P. (2016). Gas adsorption properties of ZSM-5 zeolites heated to extreme temperatures. *Ceramics International*, 42 (14), 15423-15431. https://doi.org/10.1016/j.ceramint.2016.06.193

Petrik, L. F. (2009). The influence of cation, anion and water content on the rate of formation and pore size distribution of zeolite ZSM-5. *South African Journal of Science*, 105 (7-8), 251-257.

Petrik, L. F., O'Connor, C. T., & Schwarz, S. (1995). The influence of various synthesis parameters on the morphology and crystal size of ZSM-5 and the relationship between morphology and crystal size and propene oligomerization activity. In Catalysis by Microporous Materials. Edited by Beyer, H. K., Karge, H. G., Kiricsi, I., & Nagy, J. B. https://doi.org/10.1016/S0167-2991(06)81263-2

Pluth, J. J., & Smith, J. V. (1980). Accurate redetermination of crystal structure of dehydrated zeolite A. Absence of near zero coordination of sodium. Refinement of silicon, aluminum-ordered superstructure. *Journal of the American Chemical Society*, 102 (14), 4704-4708. https://doi.org/10.1021/ja00534a024

Psycharis, V., Perdikatsis, V., & Christidis, G. (2004). Crystal structure and rietveld refinement of zeolite A synthesized from fine-grained perlite waste materials. *Bulletin of the Geological Society of Greece*, 36 (1), 121. https://doi.org/10.12681/bgsg.16591

Querol, X., Moreno, N., Umaña, J. C., Alastuey, A., Hernández, E., López-Soler, A., & Plana, F. (2002). Synthesis of zeolites from coal fly ash: An overview. *International Journal of Coal Geology*, 50 (1), 413-423. https://doi.org/10.1016/S0166-5162(02)00124-6

Reed, T. B., & Breck, D. W. (1956). Crystalline Zeolites. II. Crystal Structure of Synthetic Zeolite, Type A. *Journal of the American Chemical Society*, 78 (23), 5972-5977. https://doi.org/10.1021/ja01604a002

Ren, N., Yang, Z.-J., Lv, X.-C., Shi, J., Zhang, Y.-H., & Tang, Y. (2010). A seed surface crystallization approach for rapid synthesis of submicron ZSM-5 zeolite with controllable crystal size and morphology. *Microporous and Mesoporous Materials*, 131 (1), 103-114. https://doi.org/10.1016/j.micromeso.2009.12.009

Reyes, C. A. R., Williams, C., & Alarcón, O. M. C. (2013). Nucleation and growth process of sodalite and cancrinite from kaolinite-rich clay under low-temperature hydrothermal conditions. *Materials Research*, 16 (2), 424-438. https://doi.org/10.1590/S1516-14392013005000010

Rouessac, F. & Rouessac, A. (2013) Chemical Analysis: Modern Instrumentation Methods and Techniques. England: John Wiley & Sons, Inc.

Rudnick, R. L., & Gao, S. (2003). Composition of the continental crust. *Treatise on Geochemistry*, 3, 1-64. https://doi.org/10.1016/B0-08-043751-6/03016-4

Sartbaeva, A., Gatta, G. D., & Wells, S. A. (2008). Flexibility window controls pressure-induced phase transition in analcime. *EPL (Europhysics Letters)*, 83 (2), 26002-26006. https://doi.org/10.1209/0295-5075/83/26002

Sartbaeva, Asel, Wells, S. A., Treacy, M. M. J., & Thorpe, M. F. (2006). The flexibility window in zeolites. *Nature Materials*, 5 (12), 962-965. https://doi.org/10.1038/nmat1784

Sashkina, K. A., Qi, Z., Wu, W., Ayupov, A. B., Lysikov, A. I., & Parkhomchuk, E. V. (2017). The effect of H_2O/SiO_2 ratio in precursor solution on the crystal size and morphology of zeolite ZSM-5. *Microporous and Mesoporous Materials*, 244, 93-100. https://doi.org/10.1016/j.micromeso.2017.02.060

Sedres, G. (2016). Recovery of SiO_2 and Al_2O_3 from coal fly ash (MSc Thesis, University of the Western Cape). Retrieved June 28, 2019 from http://etd.uwc.ac.za/handle/11394/5651

Shaheen, S. M., Hooda, P. S., & Tsadilas, C. D. (2014). Opportunities and challenges in the use of coal fly ash for soil improvements-a review. *Journal of Environmental Management*, 145, 249-267. https://doi.org/10.1016/j.jenvman.2014.07.005

Shaikh, A. A., Joshi, P. N., Jacob, N. E., & Shiralkar, V. P. (1993). Direct hydrothermal crystallization of high-silica large-pore mordenite. *Zeolites*, 13 (7), 511-517. https://doi.org/10.1016/0144-2449(93)90227-T

Shigemoto, N., Hayashi, H., & Miyaura, K. (1993). Selective formation of Na-X zeolite from coal fly ash by fusion with sodium hydroxide prior to hydrothermal reaction. *Journal of Materials Science*, 28 (17), 4781-4786. https://doi.org/10.1007/BF00414272

Shigemoto, N., Sugiyama, S., Hayashi, H., & Miyaura, K. (1995). Characterization of Na-X, Na-A, and coal fly ash zeolites and their amorphous precursors by IR, MAS NMR and XPS. *Journal of Materials Science*, 30 (22), 5777-5783. https://doi.org/10.1007/BF00356720

Shoumkova, A., & Stoyanova, V. (2012). Zeolites formation by hydrothermal alkali activation of coal fly ash from thermal power station "Maritsa 3", Bulgaria. *Fuel*, 103, 533-541. https://doi.org/10.1016/j.fuel.2012.07.076

Shukla, D. B., & Pandya, V. P. (1989). Estimation of crystalline phase in ZSM-5 zeolites by infrared spectroscopy. *Journal of Chemical Technology & Biotechnology*, 44 (2), 147-154. https://doi.org/10.1002/jctb.280440206

Silva, J. P. P., Baltar, C. a. M., Gonzaga, R. S. G., Peres, A. E. C., & Leite, J. Y. P. (2012). Identification of sodium silicate species used as flotation depressants. *Minerals & Metallurgical Processing Journal*, 29 (4), 207-210.

Sing, K. S. W. (1982). Reporting physisorption data for gas/solid systems with special reference to the determination of surface area and porosity (Provisional). *Pure and Applied Chemistry*, 54 (11), 2201-2218. https://doi.org/10.1351/pac198254112201

Singh, B. K., Kim, Y., Baek, S. B., Meena, A., Sultan, S., Kwak, J. H., & Kim, K. S. (2018). Template free facile synthesis of mesoporous mordenite for bulky molecular catalytic reactions. *Journal of Industrial and Engineering Chemistry*, 57, 363-369. https://doi.org/10.1016/j.jiec.2017.08.044

Singh, R., & Dutta, P. K. (2003). MFI: A case study of zeolite synthesis. In Handbook of Zeolite Science and Technology. Edited by Auerbach, S. M., Carrado, K. A., & Dutta, P. K. The United States of America: Marcel Dekker, Inc.

Sklenak, S., Dědeček, J., Li, C., Wichterlová, B., Gábová, V., Sierka, M., & Sauer, J. (2009). Aluminium siting in the ZSM-5 framework by combination of high resolution 27Al NMR and DFT/MM calculations. *Physical Chemistry Chemical Physics*, 11 (8), 1237-1247. https://doi.org/10.1039/B807755J

Šolcová, O., Matějová, L., Topka, P., Musilová, Z., & Schneider, P. (2011). Comparison of textural information from argon (87 K) and nitrogen (77 K) physisorption. *Journal of Porous Materials*, 18 (5), 557-565. https://doi.org/10.1007/s10934-010-9409-x

Tao, Y., Kanoh, H., & Kaneko, K. (2006). Developments and structures of mesopores in alkaline-treated ZSM-5 zeolites. *Adsorption*, 12 (5), 309-316. https://doi.org/10.1007/s10450-006-0561-1

Terasaki, O., Ohsuna, T., Liu, Z., Sakamoto, Y., Ruan, J., & Che, S. (2007). Structural study of porous materials by electron microscopy. In Introduction to Zeolite Science and Practice. Edited by Čejka, J., van Bekkum, H., Corma, A., & Schüth, F. The Netherlands: Elsevier B. V. https://doi.org/10.1016/S0167-2991(07)80802-0

Thommes, M. (2007). Textural characterization of zeolites and ordered mesoporous materials by physical adsorption. In Introduction to Zeolite Science and Practice. Edited by Čejka, J., van Bekkum, H., Corma, A., & Schüth, F. The Netherlands: Elsevier B. V. https://doi.org/10.1016/S0167-2991(07)80803-2

Thommes, M., Kaneko, K., Neimark, A. V., Olivier, J. P., Rodriguez-Reinoso, F., Rouquerol, J., & Sing, K. S. W. (2015). Physisorption of gases, with special reference to the evaluation of surface area and pore size distribution (IUPAC Technical Report). *Pure and Applied Chemistry*, 87 (9-10), 1051-1069. https://doi.org/10.1515/pac-2014-1117

Todorova, T. D., & Kalvachev, Y. A. (2015). Seed-mediated approach to size-controlled synthesis of a mordenite type zeolite from organic template free initial gel. *Bulgarian Chemical Communications*, 47 (1), 409-416.

Treacy, M. M. J., & Higgins, J. B. (2007). Collection of simulated XRD powder patterns for zeolites. 5th Edition. The Netherlands: Elsevier B.V.

Ueda, S., Murata, H., Koizumi, M., & Nishimura, H. (1980). Crystallization of mordenite from aqueous solutions. *American Mineralogist*, 65, 1012-1019.

Valdés, M. G., Pérez-Cordoves, A. I., & Díaz-García, M. E. (2006). Zeolites and zeolite-based materials in analytical chemistry. *Trends in Analytical Chemistry*, 1 (25), 24-30. https://doi.org/10.1016/j.trac.2005.04.016

Valtchev, V. P., Faust, A.-C., & Lézervant, J. (2004). Rapid synthesis of silicalite-1 nanocrystals by conventional heating. *Microporous and Mesoporous Materials*, 68 (1), 91-95. https://doi.org/10.1016/j.micromeso.2003.11.018

van den Broeke, L. J. P., Bakker, W. J. W., Kapteijn, F., & Moulijn, J. A. (1999). Transport and separation properties of a silicalite-1 membrane-I. Operating conditions. *Chemical Engineering Science*, 54 (2), 245-258. https://doi.org/10.1016/S0009-2509(98)00241-3

van Hooff, J. H. C., & Roelofsen, J. W. (1991). Techniques of zeolite characterization. In Introduction to Zeolite Science and Practice. Edited by van Bekkum, H., Flanigen, E. M., & Jansen, J. C. The Netherlands: Elsevier B. V. https://doi.org/10.1016/S0167-2991(08)63605-8

van Santen, R. A., & Vogel, D. L. (1989). Lattice dynamics of zeolites. *Advances in Solid-State Chemistry*, 1, 151-224.

Vichaphund, S., Aht-Ong, D., Sricharoenchaikul, V., & Atong, D. (2014). Characteristic of fly ash derived-zeolite and its catalytic performance for fast pyrolysis of Jatropha waste. *Environmental Technology*, 35 (17-20), 2254-2261. https://doi.org/10.1080/09593330.2014.900118

Vichaphund, S., Sricharoenchaikul, V., & Atong, D. (2017). Utilization of fly ash-derived H-ZSM-5: catalytic pyrolysis of Jatropha wastes in a fixed-bed reactor. *Environmental Technology*, 38 (13-14), 1660-1672. https://doi.org/10.1080/09593330.2016.1244567

Wang, L., Sang, S., Meng, S., Zhang, Y., Qi, Y., & Liu, Z. (2007). Direct synthesis of Zn-ZSM-5 with novel morphology. *Materials Letters*, 61 (8), 1675-1678. https://doi.org/10.1016/j.matlet.2006.07.097

Wang, Yan, Ma, J., Ren, F., Du, J., & Li, R. (2017). Hierarchical architectures of ZSM-5 nanocrystalline aggregates with particular catalysis for lager molecule reaction. *Microporous and Mesoporous Materials*, 240, 22-30. https://doi.org/10.1016/j.micromeso.2016.10.051

Wang, Yeqing, Wu, Q., Meng, X., & Xiao, F.-S. (2017). Insights into the organotemplate-free synthesis of zeolite catalysts. *Engineering*, 3 (4), 567-574. https://doi.org/10.1016/J.ENG.2017.03.029

Wdowin, M., Franus, M., Panek, R., Badura, L., & Franus, W. (2014). The conversion technology of fly ash into zeolites. *Clean Technologies and Environmental Policy*, 16 (6), 1217-1223. https://doi.org/10.1007/s10098-014-0719-6

Weitkamp, J. (2000). Zeolites and catalysis. *Solid State Ionics*, 131 (1-2), 175-188. https://doi.org/10.1016/S0167-2738(00)00632-9

Weitkamp, J., & Hunger, M. (2007). Acid and base catalysis on zeolites. In Introduction to Zeolite Science and Practice. Edited by Čejka, J., van Bekkum, H., Corma, A., & Schüth, F. The Netherlands: Elsevier B. V. https://doi.org/10.1016/S0167-2991(07)80810-X

Wells, S. A., Sartbaeva, A., & Gatta, G. D. (2011). Flexibility windows and phase transitions of ordered and disordered ANA framework zeolites. *EPL (Europhysics Letters)*, 94 (5), 56001-56005. https://doi.org/10.1209/0295-5075/94/56001

Wells, S. A, Dove, M. T., & Tucker, M. G. (2002). Finding best-fit polyhedral rotations with geometric algebra. *Journal of Physics: Condensed Matter*, 14 (17), 4567-4584. https://doi.org/10.1088/0953-8984/14/17/327

Wells, S. A., Leung, K. M., Edwards, P. P., & Sartbaeva, A. (2015). Flexibility windows in faujasite with explicit water and methanol extra-framework content. *Dalton Transactions*, 44 (13), 5978-5984. https://doi.org/10.1039/c4dt03150d

Wells, S. A., Leung, K. M., Edwards, P. P., Tucker, M. G., & Sartbaeva, A. (2017). Defining the flexibility window in ordered aluminosilicate zeolites. *Royal Society Open Science*, 4 (9), 170757-170764. https://doi.org/10.1098/rsos.170757

Wells, S. A., & Sartbaeva, A. (2012). Template-based geometric simulation of flexible frameworks. *Materials*, 5 (3), 415-431. https://doi.org/10.3390/ma5030415

Wells, S. A., & Sartbaeva, A. (2015). GASP: Software for geometric simulations of flexibility in polyhedral and molecular framework structures. *Molecular Simulation*, 41 (16-17), 1409-1421. https://doi.org/10.1080/08927022.2015.1032277

Wu, H., Liu, M., Tan, W., Hou, K., Zhang, A., Wang, Y., & Guo, X. (2014). Effect of ZSM-5 zeolite morphology on the catalytic performance of the alkylation of toluene with methanol. *Journal of Energy Chemistry*, 23 (4), 491-497. https://doi.org/10.1016/S2095-4956(14)60176-5

Xie, J., Huang, M., & Kaliaguine, S. (1994). Base and acid sites in alkaline earth cation-exchanged X zeolites. *Catalysis Letters*, 29 (3-4), 281-291. https://doi.org/10.1007/BF00807107

Xu, R., Pang, W., Yu, J., Huo, Q., & Chen, J. (2007). Chemistry of Zeolites and Related Porous Materials: Synthesis and Structure. Singapore: John Wiley & Sons, Inc.

Yang, R., Meng, F., Wang, X., & Wang, Y. (2011). Influence of Na^+ on the synthesis of silicalite-1 catalysts for use in the vapor phase Beckmann rearrangement of cyclohexanone oxime. *Frontiers of Chemical Science and Engineering*, 5 (4), 401-408. https://doi.org/10.1007/s11705-011-1129-5

Yang, X., Roonasi, P., & Holmgren, A. (2008). A study of sodium silicate in aqueous solution and sorbed by synthetic magnetite using in situ ATR-FTIR spectroscopy. *Journal of Colloid and Interface Science*, 328 (1), 41-47. https://doi.org/10.1016/j.jcis.2008.08.061

Yaping, Y., Xiaoqiang, Z., Weilan, Q., & Mingwen, W. (2008). Synthesis of pure zeolites from supersaturated silicon and aluminum alkali extracts from fused coal fly ash. *Fuel*, 87 (10-11), 1880-1886. https://doi.org/10.1016/j.fuel.2007.12.002

Yu, D., Fu, M., Yuan, Y., Song, Y., Chen, J., & Fang, Y. (2016). One-step synthesis of hierarchical-structured ZSM-5 zeolite. *Journal of Fuel Chemistry and Technology*, 44 (11), 1363-1369. https://doi.org/10.1016/S1872-5813(16)30059-7

Yu, J. (2007). Synthesis of zeolites. In Introduction to Zeolite Science and Practice. Edited by Čejka, J., van Bekkum, H., Corma, A., & Schüth, F. The Netherlands: Elsevier B. V. https://doi.org/10.1016/S0167-2991(07)80791-9

Zhang, J., Li, X., Liu, J., & Wang, C. (2019). A comparative study of MFI zeolite derived from different silica sources: Synthesis, characterization and catalytic performance. *Catalysts*, 9 (1), 13-26. https://doi.org/10.3390/catal9010013

Zhang, Lei, Laak, A. N. C. van, Jongh, P. E. de, & Jong, K. P. de. (2009). Synthesis of large mordenite crystals with different aspect ratios. *Microporous and Mesoporous Materials*, 126 (1), 115-124. https://doi.org/10.1016/j.micromeso.2009.05.034

Zhang, Ling, Xie, S., Xin, W., Li, X., Liu, S., & Xu, L. (2011). Crystallization and morphology of mordenite zeolite influenced by various parameters in organic-free synthesis. *Materials Research Bulletin*, 46 (6), 894-900. https://doi.org/10.1016/j.materresbull.2011.02.018

Zhang, X., Wang, J., Liu, H., Liu, C., & Yeung, K. (2003). Factors affecting the synthesis of hetero-atom zeolite Fe-ZSM-5 membrane. *Separation and Purification Technology*, 32 (1-3), 151-158. https://doi.org/10.1016/S1383-5866(03)00028-5

Zhidomirov, G. M., Shubin, A. A., Larin, A. V., Malykhin, S. E., & Rybakov, A. A. (2012). Molecular models of the stabilization of bivalent metal cations in zeolite catalysts. In Practical Aspects of Computational Chemistry I. Edited by Leszczynski, J., & Shukla, M. K. https://doi.org/10.1007/978-94-007-0919-5_20

Appendix

Appendix A: FTIR data for as-synthesised zeolite samples

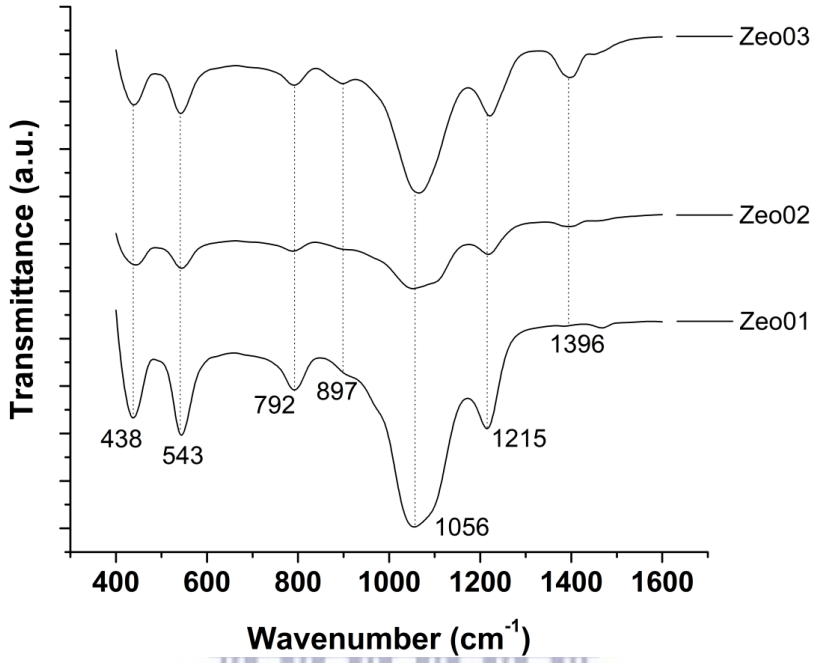

Figure A1: FTIR spectra of as-synthesised zeolite samples Zeo01-03 crystallised at a hydrothermal temperature of 160 °C for 72 hours.

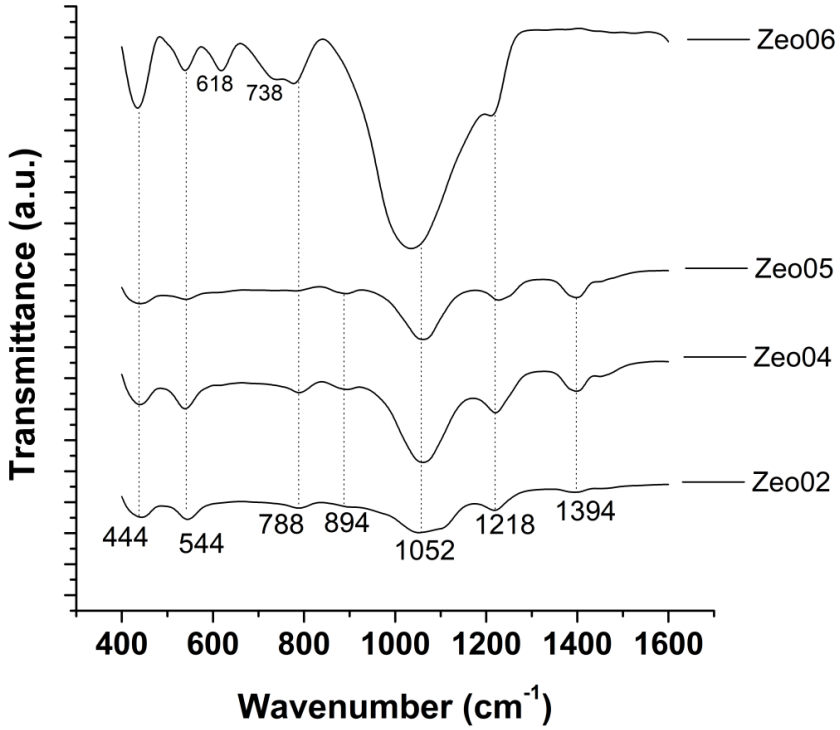

Figure A2: FTIR spectra of as-synthesised zeolite samples Zeo02 and Zeo04-06 crystallised at a hydrothermal temperature of 160 °C for 72 hours.

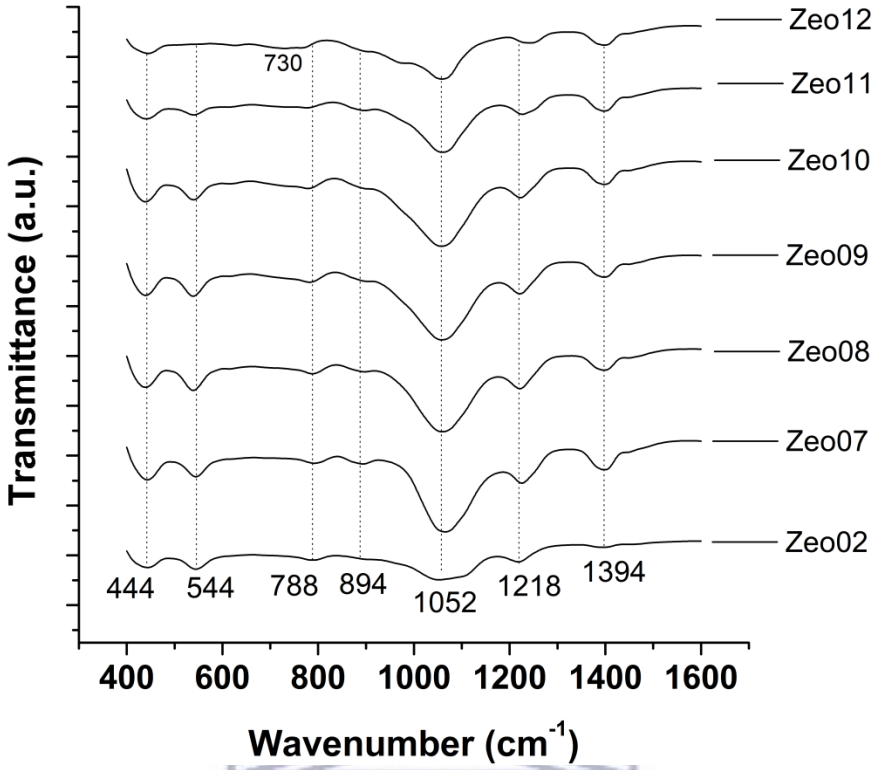

Figure A3: FTIR spectra of as-synthesised zeolite samples Zeo02 and Zeo07-12 crystallised at a hydrothermal temperature of 160 °C for 72 hours.

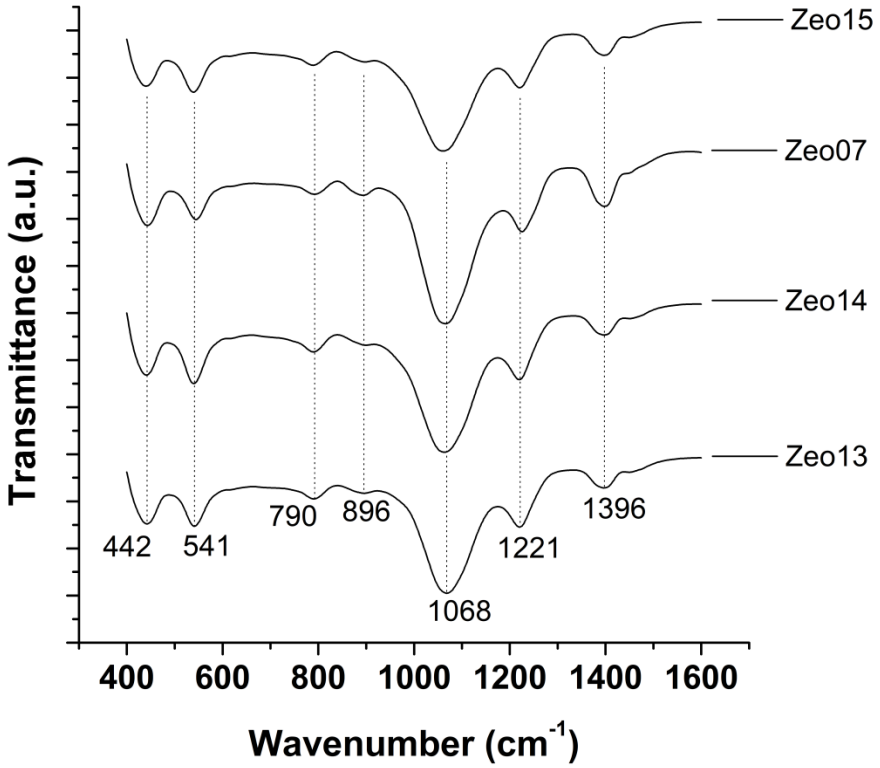

Figure A4: FTIR spectra of as-synthesised zeolite samples Zeo07 and Zeo13-15 crystallised at a hydrothermal temperature of 160 °C for 72 hours.

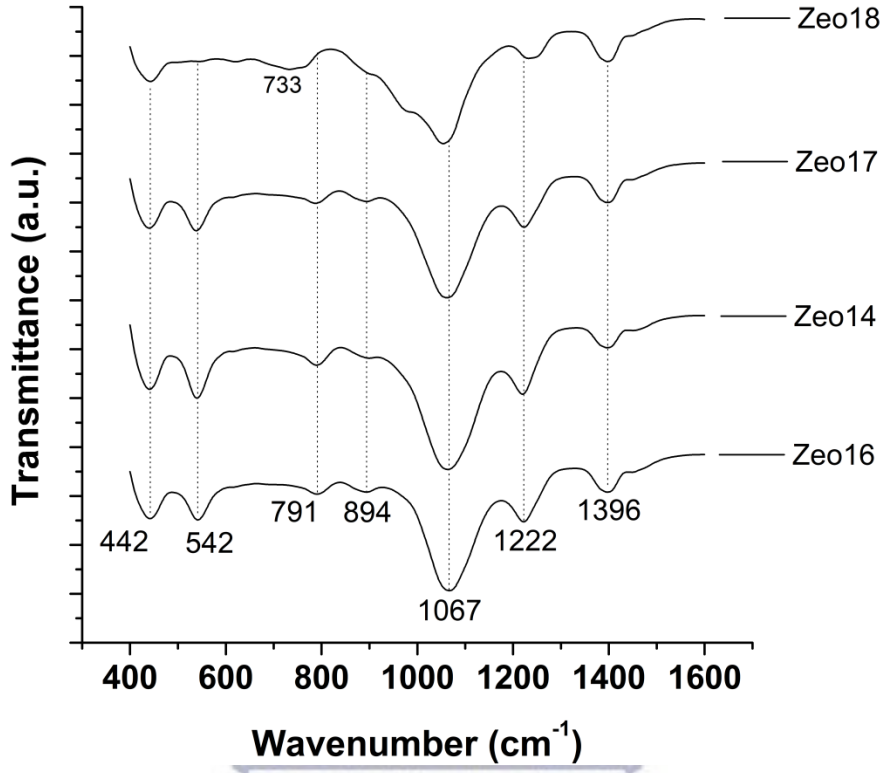

Figure A5: FTIR spectra of as-synthesised zeolite samples Zeo14 and Zeo16-18 crystallised at a hydrothermal temperature of 160 °C for 72 hours.

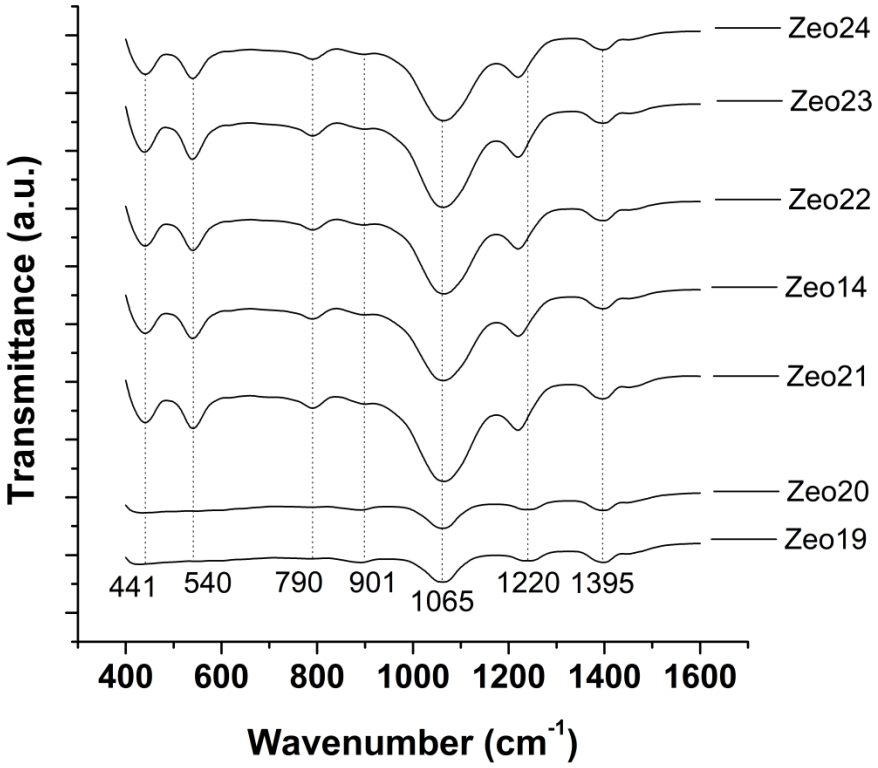

Figure A6: FTIR spectra of as-synthesised zeolite samples Zeo14 and Zeo19-24 crystallised at a hydrothermal temperature of 160 °C for varying time periods.

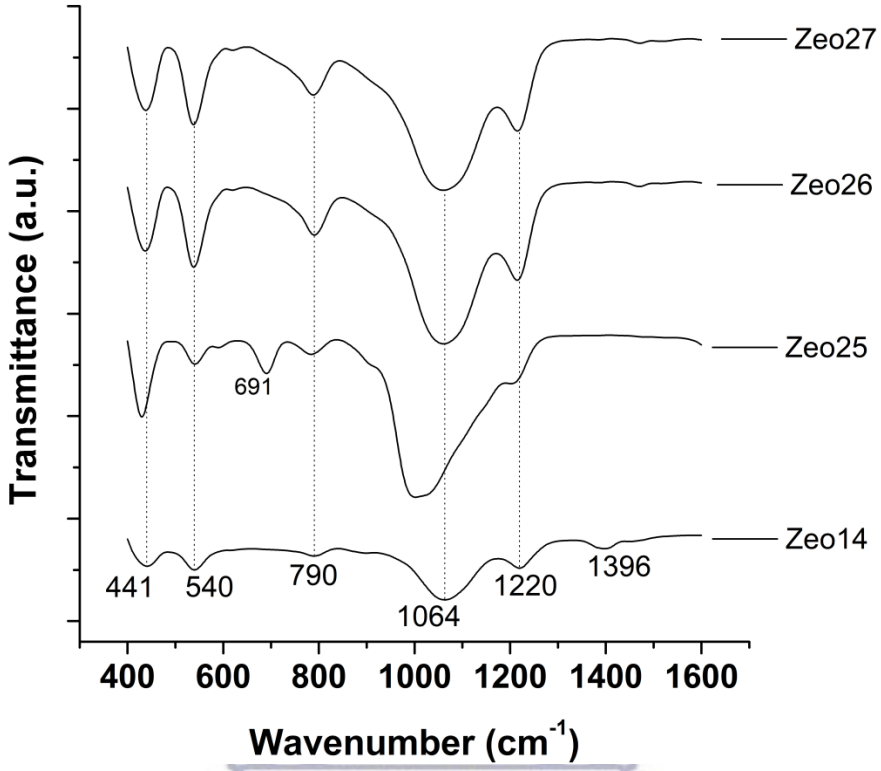

Figure A7: FTIR spectra of as-synthesised zeolite samples Zeo14 and Zeo25-27 crystallised at a hydrothermal temperature of 160 °C for 72 hours.

Appendix B: BET data for selected Na-zeolite samples

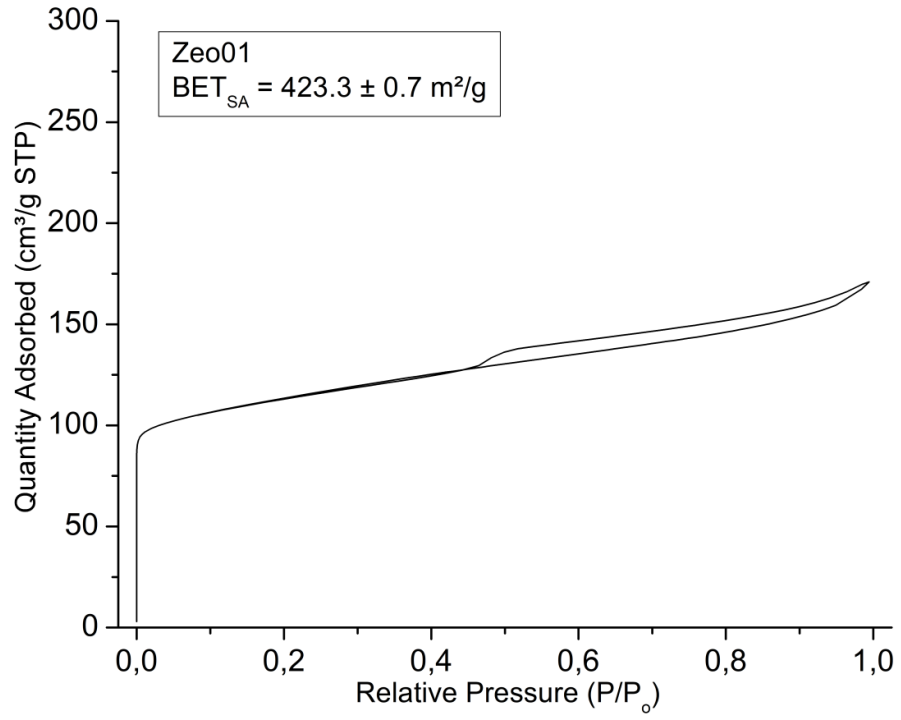

Figure B1: Nitrogen isotherm of as-synthesised zeolite sample Zeo01 crystallised at a hydrothermal temperature of 160 °C for 72 hours.

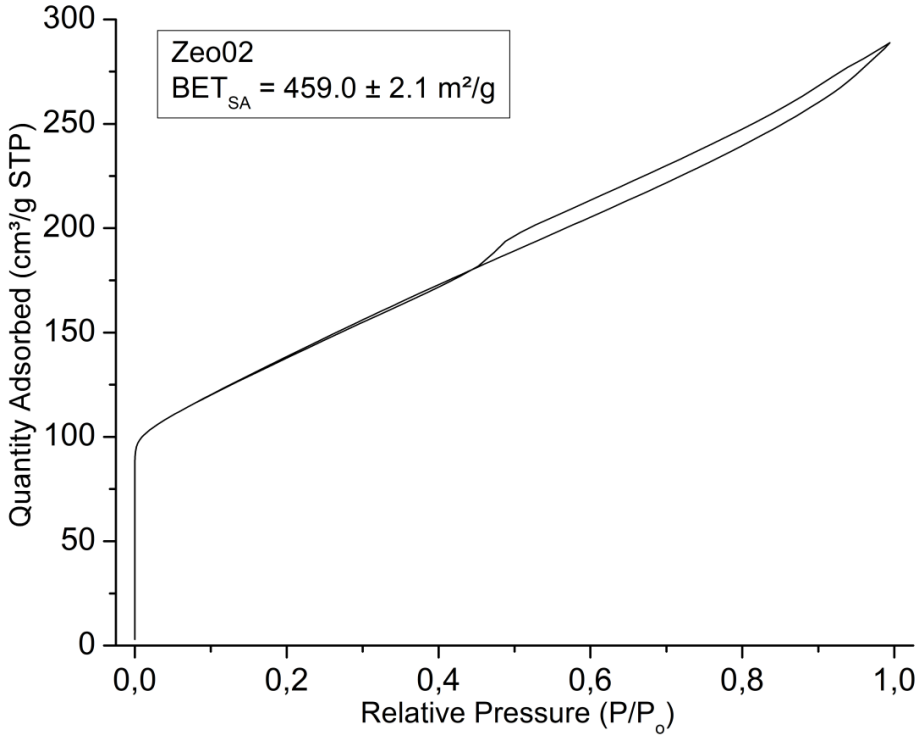

Figure B2: Nitrogen isotherm of as-synthesised zeolite sample Zeo02 crystallised at a hydrothermal temperature of 160 °C for 72 hours.

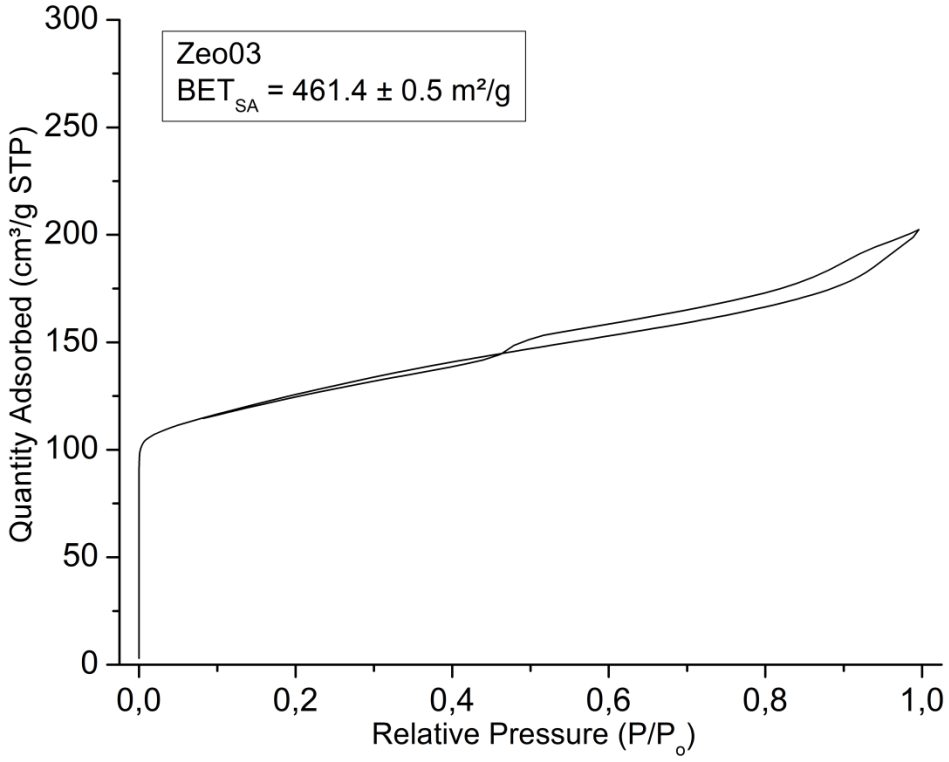

Figure B3: Nitrogen isotherm of as-synthesised zeolite sample Zeo03 crystallised at a hydrothermal temperature of 160 °C for 72 hours.

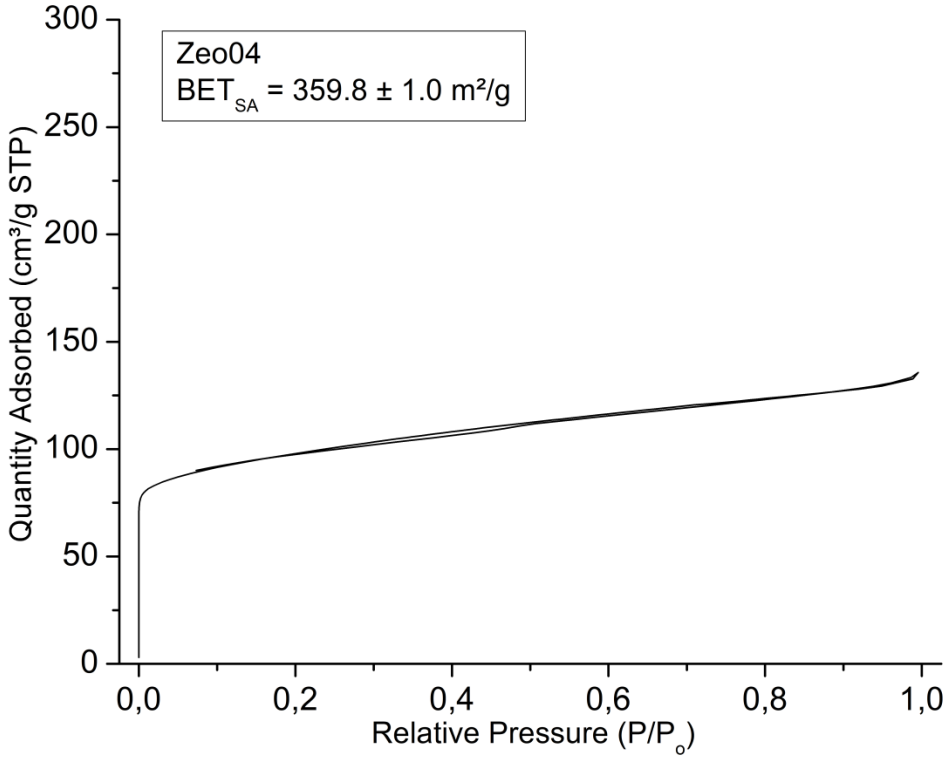

Figure B4: Nitrogen isotherm of as-synthesised zeolite sample Zeo04 crystallised at a hydrothermal temperature of 160 °C for 72 hours.

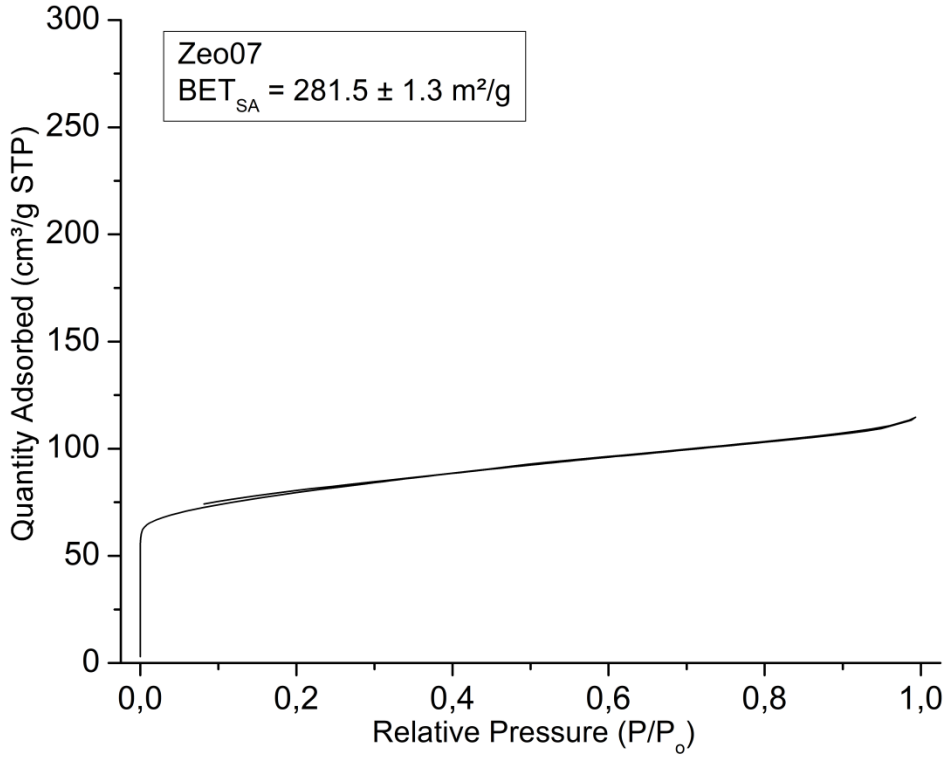

Figure B5: Nitrogen isotherm of as-synthesised zeolite sample Zeo07 crystallised at a hydrothermal temperature of 160 °C for 72 hours.

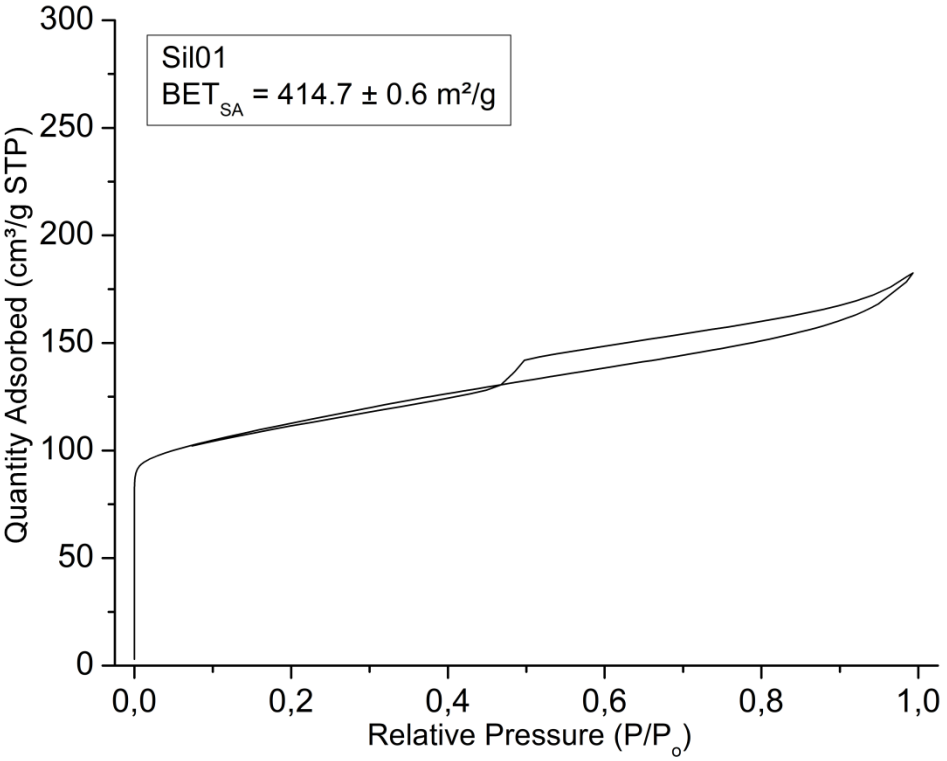

Figure B6: Nitrogen isotherm of as-synthesised zeosil sample Sil01 crystallised at a hydrothermal temperature of 170 °C for 48 hours.